



T.C.

ÇANAKKALE ONSEKİZ MART ÜNİVERSİTESİ
LİSANSÜSTÜ EĞİTİM ENSTİTÜSÜ

***CANAKKALE ONSEKİZ MART UNIVERSITY
JOURNAL OF ADVANCED
RESEARCH IN NATURAL AND
APPLIED SCIENCES***



ISSN 2757-5195

**Journal of Advanced Research in Natural
and Applied Sciences**

e-ISSN: 2757-5195

Volume 10 / Issue 1

Cilt 10 / Sayı 1

2024-Mart/March

Yayımcı / Publisher: Çanakkale Onsekiz Mart Üniversitesi

Rektör / Rector: Prof. Dr. R. Cüneyt ERENOĞLU

Baş Editör / Editor-in-Chief

Doç. Dr. Filiz UĞUR NİGİZ

Sayı Editörleri / Issue Editors

Doç. Dr. Ayça AYDOĞDU

Doç. Dr. Tuğba GÜNGÖR

Doç. Dr. Mehmet Ali YÜCEL

Doç. Dr. Doğukan TAŞER

Dr. Öğr. Üyesi Şebnem ÖNDER

Dr. Öğr. Üyesi Gülçin ÖZCAN ATEŞ

Doç. Dr. Deniz ŞANLIYÜKSEL YÜCEL

Dr. Öğr. Üyesi İsmail Onur TUNÇ

Prof. Dr. Tijen Ennil BEKTAŞ

Doç. Dr. Serdar ENGİNOĞLU

Doç. Dr. Alper SAĞLIK

Doç. Dr. Ali Tolga ÖZDEN

Dil Editörü / Language Editor

Doç. Dr. Sercan Hamza BAĞLAMA

Mizanpaj Editörü / Layout Editor

Burak ARSLAN

Yayın Editörü / Production Editor

Deniz FİDAN

Önsöz:

Journal of Advanced Research in Natural and Applied Sciences Dergisi Fen, Mühendislik, Doğa ve Temel bilimler alanlarında daha önce yayımlanmamış orijinal araştırma makalesi, derleme yazılar, teknik not türünde araştırmaları yayınlayan ulusal ve uluslararası indekslerde taranan, hakemli ve bilimsel bir dergidir. Journal of Advanced Research in Natural and Applied Sciences Dergisi Mart, Haziran, Eylül, Aralık olmak üzere yılda dört sayı yayınlanacaktır. Tr-Dizin’de taranan Journal of Advanced Research in Natural and Applied Sciences Dergisi’nin 10. cilt 1. sayısında 19 adet araştırma makalesi yayına kabul edilmiştir.

	<p>TÜBİTAK TR DİZİN tarafından taranmaktadır. Indexed by TR-DİZİN Database.</p>
	<p>TÜBİTAK-ULAKBİM DergiPark Akademik tarafından yayımlanmaktadır. Published by TÜBİTAK-ULAKBİM Turkish Journal Park Academic Database.</p>
	<p>CROSSREF® veri tabanı tarafından taranmakta ve makaleler DOI numarası ile yayımlanmaktadır. Indexed by CROSSREF® Database and articles are published with DOI number.</p>
	<p>Google Scholar'da ve SOBIAD'da taranmaktadır. Indexed by Google Scholar and SOBIAD Database.</p>

İletişim Adresi / Publisher Address

Çanakkale Onsekiz Mart Üniversitesi Lisansüstü Eğitim Enstitüsü
Terzioğlu Yerleşkesi Çanakkale (Sağlık Hizmetleri Meslek Yüksekokulu Binası)

Tel: 0286 218 05 23

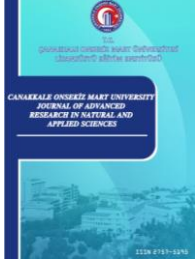
Belgegeçer / Fax: 0286 218 05 24

E-posta / E-mail: jarnas.journal@gmail.com

Dergi Web Sayfası / Journal Home Page:

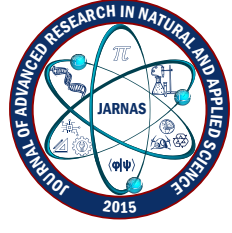
<http://jarna.dergi.comu.edu.tr/>

<https://dergipark.org.tr/tr/pub/jarnas>



CONTENTS / İÇİNDEKİLER
(2024, 10:1)

No	Articles & Authors / Makaleler & Yazarlar	Pages / Sayfa No
1	Effects of IL-6 and TNF- α Cytokines on Cell Proliferation in Androgen Dependent/Independent Prostate Cancer Cell Lines Serhad Onat*, Sümeyye Aydoğan Türkoğlu, Feray Köçkar Research/Araştırma	1-8
2	Doğu Anadolu Gözlemevi (DAG) Yerleşkesi'nin Boltwood Bulut Sensörü II (BWCS II) ile Bulutluluk Analizi Esragül Atalay*, İlham Nasıroğlu, Cahit Yeşilyaprak Research/Araştırma	9-20
3	Corrosion Behaviors' Investigation of Carbide Coatings Developed for Sulphuric Acid Recovery Systems Erhan Özkan* Research/Araştırma	21-32
4	Changes in Plant Nutrient Concentration of Olive (<i>Olea europaea</i> L.) Leaves after Different Rates of Humic Acid Application Sertaç Uyanık, Ali Sümer* Research/Araştırma	33-44
5	Single Laboratory Validation of Four Methods for Quantification of HMF in Honey Elif Yıldız, Abdullah Tahir Bayraç* Research/Araştırma	45-59
6	Uydu Verisi ve CBS ile Van Gölü Klorofil-a Dinamiklerinin İzlenmesi Ufuk Tarı*, Nazlı Olğun Kıyak Research/Araştırma	60-79



Çanakkale Onsekiz Mart University Journal of Advanced Research in Natural and Applied Sciences

Mart (March) 2024 / Cilt (Volume) 10 / Sayı (Issue) 1 / e-ISSN 2757-5195

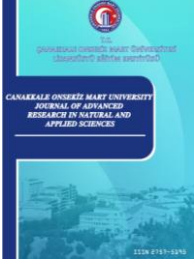
7	On the Synchronizability of Quadratic Integrate and Fire Neurons Koray Çiftçi* Research/Araştırma	80-90
8	Soil Contamination by Metals/Metalloids around an Industrial Region and Associated Human Health Risk Assessment Hale Demirtepe* Research/Araştırma	91-105
9	Disposable Voltammetric Determination of Celestine Blue at a Pencil Graphite Electrode Mehmet Güneş* Research/Araştırma	106-115
10	Anticancer, Antioxidant, Antimicrobial Activities, and HPLC Analysis of Alcoholic Extracts of <i>Parthenocissus quinquefolia</i> L. Plant Collected from Çanakkale Ferah Cömert Önder*, Sevil Kalın, Özlem Maraba, Alper Önder, Pınar Ilgın, Ersin Karabacak Research/Araştırma	116-133
11	Community-Based Strategies for Disaster Preparedness in Mauritius Henna Helvina Neerunjun* Research/Araştırma	134-149
12	<i>In vitro</i> Allelopathic Potential of Leaf Water Extracts of <i>Plantago lanceolata</i> and <i>P. major</i> on the Germination of Some Crops Onur Yaraş, Nadim Yılmaz* Research/Araştırma	150-160



Çanakkale Onsekiz Mart University Journal of Advanced Research in Natural and Applied Sciences

Mart (March) 2024 / Cilt (Volume) 10 / Sayı (Issue) 1 / e-ISSN 2757-5195

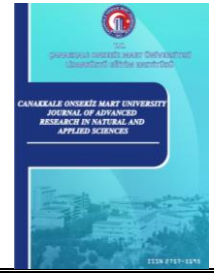
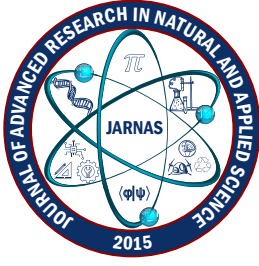
13	Correlating Measured SPT-N, Shear Wave Velocity and Liquid Limit Values in Melekli Region, Iğdır (Türkiye) Yusuf Guzel* Research/Araştırma	161-174
14	Contribution to the Molecular Phylogeny of Anthribidae (Coleoptera: Curculioniodea) Inferred from COI Sequences Polen Döngel*, Ali Nafiz Ekiz Research/Araştırma	175-181
15	Heterogeneous Photo-Fenton-like Degradation of Oxytetracycline Containing Wastewater Ceren Orak*, Gülin Ersöz Research/Araştırma	182-189
16	Polielektrolitlerin Molekül Ağırlığı ve Harman Oranının Çok Tabakalı Filmlerin Gelişimine Etkisinin ve İlaç Adsorpsiyon/Desorpsiyon Uygulamalarında Kullanımlarının QCM-D Tekniğiyle Takibi Dilara Yılmaz-Ayıkut, Öznur Yolaçan, Hüseyin Deligöz* Research/Araştırma	190-206
17	Recent Engineering Applications for Noise Reduction in an Automotive Industry Ülge Taş*, Ender Pak, Berkay Uğur Research/Araştırma	207-217
18	Effect of Venlafaxine on The Vitamins Contents of <i>Saccharomyces Cerevisiae</i> (NRRLY-12632) Meltem Çakmak, Dursun Özer, Fikret Karataş*, Sinan Saydam Research/Araştırma	218-227






Çanakkale Onsekiz Mart University Journal of Advanced Research in Natural and Applied Sciences

Mart (March) 2024 / Cilt (Volume) 10 / Sayı (Issue) 1 / e-ISSN 2757-5195

19	Assessment of Construction Site Management Practices: A Case Study of a Construction Project in Hargeisa Abdirisak Mohamed Abdillahi*, Zübeyde Özlem Parlak Biçer, Savaş Bayram Research/Araştırma	228-242
----	--	---------



Effects of IL-6 and TNF- α Cytokines on Cell Proliferation in Androgen Dependent/Independent Prostate Cancer Cell Lines

Serhad Onat¹ , Sümeyye Aydoğan Türkoğlu² , Feray Köçkar³ 

^{1,2,3}Department of Molecular Biology and Genetics, Faculty of Science and Letters, Balıkesir University, Balıkesir, Türkiye

Article History

Received: 12 Apr 2023

Accepted: 21 Aug 2023

Published: 15 Mar 2024

Research Article

Abstract – Prostate cancer is the second most common types of cancer among men worldwide. Prostate cancer, caused by abnormal and uncontrolled growth of the cells that make up the prostate tissue, is second only to related deaths in men. Cytokines, which have a significant impact on the response of the immune system, play an active role in the development of prostate cancer. This study determined the effect of proinflammatory cytokines, IL-6 and TNF- α on the proliferation of prostate cancer (PC α) cell lines. MTT test was used for the effect of cytokines applied at different doses and hours on cell viability. According to our results, IL-6 cytokine caused a high increase in proliferation in androgen-dependent LNCaP cells, while androgen-independent PC-3 cells showed different proliferative effects in time and dose-dependent manner. TNF- α cytokine had a negative effect on the proliferation of androgen-dependent LNCaP cells, while it increased the proliferation level of androgen-independent PC-3 cells. These results show that the effects of cell lines-on the proliferation of cells are different depending on their androgen sensitivity, which will be used in different cytokinetic studies to determine the inflammatory response to treat prostate cancer. It is especially important to consider this condition during the advancement of prostate cancer treatment strategies.

Keywords – Cytokine, IL-6, prostate cancer, proliferation, TNF- α

1. Introduction

Prostate cancer is the second most common cancer in men, according to data from the World Health Organization for 2020 [1]. The prostate gland, part of the male reproductive system, is a malignant tumor structure that occurs by the uncontrolled and abnormal proliferation of cells [2]. The greatest advances in the identification and treatment of prostate cancer were accelerated by the discovery of prostate-specific antigen (PSA) from the mid-1970s onwards. A relationship has been established between the follow-up of PSA from patient serums and the prognosis of patients with cancer [3]. Prostate cancer, a highly complex disease that exhibits heterogeneity at pathological, genomic, and molecular levels, is a multi-stage process that can begin with carcinoma and then turn into castration-resistant prostate cancer (CRPC), and finally continue with a metastatic prostate tumor [4]. Normal prostate tissues need androgen and androgen receptors (AR) for their development. Suppressing the AR pathway is often a common method for treating prostate cancer. Although surgical intervention and radiation for localized prostate cancer are effective treatment options, suppression of the AR pathway remains the first treatment option in metastatic prostate cancer [5].

As with many types of cancer, cytokines have a highly significant effect on prostate cancer. Cytokines directly or indirectly regulate the growth, invasiveness, and metastasis of tumor cells. They affect tumor formation by

¹serhad.onat@balikesir.edu.tr (Corresponding Author); ²saydogan@balikesir.edu.tr; ³fkockar@balikesir.edu.tr

inducing angiogenesis in the cancer microenvironment. It has been determined by studies that many different cytokines play an effective role as regulators in prostate cancer metastasis [6]. These studies have found that IL-6 plays a role in the mechanism of prostate cancer, due to the presence of a receptor of IL-6 cytokine in the prostate cancer cell lines [7]. Another cytokine tumor necrosis factor alpha (TNF- α), which is actively involved in cancer metastases, is a multifunction proinflammatory cytokine [8]. Studies have shown that TNF- α regulates many critical processes of tumor progression, such as DNA damage, oncogenic activation, and tumor metastasis [9]. TNF- α levels in the serum of prostate cancer patients have been reported in studies showing a positive correlation with the prognosis of the disease [10].

Localized and metastatic prostate cancers could be androgen-dependent or -independent. The presence or absence of androgen differs in prostate cancer treatment processes. On the other hand, IL-6 and TNF- α are prostate cancer inflammatory cytokines and have effects on cancer processes [11]. Androgen-dependent and androgen-independent prostate cancers especially differ in their responses to chemotherapeutic agents in clinical processes [12].

Considering the androgen-dependent and androgen-independent prostate cancer, the aim of this study is to comparatively analyze the effects of IL-6 and TNF- α , which are also important for prostate cancer, on cell proliferation. Therefore, in our study, the effects of IL-6 and TNF- α cytokines on androgen-dependent (LNCaP) and the androgen-independent (PC-3) PC α cell lines were investigated at different doses (10 ng/mL, 20 ng/mL, and 40 ng/mL) and at different administration times (24, 48, and 72 hours). In this study, considering that the effects of cytokines on cells could be different at different concentrations, it is planned to evaluate the effects of cytokine application at various concentrations on cells.

2. Materials and Methods

2.1. Cell Culture

Androgen-dependent LNCaP and androgen-independent PC α cells, PC-3 cells, were used for the study. RPMI-1640 (Gibco) was used for the LNCaP cell line and DMEM High Glucose (Gibco) mediums were used for PC-3 cells for the growing conditions. 10% Fetal Calf serum (FCS) was added to this medium containing glutamine. 1 mL of LNCaP and PC α cells are suspension stored in a -80°C refrigerator was taken from -80°C and the cell brought to the culture laboratory. After the cell suspension is thawed at 37 °C, then 6 mL of medium. Dissolved cells in a centrifuge at 1000 rpm for 5 min. centrifuged. After centrifugation, the supernatant is discarded, and the remaining pellet is taken into 10 mL medium by pipetting. The cells were incubated in 37°C incubators with 5% CO₂. Cell cultures with flask occupancy above 80% were regularly passaged [13].

2.2. Cell Viability Assay

In experimental studies, cell counts were performed with trypan blue and a hemocytometer counter to use adequate amounts of cells. For this process, the cells removed from the flasks were centrifuged for 5 minutes at 1000 rpm and then dissolved to become homogeneous in the 10 mL medium containing 10% FCS. To distinguish between living and dead cells, the 10 μ L of cell mix was incubated at room temperature for 5 minutes with an equal volume of trypan blue (1:1 dilution rate). This process eventually calculated the number of living cells in mL by counting living cells. (Total live cells/mL = Hemocytometer count result \times 2 \times 10⁴) [14].

2.3. Cytokine Treatment

8,000 cells per well were plated out into 96-well plates. The cells were incubated over-night to attach to the surface. After O/N incubation, the medium of the cells was refreshed with DMEM containing 0.1% BSA. After 1 hour, IL-6 (Peprotech, 200-06) and TNF- α (Peprotech, 300-01A) cytokines were administered with final concentrations of 10 ng/mL, 20 ng/mL, and 40 ng/mL per well. Plates were incubated for 24, 48, and 72 hours at 37°C with 5% CO₂ [14].

2.4. MTT

At the end of the time points, MTT dye was performed into each well of 96 well plates and cells were incubated for 4 hours at 37°C in an environment containing 5% CO₂. After the incubation, the medium was removed, adding 200 μ L isopropanol containing 4mM HCl to each well. Each well was measured by a UV spectrophotometer at the wavelength of 550 nm and the results were analyzed in the program [15].

2.5. Statistical Analyses

All experimental sets were run in 3 replicates and the data obtained were statistically analyzed with GraphPad Prism 8.0.2 (GraphPad Software, San Diego, CA, USA). Statistical values were stated as mean \pm SD, and the results were evaluated with the one-way ANOVA method. Situations, where it is $p \leq 0,05$ in the assessment, have been considered meaningful.

3. Results and Discussion

Proinflammatory cytokines were thoroughly investigated due to their different roles in prostate cancer, such as proliferation, apoptosis, migration, invasion, and regulation of angiogenesis. One of these cytokines, IL-6, is an upregulated cytokine in prostate cancer [16]. The positive or negative effects of IL-6 on the proliferation of cancer cells can be explained by differences in the activation of serum or autocrine cycles [17]. Most information on the regulation of the cell cycle by IL-6 in prostate cancer was obtained from studies with LNCaP cells. However, our study investigated the effect of cytokines on the proliferation of the cell using androgen-independent and dependent cell lines. At the same time, prostate cancer cells were exposed to different doses in different time periods, and the effect of cytokine on cell proliferation was determined to be time and dose dependent. It has been determined that some inflammatory agents used in androgen-independent prostate cancer cell lines have effects on IL-6 and TNF- α cytokines at different doses [18]. It has been reported that different chemotherapeutic agents trigger oxidative stress, apoptosis, and inflammation in a dose-dependent manner in prostate cancer cell lines [19].

In our study, IL-6 and TNF- α cytokines were applied to androgen-dependent LNCaP and androgen-independent PC-3 PC α cell lines for 24, 48, and 72 hours, with a final concentration of 10 ng/mL, 20 ng/mL, and 40 ng/mL percentage (%) viability were calculated based on cell lines.

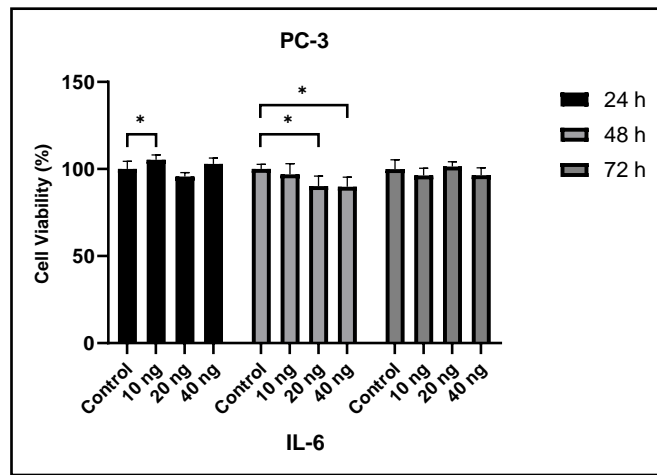


Figure 1. The effect of IL-6 cytokines on PC-3 cell viability ($p > 0.05$ (Not significant), $p \leq 0.05$ (*Significant), $p \leq 0.01$ (**Very significant), $p \leq 0.001$ (***)Very significant))

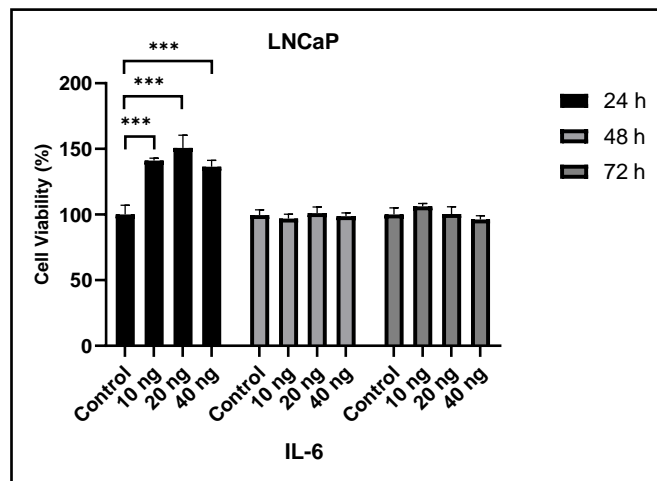


Figure 2. The effect of IL-6 cytokines on LNCaP cell viability ($p > 0.05$ (Not significant), $p \leq 0.05$ (*Significant), $p \leq 0.01$ (**Very significant), $p \leq 0.001$ (***)Very significant))

The results from the first part of our study showed statistically significant results in the androgen-independent cell line administered IL-6 cytokine for 24 and 48 hours. According to these results, the proliferation level in PC-3 cells increased in the first 24 h, but only 48 h hours cell proliferation decreased time and dose-dependent manner. However, while increases or decreases in cell proliferation have been determined for 72 h, statistically significant results have not been achieved (Figure 1).

In LNCaP cells, which have an androgen-dependent cell line, IL-6 is applied with same doses in different times. The first 24 h of the experiment showed that the level of cell proliferation increased by approximately 50%. Depending on the cytokine doses, the proliferation in LNCaP cells increased at a statistically significant rate. In the case of 48- and 72-hours experimental groups, no statistically significant results were achieved in terms of cell proliferation (Figure 2). Our results indicate that IL-6 cytokine led to the proliferation of the cell lines depending on the cell's androgen sensitivity. Our results confirm that the proliferation of IL-6 cytokine in the prostate cancer cell line increases the proliferation rate in cells that may have an androgen response [20,21]. In the literature, in hormone-independent prostate cancer, HER-2/neu tyrosine kinase is stated to have modulated the signal of the androgen receptor [22]. Another study showed that androgen absence induces N-cadherin, increasing the metastasis of prostate cancer [23]. Studies show that IL-6 cytokine organizes androgen

receptor activity and PC α cell growth supports differences in proliferation in androgen dependent/independent cell lines [24-26].

Some studies report that TNF- α cytokine acts as inductive or suppressive in the development of different types of cancer [27]. Studies with TNF- α cytokine implies that it has an important role in the advance processes of prostate cancer [28,29]. The high levels of TNF- α cytokine were identified in serums of patients whose prostate cancer prognosis was progressing poorly [10]. It is also thought that there is a study showing that TNF- α inhibits androgen dependence in prostate cancer. TNF- α cytokine may take a role in the start of an androgen-independent condition in prostate cancer, in this case an androgen-independent process can be initiated [30].

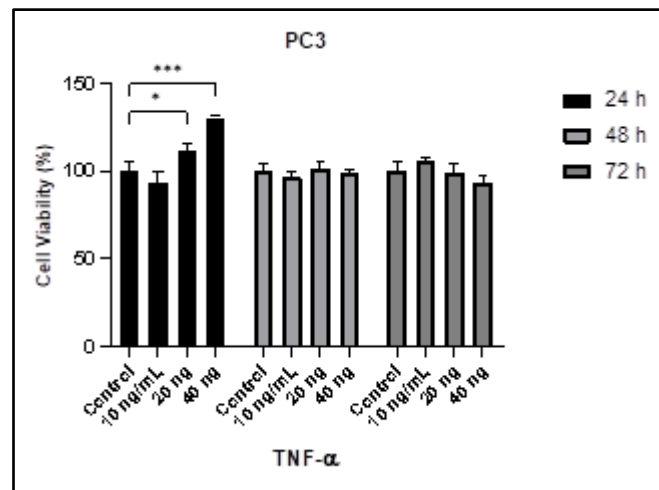


Figure 3. The effect of TNF- α cytokines on PC-3 cell viability ($p > 0.05$ (Not significant), $p \leq 0.05$ (*Significant), $p \leq 0.01$ (**Very significant), $p \leq 0.001$ (***)Very significant))

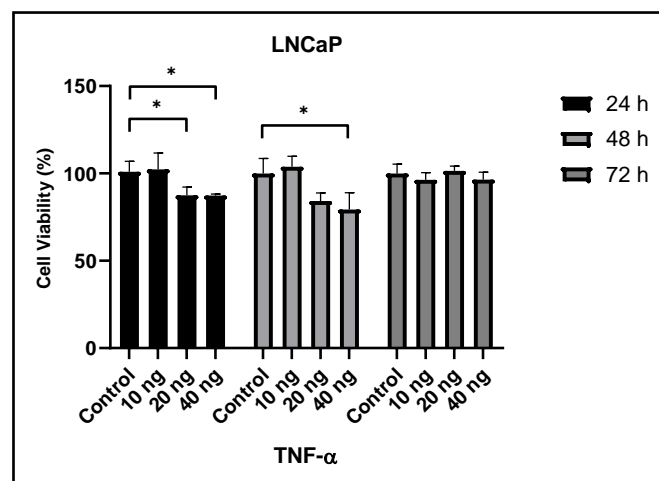


Figure 4. The effect of TNF- α cytokines on LNCaP cell viability ($p > 0.05$ (Not significant), $p \leq 0.05$ (*Significant), $p \leq 0.01$ (**Very significant), $p \leq 0.001$ (***)Very significant))

In our study, TNF- α cytokine caused the proliferation in the first 24 h in the androgen-independent PC-3 cells depending on the dose. Statistically meaningful the level of proliferation has been obtained at 20 ng/mL and 40 ng/mL of TNF- α . No statistically significant results were achieved for 48 and 72 hours (Figure 3). Similarly, when TNF- α cytokines are applied to androgen-dependent cell line, LNCaP cells at the same time and doses, the cell proliferation level decreases with 20 ng/mL and 40 ng/mL doses for 24 h and 40 ng/mL for 48 h (Figure 4). In LNCaP cells, there is no meaningful change for 72 hours of cytokine application in terms of proliferation level. Studies in literature have found that TNF- α suppresses androgen sensitivity in an androgen-dependent

prostate cancer cell line and induces the AR-mediated transcriptional activation of the TGF-beta signal [31,32]. Differences in the proliferation levels of cells were determined based on differences in the dose and time differences. Statistically meaningful results were not achieved, especially during 72 hours in all cell lines and in different cytokines applied. This is attributed to the fact that cytokines have lost their effectiveness during long incubation times. Cytokines administered have been confirmed to have different effects on cell proliferation based on cells' androgen sensitivity levels [33].

4. Conclusion

This study showed that proinflammatory cytokines applied to prostate cancer cell lines, which are androgen dependent/independent, had different effects on the proliferation of cells. The IL-6 cytokine applied to our study significantly increased the proliferation in the androgen-dependent LNCaP cells, but the proliferation in the androgen-independent PC-3 cell line varies depending on the cytokine application dose and time points. In the first 24 hours of a cytokine application to PC-3 cells, the proliferation of the cell increased while in the 48 hours, the proliferation decreased in the cytokine application. TNF- α cytokines used for the same doses and time points have been determined to reduce proliferation in androgen-dependent LNCaP cells but increase proliferation in the androgen-independent PC-3 cell lines. As a result, IL6 and TNF- α cytokines show differential effects on cell proliferation in androgen-dependent and androgen-independent prostate cancer cell lines at different concentrations and time intervals.

Author Contributions

The first author collected data and performed the experiment and wrote the paper. The second author performed data analysis and interpretation. The third author planned the analysis and wrote the article. All authors edited the paper and read and approved the final version. This paper is derived from the first author's doctoral dissertation supervised by the third author.

Conflicts of Interest

All the authors declare no conflict of interest.

Acknowledgement

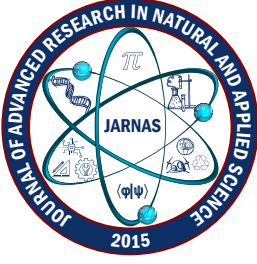
Serhad Onat was supported by Turkish Higher Education Council's 100/2000 PhD scholarship program between 2018-2022 years and by 2211-A National PhD Scholarship Program by the Scientific and Technological Research Council of Turkey (TÜBİTAK).

References




- [1] M. Daniyal, Z. A. Siddiqui, M. Akram, H. M. Asif, S. Sultana, A. Khan, *Epidemiology, etiology, diagnosis and treatment of prostate cancer*, Asian Pacific Journal of Cancer Prevention: APJCP 15 (22) (2014) 9575–9578.
- [2] S. Sandhu, C. M. Moore, E. Chiong, H. Beltran, R. G. Bristow, S. G. Williams, *Prostate cancer*. The Lancet 398 (10305) (2021) 1075–1090.
- [3] B. J. Feldman, D. Feldman, *The development of androgen-independent prostate cancer*, Nature Reviews Cancer 1 (1) (2001) 34–45.

- [4] M. M. Shen, C. Abate-Shen, *Molecular genetics of prostate cancer: New prospects for old challenges*, Genes & Development 24 (18) (2010) 1967–2000.
- [5] T. Karantanos, P. G. Corn, T. C. Thompson, *Prostate cancer progression after androgen deprivation therapy: Mechanisms of castrate resistance and novel therapeutic approaches*, Oncogene 32 (49) (2013) 5501–5511.
- [6] T. O. Adekoya, R. M. Richardson, *Cytokines and chemokines as mediators of prostate cancer metastasis*, International Journal of Molecular Sciences 21 (12) (2020) Article Number 4449 29 pages.
- [7] C. B. Siegall, G. Schwab, R. P. Nordan, D. J. FitzGerald, I. Pastan, *Expression of the interleukin 6 receptor and interleukin 6 in prostate carcinoma cells*, Cancer Research 50 (24) (1990) 7786–7788.
- [8] F. Balkwill, *Tumour necrosis factor and cancer*, Nature Reviews Cancer 9 (5) (2009) 361–371.
- [9] H. Wang, R. Fang, X. F. Wang, F. Zhang, D. Y. Chen, B. Zhou, H. S. Wang, S. H. Cai, J. Du, *Stabilization of Snail through AKT/GSK-3 β signaling pathway is required for TNF- α -induced epithelial-mesenchymal transition in prostate cancer PC3 cells*, European Journal of Pharmacology 714 (1-3) (2013) 48–55.
- [10] V. Michalaki, K. Syrigos, P. Charles, J. Waxman, *Serum levels of IL-6 and TNF-alpha correlate with clinicopathological features and patient survival in patients with prostate cancer*, British Journal of Cancer 90 (12) (2004) 2312–2316.
- [11] R. Nader, J. E. Amm, J. B. Aragon-Ching, *Role of chemotherapy in prostate cancer*, Asian Journal of Andrology 20 (3) (2018) 221–229.
- [12] J. Zhou, H. Chen, Y. Wu, B. Shi, J. Ding, J. Qi, *Plasma IL-6 and TNF- α levels correlate significantly with grading changes in localized prostate cancer*, Prostate 82 (5) (2022) 531–539.
- [13] S. A. Türkoğlu, F. Koçkar, *SPI and USF differentially regulate ADAMTS1 gene expression under normoxic and hypoxic conditions in hepatoma cells*, Gene 575 (1) (2016) 48–57.
- [14] E. Tokay, R. I. Sağkan, F. Koçkar, *TNF- α induces URG-4/URGCP gene expression in hepatoma cells through starvation dependent manner*, Biochemical Genetics 59 (1) (2021) 300–314.
- [15] N. Hacıoğlu, T. Güngör, E. Tokay, F. C. Önder, M. Ay, F. Köçkar, *Synthesis and biological evaluation of 2,4,6-trinitroaniline derivatives as potent antitumor agents*, Monatshefte für Chemie-Chemical Monthly 151 (10) (2020) 1629–164.
- [16] M. T. Spiotto, T. D. Chung, *STAT3 mediates IL-6-induced neuroendocrine differentiation in prostate cancer cells*, The Prostate 42 (3) (2000) 186–195.
- [17] Z. Culig, M. Pühr, *Interleukin-6: A multifunctional targetable cytokine in human prostate cancer*, Molecular and Cellular Endocrinology 360 (1-2) (2012) 52–58.
- [18] C. Hacıoğlu, S. Kaçar, F. Kar, G. Kanbak, V. Şahintürk, *Concentration-dependent effects of zinc sulfate on DU-145 human prostate cancer cell line: Oxidative, apoptotic, inflammatory, and morphological analyzes*, Biological Trace Element Research 195 (2) (2020) 436–444.
- [19] F. Kar, C. Hacıoğlu, S. Kaçar, V. Şahintürk, G. Kanbak, *Betaine suppresses cell proliferation by increasing oxidative stress-mediated apoptosis and inflammation in DU-145 human prostate cancer cell line*, Cell Stress Chaperones 24 (5) (2019) 871–881.
- [20] T. Chen, L. H. Wang, W. L. Farrar, *Interleukin 6 activates androgen receptor-mediated gene expression through a signal transducer and activator of transcription 3-dependent pathway in LNCaP prostate cancer cells*, Cancer Research 60 (8) (2000) 2132–2135.
- [21] D. Giri, M. Özen, M. Ittmann, *Interleukin-6 is an autocrine growth factor in human prostate cancer*, The American Journal of Pathology 159 (6) (2001) 2159–2165.

- [22] N. Craft, Y. Shostak, M. Carey, C. L. Sawyers, *A mechanism for hormone-independent prostate cancer through modulation of androgen receptor signaling by the HER-2/neu tyrosine kinase*, *Nature Medicine* 5 (3) (1999) 280–285.
- [23] K. Jennbacken, T. Tesan, W. Wang, H. Gustavsson, J. E. Damber, K. Welén, *N-cadherin increases after androgen deprivation and is associated with metastasis in prostate cancer*, *Endocrine-Related Cancer* 17 (2) (2010) 469–479.
- [24] Z. Culig, G. Bartsch, A. Hobisch, *Interleukin-6 regulates androgen receptor activity and prostate cancer cell growth*, *Molecular and Cellular Endocrinology* 197 (1-2) (2002) 231–238.
- [25] F. R. Santer, K. Malinowska, Z. Culig, I. T. Cavarretta, *Interleukin-6 trans-signalling differentially regulates proliferation, migration, adhesion and maspin expression in human prostate cancer cells*, *Endocrine-Related Cancer* 17 (1) (2010) 241–253.
- [26] W. Lou, Z. Ni, K. Dyer, D. J. Tweardy, A. C. Gao, *Interleukin-6 induces prostate cancer cell growth accompanied by activation of stat3 signaling pathway*, *The Prostate* 42 (3) (2000) 239–242.
- [27] G. Rodríguez-Berriguete, B. Fraile, R. Paniagua, P. Aller, M. Royuela, *Expression of NF- κ B-related proteins and their modulation during TNF- α -provoked apoptosis in prostate cancer cells*, *The Prostate* 72 (1) (2012) 40–50.
- [28] S. Harada, E. T. Keller, N. Fujimoto, K. Koshida, M. Namiki, T. Matsumoto, A. Mizokami, *Long-term exposure of tumor necrosis factor alpha causes hypersensitivity to androgen and anti-androgen withdrawal phenomenon in LNCaP prostate cancer cells*, *The Prostate* 46 (4) (2001) 319–326.
- [29] Y. Nakajima, A. M. DelliPizzi, C. Mallouh, N. R. Ferreri, *TNF-mediated cytotoxicity and resistance in human prostate cancer cell lines*, *The Prostate* 29 (5) (1996) 296–302.
- [30] D. Yu, Y. Zhong, X. Li, Y. Li, X. Li, J. Cao, H. Fan, Y. Yuan, Z. Ji, B. Qiao, J.-G. Wen, M. Zhang, G. Kvalheim, J. M. Nesland, Z. Suo, *ILs-3, 6 and 11 increase, but ILs-10 and 24 decrease stemness of human prostate cancer cells in vitro*, *Oncotarget* 6 (40) (2015) 42687–42703.
- [31] H. G. Van der Poel, *Androgen receptor and TGFbeta1/Smad signaling are mutually inhibitory in prostate cancer*, *European Urology* 48 (6) (2005) 1051–1058.
- [32] A. Mizokami, A. Gotoh, H. Yamada, E. T. Keller, T. Matsumoto, *Tumor necrosis factor-alpha represses androgen sensitivity in the LNCaP prostate cancer cell line*, *The Journal of Urology* 164 (3) (2000) 800–805.
- [33] P. C. Smith, A. Hobisch, D. L. Lin, Z. Culig, E. T. Keller, *Interleukin-6 and prostate cancer progression*, *Cytokine & Growth Factor Reviews* 12 (1) (2001) 33–40.



Doğu Anadolu Gözlemevi (DAG) Yerleşkesi'nin Boltwood Bulut Sensörü II (BWCS II) ile Bulutluluk Analizi

Esragül Atalay¹ , İlham Nasıroğlu² , Cahit Yeşilyaprak³ 

^{1,2,3}Astronomi ve Uzay Bilimleri Bölümü, Fen Fakültesi, Atatürk Üniversitesi, Erzurum, Türkiye

³Astrofizik Araştırma ve Uygulama Merkez, Atatürk Üniversitesi, Erzurum, Türkiye

Makale Tarihiçesi

Gönderim: 10 Mayıs 2023

Kabul: 5 Eylül 2023

Yayın: 15 Mart 2024

Araştırma Makalesi

Öz – Yer tabanlı astronomik gözlemlerde, gözlemevi ve yerleşkesindeki cihazların doğru çalışması ve verimli bir gözlem sonucu elde edilmesi için nem, rüzgâr, yağış, bulutluluk gibi meteorolojik olaylar büyük önem taşımaktadır. Bu nedenle gözlemevinin kurulacağı yerleşkenin koşullarının meteorolojik olarak uygun olması gerekmektedir. Bu çalışma kapsamında, 2011 yılında Astrofizik Araştırma ve Uygulama Merkezi (ATASAM, Erzurum) tarafından başlatılan ve kurulumu devam etmekte olan Doğu Anadolu Gözlemevi (DAG) yerleşkesinin bulutluluk özelliklerinin belirlenmesi sonrasında kontrolünün devam edilmesi amaçlanmıştır. DAG, faaliyete geçtiğinde 4m çapıyla Türkiye'nin en büyük optik ve ilk kızılötesi teleskobuna sahip olacaktır. DAG'ın bulutluluk durumunun incelenmesi için yerleşkede bulunan Boltwood Bulut Sensör II (BWCS II) meteorolojik cihazından alınan ölçümler kullanılarak analizler gerçekleştirilmiştir. Öncelikle BWCS II'den elde edilen verinin güvenilirliği için DAG yerleşkesinde bulunan ve Meteoroloji Bölge Müdürlüğü tarafından kalibre edilen Vaisala cihazı kullanılarak ölçümlerin doğruluğu kontrol edilmiştir. Vaisala cihazından alınan ölçümler ile yapılan karşılaştırmalar sonucunda BWCS II'nin sıcaklık, nem ve çiy noktası ölçümlerini doğru yaptığı tespit edilmiştir. Yerleşkenin 2019 ve 2020 yıllarına ait günlük, aylık, mevsimlik ve toplamda yıllık olarak bulutluluk durumu incelenmiştir. BWCS II veriden elde edilen sonuçlara bakıldığında yerleşkenin bulutluluk durumunun yıl içerisinde %58,2 oranında açık olduğu bulunmuştur. Bu değer, BWCS II'nin veri sıklığı ve veri kaybı da dikkate alındığında gözlemler için iyi bir sonuç olduğunu göstermiştir.

Anahtar Kelimeler – Atmosfer, Boltwood Bulut Sensör II, bulutluluk, DAG, gökyüzü sıcaklığı

Cloudiness Analysis with Boltwood Cloud Sensor II (BWCS II) over Eastern Anatolia Observatory (DAG) Site

^{1,2,3}Department of Astronomy and Space Sciences, Science Faculty, Atatürk University, Erzurum, Türkiye

³Astrophysic Research and Application Center (ATASAM), Atatürk University, Erzurum, Türkiye

Article History

Received: 10 May 2023

Accepted: 5 Sep 2023

Published: 15 Mar 2024

Research Article

Abstract – In ground-based astronomical observations, meteorological events such as humidity, wind, precipitation, and cloudiness are of great importance for the proper operation of the devices in the observatory and to obtain an efficient observation result. Therefore, the site conditions of the observatory should be suitable meteorologically. This study aims to continue the control of the Eastern Anatolia Observatory (DAG) site which was started by the Astrophysics Research and Application Center (ATASAM, Erzurum) in 2011 and continues to be established after determining the cloudiness characteristics. DAG is Turkey's first infrared and the largest optical telescope with a diameter of 4m. For the cloudiness of the DAG, analyses were made with the measurements taken from the Boltwood Cloud Sensor II (BWCS II) meteorological device located at the site. First of all, for the reliability of the data obtained from BWCS II, the accuracy of the measurements was checked using the Vaisala device, which is located on the DAG site and was calibrated by the Regional Directorate of Meteorology. Vaisala data showed that the BWCS II provides accurate temperature, humidity, and dew point

measurements. The daily, monthly, seasonal, and total annual cloudiness of the site for the years 2019 and 2020 was examined. Looking at the results obtained from the BWCS II data, it was seen that the site's cloudiness was 58.2% clear throughout the year. Considering the data frequency and data loss of BWCS II, showed that there was a good result for the observations.

Keywords – Atmosphere, Boltwood Cloud Sensor II, cloudiness, DAG, sky temperature

1. Giriş

Astronomi gök cisimlerinden gelen ışığı inceleyerek cisimlerin fiziksel ve kimyasal özelliklerini araştıran bilim dalıdır. Gök cisimleri elektromanyetik tayfın bütün dalga boylarında ışınım yapmasına rağmen, Dünya atmosferi gök cisimlerinden gelen tüm ışığı geçirmez. Bu nedenle yer atmosferi yer bazlı bir astronomik gözleminde yapılan astronomik gözlemleri kısıtlar veya tamamen engeller. Yeryüzüne kurulan teleskopların ortak sorunlarının başında yer atmosferinin sönmeme (saçılma ve soğurma) etkisi gelir. Bunun yanı sıra yeryüzündeki ışık kirliliği (aydınlatma sistemlerinin yanlış kullanımı), meteorolojik, atmosferik ve çevresel kirlilikler de astronomik gözlemler açısından büyük bir engel teşkil eder. Sadece radyo astronomide bulut, rüzgâr, yağış gibi hava şartları gözlem yapılmasına engel değildir. Ancak radyo astronomi hariç yer tabanlı gözlemler için hava şartları çok önemlidir ve birincil atmosferik parametre de bulutluluktur. Bulutlu havalarda bulut türü, konumu ve miktarı gözlem yapılmasına pek fazla olanak sağlamayabilir. Ayrıca bulut, nem, rüzgâr ve yağış gibi meteorolojik şartların bilinmesi yerleşkedeki cihazların verimli çalışmasına da katkı sağlar.

Astronomik gözlemlerin yapılabilmesi için bulut türü, miktarı ve değişimi gibi etkenler büyük bir öneme sahiptir. Bulutun tespit edilmesi, gözlem yapılacağı zamandaki bulut durumu bilgisi, astronomik gözlemler açısından önemi, hangi gece gözlem yapılıp yapılmayacağı ya da gökyüzünün hangi bölgelerinde ne kadar süreyle gözlem yapılabileceği bilgisiyle gözlem planı oluşturulabilir. Bu sayede teleskobun gözlem zamanı da verimli kullanılmış olur. Bulut modelleri, gri gövdeli yarısaydam yayıcılar olarak yapılır. Alçak ve orta bulut çok yayıcı olduklarından kolay algılanır. Yüksek seviyeli bulut ise daha az yayıcıdır ve tespit edilemez ama düşük sıcaklıkları nedeniyle gökyüzü ışımasını üzerinde minimum da olsa etkileri vardır [1].

Bulut örtüsü gözlemleri 100 yılı aşkın süredir rasatçılar aracılığı ile yapılmaktadır. Gelişen teknolojiyle birlikte bulut durumunun tespiti ve ölçümü için otomatik gözlemler yapacak cihazlar geliştirilmiştir. Uydu ölçümleri, yer tabanlı ölçüm cihazları gibi birçok teknolojik sistem geliştirilmiş ve ölçümler hem otomatik hem de daha kolay ve güvenilir bir hal almıştır. Gelişen uydu sistemlerinde de veri erişimi, kullanım yükü, çözünürlük, ölçüm hataları gibi dezavantaj oluşturan durumlar vardır [2]. Fakat yine de bu sistemlerin gelişmesi bulut gözlemlerini bambaşka bir boyuta taşımıştır. Özellikle astronomik gözlemlerde anlık durum bilgisi için yerleşkede bulunan yer tabanlı gözlem sistemleri oldukça işe yaramakta ve işleri daha kolay ve güvenilir hale getirmektedir. Atmosferde bulutluluğun hızlı değişim göstermesi nedeniyle sık bulut ölçümlerine ihtiyaç vardır. Ayrıca bulut tespitinde elektromanyetik spektrumun kullanılan dalga boyu aralığı önemlidir. Görünür bantta çalışan CCD kameralı görüntüleyiciler düşük maliyetli olmalarına rağmen bulut algılamada, Ay'ın konumu/evresi, ışık kirliliği ve diğer meteorolojik parametrelerden etkilendikleri için IR (Infrared-Kızılötesi) aralığında çalışan aletler kadar etkili ve güvenilir değildirler [3]. Son yıllarda yaygın olarak kullanılan sinoptik gözlem (Dünya'nın her yerinden aynı anda, 6 saat arayla günde toplam 4 defa yapılan gözlemdir) raporları, bulut bilgisi için tüm Dünya'da ana kaynak olmuştur. Günümüzde ise 1995'ten bu yana havaalanlarında bulut örtüsü ve yüksekliğini ölçen "Otomatik Yüzey Gözlem Sistemleri (ASOS)" kullanılmaktadır [4]. 2005'ten bu yana Hollanda Kraliyet Meteoroloji Enstitüsünde (KNMI) kızılötesi ölçüm yapan bir aletten oluşan ve uzun dalga ışınımını ölçen "Temel Yüzey Işınım Ağı (BSRN)" kullanılmaktadır [5]. Atmosferik Fizik Enstitüsü tarafından "Taramalı Kızıl Ötesi Görüntüleme Sistemi (SIRIS)" adı verilen ve 8–12 μ IR dalga boyu aralığında ölçüm yapan ve termal parlaklık sıcaklığını ölçen bir sistem geliştirilmiştir [6]. Son yıllarda ise yer tabanlı

ölçümler, uydu ve radar ölçümleri gibi araçlarla atmosferik değerler elde edilmektedir. Bu ölçümler tarım, ulaşım ve astronomi gibi birçok farklı alanda kullanılmaktadır [7].

Bu çalışma kapsamında, 39.760 Kuzey enlemi, 41.230 Doğu boylamında ve ~3170 m yükseltide yer alan Erzurum Konaklı Karakaya Tepeleri'ne kurulmakta olan DAG'ın bulunduğu yerleşkedeki BWCS II meteorolojik cihazıyla yapılan ölçümler ile bulutluluk durumu analiz edilmiştir.

2. Materyal ve Yöntem

2.1. Materyal

Gök cisimlerinden gelen enerji, atmosferden geçerken saçılma, soğurulma ve kırılma gibi çeşitli etkilere maruz kaldığı için yeryüzünden yapılan astronomik gözlemleri olumsuz etkiler. Ancak söz konusu etkiler yükseklik arttıkça yoğunluğun azalmasından dolayı yükselti ile ters orantılıdır. Bu nedenle, özellikle büyük çaplı teleskoplara sahip olacak olan gözlemevleri için yer seçimi çalışmaları yapılırken yüksek rakım tercih edilir. Gözlemevi yerleşkelerinde bulunması beklenen başlıca özellikler arasında; açık gece sayısının fazla olması, düşük astronomik görüş değerleri, ışık kirliliğinin olmaması, düşük aerosol miktarı, kararlı rüzgâr hızı ve yönü, yüksek rakım (ince ve temiz atmosfer tabakası) ve düşük nem şeklinde sıralanabilir. Teleskop barındıracak olan bir gözlemevi inşa etmeden önce; gözlemevi yerleşkesinde olması gereken özellikler dikkate alınır ve yer seçim çalışmaları yapılır. Özellikle büyük çaplı teleskoplar barındıran gözlemevi için bunlar büyük önem arz etmektedir. Ayrıca gözlemevi kurulabilmesi için yerleşkesinin altyapısı da önemli bir parametredir. Karakaya Tepeleri, rakımı (3170 m) ve şehrin bu tepelerin kuzeyinde kalmasından (şehrin genişleme yönünün aksine düşmesi yani ışık kirliliğinden şimdilik uzak olmasından) dolayı gözlemevi için uygun olduğuna karar verilerek yerleşke (2.510.000 m² alana sahip) Atatürk Üniversitesi'ne tahsis edilmiştir. DAG projesi kapsamında yapılmakta olan gözlemevi, Türkiye'nin ilk IR (NIR, <3 mikron) ve optik en büyük teleskobu (4m çaplı) olacaktır [8].

Bu çalışma kapsamında, çeşitli sensörler bulunduran aygıt(lar) kullanılarak, DAG yerleşkesinin bulutluluk analizi yapılmıştır. BWCS II meteorolojik aygıtı, kalibrasyonu Meteoroloji Genel Müdürlüğü (MGM) tarafından yapılmış olan Vaisala meteorolojik aygıtı ile karşılaştırılarak doğruluğu test edilmiştir. Bu iki meteorolojik aygıt DAG yerleşkesinde kurulmuş olan DIMM (Differential Image Motion Monitor) kulesi üzerinde bulunmaktadır. DIMM kulesi, 2012 yılında DAG yerleşkesine kurulmuş ve 7 m yüksekliğe sahiptir [9].

2.1.1. Boltwood Bulutluluk Sensörü

BWCS II, 8-14 μ dalga boyu aralığındaki gökyüzünün IR ışınımını algılayıp bulutluluk değerini ölçmek için tasarlanmış bir cihazdır. DAG yerleşkesine kurulan BWCS II, Şekil 1'de görüldüğü gibi 10 derecelik bir zenit uzaklığına sahip olacak şekilde güneye doğru yönlendirilmiştir. Bunun nedeni, yağmur ve kar gibi hava koşullarında aygıtın üzerine düşen suyun ıslaklık sensörünün yüzeyinden akmasını sağlamaktır. Ayrıca içerisinde yere doğru bakan gün ışığı sensörünün de doğru çalışması için görüş alanında bina, ağaç gibi nesnelerin olmaması ve zeminin yansıtıcı olmaması gerekmektedir [10].



Şekil 1. DAG yerleşkesinde bulunan Boltwood Bulutluluk Sensörü

BWCS II kızılötesi bir sensörle radyal ısıyı ölçerek bulut miktarını verebilir [11]. Bulut ölçümü yapmak için gelen ışınımı ölçerek gökyüzü sıcaklığı (T_{sky}) adı verilen sıcaklığa dönüştürür ve daha sonra da ortam sıcaklığını (T_{amb}) ölçüp iki sıcaklık değerini karşılaştırır. T_{sky} 'yi cihazın gökyüzüne bakan ucunda bulunan bir termopil sensör ile ölçer. T_{amb} 'yi ise cihazın gün ışığını doğrudan görmeyen yere bakan kısmında bulunan bir termistör yardımıyla ölçer. Daha sonra T_{sky} 'dan T_{amb} 'yi çıkararak aradaki farktan bulutluluk değerini, açık, bulutlu, çok bulutlu şeklinde verir. Genellikle farkın 0 ila -20 °C olduğu aralık bulutlu ve -50 °C'ye kadar düşük olduğu aralık ise açık gökyüzünü gösterir. Yani iki sıcaklık arasında fark ne kadar yüksek olursa gökyüzünün bulutlu olma ihtimali o kadar azdır [12]. BWCS II'nin çalışma kapsamında esas kullanım amacı, DAG yerleşkesi için gökyüzünün bulutluluk değerini elde etmektir. Bulutluluk durumu (cloudcon: cloud condition) için Tablo 1'de gösterildiği gibi cihaz $T_{sky} - T_{amb}$ farkına göre 4 farklı kategorik değer üretir.

Tablo 1. BWCS II'den elde edilen sıcaklık farkına göre cloudcon değerleri ve anlamları

Cloudcon Değeri	Değerlerin Anlamı	Sıcaklık farkı aralığı
0	Ölçüm yapılamamış	$\pm 999,9$ ve ± 998
1	Açık	-60 ile -25
2	Bulutlu	-25 ile -10
3	Kapalı	-10 'dan büyük

2.1.2. Gökyüzü Sıcaklığı (T_{sky})

Güneş, Dünya'nın en önemli enerji kaynağı olup enerjisi çeşitli dalga boylarında elektromanyetik dalgalar halinde yeryüzüne ulaşır. Güneş'ten gelen enerjinin tayfsal dağılımı sabittir fakat atmosferden geçip yeryüzüne gelene kadar kırılma, yansıma, soğurulma, saçılma gibi etkilere uğrar. Güneş'ten gelen enerjinin bir kısmını soğuran atmosfer, kara cisim gibi davranarak bu enerjiyi elektromanyetik ışınım halinde yayar. Bu ışınım karşılık gelen sıcaklık ise gökyüzü sıcaklığı (T_{sky}) olarak ifade edilir. Bulut atmosferde bir bariyer gibi davranarak yerden yayılan IR ışınımı geri yansır. Bu ışınım ölçülerek T_{sky} hesaplanır. Alınan veriye göre de gökyüzünün bulutluluk durumu hakkında bilgi elde edilir [13]. Yer ve gökyüzü arasındaki ışınım değişimleri, alınan global (toplam) ve yaygın Güneş ışınımına, hava sıcaklığına, neme ve rüzgâr yoğunluğuna konveksiyonla bağlı olacaktır [14].

T_{sky} , kara cisim sıcaklığı pirometre adı verilen IR termometre ile ölçülebilir. T_{sky} 'ı ölçmek ve bulut tespiti yapmak için dar bir görüş alanına sahiptir. Bu cihazın içinde sadece uzun dalga ışınımını ölçen termopil bulunur. Bu ışınım, sensöre gelen ve sensörden giden uzun dalga ışınım akısı arasındaki net ışınımı (R_{sky}) algılayıp voltaja dönüştürerek ölçer [15]. Elde edilen değer Stefan-Boltzmann yasası kullanılarak bir sıcaklık değerine çevrilir ve bu da “gökyüzü sıcaklığı” değeridir [16].

Bulut tespiti için ilk akla gelen, Ashley ve Jurcevic [17] yaptıkları çalışmadır. Bu çalışmayla, bulutun IR emisyonundan belirlenebileceğini ve bulutlu bölgenin daha fazla sinyal üreteceğini göstermişlerdir. İlerleyen zamanda bu çalışmadan yola çıkarak buluttan gelen sinyalin temel parametresi olan sıcaklığın, bulutun yüksekliği ve optik kalınlığına (veya emisyonuna), yerin sıcaklığına ve neme bağlı olduğu ile ilgili IR bulut detektör çalışmaları Clay [18] ve Buchley vd. [19] tarafından açıklanmıştır. Açık gökyüzünde bulutun varlığı gelişmiş bir sinyal üreterek bulut detektörlerinin gökyüzü sıcaklığına tepki veren IR sensöre dayalı cihazlar geliştirilmesi sağlanmıştır [18]. Clay [18], IR algılayıcı olarak termopil sensör kullanmıştır. Radyometrenin performansı üzerindeki etkilere izin vererek cihazın sıcaklığı kalibre edilir ve burada cihaz sıcaklığındaki 10 °C'lik bir değişiklik için belirtilen sıcaklıkta 1°C'lik değişiklik yapılır [18].

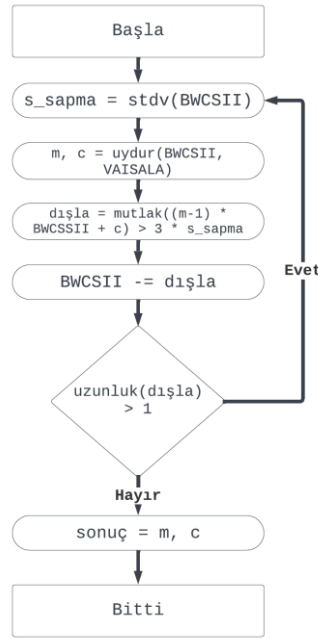
2.2. Yöntem

Bu çalışmada veri analizi için günümüzde popüler olarak kullanılan Python 3.13 programlama dili ve onun kütüphanelerinden faydalanılmıştır. BWCS II'den elde edilen, yalın metin biçiminde depolanmış ölçüm değerleri bir veri tabanına aktararak işlemler hızlandırmıştır. Veri tabanından veriyi aktarma, okuma ve ön işlem gibi işlem aşamalarında pandas kütüphanesinden faydalanılmıştır. Veride istatistiki hesapların tamamı (ortalama, ortanca, en küçük değer, en büyük değer gibi) Python'ın numpy ve pandas kütüphaneleri kullanılarak yapılmıştır. Veri uydurmalar (lineer fit gibi) için Python'ın scipy kütüphanesinden yararlanılmıştır. Zaman hesabı için Python'ın varsayılan kütüphanesi olan datetime yerine astropy kütüphanesi tercih edilmiştir. Veriyi görselleştirmek için ise, Python'ın matplotlib kütüphanesi kullanılmıştır.

DAG yerleşkesinin meteorolojik ölçümleri, yerleşkede bulunan AWOS, DAVIS, VAISALA, ASC ve BWCS II meteorolojik cihazları ile düzenli olarak alınmakta ve kaydedilmektedir. Bu çalışma kapsamında ise yerleşkenin bulutluluk durumu bilgileri için BWCS II cihazından alınan veri analiz edilmiştir. Analizi yapılan veri 2019 ve 2020 yıllarını kapsamaktadır. Veri analizine başlanmadan önce BWCS II'nin ölçümlerinin doğruluğu test edilmiştir. Sözü geçen verinin ayıklanması için alet uyarıları ve teorik limit hesaplanması olmak üzere iki yöntem kullanılmıştır. Alet uyarıları, adından da anlaşılacağı gibi, cihazın kendi verisi içinde, her sensör için verdiği bayrak (flag) değeri vardır. Örnek olarak bulutluluk için; 0, 1, 2, 3 olmak üzere 4 bayrak değeri verilmektedir. Burada; “0” bilinmiyor, “1” açık, “2” bulutlu, “3” kapalı olduğunu gösterir. Çalışmamızda doğal olarak “0” bayrak değerine sahip ölçümler dışlanmıştır. Teorik limitler ise, BWCS II'nin ölçüm yaptığı dalga boyu aralığı bilindiğinden, söz konusu aralığın dışında kalan gökyüzü sıcaklığı ölçümleri de dikkate alınmamıştır.

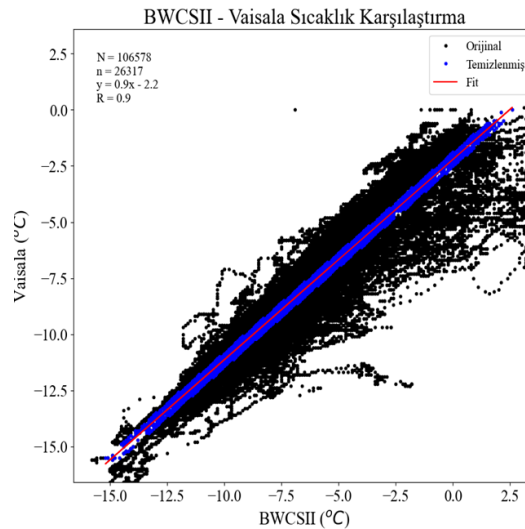
DAG yerleşkesinde bulunan VAISALA cihazının bakımı periyodik olarak MGM tarafından yapılmakta ve dolayısıyla güvenilir ölçüm sağlamaktadır. Bu nedenle BWCS II ve VAISALA meteorolojik aygıtlarının ortak olan ölçüm veri kullanılarak BWCS II'nin ölçümlerinin doğruluğuna bakılmıştır. İki cihazdan alınan ortak veri (sıcaklık, nem, çiy noktası ve rüzgâr hızıdır) için korelasyon analizinden faydalanılmıştır. Karşılaştırma verisi, BWCS II'nin sıcaklık verisinin alındığı zamana en yakın (5 saniyelik hata içerisinde kalan) VAISALA sıcaklık verisinin tespiti ile elde edilmiştir. Daha sonra söz konusu veri setine doğrusal fit uygulanmıştır. Bu doğrusal fite, BWCS II ölçümlerinin standart sapmasının (SIGMA) 3 katından daha uzaktaki veri dikkate alınmamıştır.

Bu işlem atılan (dışlanan) hiçbir veri kalmayınca kadar tekrarlanmıştır. Şekil 2’de akış şemasında karşılaştırmanın nasıl yapıldığı gösterilmiştir.



Şekil 2. BWCS II ve Vaisala Sıcaklık karşılaştırması için kullandığımız akış şeması

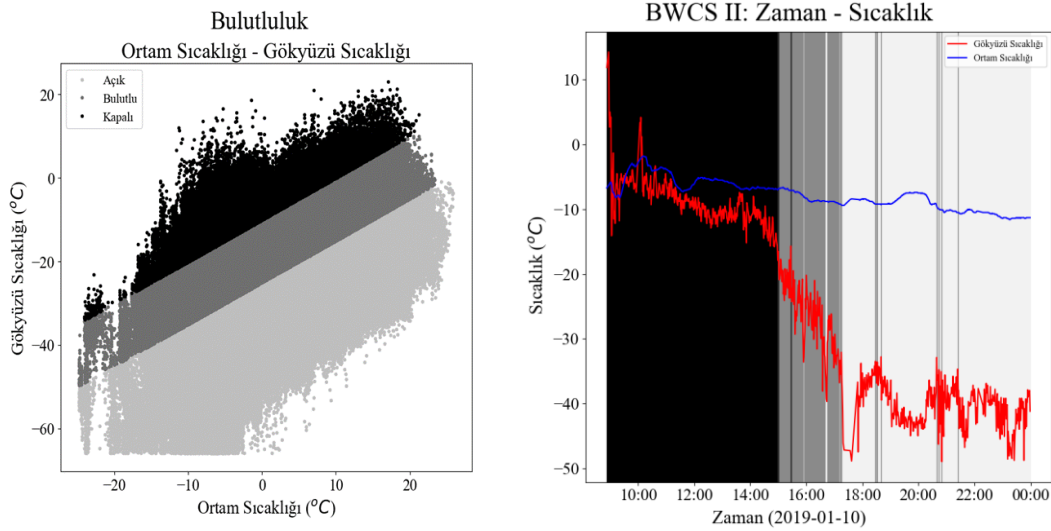
Aşağıda Şekil 3’te her iki cihazdan elde edilen sıcaklık değerlerinin bir karşılaştırılması verilmiştir. BWCS II’nin ölçtüğü sıcaklık değerlerinden bulutluluk hesaplandığı için de sıcaklık ölçümleri ele alınmıştır. Şekilde iki nicelik arasındaki korelasyonun niceliği verilmiştir. Grafikten iki cihazın sıcaklık değerleri arasında yüksek korelasyon ($R=0.9$) olduğu görülebilir. Sıcaklıklar arasındaki lineer denklem, $y = 0.9x - 2.2$ ile $R = 0.9$ hesaplanmışken, nem için bu değerler $y = 1.0x + 2.9$ ile $R = 1$ olarak hesaplanmıştır. Ayrıca ASC (All Sky Camera) görüntüleri ile de bulutluluk durumu karşılaştırması yapılarak cihazın güvenilirliğine karar verilmiştir.



Şekil 3. BWCS II ve Vaisala Sıcaklık karşılaştırması

Astronomik bir gözlemin yapılabilmesi için gökyüzünün açık olması gerekmektedir ve dolayısıyla bulutluluk durumu büyük önem arz etmektedir. Bu bilginin önceden bilinmesi gözlem zamanının verimli kullanılması açısından oldukça önemlidir. Bu nedenle gözlemlerinde meteorolojik cihazlara da yer verilmektedir. Bir gözlemevi kurulmadan önce yer seçim çalışmaları yapılmaktadır. Yer seçimi çalışmalarında açık gün sayısının

fazlalığı önemli kriterlerden birisidir. Ayrıca kurulu bir gözlemevinin zaman içerisinde atmosferik şartlarının değişebilme ihtimali de vardır. Bunun için astronomik gözlemleri için bu tür çalışmalar periyodik olarak yapılmalıdır. Açık gün sayısını ve dolayısıyla potansiyel astronomik gözlem sayısını doğru bir şekilde belirlemek için güvenilir veri ile bulutluluk analizleri yapılmalıdır. Bu nedenlerle bu çalışmada DAG yerleşkesinde bulunan BWCS II'ye ait 2019 ve 2020 yıllarının veri kullanılarak yerleşkenin bulutluluk analizleri yapılmıştır.



Şekil 4. Gökyüzü sıcaklığına karşı ortam sıcaklığından elde edilen bulutluluk durumu (sol panel), sıcaklık farkından elde edilen bir günlük bulutluluk durumu (sağ panel)

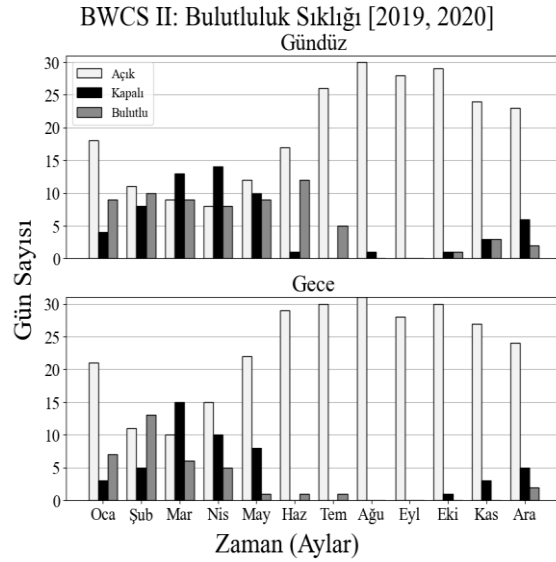
Şekil 4 sol grafikte 2019 – 2020 yılları için T_{sky} 'ya karşılık T_{amb} grafiğinden elde ettiğimiz bulutluluk durumu verilmiştir. Grafik incelendiğinde iki sıcaklık arasındaki farktan bulutluluk durumu açık, bulutlu ve kapalı olduğu aralıklar görülmektedir. Şekilde de görüldüğü gibi aradaki sıcaklık farkı $-25\text{ }^{\circ}\text{C}$ 'den küçük olduğunda gökyüzünün açık, -25 ile $-10\text{ }^{\circ}\text{C}$ arasında bulutlu ve -10 'dan büyük olduğu durumlarda ise tamamen kapalı olduğu görülmektedir. Yani İki sıcaklık arasındaki fark ne kadar büyükse gökyüzünün o kadar açık olduğu anlaşılır. Bu durumu daha iyi gösterebilmek için ayrıca sağ grafikte sadece bir günlük olarak incelenmiştir. Bunun için veri arasından en uygun gün yani gün içerisinde iki sıcaklık farkının en çok değişime uğradığı gün seçilmiştir. Şekil incelendiğinde iki sıcaklık değeri birbirine yaklaştıkça gökyüzünde bulut durumunun oluştuğu, fark arttıkça ise gökyüzünün daha berrak hale geldiği görülmektedir. Anlık da olsa bulutluluk arttığında sıcaklık değişiminin yaşandığı görülmektedir.

Astronomik gözlemlerde gece gökyüzü durumunun önemli olmasından dolayı veri gece ve gündüz olmak üzere iki ayrı şekilde incelenmiştir. Gece ve gündüz ayrımı her gün için astronomik tan zamanları hesaplanarak belirlenmiştir.

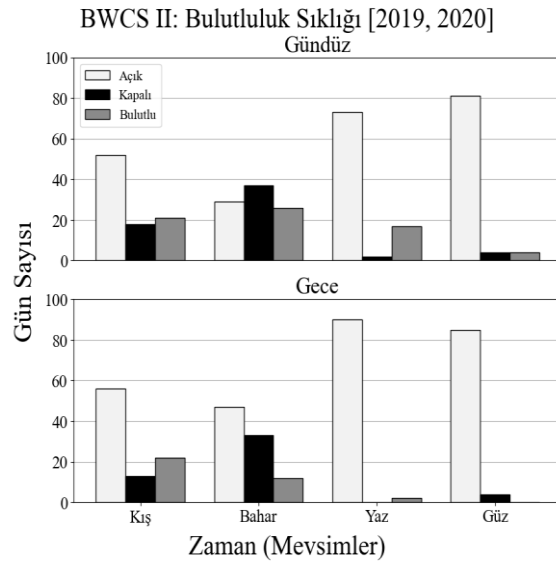
3. Bulgular ve Tartışma

Astronomide gece ve gündüz farklı gözlem türleri ve planları yapıldığı için bulut değerleri de gece ve gündüz olarak ayrı incelenmiştir. Bulutlu gün sayısı Şekil 5'te görüldüğü gibi gece ve gündüz ayrımı yapılarak aylık olarak verilmiştir. Benzer şekilde mevsimlik değişimler Şekil 6'da verilmiştir. Aylık ve mevsimlik grafiklerin değerleri de Tablo 2 ve Tablo 3'te verilmiştir. Şekil 5 incelendiğinde hem gece hem de gündüz için Temmuz, Ağustos, Eylül, Ekim, Kasım ve Aralık ayları havanın en fazla açık olduğu gün sayısına sahiptir. Ayrıca Ocak ve Haziran aylarında açık gün sayısının da yüksek olduğu görülebilir. En fazla kapalı gün olan aylar ise Mart, Nisan ve Mayıs olarak hesaplanmıştır. Ağustos ayında açık gün sayısı 30'a kadar çıkmıştır. Nisan ayında ise

açık gün sayısı 7'ye düşerek en az açık gün olan ay olduğu görülmektedir. Şekil 6 mevsimlik değerler incelendiğinde yaz ve güz mevsiminin açık gün sayısının fazla olduğu, bahar mevsiminde ise 30 günün biraz altına düştüğü görülmektedir. Özellikle yaz ve güz aylarında neredeyse 202'den az açık gün sayısı olmadığı görülmektedir. Bu değerlerin gece ile gündüz pek değişmediği görülmektedir. Tablo 2 ve Tablo 3'te aylık ve mevsimlik bulutluluk durumları gece ve gündüz olarak ayrı ayrı verilmiştir. Astronomik gözlemler için gece gökyüzünün açık olması gerekmektedir.



Şekil 5. DAG yerleşkesinde bulunan BWCS II'den alınan aylara göre bulutluluk sıklığı



Şekil 6. DAG yerleşkesinde bulunan BWCS II'den alınan mevsimlere göre bulutluluk sıklığı

Tablo 2 incelendiğinde gece zamanı bulutluluk durumu (ortalama %65) gündüz açık bulutluluk durumu (%51) yüksek olup gece ve gündüz kapalı değerler sırasıyla %16 ve %20 olarak hesaplanmıştır. Ortalama bulutlu değerler ise gece ve gündüz için sırasıyla %20 ve %29 olarak hesaplanmıştır. Astronomik gözlemlerin gece yapılması nedeniyle bu durum yerleşke için oldukça önemlidir. Veri setine yıllık olarak bakıldığında 2020 yılında açık hem gece (%68) hem de gündüz (%58) değerleri 2019 yılına ait değerlere (gece %62 ve gündüz %44) göre yüksek gerçekleşmiştir. Başka bir ifadeyle 2019 yılında kapalı ve bulutlu gün sayısı daha yüksek hesaplanmıştır. Gece zamanı için maksimum açık sayısı 2019 yılında %90.8 ile Ağustos ayında iken 2020 yılında %94.1 ile Ekim ayında hesaplanmıştır. Benzer şekilde minimum açık sayısı 2019 yılında %18.7 ile

Şubat ayında iken 2020 yılında %37.2 ile yine Şubat ayında gerçekleşmiştir. Gece zamanı için maksimum kapalı sayısı 2019 yılında %34.7 (Şubat) iken 2020 yılında %33.7 (Şubat) olarak hesaplanmıştır. Benzer şekilde gündüz değerleri ve daha fazla ayrıntı için Tablo 2'ye bakınız.

Tablo 2. Aylara göre gökyüzünün bulutluluk durumu

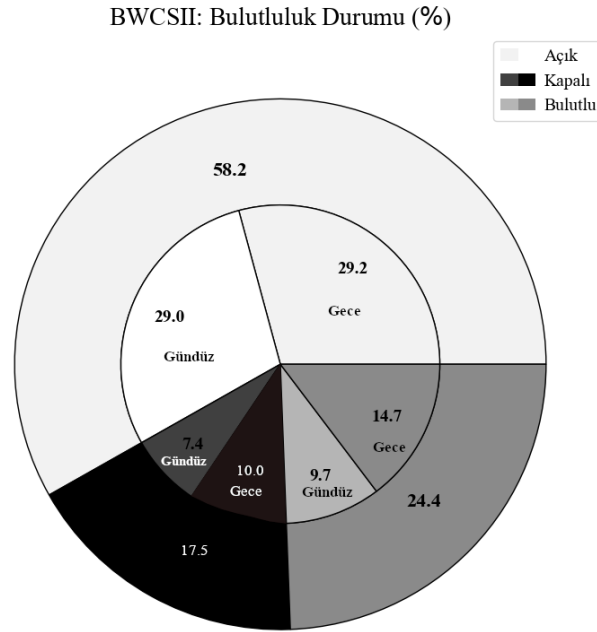
Yıl	Ay	Gece			Gündüz		
		Açık (%)	Bulutlu (%)	Kapalı (%)	Açık (%)	Bulutlu (%)	Kapalı (%)
2019	1	31.9	40.1	27.9	18.4	45.8	35.7
	2	18.7	46.6	34.7	15.1	43.9	41
	3	26.6	43.2	30.2	12.7	44.2	43
	4	52.8	25.3	21.9	24.3	39.6	36.2
	5	77.5	11.8	10.7	29.8	44.7	25.4
	6	72.7	19.8	7.5	39.8	48	12.2
	7	86.2	9.9	3.9	64.7	30.8	4.5
	8	90.8	7.2	2	71.7	25.1	3.3
	9	84.3	9.5	6.3	68.2	23.1	8.8
	10	74.8	14.8	10.5	63.5	21.6	14.9
	11	65.2	17.3	17.4	61.8	18.7	19.6
	12	56.7	18.4	24.9	60.2	16.4	23.4
2020	1	50.7	29.8	19.6	51.6	25.8	22.7
	2	37.2	43.2	19.6	31.1	38.1	30.8
	3	41.9	24.5	33.7	39.2	25.7	35.1
	4	45.6	22.9	31.5	31.7	27.1	41.2
	5	63.4	13.2	23.4	43.4	30.6	26
	6	86.3	11.2	2.5	56.3	36.4	7.3
	7	88.8	9.7	1.5	64.2	29.8	6
	8	87.9	7	5.1	75.7	19.2	5.1
	9	93.6	4.1	2.3	82.3	16.8	0.9
	10	94.1	3.1	2.8	87.7	10.1	2.3
	11	69	18.7	12.2	67.7	17.8	14.5
	12	59.4	19.3	21.3	62.9	11.2	25.9

Tablo 3. Mevsimlere göre gökyüzünün bulutluluk durumu

Yıl	Mevsim	Gece			Gündüz		
		Açık (%)	Bulutlu (%)	Kapalı (%)	Açık (%)	Bulutlu (%)	Kapalı (%)
2019	Kış	25	43.5	31.5	16.6	44.7	38.7
	Bahar	49.3	28.6	22.1	22.3	42.8	34.9
	Yaz	84.4	11.5	4.1	59.9	33.8	6.3
	Güz	75.2	13.8	11	65	21.6	13.5
2020	Kış	48.5	30.5	21	46.9	27.6	25.5
	Bahar	49.4	20.6	29.9	38.1	27.9	33.9
	Yaz	87.7	9.2	3.2	65.3	28.6	6.1
	Güz	85.1	8.9	6	79.9	14.7	5.4

Tablo 3'ten mevsimsel değerler incelendiğinde açık değerler yaz ve güz mevsimlerinde yüksek iken bahar ve kış mevsimlerinde daha düşük ölçülmüştür. En küçük açık değeri %25 ile 2019 Kış mevsimi iken en yüksek açık sayısı %87.7 ile 2020 Yaz mevsimi olarak gerçekleşmiştir. Genel olarak Kış ve Bahar mevsimlerinde

kapalı ve bulutlu değerleri yüksek olup daha az sayıda astronomik gözlem zamanı ve diğer mevsimlerde daha az bulutluluk ve daha fazla astronomik gözlem fırsatları olacaktır.



Şekil 7. DAG yerleşkesinde bulunan BWCS II'den alınan bulutluluk durumu

Şekil 7'de ise toplam bulutluluk durumu yüzde oranlarla verilmiştir. Şekil 7'deki bulutluluk durumunu incelediğinde açık günlerin %58.2 olduğu ve bunun %29.2'sinin gece, %29'unun da gündüz olduğu görülmektedir. Aynı şekilde gökyüzünün kapalı (çok bulutlu) olduğu durum için %10 gece, %7.4 gündüz olarak toplamda %17.5 olduğu görülmektedir. Benzer şekilde yerleşkenin bulunduğu alanda gökyüzünün bulutlu olması durumunun %14.7 gece ve %9.7 gündüz olarak toplamda %24 olduğu görülmektedir.

4. Sonuçlar

DAG için daha önce yer çalışmaları yapılmış ve 3170 m yükseklikte olan Erzurum Konaklı/Karakaya Tepeleri'nin IR gözlemleri için uygun olduğu belirlenmiştir. BWCS II ile elde edilen veri analiz edilmiş ve yerleşkenin astronomik gözlemler için bazı özellikleri belirlenmiştir. Bu çalışma ilk ışığını almaya hazırlanan DAG için yerinde ölçümlerle yerleşke atmosferini bulutluluk bakımından analiz eden en son çalışmadır. Bu çalışma hem yerleşkenin güncel karakteristik durumunu ortaya koymakta hem de cihaz ve ölçüm yöntemleri ile ilgili bilgiler sunmaktadır.

Yapılan analizlerde gökyüzü ve ortam sıcaklığı ölçümleri kullanılmıştır. Özellikle IR bölgede gözlem yapacak teleskoplar için IR ışınının su buharı tarafından soğurulması nedeniyle nem ve bulutluluk durumu çok önemlidir. Bulutluluk durumu için üç farklı durum söz konusudur. Bunlar açık, bulutlu ve kapalı olarak verilmiştir. Analizler sonucunda toplam açık gün değerinin %58.2, bulutlu olarak ölçülen değer %24.3 ve kapalı olarak ölçülen değerlerin ise %17.5 olduğu görülmüştür. Özellikle yaz aylarında havanın %87'sinden fazlasının açık olduğu görülmüştür. Bulutluluk durumu incelendiğinde yüksek bulut değerlerinin daha çok gündüz olduğu ve düşük bulut değerlerinin gece olduğu görülmüştür. Ayrıca 2020 yılında açık gün sayısının daha fazla olduğu yani bulutluluk durumu önceki yıla göre azalma göstermiştir.

Analizler sonucunda bulutluluk durumunun incelenmesiyle %58'den fazla açık değerlerin olduğu görülmüştür. Yapılan tüm analizler sonucunda DAG yerleşkesinin hem görsel hem de IR gözlemleri için gerekli hava koşullarına sahip oldukça iyi bir gökyüzüne sahip olduğunu görülmüştür.

Yazar Katkıları

Tüm yazarlar çalışmanın konusunun belirlenmesi, yürütülmesi, planlanması ve sonuçların değerlendirilerek çalışmanın makale haline getirilmesini sağlamıştır. Birinci yazar çalışmanın yönteminin belirlenip materyalinin hazırlanmasını sağlamış ve analizleri gerçekleştirmiştir. Tüm yazarlar makalenin son halini okuyup onaylamıştır. Bu makale, ilk yazarın ikinci yazar danışmanlığındaki yüksek lisans tezinden üretilmiştir.

Çıkar Çatışması

Yazarlar hiçbir çıkar çatışması olmadığını beyan etmektedir.

Teşekkür

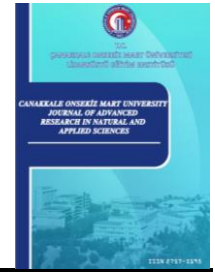
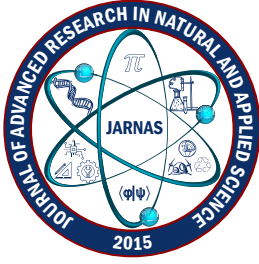
Atatürk Üniversitesi Astrofizik Araştırma ve Uygulama Merkezi (ATASAM)'ne desteklerinden dolayı teşekkür ederiz. Bu çalışma, Doğu Anadolu Gözlemevi (DAG) Projesi tarafından desteklenmiştir. Proje No: 2011K120230

Kaynaklar

- [1] P. Berdahl, R. Fromberg, *The thermal radiance of clear skies*, Solar Energy 29 (4) (1982) 299–314.
- [2] C. N. Long, J. M. Sabburg, J. Calbó, D. Pagès, *Retrieving cloud characteristics from ground-based daytime color all-sky images*, Journal of Atmospheric and Oceanic Technology 23 (5) (2006) 633–652.
- [3] D. Pérez-Ramírez, R. J. Nemiroff, J. B. Rafert, *Nightskylive.net: The night sky live project*, Astronomische Nachrichten: Astronomical Notes 325 (6-8) (2004) 568–570.
- [4] B. Dürr, R. Philipona, *Automatic cloud amount detection by surface longwave downward radiation measurements*, Journal of Geophysical Research: Atmospheres 109 (D5) (2004) 9 pages.
- [5] R. Boers, M. J. De Haij, W. M. F. Wauben, H. K. Baltink, L. H. Van Uft, M. Savenije, C. N. Long, *Optimized fractional cloudiness determination from five ground-based remote sensing techniques*, Journal of Geophysical Research: Atmospheres, 115 (D24) (2010) 16 pages.
- [6] W. X. Zhang, D. R. Lü, Y. L. Chang, *A feasibility study of cloud base height remote sensing by simulating ground-based thermal infrared brightness temperature measurements*, Chinese Journal of Geophysics 50 (2) (2007) 339–350.
- [7] K. Kaba, C. Yeşilyaprak, *Validation of CM SAF Cloud Fractional Cover (CFC) Data and Analysis of CM SAF CFC Data for the Eastern Anatolia Observatory (DAG) Site*, Journal of Advanced Research in Natural and Applied Sciences 7 (3) (2021) 304–318.
- [8] Atatürk Üniversitesi Astrofizik Araştırma ve Uygulama Merkezi (ATASAM), DAG Özet (2020), <https://atasam.atauni.edu.tr/dag/>, 10 Mayıs 2023 tarihinde erişildi.
- [9] Y. Güney, *The atmospheric seeing measurements for eastern Anatolia observatory site*, Doctoral Dissertation Atatürk University, (2021) Erzurum.
- [10] Diffraction Limited, Cloud Sensor II User's Manual (2012), <https://diffractionlimited.com/wp-content/uploads/2016/04/Cloud-SensorII-Users-Manual.pdf>, 10 Mayıs 2023 tarihinde erişildi.
- [11] Y.-H. Bae, J. H. Jo, H.-S. Yim, Y.-S. Park, S.-Y. Park, H. K. Moon, Y.-J. Choi, H.-J. Jang, D.-G. Roh, J. Choi, M. Park, S. Cho, M.-J. Kim, E.-J. Choi, J.-H. Park, *Correlation Between the "seeing FWHM" of Satellite Optical Observations and Meteorological Data at the OWL-Net Station, Mongolia Journal of*

Astronomy and Space Sciences 33 (2) (2016) 137–146.

- [12] A. Gwynne, *Cloud detection system for the Mt Kent observatory*, Bachelor's Thesis University of Southern Queensland (2005) Toowoomba.
- [13] R. Sloan, J. H. Shaw, D. Williams, *Infrared emission spectrum of the atmosphere*, Journal of the Optical Society of America 45 (6) (1955) 455–460.
- [14] L. Adelard, F. Pignolet-Tardan, T. Mara, P. Lauret, F. Garde, H. Boyer, *Sky temperature modelisation and applications in building simulation*, Renewable Energy 15 (1-4) (1998) 4188–430.
- [15] O. Gliah, B. Kruczek, S. G. Etemad, J. Thibault, *The effective sky temperature: an enigmatic concept*, Heat and Mass Transfer 47 (9) (2011) 1171–1180.
- [16] R. Tang, Y. Etzion, I. A. Meir, *Estimates of clear night sky emissivity in the Negev Highlands, Israel*, Energy Conversion and Management 45 (11-12) (2004) 1831–1843.
- [17] M. C. B. Ashley, J. S. Jurcevic, *A cloud detector for automated telescopes*, Publications of the Astronomical Society of Australia 9 (2) (1991) 334–335.
- [18] R. Clay, *Cloud monitoring for large cosmic ray sites*, in: D. Kieda, M. Salamon, B. Dingus (Eds.), 26th International Cosmic Ray Conference (ICRC26), Salt Lake City, Utah, 1999, p. 421.
- [19] D. J. Buckley, M. C. Dorrington, P. J. Edwards, T. J. L. McComb, S. P. Tummey, K. E. Turver, *Measurement of sky clarity using MIR radiometers as an adjunct to atmospheric Čerenkov radiation measurements*, Experimental Astronomy 9 (4) (1999) 237–249.



Corrosion Behaviors' Investigation of Carbide Coatings Developed for Sulphuric Acid Recovery Systems

Erhan Özkan¹ 

¹Dikkan R&D Center, İzmir, Türkiye

Article History

Received: 22 Jun 2023

Accepted: 28 Sep 2023

Published: 15 Mar 2024

Research Article

Abstract – In this study, corrosion resistance of cobalt and nickel, which are known to have high corrosion resistance, reinforced tungsten carbide coatings applied to low carbon stainless steel material surfaces to reduce corrosion-induced losses in sulphuric acid recovery systems were investigated. During the recovery of sulphuric acid, aggressive sulphur systems in the baths cause the metal surface to dissolve and therefore a high amount of material loss occurs. In order to minimize corrosion induced material loss, 316 L stainless steel surfaces were coated with an interlayer of 95% nickel and 5% aluminium alloy, and then tungsten carbide coatings were synthesized on the surfaces of substrate materials reinforced with 13% cobalt and 13% nickel, respectively by thermal spraying method to further reduce the corrosion rate. Characterization of the produced coatings were carried out by X-ray diffraction (XRD), scanning electron microscope (SEM), optical microscope, image analyzer, and surface roughness device. The standard potentiodynamic polarization characteristics of the coatings for 1M H₂SO₄ solution at room temperature were investigated with a potentiostat/galvanostat device. As the obtained results, nickel reinforced tungsten carbide coatings with nickel aluminium interlayer showed the highest corrosion resistance against sulfuric acid environment with 0,41 mm/year corrosion rate. As a result of the article, the corrosion resistance of 316L stainless steels in sulfuric acid systems was improved by 5.02 and 3.15 times, respectively.

Keywords – Cobalt and nickel reinforcements, HVOF surface coating, stainless steel, sulphuric acid corrosion, tungsten carbide coatings

1. Introduction

The most important problem encountered in sulfuric acid recovery plants is the presence of aggressive environments such as hydrogen sulfide and carbon dioxide, which cause corrosion damage to the materials [1]. Sulfuric acid (H₂SO₄) stands out as a chemical that is frequently found in structures in the petrochemical industry. The occurrence of sulfuric acid in the structures can be briefly summarized as follows: In converters, SO₂ from the raw material is oxidized to SO₃:



The gas in the reactors is exposed to high temperatures and as a result, it reacts with the water in the environment, causing the formation of sulfuric acid:



Recycling facilities are of critical importance in terms of actively positioning sustainable ecosystem processes, which are one of the important issues of today, in the organization [2]. Sulfuric acid formed because of the above chemical reactions creates an aggressive corrosive environment in the main lines of petrochemical

¹erhanozkan81@icloud.com (Corresponding Author)

industries and especially in sulfuric acid recovery plants [3]. Protecting metallic surfaces in recycling plants from corrosion, surface modifications of metals have come to the fore [4]. The corrosion resistance of materials can be increased by changing and improving the surface morphology and microstructure [5]. Changing the surface chemistry of materials; carburizing, nitriding, carbonitriding, boriding, siliconization and chroming processes are carried out [6]. In addition to all these, surface coating processes with thermal spraying have recently played a role in increasing the corrosion resistance of metallic surfaces to slow down the corrosion rate and make the surface corrosion resistance more effective [7].

Thermal spraying processes are carried out with spray guns to protect the main material surface from environmental conditions, to prevent corrosion, and to improve material surface properties [8]. After the coating material is melted with the energy used in the gun, it is thrown onto the material surface at high speed and the coating process is performed [9]. According to the type of energy supplied to the gun, there are two basic types of guns: guns that use electrical energy and guns that work with flame heating [10]. There are three types of gun systems that provide the energy required for melting fuel used flame like, flame spraying, spraying-fusing and HVOF (High Velocity Oxy-Fuel). Among these methods, especially the coatings produced with HVOF show very good adhesion and cohesion properties, as well as being very hard, making this method more advantageous than other methods [11]. Besides all these advantages, the formation of holes, pores, and micro-cracks because of high-temperature particles hitting the substrate surface at high speed can be counted among the disadvantages of this method [12]. These pores, cracks and holes have a negative effect on the corrosion behavior of the material [13]. In a corrosive environment, these structures act as channels between the coating and the substrate, causing the substrate material to be exposed to the corrosive environment [14]. This situation increases the diffusion of the corrosive environment and causes faster damage to the litter material [15]. To prevent this, systems have been developed by creating a buffer layer on the coatings [16]. Interlayers provide great advantages in preventing formations such as capillary cracks and porosity, which reduce corrosion resistance.

Due to its chemical content, 316 L quality stainless steels are widely used in systems that are expected to be resistant to aqueous corrosion, such as sea water and acidic solutions. It is defined as 1.4404 or X2CrNiMo17-12-2 according to EN, which is called European Norm Standards, and as S31603 according to UNS. The weakness of this product is that it cannot perform adequately in environments with more aggressive corrosion. For this reason, stainless steels called duplex stainless steel and defined as 1.4462 in the standard are widely used instead of 316 L stainless steel, but since the production of this type of steel is not common in our country, it is possible to obtain it from abroad. On the other hand, it is of critical importance for the sector to reduce the need for duplex quality stainless steels by improving the surface properties of 316 L quality stainless steel, which is widely produced in our country. In this study, the corrosion behavior of 316 L stainless steels, which are widely used in sulfuric acid recovery facilities in our country, with HVOF technique, and the surfaces coated with NiAl, WC-Co and WC-Ni in 1 M H₂SO₄ solution with standard potentiodynamic methods were investigated. Due to their high temperature resistance up to 1100 °C, NiAl coating was preferred as a buffer layer. Moreover, nickel-cobalt binary alloy coatings are widely used in qualified industries due to their properties such as high strength, corrosion, and wear resistance [17-19]. According to the results obtained, the records of increasing the service life of tungsten carbide coated stainless steels reinforced with different alloys in a corrosive environment were shared in detail. With these data, a roadmap has been presented regarding the basis of domestic and national solutions that will provide import substitution. In addition, information on the HVOF coating parameters, the porosity of the coating surfaces, the surface thicknesses and the corrosion behavior of the thicknesses and their interaction and changes were given in detail.

2. Materials and Methods

Experimental work steps consist of HVOF coating, characterization and analysis of coatings, corrosion tests, surface investigation and porosity determination. In Figure 1, there is a work-flow chart in which the experimental studies are symbolized as a single block.



Figure 1. Experimental work phases work-flow chart

2.1. HVOF Coating

316 L stainless steel samples with 50x50x2 mm dimensions were used as substrate material. Table 1 shows the mechanical properties of 316 L stainless steel, which is preferred as the substrate material.

Table 1. Mechanical properties of 316 L stainless steel material

Yield Strength (MPa)	Tensile Strength (MPa)	Hardness HRC
Min 170	Min 485	Max 22

Surface preparation of the samples to be used in the HVOF technique is an important step. This is because the adhesion of the coatings is directly related to the surface roughness and is controlled by the type of blast, pressure, angle, distance, time, and sandblast nozzle (hole size). Increasing the adhesion strength of the coating to the material surface, the material surface was sandblasted before proceeding to the HVOF thermal spray process. High hardness alumina particles were impinged on the material at high speed, increasing the roughness rate on the surface and increasing the number and size of asperities on the surface with increasing roughness. The particle coming to the surface during the spraying process clings to these asperities and attaches itself to this point mechanically and physically. High bond strength can only be achieved with the high roughness created. Therefore, the adhesion strength of the coating powders to the substrate surface increases. This was done with 35 grit alumina powders for 30 seconds using 400 kPa compressed air. HVOF process was carried out with Oerlikon Diamond Jet 2600 DJH brand system (Figure 2).



Figure 2. HVOF spray gun

Many carbide compositions, such as WC-based cermet carbides, have been successfully coated for the last 20 years using HVOF methods. Today these materials are used in the production of critical parts (piston and shaft, etc.) belonging to the aviation industry. HVOF coated WC-based cermet materials provide excellent toughness and high hardness. Moreover, WC-Co and WC-Ni cermet surface coatings are high hardness, wear resistance, widely used in many engineering parts as they have thermal stability and corrosion resistance. NiAl interlayer coatings were preferred because of their tribological properties. They have a critical role for the increasing

scratch resistance of the WC-based cermet carbides such as Co and Ni. Therefore, coating was obtained with conventional sintered powders with a grain size of 14 μm in the ratios of 13% by weight Co, 87% WC and 13% by weight Ni, 87% WC interlayer coating containing nickel and aluminium was carried out. The literature and previous studies were used to determine the content of the interlayer, and accordingly, NiAl powder containing 95% Ni and 5% Al by weight was used as the bond coating. The parameters of NiAl bond coating and WC-based two coatings are given in Table 2.

Table 2. Sputtering parameters of the HVOF process

Parameters	Values	
	NiAl	WC-based coatings
Oxygen flow (1 min^{-1})	120	240
Fuel gas (hydrogen) flow (1 min^{-1})	300	600
Carrier gas (nitrogen) flow (1 min^{-1})	18	18
Spray distance (mm)	250	250
Substrate velocity (in the horizontal plane) (m s^{-1})	1	1
Gun velocity (in the vertical plane) (mm s^{-1})	5	5
Number of layers	20	20

2.2. Characterization and Analysis of Coatings

The characterization of the crystal structures of the coatings and the determination of the phases they contain were carried out with Rigaku D/Max-2200/PC model X-ray diffractometer, Cu-K α (wavelength, $\lambda=0.15418 \text{ nm}$) radiation.

The surface morphologies of the coatings, the structure and distribution of the particles, and their homogeneity at high magnifications were observed with a JEOL JJM 6060 scanning electron microscope (SEM). The coating thicknesses were measured with the LUCIA 4.21 image analyzer by placing the samples in a horizontal position.

Studies on the determination of the effect of surface roughness on adhesion and corrosion resistance and the comparison of post-corrosion surface roughness compared to the pre-corrosion situation were carried out with Mitutoyo SJ-301 device.

2.3. Corrosion Tests

Corrosion tests were carried out with GAMRY PC4/750 potentiostat/galvanostat. NiAl, WCCo/NiAl and WCNi/NiAl coated 316 L stainless steel samples were ultrasonically cleaned in acetone for 15 minutes before testing. Coatings with a surface area of 50x50 mm were placed in the corrosion cell by insulating only the coating surfaces in contact with the liquid. A 3-electrode system was used as a corrosion cell. Saturated calomel electrode (SCE) reference electrode, graphite rod auxiliary electrode and coated 316 L stainless steel samples were used as working electrodes. All experiments were carried out in 1 M H₂SO₄ solution and at temperatures between 24-27 °C. After the samples were placed in the solution, they were kept until they reached the open circuit potential (OCP). This value is defined as the value at which materials reach a constant potential. After this waiting, anodic polarization studies were carried out by applying potential to the coatings from below the open circuit potentials (approximately -500 mV) up to 4 V at a scanning rate of 5 mV s⁻¹.

The porosity of HVOF coatings was determined by electrochemical methods. The porosity of the coatings was calculated using the following equation [20].

$$F = \frac{R_{p,m}}{R_p} \log \left(\frac{-|\Delta E_{cor}|}{\beta a} \right) \quad (2.1)$$

The F in the equation gives the total porosity ratio in the coating. $R_{p,m}$ is the polarization resistance of the base material, R_p is the measured polarization resistance of the coating, ΔE_{cor} is the difference between the corrosion potentials of the base material and the coated material, and βa is the Anodic Tafel Slope of the base material.

After the corrosion tests, the corrosion rate was calculated in mm/year using the formula given below, using Faraday's Law, in order to meet the requirements of the ASTM G-102 standard.

$$CR = \frac{K \times W}{A \times T \times D} \quad (2.2)$$

3. Results and Discussion

3.1. Results

3.1.1. Phase Analysis and Microstructure

Figure 3 shows the XRD patterns of coatings synthesized with the NiAl interstage on stainless steel by the HVOF technique. The coatings' XRD patterns are defined as WC-Co/NiAl and WC-Ni/NiAl. WC-Ni/NiAl coatings included WC, W_2C , W, Ni, NiAl, Ni_3Al and FeNi phases. On the other hand, WC-Co, and WC, W_2C , W, Co, CoW_9C , $Co_8W_9C_4$, NiAl, Ni_3Al and FeNi phases were determined in the WC-Co/NiAl coatings. It has been observed that the WC, W_2C , W, C, Ni_3Al , FeNi phases were common in WC-Co/NiAl and WC-Ni/NiAl coatings. W_2C and metallic W phases obtained after deposition in both WC-based layers were formed by carbon loss during the coating process. Due to the NiAl bond layer on the substrate material, the presence of NiAl and Ni_3Al phases was observed in both samples. Islak and Buytoz [21] found similar findings in their study in 2013 and found that WC was the dominant phase in tungsten carbide reinforced coatings made with HVOF. As a result of decarburization during the spraying process, the WC phase was transformed into the W_2C phase. As the Ni addition amount increased, the intensities of the phases formed by W, C and Co elements decreased in a trace amount. Carbon, which is possible to form at high temperatures and liberated because of the decarburization of cobalt-containing phases, provided the formation of the triple $Co_8W_9C_5$ phase at very low rates [22].

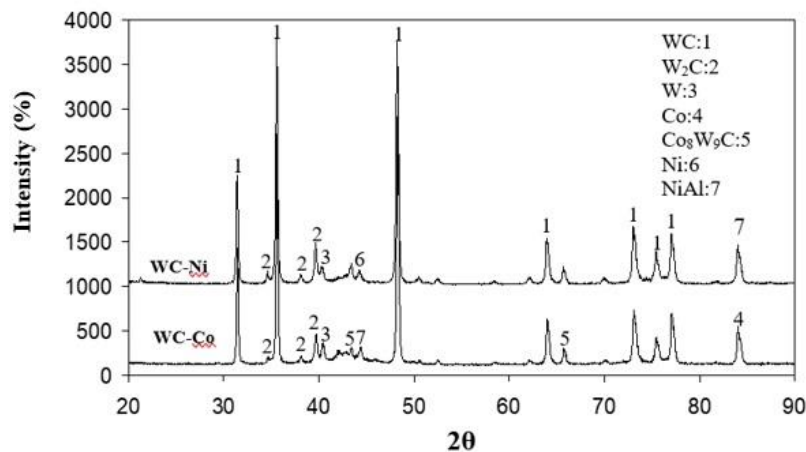


Figure 3. XRD patterns of samples coated with NiAl bond step on 316L stainless steel by HVOF technique
a) WC-Co and b) WC-Ni

A high percentage of pores, microcracks and unmelted particles were detected on the surfaces of WC-Co and WC-Ni coatings directly synthesized on 316L stainless steel without NiAl intermediate stage. The presence of these structures negatively affects corrosion, so SEM images of NiAl coated on stainless steel and WC-Co and WC-Ni coatings synthesized on this layer were evaluated and shown in Figure 4. Round particles were not observed in NiAl coatings, and this situation did not pose a great disadvantage because it is an intermediate layer, but it had a positive effect for better adhesion of the next layer. Due to the high melting temperature of the components in WC-Co coatings, the particles were synthesized in a smaller structure compared to WC-Ni coatings. The reason why the grain growth on WC-Ni coating surfaces is higher than on WC-Co coating surfaces is that the components in WC-Ni have relatively lower melting temperatures [23].

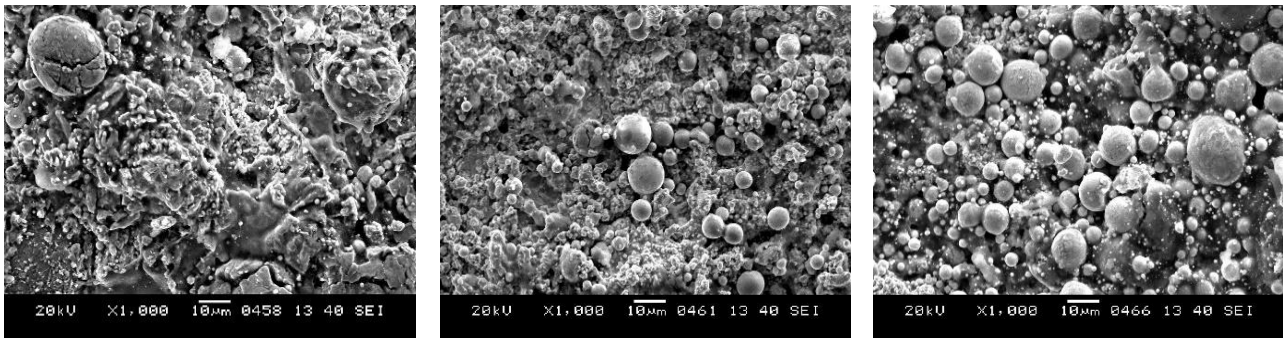


Figure 4. SEM images of coatings produced with HVOF (a) NiAl, (b) WC-Co, and (c) WC-Ni

3.1.2. Corrosion

In Figure 5, the time-dependent variation of corrosion potentials of NiAl bond coating, WC-Co and WC-Ni coatings on the main material 316 L, 316 L is given. The volt value, where the potential does not change over time, that is, the curve remains at a constant value, indicates the corrosion potential of the material (open circuit potential, equilibrium potential) [22]. By using the data in Figure 5, the equilibrium potentials of the samples were determined and scanning intervals were determined for the anodic polarization experiments, but 316 L stainless steel samples gave a more stable curve due to their bright and homogeneous surfaces. Since the NiAl bond coating surfaces are not homogeneous and have a rougher structure, it has shown a continuously decreasing curve characteristic. In Figure 4a, the absence of particle morphology in the NiAl microstructure and the heterogeneous microstructure on the surface and the inability of the curve to reach a constant potential overlap [24]. WC-Co and WC-Ni coatings, on the other hand, have a more homogeneous surface compared to NiAl and a more heterogeneous surface compared to 316 L, but when compared to each other, close curves are expected and a positive result. As a result of the comparison of the microstructures in Figure 4b and Figure 4c, the dense structure of the spherical particles on the surface confirms this data. Since an evaluation made according to the data in Figure 5 gives a misleading result, another evaluation method was preferred according to the anodic polarization curves. This situation gave similar results to literature 23 studies. The main reason for this is that the corrosion potential is a calculated potential to find the Thevenin Equivalent Voltage between any two points. Considering the distance between two points as if it is an open electrical circuit, the potential difference between those two points is determined by using the voltage values at the other ends. For this reason, the more homogeneous and smooth the system surface, the healthier and cleaner the curves will be [12].

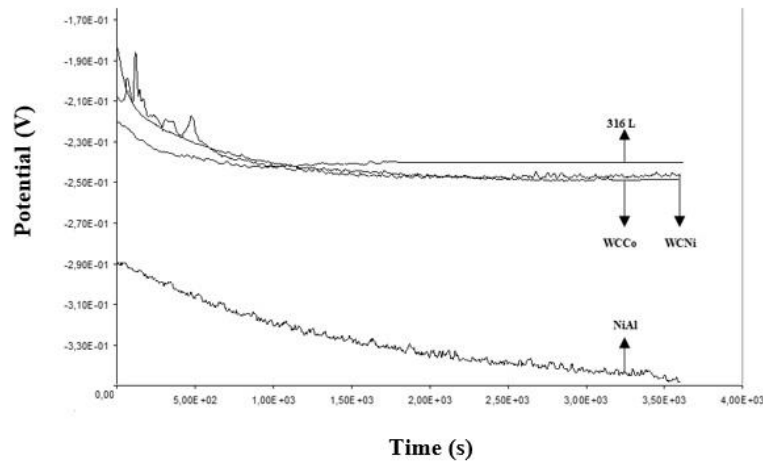


Figure 5. Time-dependent variation of corrosion potentials of substrate (316 L) and coatings (NiAl, WCCo, WCNi)

In Figure 6, the anodic polarization curves of the 316 L stainless steel sample, which is the base material, and the NiAl, WC-Co and WC-Ni coatings synthesized on it are given. The values of corrosion current (I_{cor}), corrosion potential (E_c), polarization resistance (R) and Tafel coefficients related to potentiodynamic polarization parameters are given in Table 3. Considering the Tafel curves (Figure 6) obtained in a 1 M H_2SO_4 corrosion environment, the corrosion resistance of WC-Co and WC-Ni based coating layers in the relevant corrosive environment is relatively higher compared to the substrate material, corrosion current and corrosion potential. values (Table 3). On the other hand, it was determined that the polarization resistance values were higher on the WC coated surfaces compared to the uncoated and only NiAl coated surfaces. There is a net current at the corrosion potential, but this current is not read because the total anodic current is equal to the total cathodic current. Corrosion current value is determined with this current, which is not directly measured. The current density obtained by dividing the corrosion current by the surface area of the electrode gives the corrosion rate of the metal. Since sulfuric acid affects both anodic and cathodic reactions with tungsten carbide, no great change in corrosion potentials was observed, but the corrosion current density decreased, and the polarization resistance increased. The effectiveness of HVOF coatings, calculated according to the corrosion current density and polarization resistance, increased as the corrosion resistance of the reinforcement material increased. The fact that the tungsten carbide efficiency obtained according to the polarization resistance and current density is similar, shows that there is a parallelism in the decrease of current and increase in resistance [11].

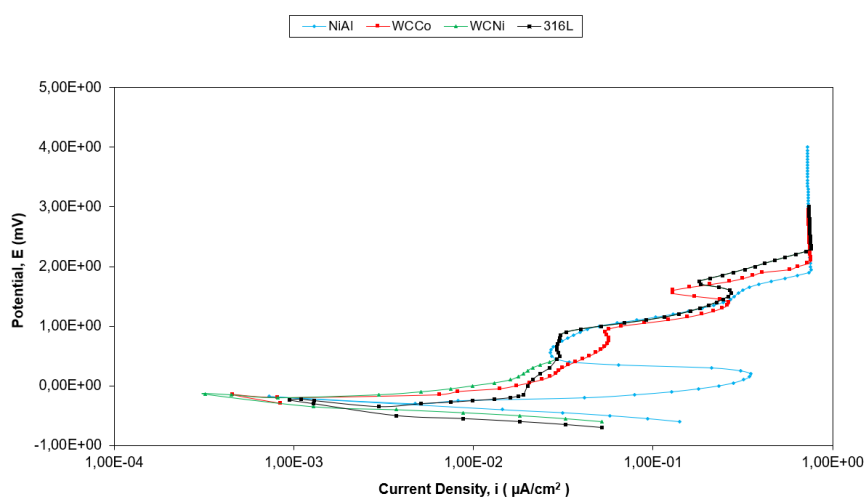


Figure 6. Anodic polarization curves of the samples

The slope values have been taken from the anodic and cathodic Tafel Polarization Curves, and it has been observed that there was correlation between the porosity values. Corrosion current was measured lower by coating 316L stainless steels. In all the results obtained, β_a was greater than β_c . This is an indication that oxide films protect the base material anodically [25]. The corrosion rate decreased by coating the surfaces with tungsten carbide. According to the results from Table 3, WC-Ni is the coating with the highest corrosion resistance, while the WC-Co coated material has a corrosion resistance close to WC-Ni. NiAl coating, on the other hand, has a lower corrosion resistance than WC-Ni and WC-Co but better than 316 L. The relationship between the advancement mechanism of the resulting structure and porosity has been established. It has been observed that WC-Ni and WC-Co coatings corroded in proportion to porosity, but NiAl interlayer coatings had the lowest corrosion resistance. Explaining this situation, porosity distribution should also be taken into consideration. Porosities that were small and homogeneously distributed throughout the coating structure cannot prevent the crystals formed because of the corrosion from progressing. Large porosities cannot prevent the crystals formed regarding to the corrosion. However, local porosities formation in crystals have been observed. This condition has a role in hindering progress [24].

Table 3. Electrochemical measurements of coatings in 1M H₂SO₄ solution at 25 °C

Sample	E _c (mV)	β _c (mV)	β _a (mV)	I _{cor} (A)	Pol.Res. (R) (Ω)	Porosity (%)
316L	-240	31,87	256,6	94,6 x 10 ⁻⁵	4,83 x 10 ⁶	-
NiAl	-180	309,4	312,3	72,7 x 10 ⁻⁵	3,90 x 10 ⁶	8,24
WC-Co	-150	283,9	375,0	45,9 x 10 ⁻⁵	2,66 x 10 ⁶	6,58
WC-Ni	-140	31,87	256,6	32,2 x 10 ⁻⁵	1,83 x 10 ⁶	7,61

In order to compare the corrosion resistance of WC-Ni and WC-Co coatings more concretely, porosity values were considered. When the porosity amounts calculated by electrochemical methods were compared, it was observed that WC-Ni with larger nucleation had a higher porosity than WC-Co and this observation was confirmed by SEM pictures, but this research made from a small surface does not reveal a very accurate comparison criterion [23]. For this reason, the corrosion rates of WC-Ni and WC-Co coatings calculated with ASTM G-102 Faraday's Law are given in Table 4.

Table 4. Corrosion rate values of NiAl, WC-Ni, and WC-Co coatings

Sample	Corrosion Density (μA/cm ²)	Corrosion Rate (mm/year)
NiAl	22,72	2,05
WC-Co	14,30	1,29
WC-Ni	11,90	0,41

WC-Ni coating, calculated by Faraday's Law, has a lower corrosion rate of 14,6% compared to WC-Co. In other words, WC-Ni coated 316 L material will lose 0,88 mm less material due to corrosion in 1 M concentration H₂SO₄ solution in 1 year compared to WC-Co coated material. Determining the corrosion rate, which is defined as the amount of metal dissolving per unit time, is important for determining the corrosion resistance of metals and their alloys. Corrosion rate is measured quantitatively by mass loss, Tafel extrapolation method, linear polarization method and alternating current impedance measurement. Homogeneous mass loss measurement is one of the most accurate methods that will give a healthy and accurate result in determining the corrosion rate [25]. Although the reliability of Table 4 data is higher, its overlap with Table 3 data indicates a healthy comparison.

In Figure 7, SEM images taken after the corrosion test of the coatings are given. According to these images, it is clearly seen that the morphology of the coating has changed and especially the particle structure has deteriorated after the corrosion test. Along with the increase in the amount of Co in the WC-Co alloy coating electrolyte, an increase in the amount of Co% in the coating layer was observed. A decrease of % Co of WC-

Co alloy was determined with the increase of % Co. The mass fraction of cobalt in the coating is always greater than the concentration of Co^{+2} ions in the electrolyte. This is related to the unusual behavior of the WC-Co alloy coating, which is consistent with the results of previous researchers, and explains the reason for the particles remaining spherical after corrosion in Figure 7b [24].

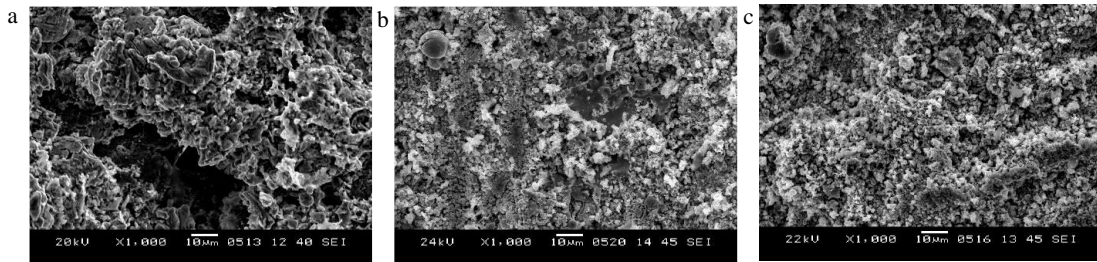


Figure 7. SEM images of coatings after corrosion test (a) NiAl, (b) WC-Co, and (c) WC-Ni

From the images in Figure 7, it cannot be concluded which coating alone suffers more material loss due to corrosion. From the SEM images, only the deformation occurring in the morphology before and after corrosion is detected, microstructure change, and thickness measurement should be made from the section to see the corrosion effect [15]. In order to reach this conclusion, the images given in Figure 8 provide a more accurate comparison.

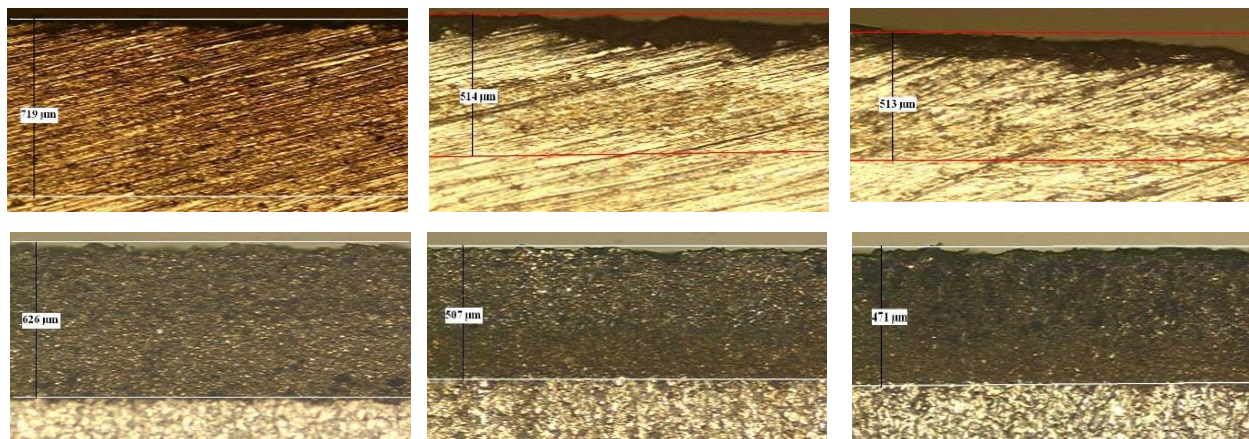


Figure 8. The view of the pre-corrosion and post-corrosion sections of the coatings and the measurement of the coating thickness (a) NiAl (P.C.) (b) NiAl (A.C.) (c) WCNi (P.C.) (d) WCNi (A.C.) (e) WCCo (P.C.) and (f) WCCo (A.C.) *(P.C.: Pre-Corrosion, A.C: Post-Corrosion)

Since the stoichiometric weights of the compared materials are close to each other, a relationship to be established between the weight loss and the amount of wear on the surface will not be very misleading [13]. The results of the thickness change in Table 5 and the corrosion rate and mass loss data exactly match. Accordingly, the most corrosion resistant nickel-reinforced tungsten carbide coating was determined.

Table 5. Changes in coating thickness

Sample	Pre-Corrosion	Post-Corrosion	Change in Thickness (%)
NiAl	719 µm	626 µm	12,93
WCNi	514 µm	507 µm	1,36
WCCo	513 µm	471 µm	8,19

3.2. Discussion

Phase analysis, microstructure control and electrochemical corrosion properties of WC-Ni/NiAl and WC-Co/NiAl samples coated with HVOF were investigated to improve the corrosion resistance and increase the

service life of 316 L stainless steel materials, which are widely used in sulfuric acid recovery plants, and the following results were obtained:

- WC-Co and WC-Ni coatings applied directly on 316 L material with the HVOF method were not coated alone due to their negative surface properties but were coated with NiAl interlayer to obtain positive surface properties.
- According to XRD results, W_2C and metallic W phases obtained after deposition in both WC-based layers were formed by carbon loss during the coating process.
- It was observed that NiAl and Ni_3Al phases were common in both samples due to the NiAl bond layer on the substrate.
- The corrosion potentials of NiAl, WC-Co/NiAl, WC-Ni/NiAl coatings and 316 L stainless steel were measured as -180, -150, -140 and -240 mV, respectively. Among the coatings, WC-Ni/NiAl was found to have the highest corrosion resistance against the sulfuric acid environment.
- The porosity ratios of the coatings were determined as 8,24% for NiAl, 6,58% for WC-Co and 7,61% for WC-Ni in the measurements made by electrochemical methods, but this calculation method is a method that can be widely used because it includes a small area. It cannot be preferred; it only gives an idea among the materials to be compared.
- The increase in the surface roughness caused a decrease in the polarization resistance of the samples.
- While the pre-corrosion thicknesses of NiAl, WC-Ni, WC-Co coatings were 719, 514 and 513 μm , respectively, these values were measured as 626, 507 and 471 μm after corrosion.

4. Conclusion

As a result, tungsten carbide-based, nickel and cobalt reinforced coatings have been successfully synthesized on 316 L stainless steel surfaces by HVOF method. The tungsten carbide phase naturally predominates in the XRD patterns. In SEM photographs, it was determined that the coatings covered the entire substrate homogeneously and were effective in anodic protection. The corrosion potentials of NiAl, WC-Co/NiAl, WC-Ni/NiAl coatings and 316 L stainless steel were measured as -180, -150, -140 and -240 mv, respectively. Among the coatings, WC-Ni/NiAl was found to have the highest corrosion resistance against sulfuric acid environment. As a result of detailed investigations of corrosion behavior, nickel-reinforced tungsten carbide coatings gave the best corrosion resistance with 0,41 mm/year corrosion rate. Due to the preference of HVOF technique, in which the parameters can be kept under stable control, certain increase or decrease in the measured values have been observed [15]. In addition, applying coatings to well-polished 316L stainless steel surfaces was another application example that supports this issue [22]. In our country, where recycling facilities have gained importance, studies are continuing to improve the material properties used in sulfuric acid recycling systems. As a result of this article, prepared for the purpose of improving the sulfuric acid corrosion resistance of 316 L quality stainless steels, an effective solution will be provided with completely national and domestic investments.

Author Contributions

The author read and approved the final version of the paper.

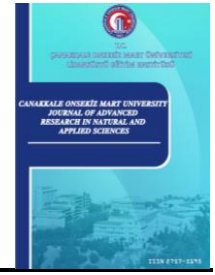
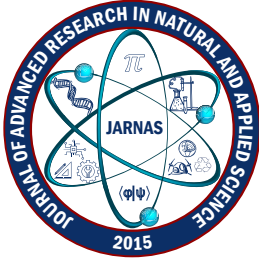
Conflicts of Interest

All the authors declare no conflict of interest.

References

- [1] U. Yurt, B. Dünder, E. Çınar, *Jeopolimer betonlarda sülfürik asit etkisinin araştırılması*, Düzce Üniversitesi Bilim ve Teknoloji Dergisi 8 (2) (2020) 1548–1561.
- [2] Ö. Tezel, S. Küçükkancabaş, E. Yıldız, *Sürdürülebilir kalkınma hedefleri bakımından atık yönetimi uygulamalarının hanehalkı tarafından değerlendirilmesi: Edirne örneği*, Trakya Üniversitesi Sosyal Bilimler Dergisi 22 (2) (2020) 941–957.
- [3] İ. Dehri, M. Özcan, H. Sözüsağlam, (2000). *Polyester kaplamalı galvanize çelik üzerine SO₂ ve NH₃ gazlarının korozyif etkilerinin EIS yöntemi ile belirlenmesi*, VII. Uluslar Arası Korozyon Sempozyumu, İstanbul, 2000, p. 246.
- [4] Z. Ahmad, *Principles of Corrosion Engineering and Corrosion Control*, Butterworth-Heinemann, Oxford, 2006.
- [5] P. R. Roberge, *Corrosion basics: An introduction*, 3rd Edition, National Association of Corrosion Engineers, Houston, 1984.
- [6] J. Stokes, *The Theory and Application of the HVOF Thermal Spray Process*, Dublin City University, Dublin, 2005.
- [7] H. Çuğ H, M. E. E. Erhaima, *Effect of Mn and Zr addition on microstructure, wear and corrosion behavior of Ti-6Al-4V composite biomaterials produced by powder metallurgy*, Manufacturing Technologies and Applications 2 (2) (2021) 41–48.
- [8] H. V. Özkavak, Ş. Ş. Özcan, *yüksek hızlı oksitasyon (HVOF) yöntemiyle kaplanmış çelik ve alüminyum alaşımlarının aşınma özelliklerinin taguchi metoduyla optimizasyonu*, BEÜ Fen Bilimleri Dergisi 9 (2) (2020) 931–942.
- [9] G. Koga, R. Schulz, S. Savoie, A. Nascimento, Y. Drolet, C. Bolfarini, C. Kiminami, W. Botta, *Microstructure and wear behavior of Fe-based amorphous HVOF coatings produced from commercial precursors*, Surface and Coatings Technology 309 (2017) 938–944.
- [10] A. K. Lakshminarayanan, V. E. Annamalai, K. Elangovan, *Identification of optimum friction stir spot welding process parameters controlling the properties of low carbon automotive steel joints*, Jmaterrestech 4 (3) (2015) 262–272.
- [11] G. Singh, N. Bala, V. Chawla, *High temperature oxidation behaviour of HVOF thermally sprayed NiCrAlY coating on T-91 boiler tube steel*, Materialstoday: Proceedings, 4 (4) (2017) 5259–5265.
- [12] T. S. Sidhu, S. Prakash, R.D. Agrawal, *State of the Art of HVOF Coating Investigations—A Review*, Marine Technology Society Journal, 39 (2) (2017) 53–64.
- [13] N. Singh, G. Vinay, D. Mahajan, *Cavitation erosion mechanisms of HVOF-sprayed Ni-based cermet coatings in 3.5% NaCl environment*, Surface and Coatings Technology, 434 (9) (2022) 128194.
- [14] S. Candan, *An investigation on corrosion behaviour of pressure infiltrated Al–Mg alloy/SiCp composites*, Corrosion Science 51 (6) (2009) 1392–1398.
- [15] H. M. Zakaria, *Microstructural and corrosion behavior of Al/SiC metal matrix composites*, Ain Shams Engineering Journal, 5 (3) (2014) 831–838.
- [16] Y. H. Yoo, D. P. Le, J. G. Kim, S. K. Kim, P. V. Vinh, *Corrosion behavior of TiN, TiAlN, TiAlSiN thin films deposited on tool steel in the 3.5 wt.% NaCl solution*, Thin Solid Films 516 (11) (2008) 3544–3548.

- [17] M. Ishikawa, H. Enomoto, M. Matsuoka, C. Iwakura, *Effect of tetraborate ions on electrodeposition of nickel-copper alloy from a pyrophosphate bath*, *Electrochimica Acta* 39 (14) (1994) 2153–2157.
- [18] G. Qiao, T. Jing, N. Wang, Y. Gao, X. Zhao, J. Zhou, W. Wang, *Effect of current density on microstructure and properties of bulk nanocrystalline Ni–Co alloys prepared by JED*, *Journal of The Electrochemical Society*, 153 (5) (2006) C305–C308.
- [19] C. U. Atuanya, D. I. Ekweghiariri, *Experimental correlation between varying processing properties and wear behaviour of ternary Ni-Co-SiO₂ composites coating of mild steel*, *The International Journal of Advanced Manufacturing Technology*, 88 (9–12) (2017) 2581–2588.
- [20] B. C. Oberländer, E. Lugscheider, *Comparison of properties of coatings produced by laser cladding and conventional methods*, *Materials Science and Technology* 8 (8) (1992) 657–665.
- [21] S. Islak, S. Buytoz, *Microstructure properties of HVOF-sprayed NiCrBSi/WCCo-based composite coatings on AISI 1040 steel*, *Optoelectronics and Advanced Materials–Rapid Communications* 7 (11–12) (2013) 900–903.
- [22] D. A. Stewart, P. H. Shipway, D. G. McCartney, (1999). *Abrasive wear behaviour of conventional and nanocomposite HVOF-sprayed WC-Co coatings*, *Wear* 225-229 (2) 789–798.
- [23] C. Lupi, A. Dell'Era, M. Pasquali, P. Imperatori, *Composition, morphology, structural aspects and electrochemical properties of Ni–Co alloy coatings*, *Surface and Coatings Technology* 205 (23–24) (2011) 5394–5399.
- [24] L. Wang, Y. Gao, Q. Xue, H. Liu, T. Xu, *Microstructure and tribological properties of electrodeposited Ni–Co alloy deposits*, *Applied Surface Science* 242 (3–4) (2005) 326–332.
- [25] R. Sruthi, G. S. Rampradheep, K. Raja, *A review on natural plant extract as a green inhibitor for steel corrosion resistance*. *International Journal of Advanced Science and Technology* 29 (3) (2020) 3529–3550.



Changes in Plant Nutrient Concentration of Olive (*Olea europaea* L.) Leaves after Different Rates of Humic Acid Application

Sertaç Uyanık¹ , Ali Sümer² 

^{1,2}Department of Soil Science and Plant Nutrition, Faculty of Agriculture, Çanakkale Onsekiz Mart University, Çanakkale, Türkiye

Article History

Received: 7 Jul 2023

Accepted: 9 Oct 2023

Published: 15 Mar 2024

Research Article

Abstract – This research was a one-year study to investigate how increasing rates of humic acid affect the nutrient elements [Nitrogen (N), phosphorus (P), potassium (K), calcium (Ca), magnesium (Mg), iron (Fe), manganese (Mn), zinc (Zn) and copper (Cu)] of olive trees (*Olea europaea*) of 14 years old found in a private cultivation land located in Bozköy of Geyikli, Çanakkale (Latitude 35 S 431667, Longitude 4409876) in 2018. The humic acid used was a suspension of 15% humic and fulvic acid, which was a commercial product (Blackjak SC, pH 4-6). Different concentrations of humic acid [0 (control), 50, 100, 200, 400 mL tree⁻¹] were applied directly to soil of 20-30 cm depth under canopy projection of trees after dissolving in 10 L of water in April. A randomized block design with four replicates and five doses was adopted on 20 trees. 200 leaf samples were taken in December from annual shoot tips as reciprocal leaf couples and nutrient element analyses were carried out. The macronutrient elements N and P significantly increased upon all humic acid applications. However, the changes in the elements K, Ca, Mg, Fe, Zn, and Mn were insignificant in all applications. Humic acid at all concentrations decreased copper in leaves. As a result, addition to routine farmer fertilization, humic acid application at the rate of 50 ml tree⁻¹ was determined to be the sufficient dose for olive trees. Moreover, this mentioned dose is considered to be the most economical dose besides being the most suitable one.

Keywords – Çanakkale-Geyikli, humic acid, leaf concentration, olive, plant nutrient elements

1. Introduction

The Olive tree has been the symbol of peace. Olive production is very important for the economy of the region in Türkiye. The history of olive tree, which is one of the earliest plants cultivated, goes back to 6000 years ago [1]. Olive is one of the shrub species of *Olea* genus belonging to the Oleaceae family. It is the only species with edible fruit [2]. *Olea europaea* has been switched to cultivar *Sativa* through cutting first time in history in 4000 BC in Türkiye which is among the Mediterranean countries [3].

Mediterranean countries meet around 90% of the world's olive needs. There are about 900 million olive trees on 90 million hectares on the planet. The number of trees increases day by day with the establishment of new orchards in other countries with an available climate. The most effective countries for olive production are Spain (38.6%), Italy (14.4%), Greece (9.8%), Türkiye (8.2%), and other Mediterranean countries [4]. The leading cities for olive production are İzmir, Aydın, Çanakkale, Bursa, Balıkesir, Muğla, and Gaziantep. Regionally, the Aegean region is the leading one, followed by the Mediterranean, Marmara, and Southeastern Anatolia. Apart from these regions, olive is cultivated in Blacksea region where Mediterranean climate prevails [3].

Olive cultivation has been preserved as the leading sector besides tourism in Geyikli region of Çanakkale

¹sertacuyanik017@gmail.com; ²sumer@comu.edu.tr (Corresponding Author)

province. Olive cultivation is not only a commercial activity, but also a hereditary culture ongoing for centuries. The demand for olive and olive oil is increasing in Türkiye. Chemical fertilizers have been used unconsciously to increase the yield per unit area. This study will be helpful in terms of informing the producers of the region where olive is intensely produced about the effects of humic acid application on increase of soil organic matter (OM) and yield and quality of olive plants. Humic acid, which is an OM itself, is known to enhance the efficiency of current plant nutrient elements in soil. Moreover, it increases the permeability of cell membrane and hence eases the uptake of plant nutrient elements [5]. Enhancement of durability of plants against disease and pests under stress conditions, ventilation of soil and its water retention, and development of microorganisms in soil can be achieved by humic acid applications. Thanks to humic acid, uptake of elements such as iron (Fe), zinc (Zn), phosphorus (P), nitrogen (N), and potassium (K) gets easier, accumulation of salt in soil is inhibited, and positive effects on ventilation of soil and enhancement of the structure of heavily loam soils can be observed. An increase in yield forming elements facilitates the uptake of micronutrient elements, especially Zn, which can be achieved with humic acid in many plants such as wheat [6,7]. This research aimed to investigate the effects of different rates of humic acid application on the nutrition elements of olive leaves.

2. Materials and Methods

The plant materials in this study were Ayvalık oil-type 14 years old olive trees planted in intervals of 7x7 m located in Bozköy, Geyikli region of Çanakkale Province (39° 50' 13" N, 26° 12' 4" E). Humic acid of a commercial brand (Blackjak SC, pH 4-6) was applied to the soil of olive trees. A single-year application of humic acid was carried out in 2018 to investigate the effect of humic acid on the nutrient element contents of olive leaves. Soil samples were taken in February from a depth of 0-30 cm from the crown projection of the trees representing the experimental area. Before the humic acid application, 0.5 kg tree⁻¹ potassium sulphate (K₂SO₄), 0.5 kg tree⁻¹ monoammonium phosphate (MAP) in November and 1 kg tree⁻¹ ammonium sulphate [(NH₄)₂SO₄] in April were routinely applied to all trees. The trial was conducted according to randomized block design with 4 replicates. Humic acid of rates 0 (control), 50, 100, 200, 400 mL tree⁻¹ were applied to 20-30 cm depth under the tree crown projection by diluting in 10 L of water in April.

From each tree used in the trial, 200 leaves were obtained according to [8]. Sampling of couple of leaves from the annual shoots was carried out from all four sides of the trees. Samples leaves were dried at 65 °C for 48 hours, and after that, they were grinded. The dried leaves were extracted with dry decomposition method and from the annual shoots and elements were detected with ICP-OES (Inductively Coupled Plasma-Optical Emission Spectrometer, Perkin Elmer OPTIMA-5300 DV) device [9].

Variance analysis was carried out on the data according to randomized block design model [10]. Significance analysis was carried out according to *F* test using JMP statistical package program, and means were compared by Duncan multiple comparison test ($\alpha < 0.05$).

3. Results and Discussion

3.1. Soil Analysis Results

The analysis results of the soil of the experimental area are given in Table 1. The soil texture has been classified as “sandy clay loam” according to the physical analysis data. The soil has the characteristics of general soil texture of Aegean Region [11]. Olive trees can grow in a wide pH range; therefore, the soil of the region has a suitable pH range [12]. There is no saltiness problem when the soil of the trial area’s total salt limit values

was evaluated according to [13]. The lime content was intermediate according to [14]. The soil was insufficient in terms of OM according to [15]. Extractable P concentration was low according to [14]. According to [16], K concentration was sufficient, Ca was sufficient and Mg element was low.

The extractable Fe of the soil was sufficient according to [17]. Extractable Cu content was detected to be sufficient according to [18]. Extractable Mn was sufficient and extractable Zn was low according to [16].

Table 1. Chemical and physical analysis values of the soil of the study area

Soil Texture			EC (%)	CaCO ₃ (%)	OM (%)	pH
Sand (%)	Silt (%)	Clay (%)				
64	7	29	0.06	8.05	0.69	7.51
Sandy Clay Loam			Non-saline	Calcareous	Very low	Slightly-Alkaline
Macro Element Content						
N (g kg ⁻¹)	P (mg kg ⁻¹)	K (mg kg ⁻¹)		Ca (mg kg ⁻¹)	Mg (mg kg ⁻¹)	
0.30	5.62	180.71		3637.53	59.87	
Low	Low	Sufficient		Sufficient	Low	
Micro Element Content						
Fe (mg kg ⁻¹)		Mn (mg kg ⁻¹)		Zn (mg kg ⁻¹)	Cu (mg kg ⁻¹)	
7.12		8.49		0.12	1.35	
Sufficient		Sufficient		Low	Sufficient	

3.2. Effect of Humic Acid on N Concentration

Compared to the control trial (13.52 g kg⁻¹) the N concentration in olive leaves was detected to be 17.83, 17.8, 18.33 and 17.68 g kg⁻¹ with increasing rates of humic acid (Figure 1). All the humic acid applications significantly increased the leaf N concentrations compared to the control ($P < 0.001$), and these increases were as follows: 31.87%, 31.95%, 35.57%, and 30.76%, respectively (Figure 1).

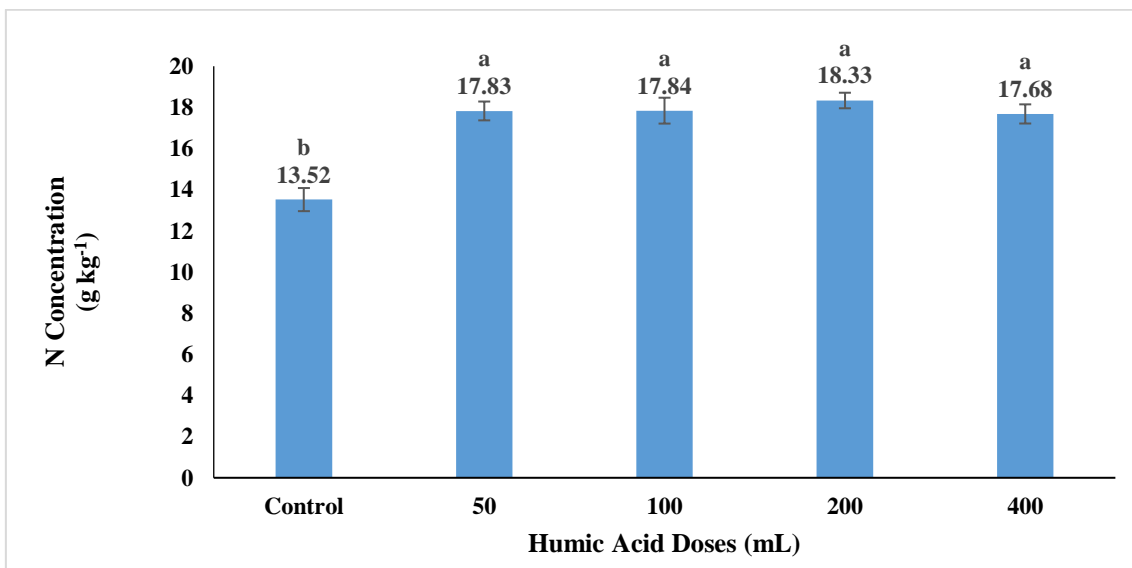


Figure 1. The effect of humic acid applied to the soil at increasing rates on leaf N concentration

N is an important element for olives. N is required the most at the flowering stage and the need continues till the hardening of the seed. Fertilizer applications make N reach a sufficient level and this will affect shoot development, fruit amount and yield parameters [8]. The results of our study were obtained from other studies, too. Sözüdoğru et al. [19] researched the effects of humic acid applied to the soil on the nutrient element concentrations in beans. As a result, the concentrations of N and P were found to increase. Eryüce [8] reported the N concentration of olive leaves in the Ayvalık region to be 1.10-1.87%, which shows that our results are compatible with the literature. The study by Reuter and Robinson [20] reported the optimum leaf N

concentration in olive trees to be between 1.5-2%. Ali [21] reported the same value which is also 1.54%. Figure 1 showed that the leaf N concentration of the control plants remained below the optimum limit values, but with the addition of humic acid, it was within the range of the optimum values according to [20,21].

3.3. Effect of Humic Acid on Leaf P Concentration

When compared to the control (0.90 g kg^{-1}), the P concentration in olive leaves was detected to be 1.40, 1.46, 1.27, and 1.24 g kg^{-1} upon increasing rates of humic acid applications, respectively. All the humic acid applications increased the leaf P concentrations significantly ($P < 0.001$), and the increases were as follows: 56.17%, 62.18%, 41.6%, and 37.49%, respectively (Figure 2). The study by Reuter and Robinson [20] reported the optimum leaf P concentration in olive trees to be between 0.1- 0.3%. Figure 2 showed that the leaf P concentration of the control plants remained below the optimum limit values, but with the addition of humic acid, it was within the range of the optimum values according to [20].

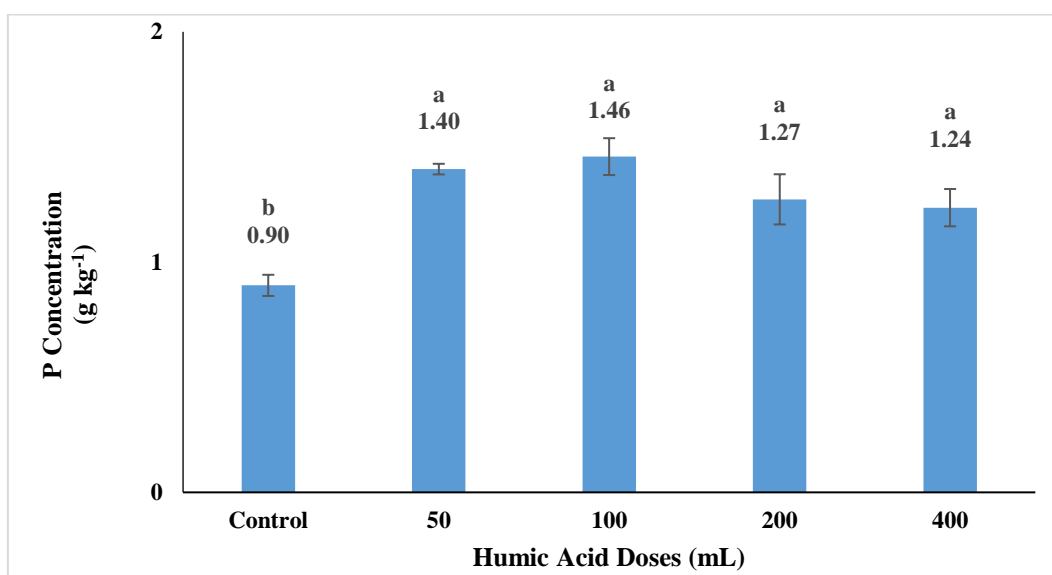


Figure 2. The effect of humic acid applied to the soil at increasing rates on leaf P concentration

Phosphorus plays an important role in formation of flowers, fruit setting and hence in decreasing the periodicity effect in olive plants [22]. Although the level of P in soil was not sufficient (Table 1), the concentration of P significantly increased with the application of humic acid, even in the first year of this study (Figure 2).

Similar results to the results of our study were detected by other researchers. Wang et al. [23] reported that when humic acid was applied to the soil together with P, P fixation was inhibited, and available P concentration was increased and also product yield increased together with the increased uptake of P by plant. Moreno et al. [5] reported that OM in soil formed compounds with Ca in soil and thus increased available P in soil, which increased plant nutrient content. In another study, Adak [24] investigated the effect of different ratios of vermicompost on nutrient elements of tomato and pepper. They reported that increasing rates of vermicompost positively affected the leaf P concentrations of pepper plants.

3.4. Effect of Humic Acid on Leaf K Concentration

Compared to the control (11.49 g kg^{-1}) the K concentrations of olive leaves were 12.26, 12.49, 12.38, and 11.39 g kg^{-1} upon increasing doses of humic acid (Figure 3). When the changes were analyzed, 50, 100, and 200 mL tree^{-1} humic acid applications increased leaf K concentrations by 6.7%, 8.62%, and 7.73% compared to the control; however, the highest humic acid dose of 400 mL tree^{-1} caused a negative change of 0.94%, but

this change was not statistically significant (Figure 3). As seen in Table 1, the sufficient level of K in trial soil might have been the reason for a non-significant change in leaf K levels.

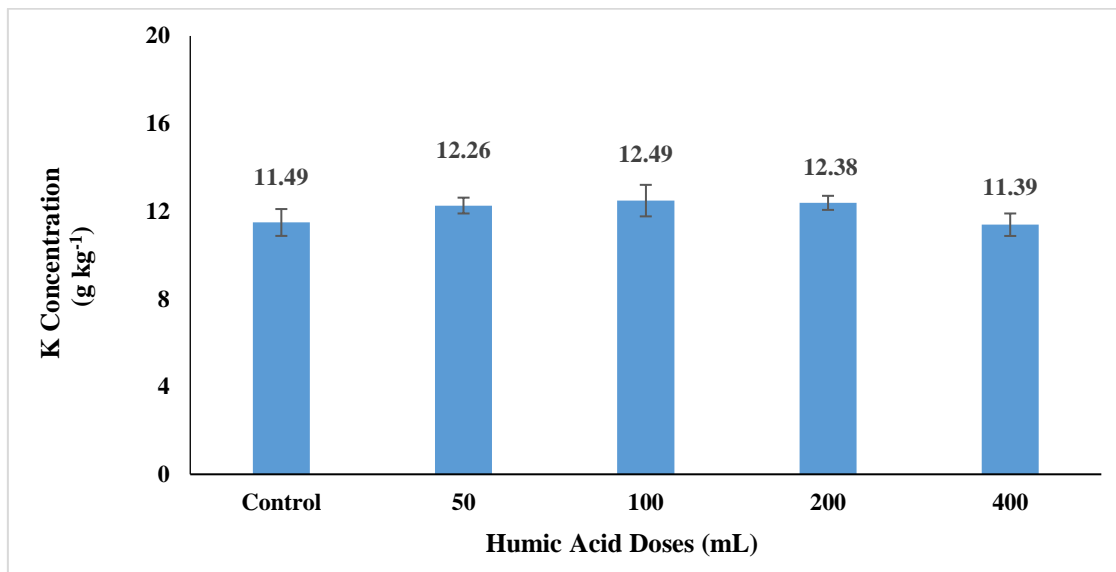


Figure 3. The effect of humic acid applied to the soil at increasing rates on leaf K concentration

Potassium is a very important nutrient element in olive cultivation. Fruit length, number of fruits, and fruit meat-seed ratio are directly related to the K nutrition. Moreover, deficiency of K increases the sensitivity of the plant to heat changes and negatively affects the product quality [25].

Similar results were reported by other researchers. Müftüoğlu and Alak [26] investigated the effects of humic acid applied to the soil in increasing doses on plant length, shoot diameter, and total K in the root and shoot of Helen-type maize plant. As the applied humic acid concentration increased, the K amount uptake by plant increased but the increase was not statistically significant. Turan et al. [27] investigated the humic acid applied on leaves on maize development and plant nutrient element content under salty conditions. The results showed an increase in plant K yet were non-significant. In another study, Çelik et al. [28] applied humic acid on the leaves under salty and limy conditions and investigated the uptake of nutrient elements by the plant. Results revealed an increase in K uptake, but it was again statistically non-significant.

Doran et al. [29], in their study with Halhalı-type olive, reported that the olive leaf K concentration was between 1.2-1.5%. The study of Reuter and Robinson [20] reported that the optimum K concentrations in olive trees were > 0.8%. Ali [21] reported a similar value as 0.87%. The leaf K concentrations in our study were between 1.13-1.24% which were similar with the findings of [20,21].

3.5. Effect of Humic Acid on Leaf Ca Concentration

Compared to the control (19.60 g kg⁻¹), the Ca concentrations in olive leaves were 19.79, 19.13, 19.34, and 18.13 g kg⁻¹ upon increasing rates of humic acid doses (Figure 4). The Ca concentration increased by 0.93% upon 50 mL tree⁻¹ application. On the other hand, 100, 200 and 400 mL tree⁻¹ humic acid applications decreased the Ca concentration of leaves, and the decreases were 2.4%, 1.32% and 7.5%, respectively, and they were not statistically significant (Figure 4). The trial soil Ca content was sufficient as seen in Table 1 which might have resulted in no change in the Ca concentrations of leaves. Similar results were obtained by other researchers. Sözüdoğru et al. [19] applied different doses of humic acid to the soil of bean plants and investigated the nutrient elements and reported that humic acid was not effective in the uptake of Ca.

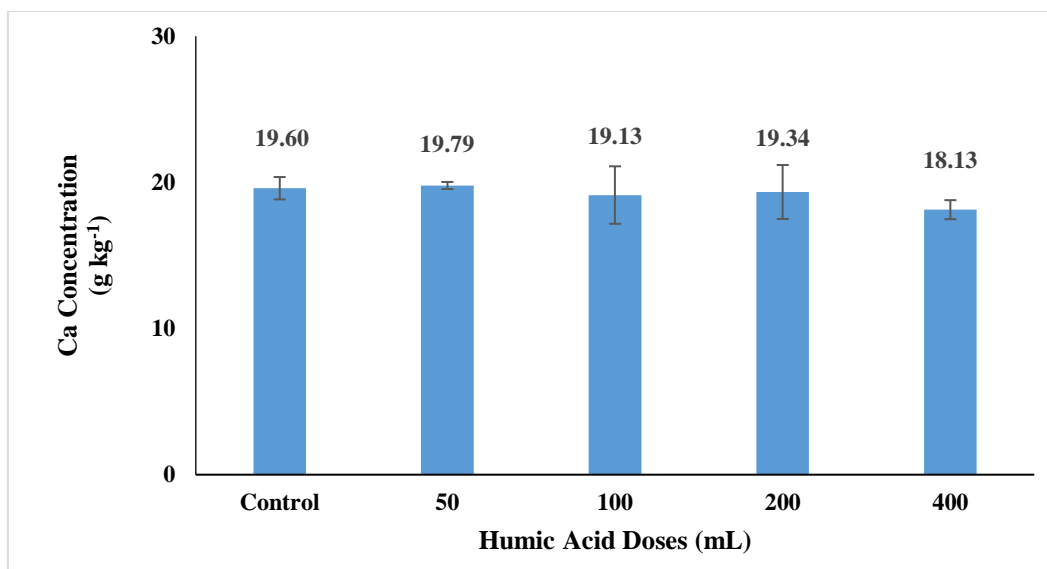


Figure 4. The effect of humic acid applied to the soil at increasing rates on leaf Ca concentration

Demir et al. [30] investigated the effect of different organic fertilizers and NPK fertilizers on nutrient element concentrations of tomato fruit and found that Ca concentration was not statistically different than the control. Eryüce [8] researched Ayvalık-type of olive and found that Ca concentration can change between 0.88-2.14%. Soyergin [31] reported that Ca concentration was between 1.26-2.94% in Gemlik-type olive. Seferoğlu [32] conducted a study on two different regions and found that leaf Ca concentrations were 1.10-1.80% in Ayvalık region, while 1.00-1.20% in Edremit region. The study of Reuter and Robinson [20] reported the optimum Ca concentrations of olive trees as >1.0 . Ali [21] reported a similar value as 1.48%. In our study, leaf Ca concentrations were found to be between 1.81-1.97%, which were compatible with results from [20,33].

3.6. Effect of Humic Acid on Leaf Mg Concentration

Compared to the control condition (1.52 g kg^{-1}), the Mg concentrations in olive leaves were 60, 1.68, 1.65, and 1.56 g kg^{-1} upon application of increasing rates of humic acid (Figure 5). The applications of 50, 100, 200 and 400 mL tree^{-1} humic acid increased the leaf Mg concentrations, and the changes were 33%, 10.86%, 8.82%, and 2.76%, respectively. However, the changes were not statistically significant (Figure 5). Similar results were reported by other researchers. Demirtaş et al. [34] used different doses of municipal waste compost for greenhouse cultivation of tomatoes. Compared to the control, they found that increase in Mg concentrations was not statistically significant. Demir et al. [30] investigated how different organic fertilizers and NPK fertilizers affected tomatoes, and again the increase in Mg concentrations was not found to be statistically significant. Eryüce [8] studied Ayvalık-type olive and reported that leaf Mg concentrations were between 0.12-0.37%. Püskülcü [35] found that leaf Mg concentrations of Memecik-type olive were changing between 0.22-0.34%. Soyergin [31] reported leaf Mg concentrations of Gemlik-type olive to be 0.12-0.37%. Seferoğlu [32] also worked on Ayvalık-type olive and reported the Mg concentrations changing between 0.15-0.31%. In our study, the Mg concentrations were between 0.15-0.16%, and inside limit values according to [20,33]. The trial soil Mg was low (Table 1). The Mg concentration tended to increase with humic acid applications, and it is expected that with humic acid applications, the effects will be more visible in the upcoming years.

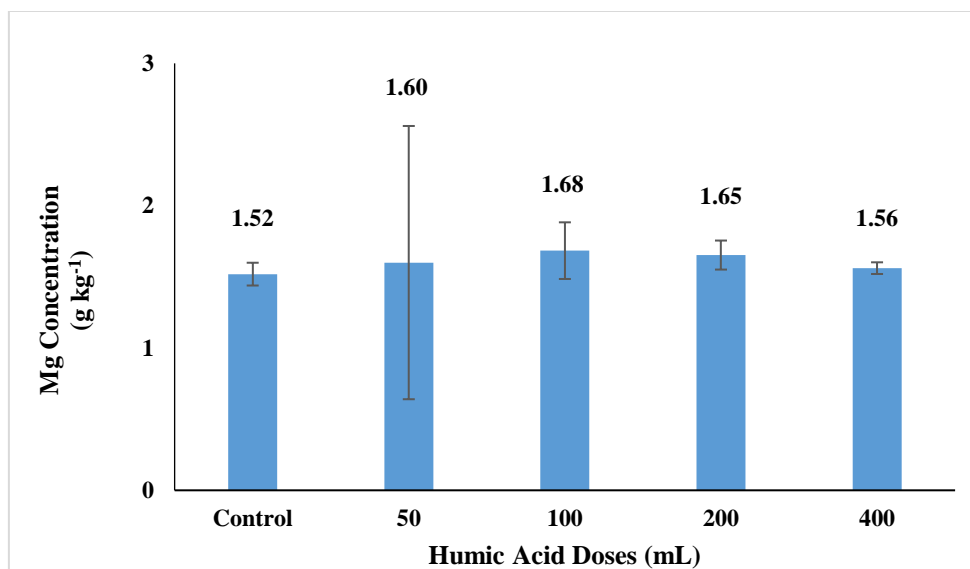


Figure 5. The effect of humic acid applied to the soil at increasing rates on leaf Mg concentration

3.7. Effect of Humic Acid on Leaf Fe Concentration

When compared to the control (111.85 mg kg⁻¹) the Fe concentrations in the leaves of olive trees were 103.87, 103.85, 103.25, and 94.55 mg kg⁻¹ upon increasing doses of humic acid applications (Figure 6). In the order of the applied humic acid (50, 100, 200, and 400 mL tree⁻¹) the decrease of Fe concentrations were as follows: 7.13%, 7.15%, 7.68%, and 15.46%, and they were not statistically significant (Figure 6).

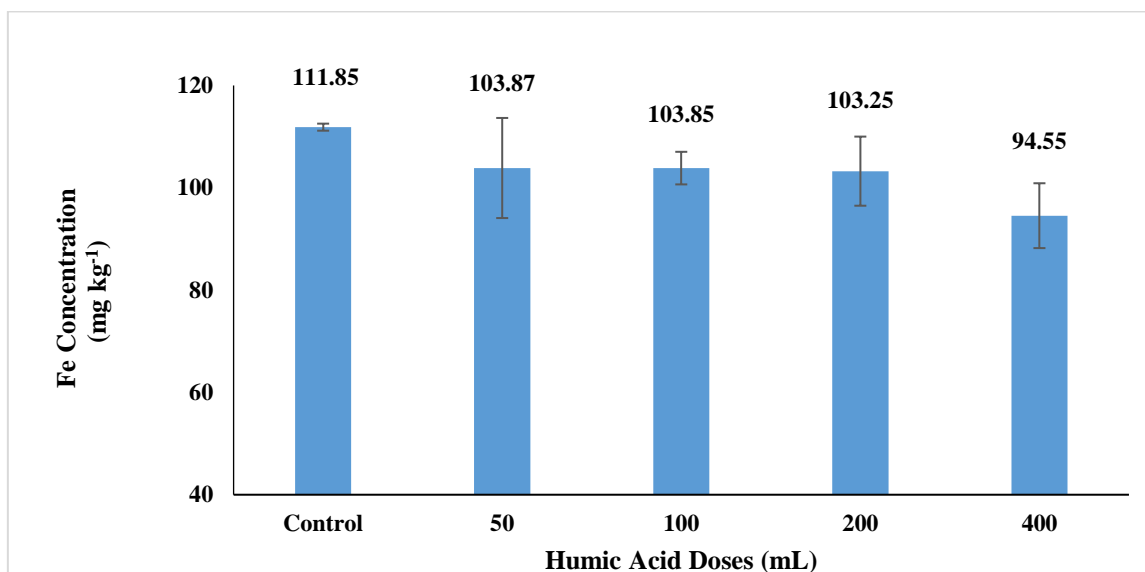


Figure 6. The effect of humic acid applied to the soil at increasing rates on leaf Fe concentration

Demir et al. [30] could not report a change in Fe concentrations upon applications of different organic fertilizers and NPK fertilizers. Humic acid of low pH (pH 4-6) applied to the soil was expected to increase the Fe availability, however, there was no significant change. On the contrary, there was a decrease in Fe concentration as seen in Figure 6. Seferoğlu [32] found the Fe concentrations in Ayvalık-type olive in Ayvalık region to be between 55-115 mg kg⁻¹, and between 60-140 mg kg⁻¹ in Edremit region. Soyergin et al. [36] reported the Fe concentration of Gemlik-type olive to be 88-280 mg kg⁻¹. In our study, the Fe concentrations were between 94.55-111.85 mg kg⁻¹, and they were compatible with the literatures. The detected Fe concentrations were inside the limit values according to [20,33].

3.8. Effect of Humic Acid on Leaf Mn Concentration

Compared to the control (45.44 mg kg⁻¹) the Mn concentrations of olive leaves upon increasing rates of humic acid applications were found to be 51.60, 52.43, 52.53, and 50.29 mg kg⁻¹ (Figure 7). All the applications increased the Mn concentrations compared to the control at 13.55%, 15.37%, 15.6%, and 10.68% in the order of humic acid concentrations respectively, however, the results were not statistically significant (Figure 7).

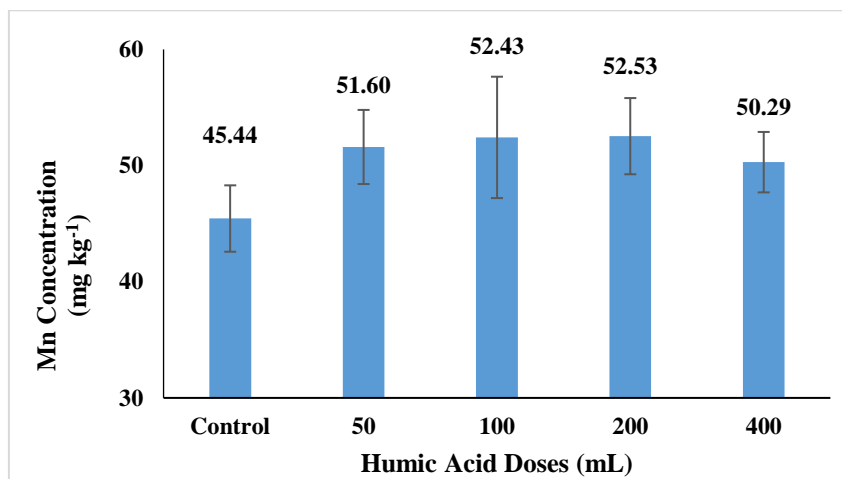


Figure 7. The effect of humic acid applied to the soil at increasing rates on leaf Mn concentration

Similar results were observed by different researchers. Demir et al. [30] investigated the effects of different organic materials and NPK fertilizers on tomatoes and found that their effect on Mn concentration was not significant. Demirtaş et al. [37] investigated the effects of plant-based liquid organic fertilization of tomatoes and found that its effect on Mn concentration was not statistically significant. Şahin [38] found the Mn concentrations in leaves of olives of organic cultivation to be 49.75-61.33 mg kg⁻¹. In our study, the Mn concentrations were found to be 45.44-52.53 mg kg⁻¹ which are inside the limit values according to [20,21,33].

3.9. Effect of Humic Acid on Leaf Zn Concentration

Compared to the control (15.79 mg kg⁻¹) the results of applying increasing doses of humic acid were 16.36, 18.01, 17.24, and 15.32 mg kg⁻¹ Zn in leaves of olive (Figure 8). Compared to the control, 50, 100, and 200 mL tree⁻¹ humic acid increased the Zn concentration in leaves by 3.6%, 14.05%, and 9.18%, respectively; however, 400 mL tree⁻¹ humic acid decreased Zn as 2.97%. these changes were not found to be statistically significant (Figure 8).

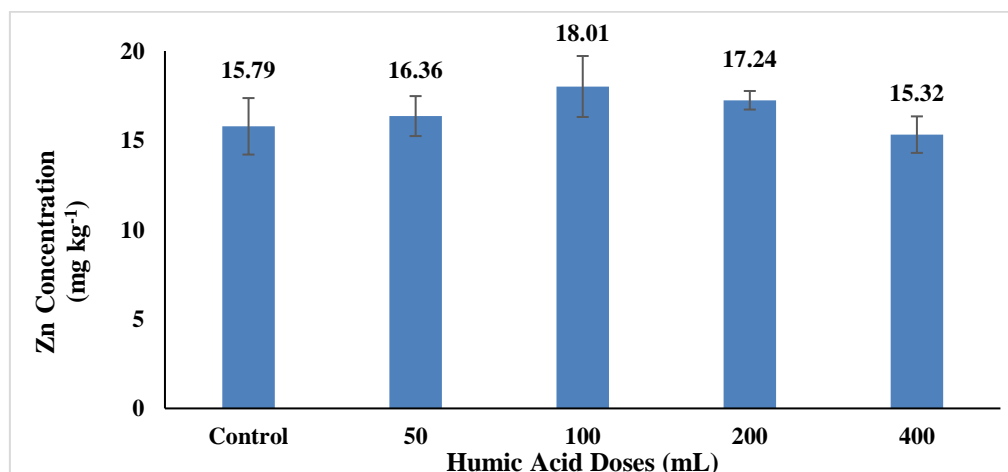


Figure 8. The effect of humic acid applied to the soil at increasing rates on leaf Zn concentration

Similar results were obtained by other researchers. Demir et al. [30] found that different organic materials and NPK fertilizers did not significantly affect the Zn concentration tomato compared to the control condition. Demirtaş et al. [37] investigated the effects of plant-based liquid fertilizer on plant nutrient elements in the tomato plant. Similarly, they did not find a statistically significant change in Zn concentrations. Tokay and Yaşar [39] reported that Zn levels significantly play an important role in olive fruit development.

Şahin [38] conducted a study on organic olive cultivation and found that the Zn concentrations as 16.78-132.81 mg kg⁻¹. Our study reported the Zn concentrations as 15.32-18.01 mg kg⁻¹ which are inside the limit values according to [20,33].

3.10. Effect of Humic Acid on Leaf Cu Concentration

Compared to the control condition (37.16 mg kg⁻¹) the Cu concentrations in olive leaves were 14.69, 17.50, 22.05, and 13.39 mg kg⁻¹ upon increasing doses of humic acid applications (Figure 9). The Cu contents significantly decreased in the left upon applications of all the humic acid doses, and these changes were as follows compared to the control: 60.48%, 52.92%, 40.67%, and 63.98% (Figure 9). Sözüdoğru et al. [19] investigated the effects of humic acid on nutrient elements of plants and found that humic acid did not affect Cu uptake, which was in contrast to our study. Şahin [38] reported the Cu contents to be 17.40-25.54 mg kg⁻¹ in the study conducted on organic cultivation olive gardens. The results of our study revealed that leaf Cu values were between 15.39-37.16 mg kg⁻¹ being inside the limit value according to [20,21,33].

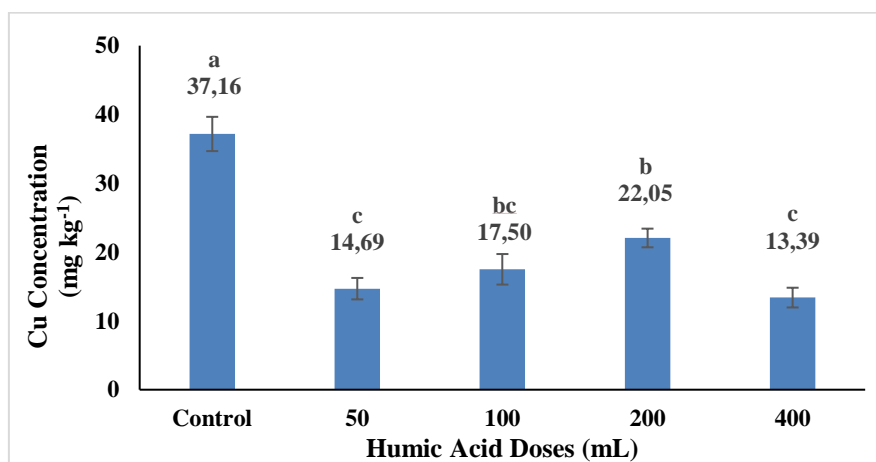


Figure 9. The effect of humic acid applied to the soil at increasing rates on leaf Cu concentration

4. Conclusion

This experiment was carried out on Ayvalık oil-type olive trees of age 14 in Bozköy located in Geyikli region of the city Çanakkale in field conditions for the year according to randomized block design. Increasing rates of humic acid increased the N and P nutrient elements, and decreased Cu concentration, while the concentrations of Ca, K, Mg, Fe, Mn, and Zn did not change. The concentrations of all the nutrient elements stayed inside the suggested limit values. Humic acid application is an important contributor to the increase of OM in soil. Although a decrease in Cu values and an increase in Fe values were observed, both elements were inside the acceptable leaf limit values. However, these micronutrient elements should be applied to the soil or leaves in case these values decrease over time. In this study, olive leaf N and P concentrations in routine farmer fertilization remain below the limit value, and with the addition of humic acid, they are within the optimum limit values. The findings of the current study show that humic acid application at the rate of 50 ml tree⁻¹ is sufficient for olive tree nutrition. Moreover, this dose is economically proper for the farmers. Since the olive

tree is perennial with a deep root structure, continuous humic acid applications are thought to be positive in terms of macro and micronutrient elements for the plant. The deficiency of N and P concentrations in the soil of Türkiye can be eliminated by the addition of humic acid. Our study is a two-year study, and the results will be shared to inform the producers of the region.

Author Contributions

Both authors devised the main conceptual ideas and developed the theoretical framework. The second author conceived and designed the analysis and wrote the article. The second author also performed the experiment and necessary analyses under the supervision of the first author. All authors read and approved the final version of the paper. This paper is derived from the first author's master's thesis supervised by the first author.

Conflicts of Interest

All the authors declare no conflict of interest.

Acknowledgement

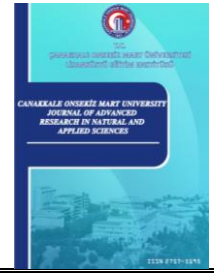
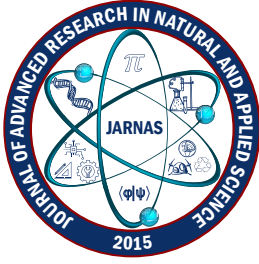
We would like to thank Dr. İrfan Uyanık for allocating the land for the realization of this study.

References



- [1] N. Kaleci, M. A. Gündoğdu, E. Doğan, O. Nergis, *Bazı yabancı kökenli zeytin çeşitlerinin olgunlaşma süresince pomolojik ve bazı biyokimyasal özelliklerindeki değişimlerin incelenmesi*, *Zeytin Bilimi* 6 (2) (2016) 119-124.
- [2] S. Lavee, *Aims, methods, and advances in breeding of new olive (*olea euroaea* L.) cultivars*, in: L. Rallo, J. M. Caballero, R. Fernández-Escobar (Eds.), *ISHS Acta Horticulturae 286 International Symposium on Olive Growing*, Cordoba, 1990, pp. 23–36.
- [3] A. Ünsal, *The Immortal Tree - Olives and Olive Oil in Türkiye* (in Turkish), 7th Edition, Yapı Kredi Yayınları, İstanbul, 2008.
- [4] G. Yıldırım, *Nutritional status of olive plantations in Camarasi village in Aydin-Karacasu*, Master's Thesis Ege University (2019) İzmir.
- [5] E. C. Moreno, W.L. Lindsay, G. Osborn, *Reactions of dicalcium phosphate dihydrate in soils*, *Soil Science* 90 (1) (1960) 58–68.
- [6] M. Kaya, M. Atak, C. Y. Çiftçi, S. Ünver, *Effects of Zinc and Humic Acid Applications on Yield and Some Yield Components of Bread Wheat (*Triticum aestivum* L.)*, *Süleyman Demirel University Journal of Natural and Applied Sciences* 9 (3) (2005) 8 pages.
- [7] A. Turhan, B. B. Aşık, H. Kuşçu, *The influence of irrigation water salinity and humic acid on nutrient contents of onion (*Allium cepa* L.)*, *Journal of Agricultural Sciences* 26 (2) (2020) 147–153.
- [8] N. Eryüce, *Ayvalık bölgesi yağlık zeytin çeşidi yapraklarında bazı besin elementlerinde bir vegetasyon periyodu içindeki değişimler*, *Ege Journal of Agricultural Research* 17 (2) (1980) 209–221.
- [9] N. M. Müftüoğlu, C. Türkmen, Y. Çıkılı, *Toprak ve bitkide verimlilik analizleri* (in Turkish), 2nd Edition, Nobel Yayın Dağıtım, Ankara, 2014.
- [10] M. Mendeş, *Uygulamalı bilimler için istatistik ve araştırma yöntemleri*, Kriter Yayınevi, İstanbul, 2012.

- [11] I. Atalay, *Red Mediterranean soils in some karstic regions of Taurus mountains Turkey*, Catena 28 (3-4) (1997) 247–260.
- [12] R. Gucci, E. Lodolini, H.F. Rapoport, *Productivity of olive trees with different water status and crop load*, Journal of Horticultural Science & Biotechnology 82 (4) (2007) 648–656.
- [13] E. V. Maas, *Salt tolerance of plants*, in: B. R. Christie (Ed.), CRC Handbook of Plant Science in Agriculture, Vol. 2 of CRC Series in Agriculture, CRC Press, Boca Raton, 2019, pp. 57-76.
- [14] A. N. Ülgen, N. Yurtsever, *Türkiye gübre ve gübreleme rehberi*, Tarım Orman ve Köyişleri Bakanlığı Toprak ve Gübre Araştırma Enstitüsü Müdürlüğü, Ankara, 1995.
- [15] H. W. Smith, M. D. Weldon, *A comparison of some methods for the determination of soil organic matter*, Soil Science Society American Proceeding 5 (C) (1941) 177–182.
- [16] M. Sillanpää, *Micronutrient assessment at the country level: An international study*, FAO, Rome, 1990.
- [17] W. L. Lindsay, W. L. Norvell, *Development of a DTPA soil test zinc, iron, manganese and copper*, Soil Science Society of America Journal 42 (30) (1978) 421–428.
- [18] W. L. Lindsay, W. A. Norvell, *Development of a DTPA soil test for zinc, iron, manganese, and copper*, Soil Science Society of America Journal 42 (3) (1978) 421-428.
- [19] S. Sözüdoğru, A. C Kütük, R. Yalçın, S. Usta, *Humik asidin fasulye bitkisinin gelişimi ve besin maddeleri alımı üzerine etkisi*, Ankara Üniversitesi Ziraat Fakültesi Bilimsel Araştırma ve İncelemeler (1996) 1–25.
- [20] D. Reuter, J. B. Robinson, *Plant analysis: An interpretation manual*, CSIRO publishing, Melbourne, 1997
- [21] M. A. Ali, *Establishment of nutrient sufficiency ranges in olive using boundary-line approach*, Journal of Plant Nutrition 46 (3) (2023) 453–461.
- [22] N. S. Mordoğan, Ş. Ceylan, *Effect of organic fertilization on yield and micro element content of olive trees growing in sandy soil texture*, Ege Journal of Agricultural Research, 54 (4) (2017) 413–419.
- [23] X. J. Wang, Z. Q. Wang, S. G. Li, *The effect of humic acids on the availability of phosphorus fertilisers in alkaline soils*, Soil Use and Management 11 (2) (1995) 99–102.
- [24] Ş. E. Adak, *The effect of vermicompost on growth and nutrient element content of tomatoes and peppers*, Master's Thesis Namık Kemal University (2016) Tekirdağ.
- [25] N. Özbek, *Meyve ağaçlarının gübrenmesi*, Tarım ve Orman Bakanlığı Yayınları, Ankara, 1981.
- [26] N. M. Müftüoğlu, H. C. Alak, *Effect of Humic Acid Applications on Available Potassium*, COMU Journal of Agriculture Faculty 2 (2) (2014) 61–66.
- [27] M. A. Turan, B. B. Aşık, H. Çelik, A. V. Katkat, *Effect of foliar applied humic acid on growth and some nutrient elements uptake of maize plant under salinity conditions*, Sakarya University Journal of Science 14 (1) (2012) 529–539.
- [28] H. Çelik, B. B. Aşık, M. A. Turan, A. V. Katkat, *Effects of foliar applied humic acid on growth and some nutrient uptake of maize under saline and calcareous soil conditions*, Sakarya University Journal of Science 14 (1) (2012) 549–561.
- [29] G. Doran, Y.K. Koca, B. Pekkolay, M. Mungan, *The nutrient status of the olive trees grown in Derik province*, Mediterranean Agricultural Sciences 21 (1) (2008) 131–138.
- [30] H. Demir, A. Topuz, M. Gölcüklü, E. Polat, F. Özdemir, H. Şahin, *The effect of different organic fertilizers on the mineral contents of tomato grown in organic farming*, Mediterranean Agricultural Sciences 16 (1) (2003) 19–25.

- [31] S. Soyergin, *Studies on nutrient contents and seasonal element fluctuations of the olive variety gemlik in Bursa area*, Doctoral Dissertation Uludağ University (1993) Bursa.
- [32] S. Seferoğlu, *Relationship between fertility status and some of quality aspects of "Ayvalık" c.v. olive orchards grown in Ayvalık and Edremit regions*, Doctoral Dissertation Ege University (1997) İzmir.
- [33] G. Haspolat, *Effects of foliar applications of the fertilizers chelated with KNO_3 , $ZnSO_4$, and $MgSO_4$ biologically and plastic mulching on vegetative growth and fruit yield in gemlik olive variety*, Master's Thesis Çukurova University (2006) Adana.
- [34] E. I. Demirtaş, F. Öktüren, A. N. Arı, *Örtüaltı domates yetiştiriciliğinde kentsel katı atık kompostu kullanımının bakiye etkilerinin belirlenmesi*. Süleyman Demirel Üniversitesi Ziraat Fakültesi Dergisi 8 (2) (2013) 23-35.
- [35] G. Püskülcü, *Memecik zeytin çeşidinde makro ve mikro besin elementlerinin mevsimsel değişimlerinin incelenmesi*, Master's Thesis Ege University (1981) İzmir.
- [36] S. Soyergin, I. Moltay, C. Genç, A. E. Fidan, A. R. Sutçu, *Nutrient status of olives grown in the marmara region*. IV International Symposium on Olive Growing, ISHS Acta Horticulturae 586 (2012) 375-379.
- [37] E. I. Demirtaş, F. Asri, C. F. Özkan, N. Arı, *Effects of organic and chemical fertilizer on plant nutritional status and soil fertility of tomatoes grown under greenhouse condition*, Batı Akdeniz Tarımsal Araştırma Enstitüsü Derim Dergisi 29 (1) (2012) 9-22.
- [38] G. Şahin, *The effects of different doses of fertilizers in organic olive growing on soil paramaters, contents of plant nutrients and oil quality*, Master's Thesis Adnan Menderes University (2013) Aydın.
- [39] F. Tokay, S. B. Yaşar, *Topraktaki hümik asit miktarına bağlı olarak zeytin toprağı, zeytin yaprağı ve zeytinin meyvesinde çinko miktarının değişimi*, in: M. Demir (Ed.), I. Ulusal Zeytin Öğrenci Kongresi, Edremit-Balıkesir, 2008, pp. 219-223.



Single Laboratory Validation of Four Methods for Quantification of HMF in Honey

Elif Yıldız¹ , Abdullah Tahir Bayrac² 

¹Institute of Immunology and Immunotherapy, University of Birmingham, Birmingham, United Kingdom

^{1,2}Department of Bioengineering, Faculty of Engineering, Karamanoğlu Mehmetbey University, Karaman, Türkiye

Article History

Received: 10 Aug 2023

Accepted: 23 Oct 2023

Published: 15 Mar 2024

Research Article

Abstract – Hydroxymethylfurfural or 5-(hydroxymethyl)-2-furaldehyde (HMF) has been absent or found in honey naturally at very low amount. It is formed in honey mainly by heating process and improper storage conditions. HMF has been reported to have cytotoxic, carcinogenic, and mutagenic effects and thus regulatory agencies in many countries impose restrictions on its maximum levels in honey. Validated methods have been required for effective and specific detection and quantification of HMF in food samples. In this study, a single laboratory validation study was conducted on four quantification methods: direct spectral analysis, High Performance Liquid Chromatography (HPLC) analysis, Seliwanoff and Winkler methods. All methods showed linearity with the lowest R^2 value of 0.992. Two method performance parameters, accuracy, and precision were satisfied by each four methods with recovery values at 98.2%, 100.2%, 102.5% and 103.3% and RSD_r (relative standard deviation) % values at 6.97%, 6.19%, 2.87% and 0.90% for spectral analysis, Seliwanoff, HPLC and Winkler methods, respectively. Based on the measurement uncertainties of four quantification methods, honey samples spiked with HMF at the final concentration of 0.004mg/0.1g were reported as 0.004 mg/0.1g \pm 0.00025 mg/0.1g by spectral analysis, 0.0036 mg/0.1g \pm 0.000691 mg/0.1g by Seliwanoff method, 0.004 mg/0.1g \pm 0.00045 mg/0.1g by HPLC and 0.0039 mg/0.1g \pm 0.00022 mg/0.1g by Winkler methods ($k=2$, confidence level of 95%). The validated methods can quantify HMF in honey with a target concentration of 0.004 mg/0.1g, specifically and accurately.

Keywords – HMF, honey, method validation, Seliwanoff, uncertainty

1. Introduction

An organic compound, 5-(hydroxymethyl)-2-furaldehyde (HMF), is a water soluble furanic compound produced by the dehydration reaction of sugar molecules, especially fructose and sucrose under acidic conditions. It is formed in sugar containing foods by a non-enzymatic browning reaction or dehydration of hexoses as a result of heating or improper and longer storage [1,2]. Since it is not found in fresh and untreated foods, the presence of HMF in food indicates excessive heat-treatment, spoilage, and possible adulteration of food products with other sugars or syrups. Fresh honey generally does not contain HMF while its concentration increases during heating process or storage [3]. Thus, the presence of HMF in honey is an indicative of honey quality. Previous studies have indicated the negative effects of HMF in humans and animals [4-7]. It has been reported that administration of HMF at certain concentrations lead to skin lesions or tumors in rats [8-10]. Lee et al. [11] presented the mutagenicity of HMF via sulfonation of its allylic hydroxyl functional group in rat. Monien et al. [12] showed the hepatocarcinogenic activity of HMF due to its reaction with DNA. Due to these cytotoxic, carcinogenic, and mutagenic effects of HMF, Codex Alimentarius Alinorm 01/25 [13] establish a

¹elifhane7@gmail.com; ²bayrac@kmu.edu.tr (Corresponding Author)

maximum HMF content as 80mg/kg in honey. European Union Council Directive 2001/110/EC [14] also set the limit of 40 mg/kg HMF in honey (80 mg/kg of HMF for honey produced in tropical regions). According to the Turkish Food Codex Honey Communique 2020/7 [15], the maximum amount of HMF in honey is 40 mg/kg while originating from tropical regions is 80 mg/kg. Since HMF is a quality marker indicating improper storage, heating treatment or other adulterations in honey, quantitative analysis methods have been playing an important role for ensuring food safety. There have been different methods proposed for the quantification of HMF in literature [16-21]; however, according to the International Honey Commission (IHC) [22] and High Performance Liquid Chromatography (HPLC) [23], Winkler [24] and White [25] methods have been applicable for HMF determination in honey. HPLC methods have been validated [26] thus far and also comparative studies have been conducted with Winkler and White methods [27] to provide reliable and accurate results.

In this study, two new spectral methods were used for the quantification of HMF in honey in addition to HPLC and Winkler methods approved by IHC. Direct use of spectrophotometer at 284 nm (without any reactive reagents) provided an easy way for determination of HMF without any interference present in honey. Another spectral method, Seliwanoff method, depended on the measurement of the absorbance of colored products formed from the reaction between resorcinol and HMF. Winkler method, Seliwanoff method, direct spectral measurement and HPLC analysis were compared based on validation parameters. Their responses to honey samples spiked with HMF and honey samples after thermal process were evaluated. These four methods were validated by a single laboratory validation study and all method performance parameters were found in the range of acceptable limits. Moreover, measurement uncertainties were calculated for all methods at the maximum acceptable limit of HMF allowed for honey. Thus far, this is the first study that compares the performances of four different methods for determination of HMF in honey.

2. Materials and Methods

2.1. Reaction Reagents and Solutions

The chemicals used in this study (HMF (analytical standard, $\geq 98.0\%$), furfural ($\geq 98.0\%$), resorcinol (99.0%), *p*-toluidine (99.0%), barbituric acid (99.0%), fructose ($\geq 98.0\%$), galactose ($\geq 98.0\%$), sucrose ($\geq 98.0\%$), glucose ($\geq 98.0\%$), HCl, acetic acid ($\geq 99.0\%$), 2-propanol ($\geq 99.0\%$), and methanol (HPLC grade, $\geq 99.0\%$) were purchased from Sigma-Aldrich (St Louis, MO, USA).

HMF stock solution was prepared by dissolving 0.01 g of HMF in 1 mL of distilled water. HMF intermediate standard solutions were prepared by diluting HMF stock solution with distilled water to have final concentration of 0.001mg/g, 0.002mg/g, 0.003mg/g, 0.004mg/g, 0.005mg/g and 0.006mg/g. Both stock and intermediate standard solutions were kept at 4°C and in dark till use. Fructose solutions at 0.57 mg/mL, 5.7 mg/mL and 57 mg/mL concentrations were prepared separately in 0.1%, 0.5% and 1.0% HCl solution and heated at 80°C for 4, 7, 9, 11, and 13 min. After heat treatment, fructose solutions were measured by UV-Vis spectrophotometer (Shimadzu UV-1800, Kyoto, Japan) at 284 nm. The yield (Y_{HMF}) of dehydration reaction was calculated by (2.1). Galactose, glucose, and sucrose were used as negative control in selectivity analysis.

$$Y_{\text{HMF}}(\%) = \frac{\text{moles of HMF produced}}{\text{moles of initial fructose}} \times 100 \quad (2.1)$$

Seliwanoff test reagent for HMF detection, resorcinol, was prepared in 15% HCl solution to have final concentration of 5 mg/mL. Winkler test reagent, *p*-toluidine, was prepared in acetic acid (1 g/mL) and diluted to 100 mL with 2-propanol. Barbituric acid solution at 0.5% was used for sample solution. The reagent

solutions were kept in the dark till use.

2.2. Samples

Honey samples used in this study were taken from local markets in Turkey. They were made from flower nectar and had a Brix^o value of 75. Honey samples were prepared by suspending 2.0 g of honey in 10 mL of water. For quantification of HMF, honey samples were spiked with known amount of HMF (0.001 mg/g, 0.002 mg/g, 0.003 mg/g, 0.004 mg/g, 0.005 mg/g and 0.006 mg/g) and analyzed by four methods. The honey samples without addition of HMF were used as negative controls. Moreover, honey samples were heated at 50°C, 70°C and 90°C for 10, 30, 60, 90, 120, 720 and 1440 min and further analyzed by four methods to quantify HMF in heat-treated samples.

2.3. Methods

2.3.1. Spectral Analysis

HMF intermediate standard solutions at concentrations of 0.001 mg/g, 0.002 mg/g, 0.003 mg/g, 0.004 mg/g, 0.005 mg/g and 0.006 mg/g were analyzed by UV-Vis spectrophotometer (Shimadzu UV-1800, Kyoto, Japan) at 284 nm. All analysis was performed in triplicate and absorbance values of all standard solutions were given in mean \pm standard deviations. Based on data, spectral calibration curve was constructed, and the equation of spectral calibration curve was used in further quantification experiments of HMF.

2.3.2. HPLC Analysis

HMF intermediate standard solutions and dehydration products at concentrations of 0.001 mg/g, 0.002 mg/g, 0.003 mg/g, 0.004 mg/g, 0.005 mg/g and 0.006 mg/g were analyzed by HPLC (Agilent 1260 Infinity, Agilent Technologies, USA) configured with 1260 Infinity II Quaternary pump, standard autosampler and degasser using a method proposed by Elmastaş et al. [28]. C18 column (250 mm x 4.6 mm, 5 μ m particles) was used with DAD detector for quantification of HMF at 285 nm. Samples were injected through the column at the flow rate of 1.0 mL/min at 25°C with mobile phase of methanol: water (10:90, v:v). Honey samples were homogenized in water and filtered through a 0.45 μ m filter before HPLC analysis. Each sample was analyzed in triplicate.

2.3.3. Winkler Method

Winkler method is another spectrophotometric method used for HMF analysis in honey samples. The determination of HMF by Winkler protocols depends on the measurement of absorbance values of test samples and reference solutions at 550 nm [24]. For test samples, 500 μ L of both standard HMF and dehydration products were mixed separately with 500 μ L of *p*-toluidine solution and 100 μ L of barbituric acid solution, while, for reference samples, 100 μ L of water was added instead of barbituric acid to *p*-toluidine: sample (1:1) mixture. The absorbance of sample solutions was measured against reference solutions at 550 nm. The calibration curves were constructed both for standard HMF solutions and dehydration products. For both spiked and heated honey samples, 10 g of each sample was suspended in 20 mL of water and then the same procedure explained above was applied. The amount of HMF in honey samples were obtained from the equation of calibration curve.

2.3.4. Seliwanoff Method

The third spectrophotometric method for determination of HMF was based on Seliwanoff analysis. The reaction parameters were optimized by evaluating the effects of resorcinol concentration and heating time. The resorcinol solution at final concentrations of 2.5 mg/mL, 3.75 mg/mL and 5 mg/mL were mixed with dehydration products (1:1 volume ratio) and heated at 100°C separately for 3 and 5 min. The absorbance of heated solutions was measured at 520 nm. At optimum conditions previously determined (2.5 mg/mL resorcinol solution and 5 min-heating), different concentrations of HMF intermediate standard solutions and dehydration products were tested by this assay and calibration curves were constructed based on their absorbance values at 520 nm against HMF concentrations. The optimized Seliwanoff method was assayed on honey samples spiked with HMF at different concentrations and heated honey samples for the quantification of HMF in samples. Basically, 500 µL of honey samples homogenized in water was added to the equal volume of resorcinol solution and heated at 100°C for 5 min. The absorbance at 520 nm was recorded for each sample. HMF in spiked and heated honey samples were quantified by regression equations of calibration curves.

2.4. Method Validation

Single laboratory validation of four methods for the quantification of HMF in honey was performed according to the International Organization for Standardization (ISO) 5725-2 [29]. Method validation parameters (selectivity, linearity, LOD, LOQ, precision and accuracy) were evaluated for all four methods.

The selectivity of methods to HMF was evaluated by testing other sugar samples at optimum conditions of each method. Galactose, sucrose, fructose, and glucose solutions at concentration of 0.004mg/g were analyzed spectrophotometrically at 284 nm, at 550 nm with *p*-toluidine and barbituric acid, at 520 nm with resorcinol reagent, and at 285 nm by chromatographic method. The calibration curves obtained by plotting absorbance of samples at 284nm, 520 nm and 550 nm and peak areas of samples at 285 nm against HMF concentrations gave information about the linearity of these methods. The equations described by $y = ax + b$ were evaluated in the concentration range in the study and R^2 values indicated the sensitivity of the measurements. LOD and LOQ values of all four methods were calculated based on the standard deviations of blank samples. LOD was represented as three times the standard deviation of blank whereas LOQ was represented as ten times the standard deviation of blank. The repeatability was the measure of the precision of four methods in this study. The HMF solution at the concentration of 0.004 mg/0.1g was prepared as three replicates and analyzed by four methods in triplicate. The standard deviation (S_r) and relative standard deviation (RSD_r) were calculated based on the response of four methods. The accepted precision limit was the repeatability value lower than 20% in this study. The accuracy referred as the closeness of results to the true value was evaluated by recovery parameter. The HMF solution at the concentration of 0.004 mg/0.1g was prepared as three replicates and analyzed by four methods in triplicate. The percentage recovery (%) was calculated for each sample analyzed by each method. The accepted accuracy limit was the recovery values of 70-120% for all methods.

2.5. Measurement Uncertainty

All validation data was used for the calculation of measurement uncertainty of four methods. The uncertainties from calibration curve (U_{calib}), repeatability (U_{RSr}) and accuracy (U_{Rec}) were selected as main sources of uncertainty in these methods and their equations were given below (2.2-2.5).

$$U_{calib} = \frac{s}{b_1} \sqrt{\left(\left(\frac{1}{p} \right) + \left(\frac{1}{m} \right) + \left(\frac{(c_0 - c')^2}{s_{xx}} \right) \right)} \quad (2.2)$$

$$U(RSD)_r = \sqrt{\frac{RSD^2}{n}} \quad (2.3)$$

$$U(Rec) = Rec \sqrt{\left(\frac{s_{obs}^2}{n \times c_{obs}^2} \right)} \quad (2.4)$$

$$U = \sqrt{U_{calib}^2 + U_{Rec}^2 + U_{RSD_r}^2} \quad (2.5)$$

where s represented the standard deviation of residuals of calibration curve; b_1 represented the slope of the calibration curve; p was the number of measurements; m was the number of standards used for calibration curve; c_0 was calculated concentration from calibration curve; c' was the mean of concentrations of standard; n was the number of repetitions in repeatability calculations; Rec was recovery value and U was the combined uncertainty. The uncertainty results were given for four methods as extended uncertainty by multiplying the combined uncertainty with coverage factor, k ($k = 2$, for a confidence level of 95%).

3. Results and Discussion

In this study, the four methods for HMF quantification were validated by single laboratory validation study and all method performance parameters and measurement uncertainties were evaluated for all methods [30].

3.1. Fructose Dehydration to HMF

HMF, a cyclic aldehyde, is formed in honey at lower pH by the degradation of reducing sugar through the Maillard reaction as a result of heat treatment or long storage of honey. The presence of HMF or the increase in its amount due to heating or improper storage is used as an indicator of honey quality [1,3,31]. The HMF formation in honey depends on certain factors such as temperature, pH [32], moisture content [33], water activity and mineral content of honey [25], however, the main factor affecting the rate of HMF formation is the ratio of fructose to glucose [34,35]. Due to lower reactivity of glucose at lower pH and its slower enolization which is the rate-limiting step for 5-HMF formation, the dehydration of fructose yields more HMF than glucose [31]. Therefore, fructose solutions prepared in 0.1%, 0.5%, and 1.0% HCL solution at different initial concentrations were used for HMF formation after heating at 80°C. Based on higher yield (Y_{HMF}) of dehydration reaction, the optimum conditions for HMF production from fructose was set as 57 mg/mL of initial fructose in 0.5% HCL solution. HMF formed in solution was used as a sample in method validation studies together with standard HMF solutions in subsequent experiments. This solution was used to represent a heat-treated or long-term stored honey sample to test the four methods for the determination of HMF.

3.2. Spectral Analysis

The spectral analysis of HMF was performed by a UV-Vis spectrophotometer at 284 nm. Both standard HMF solutions and HMF solutions formed via fructose dehydration were used for the construction of calibration curves (Figure 1A & B). The calibration curve of standard HMF solutions gave the equation of $y = 139.4x - 0.133$ ($R^2 = 0.993$) (Figure 1A) which was found to follow Beer's law in the concentrations range of 0.001-1 mg/L. Turner et al. [36] stated that the molecular absorption coefficient of HMF was calculated as 16.830 liters mole⁻¹ cm⁻¹ (or 16.830 M⁻¹ cm⁻¹). When converted to a coefficient based on molecular weight, it became 133.57 L g⁻¹ cm⁻¹. In another study, direct spectrophotometric method was used for the determination

of HMF, and it was reported that the molar absorption coefficient was $16070 \text{ M}^{-1} \text{ cm}^{-1}$ at 284 nm [37]. If converted into a coefficient based on molecular weight it was found as $127.54 \text{ L g}^{-1} \text{ cm}^{-1}$. The slope of the calibration curve in this study was 139.4 and the extinction coefficient converted to gram of HMF was close to other values described previously in literature so that calibration curve constructed with the use of standard HMF solution at 284 nm was applicable for the quantification of HMF.

HMF solutions formed by the dehydration of fructose (57 mg/mL in 0.5% HCL at 80°C) contained HMF at the concentration of 0.002, 0.003, 0.004, 0.005 and 0.006 mg/0,1g after heating for 4, 7, 9, 11 and 13 min, respectively. The calibration curve generated by plotting the concentration of HMF versus their absorbance at 284nm was an equation of $y = 149.2x - 0.207$ ($R^2 = 0.992$) (Figure 1B). According to “Harmonized Methods of the International Honey Commission” [38], the theoretical factor based on molar extinction coefficient was 149.7 to quantify HMF in honey spectrophotometrically. When compared with the slope of the calibration curve constructed by fructose dehydration’s products, it was observed that they were not significantly different from each other. Based on these results, it was concluded that these two calibration curves can be used for direct spectral determination of HMF in aqueous solution and honey.

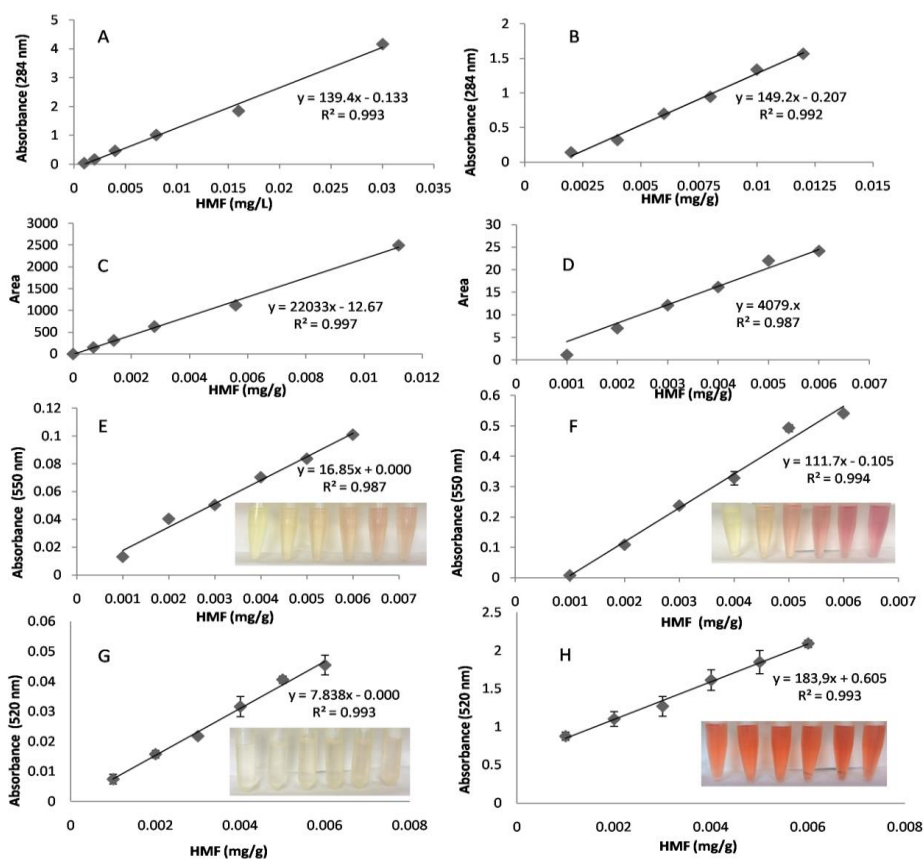


Figure 1. Correlations between HMF concentration and method response obtained by A& B) direct spectrophotometer; C&D) HPLC; E&F) Winkler method and G&H) Seliwanoff method in standard HMF solutions and fructose dehydrated products (n=3) (inlet images were digital images of products formed by reaction between HMF and Winkler/Seliwanoff reactive)

3.3. HPLC Analysis

Generally, analytical method has been preferred for HMF quantification due to its higher sensitivity and the lack of toxic compounds like *p*-toluidine used in Winkler method. Moreover, it was found that the presence of interferences in honey affected the accuracy of spectrophotometric methods [23,27,39]. Therefore, the

accuracy and sensitivity of spectral methods used in this study was compared with the results from HPLC analysis. The chromatographic determination was carried out with both standard HMF solutions and HMF solutions produced via fructose dehydration. As shown in Figure 1C and D, the calibration curves constructed with standard solutions and dehydration products in the range of 0.001-0.006 mg/0.1g gave the standard equations of $y = 22033x - 12.67$ ($R^2=0.997$) and $y = 4079x$ ($R^2=0.987$), respectively.

3.4. Winkler Method

Winkler method is one of the methods recommended by the International Honey Commission for the quantification of HMF [22]. The method principle depends on the formation of colored product after reaction between HMF, barbituric acid and *p*-toluidine and quantitative determination by measuring its absorbance at 550 nm [24]. Although Winkler method is not preferred because of the use of carcinogen *p*-toluidine, it provides advantages in terms of analysis cost and time as compared to HPLC method [40].

In this study, in order to determine the concentration of HMF in honey, two calibration curves were constructed by plotting the absorbance values of reaction products at 550 nm versus the concentration of standard HMF solutions or HMF in dehydrated fructose solutions. As shown in Figure 1E and F, the equations of calibration were $y = 16.58x + 0.0001$ ($R^2=0.987$) and $y = 111.7x - 0.105$ ($R^2=0.994$) and the slopes of the equation represented the extinction coefficients of colored products under the experimental conditions in this study. According to R^2 values, the calibration curve obtained from fructose dehydration products more accurately represented the experimental responses. Since it better represented the honey sample than standard HMF solutions, it was concluded that the calibration curve constructed by dehydration products could be used for HMF analysis in honey samples by Winkler method.

In addition to absorbance measurement, visual analysis of colored products formed in the presence of toluidine and barbituric acid was performed. The formation of red color was more obvious in dehydration products with increasing HMF content (inlet image in Figure 1E) than standard HMF solutions (inlet image in Figure 1F). As seen in digital images of red colored products and their intensities, Winkler reaction gave more clear result dehydration products with increasing HMF content.

3.5. Seliwanoff Method

The last method tested for HMF quantification in this study was Seliwanoff method. The principle of Seliwanoff method is the condensation reaction of HMF produced by three dehydration reactions between monosaccharide and resorcinol to produce a colored product, xanthenoid. Since ketoses give Seliwanoff reaction faster than aldoses, this test is mainly used for the discrimination of aldoses and ketoses. Under acidic conditions fructose is dehydrated and this dehydrated product reacts with resorcinol in a condensation reaction to give a cheery red colored product. In this study, therefore, the quantification of HMF was performed both by spectrophotometric measurements and color analysis of colored reaction product.

Before construction of calibration curves and testing real samples, resorcinol concentration and heating time were optimized with HMF solutions produced via fructose dehydration. Reaction solutions containing 0.001, 0.002, 0.003, 0.004, 0.005 and 0.006 mg/0.1g of dehydrated products and resorcinol solutions at 2.5 mg/mL, 3.75 mg/mL and 5 mg/mL were heated for 3 min and, the absorbance values of colored products were in the range of 0.1-0.25 (Figure S1A). With the increases in HMF concentration, the absorbances of colored product increased for all concentrations of resorcinol. As seen from graph and observed from the color intensities of HMF solutions at 0.004 mg/0.1g (inlet image in Figure S1A), the resorcinol solution at 5 mg/mL gave highest

absorbance value with more intense pinkish color. When heating was applied for 5 min, absorbance values increased to approximately five times the 3-minute reaction results and color intensities of reaction products became more intense (Figure S1B). Seliwanoff reaction between HMF solutions and 2.5 mg/mL of resorcinol gave higher absorbance values with higher slope as compared with other resorcinol solutions. As a result, optimum parameters for Seliwanoff method were determined as 2.5 mg/mL and 5 min for resorcinol concentration and heating time, respectively.

For HMF quantification, calibration curves for both standard HMF solutions and HMF solutions produced via fructose dehydration were constructed following optimization studies. As seen in Figure 1G and 1H, linear relationships between HMF concentration and absorbance value of colored reaction product were represented by regression equation of $y = 7.838x + 0.0001$ ($R^2=0.993$) and $183.9x + 0.605$ ($R^2=0.993$) after reaction with standard HMF solutions and dehydrated product, respectively. When standard HMF solutions were analyzed by Seliwanoff test, the absorbance values of each HMF concentration were considerably below than the values of corresponding solutions having fructose dehydration products. In addition, the correlation coefficient of ≥ 0.99 indicated relatively strong relationship between HMF concentrations in dehydrated products and absorbance values, thus, it was concluded that the calibration curve of dehydrated products can be used for spectral determination of HMF in honey by Seliwanoff method. Beside absorbance values, digital images of both standard samples and dehydrated products (inlet image in Figure 1G and 1H, respectively) were revealed the accuracy of use of the calibration curve of dehydrated products for HMF quantification. The clear red color formation was observed by fructose dehydrated products after reaction with Seliwanoff reagent.

3.6. Method Validation and Measurement Uncertainty

As a healthy sweetener, honey, contains fructose and glucose as main sugars and other mono-, di-, tri-, oligo- and polysaccharides [41,42] and sum of fructose, glucose and sucrose content is both quality and ripeness parameter of honey [14]. Therefore, the specificity of these four instrumental methods was evaluated with testing fructose, glucose, sucrose, and galactose under same test conditions as used for HMF.

Specificity of HPLC method is evaluated by the peak regions of interferences [44]. In this study, retention time was estimated at 9.31 min for the chromatogram of HMF standard solution. The peaks of interferences (glucose, fructose, and sucrose) were not observed in the region of HMF peak (data not shown). Moreover, the absence of interference peaks at the resolution lower than 1.5 times of peak of HMF supported the specificity of HPLC method for separation of HMF than other sugars [44-46]. Direct spectral analysis of HMF and possible interferences showed the specificity of the method by giving significantly different absorbance value for HMF than other analytes (Figure 2A). The specificity analysis of Winkler method (Figure 2B) indicated that significantly higher absorbance value was obtained for HMF as compared to the values of other sugars. The reagents of Winkler reaction formed a red colored product only if there was HMF in the solution; otherwise, the color remained similar as the initial color of reagents. In Winkler method, the possible reaction mechanisms are explained by the opening of furan ring in sugar such as HMF and fructose and forming a product with barbituric acid and p-toluidine that can absorb light in visible region [47]. Therefore, it is expected for fructose and HMF derived from furan to react with Winkler method's reactive. In this study, Winkler method was found highly specific for HMF detection and quantification under specified reaction conditions. As mentioned, the basic principle of Seliwanoff Test is the reaction between ketose dehydrated in the presence of acidic solution and resorcinol to form xanthenoid with pink color. Thus, it is expected that fructose and sucrose give positive results while galactose and glucose require more reaction time to give positive results. As shown in Figure 2C, the Seliwanoff reaction gave positive result only for HMF solution under optimized

condition. The red colored product was generated by the reaction between HMF and resorcinol reactive. Therefore, it could be concluded that with resorcinol amount and reaction time optimized in this study, Seliwanoff method was highly specific for HMF detection and quantification.

The validation of four methods for HMF analysis used in this study was carried out by determining LOD, LOQ, accuracy (recovery) and precision (repeatability) parameters and measurement uncertainties of methods based on EURACHEM Guide and ISO standard [48]. Table 1 summarized the method performance parameters at maximum limit of HMF determined by codex and uncertainty budgets of four methods. According to the Codex Alimentarius Commission Manual [49], it has been reported that the acceptable recovery values for 10 mg/kg and 100 mg/kg of analytes are in the range of 80 to 110% and 90 to 107%, respectively. Although the lowest recovery in sample with the content of 0.004mg/0.1g HMF was observed with direct spectral analysis (98%), all four methods met the acceptable criteria for the recovery.

The Codex Alimentarius Commission Manual [49] has also given the precision requirements based on Horwitz equation ($2 * C^{-0.1505}$). At mass fraction of 10 mg/kg, the calculated $RSDr$ % value is $RSDr \% \leq 22$, while it is $RSDr \% \leq 16$ for mass fraction of 100 mg/kg. In this study, $RSDr$ % values were found as 6.97%, 6.19%, 2.87% and 0.90% for spectral analysis, Seliwanoff, HPLC and Winkler methods, respectively. Therefore, it was concluded that all four methods satisfied the precision requirements at the HMF concentration of 0.004mg/0.1g. When LOD and LOQ values were compared, it was shown that the analytical method had lowest LOD and LOQ values as expected. The highest values of LOD and LOQ were 0.0004 mg/0.1 g and 0.0013 mg/0.1 g for Winkler method.

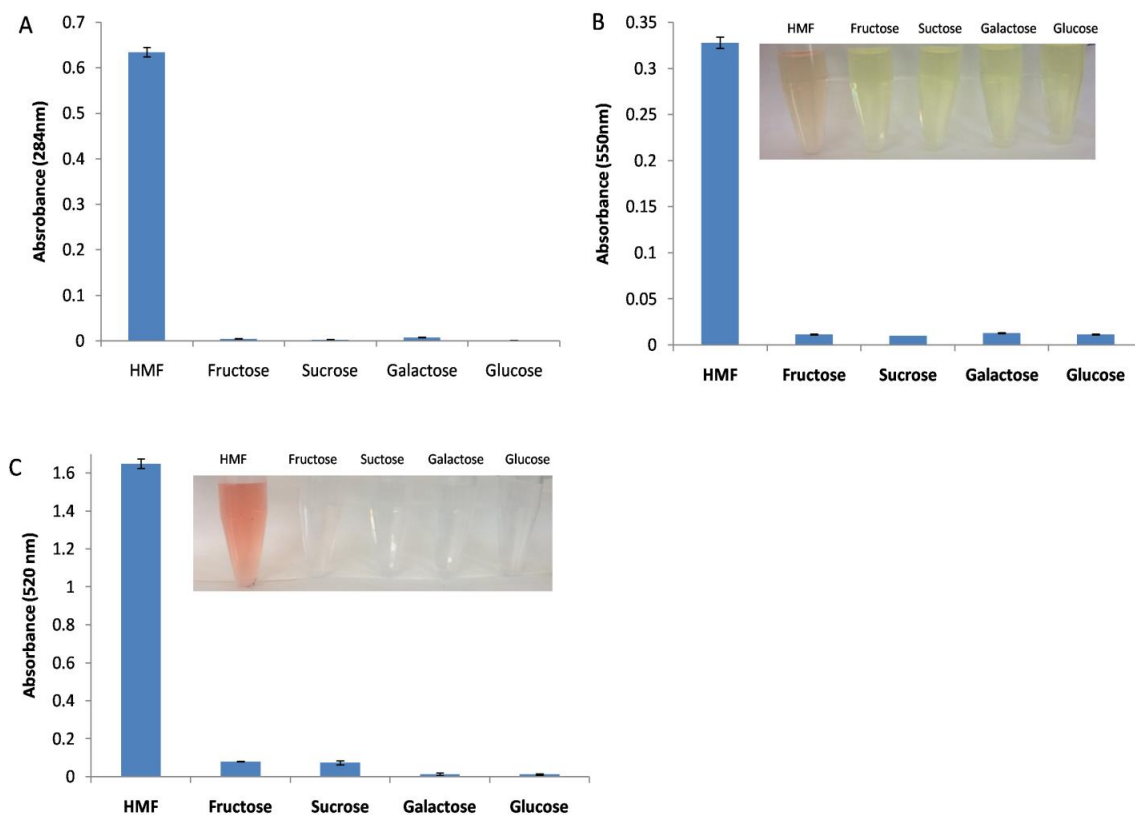


Figure 2. Specificity analysis of spectral methods for HMF; A) Direct measurement of interferences (fructose, sucrose, galactose, and glucose) by spectrophotometer at 284 nm, B) measurement by Winkler method at 550 nm, C) measurement by Seliwanoff method at 520 nm (inlet images were digital images of products formed by reaction between analytes and Winkler/Seliwanoff reactive) (n=3)

Table 1. Method performance criteria and uncertainty budgets of four methods used for the HMF determination in honey

Methods	Recovery (%)	Relative Standard deviations of repeatability (<i>RSDr</i> , %)	LOD (mg/0.1g)	LOQ (mg/0.1g)	Uncertainty of calibration curve	Uncertainty of repeatability	Uncertainty of recovery	Expanded uncertainty ^{**} , <i>U</i>
Spectral Analysis	98.2	6.97	0.0011	0.0035	0.01249	0.02793	0.02845	0.00025
HPLC Analysis	102.5	2.87	0.0004	0.0013	0.04768	0.01171	0.16971	0.00045
Winkler Method	103.3	0.90	0.0012	0.0038	0.02803	0.00369	0.00381	0.00022
Seliwanoff Method	100.2	6.19	0.0007	0.0023	0.07868	0.02525	0.02531	0.00069

^{*}Data represented the means of three measurements. P-values less than 0.5 were considered statistically significant.

^{**}with coverage factor of 2, confidence level of 95%.

Three main components contributing to uncertainty budgets were determined as uncertainty of calibration curve, recovery, and repeatability for these methods. Measurement uncertainty budgets of these methods calculated from validation data were also shown in Table 1. HMF solution at the final concentration of 0.004 mg/0.1g, therefore, were reported as 0.004 mg/0.1g \pm 0.00025 mg/0.1g, 0.0036 mg/0.1g \pm 0.000691 mg/0.1g, 0.004 mg/0.1g \pm 0.00045 mg/0.1g and 0.0039 mg/0.1g \pm 0.00022 mg/0.1g ($k=2$, confidence level of 95%) by spectral analysis, Seliwanoff method, HPLC and Winkler method, respectively. The use of calibration curve affected directly both the results of quantification and uncertainty of measurement. Since all four methods in this study analyzed the amount of HMF based on calibration curves of fructose dehydrated products, the main component of uncertainty budgets is expected to be the uncertainty of calibration curve. However, the most effective component in the uncertainty sources was the calibration curve for only Seliwanoff method. Uncertainty associated with recovery contributed more for uncertainty budgets of spectral analysis, HPLC and Winkler method which could be explained by the difference of percent recovery values from 100% (or recover values from unity).

The aim of this study was the validation of four methods for HMF determination in honey and providing their comparisons based on validation and uncertainty parameters. Previously, Zappalà et al. [27] presented a study to compare three methods for the determination of HMF in honey. It was concluded that the results of HPLC and White methods were approximately similar while it was higher when analyzed by Winkler method, and HPLC method was preferable to quantify HMF in honey due to the toxicity of Winkler reactive reagent and UV interferences in spectral analysis. A recent study described an in-house validation study based on Seliwanoff test to determine HMF in honey [50]. The proposed method had precision and accuracy in the range of 2.52–5.14% and 95.83% to 96.65%, respectively and showed a linear relationship with Winkler method and HPLC.

In this study, four methods were validated and defined for HMF quantification. Spectral analysis was used for the measurement of HMF amount directly without using any reagents. Seliwanoff method was used with resorcinol as reactive reagent which does not show any known toxicity. Besides Seliwanoff method and spectral analysis, Winkler and chromatographic method were carried out for quantitative determination of HMF after validation. Based on method performance parameters of validation study, all four methods were found to be applicable for the quantification of HMF. The measurement uncertainty of quantification of HMF by four methods based on the validation data of spiked samples was described by their linearity, recovery, and repeatability in this study. To our knowledge, this is the first study for defining direct spectral method for HMF quantification and validation of four methods to determine HMF.

3.7. Determination of HMF in Real Samples

Honey samples spiked with HMF at the final concentrations of 0.001, 0.002, 0.003, 0.004, 0.005 and 0.006 mg/0.1g were analyzed separately by four methods in this study. HPLC method was selected as reference method and spectral methods were compared with reference method. The correction factors of 0.41, 0.82 and 1.25 were used in the calculation of HMF concentrations to balance the effects of the honey matrix on the results of Spectral analysis, Seliwanoff and Winkler methods, respectively. Figure S2 represented the graph of the HMF concentrations calculated from the calibration curves of spectral analysis, Seliwanoff and Winkler methods against the HMF concentrations calculated based on the HPLC calibration curve. The comparison of the responses of three spectral methods with a chromatographic method gave the slopes of linear regression at 1.086, 1.059 and 1.062 for spectral analysis, Seliwanoff and Winkler methods, respectively. The R^2 values were ≥ 0.986 which indicated the relatively strong relationship between the results of these methods at this concentration range. Moreover, the calculated concentrations of spiked honey samples and the recovery values (%) of each method were given in Table 2. The recoveries of each method at each spiked HMF concentration were in the acceptable range of 70-120%. All these results indicated the applicability of four methods for the quantification of HMF in honey with accepted method performance criteria for recovery.

Table 2. Concentrations of HMF spiked to honey and the recoveries of four methods

HMF spiked (mg/0.1g)	Spectral analysis		Seliwanoff method		HPLC analysis		Winkler method	
	HMF (mg/0.1g)	Recovery %	HMF (mg/0.1g)	Recovery %	HMF (mg/0.1g)	Recovery %	HMF (mg/0.1g)	Recovery %
0.001	0.0011	108.7	0.0010	101.6	0.0012	118	0.0010	100
0.002	0.0023	116.2	0.0020	100.5	0.0021	105	0.0020	100.7
0.003	0.0034	114.8	0.0035	115	0.0033	110	0.0030	100.8
0.004	0.0039	98.2	0.0040	100.2	0.0041	102.5	0.0041	103.3
0.005	0.0050	98.9	0.0049	98.3	0.0047	94.6	0.0050	100.6
0.006	0.0061	102.4	0.0055	92.3	0.0056	93.3	0.0055	92.3

HMF is also used as heating index of honey and its concentration has been changed by temperature and heating time. Karabournioti and Zervalaki [51] showed that incubation of honey samples at 35°C, 45°C, 55°C and 65°C for 24 hours changed the initial HMF concentration from 2.25 mg/kg to 3.45, 3.75, 4.35 and 19.00 mg/kg, respectively. They concluded that temperature higher than 55°C resulted in a significant increase in HMF concentration regardless of the exposure time, but still lower than that recommended by international standards and codex. Another study reported that heating floral honey at 100°C for 75 and 90 minutes yielded HMF concentrations of 55.41 and 73.78 mg/kg [52]. Therefore, besides spiked honey samples, heated honey samples were analyzed in this study in order to evaluate the effectiveness of these methods for the quantification of HMF in real samples. The initial concentration of HMF in honey was lower than the detection limits of spectral methods. Three different temperatures were set and HMF concentrations were determined at certain time intervals by spectral methods. Table S1 summarized HMF concentrations produced upon heat treatment at 50°C, 70°C and 90°C. Figure S3 also showed the effect of heating temperature and time on HMF content of honey samples. Heating process at 50°C did not yield a HMF concentration higher than 40 mg/kg which is the maximum limit for HMF allowed in honey by Codex and EU directive [13,53]. However, even after 10 min of heat treatment at 70°C and 90°C, the amounts of HMF exceeded this maximum limit in honey. Moreover, these concentrations calculated by the calibration curves of each spectral method was not significantly different from each other which mean that spectral analysis, Seliwanoff method and Winkler method could be applicable for detection of HMF in heated honey.

4. Conclusion

In this study, three spectral methods and HPLC were used to evaluate HMF concentration in honey. These four methods were validated by single laboratory validation study. The measurement uncertainties were calculated for all methods at the maximum acceptable limit of HMF allowed for honey. The method validation and uncertainty results prove that these methods can be successfully used to determine HMF content in honey.

Author Contributions

All the authors equally contributed to this work. This paper is derived from the first author's master's thesis supervised by the second author. They all read and approved the final version of the paper.

Conflicts of Interest

All the authors declare no conflict of interest.

Supplementary Material

<https://dergipark.org.tr/en/download/journal-file/30476>

Acknowledgement

The authors would like to acknowledge the technical assistance provided by Karamanoğlu Mehmetbey University BILTEM and PTTO. The authors would like to thank Dr. Ceren Bayrac for her helpful input.

References

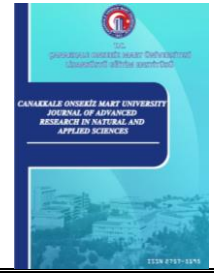
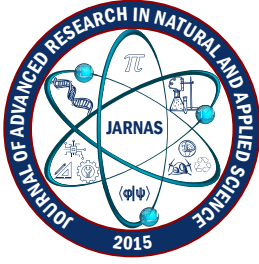
- [1] D. B. Markowicz, É. Monaro, É., Siguemoto, M. Séfora, *Maillard reaction products in processed foods: Pros and cons*, in: B. Valdez (Ed.), *Food Industrial Processes-Methods and Equipment*, London: INTECH Open Access Publisher, Rijeka, 2012, Ch. 15, pp. 281–300.
- [2] N. İçli, *Evaluation of HMF levels in unbranded flower honeys in terms of food safety*, Ankara Üniversitesi Veteriner Fakültesi Dergisi 69 (4) (2022) 431–436.
- [3] U. M. Shapla, M. Solayman, N. Alam, M. I. Khalil, S. H. Gan, *5-Hydroxymethylfurfural (HMF) levels in honey and other food products: effects on bees and human health*, *Chemistry Central Journal* 12 (2018) Article Number 35 18 pages.
- [4] C. Janzowski, V. Glaab, E. Samimi, J. Schlatter, G. Eisebbrand, *5-Hydroxymethylfurfural: Assessment of mutagenicity, DNA-damaging potential and reactivity towards cellular glutathione*, *Food and Chemical Toxicology* 38 (9) (2000) 801–809.
- [5] E. Capuano, V. Fogliano, *Acrylamide and 5-hydroxymethylfurfural (HMF): A review on metabolism, toxicity, occurrence in food and mitigation strategies*, *LWT - Food Science and Technology* 44 (4) (2011) 793–810.
- [6] M. N. Islam, M. I. Khalil, M. A. Islam, S. H. Gan, *Toxic compounds in honey*, *Journal of Applied Toxicology*, 34 (7) (2014) 733–742.
- [7] A. Apriceno, R. Bucci, A. M. Girelli, F. Marini, L. Quattrocchi, *5-Hydroxymethyl furfural determination in Italian honeys by a fast near infrared spectroscopy*, *Microchemical Journal* 143 (2018) 140–144.
- [8] M. C. Archer, W. R. Bruce, C. C. Chan, D. E. Corpet, A. Medline, L. Roncucci, D. Stamp, X. M. Zhang, *Aberrant crypt foci and microadenoma as markers for colon cancer*, *Environmental Health Perspectives*

98 (1992) 195–197.

- [9] W. R. Bruce, M. C. Archer, D. E. Corpet, A. Medline, S. Minkin, D. Stamp, Y. Yin, X.-M. Zhang, *Diet, aberrant crypt foci and colorectal cancer*, *Mutation Research* 290 (1) (1993) 111–118.
- [10] X. M. Zhang, C. C. Chan, D. Stamp, S. Minkin, M. C. Archer, W. R. Bruce, *Initiation and promotion of colonic aberrant crypt foci in rats by 5-hydroxymethyl-2-furaldehyde in thermolyzed sucrose*, *Carcinogenesis* 14 (4) (1993) 773–775.
- [11] Y. C. Lee, M. Shlyankevich, H. K. Jeong, J. S. Douglas, Y. J. Surh, *Bioactivation of 5-hydroxymethyl-2-furaldehyde to an electrophilic and mutagenically sulfuric acid ester*, *Biochemical and Biophysical Research Communications* 209 (3) (1995) 996–1002.
- [12] B. H. Monien, W. Engst, G. Barkowitz, A. Seidel, H. Glatt, *Mutagenicity of 5-hydroxymethylfurfural in V79 cells expressing human SULT1A1: identification and mass spectrometric quantification of DNA adducts formed*, *Chemical Research in Toxicology* 25 (7) (2012) 1484–92.
- [13] Joint FAO/WHO Codex Alimentarius Commission, *Codex Alimentarius: Report of the Seventh Session of the Codex Committee on Sugars ALINORM 01/25 (2000)*, https://www.fao.org/input/download/report/277/AI01_25e.pdf Accessed 28 Feb 2024
- [14] The Council of the European Union, *Council Directive 2001/110/EC relating to honey (2001)*, <https://www.fao.org/faolex/results/details/en/c/LEX-FAOC037441> Accessed 28 Feb 2024
- [15] Turkish Food Codex, *Turkish Food Codex Honey Statement 2020/7 (2020)*, <https://www.resmigazete.gov.tr/eskiler/2020/04/20200422-13.htm> Accessed 28 Feb 2024
- [16] F. J. Morales, C. Romero, S. Jiménez-Pérez, *Chromatographic determination of bound hydroxymethylfurfural as an index of milk protein glycosylation*, *Journal of Agricultural and Food Chemistry* 45 (5) (1997) 1570–1573.
- [17] G. Vanhoenacker, A. D. Villiers, K. Lazou, D. D. Keukeleire, P. Sandra, *Comparison of high-performance liquid chromatography - Mass spectroscopy and capillary electrophoresis - Mass spectroscopy for the analysis of phenolic compounds in diethyl ether extracts of red wines*, *Chromatographia* 54 (2001) 309–315.
- [18] B. M. Wagner, F. Donnarumma, R. Wintersteiger, W. Windischhofer, H. J. Leis, *Simultaneous quantitative determination of alpha-ketoglutaric acid and 5-hydroxymethylfurfural in human plasma by gas chromatography-mass spectrometry*, *Analytical and Bioanalytical Chemistry* 396 (7) (2010) 2629–2637.
- [19] D. Jöbstl, T. Husoy, J. Alexander, T. Bjellaas, E. Leitner, M. Murkovic, *Analysis of 5-hydroxymethyl-2-furoic acid (HMFA) the main metabolite of alimentary 5-hydroxymethyl-2-furfural (HMF) with HPLC and GC in urine*, *Food Chemistry* 123 (3) (2010) 814–818.
- [20] S.-M. Lin, J.-Y. Wu, C. Su, S. Ferng, C.-Y. Lo, R. Y.-Y. Chiou, *Identification and mode of action of 5-hydroxymethyl-2-furfural (5-HMF) and 1-methyl-1,2,3,4-tetrahydro- β -carboline-3-carboxylic acid (MTCA) as potent xanthine oxidase inhibitors in vinegars*, *Journal of Agricultural and Food Chemistry* 60 (39) (2012) 9856–9862.
- [21] Y. Huang, C. Li, H. Hu, Y. Wang, M. Shen, S. Nie, J. Chen, M. Zeng, M. Xie, *Simultaneous Determination of Acrylamide and 5-Hydroxymethylfurfural in Heat-Processed Foods Employing Enhanced Matrix Removal-Lipid as a New Dispersive Solid-Phase Extraction Sorbent Followed by Liquid Chromatography-Tandem Mass Spectrometry*. *Journal of Agricultural and Food Chemistry* 67 (17) (2019) 5017–5025.
- [22] S. Bogdanov, C. Lüllmann, P. Martin, W. von der Ohe, H. Russmann, G. Vorwohl, L. P. Oddo, A.-G. Sabatini, G. L. Marazzan, R. Piro, C. Flamini, M. Morlot, J. Lhéritier, R. Borneck, P. Marioleas, A.

- Tsigouri, J. Kerkvliet, A. Ortiz, T. Ivanov, B. D'Arcy, B. Mossel, P. Vit, *Honey Quality and International Regulatory Standards: Review by the International Honey Commission*, *Bee World* 80 (2) (1999) 61–69.
- [23] H. J. Jeuring, F. J. E. M. Koppers, *High performance liquid chromatography of furfural and hydroxymethylfurfural in spirits and honey*, *Journal of the Association of Official Analytical Chemists* 63 (6) (1980) 1215–1218.
- [24] O. Winkler, *Beitrag zum Nachweis und zur bestimmung von oxymethylfurfural in Honig und Kunsthonig*, *Zeitschrift für Lebensmittel Untersuchung und Forshung* 102 (3) (1955) 161–167.
- [25] J. White, *Spectrophotometric method for hydroxymethylfurfural in honey*, *Journal of the Association of Official Analytical Chemists* 62 (3) (1979) 509–514.
- [26] S. S. Virgen, S. G. Ceballos-Magana, V. D. C. Salvatierre-Stamp, M. T. Sumaya-Martinez, F. J. Martinez-Mertinez, R. Muniz-Valencia, *HPLC-DAD method development and validation for the quantification of hydroxymethylfurfural in corn chips by means of response surface optimization*, *Food Additives & Contaminants: Part A* 34 (12) (2017) 2101–2110.
- [27] M. Zappalà, B. Fallico, E. Arena, A. Verzera, *Methods for the determination of HMF in honey: A comparison*, *Food Control* 16 (3) (2005) 273–277.
- [28] A. Elmastaş, F. Aydın, A. Umaz, E. Kılınc, Y. Arslan, I. Aydın, *Determination of hydroxymethylfurfural in Turkish honeys, pekmez (grape molasses), and jam samples by high-performance liquid chromatography with diode array detection*, *Journal of Food Processing and Preservation* 46 (4) (2022) e16462 7 pages.
- [29] International Organization for Standardization, *Accuracy (trueness and precision) of measurement methods and results Part 2 ISO 5725-2 (1994)*, <https://www.iso.org/standard/36202.html> Accessed 28 Feb 2024
- [30] E. Yıldız, *Determination of hydroxymethyl furfural in honey*, Master's Thesis Karamanoğlu Mehmetbey University (2019) Karaman.
- [31] B. F. M. Kuster, *5-Hydroxymethylfurfural (HMF). A review focussing on its manufacture*, *Starch Stärke* 42 (8) (1990) 314–321.
- [32] B. Fallico, M. Zappalà, E. Arena, A. Verzera, *Effects of conditioning on HMF content in unifloral honeys*, *Food Chemistry* 85 (2) (2004) 305–313.
- [33] V. Gökmen, Ö. Ç. Açar, H. Köksel, J. Acar, *Effects of dough formula and baking conditions on acrylamide and hydroxymethylfurfural formation in cookies*, *Food Chemistry* 104 (3) (2007) 1136–1142.
- [34] H. S. Lee, S. Nagy, *Relative reactivities of sugars in the formation of 5-hydroxymethylfurfural in sugar-catalyst model systems*, *Journal of Food Processing and Preservation* 14 (3) (1990) 171–178.
- [35] Y. Román-Leshkov, J. N. Chheda, J. A. Dumesic, *Phase modifiers promote efficient production of hydroxymethylfurfural from fructose*, *Science* 312 (5782) (2006) 1933–1937.
- [36] J. H. Turner, P. A. Rebers, P. L. Barrick, R. H. Cotton, *Determination of 5-(hydroxymethyl)-2-furaldehyde and related compounds*, *Analytical Chemistry* 26 (5) (1954) 898–901.
- [37] N. Hudz, D. Leontiev, P. P. Wiczorek, *Spectral characteristics of 5-hydroxymethylfurfural as a related substance in medicinal products containing glucose*, *Pharmacia* 66 (3) (2019) 121–125.
- [38] S. Bogdanov, *Harmonised methods of the European Honey Commission (2009)*, <http://www.ihc-platform.net/ihcmethods2009.pdf> Accessed 28 Feb 2024
- [39] C. Truzzi, A. Annibaldi, S. Illuminati, C. Finale, M. Rossetti, G. Scarponi, *Determination of very low levels of 5- (hydroxymethyl)-2-furaldehyde (HMF) in natural honey: comparison between the HPLC technique and the spectrophotometric white method*, *Journal of Food Science* 77 (7) (2012) 784–90.

- [40] S. Ünüvar, *Determination of 5-hydroxymethylfurfural (5-HMF) in expired pharmaceutical syrups by using HPLC-DAD method*, Journal of the Turkish Chemical Society Section A: Chemistry 5 (3) (2018) 1431–1440.
- [41] A. Val, J. F. Huidobro, M. P. Sánchez, S. Muniategui, M. A. Fernández-Muiño, M. T. Sancho, *Enzymatic determination of galactose and lactose in honey*, Journal of Agricultural and Food Chemistry 46 (4) (1998) 1381–1385.
- [42] S. Bogdanov, T. Jurendic, R. Sieber, P. Gallmann, *Honey for nutrition and health: A review*, Journal of the American College of Nutrition 27 (6) (2008) 677–689.
- [43] A. Pascual-Maté, S. M. Osés, G. L. Marcazzan, S. Gardini, M. A. F. Muiño, M. T. Sancho, *Sugar composition and sugar-related parameters of honeys from the northern Iberian Plateau*, Journal of Food Composition and Analysis 74 (2018) 34–43.
- [44] P. Araujo, *Key aspects of analytical method validation and linearity evaluation*, Journal of Chromatography B 877 (23) (2009) 2224–2234.
- [45] E. Rozet, A. Ceccato, C. Hubert, E. Ziemons, R. Oprean, S. Rudaz, B. Boulanger, P. Hubert, *Analysis of recent pharmaceutical regulatory documents on analytical method validation*, Journal of Chromatography A 1158 (1-2) (2007) 111–125.
- [46] A. A. Ariffin, H. M. Ghazali, P. Kavousi, *Validation of a HPLC method for determination of hydroxymethylfurfural in crude palm oil*, Food Chemistry 154 (2014) 102–107.
- [47] M. I. Milani, E. L. Rossini, K. Castoldi, L. Pezza, H. R. Pezza, *Paper platform for reflectometric determination of furfural and hydroxymethylfurfural in sugarcane liquor*, Microchemical Journal 133 (2017) 286–292.
- [48] S. L. Ellison, A. Williams, *Quantifying uncertainty in analytical measurement*, 3rd Edition, EURACHEM/CITAC, Teddington, 2012
- [49] Joint FAO/WHO Codex Alimentarius Commission, *Codex Alimentarius Commission Procedural Manual*, 21st Edition (2013), <http://www.fao.org/3/a-i3243e.pdf> Accessed 28 Feb 2024
- [50] A. Besir, F. Yazici, M. Mortas, O. Gul, *A novel spectrophotometric method based on Seliwanoff test to determine 5-(Hydroxymethyl) furfural (HMF) in honey: Development, in house validation and application*, LWT 139 (2021) 110602 8 pages.
- [51] S. Karabournioti, P. Zervalaki, *The effect of heating on honey HMF and invertase*, Apiacta 36 (4) (2001) 177–181.
- [52] I. Turhan, N. Tetik, M. Karhan, F. Gurel, H. R. Tavukçuoğlu, *Quality of honeys influenced by thermal treatment*, LWT - Food Science and Technology 41 (8) (2008) 1396–1399.
- [53] Turkish Food Codex, *Turkish Food Codex Honey Statement 2012/58* (2012), <https://www.resmigazete.gov.tr/eskiler/2012/07/20120727-12.htm> Accessed 28 Feb 2024



Uydu Verisi ve CBS ile Van Gölü Klorofil-a Dinamiklerinin İzlenmesi

Ufuk Tari¹ , Nazlı Olğun Kıyak² 

¹Jeoloji Mühendisliği Bölümü, Maden Fakültesi, İstanbul Teknik Üniversitesi, İstanbul, Türkiye

²Avrasya Yer Bilimleri Enstitüsü, İstanbul Teknik Üniversitesi, İstanbul, Türkiye

Öz – Dünyanın en büyük alkali gölü olan Van Gölü, fitoplankton (mikro-alg) içeriği açısından düşük organik üretimli (oligotrofik) bir yapıya sahiptir. Besin zincirinin ilk halkasını oluşturan fitoplankton yoğunluğunun belirlenmesinde en sık kullanılan parametrelerden biri klorofil-a pigmentidir. Fitoplankton ve dolayısıyla klorofil-a yoğunlaşmaları aynı zamanda su kalitesinin evsel, tarımsal ve sanayi atıkları gibi insan kaynaklı kirliliğin takibinde de kullanılmaktadır. Bu çalışmada, Van Gölü'ndeki klorofil-a konsantrasyonlarının dağılım haritaları, literatürdeki 1983-84, 2002 ve 2014 yersel ölçme verileri (spektrofotometrik yöntem ile), uydu verisi ve Coğrafi Bilgi Sistemi (CBS) metodları kullanılarak Van Gölü'ndeki temsiliet kapasitesi değerlendirilmiştir. Buna göre, klorofil-a dağılımları mekânsal olarak değişiklik göstermektedir. Gölün kuzeydoğu ve doğusundaki klorofil-a yoğunluğunun, gölün batı kesimine göre oldukça yüksek olduğu görülmektedir. Saha çalışmaları ile 2014 yılı klorofil-a yersel ölçmelerden elde edilen klorofil-a değerleri (1.7-7.8 mg/m³) kullanılarak Landsat-8 OLI algılayıcısına ait mavi bantın (562-443 nm arası dalga boyu) yeşil banta (562-482 nm arası dalga boyu) yansıma oranı ile elde edilen klorofil-a konsantrasyonunun ölçme hatalarının içerisinde kaldığı (karesel ortalama hata) ve Landsat-8 OLI algılayıcısının Van Gölü'ndeki klorofil-a konsantrasyonlarını haritalamak için uygun olduğu belirlenmiştir. Ayrıca, Van Gölü'nün farklı lokasyonlarında 1983-84 ve 2002 yıllarında klorofil-a tesbiti için yapılan yersel ölçmeler kullanılarak, CBS'de jeo-istatistik analizler gerçekleştirilmiştir. Bu çalışma ile birlikte, Van Gölü'ndeki klorofil-a'nın mekânsal dağılımlarının izlenmesinde CBS yöntemiyle kıyaslandığında uydu verisinin temsilietinin yeterli doğrulukta tahmin edilebileceği ortaya konulmuştur.

Anahtar Kelimeler – Van Gölü, klorofil-a, uzaktan algılama, Landsat-8/OLI, CBS

Monitoring the Chlorophyll-a Dynamics of Van Lake with Satellite Data and GIS

¹Department of Geological Engineering, Faculty of Mines, Istanbul Technical University, İstanbul, Türkiye

²Eurasia Institute of Earth Sciences, Istanbul Technical University, İstanbul, Türkiye

Abstract – Lake Van, the world's largest alkaline lake, is known to be a low organic production (oligotrophic) lake in terms of phytoplankton (micro-algae). Chlorophyll-a (chl-a) pigment is one of the most frequently used parameters in determining the phytoplankton, which makes up the first link of the food chain in the lakes. Phytoplankton and hence chlorophyll-a concentrations are also used for monitoring water quality and anthropogenic pollution such as domestic, agricultural, and industrial wastes. In this study, chlorophyll-a distributions of Lake Van were studied by using in situ chl-a measurements (by spectrophotometric method) found in the literature (1983-84, 2002 and 2014 data), remote sensing data and Geographic Information System (GIS) methods, and the representativeness of satellite data in the study region was evaluated. Accordingly, chl-a distributions in Lake Van varied significantly with higher chl-a concentrations found in the northeast and east of the lake compared to the western section. The differences in chl-a data from in situ measurements in field studies in 2014 (1.7-7.8 mg/m³) and the reflection ratio of the blue band (562-443 nm wavelength) to the green band (562-482 nm wavelength) of the Landsat-8 OLI sensor were found to be below the measurement errors (mean

Article History

Received: 20 Jun 2023

Accepted: 29 Oct 2023

Published: 15 Mar 2024

Research Article

¹utari@itu.edu.tr (Corresponding Author); ²nokiyak@itu.edu.tr

squared error) and which suggested the suitability of Landsat-8 OLI sensor for mapping chl-a concentrations throughout Lake Van. In addition, geo-statistical analyses were performed for the two other chl-a data sets including the 1983-84 and 2002 data, which were older than the available satellite technology. This study showed that the use of satellite data for representation for Lake Van chl-a spatial distribution is more accurate compared to GIS method.

Keywords – Lake Van, chlorophyll-a, remote sensing, Landsat-8/OLI, GIS

1. Giriş

Van Gölü, dünyanın en büyük alkali (alkalinite 155 m eq l^{-1} , pH 9.81, tuzluluk 21.4%) ve kapalı göllerinden biridir [1]. Gölün bugünkü alkali özelliği ve tuzluluğu, çevredeki volkanik kayaçların kimyasal aşınması ve buharlaşma ile oluşmuştur. Dünyada bilinen en büyük mikrobiyolit oluşumların bu gölde olduğu da bilinmektedir [2].

Van Gölü'nün bu farklı konumuyla her zaman göl ekosistemini anlamaya yönelik çalışmalar içinde hedef alanlardan biri olmuştur (Şekil 1a ve 1b). Göl ekosistemin en temel halkasını oluşturan birincil organik üretim (alg veya fitoplankton üretimi), gerek karbon döngüsünde gerekse iklim değişikliğinde oldukça önemli bir rol oynamaktadır. Fitoplankton üretimindeki aşırı artışlar, su kalitesini etkilemekte ve çevresel sorunlara sebep olabilmektedir [3-6]. Ayrıca, antropojenik ve iklim etkilerine bağlı olarak göllerdeki klorofil-a artışları ötrofikasyona neden olur [7,8]. Van Gölü'ndeki fitoplankton yoğunluğu aynı zamanda Türkiye'nin iç balıkçılığının yaklaşık %30'unu oluşturmada olan inci kefalinin (*A. tarichi*) besin zincirine de etki etmektedir. Göl seviyesi değişimlerinin inci kefalinin popülasyonu üzerindeki etkileri de güncel araştırma konuları arasında yer almaktadır [9].

Buradan hareketle, göl suyunda birincil üretimi değerlendirmek amacıyla kullanılan en yaygın parametre 'klorofil-a' yoğunlaşmasıdır. Özellikle bu yoğunlaşmanın su örneklerinde ölçülmesi nispeten kolay olmasına rağmen, belirli yerlerde su örneklerinin toplanması, çoğunlukla yoğun kaynak gerektirmekte ve bu durum mekânsal ve zamansal değişkenliği karakterize etme açısından bilimsel çalışmaları sınırlamaktadır. Ayrıca, noktasal klorofil-a ölçümleri, maalesef su kaynağının tamamını temsil etmemektedir. Bu noktada, birincil üretimin izlemesi konusunda uzaktan algılama teknolojisi yaygınca kullanılabilir. Bu teknoloji, ötrofikasyon koşullarının direkt göstergesi olan klorofil-a yoğunluk değerlerinin tahmin edilmesini uygun maliyetli ve gerçek zamanlı olarak izleme olanağı sağlamaktadır [10-16]. Özellikle, alkali göl sularında klorofil-a konsantrasyonunun mekânsal ve zamansal değişiminin izlenmesi, tatlı su ekosistemleri üzerindeki etkilerinin anlaşılması ve birincil organik üretim koşullarının tahmin edilmesi için çok önemlidir.

Su kütlelerindeki klorofil-a konsantrasyonu hem fitoplankton biokütlesinin hem de göl ötrofikasyonunun bir göstergedir [17]. Kapalı göllerde ise, genellikle su kalitesi, akaçlama (drenaj) havzasındaki kayaçların jeokimyası, akarsu girdisi, iklim koşulları ve bunlara bağlı buharlaşma/yağış oranı ve kimyasal aşınma ile de ilişkilendirilmektedir [1]. Bu noktada uzaktan algılama teknolojisi, makro-dinamik özelliklerinden dolayı büyük kolaylık sağlamak ve bundan dolayı da su kütlelerindeki klorofil-a'nın tahminine yönelik olarak da sıklıkla kullanılmaktadır.

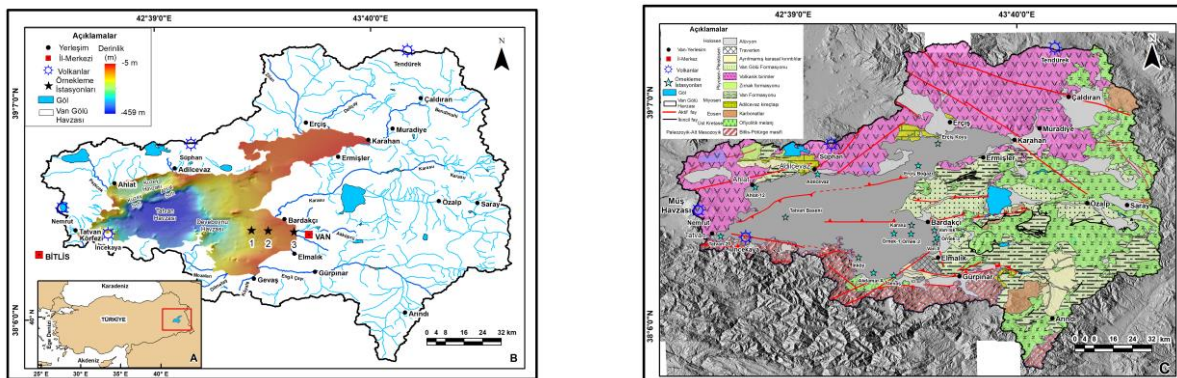
Landsat serisi uyduları, 1972 yılından beri sağladıkları görüntü arşivleri ile arazi örtüsü/kullanımı çalışmalarının yanı sıra, özellikle klorofil-a tahmini, askıda katı madde belirlenmesi, fitoplankton konsantrasyonu, alg patlaması, su yüzey sıcaklığının belirlenmesi ve makro fitlerin izlemesi gibi çalışmalarda da sıklıkla kullanılmaktadır [18-23]. Özellikle bu seriden Landsat-8 uydusuna, önceki Landsat-TM ve ETM+ uydularına ait algılayıcıların özelliklerine nazaran, yeni spektral aralıkların eklenmesi ve bunların çözünürlük özelliklerinin artırılmasıyla, su kalitesinin izlenmesi üzerine yapılan bilimsel araştırmalara katkı sağlanmıştır

[6,14,24,25]. Böylece, sucul ortamlarda Landsat-8 uydusuna ait OLI (Operational Land Imager) algılayıcısı ile çalışılması, klorofil-a düzeylerinde meydana gelen değişimlerin tahmini ve haritalanmasını mümkün kılmaktadır [26-29].

Göl suyundaki klorofil-a tahminleri, yerinde (in-situ) ölçülen klorofil-a ölçme verileri ile OLI algılayıcısına ait bantların spektral yansımaları ile birlikte çalışılan bölgeye bağlı ampirik modeller, önerilen algoritmalar ve klorofil-a verilerinin regresyon analizleri ile ilişkisi arasındaki korelasyona dayanarak yapılabilmektedir [26,28,29]. Bu yöntemler, büyük ölçüde çalışma bölgesinden elde edilen veri kümesine de bağlı olabileceği gibi, modelin uygulanabilirliği de inceleme alanı ile belirlenebilmektedir [14]. Bu çalışmada da kullanılan uydu verisine ait farklı bant kombinasyonlarının su yüzeyindeki spektral yansımaları ile ilişkili algoritmalarından biri kullanılmıştır.

Su yüzeyinin spektral yansımaları, klorofil-a tahminleri de dâhil olmak üzere, sudaki aktif maddelerin bir ifadesi olarak kullanılır [30]. Klorofil, elektromanyetik spektrumun görünür bölümünde bulunan mavi ve kırmızı ışığın emilip, yeşil ışığı yansıtma özelliği kullanılarak tespit edilmektedir. Özellikle, klorofil-a konsantrasyon tahmininde klorofilin bu özellikleri göz önünde bulundurularak, klorofil-a'nın yansımalarına duyarlı farklı bant kombinasyonları kullanılır. Farklı çalışmalarda bu bant kombinasyonlarına dayalı olarak pek çok algoritma önerilmiştir [31-35]. Bu çalışmalar genellikle sucul ortamlarda (ör. göl, deniz veya okyanus sularında) görünür yeşil renkte klorofil-a yansıma değeri ~ 565 nm [34] iken, kızılötesine yakın dalga boyları için yansıma değerinin ~ 700 nm olduğu önerilmiştir [33]. Atmosferden kaynaklanan etkiler de minimize edildiğinde, kullanılan spektral bant oranları ile daha yüksek doğrulukta klorofil-a tahminleri yapılabilmektedir [14,19,36]. Böylece, klorofil-a yansıma değerlerini belirlemek için kullanılan en yaygın algoritmalar, genellikle ~ 675 - 700 nm dalga boyları arasında yer alan spektral bantlardan seçilmektedir [37]. Bu çalışmada, gölde toplanan klorofil-a yersel ölçme verileri, örnekleme lokasyonu ve tarihi ile birlikte, bulutsuz koşullar altında elde edilen eş zamanlı Landsat-8 OLI uydu görüntüsü kullanılmıştır. Daha sonra, Ha [14] tarafından önerilen farklı bant kombinasyon modelleri arasından en uygun klorofil-a tahmin algoritması seçilerek uygulanmıştır.

Bununla beraber, klorofil-a konsantrasyonunun mekânsal ve zamansal değişimleri CBS analizleri (ör. ters mesafe ağırlıklandırma-IDW metodu) kullanılarak da tahmin edilebilmektedir [38,39]. Bu kapsamda, Van Gölü'nde farklı zamanlarda (sırasıyla, 1983-1984 ve 2002 yıllarına ait farklı aylar) elde edilen klorofil-a ölçme değerleri kullanılarak [40,41], göldeki klorofil-a konsantrasyonuna ait eğilim ve mekânsal dağılımlar belirlenmeye çalışılmıştır. Bu kapsamda, ilgili yıllara ait farklı sezonlarda (yaz ve kış dönemi) toplanan ölçmeler, CBS'nde analiz edilerek, klorofil-a konsantrasyonuna ait değişimler ile uydu verisinden elde edilen bulguların karşılaştırılması hedeflenmiştir.



Şekil 1. a) Çalışma alanının yer bulduru haritası b) Van Gölü Havzası'nın önemli akarsuları ve batimetrisi [42]'den (bu çalışmadaki örnekleme lokasyonları yıldız işareti ile gösterilmiştir), c) Jeoloji haritası ([43]'den derlenmiştir)

Van Gölü'nün kapalı bir havza oluşu iklim kayıtlarının korunmasını sağlamaktadır ve bu nedenle geçmiş iklim ve çevresel değişimleri anlamak için göl çökelleri oldukça detaylı araştırılmıştır [44-48]. Son araştırmalarda, göl sularının çeşitli su kalitesi parametrelerinin mevsimsel değişimleri birbiriyle korelasyonları incelenmiştir [49]. Ancak, göldeki besin zincirinin ilk halkası oluşturan fitoplanktonların yoğunlaşmalarının en yaygın göstergesi olan klorofil-a ölçümleri az sayıda çalışmada, farklı tarih ve lokasyonlarda kısıtlı olarak gerçekleştirilmiştir [40,41,50]. Van Gölü'nde klorofil-a konsantrasyonunun uzaktan algılama teknolojisi ile izlenmesine yönelik güncel çalışmalara fazla rastlanmadığı gibi gölün organik kirliliğinin tespiti üzerine yapılanlar da çok sınırlıdır [40,41,49,50]. Bu çalışmada, Van Gölü'nde gerçekleştirilmiş olan kısıtlı sayıdaki klorofil-a yersel ölçüm verileri kullanılarak klorofil-a yoğunlaşmalarının göldeki mekânsal dağılımı CBS (1983-84 ve 2002 verileri) ve uzaktan algılama (2014 verisi) kullanılarak incelenmiştir. Elde edilen bulgular doğrultusunda, kullanılan yöntemlerin Van Gölü klorofil-a araştırmaları açısından avantaj/dezavantajları değerlendirilmiştir.

Araştırma alanı olan Van Gölü, denizden oldukça yüksek (1648 m), Doğu Anadolu yüksek platosu üzerinde yer almaktadır. BGB-DKD yönünde yaklaşık 130 km'lik uzanımı ile, dünyanın en büyük dördüncü kapalı (hacmi, 607 km³; yüzey alanı, 3574 km²; maksimum derinliği, 460 m) ve alkali (soda) gölüdür [47,51]. Ayrıca, Anadolu, Avrasya ile Arap levhaları arasındaki çarpışma zonunda bulunan ve konumu itibarıyla de tektonizmanın oldukça aktif olduğu (bölgedeki son sismik aktivite 2011 M_w=7.1 büyüklüğündeki Van depremi) bir bölgede yer almaktadır [51-55]. Gölün hemen yakınında yer alan Nemrut Dağı (3050 m) ve Süphan Dağı (3800 m) olarak bilinen yarı aktif iki yanardağ ile İncekaya (400 m) volkanik krateri yükselir [52].

Van Gölü Havzası, batısında yer alan Muş Havzası'nın devamı niteliğinde olup Muş Havzası'ndan Nemrut Volkan'ının yaklaşık günümüzden 500-600 bin yıl önce püskürmeye başlamasıyla ayrılmıştır. Bu yaş verisi, daha sonra gölde yapılan karotlu sondaj çalışmalarında elde edilen karottaki örneklerden yapılan yaş analizleri ile de doğrulanmıştır [42,44,47,51]. Bölgesel olarak meydana gelen bu tektonik ve volkanik olaylar gölün taban morfolojisinin de farklı şekillenmesine (sırt, havza ve şelf gibi) neden olmuştur (Şekil 1b).

Van Gölü Havzası'nı oluşturan jeolojik birimler ise genellikle havzanın batısı ve kuzeyinde yüzeyleyen Kuvaterner yaşlı Nemrut ve Süphan volkanikleri, Neojen volkanik kayaları ile Miyosen yaşlı klastik ve karbonatlı çökeller ile temsil edilir (Şekil 1c). Doğusundaki birimler ise, Doğu Anadolu Yığılma Karmaşığı'nı oluşturan Pliyosen çökelleri ve Üst Kretase-Oligosen yaşlı fliş ve ofiyolitik melanj ile güneyinde yer alan Bitlis Masifi'nin Paleozoik yaşlı metamorfik kayalardan oluşur [52,53,56].

Gölün çevresinde yüzeyleyen volkanik kayaçların kimyasal ayrışması ve buharlaşması ile gölde meydana gelen hidrotermal aktivite sonucu, bugünkü göl suyunun aşırı alkali özelliğini ve tuzluluğunu oluşturmuştur. Bu durum, gölün dünyanın en büyük soda gölü olmasını da sağlamıştır [1,2,57]

Van Gölü hem coğrafi konumu hem de kapalı bir havza oluşu nedeniyle iklim değişimlerine duyarlıdır [45,46,48,58]. Bu durum, gölün iklimsel değişimlere (yağış, buharlaşma, göl seviyesi değişimleri gibi) dolayısıyla hidrolojik rejiminin değişmesine de duyarlı bir şekilde tepki verdiğini göstermektedir. Göl çevresinde yüksek göl seviyelerini işaret eden Pleyistosen yaşlı teraslar (~ 107 m'ye varan) ve çökellerinin bulunması da son 20 bin yılda birkaç yüz metreye kadar göl seviyesinde değişikliklerin meydana geldiğini göstermektedir [59,60]. Ayrıca, Van Gölü'nde günümüzde su seviyesi yükselmesinin Van Gölü'nde derin suyun yenilenmesini engellediğini ve böylece 300 m'nin altındaki derinliklerde anoksik koşulların oluştuğunu da göstermiştir [1,44].

Van Bölgesi'nde günümüzde karasal iklimin etkisiyle kışlar soğuk ve yağışlı, yazlar ılık ve kurak geçer. Gölün

yüzeysel su sıcaklıkları yaz aylarında 21-25 °C, kışın ise 2-7 °C arasında değişmektedir [44]. Yıllık yağış miktarı ~ 400-600 mm/yıl arasındadır. Bölgede rüzgâr, çoğunlukla güneybatıdan esmektedir. Bu durum kış ile ilkbahar boyunca da yağıştan sorumlu nemli havayı sağlamaktadır. Yazın özellikle Temmuz ve Ağustos aylarında ortalama 20 °C gündüz sıcaklıkları ve kuzey rüzgârları ile de kuru bir hava hakimdir [57].

Yaklaşık 16.000 km²'lik bir alanı kaplayan Van Gölü'nün kapalı havzası, çevresindeki yüksek dağlardan kaynaklı göle sürekli akan çeşitli akarsular ile beslenen kapalı bir drenaj sistemine sahiptir (Şekil 1b). Bu drenaj havzasında çoğunlukla gölü besleyen akarsular, kuzeyden Zilan, Deliçay ve Bendimahi, doğudan Karasu, Moralı ve Engil, batıdan Ovakışla, Tatvan yakınlarından Güzel ve Ahlat yakınlarından da Papicek (Süfrefor) akarsularıdır (Şekil 1b). Göle doğrudan yağış ve akarsu girdisi ile toplam tatlı su girişi yılda 4.2 km³'tür. Buharlaşma (~3.8 km³/yıl), yıllık göl seviyesi salınımları (0.9 m'ye kadar) ve akarsu girdisi, gölü kontrol eden en önemli süreçlerdir. Bu akarsular, gölün havzasında birikmekte olan önemli miktardaki sediman taşımının yanı sıra geçtikleri bölgenin arazi özelliklerine göre su kalitesinin değişim göstermesini de sağlamaktadır [1,42].

Havzaya yağışlar çoğunlukla kışın kar ve yağmur, ilkbaharda akarsu girdisi olarak görülür [57]. Göle tatlı su girişi, ilkbaharın sonlarında ve yaz başında çevresindeki dağlarda bulunan karın erimesiyle maksimum seviyelere ulaşır. 1944 yılından bu yana göl seviyesinde yapılan ölçümlere bakıldığında Ocak 1963'te ölçülen en düşük seviyesi 1646.69 m iken, Haziran 1995'te ölçülen en yüksek seviyesi 1650.55 m olarak kaydedilmiştir. 1944-2000 yılları arasında yıllık ortalama seviyeler temel alındığında ise göl seviyesinin en yüksek 1650.55 m ve en düşük ise, 1646.69 m tespit edilmiştir. Bu farkın kaydedildiği yıllar arasında da ~ 4 m lik değişim söz konusudur. Bu durum, Van Gölü'nün göl seviyesinin son 90 bin yıl içindeki değişimlerinin araştırıldığı çökel çalışmasında göl seviyesinin mevsimsel değişimin etkisiyle yıllık ortalama ~42 cm değiştiğini gösterilmiştir [46].

2. Materyal ve Yöntem

Bu çalışmanın amacı, göl ekosistem ve çevresel kirlilik açısından önemli bir alan olan Van Gölü'ndeki klorofil-a konsantrasyonunun mekânsal ve zamansal olarak uydu verisi ve CBS metodu ile değerlendirilmiştir. Bu amaç doğrultusunda görsel ve kantitatif verilerin değerlendirilmesine yönelik analizler yapılmıştır. Bu analizler için uygulanan yöntemler yayınlanmış ve kabul görmüş hipotezler uygulanarak karşılaştırılmış ve sonuçları yorumlanmıştır.

2.1. Klorofil-a Ölçüm Verileri

Van Gölünde gerçekleştirilmiş olan ölçme verileri Tablo 1'de sunulmuştur. Spektrofotometrik yöntemle gerçekleştirilen klorofil-a ölçmeleri sırasıyla 1983-84 [40], 2002 [41] ve 2014 [50] yıllarında gerçekleştirilmiştir (Şekil 2).



Şekil 2. Van Gölü seferinde Temmuz 2014'te gerçekleştirilen arazi çalışması sırasında yapılan ölçme ve filtrelemeler

Toplanan su örneklerindeki klorofil-a ölçmeleri, 0.7 µm cam fiberden geçirilen örneklerden %95 aseton filtre pigment ekstrasyonu yöntemi ile spektrofotometrede ölçülmüştür. Bunun için pigment özünün en yüksek yoğunluk ölçmeleri sırasıyla A630, A647, A664 ve A750 nm dalga boyunda gerçekleştirilmiştir. Daha sonra da klorofil-a yoğunluk değerleri için aşağıdaki denklem 2.1 uygulanarak mg/m³ cinsinden değerler elde edilmiştir (bkz. Tablo 1).

$$Chlorophyll - a \left(\frac{mg}{m^3} \right) = \frac{[11.85(A664 - A750) - 1.54(A647 - A750) - 0.08(A630 - A750) \times v]}{[V \times Z]} \quad (2.1)$$

A630, A647, A664 ve A750; farklı dalga boylarında ölçülen optik yoğunluk, v; pigment özünün ml cinsinden hacmi, V; litre olarak filtrelenen numunenin litre cinsinden hacmi ve Z; cam küvetin cm cinsinden uzunluğudur.

Tablo 1. Van Gölü'nün farklı lokasyonlarında yapılan klorofil-a ölçmeleri (mg/m³)

İstasyon	Enlem	Boylam	Derinlik (m)	Klorofil-a (mg/m ³)					Kaynakça
				10-13 Haziran 1983	8-11 Eylül 1983	1-4 Haziran 1984			
Tatvan Boğazı	42 ^o .7065	38 ^o .6453	0.5	0.12	0.07	0.52			Tuğrul vd.1984
			20	-	0.12	0.82			
			50	0.32	-	-			
Erciş Koyu	43 ^o .3831	38 ^o .9786	0.5	0.52	0.11	2.0			Tuğrul vd.1984
			5	-	-	3.9			
			10	0.64	0.08	-			
Erciş Boğazı	43 ^o .2186	38 ^o .8315	0.5	0.54	0.04	0.94			Tuğrul vd.1984
			10	0.70	-	-			
			20	-	0.14	0.48			
			30	0.46	-	-			
Ahlat	42 ^o .4775	38 ^o .7329	0.5	0.12	0.08	0.59			Tuğrul vd.1984
			20	0.23	0.13	0.87			
Gevaş	43 ^o .1071	38 ^o .3319	0.5	0.15	0.07	0.58			Tuğrul vd.1984
			20	0.14	0.19	0.92			
			50	0.07	-	-			
Adilcevaz	42 ^o .7610	38 ^o .7933	0.5	0.43	0.09	0.71			Tuğrul vd.1984
			10	0.46	0.14	0.78			
Van	43 ^o .3032	38 ^o .5042	0.5	0.23	0.08	0.41			Tuğrul vd.1984
			10	0.32	0.05	0.72			
Tatvan	42 ^o .3200	38 ^o .5105	0.5	0.22	0.41	0.63			Tuğrul vd.1984
			10	0.26	0.38	0.65			
				13 Ocak 2002	25 Ocak 2002	09 Şubat 2002	03 Mart 2002	17 Mart 2002	
Karasu	43 ^o .1887	38 ^o .5608	0.1	-	1.61	1.46	0.87	0.75	Cüreoğlu, 2002
Van İsk.	43 ^o .2925	38 ^o .5364	0.1	-	1.18	0.92	0.99	0.70	Cüreoğlu, 2002
İnköy	42 ^o .9469	38 ^o .4136	0.1	1.38	1.24	0.85	1.03	1.31	Cüreoğlu, 2002
Akdamar	43 ^o .0148	38 ^o .3443	0.1	1.39	1.28	0.68	1.14	1.73	Cüreoğlu, 2002
				07 Nisan 2002	21 Nisan 2002	05 Mayıs 2002			
Karasu	43 ^o .1887	38 ^o .5608	0.1	0.98	0.98	0.83	0.87		Cüreoğlu, 2002
Van İsk.	43 ^o .2925	38 ^o .5364	0.1	1.16	1.16	1.25	1.24		Cüreoğlu, 2002
İnköy	42 ^o .9469	38 ^o .4136	0.1	1.16	1.16	1.05	0.81		Cüreoğlu, 2002
Akdamar	43 ^o .0148	38 ^o .3443	0.1	1.07	1.07	1.07	0.96		Cüreoğlu, 2002
				08 Temmuz 2014					
Örnek-1	43 ^o .1080	38 ^o .5232	0.1	1.73					Olğun-Kıyak ve Çağatay, 2015
Örnek-2	43 ^o .1863	38 ^o .5214	0.1	1.70					Olğun-Kıyak ve Çağatay, 2015
Örnek-3	43 ^o .3075	38 ^o .5161	0.1	7.79					Olğun-Kıyak ve Çağatay, 2015

2.2. CBS ile Klorofil-a Analizi

Van Gölüne ait Tablo 1’de sunulan klorofil-a ölçme verilerini kullanarak klorofil-a mekânsal dağılımları için her veri setine CBS ve uzaktan algılama yöntemi uygulanması hedeflenmiştir. Tüm veri setleri için klorofil-a çalışmalarında kullanılan farklı algılayıcılara ait uydu veri tabanları taranmıştır. Ancak 1983-84 ve 2002 verileri için yapılan uydu görüntüsü veri tabanı taramasında ilgili algılayıcılarda söz konusu yıllar için veri bulunmadığı tespit edilmiştir. Bu nedenle, 1983-84 ve 2002 klorofil-a dağılımları için sadece CBS yöntemi kullanılmıştır. Tablo 1’de sunulan ve üç istasyondan oluşan 8 Temmuz 2014 yılı klorofil-a dağılımları için en yakın tarihli uydu verisi sadece Landsat-8 OLI algılayıcısından (11 Temmuz 2014 görüntüsü) temin edilmiştir. Ancak, 2014 yılı verilerinin alındığı istasyonlara ait lokasyonların aşağıda bahsedilen CBS yönteminde uygulanacak enterpolasyona uygun olmamasından dolayı bu yıla ait veriler sadece uzaktan algılama ile elde edilen klorofil-a verilerinin doğruluk analizinde kullanılmıştır.

Klorofil-a verilerin bir araya getirilmesi, işlenmesi, yönetilmesi, görselleştirilmesi, sorgulama ve analiz edilmesi, CBS çalışmalarında çok yaygın bilinen ArcGIS Desktop 10.6.1 ESRI™ yazılımında yapılmıştır. Farklı modüller (3D Analyst, Spatial Analyst, Geostatistical Analyst gibi) barındıran özelliği ile gölde yapılan önceki çalışmalardan elde edilen klorofil-a ölçme verileri kullanılarak değerlendirilmiştir. Bu veriler, Tablo 1’de verilmiştir.

Gölde klorofil-a parametresine yönelik su örneklerinde yapılan ölçme verileri ve bu çalışmadan elde edilen bulgularla birlikte bölgede klorofil-a değişiminin nasıl bir eğilim gösterdiği mekânsal analizlerle ortaya çıkarılmıştır. Klorofil-a konsantrasyonunun tespitine yönelik olan bu bulgular, uzaktan algılama teknolojisi ile yersel ölçmelerle, spektrofotometrik yöntemlerin kullanılmasıyla elde edilmiştir.

İnceleme alanında farklı dönemlere (ve su derinliklerine) ait alınan su örneklerinden ölçülen klorofil-a değerlerine ait sonuçlar, CBS çalışmalarında kullanılan yazılımda kullanılabilecek uygun formatta kaydedilmiştir. Daha sonra her noktaya ait veri değerlerini içeren bu dosya, ilgili yazılımda hazırlanan veri katmanı ile ilişkilendirilmiştir. Böylece, “klorofil-a değerleri” ölçülen ay ve yıllar için ayrı ayrı CBS’nin analiz modüllerinden yararlanılarak değerlendirilmiştir.

CBS’de yapılan analizlerde, farklı enterpolasyon (ara değer bulma) yöntemleri kullanılmaktadır [11,61-63]. Farklı parametrelerin ayrı şekilde haritalanmasına yönelik sunulan bu yöntemlerin temel amacı, genellikle ilgili ortamdaki mekânsal dağılımların ortaya çıkarılmasıdır. IDW enterpolasyon metodu olarak bilinen bu yöntemde, bilinmeyen konumdaki değerlerin bir ağırlık fonksiyonu kullanılarak bilinen konumlar üzerinden en uygun konumun bulunmasına dayanan mekânsal bir algoritmadır [11,61-63].

İnceleme alanında CBS’de yapılan analizde, noktasal özellikte olan “klorofil-a” değerlerini enterpolasyon algoritması kullanarak mekânsal dağılımın nasıl olduğuna dair bir tahmin modeli oluşturulmuştur. Ardından ara değerler tahmin edilip, daha net analiz yapılması sağlanmıştır. Enterpolasyon yaparken kullanılan yöntemler genel olarak ikiye ayrılır: Bunlar Ters Mesafe Ağırlıklandırma (Inverse Distance Weighting, IDW) ve Kriging enterpolasyon metotlarıdır [64]. IDW enterpolasyon metodunda, veri girişi yapılmış konumlara sayısal olarak yakın ve mantıklı veriler atanması esastır. Bu metot ile enterpole edilecek noktadan uzaklaştıkça ağırlığı azaltan ve örnekleme noktalarının ağırlıklı ortalamasına göre bir mekânsal dağılım yüzeyi oluşturur. CBS analizi ile örneklenmemiş alanlarda (yeterli verinin olmadığı) istenilen öznetelik bilgilerini ve mekânsal olarak dağılımını tahmin etmek kullanılan en iyi enterpolasyon yöntemlerinden biridir. Önceden örneklenmiş klorofil-a konsantrasyon verileri nokta kaynak tabanlıdır ve CBS tekniği kullanılarak, bunlar, hücre tabanlı (grid) görüntü verilerine dönüştürülür. Böylece, değerleri bilinmeyen noktaların yakınındaki kontrol noktalarından uzak noktalara göre daha fazla etkilendiği varsayılarak oluşturulan mekânsal haritalar

üretilebilmektedir [65,66]. Çalışma bölgesinde, IDW metodu kullanılarak enterpole edilmiş ve sonuçta klorofil-a değerlerine ait verilerden alansal verilere dönüşen grid formatında katmanlar oluşturulmuştur. Hazırlanan bu veri katmanları CBS kapsamında değerlendirilerek Van Gölü'ne ait klorofil-a konsantrasyonlarının mekânsal dağılım modeli ile tematik haritaları elde edilmiştir (Şekil 4 ve 5).

2.3. Uydu Görüntüsü ile Klorofil-a Tahmin Analizi

Van Gölü klorofil-a uydu görüntü analizleri için okyanus, deniz ve göl araştırmalarında önceki çalışmalarda yaygın olarak kullanılan OLCI, SLSTR, VIIRS, MERIS, MODIS-Aqua, SeaWiFS ve OLI [12,14,15,34,41,67-69] farklı uydu veri tabanları taranmıştır. Sadece 2014 yılı verileri için Landsat-8 uydusuna ait OLI algılayıcısından uydu görüntüsü elde edilebilmiştir.

Çalışmada kullanılan Landsat-8 OLI (Seviye 2) 11.07.2014 tarihli uydu görüntüsü, Amerikan Jeoloji Servisi (USGS-Earth Explorer) internet sitesinden temin edilmiştir. Landsat-8 uydusu; OLI ve TIRS algılayıcıları ile görünür, yakın-kızılötesi, kısa dalga kızılötesi ve termal kızılötesi spektral aralıklarda görüntü almakta olup, bu aralığa bağlı olarak mekânsal çözünürlüğü 15 ile 100 metre arasında değişmektedir. Landsat-8 OLI bant 1 (kıyısıl/aerosol) veya diğer adıyla derin mavi (mavimsi) bantın (0.433-0.453 nm dalga boyu aralığı), mekânsal çözünürlüğü 30 m'dir. Söz konusu spektral bant ile su kalitesinin belirlenmesinin yanı sıra sudaki klorofil-a konsantrasyonu ile askıda katı madde, fitoplankton ve alg patlamalarını izlemek için de kullanılmaktadır [70]. Ayrıca, mavi ve mor rengi yansıttığı bilinen bu bant aralığında suyun rengindeki küçük farklılıklar belirlenebildiğinden renk yoğunluğundaki bu farklılıklar suya neyin karıştığı konusunda da bilgi çıkartılmasına olanak sağlamaktadır.

Diğer yandan, dünyanın farklı bölgelerinde bir su kütlelerinde birçok parametre belirlemek için yapılan çalışmalarda, su örneklemelerinin zamansal ve mekânsal olarak yeterli sayıda olması ve bunların uzaktan algılama yöntemi kullanılarak tahmin yapılması ile elde edilen performanslar değişkendir. Örneğin, Giardino vd. [71] İtalya'daki bir gölde klorofil-a konsantrasyonlarını belirlemek için kullandığı Landsat uydu görüntüsü ile elde edilen temsiliyet kapasitesi değerlendirildiğinde korelasyon katsayısı (R^2), 0.99 olarak elde edilmiştir. Ancak bu yüksek sayı, yalnızca 4 nokta ile elde edilen bir değerdir. Nelson vd. [72] incelenen su kütlelerinde zamana bağlı büyük değişimin olmadığı durumlarda veri alınma zamanlamaları arasındaki farkın klorofil-a tayinindeki başarıyı etkilemeyeceğini de belirtmiştir. Li vd. [65]'teki çalışmasında uzaktan algılama ve mevcut örnekleme sayısı kullanılarak yapılan optimizasyon ile su kalitesini parametrelerinin değerlendirilme aşamasında, en azından çalışılan bölgede ön bilgi olarak hizmet edebileceğini belirtmişlerdir. Buradan hareketle, bu çalışma kapsamında sınırlı sayıda ölçülen klorofil-a değerleri kullanılarak uzaktan algılama verilerine entegre edilmiştir.

Uzaktan algılama verileri ile su kalitesi belirleme amaçlı yapılan çalışmalar, genel olarak istatistik analizlerin kullanıldığı ampirik ve yarı ampirik yöntemler ile daha çok spektral bilginin teorik analizinin gerçekleştirildiği yarı analitik ve analitik yöntemler olmak üzere gruplandırılırlar [73,74]. Ampirik yöntemlerde su kalitesi parametreleri ile çeşitli bantlar, bant oranları vb. ile regresyon ya da korelasyon analizleri yapılırken, yarı ampirik yöntemlerde ise istatistiksel analizlerin yanı sıra spektral ölçümlere de ihtiyaç duyar. Bu çalışmada ampirik yöntem kullanılmış, yersel ölçümler ile uydu görüntüsünden elde edilen sonuçlar arasındaki ilişki incelenmiş ve su yüzeyindeki dağılımlar belirlenerek doğruluk analizi yapılmıştır. Ayrıca, kırmızı ve yakın kızılötesi spektral bant aralığına (655-865 nm dalga boyu) sahip Landsat TM, ETM+ ve OLI gibi multi-spektral algılayıcılar ile kırmızı ve kızılötesi spektral bant yansıma oranlarının kullanılmasının, klorofil-a'nın tahmini için uygun olmadığı da belirlenmiştir [14].

Sucul ortamlarda klorofil-a tahminine yönelik geliştirilen algoritmalar, genellikle klorofil-a'nın su yüzeyindeki bir biriminde güneş ışığının emilme (absorpsiyon) ve yansıma (reflektans) modelleri üzerine kurulmaktadır (Şekil 3). Bunlar genellikle aşağıda detayları verilen farklı iki spektral bant oranına dayanan modellerdir [19,36].

Literatürde de kabul gören bu modellerin ayrıntıları şu şekildedir (Şekil 3);

1) 440 ve 510 nm (spektral aralık) dalga boyu arası (mavi-spektral bant) bölgedeki en güçlü emilimin ilk tepe noktası ile 550 ve 555 nm dalga boyu arası (yeşil-spektral bant) bölgedeki en düşük emilimin yansıma oranı [75-77] (Şekil 3),

2) 685 ve 710 nm arası dalga boyuna sahip yakın-kızılötesi (NIR-near infrared spektral bant) bölgedeki emilimin en düşük noktası ile 670 ve 675 nm dalga boyu arası (kırmızı-spektral bant) bölgedeki ikinci en tepe noktasındaki emilimin yansıma oranı [33,78-81] (Şekil 3),

3) Son olarak, 670 ve 675 nm dalga boyu arası (kırmızı-spektral bant) bölgedeki emilimin ikinci tepe noktası ile 550 ve 555 nm dalga boyu arası (yeşil-spektral bant) bölgedeki en düşük emilimin yansıma oranı ile ifade edilen algoritmalarıdır [82] (Şekil 3).

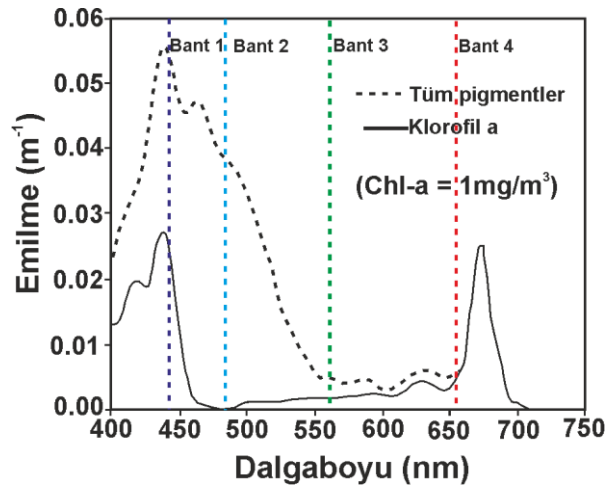
Çalışma kapsamında Landsat-8 OLI uydu görüntüsünden bilgi çıkartmak amacıyla görüntü işleme adımları SNAP (Sentinel Uygulama Platformu) ücretsiz yazılımında gerçekleştirilmiştir. Daha sonra uydu görüntüsüne, önce görüntü zenginleştirme, daha sonra da spektral bant oranlaması ilgili algoritmalar uygulanmıştır. Bu algoritmalar, klorofil-a tahmini için, iki farklı yeşil-mavi bant oranlamasıdır. [14] tarafından geliştirilen bu tahmin algoritmaları, R(562)/R(443) ve R(562)/R(483) bant oranları ile elde edilmiştir. Landsat-8 OLI algılayıcısının sadece bir adet yakın-kızılötesi bant bulunduğundan çalışmada kullanılan görüntüye bu iki bant oranları uygulanmıştır.

SNAP yazılımında bant oranlama tekniği ile uygulanan algoritma sonucunda elde edilen klorofil-a değerlerine dönüşüm aşağıdaki eşitlikler (2.2) ve (2.3) ile elde edilmiştir. Bu dönüşüm denklemi literatürde de sıklıkla kullanılan eşitliklerdir [14].

$$\text{Model 1 için; Chl-a (mg/m}^3\text{)} = ae^{b \times GrB1}; a = 0.04709, b = 4.001 \quad (2.2)$$

$$\text{Model 2 için; Chl-a (mg/m}^3\text{)} = ae^{b \times GrB2}; a = 0.008155, b = 6.081 \quad (2.3)$$

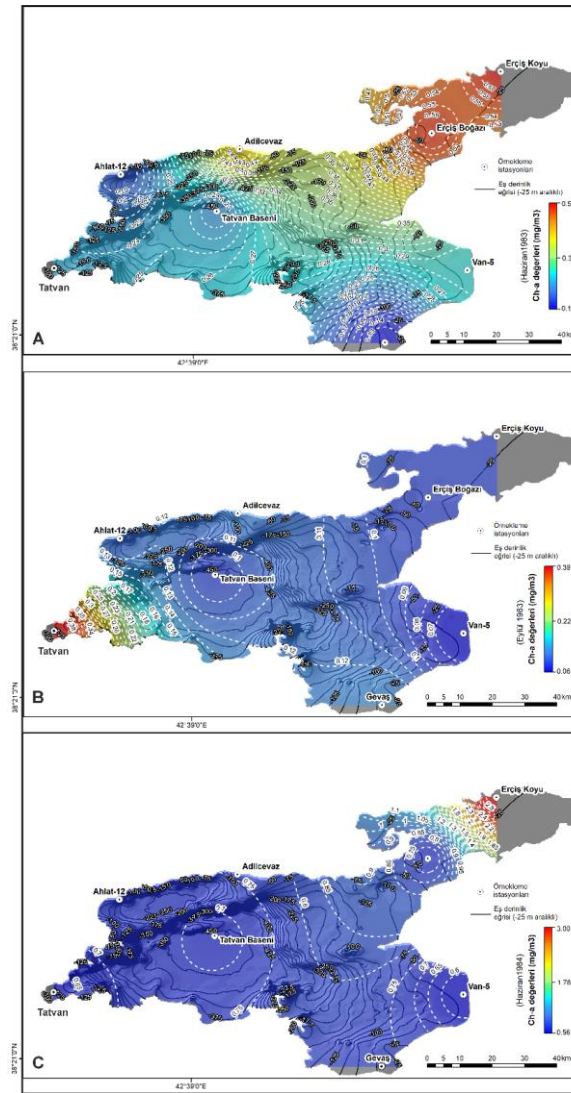
Denklemlerde kullanılan katsayılar a ve b ile e ise doğal logaritma tabanını (Euler sayısı) ifade etmektedir.



Şekil 3. Landsat-8 OLI çok bantlı uydu görüntüsünün görünür ve yakın-kızılötesi bölgelerdeki dört bantına (mavi, yeşil, kırmızı ve yakın kızılötesi spektral bantlar) ait dalga boyları ile 1 mg/m³ deki klorofil-a ve toplam pigmentin emilme miktarları ([83]'den düzenlenerek alınmıştır)

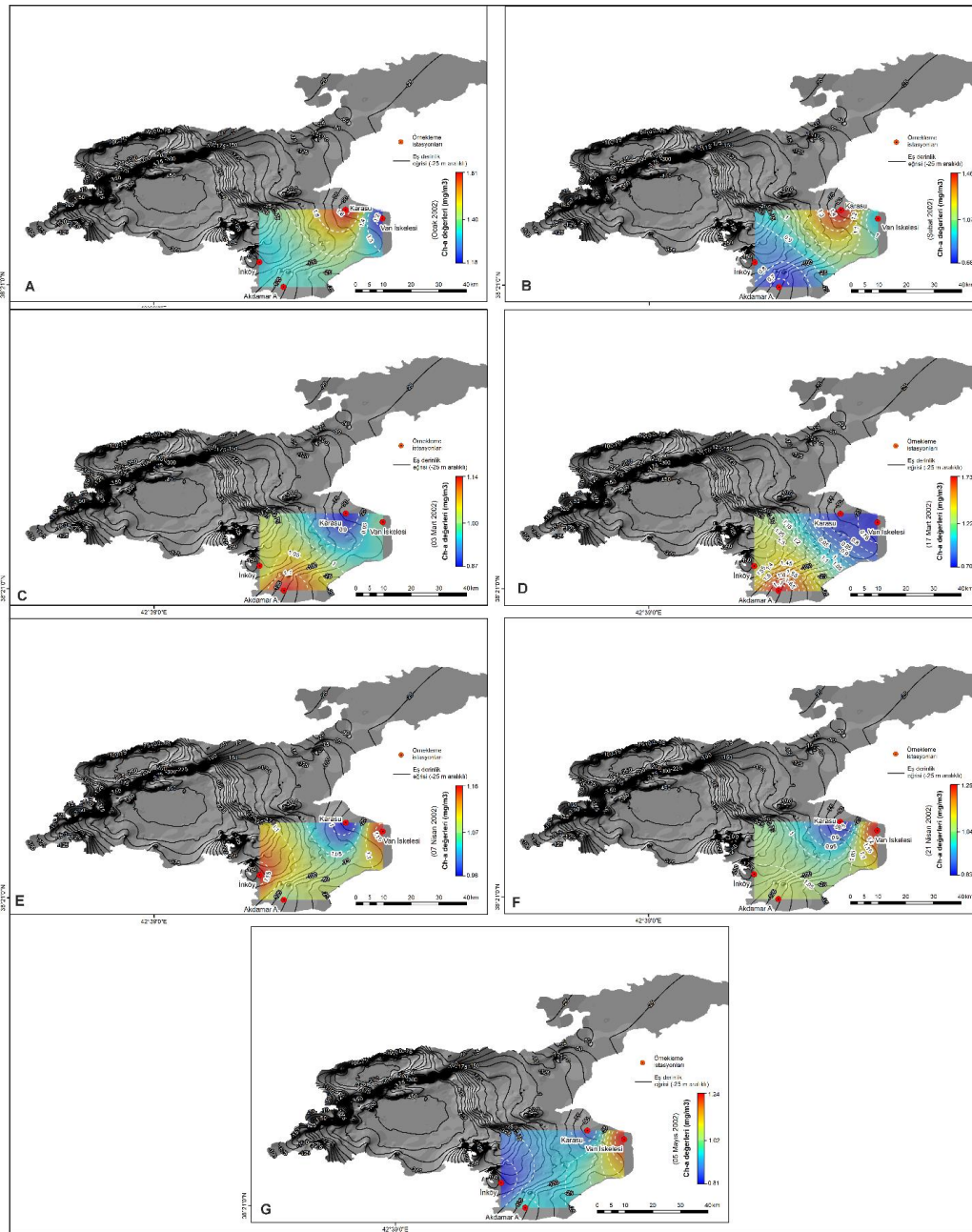
3. Bulgular ve Tartışma

Van Gölü klorofil-a mekânsal dağılımları için Tablo 1’de sunulan ölçme verileri için 1983-84 (Şekil 4) ve 2002 (Şekil 5) yılları verileri CBS yöntemi ile 2014 (Şekil 7) yılı verileri uzaktan algılama yöntemiyle incelenmiştir. 1983-84 verilerine ait ilgili çalışmanın istasyon dağılımları gölün genelini temsil edecek nitelikte olduğu gözlenmiştir (Şekil 4). Sırasıyla, Haziran 1983, Eylül 1983 ve Haziran 1984 yılları için oluşturulan klorofil-a dağılımları incelendiğinde Haziran ayında klorofil-a konsantrasyonu gölün batısında düşük iken doğusunda daha yüksektir (Şekil 4). Gölde gözlenen en yüksek klorofil-a konsantrasyonu 1.73 mg/m^3 , en düşük ise 0.06 mg/m^3 ’dür. Kış mevsiminde 1.73 mg/m^3 ile yüksek, yaz mevsiminde de 0.12 mg/m^3 ile daha düşük bir klorofil-a konsantrasyon değerleri gözlenmiştir (Şekil 4). Aynı ay için Haziran 1983 ve Haziran 1984 klorofil-a dağılımları incelendiğinde iki tarihte de gölün kuzeyinde yer alan Erciş ve yakın civarında klorofil-a yoğunlaşması olduğu görülmüştür. 1983 yılı için yaz ve sonbahar dönemi incelendiğinde sonbaharda klorofil-a değerlerinin gölün güneybatısında yer alan Tatvan bölgesinde göreceli daha yüksek olduğu gözlenmiştir (Şekil 4). En yüksek klorofil-a konsantrasyonları Haziran 1984 döneminde ($0.6-3.0 \text{ mg/m}^3$) ve en fazla kuzeyde Erciş Koyu bölgesinde gözlenmiştir (Şekil 4c). Sonbahar dönemi başını içeren Eylül ayı ile Haziran 1983 ve 1984 kıyaslandığında Eylül ayı klorofil-a değerlerinin görece düşük seviyede olduğu görülmüştür.



Şekil 4. Van Gölü’nde a) Haziran 1983, b) Eylül 1983 ve c) Haziran 1984 yıllarında elde edilen klorofil-a konsantrasyonlarının IDW metoduyla elde edilen mekânsal dağılımları

CBS yöntemiyle değerlendirilen 2002 yılı Ocak, Şubat, Mart, Nisan ve Mayıs aylarında gölün güneydoğusunda yer alan Karasu, Van, Akdamar ve İnköy kıyı ve açıklarında alınan ölçmeler Şekil 5'te sunulmuştur. İstasyon lokasyonlarının dağılımı nedeniyle, gölün sadece güney ve güneydoğu kısımlarındaki klorofil-a mekânsal dağılımları kapsamaktadır. Buna göre, örnekleme bölgesinde düşük klorofil-a değerleri 0.68-1.87 mg/m³ arasında değişmektedir. Klorofil-a konsantrasyon dağılımları incelendiğinde belirgin bir mekânsal patern izlenmemektedir. Ocak ve Şubat 2002 tarihlerinde klorofil-a yoğunluklarının kuzeyde yer alan Karasu Bölgesi'nde (Şekil 5a ve 5b), Mart 2002 döneminde ise güneyde yer alan Akdamar bölgesinde (Şekil 5c ve 5c), Nisan 2002 döneminde güneyde İnköy ile doğuda Van İskelesi (Şekil 5d ve 5e) ve Mayıs 2002 döneminde ise Van iskelesinde yüksek olduğu gözlenmektedir (Şekil 5f). 2002 yılı kış (Ocak, Şubat) ve bahar (Mart, Nisan, Mayıs) döneminde klorofil-a konsantrasyon değerleri kıyaslandığında bahar döneminde beklenen klorofil-a artışları görülmemiş ve belirgin bir fark izlenmemiştir.

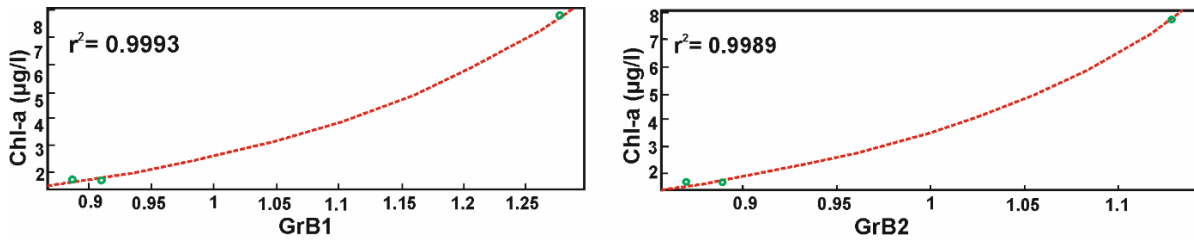


Şekil 5. Van Gölü'nde a) Ocak 2002, b) Şubat 2002, c) 03 Mart 2002, d) 17 Mart 2002, e) 07 Nisan 2002, f) 21 Nisan 2002 g) 05 Mayıs 2002 yıllarında elde edilen klorofil-a konsantrasyonlarının CBS analizi ile elde edilen mekânsal dağılımları

Temmuz 2014 dönemi için Van Gölü'nde klorofil-a tahminine yönelik olarak yapılan uzaktan algılama çalışmasında, Landsat-8 OLI algılayıcısının elektromanyetik spektrumun mavi bölgesinde, 443 nm spektral banta sahip kıyısal (coastal/aerosol) bantı (bant 1) ile ve 483 nm spektral banta sahip mavi (bant 2) bant arasındaki oran ile tespit edilmiştir. Çünkü klorofil-a'nın su yüzeyindeki bir biriminde güneş ışığını emilimi bant 1 ile ilk tepe noktasına, bant 2 ile tüm pigmentlerdeki emilim en tepe noktasına ulaşılır (Şekil 3). Yeşil ışığın yansımalarının da, 562 nm dalga boyunda yer alan bant 3 ile elde edildiği görülmüştür (Şekil 3).

Bu bilgiler ışığında göl yüzeyinde klorofil-a'nın tahmini için iki farklı yeşil-mavi spektral bant oranlamasına dayanan algoritmalar kullanılmıştır. [14] tarafından geliştirilen ve GrB1 ve GrB2 olarak adlandırılan bu tahmin algoritmaları, $R(562)/R(443)$ ve $R(562)/R(483)$ bant oranları ile elde edilmiştir (Şekil 6 ve 7).

Daha sonra iki farklı bant oranlarını ile elde edilen bu algoritmaların karşılaştırılması ve geçerli olabilmesi için aynı zaman aralığında (08 Temmuz 2014) yapılan spektral ölçme ile göldeki su örneklemeleri Landsat-8 OLI uydu görüntüsüne uygulanmıştır (Şekil 7a). Böylece her pikseldeki su yüzeyi referansları, 08 Temmuz 2014'te saha çalışmaları ile Van Gölü'nün üç farklı lokasyonunda ölçülen klorofil-a veri kümesinden elde edilen ile en iyi iki bant oranının belirlenmesi ile sağlanmıştır.



Şekil 6. Van Gölü'nde 11.07.2014 tarihinde üç istasyonda ölçülen klorofil-a değerleri ve Landsat 8/OLI görüntüsüne uygulanan GrB1 ($r^2 = 0.9993$; Karesel ortalama hata= 0.2 mg/m^3) ile GrB2 ($r^2 = 0.9989$; Karesel ortalama hata= 0.1 mg/m^3) algoritmalarından elde edilen klorofil-a tahmin değerleri arasındaki ilişki

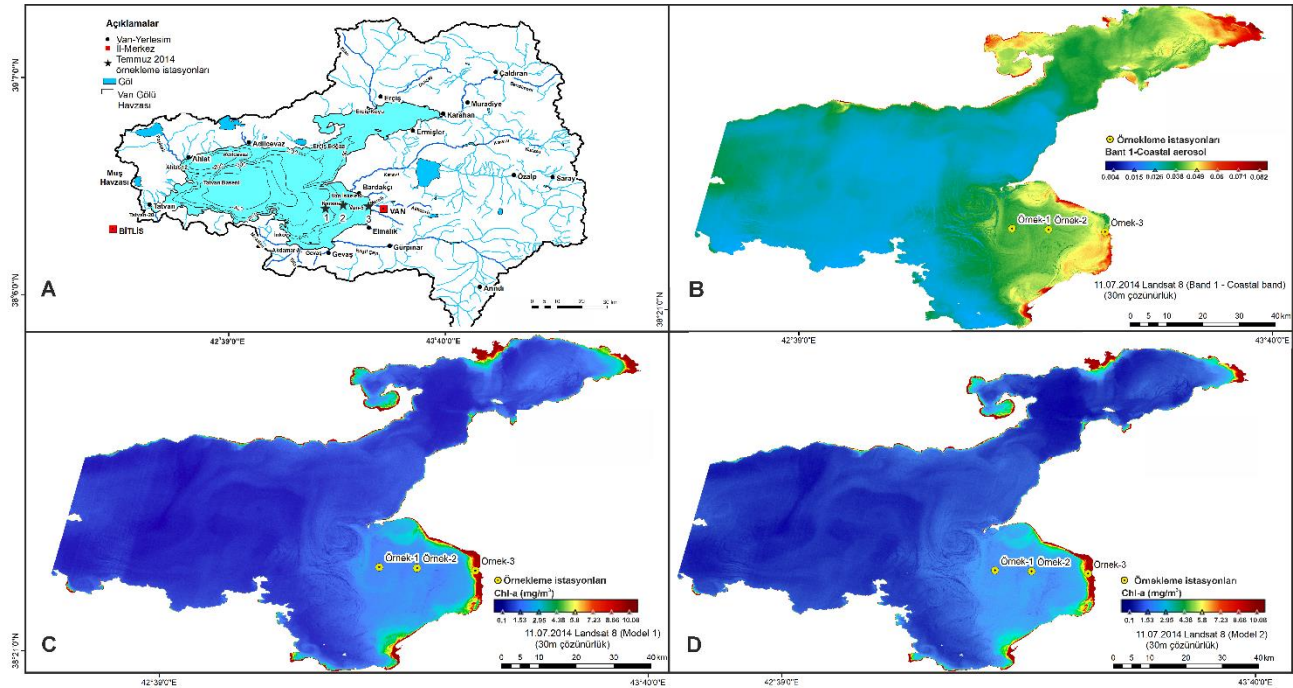
Landsat-8 OLI uydu görüntüsüne uygulanan GrB1 ve GrB2 algoritmalarından elde edilen klorofil-a tahmin değerleri $0.1\text{-}10.08 \text{ mg/m}^3$ aralığındadır (Şekil 7b ve 7c). Klorofil-a tahmini için ilgili uydu görüntüsüne iki model (farklı bant kombinasyonu) uygulanarak klorofil-a tahmin haritaları üretilmiştir (Şekil 7b ve 7c). Yersel veri olarak üç ölçme noktası kullanılarak ulaşılan bulgular birbiriyle karşılaştırılmıştır. Elde edilen veriler karşılaştırıldığında, GrB1 ve GrB2 olarak sunulan ampirik modellerin karesel ortalama hatasının 0.1 mg/m^3 'e kadar düştüğü tespit edilmiştir (Tablo 2). Bu durum, örnek sahası ortalama konsantrasyonlarının göl çapındaki ortalama konsantrasyonu temsil ettiğini de göstermektedir. Seçilen oran modelinin doğruluğu karşılaştırmak için de elde edilen konumsal doğrulukların ölçme hatalarının içerisinde kaldığı belirlenmiştir (Tablo 2).

Tablo 2. Van Gölü üç farklı lokasyonda ölçülen verileri kullanarak elde edilen klorofil-a tahmin değerleri ile iki farklı mavi-yeşil bant oranı arasındaki ilişkinin belirlenmesinde kullanılan regresyon eğrilerinin uygunluklarını gösteren parametreler

	Eşitlik	Üstel
Klorofil-a ve GrB ₁ (Tahmin modelindeki üstel eşitlik; $f(x) = ae^{bx}$ $a = 0.04709$; $b = 4.001$)	r^2	0.9993
	$F(1:8)$	-
	p -değeri	-
	Sig. (SSE)	0.01737
	Tahmini standart hata	0.1318
Klorofil-a ve GrB ₂ (Tahmin modelindeki üstel eşitlik; $f(x) = ae^{bx}$ $a = 0.008155$; $b = 6.081$)	r^2	0.9989
	$F(1:8)$	-
	p -değeri	-
	Sig. (SSE)	0.02607
	Tahmini standart hata	0.1615

Uydu verisi ile yersel ölçme verileri kıyaslandığında, Örnek-1, Örnek-2 ve Örnek-3 istasyonlarında 11 Temmuz 2014 tarihine ait Landsat-8 OLI algılayıcısı ile 1.53 mg/m^3 , 2.24 mg/m^3 ve 10 mg/m^3 üzerinde klorofil-a tahmin değerleri tespit edilirken, yersel ölçmeler ile aynı istasyonlarda 8 Temmuz 2014 tarihinde 1.73 mg/m^3 , 1.7 mg/m^3 ve 7.79 mg/m^3 olduğu görülmüştür. 2002 yılında Tablo 1'den de izlendiği üzere, Karasu ve Van İskelesi istasyonlarında 2002 yılı ilkbahar mevsimindeki klorofil-a değerlerinin, 2002 yılında diğer istasyonlarda ölçülenlere göre daha fazladır [41]. Bu çalışmada 11 Temmuz 2014 tarihli uydu verisinden elde edilen bulgulara göre bu lokasyonlara çok yakın istasyonlardan toplanan örneklerin klorofil-a değerleri de birbirine benzerdir (Şekil 7a ve 7b). Gölün doğusundaki bu bölgede klorofil-a değerlerinin fazla çıkmasının nedeni, olasılıkla Karasu akarsuyunun deşarjından kaynaklanmaktadır. Yağmurlarla beraber gelen ve mevsim itibariyle yüksek besin girdisi bulunan bu sulara klorofil-a miktarının yüksek çıkması beklenir [40,41]. Diğer önemli faktör ise Van iline yakın olan lokasyonların olasılıkla İl merkezine ait endüstriyel ve/veya kentsel atık tesislerinin yarattığı organik madde girişinin fazla olmasından dolayı klorofil-a konsantrasyonu bakımından zengin olduğu görülmüştür.

Bu çalışmada Van Gölü'ndeki klorofil-a konsantrasyonlarının belirlenmesi amaçlandığından klorofil-a'nın tahminine yönelik olarak hem Landsat-8 OLI uydu görüntüsü hem de yer ölçmeleri ile çalışılmış ve doğruluk analizi gerçekleştirilmiştir. Bant oranlaması yöntemi kullanarak oluşturulan görüntü ile tespit edilen klorofil-a değerleri, Landsat-8 OLI çok bantlı uydu görüntüsünün görünür ve yakın-kızılötesi bölgelerdeki dört bantına (mavi, yeşili kırmızı ve yakın kızılötesi) ait dalga boylarının yansımaya ve emilme miktarı ile elde edilmiştir.



Şekil 7. a) Van Gölü ve yakın çevresinin hidroloji haritası, b) 11 Temmuz 2014 yılına ait Landsat-8 OLI algılayıcısının bant 1 (kıyasal/aerosol) spektral bandına ait görüntüsü, c) Landsat-8 OLI uydu görüntüsüne GrB1 ve d) GrB2 ampirik modeller uygulanarak üretilen klorofil-a tahmin haritaları

Göllerde genellikle ötrofikasyon ve organik madde üretimi çok fazla olmasına rağmen Van Gölü'nde tespit edilen durum görece daha az olduğunu göstermektedir. Van Gölü'nün 11 Temmuz 2014 tarihli Landsat-8 OLI uydu görüntüsü ile elde edilen klorofil-a haritası izlendiği Model 1 ve Model 2 kullanılarak elde edilen klorofil-a tahmin değerleri $0.10-10.08 \text{ mg/m}^3$ aralığındadır (Şekil 7b ve 7c). İki model arasında belirgin fark izlenmemektedir. Uydu görüntüsünde, klorofil-a yoğunlaşmalarının gölün doğu kıyılarında daha fazla olduğu görülmüştür. Buna göre, en yüksek klorofil-a değerleri kuzeydoğuda Muradiye-Karahan ve kuzeyde de Erciş

Koyu ve doğuda Van ili bölgelerinde izlenmiştir (Şekil 7). Yüksek mekânsal çözünürlükte (30 m) hazırlanan tematik haritalarda göldeki yüzey akıntı ve Örnek 1 açıklarında girdapların da iyi izlendiği görülmüştür (Şekil 7b ve 7c). Ayrıca, göldeki akıntı yönlerine bakıldığında, gölün güneydoğusunda yer alan Gevaş'tan başlayan akarsu girdisi, saat yönünün tersine hareket ederek Van'a doğru ilerlemektedir (Şekil 7). Kuzeydoğu 'da Muradiye civarında gölü kuzeyden besleyen önemli akarsular (Zilan, Deliçay ve Bendimahi) bulunmaktadır (Şekil 7a). Özellikle bu bölgede Muradiye ve Erçiş civarındaki nehir suyu etkisinin yüksek klorofil-a değerleri gözlenirken, gölün güneydoğusunda yer alan Adilcevaz ve Tatvan civarında bu etkinin oldukça az olduğu görülmüştür (Şekil 7b ve 7c).

11 Temmuz 2014 yılına ait Landsat-8 OLI algılayıcısının bant 1 (kıyasal/aerosol) spektral bantına ait görüntüsü incelendiğinde klorofil-a değerlerinin en düşük olduğu değerler ($0.1-1.5 \text{ mg/m}^3$) Van Gölü'nün güneybatı kısmında yer alan Tatvan Havzası'nda (-450 m) izlenmektedir (Şekil 7b). Su derinliğinin yüzey klorofil-a değerlerine olan etkileri önceki araştırmalarda da değinilmiştir. Örneğin, Arap ve Umman Körfezlerinde MODIS Aqua uydu algılayıcısı kullanılarak gerçekleştirilen bir çalışmada, klorofil-a değerleri ile su derinliği arasında negatif bir korelasyon olduğu tespit edilmiştir [84]. Van Gölü'ndeki OLI algılayıcısı ile elde edilen en düşük klorofil-a değerlerinin batimetriye bağlı dip yansıma etkisinden kaynaklanması muhtemeldir (Şekil 7b).

4. Sonuçlar

Bu çalışmada, Van Gölü klorofil-a konsantrasyon dağılımları literatürde yer alan ölçme verileri kullanılarak CBS (IDW metodu) ve uzaktan algılama (Landsat-8 OLI algılayıcısı) metotları kullanılarak modellenmiştir. Van Gölü'nde klorofil-a ölçme verilerinin oldukça kısıtlı olduğu gözlenmiştir. 1983-84 ve 2002 yıllarına ait klorofil-a verileri IDW metodu kullanılarak mekânsal olarak incelenmiştir. 1983-84 ve 2002 yersel verileri içeren uydu görüntülerine ait veri tabanlarında klorofil-a konsantrasyonunda yaygın kullanılan hiçbir algılayıcıda bu yıllara ait uygun veri seti bulunmamıştır. 2014 yılına ait Landsat-8 OLI uydu görüntüsünden GrB1 ve GrB2 olarak adlandırılan algoritmalar kullanılarak klorofil-a tahmin değerleri bulunmuştur. Az sayıdaki 2014 yılı klorofil-a ölçmelerinin IDW metoduyla yapılan incelemede uygun olmadığı tespit edilmiştir. Klorofil-a yoğunlaşmalarının kuzeyde Erçiş kuzeydoğuda Muradiye-Karahan, doğuda Van İli ve güneydoğuda Gevaş ve İnköy açıklarında gölün batısına göre daha yüksek olduğu görülmektedir. Kullanılan iki metot kıyaslandığında, uydu verisi ile elde edilen klorofil-a konsantrasyon değerleri, sınırlı veri seti olmasına rağmen gölün genelindeki temsiliyeti yeterli doğrulukta ve yüksek çözünürlükte elde edilebilmiştir. CBS'de IDW metodu ile gölün geneline yönelik temsiliyet için geniş bir istasyon dağılımı gereklidir. Bu çalışmadaki uzaktan algılama teknolojisi kullanılarak uygulanan modeller takip edilerek önemli bir su kalitesi parametresi olan klorofil-a konsantrasyonlarının Van Gölü'ndeki zamansal ve mekânsal değişimlerinin incelenmesi tavsiye edilir.

Yazar Katkıları

İkinci yazar projeyi yönetmiştir. Her iki yazar kavramsal fikirleri tasarlamış ve teorik çerçeveyi geliştirmiştir. İkinci yazar, saha çalışmaları ile klorofil-a deneylerini gerçekleştirmiş ve birinci yazar da CBS ve uydu görüntülerinin analizini planlamış ve tasarlamıştır. Birinci yazar ve ikinci yazar bu çalışmanın bulgularını denetlemiştir. Birinci yazar, makaleyi yazmış ve temel şekil ve grafikleri hazırlamıştır. İkinci yazar makaleyi gözden geçirmiş, çalışmanın analizlerini yorumlamış ve makalenin son haline getirilmesini sağlamıştır.

Çıkar Çatışması

Yazarlar hiçbir çıkar çatışması olmadığını beyan etmektedir.

Teşekkür

Bu çalışmada kullanılan Van Gölü 2014 seferi verileri, Avrupa Birliği Marie Curie Cofund 'Environmental impacts of subaerial volcanic eruptions on alkaline lakes—A case study on Lake Van in eastern Turkey (EVOLVAN)' başlıklı projesi ve TÜBİTAK 112C001 nolu proje desteği ile elde edilmiştir. Van Gölü batimetri verileri için Dr. Deniz Çukur'a ve ICDP PaleoVan Projesi ekibine de teşekkür ederiz.

Kaynaklar

- [1] A. Reimer, G. Landmann, S. Kempe, *Lake Van, Eastern Anatolia, hydrochemistry and history*, Aquatic Geochemistry 15 (1–2) (2009) 195–222.
- [2] S. Kempe, J. Kazmierczak, G. Landmann, T. Konuk, A. Reimer, A. Lipp, *Largest known microbialites discovered in Lake Van, Turkey*, Nature 349 (6310) (1991) 605–608.
- [3] L. Daoji, D. Daler, *Ocean pollution from land-based sources: East China Sea, China*, Ambio 33 (1/2) (2004) 107–113.
- [4] S. Garrido, R. Ben-Hamadou, P. B. Oliveira, M. E. Cunha, M. A. Chícharo, C. D. Van Der Lingen, *Diet and feeding intensity of sardine *Sardina pilchardus*: Correlation with satellite-derived chlorophyll data*, Marine Ecology Progress Series 354 (2008) 245–256.
- [5] N. Olgun, S. Duggen, B. Langmann, M. Hort, C. F. Waythomas, L. Hoffmann, P. Croot, *Geochemical evidence of oceanic iron fertilization by the Kasatochi volcanic eruption in 2008 and the potential impacts on Pacific sockeye salmon*, Marine Ecology Progress Series 488 (2013) 81–88.
- [6] A. Tuzcu Kokal, N. Olgun, N. Musaoğlu, *Detection of mucilage phenomenon in the Sea of Marmara by using multi-scale satellite data*, Environmental Monitoring and Assessment 194 (585) (2022) 194–585.
- [7] X. M. Chuai, X. Chen, L. Yang, J. Zeng, A. Miao, H. Zhao, *Effects of climatic changes and anthropogenic activities on lake eutrophication in different ecoregions*, International Journal of Environmental Science and Technology 9 (2012) 503–514.
- [8] M. Nazari-Sharabian, S. Ahmad, M. Karakouzian, *Climate change and eutrophication: A short review*, Engineering, Technology and Applied Science Research 8 (6) (2018) 3668–3672.
- [9] B. Bardakçı Şener, E. M. Tıraşın, A. Ünlüoğlu, *The influence of lake level fluctuations on fisheries in Lake Van*, Journal of Limnology and Freshwater Fisheries Research, 7 (2) (2021) 157–165.
- [10] O. Holm-Hansen, M. Kahru, C. D. Hewes, S. Kawaguchi, T. Kameda, V. A. Sushin, I. Krasovski, J. Priddle, R. Korb, R. P. Hewitt, B. G. Mitchell, *Temporal and spatial distribution of chlorophyll-a in surface waters of the Scotia Sea as determined by both shipboard measurements and satellite data*, Deep-Sea Research Part II: Topical Studies in Oceanography, 51 (12-13) (2004) 1323–1331.
- [11] X. J. Wang, R. M. Liu, *Spatial analysis and eutrophication assessment for chlorophyll a in Taihu Lake*, Environmental Monitoring and Assessment 101 (1–3) (2005) 167–174.
- [12] A. Abdul-Hadi, S. Mansor, B. Pradhan, C. K. Tan, *Seasonal variability of chlorophyll-a and oceanographic conditions in Sabah waters in relation to Asian monsoon - A remote sensing study*, Environmental Monitoring and Assessment 185 (5) (2013) 3977–3991.

- [13] C. Giardino, M. Bresciani, D. Stroppiana, A. Oggioni, G. Morabito, *Optical remote sensing of lakes: An overview on Lake Maggiore*, *Journal of Limnology* 73 (1) (2014) 201–214.
- [14] N. T. T. Ha, K. Koike, M. T. Nhuan, B. D. Canh, N. T. P. Thao, M. Parsons, *Landsat 8/OLI Two bands ratio algorithm for chlorophyll-a concentration mapping in hypertrophic waters: An application to west lake in Hanoi (Vietnam)*, *IEEE Journal of Selected Topics in Applied Earth Observations and Remote Sensing* 10 (11) (2017) 4919–4929.
- [15] R. C. Trinh, C. G. Fichot, M. M. Gierach, B. Holt, N. K. Malakar, G. Hulley, J. Smith, *Application of Landsat 8 for monitoring impacts of wastewater discharge on coastal water quality*, *Frontiers in Marine Science* 4 (2017) 17 pages.
- [16] C. Cheng, Y. Wei, G. Lv, N. Xu, *Remote sensing estimation of chlorophyll-a concentration in Taihu Lake considering spatial and temporal variations*, *Environmental Monitoring and Assessment* 191 (84) (2019) 25 pages.
- [17] R. W. Johnson, R. C. Harriss, *Remote sensing for water quality and biological measurements in coastal waters*, *Photogrammetric Engineering and Remote Sensing* 46 (1) (1980) 77–85.
- [18] J. P. Verdin, *Monitoring water quality conditions in a large Western reservoir with Landsat imagery (USA)*, *Photogrammetric Engineering and Remote Sensing* 51 (3) (1985) 343–353.
- [19] A. G. Dekker, S. W. M. Peters, *The use of the thematic mapper for the analysis of eutrophic lakes: A case study in the Netherlands*, *International Journal of Remote Sensing* 14 (5) (1993) 799–821.
- [20] M. Mayo, A. Gitelson, Y. Z. Yacobi, Z. Ben-Avraham, *Chlorophyll distribution in Lake Kinneret determined from Landsat Thematic Mapper data*, *International Journal of Remote Sensing* 16 (1) (1995) 175–182.
- [21] R. K. Vincent, X. Qin, R. M. L. McKay, J. Miner, K. Czajkowski, J. Savino, T. Bridgeman, *Phycocyanin detection from LANDSAT TM data for mapping cyanobacterial blooms in Lake Erie*, *Remote Sensing of Environment* 89 (3) (2004) 381–392.
- [22] A. N. Tyler, E. Svab, T. Preston, M. Présing, W. A. Kovács, *Remote sensing of the water quality of shallow lakes: A mixture modeling approach to quantifying phytoplankton in water characterized by high-suspended sediment*, *International Journal of Remote Sensing* 27 (8) (2006) 1521–1537.
- [23] T. P. Albright, D. J. Ode, *Monitoring the dynamics of an invasive emergent macrophyte community using operational remote sensing data*, *Hydrobiologia* 661 (1) (2011) 469–474.
- [24] J. Andrzej Urbanski, A. Wochna, I. Bubak, W. Grzybowski, K. Lukawska-Matuszewska, M. Łącka, S. Śliwińska, B. Wojtasiewicz, M. Zajączkowski, *Application of Landsat 8 imagery to regional-scale assessment of lake water quality*, *International Journal of Applied Earth Observation and Geoinformation* 51 (2016) 28–36.
- [25] J. Boucher, K. C. Weathers, H. Norouzi, B. Steele, *Assessing the effectiveness of Landsat 8 chlorophyll-a retrieval algorithms for regional freshwater monitoring*, *Ecological Applications* 28 (4) (2018) 1044–1054.
- [26] J. Lim, M. Choi, *Assessment of water quality based on Landsat 8 operational land imager associated with human activities in Korea*, *Environmental Monitoring and Assessment* 187 (2015) Article Number 384 17 pages.
- [27] A. P. Yunus, J. Dou, N. Sravanthi, *Remote sensing of chlorophyll-a as a measure of red tide in Tokyo Bay using hotspot analysis*, *Remote Sensing Applications: Society and Environment* 2 (2015) 11–25.
- [28] F. S. Y. Watanabe, E. Alcântara, T. W. P. Rodrigues, N. N. Imai, C. C. F. Barbosa, L. H. da S. Rotta, *Estimation of chlorophyll-a concentration and the trophic state of the barra bonita hydroelectric reservoir using Landsat-8/OLI images*, *International Journal of Environmental Research and Public Health* 12 (9) (2015)

10391–10417.

- [29] Z. Yang, Y. Anderson, *Estimating chlorophyll-A concentration in a freshwater lake using landsat 8 imagery*, Journal of Environment and Earth Science 6 (4) (2016) 134–142.
- [30] Y. M. Li, J. Z. Huang, Y. C. Wei, W. N. Lu, *Inversing chlorophyll concentration of Taihu Lake by analytic model*, Journal of Remote Sensing-Beijing 10 (2) (2006) 2–4.
- [31] R. P. Bukata, J. E. Bruton, J. H. Jerome, S. C. Jain, H. H. Zwick, *Optical water quality model of Lake Ontario 2: Determination of chlorophyll a and suspended mineral concentrations of natural waters from submersible and low altitude optical sensors*, Applied Optics 20 (9) (1981) 1704–1714.
- [32] K. Kallio, T. Kutser, T. Hannonen, S. Koponen, J. Pulliainen, J. Vepsäläinen, T. Pyhälähti, *Retrieval of water quality from airborne imaging spectrometry of various lake types in different seasons*, Science of the Total Environment 268 (1–3) (2001) 59–77.
- [33] A. A. Gilerson, A. A. Gitelson, J. Zhou, D. Gurlin, W. Moses, I. Ioannou, S. A. Ahmed, *Algorithms for remote estimation of chlorophyll-a in coastal and inland waters using red and near-infrared bands*, Optics Express 18 (23) (2010) 24109–24125.
- [34] N. T. T. Ha, K. Koike, M. T. Nhuan, *Improved accuracy of chlorophyll-a concentration estimates from MODIS Imagery using a two-band ratio algorithm and geostatistics: As applied to the monitoring of eutrophication processes over Tien Yen Bay (Northern Vietnam)*, Remote Sensing 6 (1) (2013) 421–442.
- [35] F. Zhang, J. Li, Q. Shen, B. Zhang, C. Wu, Y. Wu, G. Wang, S. Wang, Z. Lu, *Algorithms and schemes for chlorophyll-a estimation by remote sensing and optical classification for turbid lake Taihu, China*, IEEE Journal of Selected Topics in Applied Earth Observations and Remote Sensing 8 (1) (2015) 350–364.
- [36] T. M. Lillesand, R. W. Kiefer, J. Chipman, *Remote sensing and image interpretation*, 7th edition, Wiley Company, United States, 2015.
- [37] M. H. Gholizadeh, A. M. Melesse, L. Reddi, *A comprehensive review on water quality parameters estimation using remote sensing techniques*, Sensors 16 (8) (2016) 1298 43 pages.
- [38] D. G. George, *The airborne remote sensing of phytoplankton chlorophyll in the lakes and tarns of the English Lake District*, International Journal of Remote Sensing 18 (9) (1997) 1961–1975.
- [39] R. M. Liu, X. J. Wang, C. H. Wang, Y. C. Jiang, X. W. Zhou, *Application of geo-statistics in studying spatial distribution of chlorophyll a in lakes*, Agro-environment Protection 20 (5) (2001) 308–310.
- [40] S. Tuğrul, G. Dumlu, A. Baştürk, C. İlhal, T. Balkaş, *Van Gölü özümleme kapasitesinin saptanması ve evsel nitelikli atıksu arıtımı ve deşarjı optimizasyonu*. Gebze-Kocaeli: TÜBİTAK-MAM ve İller Bankası Genel Müdürlüğü (0730018301) Yayın Numarası 145 (1984) 183 pages.
- [41] M. Cüreoğlu, *Van Gölü yüzey sularında klorofil-a değişiminin seaWIFS görüntüleri ve yer ölçümleri ile izlenmesi*, Master's Thesis Van Yüzüncü Yıl University (2002) Van.
- [42] D. Cukur, S. Krastel, H. U. Schmincke, M. Sumita, Y. Tomonaga, M. N. Çağatay, *Water level changes in Lake Van, Turkey, during the past ca. 600 ka: climatic, volcanic and tectonic controls*, Journal of Paleolimnology 52 (3) (2014) 201–214.
- [43] M. Şenel, T. Ercan, 1:500.000 ölçekli Türkiye jeoloji haritaları serisi, Van paftası, 2nd Edition, Ankara: Maden Tetkik ve Arama Genel Müdürlüğü Yayınları, Ankara, 2002.
- [44] M. Stockhecke, F. S. Anselmetti, A. F. Meydan, D. Odermatt, M. Sturm, *The annual particle cycle in Lake Van (Turkey)*, Palaeogeography, Palaeoclimatology, Palaeoecology 333–334 (2012) 148–159.
- [45] F. Barlas Şimşek, M. N. Çağatay, *Late Holocene high-resolution multi-proxy climate and environmental records from Lake Van, eastern Turkey*, Quaternary International 486 (2018) 57–72.

- [46] M. N. Çağatay, N. Öğretmen, E. Damcı, M. Stockhecke, Ü. Sancar, K. K. Eriş, S. Özeren, *Lake level and climate records of the last 90 ka from the Northern Basin of Lake Van, eastern Turkey*, *Quaternary Science Reviews* 104 (2014) 97–116.
- [47] T. Litt, N. Pickarski, G. Heumann, M. Stockhecke, P. C. Tzedakis, *A 600,000-year long continental pollen record from Lake Van, eastern Anatolia (Turkey)*, *Quaternary Science Reviews* 104 (2014) 30–41.
- [48] E. Damcı, M. N. Çağatay, *Chronological evolution of some morphological, tectonic and volcanic features in Lake Van, based on correlation of seismic and core data*, *Quaternary International* 486 (2018) 29–43.
- [49] A. Turan, A. Aldemir, *Statistical assessment of seasonal variations in water quality for different regions in Lake Van (Türkiye)*, *Environmental Monitoring and Assessment* 195 (2023) Article Number 237 18 pages.
- [50] N. Olğun Kıyak, M. N. Çağatay, *Environmental impacts of subaerial volcanic eruptions on alkaline lakes – A case study on Lake Van in eastern Turkey (EVOLVAN)*. TÜBİTAK (European Commission 7th Framework Programme funded Project-Marie Curie 2236 Co-funded Brain Circulation Scheme) TÜBİTAK (112C001) (2015).
- [51] E. T. Degens, H. K. Wong, S. Kempe, F. Kurtman, *A geological study of lake van, Eastern Turkey*, *Geologische Rundschau* 73 (2) (1984) 701–734.
- [52] M. Keskin, *Magma generation by slab steepening and breakoff beneath a subduction-accretion complex: An alternative model for collision-related volcanism in Eastern Anatolia, Turkey*, *Geophysical Research Letters* 30 (24) (2003) 8046 4 pages.
- [53] A. M. C. Şengör, M. S. Özeren, M. Keskin, M. Sakiç, A. D. Özbakir, I. Kayan, *Eastern Turkish high plateau as a small Turkic-type orogen: Implications for post-collisional crust-forming processes in Turkic-type orogens*, *Earth Science Reviews* 90 (1-2) (2008) 1–48.
- [54] O. Tüysüz, Ş. C. Genç, U. Tarı, *Van depremi kör bindirme fayının kırılmasının bir sonucu*, *Cumhuriyet Bilim Teknoloji Gazetesi* 1285 (2011) 10–11.
- [55] F. Arikan, M. N. Deviren, O. Lenk, U. Sezen, O. Arikan, *Observed Ionospheric Effects of 23 October 2011 Van, Turkey Earthquake*, *Geomatics, Natural Hazards, and Risk*, 3 (1) (2012) 1–8.
- [56] A. Sağlam Selçuk, *Evaluation of the relative tectonic activity in the eastern Lake Van basin, East Turkey*, *Geomorphology* 270 (2016) 9–21.
- [57] M. Kadioğlu, Z. Şen, E. Batur, *The greatest soda-water lake in the world and how it is influenced by climatic change*, *Annales Geophysicae* 15 (11) (1997) 1489–1497.
- [58] G. Landmann, A. Reimer, S. Kempe, *Climatically induced lake level changes at Lake Van, Turkey, during the Pleistocene/Holocene transition*, *Global Biogeochemical Cycles* 10 (4) (1996) 797–808.
- [59] S. Kempe, G. Landmann, G. Müller, *A floating varve chronology from the last glacial maximum terrace of Lake Van (Turkey)*, *Zeitschrift für Geomorphologie, Supplementband* 126 (2002) 97–114.
- [60] C. Kuzucuoglu, A. Christol, D. Muralis, A. F. Dogu, E. Akköprü, M. Fort, D. Brunstein, H. Zorer, M. Fontugne, M. Karabiyikoğlu, S. Scaillet, J. L. Reyss, H. Guillou, *Formation of the Upper Pleistocene terraces of Lake Van (Turkey)*, *Journal of Quaternary Science* 25 (7) (2010) 1124–1137.
- [61] R. Nagalakshmi, K. Prasanna, S. Prakash Chandar, *Water quality analysis using GIS interpolation method in Serthalaikadu Lagoon, east coast of India*, *Rasayan Journal of Chemistry* 9 (4) (2016) 634–640.
- [62] E. Y. Wardani, Y. Wardiatno, S. B. Agus, *Spatial distribution and biophysics chemistry characterization of Pearl Oyster farming in Semau Strait, East Nusa Tenggara*, *IOP Conference Series: Earth and Environmental Science* 54 (2017) 012069 10 pages.

- [63] M. Küçükönder, E. Kalkan, K. Cırık, *Kılavuzlu baraj gölü (Kahramanmaraş) su kalitesi ve Kanada su kalite indeksi sınıfı*, *Osmaniye Korkut Ata Üniversitesi Fen Bilimleri Enstitüsü Dergisi* 5 (1) (2022) 118–142.
- [64] D. Zimmerman, C. Pavlik, A. Ruggles, M. P. Armstrong, *An experimental comparison of ordinary and universal kriging and inverse distance weighting*, *Mathematical Geology* 31 (4) (1999) 375–390.
- [65] J. Li, L. Tian, Y. Wang, S. Jin, T. Li, X. Hou, *Optimal sampling strategy of water quality monitoring at high dynamic lakes: A remote sensing and spatial simulated annealing integrated approach*, *Science of the Total Environment* 777 (2021) 146113 14 pages.
- [66] E. Kim, S. H. Nam, C. H. Ahn, S. Lee, J. W. Koo, T. M. Hwang, *Comparison of spatial interpolation methods for distribution map an unmanned surface vehicle data for chlorophyll-a monitoring in the stream*, *Environmental Technology & Innovation* 28 (2022) 102637 11 pages.
- [67] M. G. Allan, D. P. Hamilton, B. Hicks, L. Brabyn, *Empirical and semi-analytical chlorophyll-a algorithms for multi-temporal monitoring of New Zealand lakes using Landsat*, *Environmental Monitoring and Assessment* 187 (2015) Article Number 364 24 pages.
- [68] K. Blix, K. Pálffy, V. R. Tóth, T. Eltoft, *Remote sensing of water quality parameters over Lake Balaton by using Sentinel-3 OLCI*, *Water* 10 (10) (2018) 1428 20 pages.
- [69] A. C. Blanco, A. Manuel, R. Jalbuena, K. Ticman, J. M. Medina, E. Gubatanga, A. Santos, R. Sta. Ana, E. Herrera, K. Nadaoka, *Estimation of Chl-a concentration in Laguna Lake using Sentinel-3 OLCI images*, *The International Archives of the Photogrammetry, Remote Sensing and Spatial Information Sciences* 42 (2020) 17–21.
- [70] C. D. Mobley, *Estimation of the remote-sensing reflectance from above-surface measurements*, *Applied Optics* 38 (36) (1999) 7442–7455.
- [71] C. Giardino, M. Pepe, P. A. Brivio, P. Ghezzi, E. Zilioli, *Detecting chlorophyll, Secchi disk depth and surface temperature in a sub-alpine lake using Landsat imagery*, *Science of The Total Environment* 268 (1-3) (2001) 19–29.
- [72] S. A. C. Nelson, P. A. Soranno, K. S. Cheruvilil, S. Batzli, D. Skole, *Regional assessment of lake water clarity using satellite remote sensing*, *Journal of Limnology* 62 (Suppl. 1) (2003) 27–32.
- [73] H. Wang, D. Zhao, L. Wang, F. Huang, *Advance in remote sensing of water quality*, *Marine Environmental Science* 31 (2) (2012) 285–288.
- [74] X. Wang, W. Yang, *Water quality monitoring and evaluation using remote-sensing techniques in China: A systematic review*, *Ecosystem Health and Sustainability* 5 (1) (2019) 47–56.
- [75] A. Morel, L. Prieur, *Analysis of variations in ocean color*, *Limnology and Oceanography* 22 (1977) 709–722.
- [76] H. R. Gordon, A. Y. Morel, *Remote assessment of ocean color for interpretation of satellite visible imagery*, Springer-Verlag, New York, 1983.
- [77] K. L. Carder, F. R. Chen, Z. Lee, S. K. Hawes, J. P. Cannizzaro, *MODIS Ocean Science Team Algorithm Theoretical Basis Document: Case 2 Chlorophyll-a*, University of South Florida (2003) Florida.
- [78] J. Blaustein, *The peak near 700 nm on radiance spectra of algae and water: Relationships of its magnitude and position with chlorophyll*, *International Journal of Remote Sensing* 13 (17) (1992) 3367–3373.
- [79] H. Luoheng, D. C. Rundquist, *Comparison of NIR/RED ratio and first derivative of reflectance in estimating algal-chlorophyll concentration: A case study in a turbid reservoir*, *Remote Sensing of Environment* 62 (3) (1997). 253–261.
- [80] J. F. Schalles, Y. Z. Yacobi, *Remote detection and seasonal patterns of phycocyanin, carotenoid and*

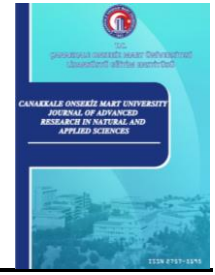
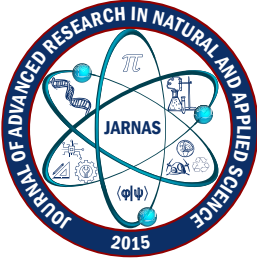
chlorophyll pigments in eutrophic waters, *Ergebnisse Der Limnologie* 55 (2000) 153–168.

[81] G. Yu, W. Yang, B. Matsushita, R. Li, Y. Oyama, T. Fukushima, *Remote estimation of chlorophyll-a in inland waters by a NIR-red-based algorithm: Validation in Asian Lakes*, *Remote Sensing* 6 (4) (2014) 3492–3510.

[82] D. C. Pierson, N. Strömbeck, *A modeling approach to evaluate preliminary remote sensing algorithms: Use of water quality data from Swedish great lakes*, *Geophysica* 36 (1–2) (2000) 177–202.

[83] J. F. Schalles, *Optical remote sensing techniques to estimate phytoplankton chlorophyll-a concentrations in coastal waters with varying suspended matter and C_{dom} concentrations*, *Remote Sensing and Digital Image Processing* 9 (2006) 27–79.

[84] K. A. Hussein, K. Al Abdouli, D. T. Ghebreyesus, P. Petchprayoon, N. O. Al Hosani, H. Sharif, *Spatiotemporal variability of chlorophyll-a and sea surface temperature, and their relationship with bathymetry over the coasts of UAE*, *Remote Sensing* 13 (13) (2021) 2447–25 pages.



On the Synchronizability of Quadratic Integrate and Fire Neurons

Koray Çiftçi¹

¹Department of Biomedical Engineering, Çorlu Faculty of Engineering, Tekirdağ Namık Kemal University, Tekirdağ, Türkiye

Abstract – Synchronization is a property of complex systems that manifests itself as the emergence of collective behavior from local interactions. Neurons are the basic building blocks of the nervous system, and in neuronal networks, the firing times of the neurons get synchronized via the electrical and chemical synapses among them. This property has been observed in both computational models and experimental studies. However, this synchronization's mechanisms have not yet been totally revealed. Here, we investigate the synchronization properties of quadratic integrate and fire (QIF) neurons from a computational modeling perspective. QIF neurons are simple yet effective models in the sense that they have the ability to capture complex behavior observed in neurons. We present analytical results concerning the spiking frequency of the QIF neurons and the relationships between membrane voltage and phase of the neurons. We give simulation results for a simple network of all-to-all coupled QIF neurons, demonstrating the effects of different types of coupling among the network members. We show that electrical and inhibitory chemical synapses play complementary roles in the formation of synchronized behavior in a neuronal network. Our results contribute to our understanding of the brain to produce cognitive abilities and coordinated action.

Article History

Received: 5 Jul 2022

Accepted: 31 Oct 2023

Published: 15 Mar 2024

Research Article

Keywords – *Integrate and fire, neuron, phase, synchronization*

1. Introduction

Computational modeling efforts in neuroscience generally seek a balance between biological realism and computational tractability. Biological realism brings complexity to the models, whereas simplicity is crucial to be able to arrive at generalizable inferences. The need for simplicity becomes even more crucial with the increasing usage of network models in neuroscience. Conductance-based models [1] can reproduce the output of many electrophysiological recordings. However, because of its inherent complexity, extending conductance-based single-neuron models to large networks of neurons is not easy. On the other hand, integrate and fire neuron models offer a great reduction in complexity but with the capability of representing the rich dynamical repertoire of neurons, especially at regions close to the firing threshold [2].

Integrate and fire neuron model is one of the earliest models in neuroscience, dating back to 1907 [3]. The model tracks the membrane potential and acts as an integrator of subthreshold stimuli. It incorporates a reset mechanism for the neuron to return to resting potential after triggering a spike [4]. Quadratic integrate and fire (QIF) neuron model is a type of integrate and fire neuron model, and it is actually the simplest form of a spiking neuron. Although simplistic in the sense that it is based on a single variable, the QIF model is widely used to model a wide range of neuronal phenomena [5], including learning [6], memory [7], and movement-induced rhythms [8]. It was also demonstrated that QIF is appropriate for modeling neural oscillations [9,10].

Neurons exhibit an oscillatory behavior [11], and a prominent feature of a neuron is its ability to synchronize

¹kciftci@nku.edu.tr (Corresponding Author)

these oscillations with other neurons [12]. This synchronization takes place under the action of synaptic couplings and is the basis of all attention [13], memory [14], coordinated action [15], and related phenomena. Although the underlying mechanisms of this synchronization are still not totally revealed, it is known that it is an emergent property with no central executive coordinating this synchronization process [16]. Thus, synchronization is a global phenomenon arising from local interactions among the neurons [17].

Oscillatory behavior and activity synchronization are not an exclusive property of neurons and are observed in many natural systems [18,19]. Observing collective behavior at different levels in living systems, from micro to macro, is possible. Therefore, it is important to discover the underlying mechanisms of this behavior to understand living systems and adapt these principles to engineering systems [20].

The synchronization characteristics of QIF neurons have already been investigated in a number of studies and the link between the Kuramoto Model [21] and the QIF model has been established [22], voltage dependence of synchronization for electrical synapses has been explored [23] and a mean field approximation for networks of QIF neurons has been proposed [24]. Recently, it has been shown that spike timing dependent plasticity allows QIF neurons to form large clusters that generate synchronous oscillations [25]. Earlier work has shown that synchronization can be achieved both with the coordinated action of inhibitory and excitatory inputs [26] or with inhibition alone [27]. A number of works have reported that inhibitory synapses increase the synchronization capability of neuronal networks [28,29]. And although electrical synapses are thought to promote synchronization in general [30], it has also been observed that anti-synchronous activity can also emerge from weak electrical coupling [31]. Thus, the joint role of electrical and inhibitory chemical coupling is still elusive. Based on these findings, in this study we particularly aim at revealing the complementary roles of inhibitory chemical synapses and electrical synapses in the formation synchronous activity in a network of QIF neurons. In the Materials and Methods, we explain the basic temporal dynamics of a single QIF neuron and the relationship between its membrane voltage and phase. This enables us to describe the neuron as an oscillator. After investigating the phase sensitivity of a neuron, we extend our analysis to a network of QIF neurons and investigate its synchronization properties under different coupling conditions. After presenting the results with discussion we conclude the paper with a summary of our results and a description of future work.

2. Materials and Methods

We first consider a single isolated neuron subject to a constant external current, but with no synaptic input. The QIF model for this neuron reads (2.1),

$$\tau \dot{v} = v^2 + \eta, \quad \text{if } v > v_p, \quad \text{then } v \leftarrow v_r \quad (2.1)$$

where, v is the membrane potential, τ is the membrane time constant and η is external current noise. Since membrane voltage increases quadratically, a resetting rule is needed, which is given as the if statement in the equation. When $\eta < 0$, the model has one stable equilibrium, which corresponds to the resting state of the neuron, i.e., $V_r = -\sqrt{\eta}$, whereas the other equilibrium point is unstable and acts as the threshold voltage for spike generation, i.e., $V_p = +\sqrt{\eta}$. In this study, we will consider the case $\eta > 0$, which corresponds to the situation where there is no equilibrium point and the neuron acts as a self-sustained oscillator. If we set $v(t = 0) = v_r$, then the time evolution of the membrane voltage may be determined by a simple separation of variables (2.2):

$$\int_{v_r}^{v(t)} \frac{1}{v'^2 + \eta} dv' = \frac{1}{\tau} \int_0^t dt' \quad (2.2)$$

which gives (2.3),

$$v(t) = \sqrt{n} \tan\left(\frac{\sqrt{n}}{\tau} t + \tan^{-1} \frac{V_r}{\sqrt{n}}\right) \quad (2.3)$$

The period of oscillation, T , may be determined by calculating the time at which $v(t) = V_p$, and is given by (2.4),

$$T = \frac{\tau}{\sqrt{n}} \left(\tan^{-1} \frac{V_p}{\sqrt{n}} - \tan^{-1} \frac{V_r}{\sqrt{n}} \right) \quad (2.4)$$

A symmetric spike resetting is generally assumed, i.e., $V_p = -V_r$, in which case the period becomes (2.5):

$$T = 2 \frac{\tau}{\sqrt{n}} \tan^{-1} \frac{V_p}{\sqrt{n}} \quad (2.5)$$

Generally, for mathematical analysis, V_p is assumed to go to infinity, and this makes the period of spike generation a simple function of membrane time constant and external current (2.6):

$$T = \frac{\pi\tau}{\sqrt{n}} \quad (2.6)$$

In practical cases, we can set $V_p \gg \sqrt{n}$ for the above equation to hold. Thence, writing $\omega = \frac{2\pi}{T} = \frac{2\sqrt{\eta}}{\tau}$, a phase variable may be introduced: $\phi = \omega t = \left(\frac{2\sqrt{\eta}}{\tau}\right) t$, which may be derived from (2.3) as (2.7),

$$\phi = 2 \arctan \frac{v}{\sqrt{n}} + \pi \quad (2.7)$$

This function may be seen as a mapping between membrane voltage and phase, which turns the neuron into a rotating oscillator on the unit circle that emits spikes when $\phi = 2\pi$.

Figure 1 shows the time course of membrane voltage and phase for a QIF neuron. Membrane voltage obeys (2.1) and the phase is calculated for each voltage value from (2.7). It may be seen that the spiking period is close to 10 s, which may be confirmed from (2.6). The membrane voltage of the neuron has fast dynamics immediately after a spike and just before the spike and a slow increase governs the rest of its temporal dynamics. On the other hand, please note the linear increase in the phase of the neuron between the spikes. Actually, we had derived the angular velocity above, and thus, the mapping given in (2.7) converts the non-linear temporal dynamics of membrane voltage to a linear phase system. We can also verify this using the chain rule (2.8):

$$\frac{d\phi}{dt} = \frac{d\phi}{dv} \frac{dv}{dt} = \frac{2}{\sqrt{\eta} \left(1 + \frac{v^2}{\eta}\right)} \frac{(v^2 + \eta)}{\tau} = 2 \frac{\sqrt{\eta}}{\tau} \quad (2.8)$$

This analysis shows that phase temporally depends on the external current and membrane time constant, and if these two parameters are constant then the phase of the neuron changes linearly between the spikes.

In our simulations, we will consider nearly identical neurons, in the sense that their membrane time constants will be identical but the external noise they are exposed to will be stochastic with a definite mean and variance.

Thus, the instantaneous change of phase will be dependent on the instantaneous noise component but can be assumed to be constant over a long time which is determined by the mean of the external noise, η .

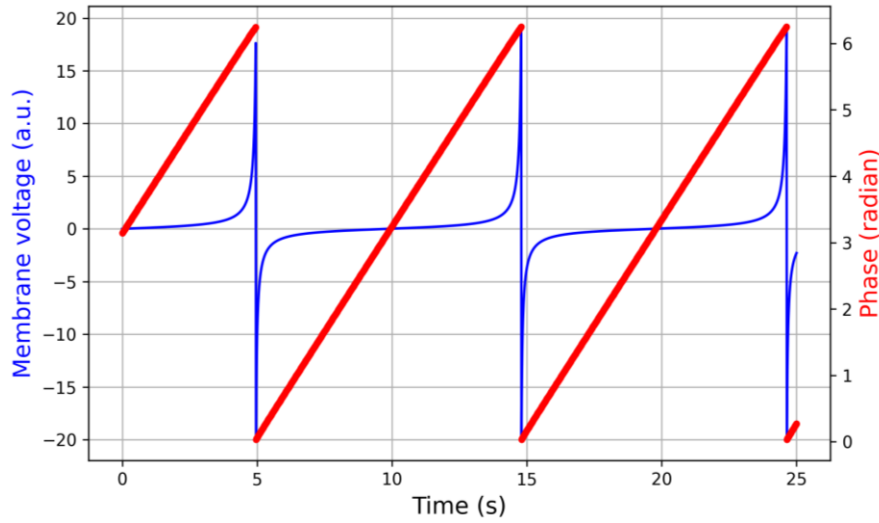


Figure 1. The time course of membrane voltage, v , for a QIF neuron with $V_p = -V_r = 20$, $\tau = 1$, and $\eta = 0.1$

2.1. Phase Sensitivity of a Neuron

The phase of a QIF neuron is a function of its membrane voltage and perturbations in this voltage cause an alteration in the phase of the neuron. In (2.7), we have noted the derivative of phase with respect to voltage (2.9):

$$\frac{d\phi}{dv} = \frac{2}{\sqrt{\eta} \left(1 + \frac{v^2}{\eta}\right)} \quad (2.9)$$

This equation tells us that the phase sensitivity depends both on the corresponding voltage and on the external noise component, and the sensitivity is maximum when $v = 0$. It is also possible to derive the sensitivity of the phase to the noise component, η , and can be shown that phase sensitivity is maximum (for a constant voltage) at $\eta = v^2$.

Phase sensitivity may be empirically determined by applying small perturbations to the membrane voltage at different phases, $\phi = \frac{t_s}{T_o}$, where T_o is the intrinsic period of the neuron and t_s is the time between the last action potential and the perturbation. We can then measure the corresponding change in the period, $\frac{(T_o - T_p)}{T_o}$, where T_p is the period in the perturbed interval. This function, relating phase to voltage perturbation is also called the phase resetting curve (PRC) of a neuron [32]. It summarizes the responses of a neuron to external inputs, from neighboring neurons or other noise components.

Figure 2 shows the analytical and numerical PRC of a QIF neuron. The two curves are in close agreement with each other, and they show that the neuron is rather insensitive to external perturbations immediately after and just before a spike, and the sensitivity is comparably much higher during the interval between these two ends. Another point to note is that phase sensitivity is always non-negative. Thus, positive perturbations will shorten the spike interval, whereas negative perturbations will cause a delay in the next spike time.

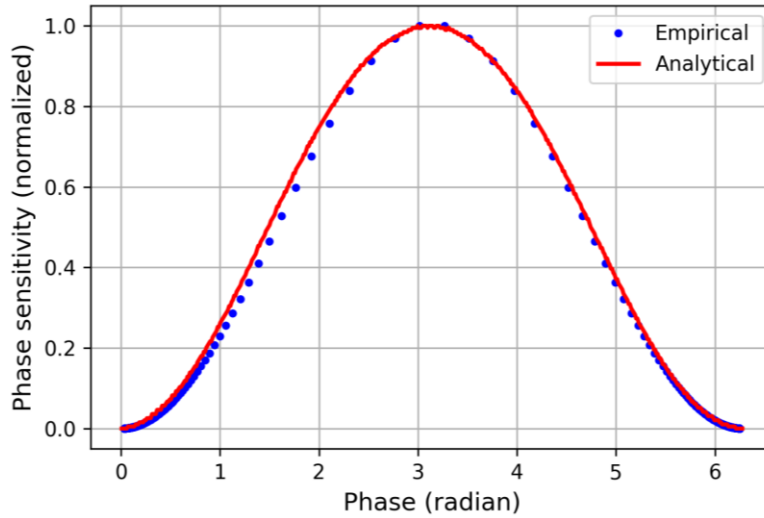


Figure 2. Analytical and empirical phase sensitivity curves for a QIF neuron. These curves show the normalized increase (or decrease) in the spiking period with an infinitesimal perturbation in the membrane voltage

2.2. A Simple Network of QIF Neurons

Neurons do not function in an isolated manner, and our main concern is the relationship among the interacting neurons. Equipped with a general understanding of phase sensitivity of a single neuron, we will now consider a network of QIF neurons, whose individual membrane voltages are evolving according to (2.10),

$$\tau \dot{v}_i = v_i^2 + \eta_i + S_i(t), \quad \text{if } v_i > v_p, \quad \text{then } v_i \leftarrow v_r \quad (2.10)$$

where $i \in \{1, 2, \dots, N\}$ indexes all-to-all coupled N neurons. $S_i(t)$, is the total time dependent synaptic input to the neuron and has two components: chemical and electrical synapses. Electrical synapses are gap junctions which permit the connected neurons to conduct electricity. In our model, electrical synapses are coupled to the neurons by the mean membrane voltage (2.11):

$$S_i^e(t) = g(\mu_v(t) - v_i), \quad \mu_v(t) = \sum_{j=1}^N v_j(t) \quad (2.10)$$

where $\mu_v(t)$ is the mean membrane voltage of the neuron population and g is a constant denoting the strength of the synaptic coupling which may be seen as the average conductance of the synaptic channels. Chemical synapses, on the other hand, are biological junctions that act through neurotransmitters, and they allow the transmission of presynaptic signals to postsynaptic neurons.

In the current model, chemical synapses are mediated by mean firing rate (2.12):

$$S_i^c(t) = \frac{C}{N} \sum_{j=1}^N \sum_k \delta(t - t_j^k) \quad (2.10)$$

where C is a constant denoting the strength of chemical couplings, t_j^k is the k^{th} spike of the j^{th} neuron, and $\delta(\cdot)$ is the *Dirac delta function*.

Electrical and chemical synapses play complementary roles in neuronal network synchronization [33]. The strength of coupling needed for synchronization depends on the relative contributions of chemical and

electrical synapses [34]. Additionally, chemical synapses may be inhibitory or excitatory. Excitatory synapses increase the activity of the postsynaptic neuron, whereas inhibitory synapses work in the reverse direction.

It has been shown that inhibitory synapses increase the synchronization capability of neuronal networks [28]. However, the exact roles of electrical and inhibitory coupling in the formation of synchronous activity is still under debate. Therefore, in this study we will only consider inhibitory chemical synapses and in order to investigate the effect of both types of coupling, we analyse the network in two different settings: 1) Only electrical coupling, 2) Inhibitory chemical coupling and electrical coupling.

3. Results and Discussion

Here, we present the results for a network of $N = 256$ all-to-all coupled neurons. Since the membrane time constant, τ , acts as an inverse multiplier of integration time in our simulations, without loss of generality, we will assume that $\tau = 1$. To keep the heterogeneity among the neurons at a low level we impose the constraint that the mean of the Gaussian noise is much larger than the standard deviation. This is also needed to satisfy the weak coupling regime between the QIF neurons. Accordingly, the external noise has a Gaussian distribution with a mean of 0.1 and a standard deviation of 0.01.

The QIF model is not directly related to physiological voltage levels. Nevertheless, to keep the voltage levels at reasonable ranges, the neurons were randomly initialized uniformly between -1 and 1 V and time courses of their membrane voltages were determined by Euler integration with time steps of 0.01 s.

3.1. Only Electrical Synapses

We first set $C = 0$ and let the network interact only through electrical synapses. Beginning from a g value of 0.01, we incrementally increased g with steps of 0.01 and check for synchronization. To quantify the synchronization, we calculated the *index of dispersion* (ratio of variance to mean) of spike intervals of the neurons.

In Figure 3, it is observable that dispersion index drops close to zero beginning from $g = 0.04$. Thus, we deduced that synchronization is achievable beginning from this value of g .

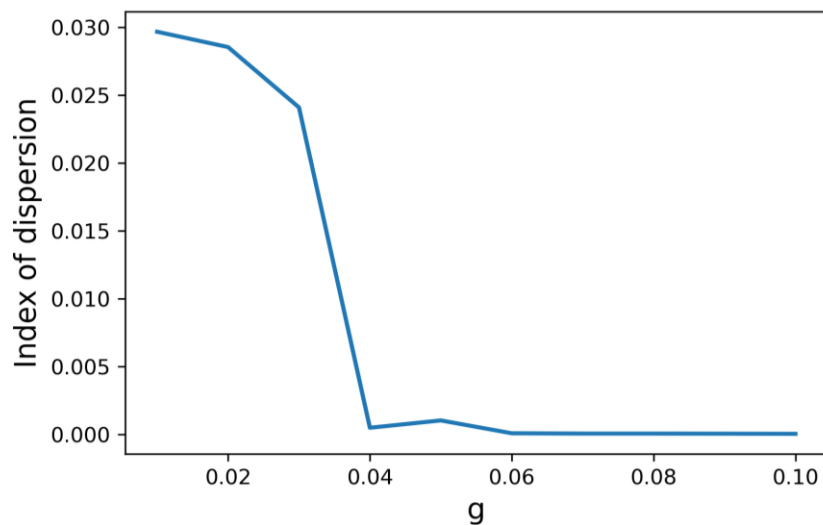


Figure 3. Index of dispersion of spiking intervals with varying electrical coupling strength. Decrease in dispersion points to the emergence of synchronization

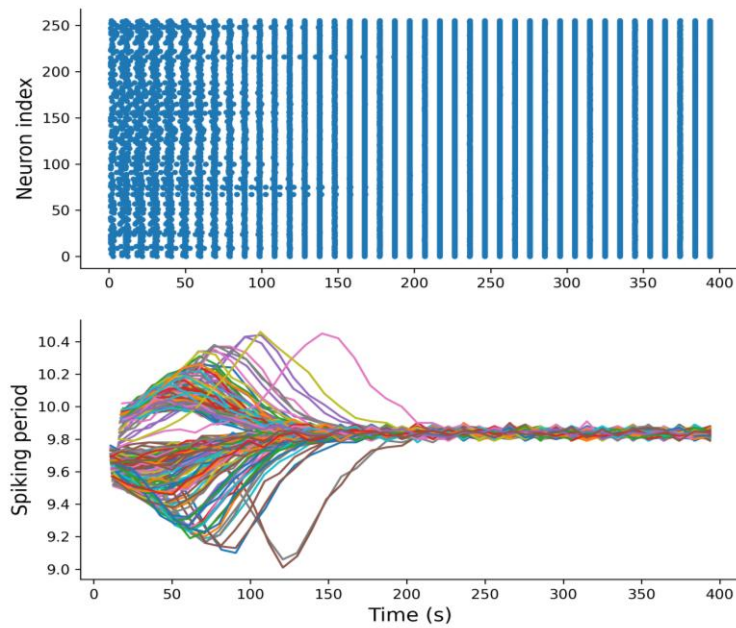


Figure 4. Top: Raster plots of neurons. Each firing of a neuron is represented as a dot at that time point. Synchronization in firings is evident as time progresses. Bottom: Evolution of spiking intervals of neurons. Spiking intervals converge as time progresses

In Figure 4, we present the raster plot and the change in the spiking periods of the neurons for $g = 0.05$. Beginning from an unsynchronized state, the neurons organize themselves towards a synchronized state. During this interval, their spiking periods converge to their intrinsic periods (~ 9.8 s). Since the external current is stochastic small fluctuations continue after convergence. Please note that this is the only achievable synchronized condition for identical neurons with electrical coupling. Since this coupling is mediated by mean membrane voltage, for those neurons whose membrane voltage is lower than the average, electrical coupling acts as an accelerator whereas for the ones that are higher than the average, coupling causes a deceleration. And as time progresses every neuron is pulled towards the mean and begins to trigger a spike at the same time. Interestingly, this pull towards synchronization also decreases the total amount of electrical coupling among the neurons. This phenomenon may be understood within the light of optimality of the brain [35]. Thus, synchronization is not achieved per se but is a state that comes out of a more general principle of energy minimization.

3.2. Inhibitory Chemical Coupling and Electrical Coupling

After investigating the role of electrical synapses on the synchronization of the neuronal network, we proceed with analyzing the combined effects of inhibitory chemical synapses and electrical synapses. Cortical circuits display a layer-specific excitation-inhibition balance in generating synchronization between neuronal assemblies [36]. In the sequel, we conjectured that a certain amount of inhibitory coupling would corroborate the synchronization capacity of the network. To be able to test this conjecture we set an electrical coupling constant of $g = 0.02$ (which is below the full synchronization level of the network). Then, we increased the inhibitory chemical coupling and checked the synchronization. We observed that the synchronization capacity increased after a certain level of inhibition, but began to decrease with further increase, which points to an optimum exhibition/inhibition ratio. In Figure 5, it may be observed that the network reaches synchronization with a larger time delay. As a further test, we lowered g and found that inhibitory coupling should also be lowered in the same amounts for synchronization (Figure 6).

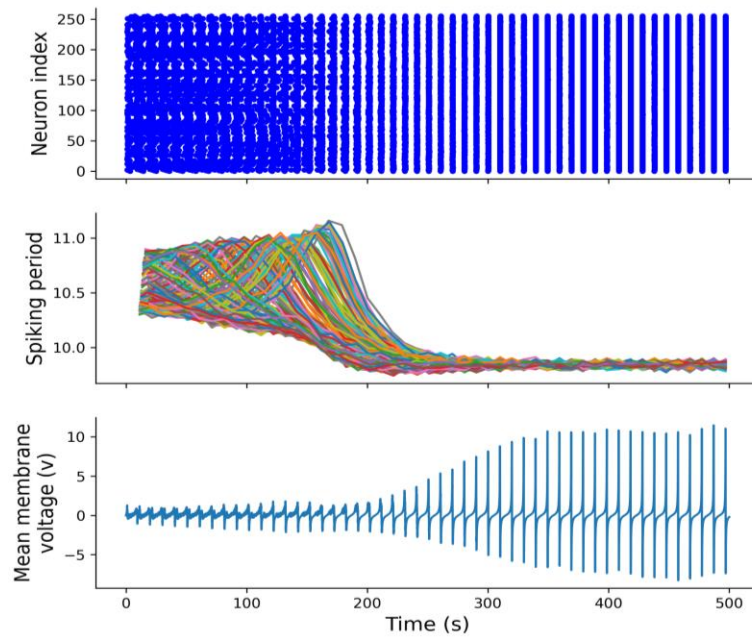


Figure 5. The definitions of the first two plots are as in Figure 4. At the bottom we included the mean membrane voltage of the population. Electrical coupling constant g is 0.02, inhibitory coupling constant $C = -0.06$. Please note that simulation time is 500 seconds

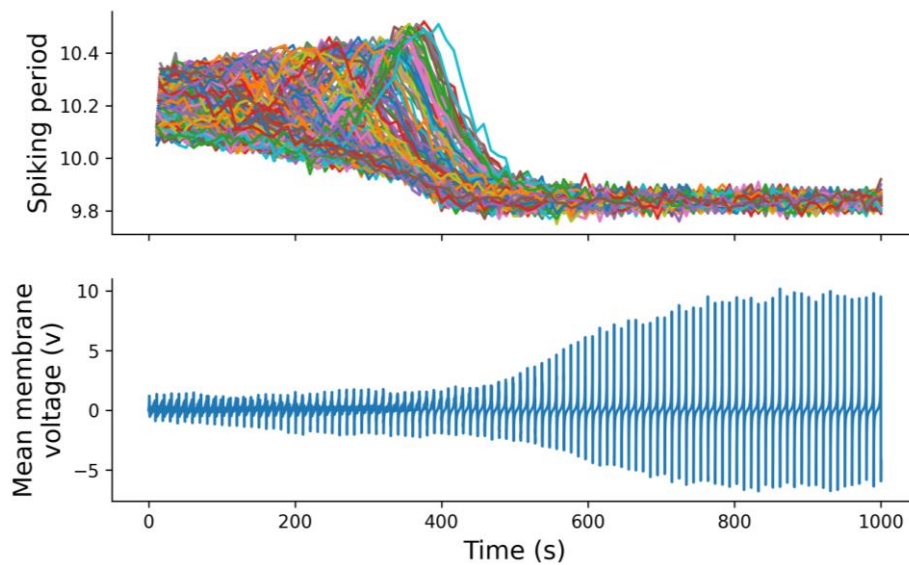


Figure 6. The definitions of the plots are as in Figure 4. Electrical coupling constant g is 0.01, inhibitory coupling constant $C = -0.12$. Please note that simulation time is 1000 seconds

4. Conclusion

In this study, we provide further evidence for the complementary roles of inhibitory chemical synapses and electrical synapses in the formation of synchronized behavior in networks of coupled neurons. First, we showed that the network may become synchronized with only electrical coupling. This synchronization takes place at a certain amount of coupling, and we also made the observation that synchronized activity also decreased the total amount of coupling among the neurons. We related this observation to the optimality of the brain hypothesis since every interaction between the neurons needs energy consumption [37]. Second, we showed that with an injection of inhibitory coupling, it may become possible for the network to arrive at full

synchronization with less electrical coupling but with a larger time delay. It has been claimed that electrical coupling had increased the robustness of inhibition induced synchronization [38]. Our results do not directly relate to this conjecture but provide an alternative look at the interplay between inhibitory and electrical coupling. Interestingly, we also observed that further increases in inhibition causes a loss in the synchronization. This point is of note since it has been reported that for a total amount of coupling either electrical coupling only or inhibition only is better at arriving neural synchrony [39]. Please note that in our simulations only electrical coupling is more efficient for driving the network towards synchrony and with the addition of inhibition this electrical coupling should be decreased. And after the network reaches synchronization, further increase in inhibition deteriorates synchrony.

This study analyzed quadratic integrate and fire neurons as use cases, however similar approaches can be extended to other neuron models. Physiologically inspired neuronal models and network structures may be used to explore the synchronization phenomenon in biologically more plausible settings.

Author Contributions

The author read and approved the final version of the paper.

Conflicts of Interest

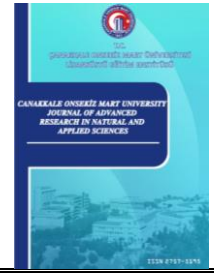
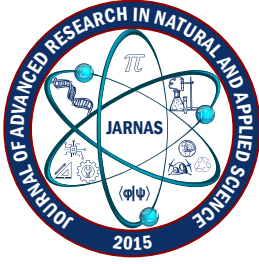
The author declares no conflict of interest.

References


- [1] A. L. Hodgkin, A. F. Huxley, *A quantitative description of membrane current and its application to conduction and excitation in nerve*, The Journal of Physiology 117 (4) (1952) 500.
- [2] R. Jolivet, T. J. Lewis, W. Gerstner, *Generalized integrate-and-fire models of neuronal activity approximate spike trains of a detailed model to a high degree of accuracy*, Journal of Neurophysiology 92 (2) (2004) 959–976.
- [3] N. Brunel, M. C. Van Rossum, *Lapicque's 1907 paper: From frogs to integrate-and-fire*, Biological Cybernetics 97 (5–6) (2007) 337–339.
- [4] A. N. Burkitt, *A review of the integrate-and-fire neuron model: I. Homogeneous synaptic input*, Biological Cybernetics 95 (2006). 1–19.
- [5] E. M. Izhikevich, *Dynamical systems in neuroscience*, MIT Press, London, 2007.
- [6] D. Mishra, A. Yadav, P. K. Kalra, *Learning with single quadratic integrate-and-fire neuron*, in: J. Wang, Z. Yi, J. M. Zurada, B. L. Lu, H. Yin, (Eds.) *Advances in Neural Networks - ISNN 2006*, Vol. 3971 of *Lecture Notes in Computer Science*, Springer, Berlin, 2006, pp. 424–429.
- [7] D. Hansel, G. Mato, *Existence and stability of persistent states in large neuronal networks*, Physical Review Letters 86 (18) (2001) 4175–4178.
- [8] Á. Byrne, M. J. Brookes, S. Coombes, *A mean field model for movement induced changes in the beta rhythm*, Journal of Computational Neuroscience 43 (2) (2017) 143–158.
- [9] G. B. Ermentrout, C. C. Chow, *Modeling neural oscillations*, Physiology and Behavior 77 (4) (2002) 629–633.
- [10] S. Keeley, Á. Byrne, A. Fenton, J. Rinzel, *Firing rate models for gamma oscillations*, Journal of Neurophysiology 121(6) (2019) 2181–2190.

- [11] G. Buzsaki, A. Draguhn, *Neuronal oscillations in cortical networks*, *Science* 304 (5679) (2004) 1926–1929.
- [12] T. Womelsdorf, J. M. Schoffelen, R. Oostenveld, W. Singer, R. Desimone, A. K. Engel, P. Fries, *Modulation of neuronal interactions through neuronal synchronization*, *Science* 316 (5831) (2007) 1609–1612.
- [13] T. Womelsdorf, P. Fries, *The role of neuronal synchronization in selective attention*, *Current Opinion in Neurobiology* 17 (2) (2007) 154–160.
- [14] N. Axmacher, F. Mormann, G. Fernández, C. E. Elger, J. Fell, *Memory formation by neuronal synchronization*, *Brain Research Reviews* 52 (1) (2006) 170–182.
- [15] J. Van Der Werf, O. Jensen, P. Fries, W. P. Medendorp, *Neuronal synchronization in human posterior parietal cortex during reach planning*, *Journal of Neuroscience* 30 (4) (2010) 1402–1412.
- [16] F. Varela, J. P. Lachaux, E. Rodriguez, J. Martinerie, *The brainweb: Phase synchronization and large-scale integration*, *Nature Reviews Neuroscience* 2 (4) (2001) 229–239.
- [17] M. V. L. Bennett, R. S. Zukin, *Electrical Coupling and Neuronal Synchronization in the Mammalian Brain*, *Neuron* 41 (4) (2004) 495–511.
- [18] S. H. Strogatz, I. Stewart, *Coupled oscillators and biological synchronization*, *Scientific American* 269 (6) (1993) 102–109.
- [19] L. Glass, *Synchronization and rhythmic processes in physiology*, *Nature* 410 (6825) (2001) 277–284.
- [20] X. Li, G. Chen, *Synchronization and desynchronization of complex dynamical networks: An engineering viewpoint*, *IEEE Transactions on Circuits and Systems I: Fundamental Theory and Applications* 50 (11) (2003) 1381–1390.
- [21] Y. Kuramoto, *Collective synchronization of pulse-coupled oscillators and excitable units*, *Physica D: Nonlinear Phenomena* 50 (1) (1991) 15–30.
- [22] P. Clusella, B. Pietras, E. Montbrió, *Kuramoto model for populations of quadratic integrate-and-fire neurons with chemical and electrical coupling*. *Chaos: An interdisciplinary, Journal of Nonlinear Science* 32 (1) (2022) 013105.
- [23] M. Jafarian, K. H. Johansson, (2019). Synchronization of quadratic integrate-and-fire spiking neurons: Constant versus voltage-dependent couplings. 2019 IEEE 58th Conference on Decision and Control (CDC), 4711-4716.
- [24] W. Ye, *Dynamics of a large-scale spiking neural network with quadratic integrate-and-fire neurons*, *Neural Plasticity* 2021 (2021) Article ID 6623926 10 pages.
- [25] I. Ratas, K. Pyragas, *Interplay of different synchronization modes and synaptic plasticity in a system of class I neurons*, *Scientific Reports* 12 (1) (2022) Article Number 19631 17 pages.
- [26] E. H. Buhl, G. Tamás, A. Fisahn, *Cholinergic activation and tonic excitation induce persistent gamma oscillations in mouse somatosensory cortex in vitro*, *The Journal of Physiology* 513 (1) (1998) 117–126.
- [27] M. Beierlein, J. R. Gibson, B. W. Connors, *A network of electrically coupled interneurons drives synchronized inhibition in neocortex*, *Nature Neuroscience* 3 (9) (2000) 904–910.
- [28] C. Van Vreeswijk, L. F. Abbott, G. Bard Ermentrout, *When inhibition not excitation synchronizes neural firing*, *Journal of computational neuroscience* 1 (4) (1994) 313–321.
- [29] M. A. Whittington, R. D. Traub, N. Kopell, B. Ermentrout, E. H. Buhl, *Inhibition-based rhythms: Experimental and mathematical observations on network dynamics*, *International Journal of Psychophysiology* 38 (3) (2000) 315–336.

- [30] R. D. Traub, *Model of synchronized population bursts in electrically coupled interneurons containing active dendritic conductances*, Journal of Computational Neuroscience 2 (1995) 283–289.
- [31] C. C. Chow, N. Kopell, *Dynamics of spiking neurons with electrical coupling*, Neural Computation 12 (7) (2000) 1643–1678.
- [32] C. C. Canavier, S. Achuthan, *Pulse coupled oscillators and the phase resetting curve*, Mathematical Biosciences 226 (2) (2010) 77–96.
- [33] N. Kopell, B. Ermentrout, *Chemical and electrical synapses perform complementary roles in the synchronization of interneuronal networks*, Proceedings of the National Academy of Sciences 101 (43) (2004) 15482–15487.
- [34] M. S. Baptista, F. M. Moukam Kakmeni, C. Grebogi, *Combined effect of chemical and electrical synapses in Hindmarsh-Rose neural networks on synchronization and the rate of information*, Physical Review E 82 (3) (2010) 036203.
- [35] L. Koban, A. Ramamoorthy, I. Konvalinka, *Why do we fall into sync with others? Interpersonal synchronization and the brain's optimization principle*, Social Neuroscience 14 (1) (2019) 1–9.
- [36] H. Adesnik, *Layer-specific excitation/inhibition balances during neuronal synchronization in the visual cortex*, The Journal of Physiology 596 (9) (2018) 1639–1657.
- [37] A. Navarrete, C. P. Van Schaik, K. Isler, *Energetics and the evolution of human brain size*, Nature 480 (7375) (2011).
- [38] J. A. White, C. C. Chow, J. Rit, C. Soto-Treviño, N. Kopell, *Synchronization and oscillatory dynamics in heterogeneous, mutually inhibited neurons*, Journal of Computational Neuroscience 5 (1) (1998) 5–16.
- [39] T. J. Lewis, J. Rinzel, *Dynamics of spiking neurons connected by both inhibitory and electrical coupling*, Journal of Computational Neuroscience 14 (3) (2003) 283–309.



Soil Contamination by Metals/Metalloids around an Industrial Region and Associated Human Health Risk Assessment

Hale Demirtepe¹ 

¹Department of Environmental Engineering, Faculty of Engineering, Izmir Institute of Technology, Izmir, Türkiye

Article History

Received: 28 Aug 2023

Accepted: 6 Nov 2023

Published: 15 Mar 2024

Research Article

Abstract – Industrial, agricultural, transportation, and waste management activities cause soil contamination by metals/metalloids. Soil contamination is an essential global concern since it poses a significant risk to human health. Particularly in areas near heavy industry, people are more prone to exposure. This study aims to determine current metal/metalloid contamination levels in soil from Aliğa industrial region and assess associated health risks. Five surface soil samples were collected from the region, representing residential, agricultural areas, and downwind of possible sources. Pollution indices were calculated to determine the metal(loid)s with anthropogenic inputs, and a human health risk assessment was conducted. As a result, significant to extreme enrichment of arsenic (As), moderate to significant enrichment of zinc (Zn) and manganese (Mn), and very high enrichment of lead (Pb) and cadmium (Cd) were observed in soil samples. Possible sources of contamination were iron and steel facilities with electric arc furnaces and oil combustion. Non-carcinogenic risk assessment revealed acceptable risks of exposure to Aliğa soils, while exposure scenarios had a great impact on estimated risks. Arsenic, chromium (Cr), and Pb appeared to be significant contributors to non-carcinogenic risk. Carcinogenic risks associated with exposure to As, Pb, Cr, cobalt (Co), and Cd in soils were evaluated to be at an acceptable level. This study only considered soil exposure pathways; hence, a comprehensive risk assessment is deemed necessary not to underestimate the risk of living around an industrial region. Nevertheless, the study provided crucial information for the current hot spots for metal(loid)s in the region and human exposure level.

Keywords – Carcinogenic risk, hazard quotient, industrial sources, soil, trace elements

1. Introduction

Anthropogenic activities such as industrial, mining, and agricultural activities, combustion of fuels, improper waste management practices, and release/use of wastewater/sewage on land lead to contamination of soil [1-3]. Among the contaminants, metals, and metalloids constitute an important class due to their resistance to degradation [1], ability to infiltrate through the soil and reach groundwater [4], and bioaccumulation in the food crops grown in the contaminated soil [5]. The presence of metal(loid)s in the soil, and accordingly, in groundwater and food crops, poses a risk to human health via several exposure pathways. Particularly due to contaminated soil, exposure can be via accidental soil ingestion, inhalation of soil fine particulates, and dermal contact with soil. Some metals are essential for body health (e.g., Zn, Cu, Mn) [1]; however, exposure to some metals, such as lead (Pb) and cadmium (Cd), has been reported to have reproductive, renal, hepatic, neurological, developmental, immunological, and hematological effects [6,7]. Arsenic (As) and cadmium (Cd) are known carcinogens (International Agency for Research on Cancer IARC-Group 1), while Pb and cobalt (Co) are probable human carcinogens [8-10]. Arsenic has also been reported to cause diabetes in children and adults and has respiratory, dermal, cardiovascular, gastrointestinal, neurological, developmental, and

¹haledemirtepe@iyte.edu.tr (Corresponding Author)

immunological effects [11,12]. Therefore, exposure to these metal(loid)s requires an in-depth investigation.

People living in regions near anthropogenic metal(loid) sources are more prone to exposure [13]. Under the influence of heavy industrial activities and traffic, the metal(loid) composition of soils has been shown to be altered compared to background soils [14-16]. Aliğa industrial region is an example of such industrial regions in Türkiye. The regional industrial activities include iron and steel plants, scrap processing plants, shipbreaking yards, a fertilizer plant, and a petrochemical plant. The region also involves ports, a railway, and a highway where heavy transportation activities exist. Due to these activities, heavy metals have been emitted to the environmental media. Previous studies conducted in the region demonstrated metal(loid) contamination of atmospheric particles [17,18], soil [14,16,19], sediments [20-23], and seawater [24], and accumulation of metals in biological matrices as well [19,25-28]. The region has another importance since three residential areas are very close to the Aliğa industrial region (Horozgediği, Çakmaklı, Bozköy), and agricultural activities, including olive tree fields, are ongoing. A study conducted to observe heavy metal contamination in soils of olive fields showed Ni, Cr, and Pb contamination in the Aliğa region [29]. The researchers also found that higher Al, Ni, and Pb levels measured in the olive leaves were possibly linked to higher soil levels of these metals [29]. This finding indicated that determining soil metal(loid) contamination is essential to assess the impacts of industrial sources on their surroundings and the associated human exposure.

This study aims to evaluate current metal(loid) contamination levels in soils around the Aliğa industrial region and assess human health risks associated with soils in the region. To the author's knowledge, the last study on soil contamination by metal(loid)s in the region was conducted in 2011 [19]. and there is no human health risk assessment study on this scope.

2. Materials and Methods

2.1. Soil Sampling and Physical-Chemical Analyses

Aliğa industrial region is located in İzmir, in western Türkiye. The region consists of several industrial facilities, including scrap processing iron-steel production facilities, steel rolling mills, a petroleum refinery, a petrochemical plant, a fertilizer plant, a natural gas-fired power plant, ship dismantling facilities, and scrap storage sites. The region also includes small residential areas (Figure 1). Soil sampling locations were selected according to the prevailing wind direction (northwest in summer, southeast in winter [14]), location of major sources, and potential receptors. Soil samples #1 and #2 were representative samples for residential areas (i.e., Horozgediği) close to the iron-steel production facilities and scrap storage sites. Soil sample #3 is downwind of major scrap processing iron and steel facilities. Lastly, soil samples #4 and #5 were collected from downwind of ports and near the road towards the port site. These two samples were also representative of agricultural areas in the region since they were collected from olive tree fields. The sampling points are depicted in Figure 1.

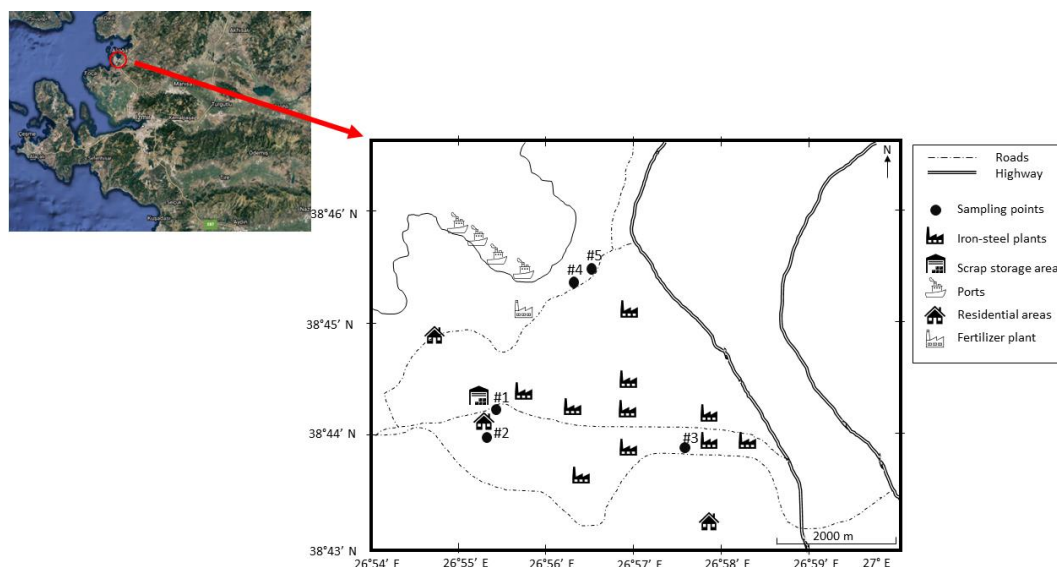


Figure 1. Location of sampling points in the Aliaga industrial region

Surface soil samples (from 0 – 10 cm) were collected in August 2021 (dry period). From every sampling location, at least five subsamples were collected from $\sim 50 \text{ m}^2$ area. After removal of vegetation where necessary, the subsamples were combined to obtain a composite sample in pre-cleaned glass jars. Collected samples were transported immediately to the laboratory at 4°C . After sieving through a 2 mm sieve, some portions of the samples were allocated for moisture content, total organic carbon and particle size analyses, and other portions for metal analysis. The moisture content of soil samples was analyzed by drying 10 g of samples in an oven at 105°C overnight. The organic matter contents were then analyzed by igniting the samples after measuring moisture content in a muffle furnace at 600°C for 4 hours. Total organic carbon analysis was conducted with Shimadzu TOC-Vcph (TNM-1 / SSM-5000A). Particle size analysis was performed by Horiba La-960 Particle Size Distribution Analyzer using the laser diffraction method. pH of the soil samples was measured in a 1:2.5 soil: water suspension using a pH meter after being soaked overnight.

2.2. Analysis of Metals/Metalloids

The soil samples were dried at room temperature overnight. Then, they were grounded by an agate mortar. Approximately 0.5 g of samples were digested in a microwave digester (MARS CEM6) after being soaked in 10 mL of HNO_3 for half an hour. The microwave program was as follows: the temperature was increased to 180°C in 15 minutes, then held there for 20 minutes and cooled back. Digested samples were analyzed for 18 metal(loid)s in an Inductively Coupled Plasma-Mass spectrometer (ICP-MS, Agilent 7500ce Octopole Reaction System). The metal(loid)s studied were lead (Pb), cadmium (Cd), molybdenum (Mo), strontium (Sr), selenium (Se), arsenic (As), zinc (Zn), copper (Cu), nickel (Ni), cobalt (Co), iron (Fe), manganese (Mn), chromium (Cr), calcium (Ca), potassium (K), magnesium (Mg), sodium (Na), and boron (B). The limits of detection for metal(loid)s were between $0.0112 \mu\text{g/L}$ (Cr) and $109 \mu\text{g/L}$ (Ca), and limits of quantitation were in the range $0.0037 \mu\text{g/L}$ (Cd) and $364 \mu\text{g/L}$ (Ca). The certified reference material analyses yielded recoveries in the range 79% (Ca) – 151% (Sr) for Supelco SQC001 and 58% (Mn) – 106% (Pb) for RTC CRM051.

2.3. Pollution Indices Calculation

Pollution indices have been mainly used to assess the degree of metal contamination in soils and sediments [15]. The most widely used pollution indices were calculated as given in (2.1)-(2.4).

$$\text{Enrichment factor}(EF) = \frac{C_n/C_{ref}}{B_n/B_{ref}} \tag{2.1}$$

$$\text{Contamination factor}(CF) = \frac{C_n}{B_n} \tag{2.2}$$

$$\text{Pollution load index}(PLI) = (CF_1 \times CF_2 \times CF_3 \times \dots \times CF_n)^{\frac{1}{n}} \tag{2.3}$$

$$\text{Geoaccumulation index}(I_{geo}) = \log_2 \frac{C_n}{1.5 \times B_n} \tag{2.4}$$

where C_n is the concentration of metal(loid) in the sample, C_{ref} is the concentration of reference metal(loid) in the sample, B_n is the concentration of metal(loid) in background soil (i.e., Earth’s crust), and B_{ref} is the concentration of reference metal(loid) in the Earth’s crust, and n is the number of metal(loid)s analyzed. In this study, Fe was chosen as the reference metal, similar to previous studies [22,23,31], and the elemental concentrations of Earth’s crust were taken from [32]. EF was commonly used to assess the degree of anthropogenic effects on soil [33]. CF was proposed by [34] to determine the pollution level of metal compared to background levels. PLI was developed by [35] as another index for pollution assessment. Lastly, I_{geo} was used to evaluate soil contamination by comparing the current levels with pre-industrial levels [36]. Table 1 represents the criteria to evaluate the pollution levels of soil samples in this study.

Table 1. Criteria to assess soil metal(loid) pollution level

Indices	Value	Assessment
EF	EF < 2	Minimal enrichment
	2 < EF < 5	Moderate enrichment
	5 < EF < 20	Significant enrichment
	20 < EF < 40	Very high enrichment
	EF ≥ 40	Extremely high enrichment
CF	CF < 1	Low contamination factor
	1 ≤ CF < 3	Moderate contamination factor
	3 ≤ CF < 6	Considerable contamination factor
PLI	CF > 6	Very high contamination factor
	PLI < 1	Not polluted
	PLI = 1	Baseline levels of pollution
I_{geo}	PLI > 1	Polluted
	$I_{geo} < 0$	Uncontaminated
	0 < I_{geo} < 1	Uncontaminated to moderately contaminated
	1 < I_{geo} < 2	Moderately contaminated
	2 < I_{geo} < 3	Moderately to strongly contaminated
	3 < I_{geo} < 4	Strongly contaminated
4 < I_{geo} < 5	Strongly to extremely contaminated	
	$I_{geo} \geq 5$	Extremely high contaminated

2.4. Human Health Risk Assessment

The presence of metal(loid)s in soil poses a risk for human health since several interaction mechanisms are possible between soil and humans. Hence, human health risk assessment (HHRA) was conducted using the methodology proposed by the United States Environmental Protection Agency (US EPA) [37]. Three exposure pathways were considered: i) accidental soil ingestion, ii) inhalation of soil particulates, and iii) dermal contact with soil. HHRA was conducted for i) children between 6 and 12 years of age, ii) female adults, and iii) male adults. For the dermal contact pathway, two scenarios were developed for children and adults: exposure during outdoor sports and gardening or farming activities for adults and exposure during playing in dry and wet soil for children. These scenarios provided evaluating one order of magnitude difference in the level of contact with soil, i.e., soil adherence to skin. The daily exposure doses (DED) were estimated for each pathway using (2.5)-(2.7), the mean of the metal(loid) concentrations, and the values presented in Table 2. Then, non-carcinogenic risk was estimated for the metal(loid)s listed in Table 3 using (2.8) since these metal(loid)s had

toxicity reference values (TRVs) defined for modes of action other than cancer. TRV is the maximum dose of a pollutant that a human can intake daily without having a health risk. Several regulatory agencies have reported TRV under various names such as no-observed adverse effect level, tolerable daily intake, and derived no or minimum effect level [38-41]. CompTox database established by the US EPA was used primarily for TRVs since this database reports data from many resources, allowing the users to select the most appropriate one [41]. When no data was available in the CompTox database, other sources (e.g., ECHA, Health Canada, and OEHHA) were used. For As, Cd, Cr, Co, and Pb, which are known and probable human carcinogens, the carcinogenic risk was assessed using (2.9). For As and Pb, oral and inhalation exposure routes were evaluated separately, while for Cd, Cr, and Co, inhalation cancer risk was estimated. Slope factors were obtained from various sources and presented in Table 3.

$$DED_{ing} \left(\frac{mg}{kg \text{ body weight} \times day} \right) = \frac{C_n \times IngR \times EF \times ED}{BW \times AT} \quad (2.5)$$

$$DED_{inh} \left(\frac{mg}{kg \text{ body weight} \times day} \right) = \frac{C_n \times InhR \times EF \times ED}{PEF \times BW \times AT} \quad (2.6)$$

$$DED_{derm} \left(\frac{mg}{kg \text{ body weight} \times day} \right) = \frac{C_n \times TBSA \times SA \times DAF \times EF \times ED}{BW \times AT} \quad (2.7)$$

$$\text{Hazard quotient } (HQ_i) = \frac{DED_i}{RfD_i} \quad (2.8)$$

$$CR_i = DED_i \times SF_i \quad (2.9)$$

Table 2. Parameters used in estimating daily exposure dose due to ingestion, inhalation, and dermal contact exposure routes

Parameter	Value	Reference
Ingestion rate (IngR – mg/day)	20 (adults)	[37]
	50 (children)	[37]
Inhalation rate (InhR – m ³ /day)	15 (adults)	[37]
	12 (children)	
Total body surface area (TBSA – m ²)	2.10 (adult male)	[37]
	1.86 (adult female)	
	1.08 (children)	
Soil adherence to skin (SA – mg/cm ²)	0.01 (adults – outdoor sports-soccer)	[42]
	0.1 (adults – gardeners, farmers)	
	0.2 (children – playing in wet soil)	
	0.04 (children – playing in dry soil)	
Dermal absorption factor (DAF)	0.03 (for As)	[39,42]
	0.01 (for Cd)	
	0.1 (for Cr, Zn)	
	0.06 (for Cu)	
	0.091 (for Ni)	
	0.001 (for all other metal(loid)s)	
Particle emission factor (PEF – m ³ /g)	1.36·10 ⁶	[43]
Exposure duration (ED – years)	24 (adults)	
	6 (children)	[37]
Exposure frequency (EF – days)	350 (adults & children)	[37]
Average time	365·ED (for non-carcinogenic)	[37]
	365·Lifetime (for carcinogenic)	
Lifetime	75 years	[37]
Body weight (BW – kg)	80 (male adults)	[37]
	70 (female adults)	
	31.8 (children)	

Table 3. Toxicity reference values and slope factors of metal(loid)s to be used in risk assessment

Metal(loid)	Toxicity reference value (TRV) (mg/kg.day)	Slope factor (mg/kg.day) ⁻¹	
		oral	inhalation
As	0.0003 [41]	1.5 [41]	27 [39]
Cd	0.001 [41]		42 [39]
Cr (total)	0.001 [39]		46 [39]
Co	1 [41]		27 [44]
Cu	0.041 [38]		
Fe	0.7 [38]		
Mn	0.14 [41]		
Ni	0.02 [41]		
Pb	0.0015 [41]	0.0085 [40]	0.042 [40]
Zn	0.9 [41]		

2.5. Data Analysis

Statistical analyses of the data were conducted using SPSS 25. Non-parametric tests were applied for correlations (Spearman correlation, r_s) due to a low number of samples. Correlations were considered significant if $p < 0.05$.

3. Results and Discussion

3.1. Physical Characteristics of Soil Samples

The collected soil samples had a moisture content of 2.86 – 5.39%, organic matter content of 6.08 – 12.4%, TOC content of 0.91 – 3.51%, and pH of 7.80 – 8.65. Sample #3 has the lowest moisture and organic contents and the highest pH (Table 4). The particle size analysis results revealed that samples #1 and 2 had silt, and others had silt loam texture, according to USDA classification. A previous study identified the soil groups in the study area [45]. According to the classification, samples #1 and #2 belonged to the non-calcareous brown soil group, #3 belonged to the colluvial soil group, and samples #4 and #5 belonged to the brown forest soil group [45].

Table 4. Moisture, organic matter, and total organic carbon content of soil samples (% w/w)

Sample #	Moisture content	OM content	TOC	pH
1	5.39	12.4	2.61	7.80
2	4.06	10.7	3.51	7.88
3	2.86	6.08	0.91	8.65
4	3.23	9.44	2.53	8.20
5	3.49	9.82	2.04	8.00

3.2. Metal(loid) Concentrations in the Soil Samples

The concentrations of metal(loid)s in soil samples are presented in Table 5. The lithophilic elements, such as Fe (mean \pm standard deviation: 26320 \pm 15105 μ g/g dry weight (dw)), Ca (18936 \pm 11952 μ g/g dw), Mg (4910 \pm 1442 μ g/g dw) and K (3047 \pm 1633 μ g/g dw), dominated the soil composition in Aliaga region, while they were lower than crustal elemental concentrations [32]. This finding was also noted by [16], who discussed

the variation concerning site-specific geological formations. Other than the lithophilic elements, Mn, Zn, Pb, and Sr had one or two orders of magnitude higher concentrations than other metal(loid)s. The industrial region has several scrap processing iron and steel facilities operating electric arc furnaces. Previous studies demonstrated that these facilities emit Zn, Fe, Pb, Mn, and Cd from their stacks [46]. Kara et al. [14] study also showed the dust emitted from the region's paved and unpaved roads, slag piles, and coal piles caused the emission of particles involving these metals into the atmosphere. Then, dry and wet deposition of atmospheric particles result in their sinking into the soil around the region. Considering the prevailing wind directions, i.e., northwest in summer, and southeast in winter [14], all sampling locations were influenced by iron and steel facilities throughout the year. Nevertheless, sampling points #1 and #2 showed the highest concentrations for Zn, Fe, Pb, Mn, and Cd, indicating the hot spots in the region. Essentially, these two sampling points showed the highest concentrations for all metal(loid)s analyzed, except for Cu, whose concentration was highest in sampling point #4.

B concentrations in the Aliğa region were previously reported by [14] as $25.5 \pm 17.8 \mu\text{g/g dw}$ around Nemrut Bay, where the samples of the present study were also collected. The present study found a very similar mean value for B ($22.7 \pm 7.77 \mu\text{g/g dw}$) to [14] study in which samples were collected in 2009. The researchers discussed this high value of B compared to other industrial and non-industrial areas of Aliğa that geothermal interferences due to groundwater use in some plants might be the reason [14]. Hence, it can be speculated that groundwater use and geothermal influences continue in the region.

Table 5. Metal(loid) concentrations in soil samples from Aliğa region ($\mu\text{g/g}$ dry weight)

Sample #	1	2	3	4	5	Mean	Median	Standard deviation
Zn	423.9	375.6	201.9	266.4	227.3	299.0	266.4	96.30
Sr	159.6	170.8	125.9	102.6	128.9	137.6	128.9	27.49
Se	0.22	0.09	ND	0.13	0.18	0.12	0.13	0.09
Pb	187.0	186.9	84.45	182.7	144.2	157.1	182.7	44.39
Ni	27.54	50.82	23.00	23.56	30.11	31.01	27.54	11.46
Na	110.8	455.1	398.9	297.1	215.1	295.4	297.1	138.5
Mo	3.08	1.85	1.77	1.67	2.55	2.18	1.85	0.61
Mn	1463	2306	1525	934.9	1066	1459	1463	536
Mg	6626	2671	5252	4662	5341	4910	5252	1442
K	1678	1622	2523	5406	4006	3047	2523	1633
Fe	24582	52371	22960	15475	16213	26320	22960	15105
Cu	34.79	45.38	25.73	87.41	30.67	44.80	34.79	24.90
Cr	42.26	98.82	34.94	37.61	39.88	50.70	39.88	27.04
Co	9.50	11.38	8.83	4.30	6.29	8.06	8.83	2.78
Cd	2.27	2.26	1.03	1.01	1.20	1.55	1.20	0.65
Ca	21153	4935	19135	12414	37043	18936	19135	11952
B	34.54	14.36	25.78	20.09	18.79	22.70	20.10	7.77
As	49.76	30.08	10.92	16.75	45.29	30.56	30.08	17.05

Although the number of samples was low, correlations between elements were investigated to observe possible common sources. Cr and Ni; Pb and Zn; Mn with Fe; As and Cd, Mo, Se; Sr with Fe, Co, and Cr correlated significantly and strongly ($r_s > 0.90$). Cr and Ni are commonly used in industries such as steel production and metal plating [47], while it is worth noting that Ni concentrations in the samples were lower than the crustal

concentrations. Correlations of Pb with Zn and Mn with Fe might show their common source being iron-steel production facilities in the area, while traffic may be another source for Pb and Zn [16]. Arsenic correlation with Cd might indicate their common source to be vehicular or industrial oil combustion [48]. Another source for As and Cd contamination might be the possible use of phosphate fertilizers, which contain these metal(loid) [49]. Moisture and organic matter contents of soil samples significantly correlated with Pb, Zn, Cr, and As concentrations ($r_s=0.90$). The organic matter content of soil influences the sorption of metals to soil, which is also dependent on soil pH and the presence of other metal ions [50]. Correlations of pH with Pb, Cd, As, Zn, and Cr were significant and strong but negative ($r_s=-0.90$). In general, as the soil pH decreases, the solubility and, hence, the mobility of metal(loid)s increases. A previous study also reported lower concentrations of Cd, Pb, and Zn in soils with a pH >8.2 than at a pH around 7.7 [51]. The inverse relationship between pH and concentration found in the present study indicated that redox potential, soil clay content, presence of competing ions, and complexation potential of metal(loid)s were essential parameters to understand the mobility and behavior of metal(loid)s in soil [51]. Nevertheless, Pb, Zn, Cr, and As can be considered the most affected metal(loid)s by the soil organic content and pH. A more precise result can be achieved by increasing the number of soil samples.

Pollution indices were calculated to assess the anthropogenic effects of metal(oids) on soil composition in the region (Figure 2). EFs calculated for As revealed extreme enrichment of soil samples #1 and 5, while significant to very high enrichment of As was observed for other samples. For soil samples #1, 4, and 5, very high enrichment of Pb and Cd were observed. Zn and Mn were moderately to significantly enriched in all samples. The contamination factor was very high for Pb, Cd, and As for all samples. Additionally, for samples #1, 2, and 4, considerable contamination of Zn was observed. Interestingly, B and Mo had moderate contamination factor for all samples. Lastly, according to geoaccumulation index calculations, soil sample #5 was extremely highly contaminated by Mn. Strong to extreme contamination by As was observed for soil sample #1, while strong contamination by Pb and Cd was observed for samples #1 and 2. To sum up, As, Pb, Cd, Zn, and Mn were evaluated as the metal(loid)s of anthropogenic origin in the Aliaga industrial region. This finding was also supported by previous studies conducted in the region [14,16]. High enrichment of metal(loid)s in soil samples #1 and 2, collected from the residential area, suggested a high potential for human exposure. PLI of samples #1 and 2 were higher than one, which supported this hypothesis. Additionally, soil samples #4 and 5 were collected from olive tree fields, and their high enrichment with these metal(loid)s can be considered a threat to agricultural products grown in the area.

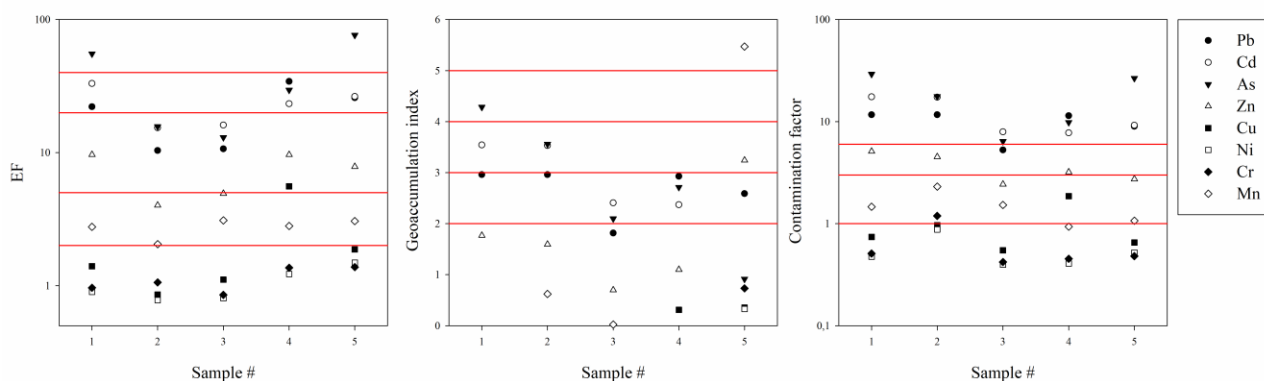


Figure 2. Enrichment factor, geoaccumulation index, and contamination factor for sampling locations in the Aliaga industrial region

Compared to the soil concentrations in Türkiye and around the world (Table 6), this study's metal(loid) concentrations were generally in the range of minimum and maximum observations. Goren et al. [52] presented a comprehensive review of soil metal concentrations from various parts of Türkiye. Compared to Turkish levels, Pb and Fe concentrations found in this study were greater than the Turkish average but lower than that of Türkiye's industrial sites. Also, the Zn and Mn concentrations of this study were greater than that of the Turkish general and industrial average. On the other hand, As, Cu, Co, Ni, and Cr concentrations were lower than the Turkish general and industrial average. Among the previous studies from the region, [16] demonstrated similar concentrations of Fe and Cu but higher concentrations of Cd, Co, Cr, Ni, and Zn. Mn and Pb levels found in this study were higher than those found by [16]. Only As concentration was comparable to that found in [14,19], while other metals were lower in this study. Another study conducted in the region focused on soil concentrations in olive tree fields [29]. Lower levels of Cd and Pb but comparable levels of Cr and Ni were observed by [29]. Two other regions where heavy industrial activities are ongoing in Türkiye, i.e., İskenderun (Hatay) and Dilovası (Kocaeli), showed higher concentrations of metal(loid)s than that of this study, except for As and Pb [30,53]. When compared to the levels from locations where industrial activities such as a Cu-smelter [13], coal-fired power plants [54], petrochemical plants [55,56], and steel production plants [57] affect environmental metal(loid) concentrations in different parts of the world, soil samples from Aliğa region showed consistently higher Pb, Zn, and Mn concentrations. For other metal(loid)s, case-specific observations have been recorded (Table 6).

Table 6. Comparison of mean metal(loid) concentrations in soil samples from around the world ($\mu\text{g/g}$ dry weight)

Location	As	Cd	Co	Cr	Cu	Fe	Mn	Ni	Pb	Zn	References
Aliğa, Türkiye (n=5)	30.56	1.55	8.06	50.7	44.8	26320	1459	31.01	157.1	299	This study
Aliğa, Türkiye (n=9)	-	2.3	23	163	45	27800	864	62	85	1092	[16]
Aliğa, Türkiye (n=13)	25.5	23.5	16.7	2	237	50900	3148	71.9	1309	6065	[14]
Aliğa, Türkiye (n=21)	27.1	2	-	-	55.7	-	-	-	237	933	[19]
Hatay, İskenderun, Türkiye (n=17)	9	2	-	798	61	-	-	1154	109	531	[30]
Dilovası, Kocaeli, Türkiye (n=49)	11	2.1	8	125	59	34628	2684	44	129	535	[53]
Konya, Türkiye (n=17)	-	0.15	-	24.98	-	-	-	34.29	20.48	-	[58]
Turkish average	188	1.55	13.9	133	72.9	18918	555	89.2	78.7	162	[52]
Türkiye's industrial soils average	500	4.25	21.1	333	588	35579	992	125	248	248	[52]
Hubei, China (n=102)	35.84	4.87	-	-	195.26	-	-	-	92.65	-	[13]
Jiangsu, China (n=105)	7.46	0.11	12.76	86.38	31.6	11600	352.8	34.93	31.41	61.16	[59]
Rostov Region, Russia (n=12)	-	0.8	-	23.64	53	-	827	58.4	41.9	108.7	[54]
Mahshahr, Iran (n=47)	0.37	3.58	-	23.64	20.88	-	-	70.89	39.65	62.98	[56]
Ulsan, Phang, Gwangyang, S.Korea (n=50)	8.3	2	9.2	30.4	24.8	28800	588.6	16.4	23.7	119	[55]
Smederevo, Serbia (n=48)	-	2.75	25.5	56.3	31.8	24620	740	80.2	40.6	77.6	[57]

3.3. Human Health Risk Assessment

HHRA was conducted to understand how soil contamination by metal(loid)s might affect local people through three main exposure pathways: accidental ingestion of soil, inhalation of soil particulates, and dermal contact with soil. Non-carcinogenic risks (HQ) have been estimated for children and adults for each metal separately. Figure 3 presents HQ values estimated for all exposure pathways where two scenarios were generated for dermal contact. The results suggested that HQs varied significantly by exposure scenario, metal(loid) species, and age. Among the exposure pathways, inhalation had the lowest HQs for all metals. A general factor of particulate emission from soil [43] was used to estimate inhalation exposure; hence, sampling of particulate matter and dust right above soil might better represent local emissions and, accordingly, the exposure dose via inhalation of soil particulates in the region. As can be seen from Figure 3, dermal contact during playing with dry and wet soil for children and during outdoor sports and farming for adults completely changed the HQ profiles. The ingestion pathway was the most significant contributor to non-carcinogenic risk for all metal(loid)s when playing with dry soil, and outdoor sports scenarios were considered. In contrast, HQ of dermal contact with soil exceeded that of ingestion pathway for As, Zn, Cr, Cu, and Ni when playing with wet soil, and farming scenarios were considered. The hazard index (HI) was also calculated by summing up the HQs of each exposure pathway for each metal(loid). For dermal contact during playing with dry soil and outdoor sports scenarios, the highest HIs of metal(loid)s were in the order: As (0.20) > Pb (0.17) > Cr (0.15) for children and As (0.04) > Pb (0.03) > Cr (0.027) for adults. However, for dermal contact during playing with wet soil and farming scenario, HI order has changed to Cr (0.41) > As (0.36) > Pb (0.17) for children and Cr (0.14) > As (0.11) > Pb (0.03) for adults. Therefore, it was recommended that exposure scenarios were carefully defined while conducting HHRA.

Examining the above-given HI values, no metal(loid) exceeded the unacceptable risk level of 1. Hence, the non-carcinogenic risk of exposure to Aliąa soil was evaluated to be acceptable under all scenarios. Comparatively, children always had a higher risk than adults due to their lower body weight and higher accidental soil ingestion rate, indicating that children are more susceptible to environmental contamination.

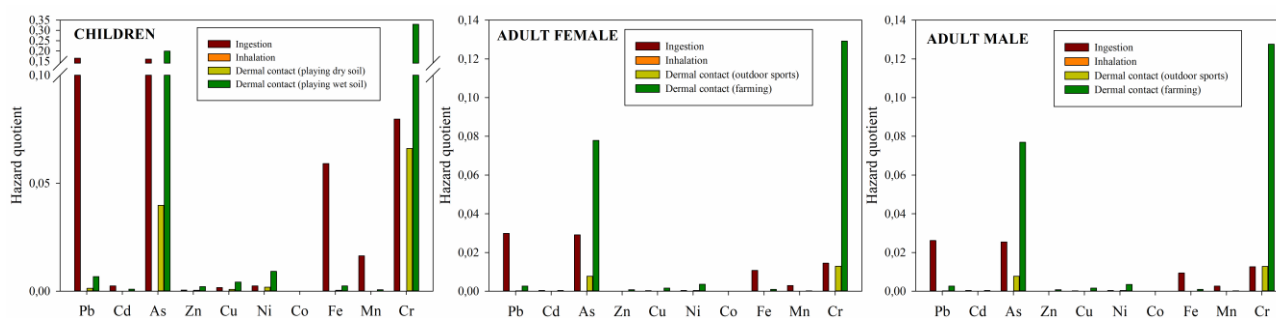


Figure 3. Hazard quotients of metal(loid)s' exposure via various pathways for children and adults

This study also estimated the carcinogenic risks of exposure to metal(loid)s in soil, considering only ingestion and inhalation pathways. CR for children via ingestion and inhalation pathways were $2.21 \cdot 10^{-5}$ and $1.76 \cdot 10^{-8}$ for As, and $1.61 \cdot 10^{-7}$ and $1.40 \cdot 10^{-10}$ for Pb, respectively. Since there are only slope factors of inhalation route for Cr, Co, and Cd, their CR for children were $4.96 \cdot 10^{-8}$, $6.35 \cdot 10^{-9}$, and $1.39 \cdot 10^{-9}$, respectively. CRs for adults were lower than those for children through the ingestion pathway, yet they were approximately two times higher than those for children through the inhalation pathway. Since all CRs estimated in this study were lower than 10^{-4} , which is the threshold for unacceptable cancer risk, the carcinogenic risk of exposure to soil metal(loid)s was evaluated to be acceptable. While As was the most important contributor to CR via the

ingestion pathway, Cr became the prominent metal(loid) in CR via the inhalation pathway. The interchange of important metal(loid)s, As, and Cr between exposure scenarios was also observed in non-carcinogenic risk assessment.

4. Conclusion

The metal(loid) concentrations of five soil samples collected from the Aliaga industrial region were dominated by lithophilic elements. However, pollution indices demonstrated moderate to extreme enrichment and strong to extremely high soil contamination of Pb, Cd, Mn, Zn, and As. Scrap processing iron and steel facilities with electric arc furnaces were the possible sources of these metal(loid)s together with oil combustion in the region. The study was deemed a pre-screening of soils in Aliaga industrial region after a ten-year research gap to understand the current hot spots. As a result, samples from residential and agricultural areas pointed out the possibility of human exposure to metal(loid)s in soil. HHRA suggested that both carcinogenic and non-carcinogenic risks were at an acceptable level. However, a considerable increase in HQ values has been observed when dermal exposure scenarios were changed. Hence, exposure scenarios should be clearly defined when conducting HHRA. Additionally, this study only considered soil exposure pathways and did not include inhalation of metal accumulating air particles or ingestion of locally grown food. It is important to conduct a comprehensive risk assessment not to underestimate the risk of living close to an industrial region. Furthermore, a more extensive sampling and analysis strategy would be essential for continuously monitoring soil contamination and assessing the risk in the area.

Author Contributions

The author read and approved the final version of the paper.

Conflicts of Interest

The author declares no conflict of interest.

Acknowledgement

The author would like to thank İzmir Institute of Technology Integrated Research Center for conducting metal(loid)s and TOC analysis (Environmental Development Application and Research Center) and particle size analysis (Center for Materials Research).

References

- [1] J. Briffa, E. Sinagra, R. Blundell, *Heavy metal pollution in the environment and their toxicological effects on humans*, Heliyon, 6 (9) (2020).
- [2] P. C. Nagajyoti, K. D. Lee, T. V. M. Sreekanth, *Heavy metals, occurrence and toxicity for plants: A review*, Environmental Chemistry Letters 8 (3) (2010) 199–216.
- [3] X. Xin, J. Shentu, T. Zhang, X. Yang, V. C. Baligar, Z. He, *Sources, indicators, and assessment of soil contamination by potentially toxic metals*. Sustainability (Switzerland) 14 (23) (2022).
- [4] G. Chen, G. Zeng, C. Du, D. Huang, L. Tang, L. Wang, G. Shen, *Transfer of heavy metals from compost to red soil and groundwater under simulated rainfall conditions*, Journal of Hazardous Materials 181 (1–3) (2010) 211–216.

- [5] P. K. Rai, S. S. Lee, M. Zhang, Y. F. Tsang, K. H. Kim, Heavy metals in food crops: Health risks, fate, mechanisms, and management, *Environment International*, 125 (2019) 365–385.
- [6] ATSDR, Toxicological Profile for Cadmium, Atlanta, Georgia, USA, 2012.
- [7] ATSDR, Toxicological Profile for Lead, Atlanta, Georgia, USA, 2020.
- [8] IARC, Beryllium, Cadmium, Mercury, and Exposures in the Glass Manufacturing Industry, Vol. 58 of IARC Monographs on the Evaluation of Carcinogenic Risks to Humans, UK, 1993.
- [9] IARC, Arsenic, metals, fibres, and dusts, Vol. 100C of IARC Monographs on the Evaluation of Carcinogenic Risks to Humans, Lyon, France, 2012.
- [10] IARC, Cobalt, Antimony Compounds, and Weapons-grade Tungsten Alloy, Vol. 131 of IARC Monographs on the Identification of Carcinogenic Hazards to Humans, Lyon, France, 2023.
- [11] ATSDR, Toxicological Profile for Arsenic, Atlanta, Georgia, USA, 2007.
- [12] ATSDR, Addendum to the Toxicological Profile for Arsenic, Atlanta, Georgia, USA, 2016.
- [13] L. M. Cai, Q. S. Wang, J. Luo, L. G. Chen, R. L. Zhu, S. Wang, C. H. Tang, *Heavy metal contamination and health risk assessment for children near a large Cu-smelter in central China*, *Science of the Total Environment*, 650 (2019) 725–733.
- [14] M. Kara, Y. Dumanoglu, H. Altiok, T. Elbir, M. Odabasi, A. Bayram, *Spatial distribution and source identification of trace elements in topsoil from heavily industrialized region, Aliaga, Turkey*, *Environmental Monitoring and Assessment* 186 (10) (2014) 6017–6038.
- [15] H. D. Weissmannová, J. Pavlovský, *Indices of soil contamination by heavy metals – methodology of calculation for pollution assessment (minireview)*, *Environmental Monitoring and Assessment*, 189 (12) (2017).
- [16] S. Yatkin, A. Bayram, *Investigation of chemical compositions of urban, industrial, agricultural, and rural top-soils in İzmir, Turkey*, *Clean - Soil, Air, Water* 39 (6) (2011) 522–529.
- [17] B. Cetin, S. Yatkin, A. Bayram, M. Odabasi, *Ambient concentrations and source apportionment of PCBs and trace elements around an industrial area in Izmir, Turkey*, *Chemosphere* 69 (8) (2007) 1267–1277.
- [18] M. Kara, Y. Dumanoglu, H. Altiok, T. Elbir, M. Odabasi, A. Bayram, *Seasonal and spatial variations of atmospheric trace elemental deposition in the Aliaga industrial region, Turkey*, *Atmospheric Research* 149 (2014) 204–216.
- [19] M. Odabasi, D. Tolunay, M. Kara, E. Ozgunerge Falay, G. Tuna, H. Altiok, Y. Dumanoglu, A. Bayram, T. Elbir, *Investigation of spatial and historical variations of air pollution around an industrial region using trace and macro elements in tree components*, *Science of the Total Environment* 550 (2016) 1010–1021.
- [20] E. Esen, F. Kucuksezgin, E. Uluturhan, *Assessment of trace metal pollution in surface sediments of Nemrut Bay, Aegean Sea*, *Environmental Monitoring and Assessment* 160 (1–4) (2010) 257–266.
- [21] G. Neşer, A. Kontas, D. Ünsalan, E. Uluturhan, O. Altay, E. Darilmaz, F. Küçüksezgin, N. Tekoğul, F. Yercan, *Heavy metals contamination levels at the Coast of Aliaga (Turkey) ship recycling zone*, *Marine Pollution Bulletin*, 64 (4) (2012) 882–887.
- [22] E. Tunca, M. Aydın, Ü. A. Şahin, *An ecological risk investigation of marine sediment from the northern Mediterranean coasts (Aegean Sea) using multiple methods of pollution determination*, *Environmental Science and Pollution Research*, 25 (8) (2018) 7487–7503.
- [23] A. Yılmaz, B. Karacık, S. D. Yakan, B. Henkelmann, K. W. Schramm, O. S. Okay, *Organic and heavy metal pollution in shipbreaking yards*, *Ocean Engineering* 123 (2016) 452–457.

- [24] M. Kara, Y. Dumanoglu, H. Altiook, T. Elbir, M. Odabasi, A. Bayram, *Spatial variation of trace elements in seawater and sediment samples in a heavily industrialized region*, Environmental Earth Sciences 73 (1) (2015) 405–421.
- [25] H. Aydın, E. E. Yürür, S. Uzar, F. Küçüksezgin, *Endüstriyel kirliliğin etkisindeki Aliğa ve Nemrut Körfezi modern dinoflagellat kist topluluğu*, Turkish Journal of Fisheries and Aquatic Sciences 15 (2) (2015) 543–554.
- [26] M. Aydın, E. Tunca, Ü. Alver Şahin, *Effects of anthropological factors on the metal accumulation profiles of sea cucumbers in near industrial and residential coastlines of İzmir, Turkey*, International Journal of Environmental Analytical Chemistry 97 (4) (2017) 368–382.
- [27] D. Ozkan, M. Dagdeviren, S. Katalay, A. Guner, N. Ü. K. Yavaşoğlu, *Multi-biomarker responses after exposure to pollution in the Mediterranean mussels (mytilus galloprovincialis l.) in the Aegean Coast of Turkey*, Bulletin of Environmental Contamination and Toxicology 98 (1) (2017) 46–52.
- [28] I. Pazi, L. T. Gonul, F. Kucuksezgin, G. Avaz, L. Tolun, A. Unluoglu, Y. Karaaslan, S. M. Guver, A. Koc Orhon, E. Siltu, G. Olmez, *Potential risk assessment of metals in edible fish species for human consumption from the Eastern Aegean Sea*, Marine Pollution Bulletin, 120 (1–2) (2017) 409–413.
- [29] B. Çolak Esetlili, T. Pekcan, E. Aydoğdu, S. Turan, D. Anaç, *Natural radionuclides and heavy metal contents in the olive (Olea Europaea L.) groves of Northwestern Anatolia*, Journal of Tekirdag Agricultural Faculty 16 (2) (2019) 260–269.
- [30] M. Odabasi, A. Bayram, T. Elbir, R. Seyfioglu, Y. Dumanoglu, S. Ornektekin, *Investigation of soil concentrations of persistent organic pollutants, trace elements, and anions due to iron–steel plant emissions in an industrial region in Turkey*, Water, Air and Soil Pollution 213 (1–4) (2010) 375–388.
- [31] A. O. Famuyiwa, C. M. Davidson, A. O. Oyeyiola, S. Ande, Y. Lanre-Iyanda, S. O. Babajide, *Pollution characteristics and health risk assessment of potentially toxic elements in school playground soils: A case study of Lagos, Nigeria*, Human and Ecological Risk Assessment 25 (7) (2019) 1729–1744.
- [32] A. A. Yaroshevsky, *Abundances of chemical elements in the Earth's crust*, Geochemistry International 44 (1) (2006) 48–55.
- [33] R. A. Sutherland, *Bed sediment-associated trace metals in an urban stream, Oahu, Hawaii*, Cases and Solutions Environmental Geology 39 (6) (2000).
- [34] L. Hakanson, *An ecological risk index for aquatic pollution control. a sedimentological approach*, Water Research 14 (8) (1980) 975–1001.
- [35] D. L. Tomlinson, J. G. Wilson, C. R. Harris, D. W. Jeffrey, *Problems in the assessment of heavy-metal levels in estuaries and the formation of a pollution index*, Helgoländer Meeresuntersuchungen, 33 (1980) 566–575.
- [36] G. Müller, *Index of geoaccumulation in sediments of the Rhine River*, GeoJournal 2 (1969) 108–118.
- [37] US EPA, Exposure Factors Handbook: 2011 Edition, National Center for Environmental Assessment, Washington, DC, USA, 2011.
- [38] ECHA, European Chemicals Agency Information on Chemicals, <https://echa.europa.eu/information-on-chemicals>, Accessed 28 Aug 2023.
- [39] Health Canada, Toxicological Reference Values (TRVs) and Chemical-Specific Factors, Version 2.0, Part II of Federal Contaminated Site Risk Assessment in Canada, Ottawa, Ontario, Canada, 2010.
- [40] OEHHA, California Office of Environmental Health Hazard Assessment, <https://oehha.ca.gov/chemicals>, Accessed 28 Aug 2023.

- [41] US EPA, CompTox Chemicals Dashboard, <https://comptox.epa.gov/dashboard/>, Accessed 28 Aug 2023.
- [42] US EPA, Example Exposure Scenarios, National Center for Environmental Assessment, Washington, DC, USA, 2004.
- [43] US EPA, Supplemental Guidance for Developing Soil Screening Levels for Superfund Sites, Washington DC, USA, 2002.
- [44] OEHHA, Cobalt and Cobalt Compounds Cancer Inhalation Unit Risk Factors, California, USA, 2020.
- [45] İ. Eroğlu, R. Bozyiğit, *The natural and humanitarian factors affecting the land use in Aliğa, Marmara Coğrafya Dergisi* 27 (2013) 353–400.
- [46] S. Yatkin, A. Bayram, *Determination of major natural and anthropogenic source profiles for particulate matter and trace elements in Izmir, Turkey*, *Chemosphere*, 71 (4) (2008) 685–696.
- [47] H. Zhao, Y. Wu, X. Lan, Y. Yang, X. Wu, L. Du, *Comprehensive assessment of harmful heavy metals in contaminated soil in order to score pollution level*, *Scientific Reports*, 12(1) (2022).
- [48] M. Mansha, B. Ghauri, S. Rahman, A. Amman, *Characterization and source apportionment of ambient air particulate matter (PM_{2.5}) in Karachi*, *Science of the Total Environment*, 425 (2012) 176–183.
- [49] W. Jiao, W. Chen, A. C. Chang, A. L. Page, *Environmental risks of trace elements associated with long-term phosphate fertilizers applications: A review*, *Environmental Pollution* 168 (2012) 44–53.
- [50] M. M. Nederlof, W. H. Van Riemsdijk, *Effect of natural organic matter and pH on the bioavailability of metal ions in soils*, in: P. M. Huang, J. Berthelin, J. M. Bollag, W. B. McGill, A. L. Page (Eds.), *Environmental Impact of Soil Component Interactions: Metals, Other Inorganics, and Microbial Activities Volume II*, CRC Press, London, 1995, Ch. 7, pp. 75–86.
- [51] A. Kicińska, R. Pomykała, M. Izquierdo-Diaz, *Changes in soil pH and mobility of heavy metals in contaminated soils*, *European Journal of Soil Science*, 73 (1) (2022).
- [52] A. Y. Goren, M. Genisoglu, Y. Kazanclı, S. C. Sofuoğlu, *Countrywide spatial variation of potentially toxic element contamination in soils of Turkey and assessment of population health risks for nondietary ingestion*, *ACS Omega* 7(41) (2022) 36457–36467.
- [53] B. Cetin, *Soil concentrations and source apportionment of polybrominated diphenyl ethers (PBDEs) and trace elements around a heavily industrialized area in Kocaeli, Turkey*, *Environmental Science and Pollution Research International* 21 (13) (2014) 8284–8293.
- [54] T. Minkina, E. Konstantinova, T. Bauer, S. Mandzhieva, S. Sushkova, V. Chaplygin, M. Burachevskaya, O. Nazarenko, R. Kizilkaya, C. Gülser, A. Maksimov, *Environmental and human health risk assessment of potentially toxic elements in soils around the largest coal-fired power station in Southern Russia*, *Environmental Geochemistry and Health* 43(6) (2021) 2285–2300.
- [55] I. G. Cho, M. K. Park, H. K. Cho, J. W. Jeon, S. E. Lee, S. D. Choi, *Characteristics of metal contamination in paddy soils from three industrial cities in South Korea*, *Environmental Geochemistry and Health* 41 (5) (2019) 1895–1907.
- [56] F. Nikfar, S. Sabzalipour, A. Gholami, A. Nazarpour, *Carcinogenic risk assessment, health endpoint and source identification of heavy metals in Mahshahr, Iran*, *Toxin Reviews* 42 (1) (2023) 132–145.
- [57] R. Dragović, B. Gajić, S. Dragović, M. Dordević, M. Dordević, N. Mihailović, A. Onjia, *Assessment of the impact of geographical factors on the spatial distribution of heavy metals in soils around the steel production facility in Smederevo (Serbia)*, *Journal of Cleaner Production* 84 (1) (2014) 550–562.
- [58] A. Ozturk, O. K. Arici, *Carcinogenic-potential ecological risk assessment of soils and wheat in the eastern region of Konya (Turkey)*, *Environmental Science and Pollution Research* 28 (2021) 15471–15484.

- [59] Y. Jiang, S. Chao, J. Liu, Y. Yang, Y. Chen, A. Zhang, H. Cao, *Source apportionment and health risk assessment of heavy metals in soil for a township in Jiangsu Province, China*, Chemosphere 168 (2017) 1658–1668.



Disposable Voltammetric Determination of Celestine Blue at a Pencil Graphite Electrode

Mehmet Güneş¹ 

¹Department of Chemistry, Faculty of Science, Çanakkale Onsekiz Mart University, Çanakkale, Türkiye

¹High School of Kanuni Anatolian Imam Hatip, Aksaray, Türkiye

Abstract – The proposed study describes a novel and disposable voltammetric sensor that designed for the sensitive determination of celestine blue (CelsB) using a pencil graphite electrode (PGE). The electrochemical characterization study of the designed sensor was performed by recording the cyclic voltammograms (CVs) and electrochemical impedance (EI) curves in 5.0 mM of $\text{Fe}(\text{CN})_6^{3-/4-}$ including 0.10 M of KCl, and compared with the other carbon-based electrodes such as carbon paste (CPE) and glassy carbon (GCE) electrodes. The electrochemical behaviour of CelsB was examined at different carbon-based electrodes including PGE, CPE, and GCE by the cyclic voltammetric (CV) method. The recorded CVs showed that the remarkable response obtained at PGE toward oxidation of CelsB. Moreover, the PGE shows a wide linear range (4.0 – 150 μM) and detects the CelsB with a notable limit of detection (1.21 μM). In addition, the results from the interference studies proved that the PGE enables selective voltammetric determination of CelsB in presence of various species. A feasibility study for CelsB sensor was also tested on tap water and cherry apple juice samples and the recovery values obtained between 96.2 – 103 % with high precision and accuracy indicated that the PGE shows an acceptable and good applicability to real samples.

Article History

Received: 1 Oct 2023

Accepted: 21 Nov 2023

Published: 15 Mar 2024

Research Article

Keywords – Celestine blue, electrochemistry, pencil graphite electrode, sensors, voltammetry

1. Introduction

Dyes have been used as an important component in leather, paper, textile, and pharmaceutical products. As a result, the widespread use of dyestuffs induced soil and water pollution [1-4]. The CelsB which is soluble in water and classified as an essential oxyazine group dye, shows good mediator properties due to its high electron transfer properties (Figure 1) [5]. The CelsB has a non-complex structure, and it is structurally positively charged property [6]. On the other hand, it causes harmful effects on human health [7-9]. It has also been expressed that the extreme use of azo dyes [10] may cause mutagenic, hyperactivity, and carcinogenic impacts in children [11]. According to the information mentioned above, the rapid, selective, and sensitive determinations of CelsB have a great importance on humans and the environment. It may be stated that the electrochemical oxidation and reduction of CelsB proceeds with the exchange of two protons and two electrons via catechol groups [7].

¹m.gunes@outlook.com (Corresponding Author)

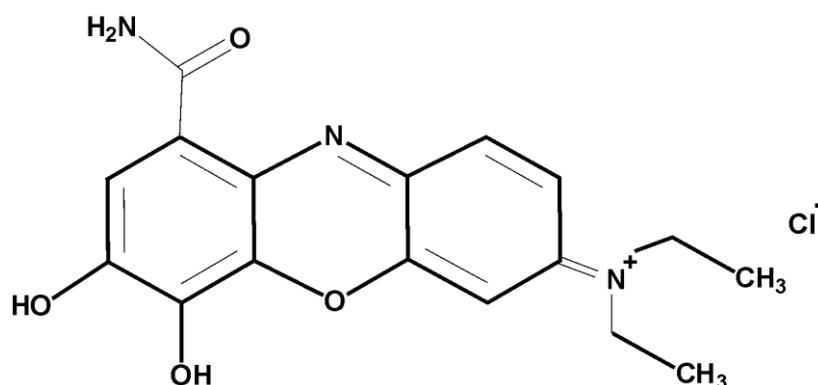


Figure 1. Structure of molecular CelsB [5]

Electrochemical methods are still attractive due to their cheapness, high sensitivity, mobility, selectivity, speedy response, easy instrumentation, ability to be miniaturized properties [12,13]. Various carbon-based electrodes, such as PGE, CPE, and GCE have been widely used in the design of electrochemical sensors [14]. The GCE is expensive and includes hard and time-consuming surface cleaning and polishing procedures. The other commonly used electrode, CPE has a renewable surface and cost-effective, but it also includes hard preparation steps and the same limitations mentioned above [15]. Among these electrodes, the PGE attracts great attention due to its many advantageous properties. These features can be listed as follows; disposability, low-priced, pretty reactive, renewable surface, less toxicity, extensive potential range, well mechanical rigidity, and easily available [16-22].

As far as we know from the literature, there is no study that performed for the electrochemical determination of CelsB using PGE. In this study, the disposable PGE firstly was used for the sensitive and selective voltammetric detection of CelsB. Considering the recovery values obtained from the feasibility test on different samples suggested that the proposed methodology can be applied successfully in the determination of CelsB from daily samples.

2. Materials and Methods

2.1. Apparatus and Chemicals

All electrochemical measurements were performed using a Galvano plot GX203 analyzer originating in Türkiye. Experiments were carried out by choosing RE5B-BASI Ag/AgCl_(saturated KCl) (Diameter size: 6.0 mm) as the reference electrode, MW1032-BASI Pt wire (Diameter size: 0.50 mm) as the counter electrode, and pencil graphite as the working electrode in the cell of the conventional triple electrode system where the experiment was conducted. All electrochemical measurements were evaluated for the PGE (The used length is 1.0 cm that equals to 0.159 cm² of geometric area (A_G), CPE (BASI, Diameter size: 2.87 mm), GCE (BASI, Diameter size: 3.0 mm). A pH meter device (HI-221 Hanna) including a unified glass electrode system was used to regulate Britton-Robinson buffer solutions (BRBS) at different pHs. The pure water was generated from the device of Q7B Elga option. Celestine blue (97%, C₁₇H₁₈N₃O₄Cl, 363.80 g mol⁻¹), citric acid, D(+)-glucose, tartrazine (Tz), quinoline yellow (QY), and brilliant blue (BB) were purchased from Aldrich. K₃[Fe(CN)₆] and dopamine hydrochloride (DA), were provided from Alfa Aesar. KNO₃, Na₂SO₄, Na₂CO₃, CaCl₂.2H₂O, Mg₂SO₄.7H₂O, Na₂HPO₄, NaH₂PO₄ MgCl₂, KCl, NaCl, CH₃COOH, NaOH, H₃BO₃, H₃PO₄, K₄[Fe(CN)₆].2H₂O, L-ascorbic acid (L-AA), fructose, and were provided from Merck company.

2.2. Electrochemical Experiments

The CPE used in the experimental study was prepared by filling the CPE body after obtaining a paste consistency with mineral oil (25%) and graphite powder (75%). Before use, GCE was cleaned with alumina slurry (0.30 μm) and polished. Then, resulted electrode was left in an ultrasonic bath in ethanol and water for 10 minutes to remove the trace of impurities. EI curves of PGE, GCE, and CPE (frequency range of 0.10 – 100000 Hz) were recorded in 5.0 mM of $\text{Fe}(\text{CN})_6^{3-/4-}$ solution that contains 0.10 M KCl. Cyclic voltammetric responses of 16 μM CelsB at the mentioned electrodes were recorded in pH 5.0 BRBS containing KCl. The effect of pH and scan rate on electrochemical response of CelsB was examined from the recorded CVs of 50 μM CelsB.

2.3. Real Sample Study

To determine the CelsB in tap water and cherry apple juice samples, known (5 and 10 μM) concentrations of CelsB were spiked into both samples. Afterward, the standard additions were performed from the 5.0 mM standard CelsB solution, and CVs were recorded. Recovery values were calculated for the samples.

3. Results and Discussion

3.1. Characterization Studies

Electrochemical impedance spectroscopy (EIS) is a useful method for the examination of the surface conductivity properties of electrodes. The semicircle part of the curves corresponds to charge transfer resistance (R_{ct}) directly related with the surface conductivity at high frequencies, and the linear part is related with the diffusion [23,24]. The PGE, CPE, and GCE are electrochemically characterized by the recording of the CVs (Figure 2A) and EI curves (Figure 2B) of 5.0 mM of $\text{Fe}(\text{CN})_6^{3-/4-}$ solution that contains 0.10 M KCl.

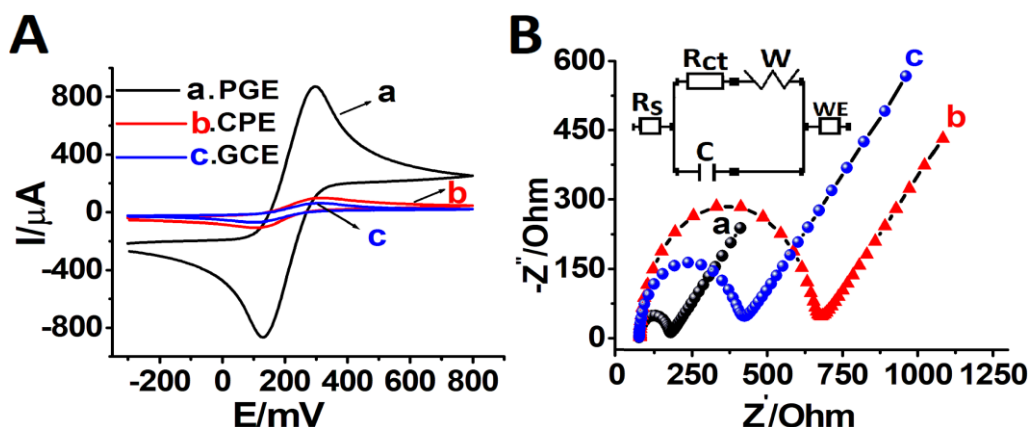


Figure 2. A) CVs and B) EI curves for 5.0 mM of $\text{Fe}(\text{CN})_6^{3-/4-}$ solution contains 0.10 M KCl at (a) PGE, (b) CPE, and (c) GCE, the inset of Figure B is the electrochemical impedance circuit model: (C: Capacitance for double-layer; R_s : Ohmic resistance; WE: Working electrode ; W: Warburg impedance, (Scan rate (S.rate): 50 mV/s)

As can be seen in Figure 2A, the oxidation (E_a) and reduction (E_c) peak currents of different carbon-originated electrodes (CPE and GCE) are significantly lower than that obtained with PGE (Table 1). The reversibility of the peaks belongs to $\text{Fe}(\text{CN})_6^{3-/4-}$ higher ($\Delta E = 173$ mV) than those obtained at CPE and GCE and its surface exhibits better conductivity ($R_{ct} = 96$ ohm). The PGE shows high voltammetric response and better conductivity among the other electrodes. Because, the PGE has a composite structure including graphite and clay that

provides larger electroactive surface. Therefore, this structural property may have improved the electron transfer between PGE and $\text{Fe}(\text{CN})_6^{3-/4-}$ [25].

Table 1. CV and EIS responses obtained as a result of the characterization studies of the electrodes

WE	Results from the recorded CVs				Results from the recorded EI curves	
	E_a (mV)	E_c (mV)	ΔE (mV)	I_a (μA)	I_c (μA)	R_{ct} (Ohm)
PGE	299	126	173	885	871	96
CPE	325	110	215	94	95	574
GCE	309	100	209	98	97	310

3.2. Investigation of the Electrochemical Behavior of CelsB

The recorded CVs for $16\mu\text{M}$ CelsB in BRBS (pH 5.0) at the PGE, CPE, and GCE was given in Figure 3. The recorded CVs indicate that the irreversible oxidation of CelsB observed at 746, 800, and 708 mV at the PGE, CPE, and GCE, respectively. Moreover, the highest voltammetric response based on the irreversible oxidation of CelsB obtained with PGE. The best voltammetric response observed at PGE are attributed to the porous composite structure that leads an increase in electroactive surface area of PGE. In other words, the electron transfer between CelsB and PGE on the surface of PGE improved [25]. Therefore, the PGE was selected for the determination of CelsB according to its highest response.

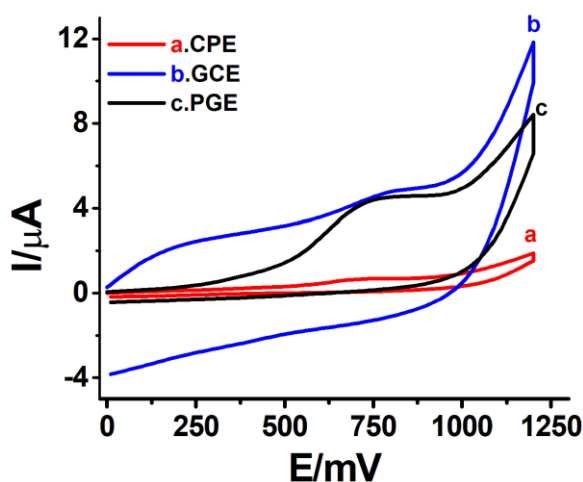


Figure 3. CVs of $16\mu\text{M}$ CelsB electrochemical responses at (a) CPE, (b) GCE, and (c) PGE in BRBS (pH 5.0) at S.rate 50 mV/s

3.3. The Effect of pH

The CV method was used to determine the most suitable supporting electrolyte developed for the determination of CelsB. For this aim, CVs of $50\mu\text{M}$ CelsB in BRBS solutions with different pH values (2.0 – 6.0) were recorded at PGE (Figure 4). Because of the fact that the best electrochemical response was achieved at the pH of 5.0, this supporting electrolyte was chosen for further studies.

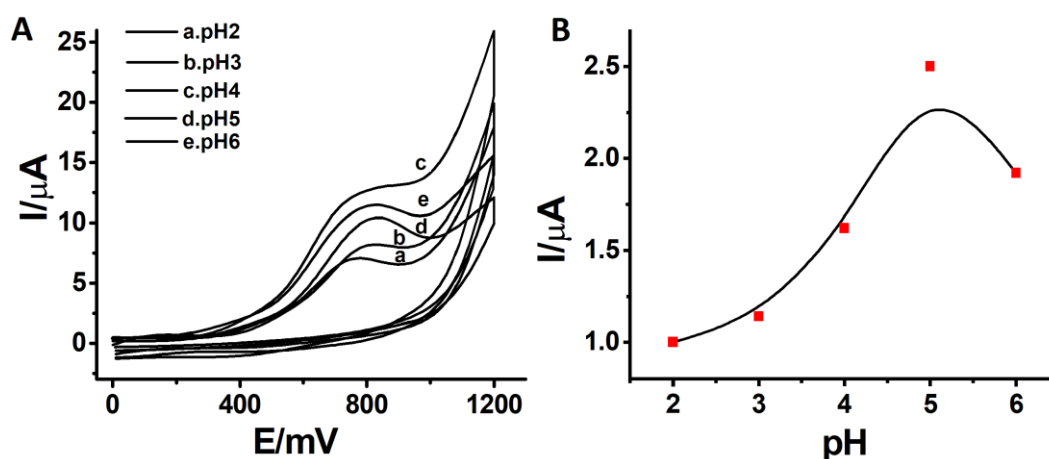


Figure 4. A) The CVs recorded for 50 μ M CelsB in various pH values (2.0 – 6.0) of BRBS (Potential range: 0 – 1200 mV, S.rate: 50 mV/s) and B) pH versus current graph

3.4. The Influence of Scan Rate

The influence of scan rate on the voltammetric response of CelsB was investigated by recording the CVs 50 μ M CelsB in BRBS (pH 5.0) at enhanced scan rates ranging from 10 to 600 mV/s (Figure 5). The effect of scan rate on peak current among 10 and 600 mV/s was investigated using the CV method of 50 μ M CelsB in pH 5.0 BRBS. As can be understood from the given Figure, the voltammetric response based on the oxidation peak current of CelsB enhances by the increasing of scan rate. In addition, the high linearity ($R^2 = 0.9977$) between the $I_a(\mu\text{A})$ vs. square root of scan rate generated from the recorded CVs confirms that the irreversible oxidation of CelsB occurs with a diffusion-controlled process [25-28].

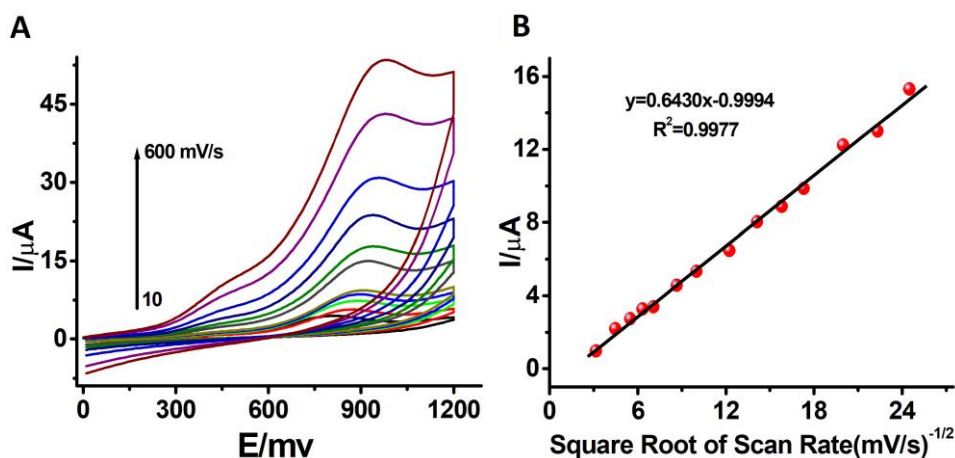


Figure 5. A) CV responses acquired from PGE against 50 μ M CelsB at different S.rate (10-600 mV/s) at pH 5 (BRBS) potential range: 0 – 1200 mV, B) the linear variation of the square root of the scan rate versus the oxidation peak currents of CelsB

3.5. The Cyclic Voltammetric Determination of CelsB

The determination of CelsB performed by CV technique. Figures 7 and 8 show the CVs of the increased concentrations of CelsB (0 – 150 μ M). The obtained calibration curve generated from the CVs confirmed that the voltammetric response of CelsB goes linearly between 0 – 150 μ M. The LOD value was calculated according to the $3 \times \text{Std}/\text{slope}$ and was found to be 1.21 μ M (Std is the standard deviation of the minimum CelsB concentration that observes as a measurable signal; the slope was calculated from the calibration plots). The electrochemical performance of the CelsB sensor has been compared with the only study reported in

literature (Table 2) (Roushani et al., 2021). In the reported study, screen printed carbon electrode was modified with NiO nanoparticles and synthesized molecularly imprinted polymer of CelsB (CB-MIP/NiO-NPs/SPCE) for the differential pulse voltammetric determination of CelsB. Although the related sensor shows wider linear range (2.0 – 150 μM) and lower LOD (0.35 μM), the method includes significant limitations. Firstly, the SPCE is an expensive electrode material. Secondly, the synthesis of CB-MIP and the preparation of the CB-MIP/NiO-NPs/SPCE include hard and time-consuming procedures. These significant factors limit the practical usability of the designed sensor. On the other hand, the CelsB sensor based on PGE does not include these disadvantages, and provides disposable, low-cost, fast, and practical determination of CelsB. Moreover, there is a limit of study based the electrochemical determination of CelsB [2], the proposed method has the potential to be an example based on practical and low-cost electrochemical determination of CelsB that will contribute to the deficiency in this field.

The reproducibility and repeatability were examined by recording under optimized conditions. The reproducibility was examined five PGEs, and the relative standard deviation (RSD) value was found to be 4.7 %. The intra-day repeatability was researched by 10 times recording the CV responses of 8.0 μM CelsB at the same electrode and the RSD value was calculated as 4.6%. The obtained RSD values lower than 5.0% indicated that the PGE exhibits reproducible and stable intra-day voltammetric responses. Although the PGE shows poor intra-day responses, the disposable and practical use of PGE tolerates this limitation.

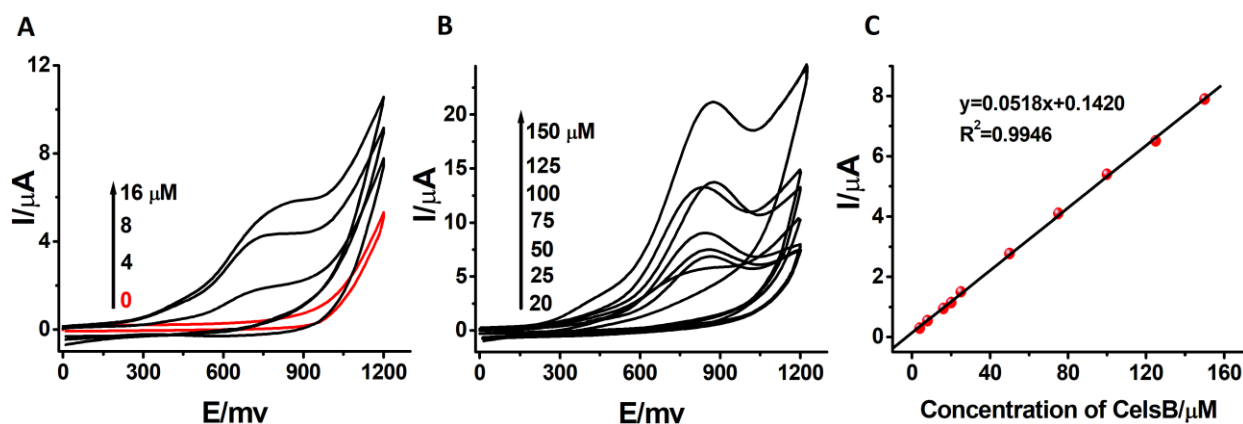


Figure 6. A) CVs from 0 to 16 μM CelsB B) CVs from 20 μM to 150 μM CelsB (BRBS pH5.0; S. rate: 50 mV/s) C) Calibration curve of CVs acquired from CelsB at increasing concentrations

Table 2. The performance comparison between electrochemical CelsB sensors

WE	Method	E_a (mV)	Linear response range (μM)	LOD (μM)	Real sample	Reference
PGE	CV	+746	4.0 – 150	1.21	Cherry apple juice, tap water	This work
CB-MIP/NiO-NPs/SPCE	DPV	-100	2.0 – 150	0.37	Waste water from textile, industry	[2]

3.6. The Selectivity to CelsB

The influence of some possible kinds of molecules and ions on the voltammetric response of 50 μM CelsB was tested under the optimized conditions. Table 3 shows that the influence of 25-fold Fructose, Na^+ , Ca^{2+} , K^+ , Mg^{2+} , NO_3^- , 10-fold SO_4^{2-} , CO_3^{2-} , 1-fold Tz, Qy, BB, Citric acid, and 0.01-fold L-AA on CelsB was found to be negligible according to the tolerance limit of 10%. According to all these results, it was found that the proposed method can be applied for selective determination of CelsB in real samples including the mentioned species.

Table 3. Influence of some possible kinds of interferences (n=3)

Interference	The amount of interference (fold)	% Alteration in voltammetric response	±SD
L-AA	0.01	+ 1.72	0.11
Citric acid	1	+ 8.15	1.13
Fructose	25	+ 5.76	0.54
Glucose	50	+ 0.90	1.74
Tz	1	- 0.80	0.16
QY	1	- 5.43	0.25
BB	1	+ 8.72	0.65
Na ⁺	25	+ 2.79	0.78
Ca ²⁺	25	+ 3.43	0.86
K ⁺	25	+ 6.34	1.50
Mg ²⁺	25	+ 8.33	1.10
NO ³⁻	25	+ 6.30	1.50
SO ₄ ²⁻	10	+ 8.10	0.78
CO ₃ ²⁻	10	+ 2.60	0.56

3.7. The Application on Real Samples

The feasibility of the method was examined in cherry apple juice and tap water samples by using the standard addition-CV techniques together. Each sample was enriched with 5 and 10 μM of CelsB and the additions from standard solution were performed and the CVs were recorded. The percentage values for the recovery of CelsB were calculated from the calibration curves that generated from the recorded CVs (Table 4). The high percentages of recovery (96.2 – 103%) found from the feasibility studies proved the high applicability of the proposed sensor on real samples.

Table 4. Results of recovery applications for the detection of CelsB using the standard addition management in real samples (n=3)

Sample	Adding (μM)	Found (μM)	RSD (%)	Recovery (%)
Tap water	5	5.05	3.09	102
	10	10.22	3.08	102.20
Cherry apple juice	5	4.81	2.60	96.20
	10	10.30	4.85	103

4. Conclusion

As a result, a novel and disposable sensor based on cyclic voltammetric determination of CelsB was performed at PGE for the first time. The proposed methodology provides fast, practical, and low-cost electrochemical determination of CelsB without including time-consuming and hard, cleaning, polishing modification, and steps. The CelsB sensor designed on PGE shows wide linear range (4.0 – 150 μM) and low LOD (1.21 μM) for the voltammetric determination of CelsB. Moreover, the proposed methodology exhibits good repeatability and reproducibility, and provides determination of CelsB in high precision and accuracy from real samples. In summary, considering that the studies upon the electrochemical detection of CelsB in the literature are quite limited, it is hoped that this study will add diversity to the existing studies in terms of cost, speed, and practicality.

Author Contributions

The author read and approved the final version of the paper.

Conflicts of Interest

The author declares no conflict of interest.

Acknowledgement

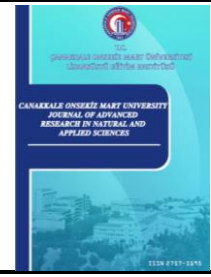
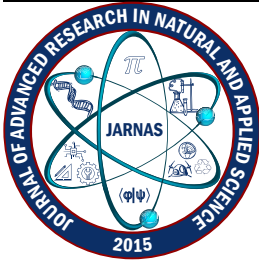
The author would like to thank Dr. Yusuf Dilgin for his support in performing this study.

References







- [1] V. Aruna Janani, D. Gokul, N. Dhivya, A. Nesarani, K. Mukilan, A. Suresh Kumar, M. Vignesh Kumar, *Optimization studies on methyl orange (MO) dye adsorption using activated carbon nanoadsorbent of ocimum basilicum linn leaves*, Journal of Nanomaterials 2023 (2023) Article ID 7969512 14 pages.
- [2] M. Roushani, Z. Saedi, Z. Mirzaei Karazan, A. Azadbakhat, *Electrochemical detection of celestine blue based on screen printed carbon electrode modified with molecular imprinted polymer and NiO nanoparticles*, Analytical and Bioanalytical Chemistry Research 8 (4) (2021) 493–504.
- [3] K. G. Akpomie, J. Conradie, *Biosorption and regeneration potentials of magnetite nanoparticle loaded solanum tuberosum peel for celestine blue dye*, International Journal of Phytoremediation 23 (4) (2021) 347–361.
- [4] P. S. Ganesh, G. Shimoga, S. H. Lee, S. Y. Kim, E. E. Ebenso, *Interference free simultaneous detection of dihydroxy benzene isomers at cost-effective and reliable celestine blue modified glassy carbon electrode*, ChemistrySelect 6 (9) (2021) 2379–2386.
- [5] Y. Chen, Y. Zhong, J. X. Ye, Y. Lei, A. L. Liu, *Facile label-free electrochemical dna biosensor for detection of osteosarcoma-related survivin gene*, Biosensors 12 (9) (2022) 747 11 pages.
- [6] A. Valipour, M. Roushani, *TiO₂ nanoparticles doped with celestine blue as a label in a sandwich immunoassay for the hepatitis C virus core antigen using a screen printed electrode*, Microchimica Acta 184 (2017) 2015–2022.
- [7] A. Noorbakhsh, M. Khakpoor, M. Rafieniya, E. Sharifi, M. Mehraza, *Highly sensitive electrochemical hydrogen peroxide sensor based on iron oxide-reduced graphene oxide-chitosan modified with DNA-celestine blue*, Electroanalysis 29 (4) (2017) 1113–1123.
- [8] E. Hamidi-Asl, J. B. Raoof, A. S. Meibodi, Z. H. Bazgir, *Celestine blue as a new indicator in electrochemical DNA biosensors*, Science China Chemistry 59 (1) (2016) 128–134.
- [9] N. Abbasi, S. A. Khan, T. A. Khan, *Response surface methodology mediated process optimization of celestine blue B uptake by novel custard apple seeds activated carbon/FeMoO₄ nanocomposite*, Journal of Water Process Engineering 43 (2021) Article ID 102267 14 pages.
- [10] M. S. Saad, L. Balasubramaniam, M. D. H. Wirzal, N. S. Abd Halim, M. R. Bilad, N. A. H. Md Nordin, F. N. Ramli, *Integrated membrane–electrocoagulation system for removal of celestine blue dyes in wastewater*, Membranes 10 (8) (2020) 184 12 pages.
- [11] K. Pliuta, A. Chebotarev, A. Pliuta, D. Snigur, *Voltammetric determination of allura red AC onto carbone-paste electrode modified by silica with embedded cetylpyridinium chloride*, Electroanalysis 33 (4) (2021) 987–992.
- [12] E. Murugan, A. Poongan, A. Dhamodharan, *Electrochemical sensing of acetaminophen, phenylephrine hydrochloride and cytosine in drugs and blood serum samples using β -AgVO₃/ZrO₂@g-C₃N₄ composite coated GC electrode*, Journal of Molecular Liquids 348 (2022) 118447 11 pages.

- [13] T. Erşan, D. G. Dilgin, E. Kumrulu, U. Kumrulu, Y. Dilgin, (2023). *Voltammetric determination of favipiravir used as an antiviral drug for the treatment of COVID-19 at pencil graphite electrode*, *Electroanalysis* 35 (4) 11 pages.
- [14] N. Sedhu, J. J. Kumar, P. Sivaguru, V. Raj, *Electrochemical detection of riboflavin in pharmaceutical and food samples using in situ electropolymerized glycine coated pencil graphite electrode*, *Journal of Electroanalytical Chemistry* 928 (2023) 117037 9 pages.
- [15] S. Karakaya, *Development of an amperometric hydrazine sensor at a disposable poly (alizarin red S) modified pencil graphite electrode*, *Monatshefte für Chemie-Chemical Monthly* 150 (2019) 1911–1920.
- [16] E. Pradeepa, Y. A. Nayaka, N. R. Manjushree, *Sensitive and selective determination of vanillin in the presence of dopamine and uric acid using low-cost and trouble-free pencil graphite electrode modified with methyl orange*, *Materials Chemistry and Physics* 296 (2023) 127180 14 pages.
- [17] L. A. Zambrano-Intriago, C. G. Amorim, A. N. Araújo, D. Gritsok, J. M. Rodríguez-Díaz, M. C. Montenegro, *Development of an inexpensive and rapidly preparable enzymatic pencil graphite biosensor for monitoring of glyphosate in waters*, *Science of The Total Environment* 855 (2023). 158865 12 pages.
- [18] N. M. Omar, E. M. Mabrouk, A. Y. El-Etre, A. I. Ali, A. M. Beltagi, *Development of a disposable pencil graphite electrode modified with poly 1,5-diaminonaphthalene for voltammetric determination of flufenamic acid*, *Journal of The Electrochemical Society* 170 (8) (2023) 087501 10 pages.
- [19] G. Önal, A. Levent, *Electrochemical evaluation and determination of vindesine used in cancer chemotherapy at disposable pencil graphite electrode by voltammetric method*, *Monatshefte für Chemie-Chemical Monthly* 154 (2) (2023) 205–213.
- [20] N. Ghaffari, K. Pokpas, E. Iwuoha, N. Jahed, *Sensitive electrochemical determination of bisphenol a using a disposable, electrodeposited antimony-graphene nanocomposite pencil graphite electrode (PGE) and differential pulse voltammetry (DPV)*, *Analytical Letters* 57 (6) (2023) 1008–1025.
- [21] F. Akter, D. C. Kabiraz, M. M. Islam, S. Ahmed, M. A. Hanif, Y. S. Kim, *Disposable pencil lead as an electrochemical transducer for monitoring catechol in river and tap water*, *Coatings* 13 (5) (2023) 913 12 pages.
- [22] R. M. Carvalho, E. R. Pedão, F. M. R. Guerbias, M. P. Tronchini, V. S. Ferreira, J. M. Petroni, B. G. Lucca, *Electrochemical study and forensic electroanalysis of fungicide benzovindiflupyr using disposable graphite pencil electrode*, *Talanta* 252 (2023) 123873 7 pages.
- [23] A. Afkhami, A. Bahiraei, T. Madrakian, *Gold nanoparticle/multi-walled carbon nanotube modified glassy carbon electrode as a sensitive voltammetric sensor for the determination of diclofenac sodium*, *Materials Science and Engineering: C* 59 (2016) 168–176.
- [24] M. Minakshi, K. Wickramaarachchi, *Electrochemical aspects of supercapacitors in perspective: from electrochemical configurations to electrode materials processing*, *Progress in Solid State Chemistry* 69 (2023) 100390 10 pages.
- [25] S. Karakaya, B. Kartal, Y. Dilgin, *Development and application of a sensitive, disposable and low-cost electrochemical sensing platform for an antimalarial drug: amodiaquine based on poly (calcein)-modified pencil graphite electrode*, *International Journal of Environmental Analytical Chemistry* 102 (17) (2020) 5136–5149.
- [26] S. Karakaya, Y. Dilgin, *The application of multi-walled carbon nanotubes modified pencil graphite electrode for voltammetric determination of favipiravir used in COVID-19 treatment*, *Monatshefte für Chemie-Chemical Monthly* 154 (2023) 729–739.

- [27] S. Ayaz, Y. Dilgin, *Flow injection amperometric determination of hydrazine based on its electrocatalytic oxidation at pyrocatechol violet modified pencil graphite electrode*, *Electrochimica Acta* 258 (2017) 1086–1095.
- [28] A. Wilson, B. Sajeevan, M. G. Gopika, A. Babu, K. M. Sreedhar, B. Saraswathyamma, *Electrochemical quantification of vanillin using hydrazine derivative modified pencil graphite electrode*, *Materials Today: Proceedings* 80 (2023) 558–563.



Anticancer, Antioxidant, Antimicrobial Activities, and HPLC Analysis of Alcoholic Extracts of *Parthenocissus quinquefolia* L. Plant Collected from Çanakkale

Ferah Cömert Önder¹ , Sevil Kalın² , Özlem Maraba³ , Alper Önder⁴ , Pınar Ilgın⁵ ,
Ersin Karabacak⁶ 

¹Department of Medical Biology, Faculty of Medicine, Çanakkale Onsekiz Mart University, Çanakkale, Türkiye

^{2,3}Department of Medical System Biology, School of Graduate Students, Çanakkale Onsekiz Mart University, Çanakkale, Türkiye

⁴Department of Chemistry, Laboratory of Inorganic Materials, Faculty of Science, Çanakkale Onsekiz Mart University, Çanakkale, Türkiye

⁵Department of Chemistry and Chemical Processing Technologies, Lapseki Vocational School, Çanakkale Onsekiz Mart University, Çanakkale, Türkiye

⁶Department of Biology, Faculty of Science, Çanakkale Onsekiz Mart University, Çanakkale, Türkiye

Abstract – This study aimed to contribute to revealing the health effects of the *Parthenocissus quinquefolia* L. (PQ) plant by examining the biological activities of various extracts of the plant. An ethnobotanical important medicinal plant, PQ belongs to the Vine family (Vitaceae) and is known for its medicinal uses. Herein, fruit and leaf alcoholic extracts of the plant exhibited anticancer activity on triple negative breast cancer (TNBC) cell lines, estrogen receptor positive (ER+) (MCF-7), and human colon adenocarcinoma (HT-29) cancer cell lines. Furthermore, fruit methanol extracts displayed strong radical scavenging activity with low IC₅₀ values such as 0.51 mg/mL, 0.80 mg/mL, 0.84 mg/mL, and 1.45 mg/mL. The highest TEAC values (18.72 mM Trolox/mg, 9.90 mM Trolox/mg, and 8.41 mM Trolox/mg) were calculated for the extracts of red leaves. The antifungal activity was determined against *Candida albicans* as fungal pathogen. The cell apoptosis with methanol extract was obtained between 20 µg/mL and 70 µg/mL for 48 h and 72 h treatments by Hoechst 33258 staining of nuclei under a fluorescence microscopy. HPLC analysis was performed for methanol extracts to determine major bioactive components. Consequently, this plant extracts may guide to new strategies and may be uses in medicinal applications for further investigations.

Article History

Received: 18 Oct 2023

Accepted: 12 Dec 2023

Published: 15 Mar 2024

Research Article

Keywords – Anticancer, Antimicrobial, Antioxidant, HPLC, *Parthenocissus quinquefolia* L.

1. Introduction

Plants are widely used worldwide in folk medicine and medicine for cancer therapy and other diseases [1]. Due to the significance of plants for human health, research on their bioactive properties has increased [2]. Compared to using traditional drugs to reduce side effects caused by chemotherapy, there are many advantages to the usage of plant-based medicines [3]. Natural antioxidants and many phytochemicals have been recently proposed against cancer therapy due to their importance in signaling pathways [4]. Plant bioactive components have a significant role in inhibiting cancer cells because of their structural diversity [5]. The harmful effects of these free radicals on cellular systems cause many diseases, such as cancer [6].

Bioactive components from the plant extracts act as antioxidants, and hereby, free radicals can be neutralized.

¹ferahcomertonder@comu.edu.tr (Corresponding Author); ²sevilkalin.1995@gmail.com; ³ozlemmaraba@gmail.com; ⁴alperonder@outlook.com; ⁵pinarilgin@comu.edu.tr; ⁶krbersin@comu.edu.tr

Phenolic compounds contain biologically active secondary metabolites with strong antioxidant and antiradical properties [7,8]. Plant-derived antioxidants have become an important research topic for the last two decades [9,10]. Oxidative stress (OS) has a key role in the stimulation of many diseases, such as immunosuppressive, diabetes mellitus, cancer, and neurodegenerative diseases. Thus, antioxidants have an important role in destroying free radicals that cause OS [11]. Phenolics play an important role against microbial activities and infections [12]. Phenolic compounds such as quercetin and ellagic acid are recognized to be beneficial to human health, reducing the risk of degenerative diseases by reducing OS [13].

Parthenocissus quinquefolia L. (PQ) belongs to the Vitaceae family and is known for its many pharmacological activities, including cancer chemoprotective effect, antimicrobial, antiviral, anti-rheumatism, arthritis, gastrointestinal, antidiabetic, diuretic, anti-inflammatory, and anti-cholesterol activities [14-16]. It was indicated that PQ was an ethnobotanical important medicinal plant with broad-spectrum biological activities, including antifungal, antibacterial, and antioxidant [14,17]. The plant's bark has been employed in traditional medicine as an expectorant and tonic. PQ roots have been used in infusions [15]. Pharmacologically active plants are a rich source of compounds with special therapeutic potentials and are still of great importance for identifying new drug leads [18].

Herein, this study focused on the biological activity studies, including anticancer, antioxidant, and antimicrobial, with various extracts of the PQ plant collected from Çanakkale/Türkiye. The morphological differences in cancer cells were determined under fluorescent microscopy. Determination of the bioactive content of methanol extracts of fruit and leaves of the plant was carried out by HPLC analysis. The flowchart is given in Figure 1.

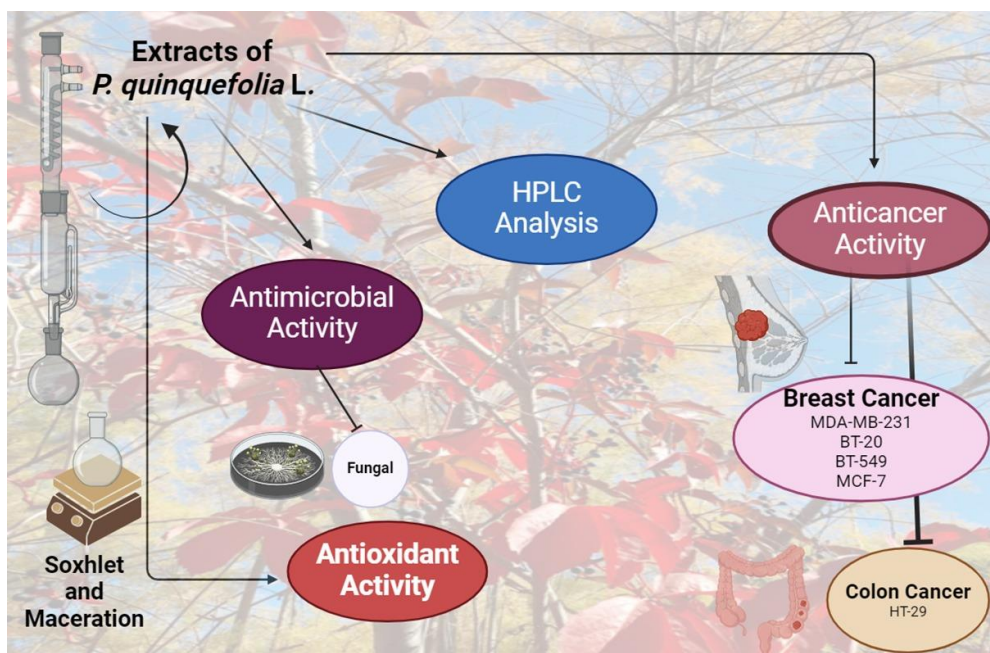


Figure 1. A representative flowchart

2. Materials and Methods

Ethanol (EtOH), *n*-hexane, ethyl acetate (EtOAc), methanol (MeOH), and dichloromethane (DCM), DPPH (2,2-diphenyl-1-picrylhydrazil), trolox, F-C reagent, and ABTS were obtained from Sigma-Merck.

2.1. Plant Preparation

This plant was collected from Çanakkale Onsekiz Mart University Terzioğlu Campus-Türkiye. The plant was identified and kept in Çanakkale Botanik Bahçesi Herbariumu (CBB 003110-Herb. Hort. Bot. Canakkalensis). The fruits and leaves were dried without direct sunlight in the air, and then ground. The photos of *PQ* were shown in Figure 2. The extracts were prepared by using Soxhlet method with *n*-hexane, DCM, EtOAc, MeOH, and EtOH:H₂O (75:25), respectively, according to our previously reported study [19]. The other extract was prepared by directly using MeOH and then ethanolic solution. Maceration was performed at room temperature by using MeOH [20]. The solvent was removed by using rotary evaporator (IKA RV10). The plant extracts were kept in the refrigerator at +4°C. The obtained extracts were given in Table 1.

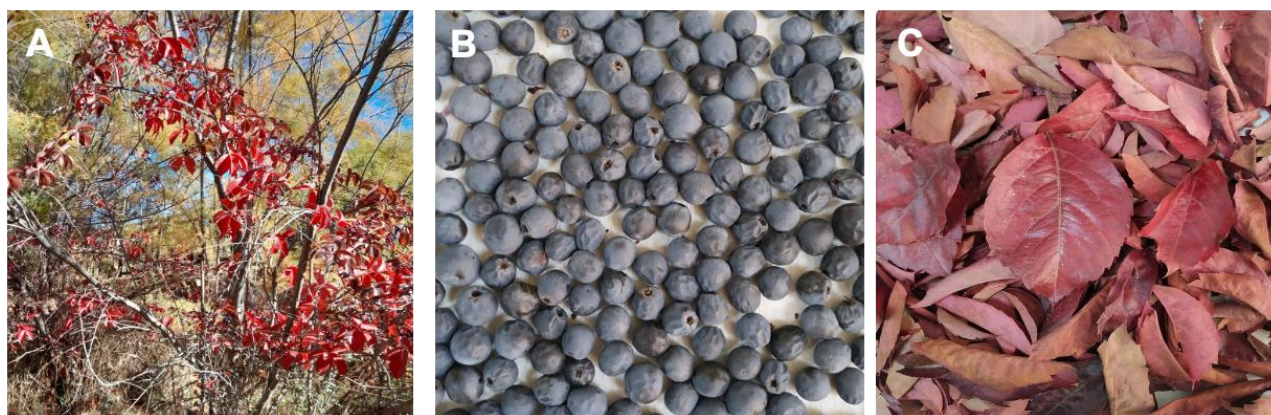


Figure 2. Photos of *PQ* were taken by the authors. A) collected from Çanakkale, B) fruits, C) red leaves

Table 1. The prepared extracts (1-7)

Extracts	Codes
MeOH extract of red leaves (gradually)	1
MeOH extract of fruits (gradually)	2
Aqueous ethanol extract after directly methanol of fruits	3
MeOH extract of fruits (maceration)	4
MeOH extract of fruits (directly)	5
MeOH extract of red leaves (directly)	6
Aqueous ethanol extract after directly methanol of red leaves	7

2.2. Anticancer Activity

2.2.1. Cell Culture

Human triple negative breast cancer cell lines (TNBC) (MDA-MB-231, BT-20, BT-549), and ER+ (MCF-7), and human colon cancer (HT-29) cell lines were gift. Dulbecco's containing 2 mM L-Glutamine Modified Eagle Medium (DMEM) was used for the cultivation. 1% Penicillin/streptomycin (PS) and 10% fetal bovine serum (FBS) were added to culture media and the cells were kept in a 37°C incubator containing 5% CO₂ incubator [21,22]. For anticancer activity, stock solutions of the extracts were prepared at 10 mg/mL.

2.2.2. Clonogenic Assay and Cell Cytotoxicity

Colony inhibition on breast and colon cancer cells were carried out. The effect of the extracts at various concentrations was examined for 8-12 days. Crystal violet was used for staining. The cytotoxicity was

determined by MTT (Thiazole Blue) assay for 48 h with time- and dose-dependent manner studies. The absorbances were measured by a plate reader (Thermo) at 570 nm. The cell viability (%) was calculated and compared to dimethyl sulfoxide (DMSO). Statistically significant results were indicated as asterisk [21-23].

2.2.3. Wound Healing Assay

The cell migration analysis was performed in 6-well plates. The cells were scratched in the middle with the help of a pipette tip and washed with phosphate buffer saline (PBS). The extracts (**1** and **2**) were applied to cancer cells. Then, microscope images were taken for different time points and the Image J program was used [21].

2.2.4. Fluorescent microscopy

The most active extract in cell-based assays was applied to cancer cells for 48 h and 72 h treatments. Paraformaldehyde (4%) was used to fix the cells and Hoechst 33258 dye was used for staining of nuclei. The morphological changes were examined under a fluorescence microscope (Zeiss AXIO Scope A1) [21,24].

2.3. Antioxidant Activity

The antioxidant capacities were investigated with DPPH and trolox equivalent antioxidant capacities (TEAC) assays according to a reported study. 10 mg/mL stock solutions were prepared for each extract and then, intermediate solutions were prepared freshly and used. All experiments were repeated three times [20].

2.3.1. DPPH Assay

To determine antioxidant capacity, stock solutions prepared in MeOH were used at 10 mg/mL concentration. IC₅₀ values were calculated by the help of measured absorbances at 517 nm [20,25].

2.3.2. TEAC Assay

The TEAC method was performed by the form of ABTS radical cation as a result of the oxidation of ABTS reagent with persulfate. TEAC values obtained at various concentrations were performed by using the Trolox standard curve [20].

2.3.3. Analysis of The Total Phenolic Amount

F-C method was used according to the previously reported study. The absorbances measured at 725 nm spectrophotometrically were used to calculate the total phenolic amount. The results were given as mg gallic acid equivalent [20].

2.4. Antimicrobial Activity

Disc diffusion method was used to examine the effect of plant extracts against various strains including *Staphylococcus aureus*-ATCC29213, *Bacillus subtilis*-ATCC6633, *Bacillus cereus*-ATCC10876, *Escherichia coli*-ATCC25952, *Pseudomonas aeruginosa*-ATCC27853. To grow bacterial strain cultures in the agar disc diffusion method, 30 g of tryptic soy broth (TSB) medium solution was prepared in 1 L water and autoclaved. To grow, 40 g of tryptic soy agar (TSA) medium solution was prepared in 1 L water and autoclaved. TSA medium is then transferred to petri dishes as 20 mL. One bead of the bacterial strain removed

from -80°C was transferred to 15 mL of TSB medium solution and incubated overnight in a shaking water bath (37°C). Solid agar petri dish 50 μL of the bacterial suspension was added to the surface and seeded with a sterile cell spreader. In these aseptic conditions, 6 mm diameter sterile discs were placed in the middle of the agar plates and mass was placed on these discs known plant extracts were placed. Petri dishes were incubated at 37°C overnight. Then, the inhibition zone diameters around the samples with a caliper were measured to determine the antimicrobial activity [26].

2.5. HPLC Analysis

To identify the major phenolic components, MeOH extracts of fruit (**2**) and red leaf (**1**) of *PQ* were used. HPLC analysis was carried out by using ACE Generix5 C18 (250x4.6 mm) 5 μm column 30°C at Igdur University Research Laboratory Practice and Research Center. The instrument conditions were given as follows: injected volume (10 μL), flow (0.8 mL/min). The DAD detector was set at wavelengths 300/200 nm and 300/4 nm. The solvent system was 83% (0.1 phosphoric acid in water) 17% (100% ACN). Standards such as catechin, isoquercitrin, baicalin, oleuropein, hesperidin, chlorogenic acid, naringin, resveratrol, quercetin, chrysin, 6-hydroxy flavone, curcumin, gallic acid, tannic acid, caffeic acid, rutin, *t*-ferulic acid, resveratrol, apigenin were used in the methods.

2.6. Statistical Analysis

Statistical analysis was performed by using GraphPad Prism.

3. Results and Discussion

3.1. Effects of Plant Extracts on Cancer Cell Cytotoxicity

MTT assay is based on the reduction of MTT tetrazolium compound and has been carried out in this study. The cytotoxic effects of these extracts on short-term cell proliferation at increasing concentrations from 40 to 200 $\mu\text{g}/\text{mL}$ for 48 h treatments were determined on TNBC, ER+ MCF-7, and HT-29 cells. The cytotoxicity of mature red leaves and fruit extracts of *PQ* contributed to reduce the inhibition of cell viability in the studied cells. We detected the antiproliferative effects of MeOH and ethanolic extracts for fruits and leaves obtained from *PQ*. According to our findings, the cytotoxic effect of extracts (**2** and **6**) in MDA-MB-231 cells at $\mu\text{g}/\text{mL}$ concentrations were obtained at higher for 48 h time-dependent. MDA-MB-231-cells were treated with Doxorubicin (Dox) (0.05 μM) for 48 h in combination therapy with the extracts, the cell viability decreased at 40 $\mu\text{g}/\text{mL}$ with the combination of the extracts (Figure 3a).

As seen in Figure 3d, cell viability in BT-549 cells was dramatically decreased by all extracts at 160 $\mu\text{g}/\text{mL}$ concentration, respectively, for 48 h as a time-dependent. According to the cancer cell cytotoxicity, we obtained the cell inhibition in BT-20 cells for 48 h, the most effective extracts were determined, and all extracts displayed high cytotoxicity at 80 $\mu\text{g}/\text{mL}$ (Figure 3f). In the light of these findings, the most significant antiproliferative effect of *PQ* on ER+ MCF-7 cells was observed at approximately 80 $\mu\text{g}/\text{mL}$ of extract **4** (Figure 3g). According to the obtained cell cytotoxicity data in HT-29 cells for 48 h, the extracts (**3** and **7**) had higher cytotoxic effects (Figure 4a,4b). Based on our above-mentioned results, plant extracts showed higher cytotoxicity in five cancer cell lines for 48 h. As far as is known, it has been reported for the first time that *PQ* plant extracts have strong cytotoxic effects against studied cancer cell lines.

According to the literature findings, Summiya et al. [10] emphasized the necessary of using *PQ* in cancer research study. The extracts of four different plant species including *PQ* were used for the cytotoxicity of different cancer cells, cell cycle arrest, and apoptosis studies [27]. In addition, anticancer activity of aqueous ethanol extract of *PQ* leaves was reported for KB cell lines in A431 and subG1 [27]. In another study involving the *P. tricuspidata* plant, cytotoxicity, antioxidant and antimicrobial activity were examined. Cytotoxicity analyses were performed on MDA-MB-361 and MDA-MB-453 cell lines [28]. Based on our findings, antiproliferative effects of *PQ* fruit and leaf extracts were observed in MeOH extracts for all breast cancer cell lines for 48 h treatments. Although the results exhibited MeOH extracts were found to be significant due to their cytotoxicity, the effect on the inhibition of colonies with ethanolic extract was determined more significant in long-term inhibition.

In a recent study, combination studies of natural bioactive compounds and doxorubicin (Dox) in various types of cancer were highlighted [29]. The combination therapy studies of Dox with curcumin [30], apigenin [31], naringenin [32] and quercetin in breast cancer cells have been reported. Furthermore, the prepared hydrogel using the *PQ* plant extract as a crosslinker reported as a potential drug-carrier in combination with Dox for cancer therapy studies [21].

3.2. Inhibition Effect of Plant Extracts on Colony Formation

To determine the effects of fruit and leaf extracts on the colony formation, a dose-dependent manner study was performed in cancer cells. Our results indicated that all extracts (**1-7**) decreased the number of colonies in TNBC MDA-MB-231 cell line at 45 $\mu\text{g/mL}$ compared to control cells (Figure 3b). To understand the role of reducing the colonies, the treatments at various volumes were performed with the extracts (**2-7**) in BT-549 cells. According to this, the results showed that all extracts inhibited the colony formation at 40 $\mu\text{g/mL}$ (Figure 3c). The extracts significantly inhibited the colony formation in BT-20 cells at 45 $\mu\text{g/mL}$. Moreover, it has been determined that extract **4** obtained by maceration has a highly strong inhibitor effect on the colony formation (Figure 3e).

The inhibitor effect of extracts (**1-6**) on ER+ MCF-7 cells was determined to be similar as BT-20 cells (Figure 3g). According to colony formation inhibition study in HT-29 colon cells, although other extracts exhibited inhibitor potential at 50 $\mu\text{g/mL}$, the extracts (**1-4**) showed the colony inhibition at 45 $\mu\text{g/mL}$ (Figure 3a). Overall, all extracts were determined with their inhibition effect on breast and colon cancer cell lines. As far as is known, we report for the first time these results may exhibit that *PQ* includes high cytotoxic compounds.

3.3. Effect of the Extracts on Cell Migration

It was used a scratch test to measure the spread of cancer cells [21]. For this purpose, highly effective MeOH extracts (**1** and **2**) were applied to HT-29 cells. Blocked the migration of HT-29 cells with extract **1** at 160 $\mu\text{g/mL}$ (24 h) and 200 $\mu\text{g/mL}$ (48 h) and extract **2** at 80 $\mu\text{g/mL}$ (24 h) and 160 $\mu\text{g/mL}$ (48 h). These results may indicate that the extracts of *PQ* can block aggressive cells for metastasis (Figure 4c).

3.4. Effect of the Extracts on Morphological Changes

Herein, the fluorescence microscopy was used for fruit MeOH extract **2** of *PQ* for the first time. Nuclei (blue) was stained with Hoechst to observe the effects of extract **2** on the morphologic changes in breast cancer cells. MDA-MB-231 and MCF-7 cells were treated with extract **2** in the increasing volumes of 20-80 $\mu\text{g/mL}$ for 48 h and 72 h and observed under a fluorescence microscopy. It was also determined that extract **2** contributed to

morphological changes on cancer cells as dose- and time-dependent. Extract 2 induced apoptosis in both cancer cells, and the apoptotic cells increased by the increasing doses of extract 2. It was the most active extract that caused the morphological changes in cancer cells (Figure 5). As is indicated in the literature, it was observed that the condensed chromatin, marginalized nuclei, and apoptotic features such as fragmentation in doxorubicin- and extract-treated cells by a fluorescence microscopy [33].

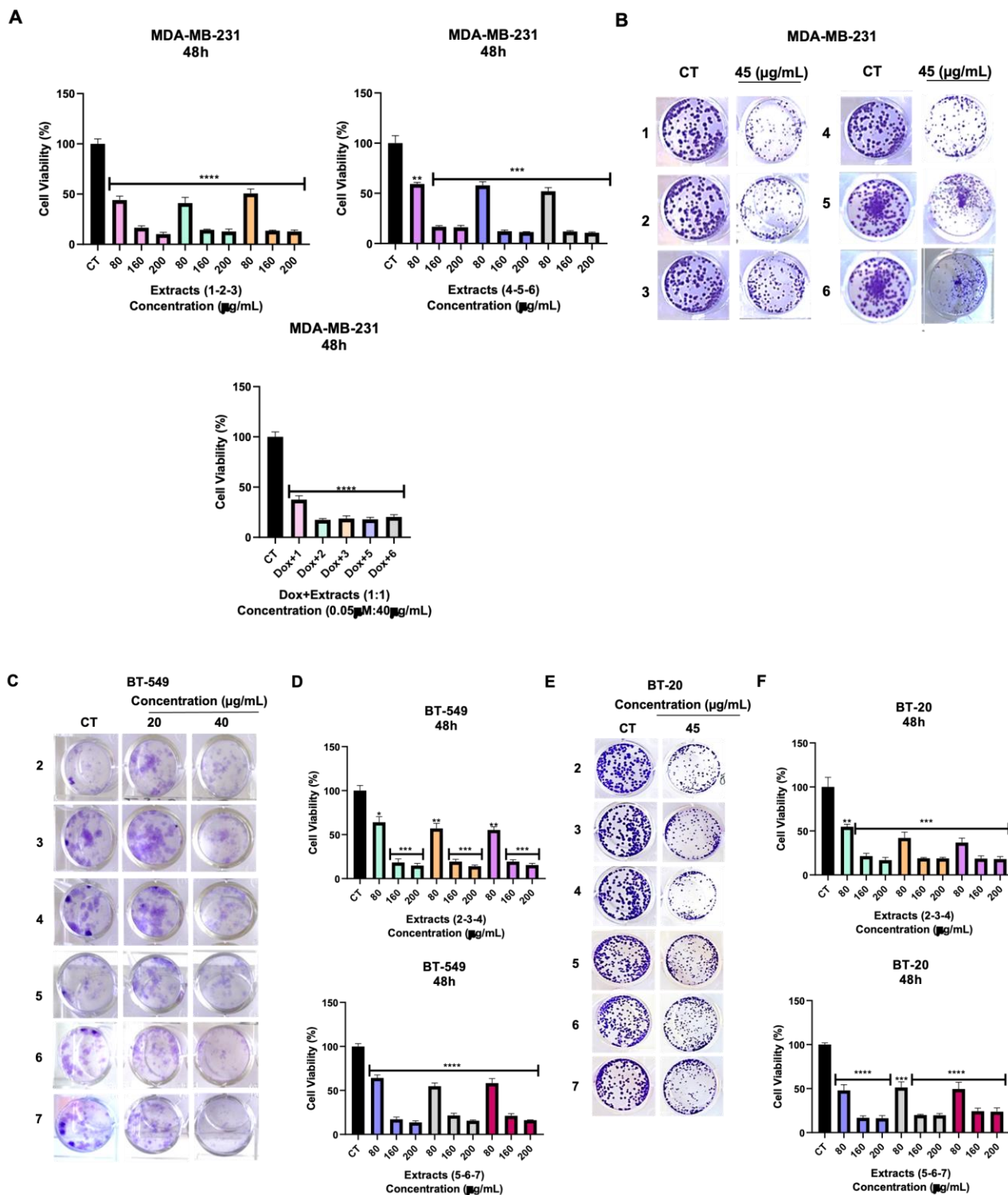


Figure 3. Cell cytotoxicity and colony inhibition assay in breast cancer cells. A,D,F,G) The extracts decreased the cell cytotoxicity with MTT assay in time- and dose-dependent manner. B,C,E,G) The colonies were dramatically inhibited by the extracts (1-7) (8-12 days)

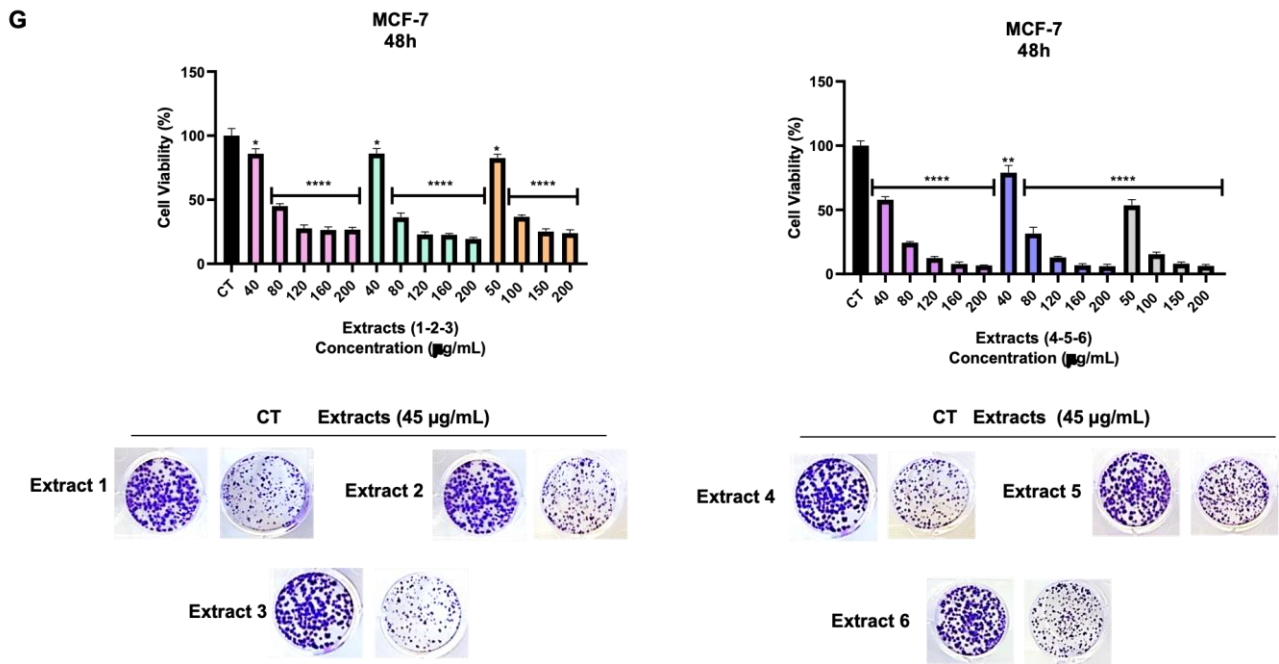


Figure 3. (Continued)

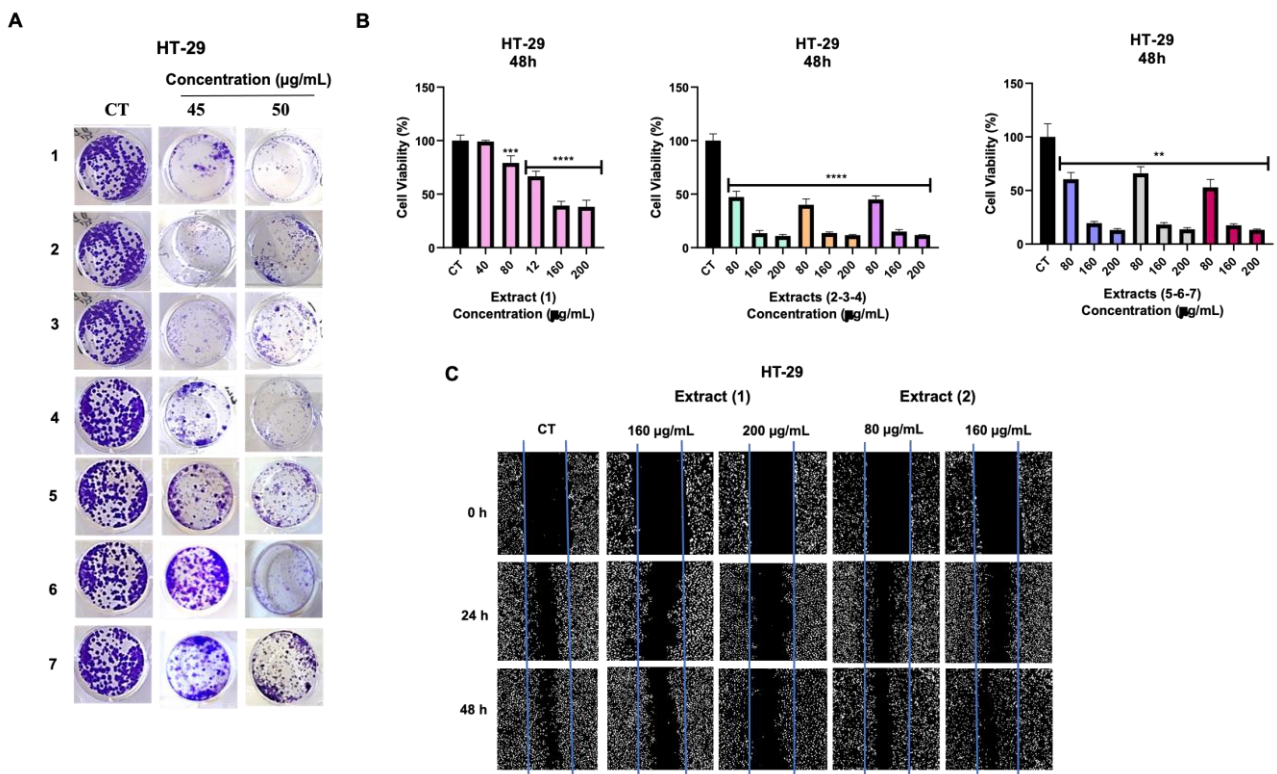


Figure 4. Cell cytotoxicity and colony formation inhibition assay in HT-29 colon cancer cells. A) The colonies were dramatically inhibited by the increasing doses of the extracts (9-12 days). B) The extracts decreased the cell cytotoxicity with MTT assay following the 48 h treatments. C) Wound healing assay in HT-29 cells. HT-29 cells were blocked by the extracts (1 and 2)

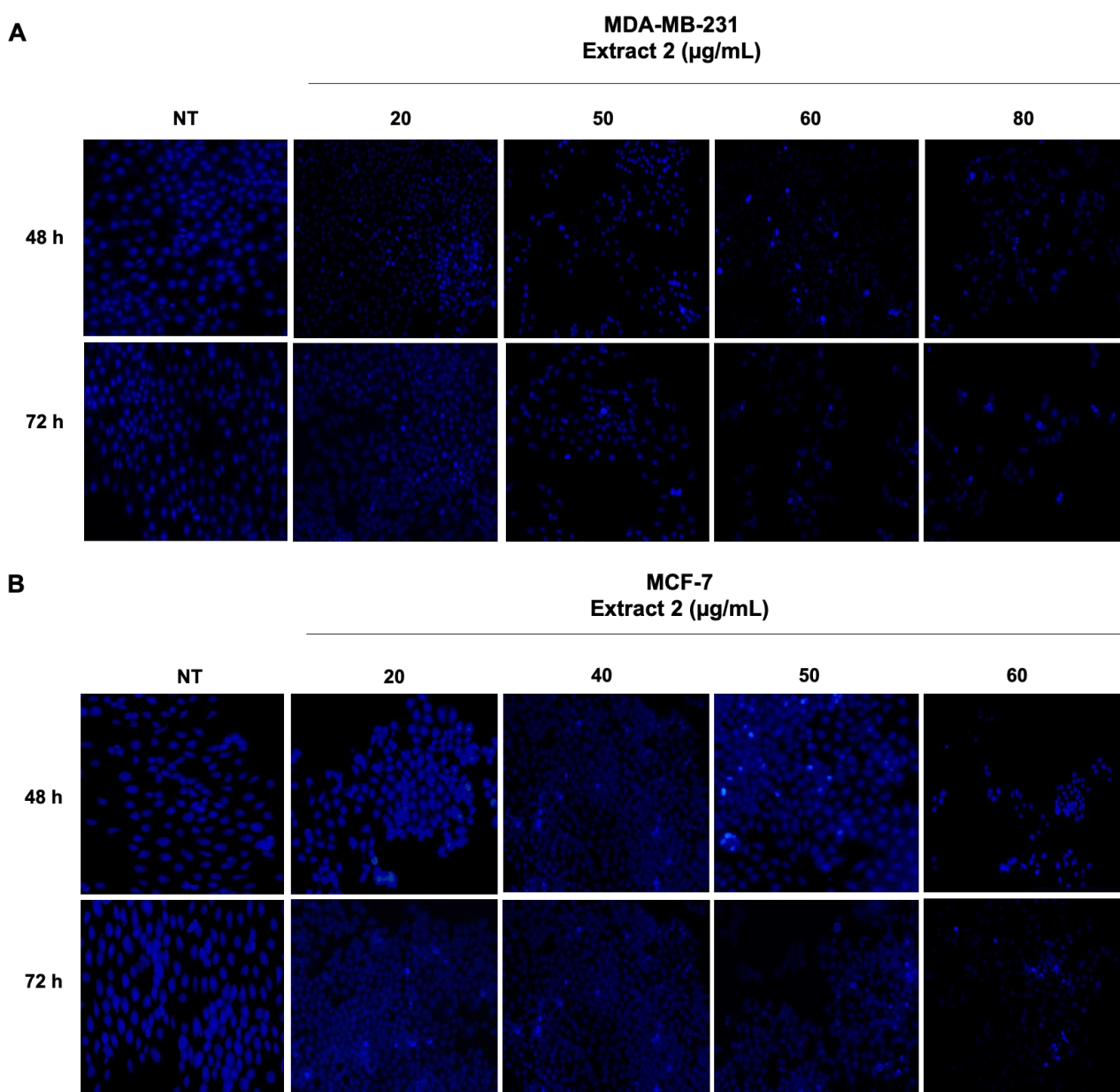


Figure 5. Morphological changes following the treatment with the extract 2 were detected by Hoechst staining under a fluorescence microscopy

3.5. Total Phenolic Content and Antioxidant Activity

In terms of phenolic component amounts, the extracts (1 and 2) were evaluated with their high phenolic amounts. However, extract 5 was determined with its low phenolic content. In this study, red leaf extracts displayed high total phenolic content. The gallic acid values in 100 µL samples of the extracts were calculated and the total phenolic component amounts were determined in 10 mg/mL extract. As a result, the extracts were determined as equivalent to gallic acid per mg extract. It is known that aqueous extracts contain glycoside linked structures. It was reported that the extracts from fruits and leaves of *PQ* plant included alkaloids, terpenoids, flavonoids, saponins, tannins, and glycoside metabolites [14,16]. The findings are given in Table 2. In DPPH analysis, the 50% inhibition values were calculated as the IC₅₀ value. Accordingly, the results show that the fruit MeOH (extract 3) and fruit MeOH maceration (extract 4) showed higher scavenging activity with the DPPH radical, respectively. However, the extracts (1, 6, 7) obtained from red leaves did not exhibit strong radical scavenging activity with DPPH analysis (Table 2).

Table 2. IC₅₀ inhibition and TEAC values and total phenolic amount of extracts

Extracts	DPPH IC ₅₀ values (mg/mL)	TEAC (mM Trolox/mg)	Total phenolic content (mg GA/10 mg extract)
1	11.82±0.32	9.90±0.21	9.40±0.49
2	0.80±0.01	0.86±0.03	9.54±0.45
3	0.51±0.11	1.33±0.03	3.17±0.11
4	0.84±0.03	0.88±0.03	1.43±0.11
5	1.45±0.06	0.46±0.02	0.57±0.08
6	12.60±0.45	8.41±0.33	2.83±0.18
7	10.22±0.36	18.72±0.31	1.52±0.33

According to the TEAC method, the highest activity was obtained from extracts (7 and 1) with 18.72±0.31 mM Trolox/mg and 9.90 ±0.21 mM Trolox/mg values, respectively. TEAC values were found to be quite low in fruit extracts. These results indicated that extracts from red leaves have more activity in TEAC analysis (Table 2). In the reported studies, the stems and leaves of *PQ* of DPPH scavenging activity were detected for aqueous (322.34±0.01) and ethanol extracts (1398.85±0.01) [34]. The DPPH assay was reported with IC₅₀ value of 13.6±0.34 µg/mL, 18.24±1.43 µg/mL, 28.84±2.20 µg/mL, and 38.28±2.79 µg/mL for aqueous, chloroform, ethanol, and *n*-hexane stem extracts, respectively, and the IC₅₀ value of 27.08±3.41 µg/mL, 19.67±0.70 µg/mL, 24.32±1.02 µg/mL, 14.25±0.65 µg/mL aqueous, chloroform, ethanol, and *n*-hexane bark extract, respectively [10]. Finally, chloroform extracts of fruits and leaves of *PQ* from Pakistan have been reported with its best antiradical activity [16].

The vine family is known for its many pharmacological activities such as cancer chemoprotective effect, antimicrobial, antiviral, anti-rheumatism, arthritis, gastrointestinal system problems, antidiabetic, diuretic, anti-inflammatory, anti-cholesterol activity. Phytochemical screening was carried out by extracting the plant collected from Iraq and Pakistan with different solvents [35,36]. A study was conducted to evaluate the antioxidant capacities of *PQ* leaves and fruits collected from Pakistan. The extracts were obtained from the fruits and leaves of the plant with the help of various solvents. Its antioxidant activity was examined by phytochemical analysis and DPPH, FRAP, TFC methods. Phytochemical screening of various extracts from *PQ* revealed the presence of its secondary metabolites (alkaloids, flavonoids, terpenoids etc.). As a result, the antioxidant potential of chloroform and ethanolic extracts was found to be higher. Thus, it has been stated that the traditional use of *PQ* leaves and fruits may be possible for the treatment of human diseases [13,14]. DPPH and FRAP antioxidant activity results of various extracts of *PQ* bark and roots collected from Pakistan were compared with standard antioxidants and plant extracts were found to have better antioxidant potential. For this reason, it has been stated that it can be used in the treatment of cancer and aging in the future [35]. DPPH, FRAP and total phenolics were determined in aqueous and ethanol extracts of the roots and leaves of the plant collected from Thailand [34].

Based on our results, the radical scavenging activities and TEAC values for the active extracts indicated that the extracts from fruits and red leaves could have promising bioactive components. The phenolic components are generally extracted with solvents in the changing polarities such as ethyl acetate, alcohol, and alcohol-water mixtures [37]. Extraction with polar solvents is resulted in the extracts containing largely phenolic components [38,39]. In order to obtain major antioxidants from various parts of plants such as leaves the effect of different solvent types such as hexane, MeOH, and EtOH was analyzed. It was found that MeOH extract

was more effective than EtOH extract in the large amount of phenolic content obtained from walnut fruits [40,41].

Analysis on the antioxidant potential is used as an indicator of phenolic content [42]. Among them, DPPH is widely used and the oldest known method. Antioxidant capacity of plant extracts can be determined with TEAC. In addition, the antioxidant activity values may also depend on various factors such as solvent and method for extraction [43]. Besides, free radicals and reactive oxygen species (ROS) have a significant impact on biological systems. OS has a role in the varying types of diseases such as cancer, Alzheimer's disease, and diabetes. Natural compounds as antioxidants from plants protect biological systems and provide human health [44]. Thus, we have thought that these active plant extracts may contribute to reducing the ROS in the biological system.

3.6. Antimicrobial Activity

To examine the inhibitory effect of plant extracts on some microorganisms that cause various infectious diseases, antimicrobial activity was determined by using the minimum inhibitory concentration measurement and disk diffusion method [45]. *S. aureus*, *B. cereus*, *E. coli*, *P. aeruginosa*, *E. faecalis*, *B. subtilis*, and *C. albicans* are microorganism strains used in the study. Bacterial growth was controlled with an empty disc (C) placed on petri dishes. It is known that many medicinal plants are traditionally used to treat diseases caused by microorganisms [46,47]. Antibacterial effects of various extracts of *PQ* plant on gram positive (*S. aureus*, *B. cereus*, *E. faecalis*, *B. subtilis*) and gram negative (*E. coli*, *P. aeruginosa*) bacterial and fungal pathogen (*C. albicans*) were evaluated and the results of the zone diameters are given in Table 3. Also, the results of a few of them (*B. cereus*, *E. coli* and *C. albicans*) are given in Figure 7. All plant extracts showed very promising results against all tested microorganisms. The antibacterial properties found in the extracts of this *PQ* may possibly be attributed to some phenolic compounds. It was determined that the effects of the plant, especially the extract 4, on various test bacteria were more effective than the other plant solutions. The main reason for the different results obtained may be due to phytochemicals (Table 3) such as flavonoids, vitamins, and sterols in the plant structure [48]. Overall, these studies show that *PQ* extracts have potential antimicrobial activity against and fungi and may serve as potential sources for the future use of these extracts as new bactericidal agents in the treatment and prevention of infections. In the literature, MeOH extract of *PQ* fruits showed antifungal effects on *A. solani* pathogen [14].

Table 3. Antimicrobial activity of the extracts of *PQ* by disc diffusion method (Zone of inhibition in mm at 300 µg/disc)

Extracts	<i>E. faecalis</i>	<i>S. aureus</i>	<i>B. cereus</i>	<i>B. subtilis</i>	<i>E.coli</i>	<i>P. aeruginosa</i>	<i>C. albicans</i>
1	8	7	8	8	8	8	8
2	7	7	9	8	7	8	7
3	8	9	9	7	NI	9	7
4	11	10	10	9	8	10	9
5	NI	8	9	NI	NI	9	7
6	8	9	9	7	NI	10	7
7	7	9	8	7	NI	9	8

NI: No inhibition zone observed.

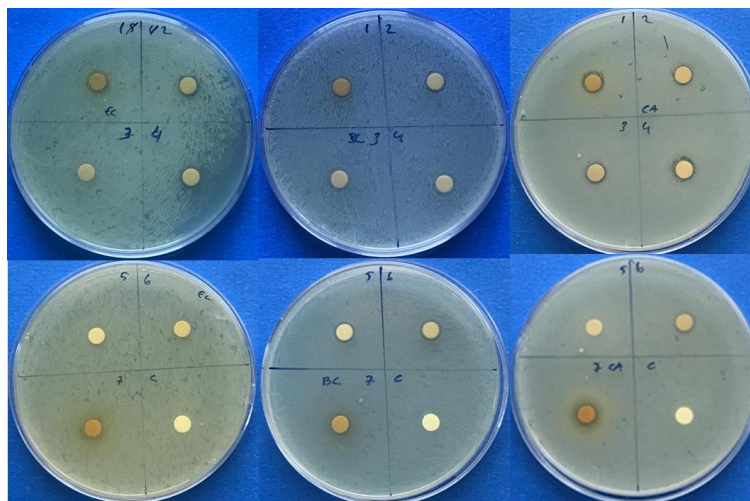


Figure 6. *E. coli*, A (1,2,3,4) and B (5,6,7,C); *B. cereus*, C (1,2,3,4) and D (5,6,7,C); *C. albicans*, E (1,2,3,4) and F (5,6,7,C) (extracts (1); (2); (3); (4); (5); (6); (7); control disk (C))

In addition, it is reported that *PQ* ethanolic extract of leaves has inhibitory effects against *A. hydrophila* (59.68%) and *A. caviae* (55.90%) which cause gastroenteritis disease [34]. In the reported antimicrobial activity study, gram-positive and -negative bacteria and fungi *S. aureus*, *S. epidermidis*, *M. luteus*, *E. faecalis*, *B. subtilis*, *B. cereus*, *E. coli*, *P. aeruginosa*, *K. pneumoniae* and *C. albicans* strains were studied [28].

3.7. The Secondary Metabolites were Determined by HPLC Analysis

Herein, the secondary metabolites in extracts (1 and 2) were determined by HPLC analysis with different methods. The phenolic contents including rutin (19.747), caffeic acid (9.671), naringin (27.546), resveratrol (32.594), quercetin (34.859), baicalin (32.594) were determined in extract 1 (Figure 7a,7b). The phenolic compounds of extract 2 were determined as rutin (19.488), naringin (27.578), resveratrol (32.404), and baicalin (32.404) (Figure 8a,8b). The retention times of phenolic contents of extract 1 were calculated as caffeic acid (9.653), isoquercitrin (27.013), naringin (29.299), resveratrol (30.545), quercetin (35.008) (Figure 9a). The retention times of phenolic contents of extract 2 were calculated as caffeic acid (9.620), ellagic acid (22.233), isoquercitrin (26.815), naringin (29.272), resveratrol (30.283) (Figure 9b).

According to HPLC studies with the *PQ* [14,36]. Mohamed et al. [14] used HPLC-UV for the determination of flavonoid compounds such as rutin and myricetin in MeOH extracts of *PQ* fruits. Spectroscopic analysis of its secondary metabolites was carried out [36]. In the other study it was reported that tropane glycosidic alkaloid, sennoside C and rutin were identified from ethanolic extracts of *PQ* obtained from petroleum ether fraction by HPLC [36]. The fruits of the plant collected from Tunisia were dried at room temperature and anthocyanins were identified by HPLC [17].

4. Conclusion

Herein, *PQ* extracts from fruits and red leaves were biologically investigated in detail. First, the extracts were performed gradually in the increasing polarity from apolar to polar solvents. Some extracts were obtained by directly polar solvents such as MeOH and aqueous EtOH or aqueous EtOH after MeOH. According to our results, all plant extracts contributed to anticancer activity in the changing doses on five different cancer cell lines for cancer therapy. As is expected, MeOH extracts of fruits displayed strong radical scavenging activity at low IC₅₀ values such as 0.51 mg/mL, 0.80 mg/mL, 0.84 mg/mL, and 1.45 mg/mL.

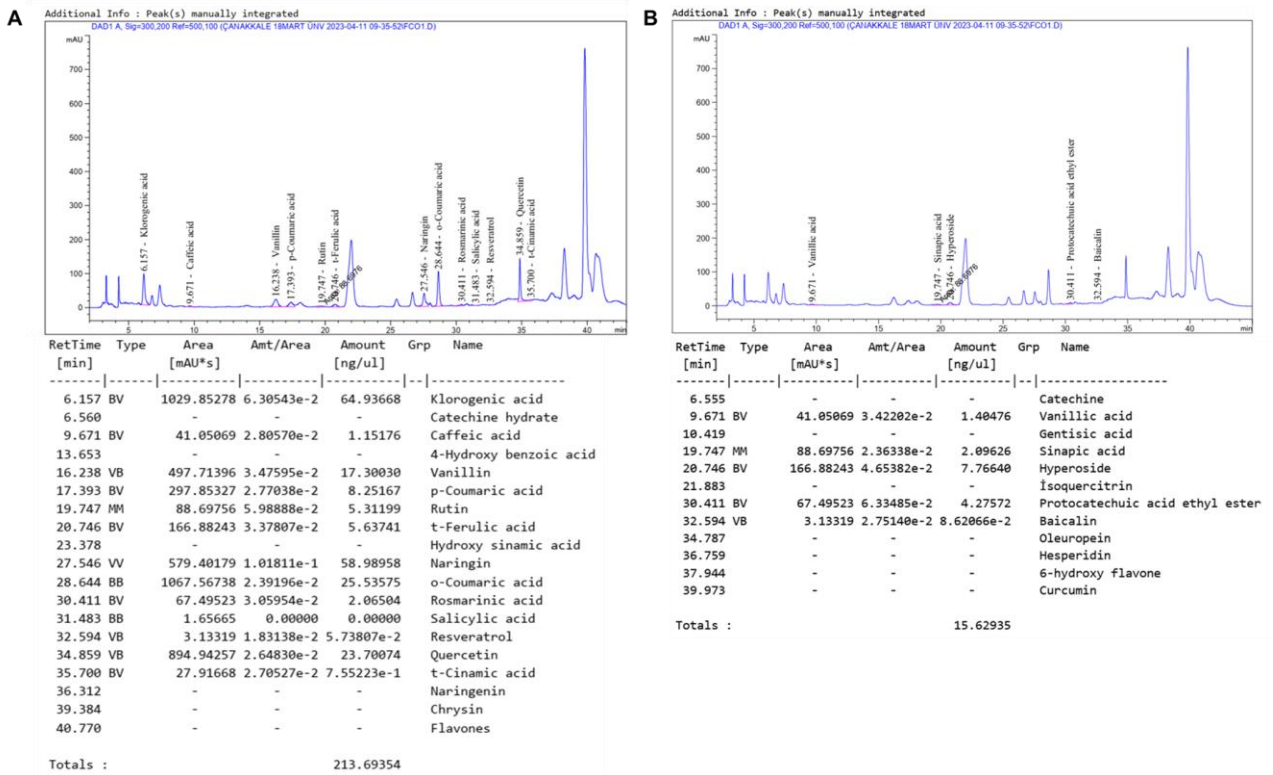


Figure 7. HPLC spectrum of extract 1

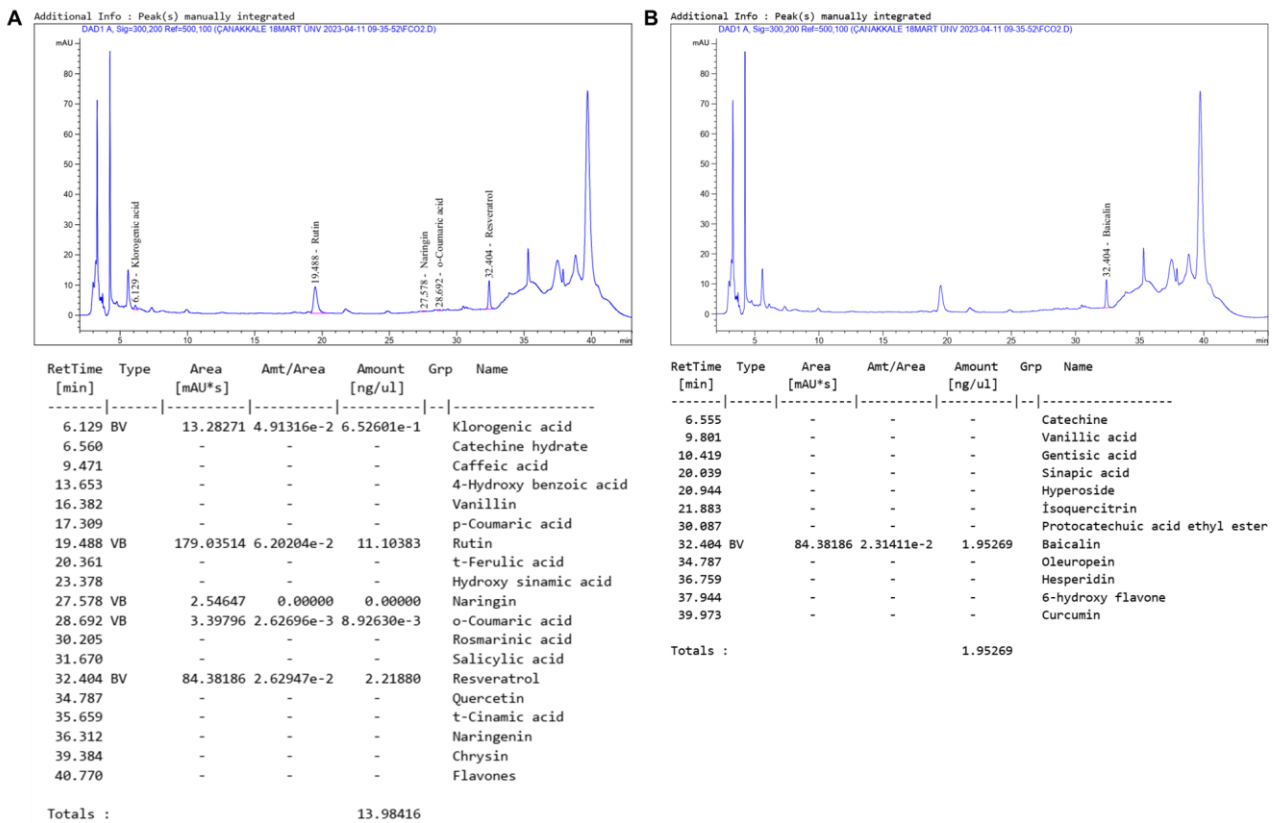


Figure 8. HPLC spectrum of extract 2 with two different methods

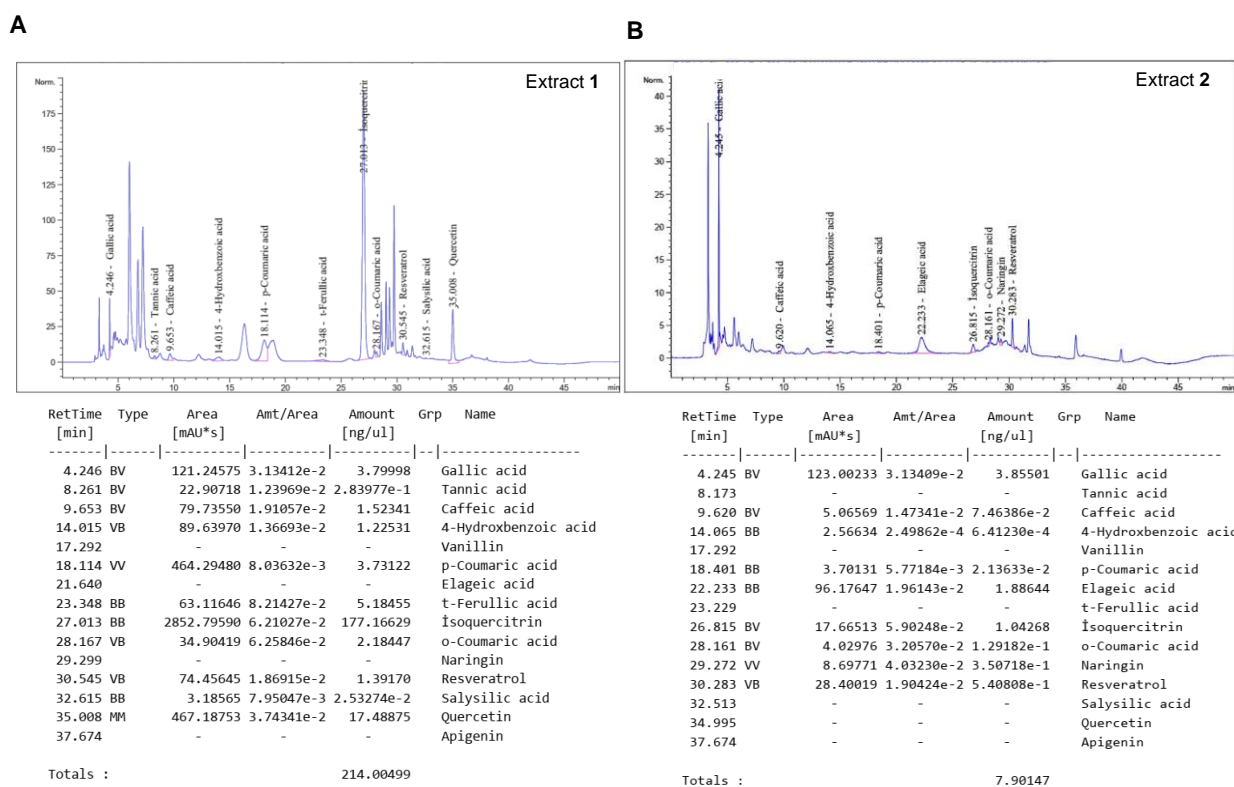


Figure 9. HPLC spectrum of extracts 1 and 2

The highest TEAC values including 18.72 mM Trolox/mg, 9.90 mM Trolox/mg, and 8.41 mM Trolox/mg were calculated for red leaf extracts. The antifungal activity was determined against *C. albicans* as a fungal pathogen. All plant extracts showed very promising results against all tested microorganisms.

In conclusion, we may emphasize that *PQ* may be a promising medicinal plant for breast and colon cancers due to the cell cytotoxicity, cell migration, and inhibition effect on colony formation. It was obtained that MeOH extracts of fruits and red leaves led to apoptosis determined by Hoechst staining in MDA-MB-231 and ER+ MCF-7 cells. Additionally, major bioactive components in plants such as rutin, quercetin, resveratrol, naringenin, catechin, curcumin were identified by HPLC analysis. As a result, bioactive components of *PQ* may contribute to further research to be used in plant-based cancer studies.

Author Contributions

The first author directed the project and supervised this study's findings. All authors analyzed the experiments. All authors contributed to the writing of the manuscript. The first, fourth, fifth, and sixth authors reviewed and edited the manuscript. All authors read and approved the final version of the manuscript.

Conflicts of Interest

All the authors declare no conflict of interest.

Acknowledgement

This work was supported by The Scientific Research Coordination Unit at Çanakkale Onsekiz Mart University, Grant number: THD-2022-4041. We thank Dr. Mehmet Ay, Dr. Hava Özyay, and Dr. Özgür Özyay for laboratory facilities, Dr. Zuhale Hamurcu for breast cancer cell lines, Dr. Tuğba Tümer for colon cancer cell line, Çanakkale Onsekiz Mart University Experimental Research Application and Research Center (ÇOMÜDAM)

for laboratory facilities, and Iğdır University Research Laboratory Practice and Research Center (ALUM) for HPLC analysis. The microorganisms were obtained from the microbiology laboratory of the Bioengineering faculty of Çanakkale Onsekiz Mart University.

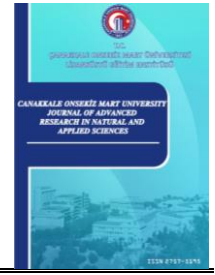
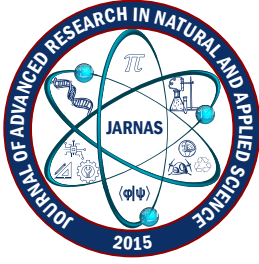
References

- [1] O. S. Nwozo, E. M. Effiong, P. M. Aja, C. G. Awuchi, *Antioxidant, phytochemical, and therapeutic properties of medicinal plants: A review*, International Journal of Food Properties 26 (1) (2022) 359–388.
- [2] M. Samtiya, R. E. Aluko, T. Dhewa, J. M. Moreno-Rojas, *Potential health benefits of plant food-derived bioactive components: An overview*, Foods 10 (4) (2021) 839 25 pages.
- [3] M. Khalid, M. Amayreh, S. Sanduka, Z. Salah, F. Al-Rimawi, G. M. Al-Mazaideh, A. A. Alanezi, F. Wedian, F. Alasmari, M. H. Faris Shalayel, *Assessment of antioxidant, antimicrobial, and anticancer activities of *Sisymbrium officinale* plant extract*, Heliyon 8 (9) (2022) e10477 6 pages.
- [4] A. S. Choudhari, P. C. Mandave, M. Deshpande, P. Ranjekar, O. Prakash, *Phytochemicals in cancer treatment: From preclinical studies to clinical practice*, Frontiers in Pharmacology 10 (2020) 1614 17 pages.
- [5] N. H. Nguyen, Q. Ta, Q. T. Pham, T. Luong, V. T. Phung, T. H. Duong, V. G. Vo, *Anticancer activity of novel plant extracts and compounds from *Adenosma bracteosum* (Bonati) in human lung and liver cancer cells*, Molecules 25 (12) (2020) 2912 16 pages.
- [6] P. Chaudhary, P. Janmeda, A. O. Docea, B. Yeskaliyeva, A. F. Abdull Razis, B. Modu, D. Calina, J. Sharifi-Rad, *Oxidative stress, free radicals and antioxidants: potential crosstalk in the pathophysiology of human diseases*, Frontiers in Chemistry 11 (2023) 1158198 24 pages.
- [7] M. Michalak, *Plant-derived antioxidants: Significance in skin health and the ageing process*, International Journal of Molecular Sciences 23 (2) (2022) 585 29 pages.
- [8] L. Shi, W. Zhao, Z. Yang, V. Subbiah, H. A. R. Suleria, *Extraction and characterization of phenolic compounds and their potential antioxidant activities*, Environmental Science and Pollution Research 29 (54) (2022) 81112–81129.
- [9] Y. Kocak, F. Altindag, E. Okumus, G. Oto, M. Hafif Bayir, S. Alparslan, *The effect of quercetin against oxidative stress and possible histopathological changes due to Bisphenol-A exposure in rat ovary*, Chronicles of Precision Medical Researchers 4 (3) (2023) 290–296.
- [10] F. Summiya, P. Anjum, K. Zaheer, S. Andleeb, S. Shabnum, M. Asma, *Phytochemical screening and antioxidant potential of *Parthenocissus quinquefolia* [L.] planch extracts of bark and stem*, Pakistan Journal of Pharmaceutical Sciences 31 (5) (2018) 1813-1816
- [11] K. Jomova, R. Raptova, S. Y. Alomar, S. H. Alwasel, E. Nepovimova, K. Kuca, M. Valko, *Reactive oxygen species, toxicity, oxidative stress, and antioxidants: Chronic diseases and aging*, Archives of Toxicology 97 (10) (2023) 2499–2574.
- [12] G. S. Četković, J. M. Čanadanović-Brunet, S. M. Djilas, V. T. Tumbas, S. L. Markov, D. D. Cvetković, *Antioxidant potential, lipid peroxidation inhibition and antimicrobial activities of *Satureja montana* L. subsp. *kitaibelii* extracts*, International Journal of Molecular Sciences 8 (10) (2007) 1013–1027.
- [13] Z.-Ud-D. Khan, S. Faisal, A. Perveen, A. A. Sardar, S. Z. Siddiqui, *Phytochemical properties and antioxidant activities of leaves and fruits extracts of *Parthenocissus Quinquefolia* (L.) planch*, Bangladesh Journal of Botany 47 (1) (2018) 33–38.
- [14] A. A. Mohamed, M. M. Salah, M. M. Z. El-Dein, M. EL-Hefny, H. M. Ali, D. A. A. Farraj, A. A. Hatamleh, M. Z. M. Salem, N. A. Ashmawy, *Ecofriendly bioagents, *Parthenocissus quinquefolia*, and*

- Plectranthus neochilus* extracts to control the early blight pathogen (*Alternaria solani*) in tomato, *Agronomy* 11 (5) (2021) 911–17 pages.
- [15] A. Zardi-Bergaouia, M. Jouinia, M. Znatia, A. El Ayeb-Zakhamab, H. B. Janneta, *Physico-chemical properties, composition and antioxidant activity of seed oil from the Tunisian Virginia Creeper (Parthenocissus quinquefolia (L.) planch)*, *Journal of the Tunisian Chemical Society* 18 (2016) 89–95.
- [16] K. Zaheer-Ud-Din, F. Summiya, P. Anjum, A. A. Sardar, S. Z. Siddiqui, *Phytochemical properties and antioxidant activities of leaves and fruits extracts of Parthenocissus quinquefolia (L.) Planch*, *Bangladesh Journal of Botany* 47 (1) (2018) 33–38.
- [17] M. B. Ticha, N. Meksi, H. E. Attia, W. Haddar, A. Guesmi, H. B. Jannet, M. F. Mhenni, *Ultrasonic extraction of Parthenocissus quinquefolia colorants: Extract identification by HPLC-MS analysis and cleaner application on the phytodyeing of natural fibres*, *Dyes and Pigments* 141 (2017) 103–111.
- [18] A. G. Atanasov, B. Waltenberger, E. M. Pferschy-Wenzig, T. Linder, C. Wawrosch, P. Uhrin, V. Temml, L. Wang, S. Schwaiger, E. H. Heiss, J. M. Rollinger, D. Schuster, J. M. Breuss, V. Bochkov, M. D. Mihovilovic, B. Kopp, R. Bauer, V. M. Dirsch, H. Stuppner, *Discovery and resupply of pharmacologically active plant-derived natural products: A review*, *Biotechnology Advances* 33 (8) (2015) 1582–1614.
- [19] Kivanç, M. R., Önder, A., Cömert Önder, F., Ilgin, P. (2023). Pektin/p(HEMA-ko-AAc) Hidrojellerine Gömülü Gümüş Nanopartiküllerin Yeşil Sentez Yöntemi olarak Parthenocissus quinquefolia L. Bitki Özütü ile Üretilmesi. *Lapseki Meslek Yüksekokulu Uygulamalı Araştırmalar Dergisi*, 4(7), 12-19. <https://dergipark.org.tr/tr/pub/ljar/issue/78716/1290920>
- [20] F. Comert Onder, M. Ay, S. D. Sarker, *Comparative study of antioxidant properties and total phenolic content of the extracts of Humulus lupulus L. and quantification of bioactive components by LC-MS/MS and GC-MS*, *Journal of Agricultural and Food Chemistry* 61 (44) (2013) 10498–10506.
- [21] F. Comert Onder, S. Kalin, A. Onder, H. Ozay, O. Ozay, *Assessment of release and anticancer effect of innovative pH-responsive and antioxidant-biodegradable hydrogel by using Parthenocissus quinquefolia L. extract as a crosslinker*, *Journal of Drug Delivery Science and Technology* 90 (5) (2023) 105113–12 pages.
- [22] F. Ozsoy, F. Comert Onder, P. Ilgin, H. Ozay, A. Onder, O. Ozay, *Self-assembled silibinin-containing phosphazene/cystamine hybrid nanospheres as biodegradable dual-drug carriers with improved anticancer activity on a breast cancer cell line*, *Materials Today Communications* 37 (2023) 107116–11 pages.
- [23] I. Fatima, N. Safdar, W. Akhtar, A. Munir, S. Saqib, A. Ayaz, S. Bahadur, A. F. Alrefaei, F. Ullah, W. Zaman, *Evaluation of potential inhibitory effects on acetylcholinesterase, pancreatic lipase, and cancer cell lines using raw leaves extracts of three fabaceae species*, *Heliyon* 9 (5) (2023) e15909–8 pages.
- [24] R. Delalat, S. A. Sadat Shandiz, B. Pakpour, *Antineoplastic effectiveness of silver nanoparticles synthesized from Onopordum acanthium L. extract (AgNPs-OAL) toward MDA-MB231 breast cancer cells*, *Molecular Biology Reports* 49 (2022) 1113–1120.
- [25] Y. Kocak, G. Oto, I. Meydan, H. Seckin, *Van bölgesinde yetişen Allium schoenoprasum L. bitkisinin toplam flavonoid, DPPH radikal söndürme, lipid peroksidasyonu ve antimikrobiyal aktivitesinin araştırılması*, *Yüzüncü Yıl Üniversitesi Tarım Bilimleri Dergisi* 30 (1) (2020) 147–155.
- [26] S. Durmuş, B. Yilmaz, M. R. Kıvanç, A. Onder, P. Ilgin, H. Ozay, O. Ozay, *Synthesis, characterization, and in vitro drug release properties of AuNPs/p (AETAC-co-VI)/Q nanocomposite hydrogels*, *Gold Bulletin* 54 (2021) 75–87.
- [27] N. Partovi, H. H. Kumleh, E. Mirzajani, M. Farhadpour, *Identification of Lilium ledebourii*

- antiproliferative compounds against skin, bone, and oral cancer cells*, Avicenna Journal of Phytomedicine 13 (6) (2023) 626–640.
- [28] T. Kundaković, T. Stanojković, M. Milenković, J. Grubin, Z. Juranić, B. Stevanović, N. Kovačević, *Cytotoxic, antioxidant, and antimicrobial activities of Ampelopsis brevipedunculata and Parthenocissus tricuspidate (VITACEAE)*, Archives of Biological Sciences Belgrade 60 (4) (2018) 641–647.
- [29] A. Elfadadny, R. F. Ragab, R. Hamada, S. K. Al Jaouni, J. Fu, S. A. Mousa, H. Ali, *Natural bioactive compounds-doxorubicin combinations targeting topoisomerase II-alpha: Anticancer efficacy and safety*, Toxicology and Applied Pharmacology 461 (2023) 116405 18 pages.
- [30] S. Saharkhiz, A. Zarepour, N. Nasri, M. Cordani, A. Zarrabi, *A comparison study between doxorubicin and curcumin co-administration and co-loading in a smart niosomal formulation for MCF-7 breast cancer therapy*, European Journal of Pharmaceutical Sciences 191 (2023) 106600 10 pages.
- [31] M. Sudhakaran, M. R. Parra, H. Stoub, K. A. Gallo, A. I. Doseff, *Apigenin by targeting hnRNPA2 sensitizes triple-negative breast cancer spheroids to doxorubicin-induced apoptosis and regulates expression of ABCC4 and ABCG2 drug efflux transporters*, Biochemical Pharmacology 182 (2020) 114259 13 pages.
- [32] B. Pateliya, V. Burade, S. Goswami, *Combining naringenin and metformin with doxorubicin enhances anticancer activity against triple-negative breast cancer in vitro and in vivo*, European Journal of Pharmacology 891 (2021) 173725 10 pages.
- [33] H. M. Shirang, B. J. Kariyil, R. John, *Anticancer potential of methanol extract of seeds of Artocarpus hirsutus in human breast cancer cell lines*, Indian Journal of Traditional Knowledge 22 (2) (2023) 390–400.
- [34] N. Rattanata, S. Daduang, S. Phaetchanla, W. Bunyatratchata, B. Promraksa, R. Tavichakorntrakool, P. Uthaiwat, P. Boonsiri, J. Daduang, *Antioxidant and antibacterial properties of selected Thai weed extracts*, Asian Pacific Journal of Tropical Biomedicine 4 (11) (2014) 890–895.
- [35] S. Faisal, A. Perveen, Z. U. Khan, A. A. Sardar, S. Shaheen, A. Manzoor, *Phytochemical screening and antioxidant potential of Parthenocissus quinquefolia (L.) plant extracts of bark and stem*, Pakistan Journal of Pharmaceutical Sciences 31 (5) (2018) 1813–1816.
- [36] N. R. Ismail, E. J. Kadhim, *Phytochemical screening and isolation of new compounds*, International Journal of Drug Delivery Technology 11 (3) (2021) 1033–1039.
- [37] J. Dai, R. J. Mumper, *Plant phenolics: extraction, analysis and their antioxidant and anticancer properties*, Molecules 15 (10) (2010) 7313–7352.
- [38] H. Hajimehdipoor, R. Shahrestani, M. Shekarchi, *Investigating the synergistic antioxidant effects of some flavonoid and phenolic compounds*, Research Journal of Pharmacognosy 1 (3) (2014) 35–40.
- [39] A. Oreopoulou, D. Tsimogiannis, V. Oreopoulou, *Extraction of polyphenols from aromatic and medicinal plants: an overview of the methods and the effect of extraction parameters*, in: R. R. Watson (Ed.), Polyphenols in Plants: Isolation, Purification and Extract Preparation, 2nd Edition, Academic Press, Cambridge, 2019, Ch. 15, pp. 243–259.
- [40] A. Altemimi, N. Lakhssassi, A. Baharlouei, D. G. Watson, D. A. Lightfoot, *Phytochemicals: Extraction, isolation, and identification of bioactive compounds from plant extracts*, Plants 6 (4) (2017) 42 23 pages.
- [41] P. Anokwuru, G. N. Anyasor, O. Ajibaye, O. Fakoya, P. Okebugwu, *Effect of extraction solvents on phenolic, flavonoid and antioxidant activities of three nigerian medicinal plants*, Nature and Science 9 (7) (2011) 53–61.
- [42] D. Stalikas, *Extraction, separation, and detection methods for phenolic acids and flavonoids*, Journal of Separation Science 30 (18) (2007) 3268–3295.

- [43] M. Kisiriko, M. Anastasiadi, L. A. Terry, A. Yasri, M. H. Beale, J. L. Ward, *Phenolics from medicinal and aromatic plants: Characterisation and potential as biostimulants and bioprotectants*, *Molecules* 26 (21) (2021) 6343–37 pages.
- [44] G. Pizzino, N. Irrera, M. Cucinotta, G. Pallio, F. Mannino, V. Arcoraci, F. Squadrito, D. Altavilla, A. Bitto, *Oxidative stress: Harms and benefits for human health*, *Oxidative Medicine and Cellular Longevity* 2017 (2017) Article ID 8416763 13 pages.
- [45] Clinical and Laboratory Standards Institute, *Laboratory documents: Development and control; Approved guideline, 5th Edition*, Clinical and Laboratory Standards Institute, 2006.
- [46] H. Hamrouni, K. B. Othman, H. Benmoussa, S. Idoudi, H. Najjaa, M. Neffati, W. Elfalleh, *Phenolic profiling, antioxidant, and antibacterial activities of selected medicinal plants from Tunisia*, *Chemistry & Biodiversity* 20 (8) (2023) e202300265 10 pages.
- [47] S. Dubale, D. Kebebe, A. Zeynudin, N. Abdissa, S. Suleman, *Phytochemical screening and antimicrobial activity evaluation of selected medicinal plants in Ethiopia*, *Journal of Experimental Pharmacology* 15 (2023) 51–62.
- [48] T. T. Cushnie, A. J. Lamb, *Recent advances in understanding the antibacterial properties of flavonoids*, *International Journal of Antimicrobial Agents* 38 (2) (2011) 99–107.



Community-Based Strategies for Disaster Preparedness in Mauritius

Henna Helvina Neerunjun¹

¹School of Mauritian and Area Studies, Mahatma Gandhi Institute, Moka, Mauritius

Abstract – Mauritius is Small Island Developing State (SIDS) of volcanic origin which lies in the South-West Indian Ocean Basin and is vulnerable to the consequences of global environmental challenges. The fourth priority action of the Sendai Framework for Disaster Risk Reduction 2015-2030 is to consolidate disaster preparedness for an effective response and to have a Build Back Better agenda that will improve recovery, rehabilitation, and reconstruction. This research aimed at examining the disaster management system in Mauritius through community-based approaches. The National Disaster Risk Reduction and Management Centre's (NDRRMC) involvement with the community living in high-risk zones was investigated. This study used quantitative data gathered from secondary sources and included the number of field training simulation exercises, training of volunteers under the Community Disaster Response Programme (CDRP), awareness campaigns and formulation of contingency plans based on documentation across Mauritius. The NDRRMC identified 109 high-risk zones across Mauritius out of which 13.7 per cent benefitted from all four forms of mitigation activities. Results indicated that contingency plans in Mauritius were evidence-based and had been developed after identification of disaster risk in selected regions, and therefore, they were limited to some types of disasters only. Findings also revealed that flooding was the most common type of simulated disaster exercise undertaken. The greatest number of field simulation exercises was carried out in Poste de Flacq. Results also demonstrated that only 38.5% of the community were exposed to disaster-related awareness campaigns, making it the least common form of disaster risk reduction (DRR) activity in Mauritius.

Article History

Received: 30 Jul 2023

Accepted: 18 Dec 2023

Published: 15 Mar 2024

Research Article

Keywords – Community-based strategies, contingency plans, disaster preparedness, simulation exercises, Mauritius

1. Introduction

Various approaches have been employed to reduce vulnerability and build the resilience of local communities to the impacts of climate change and disasters across the world. Small Island Developing State (SIDS), such as Mauritius, frequently experience natural hazards, namely, tropical cyclones, sea-level rise, storm surges, landslides, Indian Ocean waves (IOWaves) and flash floods. The National Risk Reduction and Management Policy 2020-2030 recognizes the importance of empowering our communities to strengthen their resilience, thus reducing significant economic and human losses in Mauritius [1].

The number of disasters and casualties which arise from natural hazards has increased around the world [2]. The World Risk Report of 2017 ranked Mauritius as the 13th country with the highest risk worldwide, and 7th on the list of countries having the greatest exposure to natural hazards [3]. According to the National Disaster Risk Reduction and Management Centre (NDRRMC), heavy/torrential rains result in flooding which accounts for more than 70 per cent of disaster events in the Republic of Mauritius. The estimated cost of infrastructural damages due to flooding will reach US \$ 2 billion in the Republic of Mauritius in the next 50 years [4]. Small islands such as Mauritius are increasingly prone to socio-economic losses and environmental degradation as a

¹henna.neerunun@mgi.ac.mu (Corresponding Author)

result of their geographical remoteness, heavy reliance on international markets, limited number of resources and high coastal population densities [5].

Mauritius has made tremendous efforts to maintain an acceptable level of investment in cyclone preparedness measures and its community-based disaster response teams [6]. The organizational structure of the NDRRMC consists of a full-fledged community staff in each of the District Councils and Municipal Councils across Mauritius. It ensures that the local communities are aware of the alert system and that there are regular trainings in place for torrential rains and flash floods [6].

While there have been several attempts to include Information and Communication Technology (ICT) in the different phases of disaster management process in Mauritius [7], Ruchama and Ansaram [8] concluded that community capacity building and social networking services remain the most effective techniques for disaster risk reduction in Mauritius. Although the concept of community-led approaches has emerged internationally and has been implemented by various organizations, they remain a serious challenge in many countries [9]. Several low-income countries have also adopted a bottom-up approach to disaster risk reduction by engaging communities. In Mauritius, the study of community engagement in disaster risk reduction and various other fields is limited. Betchoo [10] assessed the importance of engaging rural communities in climate change and sustainable development and emphasized the need to involve Mauritian citizens in issues affecting them directly. Community engagement was also found to be one of the positive factors which contributed to contain the outbreak of the Covid-19 pandemic in Mauritius [11].

Previous studies carried out in other SIDS such as the Caribbean Islands have demonstrated that some sectors of the communities have limited capacity to cope with natural hazards [12-14]. Betchoo [9] further highlighted that community engagement might help to understand the hindrances to an effective coordination of disaster risk reduction activities between communities and local organizations in Mauritius. Walshe et al. [15] also conducted a disaster-related study on the Mauritian society and examined the long-term cyclone memory of communities in Mauritius. Their study revealed that long intervals between natural hazards such as large tropical cyclones, may result in populations forgetting their exposure and practices of response. As a matter of fact, several authorities are being urged to address the challenge of natural hazards impacting on human settlements with the close collaboration of the local communities [16]. As an effective community engagement can make a difference in the outcome of a crisis, its successful implementation is important in order to achieve measurable and sustainable goals in disaster risk reduction in Mauritius.

2. Relevance of Capacity Building and Community-Based Approaches in DRR

Concepts of capacity building at community level in DRR have been previously applied by various scholars [17-19]. Community-Based Approaches (CBAs) are emerging rapidly as the development community comes to understand the benefits of these approaches [20,21]. For instance, CBAs take into consideration local cultures and development issues [22] such that communities are able to readily collaborate with development partners and identify risks themselves using place-specific knowledge of their local environments [23].

The occurrence of small to moderate, recurrent, and repeated threats often required the need to tap into local knowledge and capacity for organization and action [24]. Zubir and Amirrol [25] also highlighted the need for participatory involvement of the local community as one of the many aspects of DRR. People at the community or village levels are the first to suffer the adverse effects of extreme weather events regardless of whether the disaster is of national or regional proportion. They adopt coping and survival mechanisms to face and respond to the crisis well before external help from Non-Governmental Organizations (NGOs) or the Government can

reach them. On the other hand, Mc Bean and Rodgers [18] considered capacity building as a means of identifying the limitations in governmental response and developing alternative ways to overcome these barriers. Unfortunately, the roles of communities are often undervalued and at times ignored too [26]. Shah et al. [19] assessed current capacity levels of local institutions in Pakistan and found that local institutions were poorly prepared in terms of awareness and trainings. Their study concluded that one way to reduce the vulnerability of communities was to enhance the preparedness levels of local institutions through capacity building, so that they are able to provide first-hand rescue and support to the communities.

2.1. Legislations in Mauritius

Community engagement in disaster management has been one of the objectives of Hyogo Framework for Action (HFA) 2005-2015 and its successor, the Sendai Framework for Disaster Risk Reduction (SFDRR) 2015-2030. The SFDRR is a non-binding framework which intends to fill in the gaps identified in the HFA 2005-2015 and completes the disaster cycle by including response and recovery periods [27]. In order to be in line with the targets set by the SFDRR, the National Disaster Risk Reduction and Management Act 2016 in Mauritius stipulates that each local committee shall have a close collaboration with its local community under the supervision of the NDRRMC. One of the key functional areas of the NDRRMC is to mitigate the impacts of natural hazards, to prepare for measures which will minimize harm to economies and populations, to respond during emergencies and to ensure a smooth and timely recovery of affected communities. For the period 2020-2030, the NDRRMC has also worked out a NDRRM Action Plan, a Strategic Framework and a Policy to strengthen its disaster-related legislative capabilities.

2.2. Contingency Planning for Disasters in Mauritius

A contingency is a highly uncertain situation that is likely to occur shortly but may not [28]. Local authorities, therefore, devise a contingency plan which is a set of procedures and clearly defined strategies based on uncertain events which occur at different scales to coordinate operations in times of disasters [29]. While contingency planning was initially formulated to address technological hazards such as toxic spills and industrial blasts, there has been an increasing emphasis on incorporating natural hazards, such as floods, storms, and earthquakes in contingency plans [30]. Sikka et al. [31] investigated the relevance of contingency planning for agricultural practices in India to meet the challenges of extreme weather events. Hussein [32] also examined the use of contingency planning and operational plans among the Indonesian communities and how these have been approved by the community leader and integrated into the local development planning programme. Koenti [33] also adopted a contingency approach to evaluate the disaster management system in Yogyakarta in Indonesia in partnerships with government agencies, state companies, the private sector, NGOs, international institutions, and the community. However, assessing contingency plans through real-time simulation can be costly, and, if the planned scenario does not occur, the contingency plan may not be enacted [33].

Given that a well-prepared contingency plan is essential to increase the capacity of the personnel in charge, the NDRRMC in Mauritius ensures that disaster contingency plans are prepared, reviewed, and updated periodically with the involvement of relevant institutions [4].

2.3. Field Training Exercise Simulation as an Important Aspect of DRR

There is ample literature on the use of simulations in heightening awareness in several different settings [34-36]. Lizuka [17] assessed disaster training exercises in Sri Lanka in which 6709 people living in disaster affected areas had participated. Her study revealed a positive response to the training activities. The United Nations for Disaster Risk Reduction (UNDRR) has also published a training manual which provides background information on conducting simulation exercises and drills on DRR to support the Sendai Framework for Disaster Risk Reduction (SFDRR) 2015-2030. It identified different types of simulation exercises, such as tabletop exercise and drills, that would enable professional teams such as the firefighters, medical personnel and the first- responders to test their equipment, plans, procedures, skills, and knowledge.

The NDRRMC opted for disaster simulation exercises as a means of preparing community members in village and municipal council areas for flooding, landslides, and tsunami-related coastal inundation. In an attempt to support tourist welfare, this training has been extended to hotels and tourist resorts whereby regular simulation exercises involving the staff and guests have been carried out to familiarize them with local coping strategies [6].

2.4. Awareness Campaigns

Mathbor [37] examined the benefits of making effective use of social capital such as social networks, social cohesion, social interaction, and community solidarity in attenuating the impacts of natural hazards that affect coastal regions. His study emphasized the importance of conducting round-the-year awareness activities for volunteers, whilst making use of local folk media to disseminate disaster-related messages to large numbers of people. As per the NDRRM Act 2016 Section 9, the NDRRMC coordinates and monitors all disaster risk reduction and management activities through community participation and public awareness activities in Mauritius. It carries out regular sensitization campaigns on DRR since knowledge management is a fundamental component for informed decision-making and coordinated actions in all phases of disaster management.

2.5. Community Disaster Response Programmes (CDRP)

Informal volunteering has gained widespread interest in disaster management as it stimulates spontaneous responses by individuals and voluntary groups from within and outside disaster-affected communities [38]. Their study looked into the implementation of appropriate policies, legal frameworks, and institutional arrangements for integrating informal volunteers in disaster management systems in European countries such as Germany, Italy, Belgium, Hungary, Sweden, Norway, Finland, and Estonia.

The successful implementation of a mitigation project is, to some extent, dependent on community involvement [39]. Therefore, the NDRRMC introduced the Community Disaster Response Programme (CDRP) which aimed at initiating volunteers to basic safety and rescue techniques such as fire safety, rope handling, first aid, water rescue activities, basic camp management, sand bagging and team building to respond to disasters. When emergencies occur, the trained community members would be able to act strategically to provide immediate assistance to victims, give adequate support to responding authorities and set up groups of disaster management volunteers at a disaster site before the arrival of government aid. One of the objectives of the NDRRMC was to develop a culture of DRR within the population and build the capacity of the community to respond to disasters, in order to be in line with the Sendai Framework for Disaster Risk Reduction (SFDRR) 2015-2030.

2.6. Purpose of Study

The research objectives of this study are to:

- examine the various CBAs to disaster risk mitigation which have been implemented in Mauritius;
- analyze the spatial distribution of contingency plans and simulation exercises in Mauritius;
- identify the type of simulation exercise with the greatest geographical extent in Mauritius;
- identify the least and most common forms of community-based disaster related activity carried out in Mauritius.

3. Methodology

3.1. Justification of Methods

The term “local participation” became popular in disaster discourse following the mid-term evaluation of the International Decade for Natural Disaster Reduction (IDNDR) in May 1994 such that risk reduction programmes have increasingly been engaging local residents [40]. Shaw [41] also examined the success and shortcomings of CBAs in disaster management in several countries. His analysis of CBAs varied from capacity-building, legislations, stakeholder participation and community involvement, local knowledge, and effective social networking. A series of community-based DRR methods have also contributed to improve community resilience in the landslide-prone area of Wanzhou in China [42]. Therefore, this study also attempts to investigate the different CBAs that have been implemented in Mauritius and the geographical extent to which they have been carried out throughout the country.

3.2. Datasets

This study used five datasets obtained on request from secondary sources, namely governmental organizations. Four datasets pertaining to the frequency of DRR activities such as (i) field training exercises, (ii) awareness campaigns, (iii) training exercises delivered to volunteers under the Community Disaster Response Programme (CDRP) and (iv) the availability of contingency plans, were obtained from the NDRRMC. The NDRRMC identified regions which were considered as high-risk based on place-specific evidence to prioritize training and DRR activities. The fifth dataset was made available upon request from the Statistics Office Mauritius. This dataset consisted of administrative boundaries in Mauritius which included five Municipal Council Areas (MCAs) and four District Council Areas (DCAs). These were further broken down into smaller areas known as Municipal Council Wards (MCWs) for urban regions and Village Council Areas (VCAs) for rural settlements respectively. The number of yearly DRR activities carried out in each MCA/DCA was reported to the NDRRMC by the local disaster Management Coordinator who acts as the liaison officer between the MCA/DCA and the NDRRMC. Results have been displayed for 144 administrative regions, including 124 VCAs and 20 MCWs.

3.3. Methods

3.3.1. Statistical Analysis

The NDRRMC identified 109 high-risk zones across Mauritius. The percentage of regions which benefitted from the different forms of disaster mitigation activities in the high-risk areas has been calculated using a basic statistical technique.

3.3.2. Tabulation Method

The forms of disaster mitigation activities have been summarized and displayed using the tabulation method to facilitate further analysis. Results of statistical analysis have been expressed as percentages and displayed in the form of a table for ease of comparison.

3.3.3. Mapping of Results using the Geographic Information System (GIS)

The GIS analytic tool was used to show the spatial distribution of contingency plans and simulation exercises on a thematic map which portrays the urban and rural administrative regions in Mauritius. Simulation exercises have been carried out for flooding, flash floods, torrential rain, landslides, IO Wave and tsunami. A region may have benefited from a single type of simulation exercise or a combination of exercises. Each single type or combination of simulation exercises was attributed a color while the availability of a contingency plan for a specific region was denoted by a red star on the map of Mauritius. Administrative regions which have not benefited from any simulation exercise have been grouped into the ‘none’ category with a white color code. However, some of these regions may have a readily available contingency plan.

4. Results

The forms of Community-Based DRR activities were divided into four capacity- building components for each region and are presented in Table 1 below: availability of a contingency plan, community exposure to simulation exercises, awareness campaigns and disaster-related volunteering programmes (CDRP). The type of simulation exercise (if any) is also shown in Table 1.

Table 1. Forms of Community-Based DRR activities carried out by region in high-risk zones

District Council Area	SN	Name of Region	Capacity Building Components				Type of Simulation Exercise
			CDRP as at Dec 2020	Contingency Plan available as at Dec 2020	Awareness Campaigns	Simulation Exercise	
Rivière du Rempart District Council	1.	Cottage	✓	✓	×	✓	Flooding
	2.	L’Amitié	✓	✓	×	✓	Flooding
	3.	Gokoola	✓	✓	×	×	
	4.	Grand Baie	×	×	×	✓	IOWave, tsunami
	5.	Péreybère	×	×	×	✓	Flooding
	6.	Amaury	×	×	✓	×	
Savanne District Council	1..	Rivière du	✓	✓	×	✓	Flooding
	2.	Bel Ombre	✓	✓	✓	✓	Tsunami, IOWave
	3.	Rivière des	✓	✓	×	✓	Tsunami, IOWave
	4.	Surinam	×	✓	×	×	
	5.	Souillac	✓	✓	✓	✓	Landslide
	6.	Britannia	✓	✓	×	×	
	7.	Grand Bois	×	✓	×	×	
	8.	Bois Chéri	×	✓	×	×	
	9.	L’Escalier	✓	✓	×	×	
	10.	La Flora	✓	✓	×	✓	Flooding
	11.	Riv. des	×	×	×	✓	Landslide
	12.	Riambel	×	×	×	✓	Tsunami/IOWave
	13.	St-Martin	×	×	×	✓	Tsunami/IOWave
	14.	Baie du Cap	×	×	×	✓	Tsunami/IOWave

Table 1. (Continued)

District Council Area	SN Name of Region	Capacity Building Components					Type of Simulation Exercise
		CDRP as at Dec 2020	Contingency Plan available as at Dec 2020	Awareness Campaigns	Simulation Exercise		
Black River District Council	1. La Gaulette	×	✓	✓	×		
	2. Richelieu	✓	✓	✓	✓	Flooding, tsunami	
	3. Canal Dayot	✓	✓	×	✓	Flooding	
	4. Sable Noir	×	✓	×	×		
	5. Bain des Dames	✓	✓	✓	×		
	6. Pointe aux Sables	✓	✓	✓	✓	Flooding	
	7. Bambous	✓	✓	✓	✓	Flash flood, flooding	
	8. Cotteau Raffin	✓	✓	✓	×		
	9. Albion	✓	×	×	✓	Torrential Rain	
	10. Tamarin	×	×	×	✓	Tsunami	
	11. Flic-en-Flac	×	×	×	✓	Flooding, Torrential rain	
	12. Chamarel	×	×	×	✓	Landslide, Tsunami, IOWave	
	13. Petite Rivière Noire	×	×	×	✓	Tsunami	
	14. Grande Rivière Noire	×	×	×	✓	Torrential rainfall	
	15. Le Morne	×	×	×	✓	Tsunami	
	16. Cascavelle	×	×	×	✓	Flash flood	
Moka District Council	1. Morc. Sans Souci	×	✓	×	✓	Flooding	
	2. Montagne Blanche	✓	✓	✓	✓	Flooding	
	3. L'Espérance	✓	✓	×	✓	Flooding	
	4. Quartier Militaire	×	✓	×	×		
	5. La Laura	×	×	×	✓	Flooding	
	6. Moka	×	×	×	✓	Landslide	
Pamplemousses District Council	1. Fond du Sac	✓	✓	×	✓	Flooding	
	2. Cité Roma/Le Hochet	✓	✓	✓	×		
	3. Terre Rouge	✓	✓	✓	✓	Flooding	
	4. Cité Mandela	×	✓	✓	×		
	5. C. La Boue/B. Source	✓	✓	✓	×		
	6. Bois Rouge	✓	✓	✓	×		
	7. Mapou	×	×	×	✓	Torrential rain	
	8. Crève France	×	×	×	✓	Torrential rain, Landslide	
	9. Pointe aux Piments	×	×	×	✓	Tsunami/IOWave	
	10. Trou aux Biches	×	×	×	✓	IOWave/Tsunami	
	11. Abercrombie	×	×	✓	×		
	12. Notre Dame	×	×	✓	×		
	13. Triolet	×	×	✓	×		
	14. Roche Bois	×	×	✓	×		
Grand Port District Council	1. Nouvelle France	✓	✓	✓	✓	Flooding	
	2. 16 ^{ème} Mille	✓	✓	✓	×		
	3. Carreau Esnouf	✓	✓	✓	✓	Flooding	
	4. New Grove/Gros Billot	✓	✓	✓	✓	Flooding	
	5. Mare Tabac	✓	✓	✓	×		
	6. Plaine Magnien	✓	✓	✓	×		
	7. Trois Boutiques	✓	✓	✓	✓	Flooding	
	8. B. des Amourettes	×	×	×	✓	IOWave	
	9. Rivière des Créoles	×	×	×	✓	Flooding	
	10. Vieux Grand Port	✓	×	✓	✓	Flooding	
Flacq District Council	1. Clémencia	✓	✓	×	×		
	2. Bramsthan	✓	✓	×	×		
	3. Argy	×	✓	×	✓	Flashflood	
	4. Cité Débarcadère	×	✓	×	×		
	5. Poste de Flacq	✓	✓	×	✓	Flooding, Tsunami	
	6. Grand Sable	✓	✓	×	×		
	7. Belle Mare	×	×	×	✓		
	8. Quatre-Soeurs	×	×	×	✓	Landslide	
	9. G.R.S.E	×	×	×	✓	Tsunami	
	10. Centre de Flacq	×	×	×	✓	Torrential rain	
	11. Bel Air	×	×	×	✓	Flash flood	

Table 1. (Continued)

District Council Area	SN Name of Region	Capacity Building Components				Type of Simulation Exercise
		CDRP as at Dec 2020	Contingency Plan available as at Dec 2020	Awareness Campaigns	Simulation Exercise	
Curepipe Municipal Council	1. Labrasserie	×	×	×	✓	Flooding
	2. La Colombe	×	✓	✓	×	
	3. Camp Bombaye	×	✓	✓	×	
	4. Forest-Side	✓	✓	×	×	
	5. Floréal/Mangalkan	✓	✓	✓	✓	
	6. Eau-Coulée	✓	✓	✓	✓	Flooding
	7. Les Casernes	✓	✓	✓	×	
	8. Curepipe Centre	×	×	×	✓	Flooding
Beau-Bassin/Rose-Hill Municipal Council	1. Stanley	✓	✓	✓	×	
	2. Mont Roches	✓	✓	✓	✓	Flooding
	3. Barkly	✓	✓	✓	×	
	4. Chebel	✓	✓	✓	×	
	5. Coromandel	✓	✓	✓	✓	Flooding
	6. Morc. Hermitage	×	×	×	✓	Landslide
Municipal Council of Port-Louis	1. Résidence La Cure	✓	✓	✓	✓	Flooding
	2. Ste Croix	✓	✓	✓	×	
	3. Le Cornu	×	✓	✓	×	
	4. V.des Prêtres	✓	×	✓	×	
	5. Chitrakoot	×	×	×	✓	Landslide
	6. Tranquebar	×	✓	✓	×	
Municipal Council of Quatre Bornes	1. Candos	×	✓	×	✓	Landslide
	2. La Louise	×	✓	×	✓	Flooding
	3. Bassin	×	✓	×	✓	Flooding
	4. Avenue Berthaud	×	✓	×	×	
	5. Ollier	×	×	×	✓	Flooding
Municipal Council of Vacoas/Phoenix	1. Malakoff/La Marie	✓	✓	×	✓	Flooding
	2. La Caverne	✓	✓	×	✓	Flooding
	3. Prom. Père Laval	×	✓	×	✓	Flooding
	4. Henrietta	✓	✓	×	✓	Flooding
	5. Camp Belin	×	✓	×	✓	Flooding
	6. St-Paul	×	×	×	✓	Flooding
	7. Morc. Réunion	×	×	×	✓	Landslide
		51/109	68/109	42/109	70/109	

Table 2. Percentage of regions exposed to each capacity building component

Community-based disaster strategy	Capacity Building Component			
	CDRP	Availability of Contingency Plan	Awareness Campaigns	Simulation Exercise
% of high-risk areas exposed to DRR activity	46.8%	62.3%	38.5%	64.2%

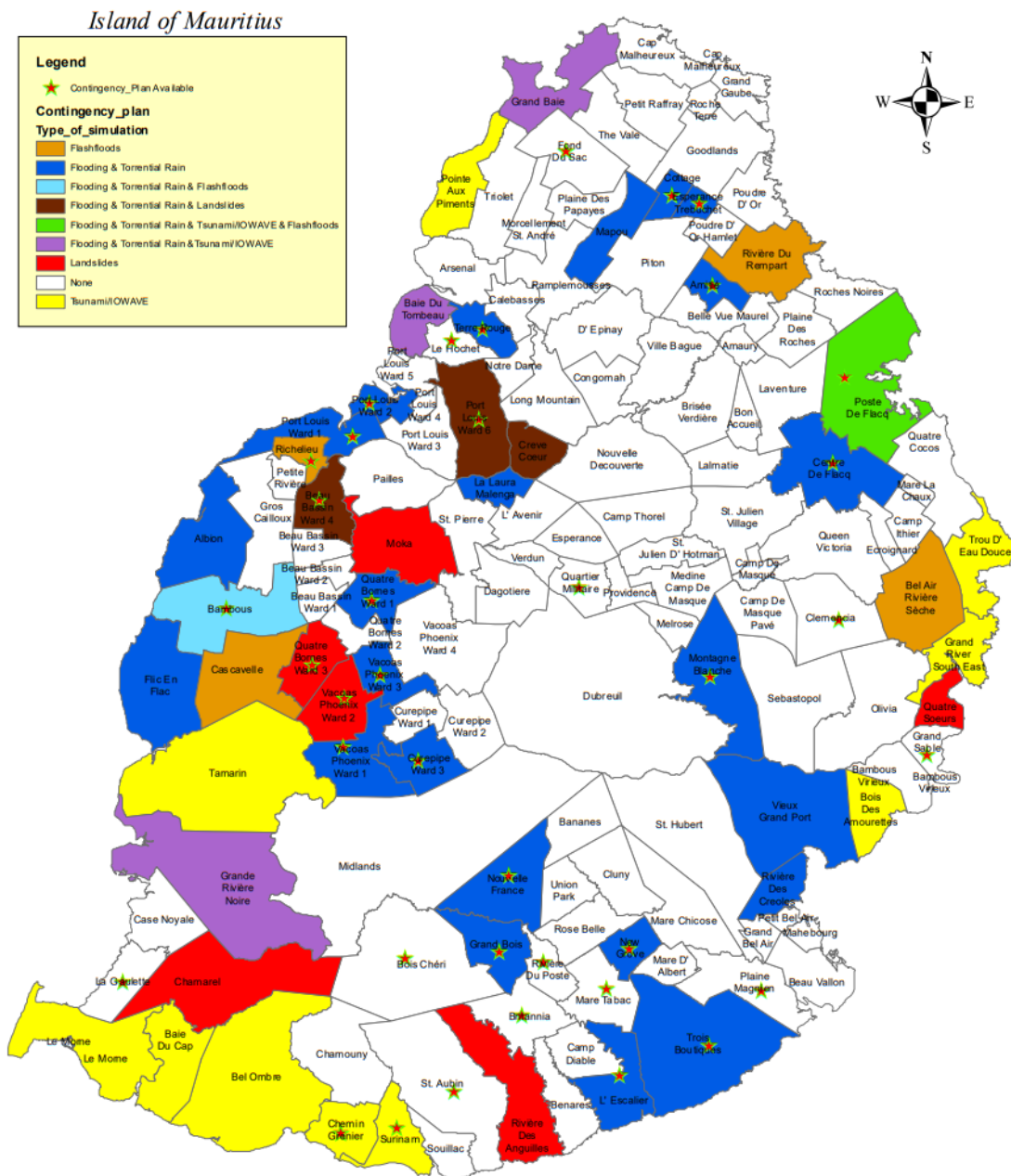


Figure 1. Spatial distribution of contingency plans and simulation exercises carried out in Mauritius as of 2020

Results showed that specific forms of community-based DRR exercises have been carried out in selected regions which have been previously identified as high-risk areas by the NDRRMC based on place-based evidence gathered from past disasters. Coastal regions have been more exposed to community-based-DRR exercises than inland regions (Figure 1). Simulation exercises have been the most frequent (64.2%) (Table 2) form of mitigation activity and flooding has been the most common simulated disaster (Figure 1).

Tsunami and IOWave simulation exercises have been carried out mostly on the South West coast, the East coast, in Tamarin on the West coast, in Baie du Tombeau and Grand Baie along the North West coast and Poste de Flacq along the North-East coast (Table 1 and Figure 1). Communities of Morcellement Réunion, Rivière des Anguilles, Quatre Sœurs, La Laura and Chamarel have benefitted from landslide-related simulation exercises. Four regions, namely Rivière du Rempart, Bel-Air Rivière Sèche, Cascavelle and Richelieu, have been exposed to simulation exercises geared towards flash floods. The greatest number of simulation exercises took place in Poste de Flacq where communities were involved in tsunami, IOWave, torrential rain and flash

floods exercises (Table 1 and Figure 1). All four forms of capacity building activities have been successfully implemented in 15 regions out of 109, but none of which was found in the Municipal Council of Vacoas/Phoenix (Table 1). The beneficiaries were Bel Ombre, Richelieu, Pointe aux sables, Bambous, Montagne Blanche, Terre rouge, Nouvelle France, Carreau Esnouf, New Grove/Gros Billot, Trois Boutiques, Floréal/Mangalkan, Eau Coulée, Mont Roches, Coromandel, and Résidence La Cure. Communities living in the mountain valleys of Port-Louis, for instance in the municipal ward 6 and in Crève Coeur, and along part of the steep-sided gorges of the Grand River North West, have been exposed to both hazardous flash flooding and landslide simulation exercises (Figure 1).

Results indicated that 62.3% of the risk-prone areas had a contingency plan ready (Table 2). In Mauritius, contingency plans are evidence-based and are limited to only some types of natural hazards. This is because contingency plans have been developed after identification of hazard risk in selected regions.

In addition, findings demonstrated that 46.8% (Table 2) of the population living in risk-prone areas have been trained under the CDRP programme in Mauritius whilst awareness campaigns remained the least common form of DRR activity (38.5%) (Table 2) carried out so far (Table 2).

5. Discussion of Findings

This study revealed that simulation exercises were the most frequent form of mitigation activity (64.2%) (Table 2) and flooding was the most common type of simulated disaster. Simulation exercises provide realistic learning situations at manageable costs [43]. Regular evaluation of the simulation exercises is required to provide evidence-based feedback on performance of all participants and to determine whether the current level of preparedness is of a satisfactory standard [44]. In another study, Gundran et al. [34] demonstrated that simulation exercises successfully enabled participants to increase their knowledge and overcome challenges in communication strategies, and to adopt these lessons to their own organizations to increase their capacity during disaster response.

Furthermore, findings indicated that 62.3% of the risk-prone areas had a readily available contingency plan (Table 2). Alexander [30] stated that contingency planning is an exploratory process which provides generic procedures for managing unforeseen impacts. According to his study, carefully constructed scenarios can help to anticipate the needs that will arise when foreseeable hazards happen. His study also emphasized the need for such plans to respond to the impacts of natural hazards, to maintain business continuity and to guide recovery and reconstruction effectively.

In addition, results demonstrated that 46.8% (Table 2) of the population living in risk-prone areas have been trained under the CDRP programme in Mauritius. Community infrastructure is essential in the post-disaster phase as shelters and an adequate number of volunteers must be provided to give assistance to the displaced households [6]. In other countries such as Sweden and Norway, community volunteering has become regulated, and volunteers are formally insured. Disaster management authorities have made extensive use of social media to register informal volunteers and to guide them through practical training exercises that focus primarily on first aid [38]. Community members who found their lives or livelihoods highly exposed to the impacts of natural hazards were more likely to actively engage themselves in disaster preparedness than those who did not [45].

In Mauritius, awareness campaigns were the least common form of DRR activity (38.5%) (Table 2) carried out so far (Table 2). Education remains one of the main priorities of the Global DRR initiatives [46,47] and raising awareness plays a key role in addressing the intricacy of adapting to climate change. Chen et al. [48]

pointed out that the traditional forms of community capacity building efforts in DRR would include access to education, training, funding, information, equipment, and food supplies, but highlighted the need to integrate scientific and technological developments of the recent decades in DRR activities because traditional resources often go underutilized due to a lack of organization [49]. However, many communities struggle to integrate scientific methods in developing DRR strategies, thus hindering adequate access to information, as scientific data requires large volumes of continuous temporal and spatial data coverage [49].

DRR activities have improved since the setting up of the NDRRMC in 2013 and have been oriented favorably towards participatory processes. These results were consistent with Haque and Uddin [50] who also stated that the landscape of disaster management has changed positively in recent decades, mainly in the low-income countries. The results were further supported by Kafle [51] who pointed out that at-risk communities should be at the center of the decision-making process and be actively engaged in the assessment and implementation of DRR measures. In another study, Bhagat [21] concluded that capacity building and training of disaster relief volunteers were the main focus of community-based disaster management since they are the first responders. Shaw [52] also identified communities as the first emergency responders in case of a disaster. He stated that there exists innovative community based DRR practices worldwide, and it is important to analyze and withdraw common lessons from them. Similarly, Yodmani [53] argued that community-based disaster risk management (CBDRM) techniques could eventually contribute to vulnerability reduction and capacity strengthening by preventing human, economic and environmental losses. Community empowerment is widely used in disaster management, and it has been used as a common method to build resilient communities by many NGOs and countries such as Indonesia, Philippines, and Bangladesh. While Rozi et al. [54] studied the contribution of religious values and local wisdom in CBAs, Badrudin [55] argued that CBAs consist of traditional relief measures whereby communities are either “victims” or “beneficiaries” of disaster relief assistance only.

Despite the massive efforts to improve public disaster education, poor levels of preparedness still prevail in many countries [56,57]. Past studies revealed that, although people knowingly live in hazardous environments, barriers to at-home-preparedness still exist, and, therefore, households’ disaster unpreparedness remains high [58,59]. Having an appropriate infrastructure such as a robust early warning system does not guarantee that most people will respond favorably to a disaster. In a study conducted by Nakamura [60], it was found that many inhabitants on the Ryukyu Islands of Japan were neither aware of the tsunami risk, nor did they know what the siren was meant for. Yadav and Barve [61] stated that CBAs can further be improved with the collaboration of relief agencies and NGOs such as the Red Cross to address gaps that overstretched government departments cannot fill. This was further supported by Gero et al. [62] who pointed out the importance of Community Based Health and First Aid in Samoa in the Pacific for successful implementation of DRR strategies. Hence, community-disaster communication and education strategies must take into consideration the community demographic characteristics such as age, education level, cultural beliefs, customs, and financial resources in terms of funding and infrastructural facilities.

6. Conclusion

This research paper identified the CBAs to Disaster Risk Reduction which have been executed in various administrative areas across Mauritius. Although the forms of CBAs varied from region to region, mobilization and awareness remained the core elements of such approaches.

O’Brien and O’Keefe [63] noted that community members are frontline actors in the disaster management process. Their active involvement in risk reduction measures helps to identify the root causes of their

vulnerability to disasters [64]. However, local communities cannot improve their resilience to natural hazards on their own. Long-term training of the personnel is also essential for sustainable community-based disaster risk reduction efforts in high risk areas. Many countries have already adopted a policy transition from a top-down process to a community-centered approach with a focus on building bridges between community members and key stakeholders [50]. Global frameworks such as the Sendai Framework for Disaster Risk Reduction 2015-2030 and UN Sustainable Development Goals 2030 also encourage active participation of community members.

Mauritius has also implemented Community-Based Disaster Management in its various laws and regulations, such as the National Disaster Risk Reduction and Management Act 2016. Rules and regulations provide guidelines on how to ensure adequate community participation when implementing disaster management activities. Ultimately, results from this study suggest that there is a need to implement the different forms of community-based disaster activities on a larger scale across Mauritius in order to maintain a reasonable level of public interest in hazard mitigation. The active engagement of community members in Mauritius may eventually enable local institutions to identify weaknesses in emergency relief operations and to learn from disaster experiences.

The main conclusions drawn from this study were:

- Four community based DRR methods have contributed to improve community resilience towards natural hazards in Mauritius, namely, community volunteering, contingency planning, simulation exercises and awareness campaigns;
- All four forms of capacity building activities have been successfully implemented in 15 regions out of 109, but none of which was found in the Municipal Council of Vacoas/Phoenix;
- There has been an extensive attempt to mitigate the impact of natural hazard events through simulation exercises;
- The most common form of simulation exercise was flooding;
- The region of Poste de Flacq along the North East coast has benefitted from the greatest number of simulation exercises;
- Exposure to awareness campaigns has been very low and can be further increased to reach out to a wider audience.

Author Contributions

The author read and approved the final version of the paper.

Conflicts of Interest

The author declares no conflict of interest.

Acknowledgement

We thank the National Disaster Risk Reduction and Management Centre (NDRRMC) for the datasets provided. This work was supported by the Higher Education Mauritius under the Individual Research Support Scheme, Grant number: ID-2021-1.

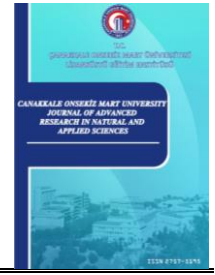
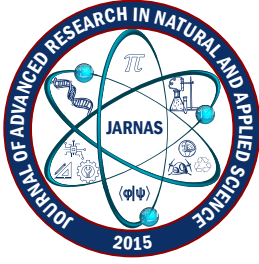
References

- [1] Ministry of Local Government and Disaster Risk Management - Republic of Mauritius, *National disaster risk reduction and management policy 2020-2030*, 2016, 26 pages.
- [2] T. A. Codreanu, A. Celenza, I. Jacobs, *Does disaster education of teenagers translate into better survival knowledge, knowledge of skills and adaptive behavioural change? A systematic literature review*, *Prehospital and Disaster Medicine* 29 (2014) 629–642.
- [3] M. Aleksandrova, D. Malerba, C. Strupat, *World Risk Report “Building Back Better” through social protection*, Bündnis Entwicklung Hilft, Bochum: Ruhr University Bochum – Institute for International Law of Peace and Armed Conflict (2001) 33–37.
- [4] National Audit Office, Ministry of Social Security, National Solidarity and Environment and Sustainable Development - Republic of Mauritius, *Performance audit report: Government response to mitigate the impact of flooding*, (2019) 1–32.
- [5] I. Kelman, J. J. West, *Climate change and small island developing states: A critical review*, *Ecological and Environmental Anthropology* 5 (1) (2009) 1–16.
- [6] Capacity for Disaster Reduction Initiative, *Mauritius: Disaster risk management: A capacity diagnosis*, (2020) 1–170.
- [7] R. K. Sungkur, A. Kissoonah, *ICT for disaster management and emergency telecoms preparation, migration and recovery for the island of Mauritius*, *Strengthening Disaster Resilience in Small States: Commonwealth Perspectives*, 2019, Ch. 4, 67–85.
- [8] E. Ruchama, K. Ansaram, *Assessment of disaster risk reduction practices in Mauritius*, in: J. M. Luetz, D. Ayal, (Eds.), *Handbook of Climate Change Management: Research, Leadership, Transformation*, 2021, pp. 3533–3559.
- [9] N. K. Betchoo, *Developing a model of community participation in disaster management in Mauritius*, *Journal of Multidisciplinary Engineering Science and Technology* 5 (12) (2018) 9172–9175.
- [10] N. K. Betchoo, *Engaging rural communities in sustainable development in Mauritius*, *Journal of Multidisciplinary Engineering Science and Technology* 2 (3) (2015) 370–375.
- [11] L. Musango, L. Veerapa Mangroo, Z. Joomaye, A. Ghurbhurrin, V. Vythelingam, E. Paul, *Key success factors of Mauritius in the fight against COVID-19*, *BMJ Global Health* 6 (3) (2021) e005372 5 pages.
- [12] I. Ferdinand, G. O’Brien, P. O’Keefe, J. Jayawickrama, *The double bind of poverty and community disaster risk reduction: A case study from the Caribbean*, *International Journal of Disaster Risk Reduction* 2 (2012) (2012) 84–94.
- [13] F. Linnekamp, A. Koedam, I. S. A. Baud, *Household vulnerability to climate change: Examining perceptions of households of flood risks in Georgetown and Paramaribo*, *Habitat International* 35 (3) (2011) 447–456.
- [14] M. Pelling, J. I. Uitto, *Small island developing states: Natural disaster vulnerability and global change*, *Global Environmental Change Part B: Environmental Hazards* 3 (2) (2001) 49–62.
- [15] R. A. Walshe, G. C. Adamson, I. Kelman, *Helices of disaster memory: How forgetting and remembering influence tropical cyclone response in Mauritius*, *International Journal of Disaster Risk Reduction* 50 (2020) 101901 13 pages.
- [16] A. Chacowry, *Community recovery and resilience building in the aftermath of flood hazards in the small island developing state of Mauritius*, Doctoral Dissertation University of Gloucestershire (2014) Cheltenham.



- [17] A. Lizuka, *Developing capacity for disaster risk reduction: Lessons learned from a case of Sri Lanka*, Progress in Disaster Science 6 (2020) 100073 7 pages.
- [18] G. McBean, C. Rodgers, *Climate hazards and disasters: The need for capacity building*, Wiley Interdisciplinary Reviews: Climate Change 1 (6) (2010) 871–884.
- [19] A. A. Shah, R. Shaw, J. Ye, M. Abid, S. M. Amir, A. K. Pervez, S. Naz, *Current capacities, preparedness and needs of local institutions in dealing with disaster risk reduction in Khyber Pakhtunkhwa, Pakistan*, International Journal of Disaster Risk Reduction 34 (2019) 165–172.
- [20] J. I. Uitto, R. Shaw, *Adaptation to changing climate: Promoting community-based approaches in the developing countries*, SANSI: An Environmental Journal for the Global Community 1 (2006) 93–107.
- [21] S. N. Bhagat, *Community-based disaster management strategy in India: An experience sharing*, PDPU Journal of Energy and Management (2013) 11–17.
- [22] J. M. Ayers, S. Huq, *The value of linking mitigation and adaptation: A case study of Bangladesh*, Environmental Management 43 (2009) 753–764.
- [23] M. K. Van Aalst, T. Cannon, I. Burton, *Community level adaptation to climate change: The potential role of participatory community risk assessment*, Global Environmental Change 18 (1) (2008) 165–179.
- [24] I. Kelman, J. Mercer, *A knowledge integration tool for disaster risk reduction including climate change*, in: M. Lopez-Carresi, M. Fordham, B. Wisner, I. Kelman, J. C. Gaillard (Eds.), *Disaster Management: International Lessons in Risk Reduction, Response and Recovery* Earthscan London, 2014, pp. 287–299.
- [25] S. S. Zubir, H. Amirrol, *Disaster risk reduction through community participation*, WIT Transactions on Ecology and the Environment 148 (2011) 195–206.
- [26] H. A. Rahman, *Community based approach towards disaster management*, Asian Journal of Environment, History and Heritage 2 (2) (2018) 55–66.
- [27] L. Pearson, M. Pelling, *The UN Sendai Framework for Disaster Risk Reduction 2015–2030: Negotiation process and prospects for science and practice*, Journal of Extreme Events 2 (1) (2015) Article Number 1571001 12 pages.
- [28] C. Van den Heuvel, L. Alison, N. Power, *Coping with uncertainty: Police strategies for resilient decision-making and action implementation*, Cognition, Technology and Work 16 (2014) 25–45.
- [29] W. B. Ten Brinke, B. Kolen, A. Dollee, H. Van Waveren, K. Wouters, *Contingency planning for large-scale floods in the Netherlands*, Journal of Contingencies and Crisis Management 18 (1) (2010) 55–69.
- [30] D. E. Alexander, *Disaster and emergency planning for preparedness, response, and recovery*, Oxford University Press, USA, 2015, 1–20.
- [31] A. K. Sikka, B. B. Rao, V. U. M. Rao, *Agricultural disaster management and contingency planning to meet the challenges of extreme weather events*, Mausam 67 (1) (2016) 155–168.
- [32] R. Husein, *Localizing disaster risk reduction: A case study of community-based disaster preparedness in Bima and Palangkaraya Indonesia*, In IOP Conference Series: Earth and Environmental Science 989 (1) (2022) 1–12.
- [33] I. J. Koenti, *Disaster management using a contingency approach in the special region of Yogyakarta*, In IOP Conference Series: Earth and Environmental Science 1030 (1) (2022) 012017 9 pages.
- [34] C. P. D. Gundran, H. Y. Lam, A. C. A. Tuazon, J. V. Cleofas, F. B. Garcia, T. E. M. Puli, M. S. I. Magdales, *Enhancing mass casualty disaster management competencies through an integrated disaster simulation training program*, International Journal of Disaster Risk Reduction 78 (2022) 103124 21 pages.

- [35] R. D. Tennyson, *Computer-based enhancements for the improvement of learning*, Annual Management AECT, Atlanta, 1987, Article ID 56806080, 14 pages.
- [36] C. K. West, J. Snellen, T. K. S. Murray, *A report on the research and development of instructional simulation*, Final Report to the Defense Systems Management College Fort Belvoir, Virginia, 1991, 1–78.
- [37] G. M. Mathbor, *Enhancement of community preparedness for natural disasters: The role of social work in building social capital for sustainable disaster relief and management*, International Social Work 50 (3) (2007) 357–369.
- [38] O. Nahkur, K. Orru, S. Hansson, P. Jukarainen, M. Myllylä, M. Krüger, M. Rhinard, *The engagement of informal volunteers in disaster management in Europe*, International Journal of Disaster Risk Reduction (2022) 103413 14 pages.
- [39] I. Buchori, A. Zaki, P. Pangi, A. W. Sejati, A. Pramitasari, Y. Liu, *Adaptation strategies and community participation in government-led mitigation projects: A comparison between urban and suburban communities in Pekalongan, Indonesia*, International Journal of Disaster Risk Reduction 81 (1) (2022) 103271 13 pages.
- [40] B. Wisner, *Five years beyond Sendai-Can we get beyond frameworks?*, International Journal of Disaster Risk Science 11 (2020) 239–249.
- [41] R. Shaw, *Overview of Community-Based Disaster Risk Reduction*, in: R. Shaw (Ed.), Vol.10 of Community-Based Disaster Risk Reduction, Community, Environment and Disaster Risk Management, Emerald Group Publishing Limited, Bingley, 2012, Ch. 2, pp. 3–17.
- [42] Y. Liu, K. Yin, L. Chen, W. Wang, Y. Liu, *A community-based disaster risk reduction system in Wanzhou, China*, International Journal of Disaster Risk Reduction 19 (2016) 379–389.
- [43] D. J. O'Reilly, D. C. Brandenburg, *Simulation and learning in disaster preparedness: A research and theory review*, Online Submission (2006) 763–770.
- [44] R. J. J. Beerens, H. Tehler, *Scoping the field of disaster exercise evaluation-A literature overview and analysis*, International Journal of Disaster Risk Reduction 19 (2016) 413–446.
- [45] D. Paton, D. Johnston, *Disasters and communities: vulnerability, resilience and preparedness*, Disaster Prevention and Management 10 (4) (2001) 270–277.
- [46] A. Amri, D. K. Bird, K. Ronan, K. Haynes, B. Towers, *Disaster risk reduction education in Indonesia: challenges and recommendations for scaling up*, Natural Hazards and Earth System Sciences (2016) 595–612.
- [47] M. Muzani, C. Setiawan, J. N. W. Schadu, A. Awida, M. Munzir, *The obstacles hierarchy of school disaster preparedness implementation in mount sinabung area, Indonesia*, Frontiers in Education 7 (2022) 842990 17 pages.
- [48] F. Chen, Z. Shirazi, L. Wang, *Building scientific capacity in disaster risk reduction for sustainable development*, Cultures of Science 4 (1) (2021) 40–54.
- [49] Organization for Economic Cooperation and Development (OECD), *The challenge of capacity development: Working towards good practice*, OECD Papers 6 (1) (2006) 1–37.
- [50] C. E. Haque, M. S. Uddin, *Disaster management discourse in Bangladesh: A shift from post-event response to the preparedness and mitigation approach through institutional partnerships*, in: J. Tiefenbacher (Ed.), Approaches to Disaster Management-Examining the Implications of Hazards, Emergencies and Disasters, IntechOpen, 2013, 1–230.
- [51] S. K. Kafle, *Integrated community-based risk reduction: An approach to building disaster resilient*

- communities, in: Annual International Workshop & Expo on Sumatra Tsunami Disaster & Recovery, 2010, 1–20.
- [52] R. Shaw, *Community based approaches of sustainable development and disaster risk reduction, in sustainable development and disaster risk reduction*, Springer, 2016, Tokyo, pp. 207–214.
- [53] S. Yodmani, *Disaster risk management and vulnerability reduction: Protecting the poor*, New York: The Center, 2001, pp. 1–36.
- [54] S. Rozi, A. R. Ritonga, J. Januar, *Local community-based disaster management: The transformation of religious and local wisdom values in preparation to deal with natural hazards in West Sumatra, Indonesia*, *Jambá: Journal of Disaster Risk Studies* 13 (1) (2021) 1–7.
- [55] A. R. Badrudin, *Issues of disaster management preparedness: A case study of directive 20 of national security council in Malaysia*, *International Journal of Business and Social Science* 3 (5) (2012) 85–92.
- [56] M. K. Lindell, D. J. Whitney, *Correlates of household seismic hazard adjustment adoption*, *Risk Analysis* 20 (1) (2000) 13–26.
- [57] D. Paton, L. Smith, D. Johnston, *Volcanic hazards: Risk perception and preparedness*, *New Zealand Journal of Psychology* 29 (2) (2000) 86–91.
- [58] N. Kapucu, *Collaborative emergency management: better community organising, better public preparedness and response*, *Disasters* 32 (2) (2008) 239–262.
- [59] D. King, *You're on your own: Community vulnerability and the need for awareness and education for predictable natural disasters*, *Journal of Contingencies and Crisis Management* 8 (4) (2000) 223–228.
- [60] M. Nakamura, *Source fault model of the 1771 Yaeyama tsunami, southern Ryukyu Islands, Japan, inferred from numerical simulation*, *Pure and Applied Geophysics* 163 (2006) 41–54.
- [61] D. K. Yadav, A. Barve, *Role of capacity building in disaster preparedness: A case of cyclone Phailin*, *Proceedings of the 17th Annual International Conference of the Society of Operations Management*, 2014, pp. 980–985.
- [62] A. Gero, K. Méheux, D. Dominey Howes, *Integrating community-based disaster risk reduction and climate change adaptation: Examples from the Pacific*, *Natural Hazards and Earth System Sciences* 11 (1) (2011) 101–113.
- [63] G. O'Brien, P. O'Keefe, *Managing adaptation to climate risk: Beyond fragmented responses*, Routledge, London (2014) 1–210.
- [64] B. Wisner, P. Blaikie, T. Cannon, I. Davis, *At risk: Natural hazards, people's vulnerability and disasters*, Routledge, London (1994) 1–134.



In vitro Allelopathic Potential of Leaf Water Extracts of *Plantago lanceolata* and *P. major* on the Germination of Some Crops

Onur Yaraş¹ , Nadim Yılmaz² 

¹Institute of Natural and Applied Sciences, Tekirdağ Namık Kemal University, Tekirdağ, Türkiye

²Department of Biology, Faculty of Arts and Sciences, Tekirdağ Namık Kemal University, Tekirdağ, Türkiye

Article History

Received: 23 Sep 2023

Accepted: 22 Dec 2023

Published: 15 Mar 2024

Research Article

Abstract – Alongside increasing productivity in plant production, reducing crop losses has become a major focus for the struggle of today's man against hunger. Allelopathy, an ecological phenomenon in which organisms interfere with each other, can be a useful strategy in agricultural systems, especially for weed management. In this study, the allelopathic effects of leaf water extracts from two weed species, *Plantago lanceolata* and *P. major*, on the seed germination of some crop plants, including wheat, sunflower, lentil, bean, carrot, radish, and purslane were investigated. *In vitro* germination assays were conducted to determine the effects of different dilutions of the stock extract on the germination rate. The results of the study showed that as the concentration of the extracts from both weeds increased, germination rates decreased in all crop plants. As to the seeds that were exposed to *P. lanceolata* extract, the ones with the most inhibited germination were carrot (11.84-100%), purslane (18.53-100%), radish (6.17-98.84%), lentil (13.77-95.56%), sunflower (17.57-94.98%), and wheat (30.12-78.31%). The seeds of beans (28.69-39.15%), on the other hand, were the least affected. Similarly, for seeds exposed to *P. major* extract, the ones with the most inhibited germination were carrot (4.67-100%), lentil (65.46-99.55%), purslane (25.09-99.24%), radish (48.69-95.51%), sunflower (43.68-93.16%), and beans (20.70-66.80%), while wheat (12.35-60.62%) seeds were the least affected. If purslane and radish are considered as weeds, our findings suggest that higher concentrations of *P. lanceolata* and *P. major* extracts can be effective bioherbicides for controlling these weeds.

Keywords – *Plantago*, allelopathy, leaf extract, seed germination, Petri dish assay

1. Introduction

The United Nations Population Division has reported that the world population reached 8 billion as of November 15, 2022, and it is projected to reach 8.5 billion by the year 2030, 9.7 billion by 2050, and 10.4 billion by 2100 [1]. Our planet will need to sustain this continuously growing population. The foundation of the essential food supply necessary for human life and existence is formed by food nutrition. Agriculture, which has been ongoing from the past until today, is the primary source of food [2], and plants constitute more than 80% of humanity's primary food sources. Furthermore, plants are indirectly related to human nutrition as they serve as the main food source for livestock [3].

In addition to efforts to increase productivity in plant-based products and obtain more crops from less land, minimizing crop losses caused by various factors has been a major challenge in combating hunger for contemporary society. There are several factors in plant production that negatively affect yield and quality, leading to crop losses. One of these factors is weed infestation, which accounts for approximately 34% of crop

¹onuryaras@gmail.com; ²nyilmazer@nku.edu.tr (Corresponding Author)

losses [4], and if left uncontrolled, can result in crop losses of up to 100% [5].

Allelopathy, an ecological phenomenon in which organisms influence each other, can be a beneficial strategy, especially in weed control, within agricultural systems [6]. Allelopathy involves the ability of plants to release certain chemical compounds (allelochemicals) that can either benefit or harm other plants, plant pathogens, and herbivorous insects. Unlike synthetic agricultural pesticides, allelochemicals can easily degrade in nature, thereby minimizing environmental damage. Additionally, allelopathy helps reduce costs in agricultural production. As the importance of effective utilization of allelopathy in agriculture is recognized, research in this field is increasing, allowing for the discovery of new and more potent allelochemicals [7,8]. In this context, this study aims to explore the allelopathic potential of two weed species, *Plantago lanceolata* and *P. major*, with a focus on the former, which has not yet been identified as exhibiting allelopathic traits.

2. Materials and Methods

2.1. Plant Material and Preparation of Extracts

The leaves of *Plantago lanceolata* and *P. major* were collected from vacant lots in the Değirmenaltı neighborhood of Süleymanpaşa district, Tekirdağ province, Türkiye, in April and May of 2022, prior to flowering. After washing the leaves with tap water, they were left to dry in a dimly lit room at room temperature, protected from dust, for several weeks. Following the drying process, the leaves were manually crushed into a powdered form [9,10]. From this material, 25 g was soaked in 250 ml of distilled water at room temperature and in darkness for 24 hours. The mixture was first filtered through a cheesecloth and then filtered twice through Whatman filter paper No. 1 [11]. The filtrate was stored in a refrigerator. Another 250 ml of distilled water was added to the residue, and it was left to soak for 24 hours at room temperature in darkness. The same procedure was followed to obtain the second filtrate, and the two filtrates were combined and stored at 4 °C as a stock extract (%5) for later use. In the experiments, concentrations of 100% (50 mg ml⁻¹), 75% (37.5 mg ml⁻¹), 50% (25 mg ml⁻¹), 25% (12.5 mg ml⁻¹), and 1% (0.5 mg ml⁻¹) of the stock extract were used.

2.2. Plant Material and Preparation of Extracts

Wheat, sunflower, lentil, bean, carrot, radish, and purslane were employed as test crops, all of which underwent allelopathy testing for *P. lanceolata*; additionally, excluding purslane, they were also tested for *P. major* allelopathy for the first time in this study. The commercial seeds of wheat, sunflower, carrot, radish, and purslane from several different brands were purchased from a local seed sales company in Tekirdağ, Türkiye. Lentil and bean seeds were obtained from a grocery store as food-grade products. Seeds that were broken, deformed, or had different colors were visually inspected and removed. Empty and underdeveloped seeds were discarded by floating in water. To eliminate the possibility of fungal or bacterial toxins affecting germination, the intact seeds were subjected to surface sterilization for two minutes with a solution of 10:1 distilled water to commercial bleach (sodium hypochlorite) (with agitation). After surface sterilization, the seeds were washed three times with distilled water. The Petri dishes, filter papers, glassware, and forceps used in the germination experiments were wrapped in aluminum foil and sterilized in an autoclave at 121 °C for 15 minutes [12]. The seeds were germinated between two filter papers in Petri dishes with a diameter of 12 cm. Depending on the seed size, a homogeneous placement of 20 (bean), 40 (wheat, sunflower, lentil), 60 (radish), 150 (carrot), and 300 (purslane) seeds was made in each Petri dish. Before sowing the seeds into the Petri dishes, the filter paper placed at the bottom of the dish was moistened with 3 ml of extract (%100, %75, %50, %25, and %1) for experimental seeds and 3 ml of distilled water for control seeds. After placing the seeds, they were covered

with filter paper, and 9 ml of the corresponding concentration of extract was added to each experimental group, while the same amount of distilled water was added to the control group. The Petri dishes were sealed and incubated at 22-24 °C in an incubator for 72 hours for wheat, sunflower, lentil, bean, radish, and purslane. Carrot seeds were allowed to germinate for 144 hours due to their late germination characteristic. At the end of the germination period, seeds with a radicle length larger than 2 mm were considered germinated [13]. The germination experiments were repeated three times.

2.3. Germination Rate and Effect Compared to Control (%)

The germination rate (%) was calculated by multiplying the ratio of the number of germinated seeds to the total number of seeds at the end of the germination period by 100 [12]. The results of the three repetitions were given as "mean ± standard error." The effect (%) of different concentrations of the extract compared to the control was calculated using the following formula [14].

$$\text{Effect (\% compared to control)} = \frac{(\text{Germination rate of the extract concentration} - \text{Germination rate of the control}) \times 100}{\text{Germination rate of the control}}$$

2.4. Statistical Analysis

The obtained findings were calculated as mean ± standard error (S.E.M.). Statistical analysis was performed using GraphPad Prism software program (GraphPad Prism Version 9, San Diego, CA, USA), and it included one-way analysis of variance (ANOVA) followed by Tukey's multiple comparisons test. A *p* value of less than 0.05 was considered statistically significant.

3. Results and Discussion

When the effects of *P. lanceolata* extract concentrations of 1%, 25%, 50%, 75%, and 100% on the germination of our test plant seeds were examined, it was determined that as the extract concentration increased, the germination rates of the seeds decreased significantly in a statistically significant manner (*p*<0.001 for all concentrations). However, the application of a 1% concentration did not show a statistically significant increase in germination rate in wheat seeds and a decrease in germination rate in radish seeds (Figure 1).

The extent to which different concentrations of *P. lanceolata* extract affected the germination of the test plant seeds compared to the control is shown in Table 1. As can also be seen from the relevant table, the seeds that were most inhibited from germinating by *P. lanceolata* extract were, in order, carrots, purslane, radishes, lentils, sunflowers, and wheat seeds. Bean seeds, on the other hand, were the least affected in terms of germination by *P. lanceolata* leaf extract.

When the effects of *P. major* extract concentrations of 1%, 25%, 50%, 75%, and 100% on the germination of the test plant seeds were evaluated, it was determined that as the extract concentration increased, the germination rates of the seeds decreased significantly in a statistically significant manner. However, it was observed that the 1% concentration of *P. major* extract increased the germination rate of wheat, lentil, bean, radish, and purslane seeds; although the increase was not statistically significant for wheat, beans, radishes, and purslane, it was significant for lentils (*p*<0.001) (Figure 2).

The extent to which different concentrations of *P. major* leaf extract affected the germination of plant seeds compared to the control is shown in Table 2. From this table, it can be seen that the seeds most inhibited from germinating by *P. major* leaf extract were, in order, carrots, lentils, purslane, radishes, sunflowers, and bean seeds. Wheat seeds, on the other hand, were the least affected in terms of germination by *P. major* leaf extract.

In recent years, there has been an increase in studies highlighting the role of allelopathy in intercropping, crop-weed, and weed-weed relationships, as well as research on the potential use of allelopathic plants in weed control. These studies have gained considerable popularity [15,16]. In this study, we investigated the potential allelopathic effects of leaf water extracts of *Plantago lanceolata* and *P. major* on the germination of seeds of crops such as wheat, sunflower, lentil, bean, and carrot, in the context of the crop-weed relationship. Additionally, we explored the possible allelopathic effects on the germination of weed seeds, specifically radish and purslane, in the context of the weed-weed relationship. To date, studies have unveiled the allelopathic effects of *Plantago major*, *P. lagopus*, *P. squarrosa*, *P. virginica*, and *P. psyllium*. Notably, investigations into the impact of *P. major* have primarily focused on the germination of purslane as a crop. Meanwhile, the allelopathic effects of *P. major* and other *Plantago* species on the germination of various weed seeds have been explored in these studies [17-20]. There has been no experimental study regarding the allelopathic properties of *P. lanceolata*, making our study the first in this regard. Nevertheless, there is only one article reporting observations made by Professor Knut Schmidtke (Dresden, Germany), an agricultural professor and co-author of the relevant article, stating that there was a significant decrease in yield when wheat (*Triticum aestivum*) was grown in a field previously inhabited by *P. lanceolata* [21].

The most common biological experiments used to determine the effects of allelochemicals and reveal the allelopathic potentials of various plant extracts are seed germination and seedling growth and development studies (including root and shoot lengths). These experiments are typically conducted using the Petri dish method in their simplest form. In seed germination studies, the germination rate is often calculated [22]. In this study as well, the allelopathic potential was determined through seed germination experiments using the Petri dish method, and the results of seed germination were presented as germination rates.

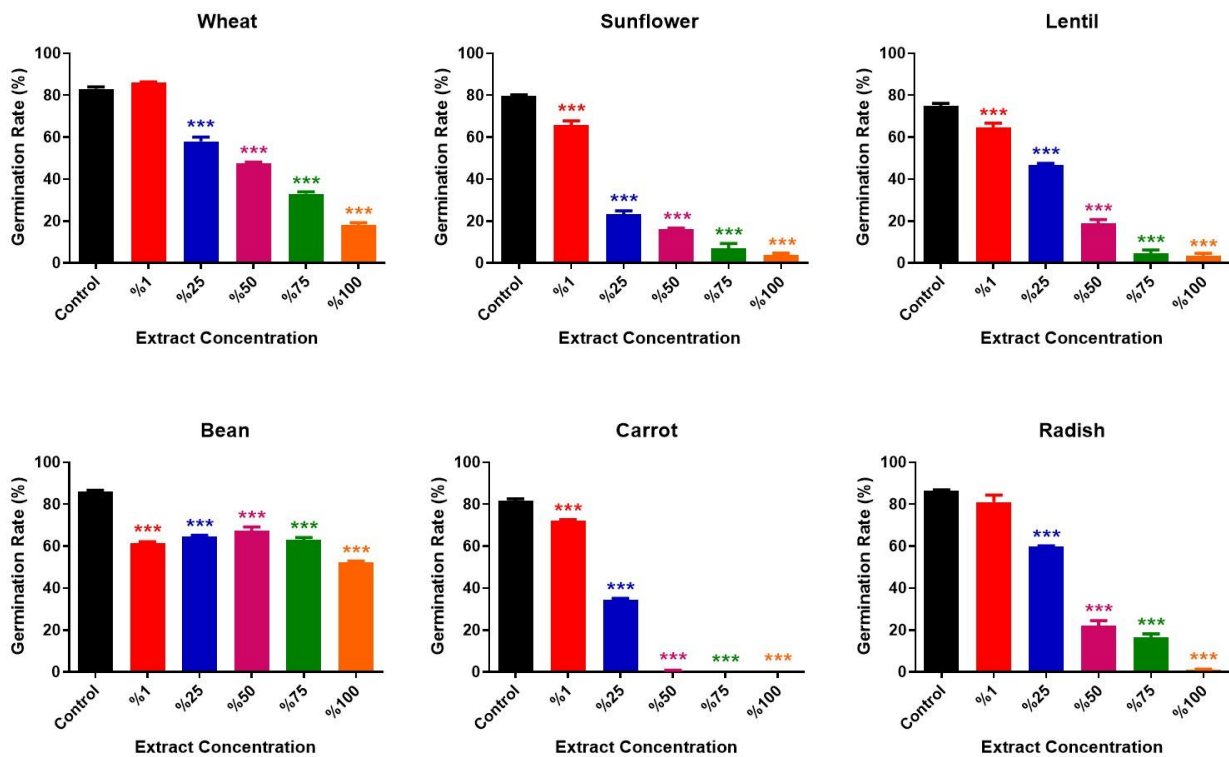


Figure 1. The effect of different concentrations (1%, 25%, 50%, 75%, and 100%) of *P. lanceolata* leaf water extract on the germination of wheat, sunflower, lentil, bean, carrot, radish, and purslane seeds. *** $p < 0.001$; statistical significance compared to the control group

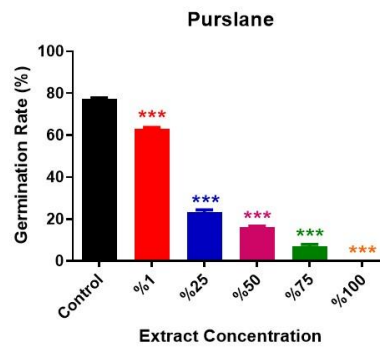


Figure 1. (Continued)

In an allelopathic study, one of the most important aspects is the selection of target species from both monocotyledonous and dicotyledonous plants to determine the potential selectivity of allelochemicals [22]. Accordingly, in the present study, both monocotyledonous (wheat) and dicotyledonous (sunflower, lentil, bean, carrot, radish, purslane) species were used as test plants.

Table 1. Effect of different concentrations of *P. lanceolata* leaf water extract compared to the control (%)

Test Plants	Germination Rates (%)*					
	Control	Extract Concentrations				
		%1	%25	%50	%75	%100
Wheat	83	86	58	47.33	33	18
The effect compared to the control		+3.61	-30.12	-42.98	-60.24	-78.31
Sunflower	79.67	65.67	23.33	16	7	4
The effect compared to the control		-17.57	-70.72	-79.92	-91.21	-94.98
Lentil	75	64.67	46.67	19	4.67	3.33
The effect compared to the control		-13.77	-37.77	-74.67	-93.77	-95.56
Bean	86	61.33	64.67	67.33	63	52.33
The effect compared to the control		-28.69	-24.80	-21.71	-26.74	-39.15
Carrot	81.67	72	34.33	0.67	0	0
The effect compared to the control		-11.84	-57.97	-99.18	-100	-100
Radish	86.33	81	59.67	22	16.33	1
The effect compared to the control		-6.17	-30.88	-74.52	-81.08	-98.84
Purslane	77.33	63	23.33	16	7	0
The effect compared to the control		-18.53	-69.83	-79.31	-90.95	-100

*Germination rates are given as "Mean". Concerning the effect compared to the control, positive (+) values indicate the promotion of germination, while negative (-) values indicate the inhibition of germination.

Most allelochemicals are hydrophilic [23] and can dissolve either completely or partially in water [24,25]. Therefore, in nature, they are usually released from the aboveground parts of plants through dew, rain, or fog droplets, either by dissolution or washing. They can exhibit their effects in this dissolved state and can also acquire allelopathic properties after being modified by soil microorganisms [26]. Consequently, in this study, water extracts were used to simulate naturally dissolved/washed allelochemicals.

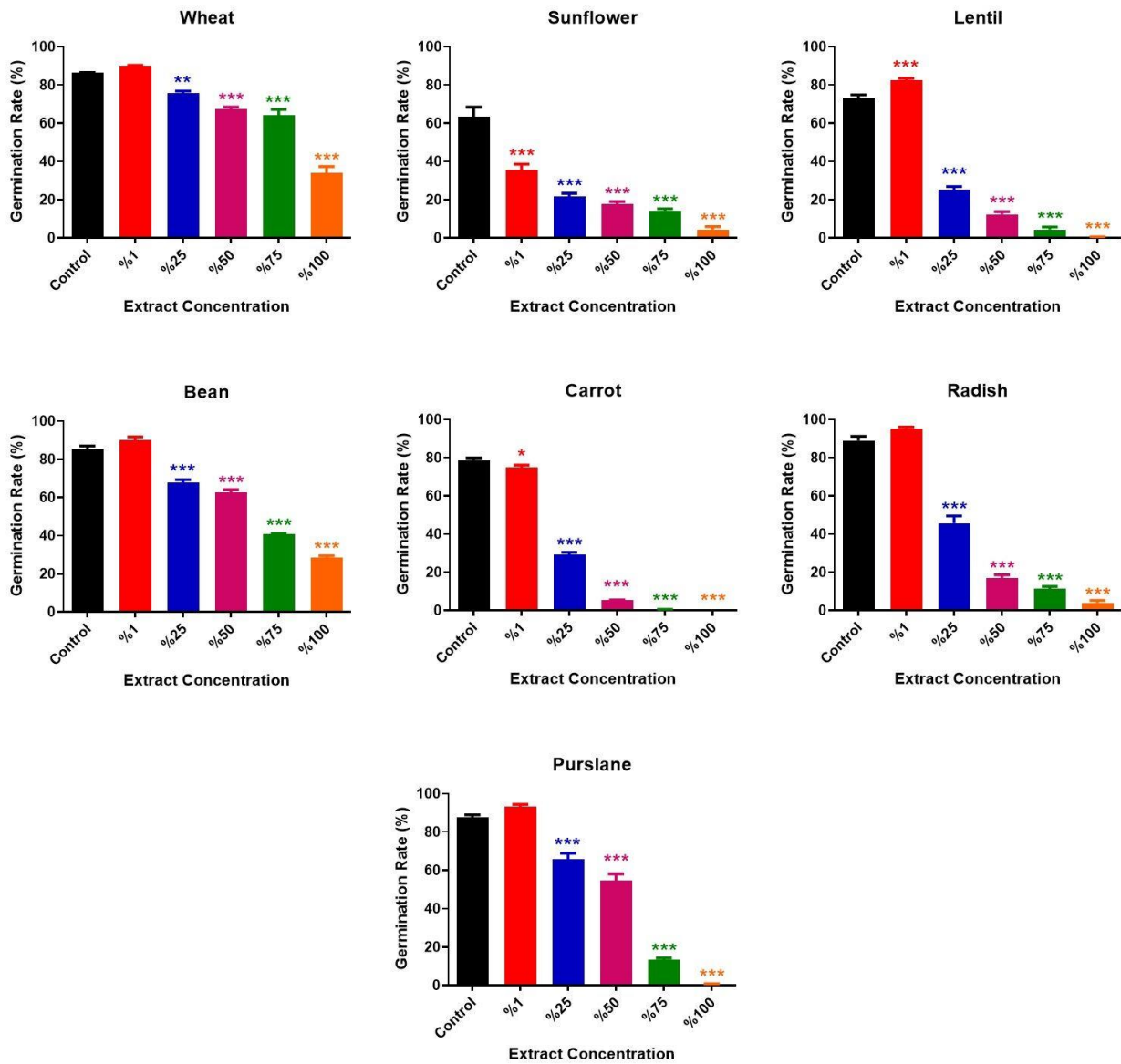


Figure 2. The effect of different concentrations (1%, 25%, 50%, 75%, and 100%) of *P. major* leaf water extract on the germination of wheat, sunflower, lentil, bean, carrot, radish, and purslane seeds. * $p < 0.05$; ** $p < 0.01$; *** $p < 0.001$; statistical significance compared to the control group

In the current study, radish and purslane were used as test plants, representing weeds. *Raphanus raphanistrum* ssp. *raphanistrum* (synonym *Raphanus sativus*) (radish) is considered one of the four worst weeds in agricultural fields worldwide [27,28]. It has the ability for vegetative reproduction (forming lateral roots from stem fragments) and can produce a large number of seeds within six weeks after germination (a single plant can produce 10,000 to 242,000 seeds.) [29-31]. Purslane, on the other hand, ranks ninth among the most dangerous weeds globally due to its ability to produce a significant number of seeds within a short period after germination [20,32]. Although commercial seeds of radish and purslane were used in this study, it has been reported that the germination success of seeds from spontaneously growing plants in nature is generally weaker than that of commercial seeds of the same plants [33]. Therefore, it is inevitable that the allelopathic effects observed in the experiments conducted in this study would be even stronger in nature.

Table 2. The effect of different concentrations of *P. major* leaf water extract compared to the control (%)

Test Plants	Germination Rates (%) [*]					
	Control	Extract Concentrations				
		% 1	%25	%50	%75	%100
Wheat	86.33	90	75.67	67.33	64	34
The effect compared to the control		+4.25	-12.35	-22.01	-25.87	-60.62
Sunflower	63.33	35.67	21.67	17.67	14	4.33
The effect compared to the control		-43.68	-65.78	-72.10	-77.89	-93.16
Lentil	73.33	82.33	25.33	12.33	4.33	0.33
The effect compared to the control		+12.27	-65.46	-83.19	-94.10	-99.55
Bean	85.33	90	67.67	62.67	40.67	28.33
The effect compared to the control		+5.47	-20.70	-26.56	-52.34	-66.80
Carrot	78.67	75	29.33	5.33	0.33	0
The effect compared to the control		-4.67	-62.72	-93.23	-99.58	-100
Radish	89	95	45.67	17	11.33	4
The effect compared to the control		+6.74	-48.69	-80.90	-87.27	-95.51
Purslane	87.67	93	65.67	54.67	13.33	0.67
The effect compared to the control		+6.08	-25.09	-37.64	-84.80	-99.24

^{*}Germination rates are given as "Mean". Concerning the effect compared to the control, positive (+) values indicate the promotion of germination, while negative (-) values indicate the inhibition of germination.

The effect of allelochemicals is highly dependent not only on the type of solvent used for extraction [34] but also on the concentration (dose) of the extract [35]. The majority of studies conducted to date have demonstrated that increasing extract concentration significantly reduces seed germination and seedling development in test plants. In some cases, it even completely inhibits them [36-41]. Consistent with the findings of these studies, as well as previous research on other *Plantago* species [17-20], the current study also observed a decrease in the germination rates of all test plants as the concentration of extracts from both weed species increased. Specifically, extracts from *P. lanceolata* at 75% (37.5 mg ml⁻¹) and 100% (50 mg ml⁻¹) concentration inhibited the germination of purslane, carrot, radish, lentil, and sunflower seeds by 90-100%. Similarly, extracts from *P. major* at 75% and 100% concentration inhibited the germination of carrot, lentil, purslane, radish, and sunflower seeds by 80-100%. In the study by Al-Obaidi [20], which supports our findings regarding purslane, the water extract of the aerial parts of *P. major* at 40 mg ml⁻¹ inhibited purslane germination by approximately 30.24%, while the lowest concentration (2.5 mg ml⁻¹) resulted in a 4.60% inhibition. However, in our study, a concentration of 75% (37.5 mg ml⁻¹), close to the 40 mg/ml concentration, led to an 84.80% inhibition of germination. It is well-established that the production of allelochemicals varies based on the environment in which plants are grown and the environmental stresses they encounter, including light, nutrients, water and temperature stress, and atmospheric CO₂ [42,43]. As a result, the differences in allelopathic effects on purslane germination observed in our study may be attributed to the diverse environmental conditions under which the *P. major* was grown, along with variations in experimental conditions. Regarding the allelopathic potential of *P. major*, it is noteworthy that the water extract of the aerial parts of *P. major* at concentrations of 10 mg ml⁻¹ and 2.5 mg ml⁻¹ inhibited the germination of *Bidens pilosa* by approximately 72.41% and 7.41%, respectively [18].

It has been found that allelochemicals can not only negatively affect the growth of certain species but also promote the germination and seedling development of the same or different species when used at different concentrations [44]. In particular, several studies have shown that low-concentration water extracts stimulate germination and growth of various crops and increase their productivity [45,46]. In this study, although the 1% extract of *P. lanceolata* appeared to promote germination in wheat and the 1% extract of *P. major* seemed

to promote germination in wheat, bean, lentil, radish, and purslane, only the promotion of lentil seed germination was statistically significant.

The *Plantago* genus contains various natural products, including iridoids, phenylpropanoid glycosides, flavonoids, tannins, triterpenes, saponins, and sterols, with iridoid glycosides being present in large quantities in *Plantago* species' leaves and above-ground parts [47]. It is known from various studies that iridoid glycosides aucubin and catalpol, found in the leaves and above-ground parts of *Plantago* [48,49], inhibit seed germination and root development [50,51]. The allelopathic effect of alfalfa (*Medicago sativa*) has been attributed to its water-soluble saponins [52]. In the current study, the observed inhibitory effect on germination is likely due to the presence of these iridoids and saponins in the leaves of *P. lanceolata* and *P. major*. It has been reported that *P. major* contains less aucubin in its leaves and above-ground parts compared to *P. lanceolata* [48]. This explains the finding in this study that the inhibitory effect on germination of *P. lanceolata* is stronger compared to *P. major*.

4. Conclusion

In conclusion, based on the data obtained from this study, the presence of *P. lanceolata* and *P. major* should be considered in fields where wheat, sunflower, lentil, bean, carrot, radish, and purslane are cultivated, both before and after sowing, to achieve high yields. Furthermore, the potential use of leaf water extracts of *P. lanceolata* and *P. major* as effective bioherbicides should be evaluated in the control of radish and purslane, which grow as weeds in agricultural fields.

Author Contributions

All the authors equally contributed to this work. This paper is derived from the first author's master's thesis supervised by the second author. They all read and approved the final version of the paper.

Conflicts of Interest

All the authors declare no conflict of interest.

Acknowledgement

We thank Dr. Ebru GÜREL GÜREVİN, Dr. Deniz EROL KUTUCU, and Gülce BAYHUN for their supports.

References

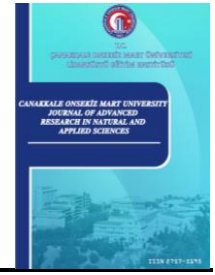
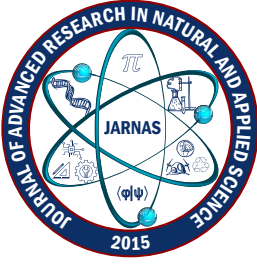
- [1] United Nations Department of Economic and Social Affairs, Population Division, World Population Prospects 2022: Summary of Result (2022), <https://www.un.org/development/desa/pd/content/World-Population-Prospects-2022>, Accessed 12 March 2023.
- [2] Ö. Demirel, O. Akveç, C. Can, *A current overview of plant biotechnology*, Euroasia Journal of Mathematics, Engineering, Natural & Medical Sciences 9 (20) (2022) 110–149.
- [3] D. M. Rizzo, M. Lichtveld, J. A. K. Mazet, E. Togami, S. A. Miller, *Plant health and its effects on food safety and security in a One Health framework: four case studies*, One Health Outlook 3 (2021) Article Number 6 9 pages.
- [4] Y. Gharde, P. K. Singh, R. P. Dubey, P. K. Gupta, *Assessment of yield and economic losses in agriculture due to weeds in India*, Crop Protection 107 (2018) 12–18.

- [5] B. S. Chauhan, *Grand challenges in weed management*, *Frontiers in Agronomy* 1 (2020) 3–4 pages.
- [6] K. Jabran, G. Mahajan, V. Sardana, B. S. Chauhan, *Allelopathy for weed control in agricultural systems*, *Crop Protection* 72 (2015) 57–65.
- [7] Y. Khamare, J. Chen, S. C. Marble, *Allelopathy and its application as a weed management tool: A review*, *Frontiers in Plant Science* 13 (2022) 1034649 17 pages.
- [8] M. Kostina-Bednarz, J. Płonka, H. Barchanska, *Allelopathy as a source of bioherbicides: challenges and prospects for sustainable agriculture*, *Reviews in Environmental Science and Biotechnology* 22 (2) (2023) 471–504.
- [9] İ. Kadioğlu, Y. Yanar, U. Asav, *Allelopathic effects of weeds extracts against seed germination of some plants*, *Journal of Environmental Biology* 26 (2) (2005) 169–173.
- [10] R. Velasco-Lezama, R. Tapia-Aguilar, R. Roman-Ramos, E. Vega-Avila, Ma. S. Perez-Gutierrez, *Effect of *Plantago major* on cell proliferation in vitro*, *Journal of Ethnopharmacology* 103 (1) (2006) 36–42.
- [11] E. Kozan, E. Küpeli, E. Yeşilada, *Evaluation of some plants used in Turkish folk medicine against parasitic infections for their in vivo anthelmintic activity*, *Journal of Ethnopharmacology* 108 (2) (2006) 211–216.
- [12] M. Ertem, M. S. Adak, *Effects on germination and viability of gibberellic acid and potassium nitrate on endemic *Verbascum linearilobum* species*, *Journal of Agricultural Faculty of Bursa Uludağ University* 36 (1) (2021) 173–195.
- [13] E. Kaçal, O. Çalışkan, A. Atak, M. Aydınli, G. Öztürk, A. Bayav, *Effects of proline and temperature applications on germination of black mulberry seeds*, *Mustafa Kemal University Journal of Agricultural Sciences* 25 (2) (2020) 181–188.
- [14] H. Önen, *Studies on some biological aspects and control methods of *Artemisia vulgaris* L.*, Doctoral Dissertation Tokat Gaziosmanpaşa University (1999) Tokat.
- [15] S. J. Meiners, C.-H. Kong, *Introduction to the special issue on allelopathy*, *Plant Ecology* 213 (12) (2012) 1857–1859.
- [16] Y. Xu, X. Chen, L. Ding, C.-H. Kong, *Allelopathy and allelochemicals in grasslands and forests*, *Forests* 14 (3) (2023) 562 22 pages.
- [17] A. Rahimi, H. R. Rahimian Mashhadi, M. R. Jahansoz, F. Sharifzade, K. Postini, *Allelopathic effect of *Plantago psyllium* on germination and growth stages of four weed species*, *Iranian Journal of Weed Science* 2 (2) (2006) 13–30.
- [18] A. M. Abd El-Gawad, I. A. Mashaly, M. E. Abu Ziada, M. R. Deweeb, *Phytotoxicity of three *Plantago* species on germination and seedling growth of hairy beggarticks (*Bidens pilosa* L.)*, *Egyptian Journal of Basic and Applied Sciences* 2 (4) (2015) 303–309.
- [19] H. Wang, Y. Zhou, Y. Chen, Q. Wang, L. Jiang, Y. Luo, *Allelopathic potential of invasive *Plantago virginica* on four lawn species*, *PLoS One* 10 (4) (2015) e0125433.
- [20] A. F. Al-Obaidi, *Phytotoxicity of *Plantago major* extracts on germination and seedling growth of purslane (*Portulaca oleracea*)*, in: J. C. Jimenez-Lopez (Ed.), *Seed Dormancy and Germination*, IntechOpen, 2020, Ch. 7, 9 pages.
- [21] M. Dietz, S. Machill, H. C. Hoffmann, K. Schmidtke, *Inhibitory effects of *Plantago lanceolata* L. on soil N mineralization*, *Plant and Soil* 368 (2013) 445–458.
- [22] B. Lotina-Hennsen, B. King-Diaz, M. I. Aguilar, M. G. Hernandez Terrones, *Plant secondary metabolites. Targets and mechanisms of allelopathy*, in: M. J. Reigosa, N. Pedrol, L. González (Eds.), *Allelopathy: A Physiological Process with Ecological Implications*, Springer, Dordrecht, 2006, Ch. 11,

pp. 229–265.

- [23] C.-H. Chou, *Introduction to allelopathy*, in: M. J. Reigosa, N. Pedrol, L. González (Eds.), *Allelopathy: A Physiological Process with Ecological Implications*, Springer, Dordrecht, 2006, Ch. 1, pp. 1–9.
- [24] D. Soltys, U. Krasuska, R. Bogatek, A. Agnieszka Gniazdowska, *Allelochemicals as Bioherbicides-Present and Perspectives*, in: A. J. Price, J. A. Kelton (Eds.), *Herbicides-Current Research and Case Studies in Use*, IntechOpen, 2013, Ch. 20, pp. 517–542.
- [25] A. A. Singh, G. Rajeswari, L. A. Nirmal, S. Jacob, *Synthesis and extraction routes of allelochemicals from plants and microbes: A review*, *Reviews in Analytical Chemistry* 40 (1) (2021) 293–311.
- [26] X. Zhu, Y. Yi, L. Huang, C. Zhang, H. Shao, *Metabolomics reveals the allelopathic potential of the invasive plant Eupatorium adenophorum*, *Plants (Basel)* 10 (7) (2021) 1473 14 pages.
- [27] A. Charbonneau, D. Tack, A. Lale, J. Goldston, M. Caple, E. Conner, O. Barazani, J. Ziffer-Berger, I. Dworkin, J. K. Conner, *Weed evolution: Genetic differentiation among wild, weedy, and crop radish*, *Evolutionary Applications* 11 (10) (2018) 1964–1974.
- [28] R. B. Vercellino, C. E. Pandolfo, M. Cantamutto, A. Presotto, *Interference of feral radish (*Raphanus sativus*) resistant to AHAS-inhibiting herbicides with oilseed rape, wheat, and sunflower*, *International Journal of Pest Management* (in press).
- [29] B. S. Chauhan, D. E. Johnson, *Seed germination ecology of *Portulaca oleracea* L.: An important weed of rice and upland crops*, *Annals of Applied Biology* 155 (1) (2009) 61–69.
- [30] C. A. Proctor, R. E. Gaussoin, Z. J. Reicher, *Vegetative reproduction potential of common purslane (*Portulaca oleracea*)*, *Weed Technology* 25 (4) (2011) 694–697.
- [31] H. M. El-Shora, M. M. Alharbi, D. B. Darwish, D. Gad, *Allelopathic potential of aqueous leaf extract of *Rumex dentatus* L. on metabolites and enzyme activities of common purslane leaves*, *Journal of Plant Interactions* 17 (1) (2022) 267–276.
- [32] S. Rashidi, A. Reza Yousefi, N. Goicoechea, M. Pouryousef, P. Moradi, S. Vitalini, M. Iriti, *Allelopathic interactions between seeds of *Portulaca oleracea* L. and crop species*, *Applied Sciences* 11 (8) (2021) 3539 11 pages.
- [33] J. A. Fernández, A. Navarro, M. J. Vicente, D. Peñapareja, V. Plana, *Effect of seed germination methods on seedling emergence and earliness of purslane (*Portulaca oleracea* L.) cultivars in a hydroponic floating system*, *Acta Horticulturae* 782 (2008) 207–212.
- [34] G. B. Williamson, D. Richardson, *Bioassays for allelopathy: Measuring treatment responses with independent controls*, *Journal of Chemical Ecology* 14 (1988) 181–187.
- [35] R. G. Belz, K. Hurlle, S. O. Duke, *Dose-Response-A challenge for allelopathy?*, *Nonlinearity in Biology, Toxicology and Medicine* 3 (2) (2005) 173–211.
- [36] S. Gülsoy, K. Özkan, A. Mert, Y. Eser, *Chemical compounds of volatile oil obtained from fruit of crimean juniper (*Juniperus excelsa*) and leaves of Turkish plateau oregano (*Origanum minutiflorum*) and allelopathic effects on germination of Anatolian black pine (*Pinus nigra* subsp. *pallasiana*)*, *Biological Diversity and Conservation* 1 (2) (2008) 105–114.
- [37] O. Aydın, N. Tursun, *Determination of allelopathic effects of some plant originated essential oils on germination and emergence of some weed seeds*, *Kahramanmaraş Sütçü İmam University Journal of Natural Sciences* 13 (1) (2010) 11–17.
- [38] M. Yılar, A. Onaran, Y. Yanar, S. Belgüzar, İ. Kadioğlu, *Herbicidal and antifungal potential of *Trachystemon orientalis* (L.) G. Don (Kaldırık)*, *Iğdır University Journal of the Institute of Science and Technology* 4 (4) (2014) 19–27.

- [39] N. Özbay, *Allelopathic effects of some herbs and medicinal plants' extracts on seed germination and seedling growth of pepper*, Turkish Journal of Agricultural and Natural Sciences 5 (1) (2018) 81–85.
- [40] M. Yılar, Y. Bayar, A. Onaran, *Chemical composition and allelopathic effect of *Origanum onites* L. essential oil*, Plant Protection Bulletin 59 (3) (2019) 71–78.
- [41] R. Karaman, C. Türkay, İ. Akgün, *Effects of oat grass juice on germination and seedling characteristics of certain weeds and cultivated plants*, Journal of Tekirdağ Agricultural Faculty 18 (2) (2021) 312–321.
- [42] H. Gawronska, A. Golsiz, *Allelopathy and Biotic Stresses*, in: M. J. Reigosz, N. Pedrol, L. González (Eds.), *Allelopathy: A Physiological Process with Ecological Implications*, Springer, Dordrecht, 2006, Ch. 10, pp. 211–227.
- [43] P. C. Bhowmik, *Bioavailability of allelochemicals in soil environment under climate change: Challenges and perspectives*, Indian Journal of Weed Science 54 (4) (2022) 389–396.
- [44] S. S. Narwal, *Allelopathy in crop production*, Scientific Publishers, Jodhpur, India, 1994.
- [45] P. Oudhia, S. S. S. Kolhe, R. S. Tirpathi, *Allelopathic effect of *Blumea lacera* L. on rice and common kharif weeds*, Oryza 35 (1998) 175–177.
- [46] Z. A. Cheema, M. Farooq, A. Khaliq, *Application of allelopathy in crop production: Success story from Pakistan*, in: Z. A. Cheema, M. Farooq, A. Wahid (Eds.), *Allelopathy: Current Trends and Future Applications*, Springer, Berlin, Heidelberg, 2013, Ch. 6, pp. 113–143.
- [47] T. Majkić, K. Bekvalac, I. Beara, *Plantain (*Plantago* L.) species as modulators of prostaglandin E₂ and thromboxane A₂ production in inflammation*, Journal of Ethnopharmacology 262 (2020) 113140 9 pages.
- [48] A. B. Samuelsen, *The traditional uses, chemical constituents and biological activities of *Plantago major* L. A review*, Journal of Ethnopharmacology 71 (1-2) (2000) 1–21.
- [49] M. Pol, K. Schmidtke, S. Lewandowska, **Plantago lanceolata*-An overview of its agronomically and healing valuable features*, Open Agriculture 6 (1) (2021) 479–488.
- [50] F. Pardo, F. Perich, R. Torres, F. Delle Monache, *Phytotoxic iridoid glucosides from the roots of *Verbascum thapsus**, Journal of Chemical Ecology 24 (1998) 645–653.
- [51] T. Wang, M. Gui, H. Liu, H. Zhao, L. Xu, M. Zha, J. Li, *Secretion of catalpol from *Rehmannia glutinosa* roots to the rhizosphere*, Acta Physiologiae Plantarum 32 (2010) 141–144.
- [52] H. Önen, *Studies on allelopathic effects of mugwort and alfalfa in Turkey: An overview*, In *Allelopathy Workshop: (Allelopathy in Turkey: Past, Present, Future)*, Atatürk Horticultural Central Research Institute, Yalova, 2006, pp. 3–21.



Correlating Measured SPT-N, Shear Wave Velocity and Liquid Limit Values in Melekli Region, Iğdır (Türkiye)

Yusuf Guzel¹

¹Department of Civil Engineering, Faculty of Engineering, Necmettin Erbakan University, Konya, Türkiye

Article History

Received: 20 Nov 2023

Accepted: 31 Dec 2023

Published: 15 Mar 2024

Research Article

Abstract – Characterization of soil layers underneath or having interaction with structures is substantially critical for the overall stability of structures under static and dynamic conditions. The main objectives in characterizing soil are mainly to determine ultimate bearing capacity, settlement, and liquefaction potential. Additionally, the dynamic behavior of soil during seismic excitation, as well as its interaction with structures, should be determined. In these regards, Standard Penetration Test blow counts (SPT-N) and shear wave velocity (V_s) values of soils obtained directly through field tests are known to reflect the soil characteristics, strongly. Therefore, any correlation between these two soil parameters is always in utmost interest. This study assesses the correlation between V_s and SPT-N values measured in Melekli region, Iğdır (Türkiye). Moreover, four existing correlations in the literature are presented. The best-fit curve for the measured data is shown to divert from the existing correlation curves, which are also significantly different from each other, for all soils, sand, and clay soils. This can be attributed to the uniqueness of correlation to the study site as geological conditions at one site differ extensively from another site. There seems to be valuable correlation between V_s and water content and liquid limit in the studied area.

Keywords – Standard penetration test, blow count, shear wave velocity, liquid limit, correlation

1. Introduction

Structures built whether on or below the ground surface are supported by the foundation soils. Determinations of foundation soil properties are necessary and vital so as to ensure the stability of structures [1]. By assessing the foundation soil features, the suitability of the soil for a project to be initiated is determined and necessary steps (foundation design, soil improvement etc), to ensure that the structures are supported safely, are projected [2].

The loads exposed by the structures cause increases in stresses within the soil bodies. As the soil layers deepen, the incremental stress caused by the structural loads diminishes. Soils layered through the deposits should be featured up to a depth at which the stress increment due to the structural loads is thought to be negligible. This depth is designed by Turkish Building Earthquake Code (TBEC, [3]) to be the highest of the two cases; (i) 1.5 times of the building width or (ii) the depth at which stress increment decreases to the 10% of the in-situ soil effective stress. For deep foundation applications, the investigation depth should be sufficient for the design of deep foundations.

Generally, one of the most widely acknowledged and used field test for soil characterization is Standard Penetration Test (SPT) [4]. This is due to its simplicity and convenience in its application. In addition, the test

¹yusufkurtdereli@hotmail.com (Corresponding Author)

is done on undisturbed soils at the field, so the complexity encountered in the laboratory tests is avoided (i.e., taking undisturbed soil samples, transferring to the laboratory, forming the field conditions, replacing to the testing machines etc.). Besides, the parameter measured through SPT strongly reflects the load bearing capacity and settlement of the soils. In order to support the findings of SPT data, Cone Penetration and Menard Pressuremeter and Dilatometer Tests can be conducted. These tests mostly cause the development of large strains in the soil body, hence, offer a more reliable prediction of soil strength as opposed to soil stiffness [5].

Soil stiffness at small strain levels, on the other hand, is calculated with more accuracy by means of shear wave velocity (V_s). V_s measurement is seen to be significant especially in dynamic site response analysis, settlement analysis and soil-structure interaction [6-8]. There are two main in-situ V_s measurement techniques available: (1) surface wave methods and (2) subsurface wave methods. The most popular surface wave methods are multi-station analysis of surface wave (MASW) [9] and two-station spectral analysis of surface wave (SASW) [10], while down-hole and cross-hole methods are recognized to be widely used subsurface methods. Surface wave methods have several advantages over subsurface wave methods: (i) non-destructive and non-invasive, (ii) eases of test conduct and (iii) no need of opening boreholes (therefore its much cheaper and less time consuming). In surface wave techniques three main procedures carried out: (i) in-situ test involving records of the surface waves, (ii) featuring the dispersion in the measured field data and (iii) attaining shear wave velocity profile from the dispersion curve [11,12].

As SPT-N and V_s are two fundamental soil properties required for characterization of soil [13,14], correlation between these two parameters is always of interest. This is due to the fact that in the absence of one for a site, the other soil property can be predicted. For this purpose, $V_{s,30}$ map for Taiwan was generated by consistently configuring the relation of V_s with SPT-N over the 257 strong motion sites [15]. An empirical formulation was developed by [16] for the relationship between V_s and SPT-N varying over the depth of Alluvial and Pliocene soil deposits in Erbaa, Türkiye. Similarly, [17] suggested the correlation from the measurements of SPT-N and V_s values at 17 different locations in Lucknow city. Another empirical correlation between SPT-N and V_s measured via downhole tests was proposed by [18]. Unique empirical formulation for separate soils within the Roorkee area was proposed [19]. In addition, it was seen that the less the fine content available in the soil, the better the correlation becomes. Moreover, different correlations for various soil types (i.e. all soils, silty soils and sandy soils) were formed by taking into account 500 SPT-N and V_s values in the Kathmandu valley, Nepal [20]. [21] developed a set of correlations for various soil conditions in the Dholera territory by including 336 SPT-N and V_s data at, in total, 58 sites. [22] utilized measurements of SPT-N and V_s values at 20 boreholes in Edirne district, Türkiye, and tested the accuracy of available empirical formulations. Equally, using soil data from 30 different locations in Varanasi city, a correlation between SPT-N and V_s was recommended and seismic site classification was made available for the site of interest [23]. Similar studies offering different correlation between SPT-N and V_s for various sites and soil conditions can be found in the studies of Anbazhagan and Bajaj [24]; Kishida and Tsai [25]; Naji, Akin, and Cabalar [26]; Shukla and Solanki [27] and Rao and Choudhury [28] amongst others.

In the current study, it is attempted to develop best-fit curve between SPT-N and V_s for a region, within the Iğdır district, Türkiye. The relationship is proposed for all soil types, clayey/silty soils, and sandy soils. Also, correlations between water content (w) and V_s and between liquid limit (LL) and V_s are configured. This paper carries on by defining the study area in the next section. Subsequently, detailed information regarding obtaining the SPT-N and V_s data is provided. Later, the correlations bounding SPT-N – V_s , w – V_s and LL – V_s are presented and discussed thoroughly. Finally, the main outputs of the study are briefly highlighted.

2. Location of the Study Area

The study area is within the Iğdır district located far-east of Türkiye (Figure 1). The district borderline is colored blue (Figure 1a). It has borders with three seismically active countries; Armenia, Nakhcivan and Iran. Iğdır district including the study area of Melekli is positioned on a plain area deposited between Mount Ararat and Caucasus Mountains in the east of Türkiye. The study area is positioned approximately between $39^{\circ}60'0''$ and $39^{\circ}56'0''$ latitudes and $44^{\circ}4'0''$ and $44^{\circ}7'0''$ longitudes, as demonstrated in Figure 1b. The soil bodies within the site are formed by quaternary alluvial soils as a result of depressions over the years from Aras River [29].

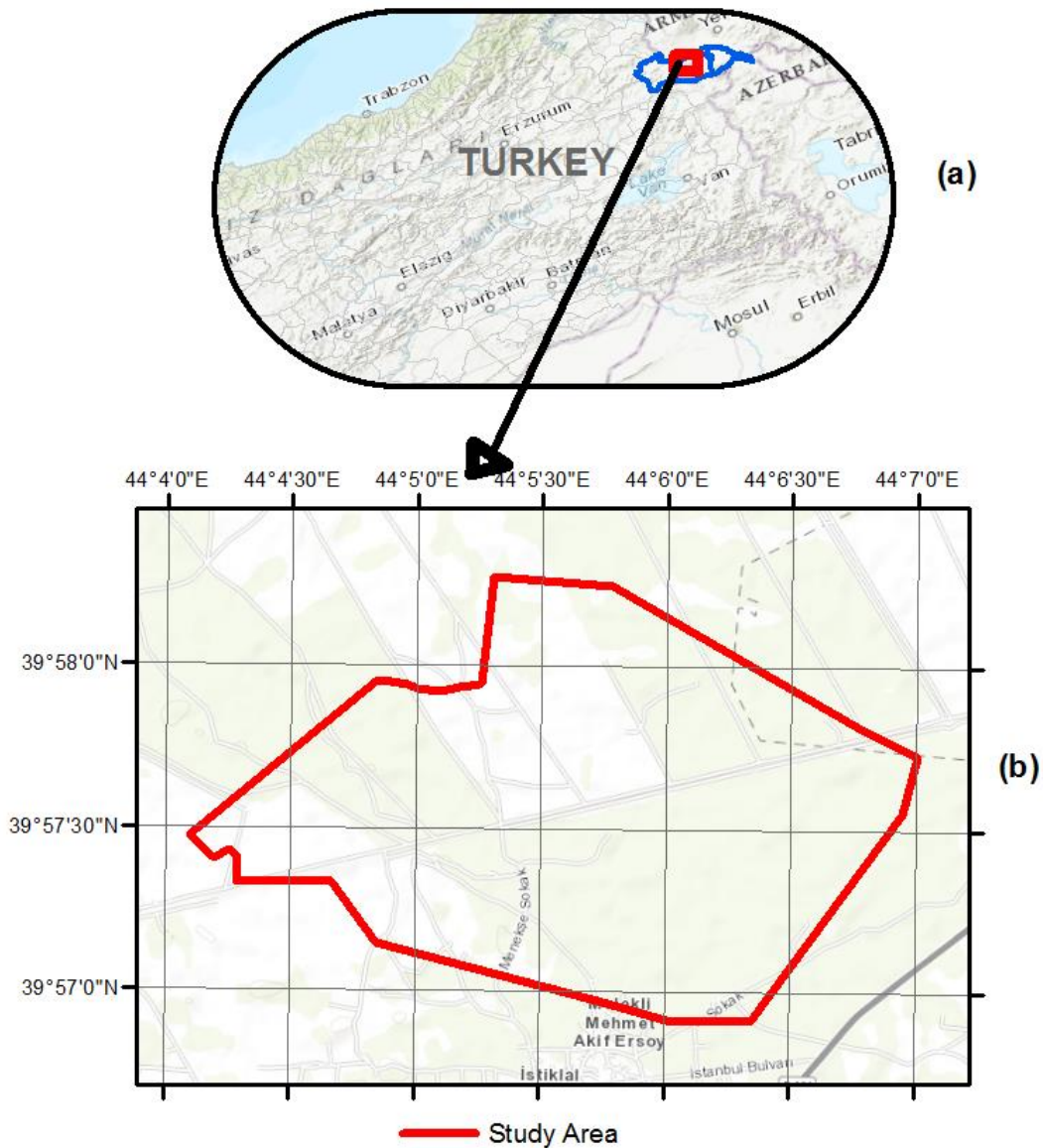


Figure 1. Location of the study area; (a) within Türkiye and Iğdır district, bordering with Armenia, Nakhcivan and Iran, (b) with precise coordinates

3. SPT-N and Shear Wave Velocity Measurements

In the study area, 50 boreholes were opened to measure the SPT-N values in every 1.5 m depth at different locations. The field tests were conducted following TS-1900-1 [30] and SPT-N values are calculated accordingly. A fluid rotary drilling machine was used with $3^{5/8}$ inch drill. All of the boreholes reach 20 m

depth while only 3 boreholes (BH-2, BH-49 and BH-50) opened up to 30 m depth from the ground surface. In total, 650 SPT-N data is considered from the opened boreholes. Locations of the boreholes are presented in Figure 2a. For the measurement of shear wave velocity (V_s) values throughout the depth, multi-station analysis of surface wave (MASW) method is used. In total, 26 MASW tests were conducted at locations distinctive than the borehole locations, as seen in Figure 2b. The V_s measurement at the locations were made up to 50 m below the ground surface.

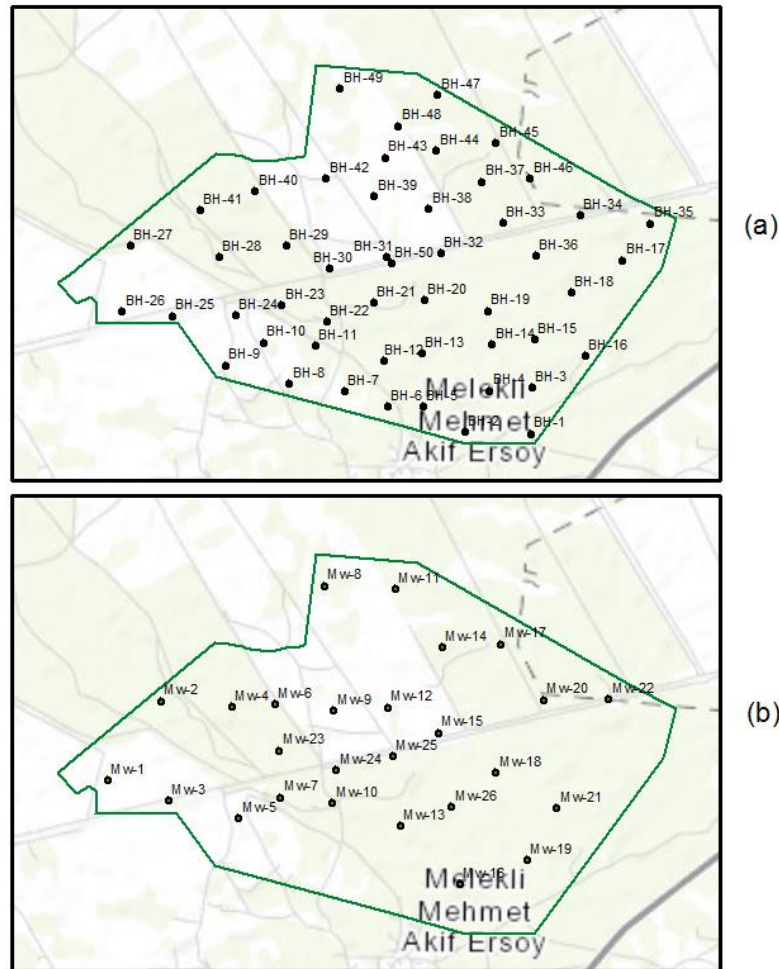


Figure 2. Locations of boreholes and MASW tests for a) SPT-N and b) shear wave velocity values

SPT-N values range from 3 to 49 within all the considered depths. SPT-N values at different depths for BH-29 and BH-44 are provided in Figure 3, aiming to demonstrate the exemplary stratigraphy and SPT-N distributions along 20 m depth in the study area. When the top 4.5 m is formed by silty sand, high plastic clay is seen up to 20 m depth in BH-29. Similarly, fine-grained highly plastic clay soil occupies the top 10.5 depth below which sand soil with silt inclusion is encountered in BH-44. In general, a majority of soil layers have fine-grained soils but there are still considerable coarse-grained soil layers available in the study area. V_s values also extend from 120 m/s to 345 m/s. Again, exemplary measured V_s values (or V_s profiles) and its changes along 50 m depth at two Mw locations are given in Figure 4. Minimum and maximum average V_s values at the top 30 m ($V_{s,30}$) are 188 m/s and 283 m/s, meaning that the investigated sites are most of the time classified as soil class C or soil class D according to Eurocode 8 [31] and Turkish Building Earthquake Code [3], respectively. The distribution of $V_{s,30}$ over the area of interest is illustrated in Figure 5.

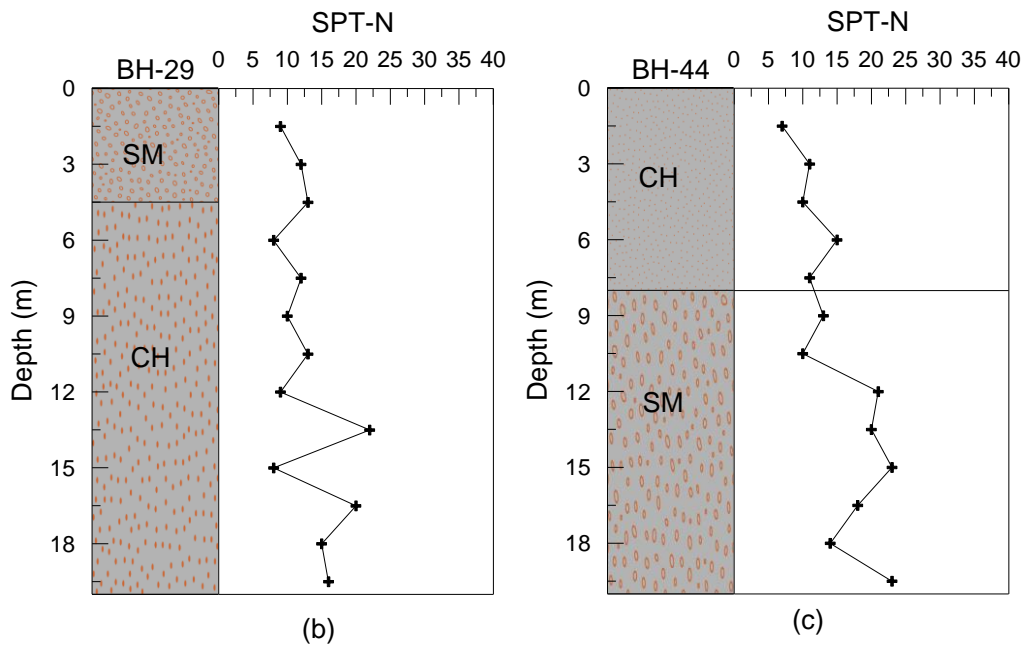


Figure 3. Distributions of SPT-N values until 20 m depth at BH-29 and BH-44

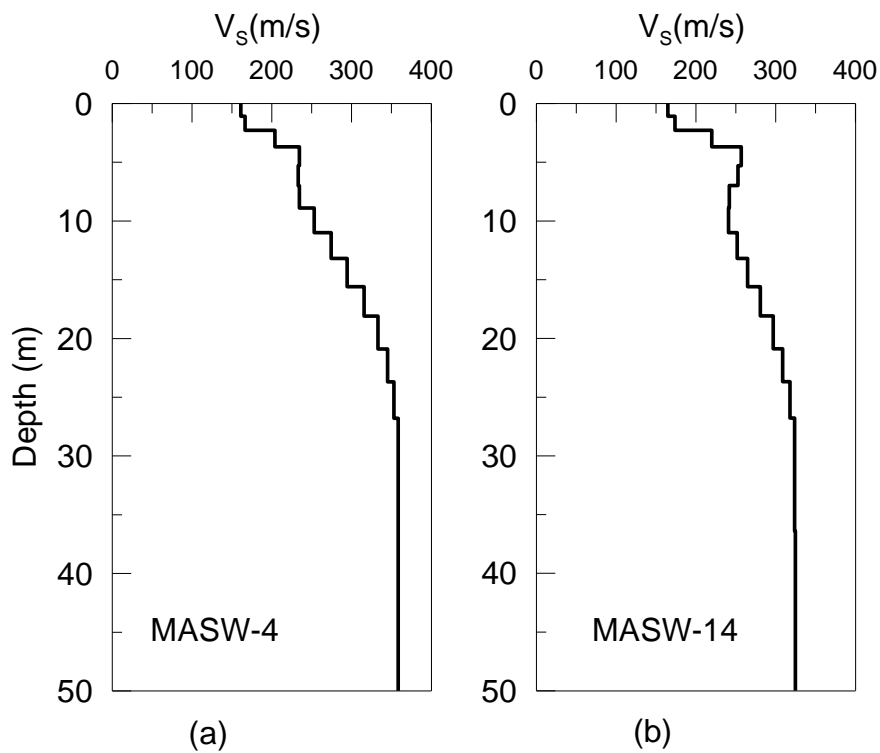


Figure 4. V_s values up to 50 m depth at two different locations (MASW-4 and MASW-14)

Table 1. Ranges of average shear wave velocity at the top 30 m ($V_{s,30}$) of soil sites determining the soil classes given in EC8 and TBEC 2018

Design code/ $V_{s,30}$ (m/s) range	>1500	760-1500	360-760	180-360	<180
EC8	A	B	C	D	
TBEC 2018	A	B	C	D	E

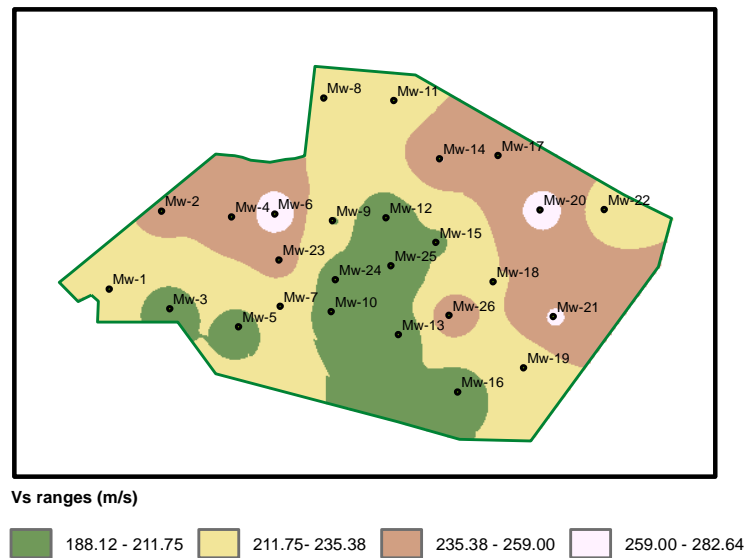


Figure 5. V_s distributions over the study area

It is important to note here that since the SPT-N and V_s measurement locations are different, the measured values cannot directly be correlated. Therefore, possible V_s values at SPT-N test locations are interpolated with inverse distance weight (IDW) method. The interpolation method estimates the desired values at a location from the measured values at known certain locations by allocating weight values based on their distances to the location of estimate. The idea of this method is the closer the distance between estimated and measured locations, the more likely the values will be similar [32]. Function governing the IDW interpolation is written as [33]:

$$Z(x) = \frac{\sum_{i=1}^n W_i Z_i}{\sum_{i=1}^n W_i} \quad (3.1)$$

$$W_i = d_i^{-u} \quad (3.2)$$

in which $Z(x)$ is the expected value at a location; Z_i is the known (measured) value at a known point; n is the total number of known values used in the interpolation; d_i is the distance between the known location and predicted location; and u is the weight power that expresses the development of weight decreases with the increase of the distances. The main component of the IDW interpolation is the power parameter, which is considered as 2. Several studies utilised IDW technique in mapping the SPT-N values along with the other soil parameters at a region. In this respect, [34] employed the Inverse Distance Weighting (IDW) technique to create spatial maps for soil type, Atterberg's limits, sulphate and chloride content, and Standard Penetration Test (SPT-N) for the Sialkot district. [35] established geotechnical maps for the Lahore region, focusing on soil types and SPT-N values using GIS. [36] created contour maps for Islamabad based on N-values and soil types. Finally, [37] developed digital maps using GIS for Islamabad, showcasing geotechnical soil characteristics, vertical profiles, and bearing capacity curves for each zone.

Additionally, several laboratory tests were conducted to determine the soil types, limit states and Atterberg limits. Mainly, sieve analyses and hydrometer tests were conducted over, in total, 333 soil samples, Casagrande and plastic tests were made over 275 soil samples retrieved from the boreholes. Moreover, the water contents of the soil samples were attained. The soil layers consist mostly of fine-grained soils, accounting for 75% of the total soil bodies, and partially of coarse-grained soils, making up 25% of the total. The fine-grained soil layers contain low or high plastic clay and silt, with some gravel and sand. The coarse-grained soil layers are mainly composed of sand, with occasional gravel, silt, and clay. The plastic limit (PL) ranges from 26.2% to

77.9%, while the liquid limit (LL) ranges from 12.4% to 42.1%. The water content of the soils varies from 1.7% above the water table to a maximum of 57% below the water table. The soil densities measured range from 17.7 kN/m³ to 19.2 kN/m³. Overall, 72 and 261 soil samples possess sandy and clayey soil types, respectively.

4. Results and Discussion

4.1. Existing Empirical Formulations

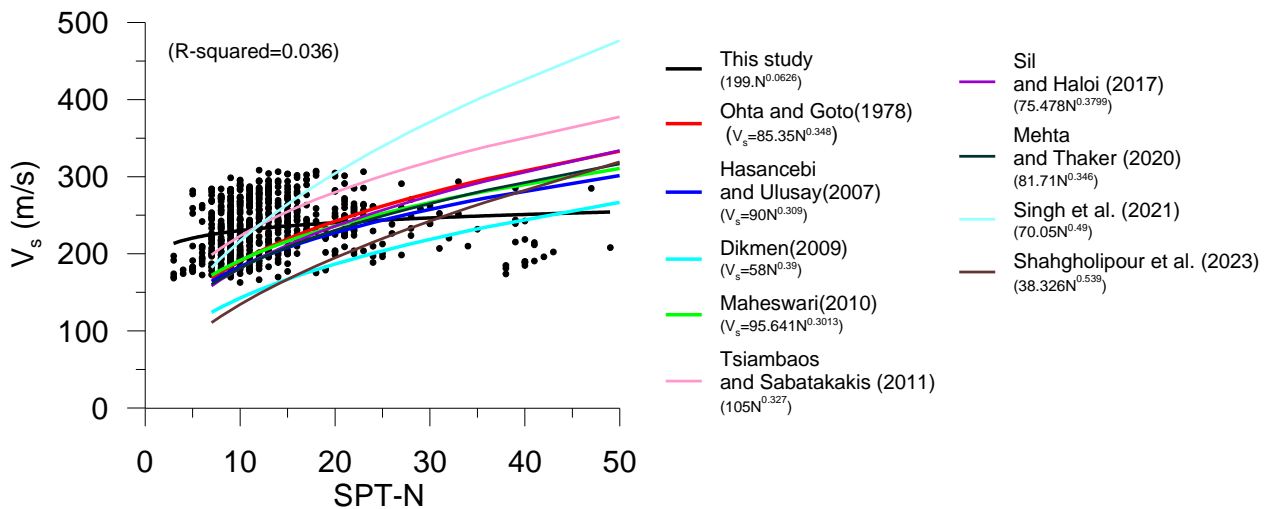
In literature, there have been numerous studies depicting the correlation between SPT-N and V_s data. Several empirical formulations given in the literature are presented in Table 2. These formulations totally involve uncorrected SPT-N values as uncorrected SPT-N values were thought to be strongly correlated with the V_s data. While in some studies the correlation was provided, separately, for all soils, sandy, silty, and clayey soils, others proposed only for all soils. Importantly, most of the time the suggested correlations were specific to the studied areas therefore does not necessarily suit the other locations [38]. Mostly, the prediction of V_s from SPT-N value is based on multiplication of a constant coefficient with powered SPT-N.

Table 2. Several existing empirical formulations representing the correlation between V_s and SPT-N given in the literature

Authors	All soils	Sand	Clay
Ohba and Toriumi [39]	$V_s=84N^{0.33}$	-	-
Athanasopoulos [40]	$V_s=107.6N^{0.36}$	-	$V_s=76.55N^{0.445}$
Ohsaki and Iwasaki [41]	$V_s=81.4N^{0.39}$	$V_s=59.4N^{0.47}$	-
Imai [42]	$V_s=91N^{0.337}$	$V_s=80.6N^{0.331}$	$V_s=102N^{0.292}$
Ohta and Goto [43]	$V_s=85.35N^{0.348}$	$V_s=88N^{0.34}$	-
Yokota, Imai, and Konno [44]	$V_s=121N^{0.27}$	-	-
Imai and Tonouchi [45]	$V_s=97N^{0.314}$	-	-
Jinan [46]	$V_s=116.1(N+0.3185)^{0.202}$	-	-
Lee [47]	-	$V_s=57.4N^{0.49}$	$V_s=144.43N^{0.31}$
Kalteziotis, Sabatakakis, and Vassiliou [48]	$V_s=76.2N^{0.24}$	$V_s=49.1N^{0.5}$	$V_s=76.6N^{0.45}$
Pitilakis, Anastasiadis, and Raptakis [49]	-	$V_s=162N^{0.178}$	-
Raptakis, Anastasiadis, Pitilakis, and Lontzetidis [50]	-	$V_s=100N^{0.24}$	$184.2N^{0.17}$
Kayabali [51]	-	$V_s= 175 + 3.5N$	-
Kyriazis Pitilakis, Raptakis, Lontzetidis, Tika-Vassilikou, and Jongmans [52]	-	$V_s=145N^{0.17}$	$V_s=162N^{0.178}$
Kiku [53]	$V_s=68.3N^{0.292}$	-	-
Hasancebi and Ulusay [54]	$V_s=90N^{0.309}$	$90.82N^{0.319}$	$97.89N^{0.269}$
Lee and Tsai [15]	$V_s=137.153N^{0.229}$	$V_s=98.07N^{0.305}$	$V_s=163.15N^{0.192}$
Dikmen [4]	$V_s=58N^{0.39}$	$73N^{0.33}$	$44N^{0.48}$
Maheswari, Boominathan, and Dodagoudar [55]	$V_s=95.641N^{0.3013}$	$100.53N^{0.263}$	$89.31N^{0.358}$
Tsiambaos and Sabatakakis [56]	$V_s=105.7N^{0.327}$	$V_s=79.7N^{0.365}$	$V_s=88.8N^{0.37}$
Anbazhagan et al. [38]	$V_s=68.96N^{0.51}$	$V_s=60.17N^{0.56}$	$V_s=106.63N^{0.39}$
Sarda Thokchom et al. [21]	$V_s=3.39N+160.5$	-	-
Sil and Haloi [57]	$V_s=75.478N^{0.3799}$	$V_s=79.217N^{0.369}$	$V_s=99.708N^{0.335}$
Mehta and Thaker [58]	$V_s=81.71N^{0.346}$	$V_s=79.81N^{0.355}$	$V_s=83.65N^{0.336}$
Singh, Duggal, and Singh [23]	$V_s=70.05N^{0.49}$	-	$V_s=74.80N^{0.47}$
Shahgholipour, Afsari, and Ghaseminejad [59]	$V_s=38.726N^{0.539}$	$V_s=42.515N^{0.496}$	$V_s=31.241N^{0.626}$

4.2. Proposed Empirical Formulations

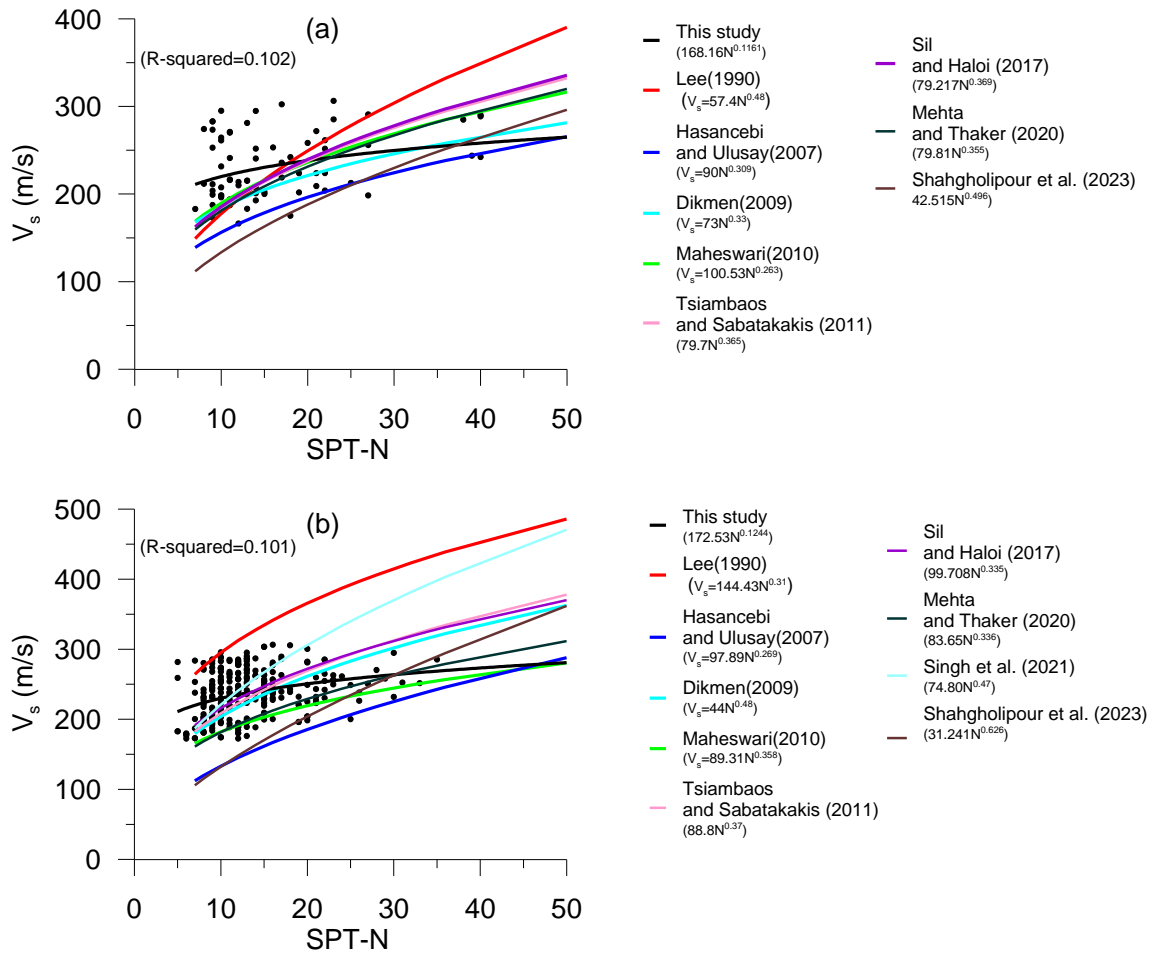
In Figure 6, pairs of SPT-N and V_s values at the same depths are presented along with the best-fit curve for all soils. In addition, the ten developed curves belonging to the empirical formulations available in the literature are plotted. The correlation within the observed data in the studied site seems to be flat. More clearly, the increase in the SPT-N data does not tend to increase the V_s drastically. Instead, it is possible to see alike V_s values for small and large SPT-N values. Therefore, the best-fit curve possesses a higher coefficient with less power value. In contrast, the curves provided in the literature are developing more linearly and they tend to smooth with the higher SPT-N values. The curves suggested by Ohta and Goto [43], Hasancebi and Ulusay [54] and Maheswari et al. [55] give always lower V_s values up to the SPT-N values of 20-25 than the best-fit curve of the available data. Above these SPT-N values, V_s predicted by the aforementioned curves are always greater than the suggestions by the current data best-fit curve. Besides, the empirical correlation suggested by Sil and Haloi [57] almost overlaps with that of Ohta and Goto [43], in particular when SPT-N value is over 30. Similarly, Mehta and Thaker [58] empirical correlation performs in line with that of Hasancebi and Ulusay [54]. The correlation produced by Dikmen [4] gives lower V_s than the best-fit from this study and from the others below the SPT-N value of 45. The empirical correlation given by Tsiambaos and Sabatakakis [56] predicts V_s values that are second highest in the plotted curves after Dikmen [4]. On the contrary, the correlation produced by Singh et al. [23] expresses the lowest V_s values against SPT-N values, especially between 16 and 44 SPT-N range, and does not match with the best-fit curve of the current data. Lastly, the suggested empirical correlation by Shahgholipour et al. [59] depicts V_s values incrementing gradually but still lower than the best fit curve up to the SPT-N value of 30.



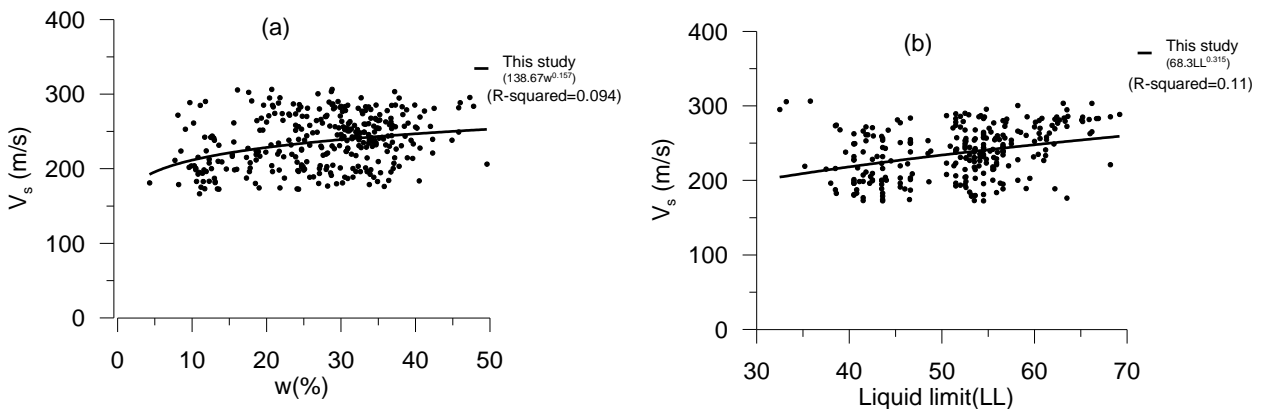
Figures 6. Best-fit curve representing the correlation, for all soils) between SPT-N and V_s data at the study site along with the suggested curves available in the literature

In Figures 7a and 7b, the correlations are separately assessed for sandy and clayey soils, respectively. Again, 9 and 10 different correlations for sandy and clayey soils given in the literature are also demonstrated for comparison purposes. The correlations proposed by Lee [47], Hasancebi and Ulusay [54], Dikmen [4] and Maheswari et al. [55] offer V_s values that are well below the best-fit curve of this study until approximately 16, 20, 34 and 50 SPT-N values (as seen in Figure 7a). Above the mentioned SPT-N values, the literature given empirical correlations always predict higher V_s values. It is, however, important to note that the inclinations of the curves by Hasancebi and Ulusay [54] and Dikmen [4] get closer to the best-fit curve of the current data by the increase of the SPT-N value. The empirical correlations by Maheswari [55] and Mehta and Thaker [58]

and by Tsiambaos and Sabatakakis [56] and Sil and Haloi [57] result in almost same V_s predictions when the formers lead to greater V_s values than the latter ones, particularly above the SPT-N value of 20.5. The suggested empirical correlation by Shahgholipour et al. [59] estimates always less V_s values up to the SPT-N value of 37.6 than the best-fit curve of the current data, above which it leads to the higher values. Similar comments can also be made for the correlations proposed by clayey soils. Nevertheless, the correlations recommended by Lee [47] and Singh et al. [23] are totally out of the given data, producing always higher V_s values (Figure 7b). In this case, the correlations proposed by Hasancebi and Ulusay [54] Maheswari [55] and Mehta and Thaker [58] incline nearer to the best-fit curve of the current data.



Figures 7. Best-fit curve representing the correlations, for (a) sandy and (b) clayey soils, between SPT-N and V_s data at the study site along with the suggested curves available in the literature



Figures 8. Correlations between (a) V_s and w and (b) V_s and LL and their best-fit curves

Predicting the V_s from the water content (w) and from the liquid limit (LL) values are also possible. Since w and LL are available for 333 and 275 soil samples, their relations with the V_s data are plotted in Figures 8a and 8b, respectively, along with the best-fit curves. While the best-fit curve for the V_s - w correlation is information of $V_s=138.67w^{0.157}$, and for the V_s -LL correlation it is represented by $V_s=68.3LL^{0.315}$. These formulations, in addition to the previously represented ones, are illustrated in Table 3.

Table 3. Relation of V_s with SPT-N and w values for all soils, sandy soils, and clayey soils

Correlation type	For all soils	For sandy soil	For clayey soil
V_s - SPT-N	$199N^{0.0626}$	$168.16N^{0.1161}$	$68.3N^{0.315}$
V_s - w	$138.67w^{0.157}$	-	-
V_s - LL	-	-	$68.3LL^{0.315}$

The correlations between SPT-N and V_s values at the studied site depicted for all soils and sandy and clayey soils are shown to be unique to this site as the empirical correlations available in the literature do not match well with the current data. In fact, the correlations in the literature also divert mostly from each other. The suggested SPT-N and V_s correlations (as well as V_s - w and V_s -LL correlations) can be useful for future site studies that may be conducted in future. They will be useful to obtain knowledge of SPT-N values and stiffness distribution for the site that are main inputs for calculating soil bearing capacity and site response analysis.

5. Conclusion

This study evaluates and proposes the correlation between V_s and SPT-N values measured at the Melekli region deposited by alluvial soils, in Türkiye. Correlations are formed for all soils, sandy soils, and clayey soils. Several existing well-known V_s prediction equations are also used for comparison purposes. In addition, the formulations for the prediction of V_s through the measured w and LL values at the site are suggested. The results of this study can be listed as follows:

- The best-fit curve representing the correlation between the V_s and SPT-N for the site is relatively flatter than the ones given in the literature for all soils.
- Similarly, the best-fit curves in the case of sand and clay soils divert considerably from the correlations given in the literature. This is, in particular, true at low SPT-N values as the diversion diminishes at higher SPT-N values with two of the existing correlations.
- In fact, the suggested correlations are significantly dissimilar in any types of soils. This can be attributed to the unique geological conditions (formations, effective stress, overconsolidation, etc) that lead to the formations of distinctive correlations between V_s and SPT-N values.
- For the studied site, it has been shown that w and LL are correlated, to some extent, with V_s as much as that correlation level with SPT-N.

Overall, development of correlation between V_s and SPT-N for a specific site cannot suit to another site. Finally, the significance of such correlation may alter from one site to another and different soil parameters (like w , LL, etc.) may also correlate reasonably well with V_s or SPT-N.

Author Contributions

The author read and approved the final version of the paper.

Conflicts of Interest

The author declares no conflict of interest.

Acknowledgement

The author thanks Dr. Muhammed Alperen Özdemir at Iğdır University (Türkiye) for attaining the geotechnical data and the Turkish Special Provincial Administration (Iğdır) for sharing the data.

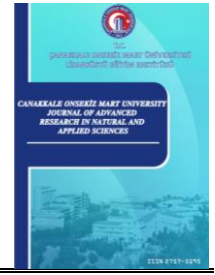
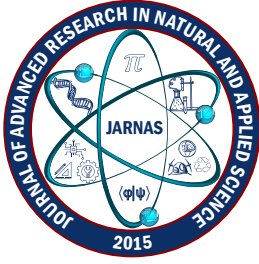
References

- [1] Ö. Yıldız, *Correlation between Spt and Pmt results for sandy and clayey soils*, Eskişehir Technical University Journal of Science Technology A-Applied Sciences 22 (2) (2021) 175–188.
- [2] S. L. Kramer, *Geotechnical earthquake engineering*, Simon & Schuster, New Jersey, 1996.
- [3] Turkish Building Earthquake Code, Deprem etkisi altında binaların tasarımı için esaslar (in Turkish), Türkiye bina deprem yönetmeliği, Ankara, 2018.
- [4] Ü. Dikmen, *Statistical correlations of shear wave velocity and penetration resistance for soils*, Journal of Geophysics and Engineering 6 (1) (2009) 61–72.
- [5] C. P. Lin, C. H. Lin, C. J. Chien, *Dispersion analysis of surface wave testing - SASW vs. MASW*, Journal of Applied Geophysics 143 (2017) 223–230.
- [6] Y. Guzel, F. Guzel, *Investigation of local site effect considering the recordings of the 08.11.2021 earthquake event in Konya, Turkey*, Natural Hazards 116 (1) (2023) 619–636.
- [7] Y. Guzel, M. Rouainia, G. Elia, *Effect of soil variability on nonlinear site response predictions: Application to the Lotung site*, Computers and Geotechnics 121 (2020) 103444 16 pages.
- [8] K. H. Stokoe, S. H. Joh, R. D. Woods, *Some contributions of in situ geophysical measurements to solving geotechnical engineering problems*, 2nd International Conference on Site Characterization (ISC-2), Porto, 2004, 19–22.
- [9] C. B. Park, R. D. Miller, J. H. Xia, *Multichannel analysis of surface waves*, Geophysics 64 (3) (1999) 800–808.
- [10] S. Nazarian, K. H. Stokoe II, *In situ shear wave velocities from spectral analysis of surface waves*, Proceedings of the Eight World Conference on Earthquake Engineering, San Francisco, 1984, pp. 31–40.
- [11] C. P. Lin, C. C. Chang, T. S. Chang, *The use of MASW method in the assessment of soil liquefaction potential*, Soil Dynamics and Earthquake Engineering 24 (9-10) (2004) 689–698.
- [12] S. Nazarian, M. R. Desai, *Automated Surface-Wave Method - field testing*, Journal of Geotechnical Engineering-Asce 119 (7) (1993) 1094–1111.
- [13] P. Anbazhagan, K. Ayush, M. E. Yadhunandan, K. Siriwanth, K. Suryanarayana, G. Sahodar, *Effective use of SPT: Hammer energy measurement and integrated subsurface investigation*, Indian Geotechnical Journal 52 (5) (2022) 1079–1096.
- [14] K. S. Vipin, T. G. Sitharam, P. Anbazhagan, *Probabilistic evaluation of seismic soil liquefaction potential based on SPT data*, Natural Hazards 53 (3) (2010) 547–560.
- [15] C.-T. Lee, B.-R. Tsai, *Mapping Vs30 in Taiwan*, Terrestrial Atmospheric and Oceanic Sciences 19 (6) (2008) 671–682.

- [16] M. K. Akin, S. L. Kramer, T. Topal, *Empirical correlations of shear wave velocity (V_s) and penetration resistance (SPT-N) for different soils in an earthquake-prone area (Erbaa-Turkey)*, Engineering Geology 119 (1-2) (2011) 1–17.
- [17] P. Anbazhagan, *Method for seismic microzonation with geotechnical aspects*, Disaster Advances 6 (4) (2013) 66–85.
- [18] M. Esfehanizadeh, F. Nabizadeh, R. Yazarloo, *Correlation between standard penetration (N-SPT) and shear wave velocity (V_s) for young coastal sands of the Caspian Sea*, Arabian Journal of Geosciences 8 (9) (2015) 7333–7341.
- [19] B. Kirar, B. K. Maheshwari, P. Muley, *Correlation between shear wave velocity (V_s) and SPT resistance (N) for Roorkee Region*, International Journal of Geosynthetics and Ground Engineering 2 (2016) Article Number 9 11 pages.
- [20] D. Gautam, *Empirical correlation between uncorrected standard penetration resistance (SPT-N) and shear wave velocity (V_s) for Kathmandu Valley, Nepal*, Geomatics Natural Hazards and Risk 8 (2) (2017) 496–508.
- [21] S. Thokchom, B. Rastogi, N. Dogra, V. Pancholi, B. Sairam, F. Bhattacharya, V. Patel, *Empirical correlation of SPT blow counts versus shear wave velocity for different types of soils in Dholera, Western India*, Natural Hazards 86 (2017) 1291–1306.
- [22] K. Dehghanian, E. Çaltılı, B. Koçak, H. M. Soysal, *Implementation of shear wave velocity and standard penetration test correlation for Edirne district, Turkey*, Journal of Sustainable Construction Materials 7 (1) (2022) 24–29.
- [23] M. Singh, S. K. Duggal, V. P. Singh, *A Study to establish regression correlation between shear wave velocity and "N"-Value for Varanasi City, India*, Proceedings of the National Academy of Sciences India Section a-Physical Sciences 91 (2) (2021) 405–417.
- [24] P. Anbazhagan, K. Bajaj, *Region-specific correlations between VS30 and time-averaged VS and SPT-N values at different depths for the indo-gangetic basin*, Indian Geotechnical Journal 50 (3) (2020) 454–472.
- [25] T. Kishida, C. C. Tsai, *Prediction model of shear wave velocity by using SPT blow counts based on the conditional probability framework*, Journal of Geotechnical and Geoenvironmental Engineering 143 (4) (2017) 10 pages.
- [26] D. M. Naji, M. K. Akin, A. F. Cabalar, *A comparative study on the V_{S30} and N_{30} based seismic site classification in Kahramanmaraş, Turkey*, Advances in Civil Engineering 2020 (2020) Article ID 8862827 15 pages.
- [27] D. Shukla, C. H. Solanki, *Estimated Empirical Correlations Between Shear Wave Velocity and SPT-N Value for Indore City Using NLR and ANN*, Indian Geotechnical Journal 50 (5) (2020) 784–800.
- [28] V. D. Rao, D. Choudhury, *Estimation of shear wave velocity and seismic site characterization for new nuclear power plant region, India*, Natural Hazards Review 21 (4) (2020) 11 pages.
- [29] M. Öztürk, V. Altay, E. Altundağ, S. Gücel, *Halophytic plant diversity of unique habitats in Turkey: Salt mine caves of Çankırı and Iğdır, Halophytes for food security in dry lands*, Elsevier, Oxford, 2016, pp. 291–315.
- [30] TS 1900-1, *İnşaat mühendisliğinde zemin laboratuvar deneyleri, Bölüm 1: Fiziksel özelliklerin tayini*, Ankara, 2006.
- [31] CEN, Eurocode 8: Design of structures for earthquake resistance–Part 1: General rules, seismic actions and rules for buildings, Brussels, 2005.

- [32] G. S. Bhunia, P. K. Shit, R. Maiti, *Comparison of GIS-based interpolation methods for spatial distribution of soil organic carbon (SOC)*, Journal of the Saudi Society of Agricultural Sciences 17 (2) (2018) 114–126.
- [33] Y. F. Xie, T. B. Chen, M. Lei, J. Yang, Q. J. Guo, B. Song, X. Y. Zhou, *Spatial distribution of soil heavy metal pollution estimated by different interpolation methods: Accuracy and uncertainty analysis*, Chemosphere 82 (3) (2011) 468–476.
- [34] Z. Ijaz, C. Zhao, N. Ijaz, Z. ur Rehman, A. Ijaz, *Spatial mapping of geotechnical soil properties at multiple depths in Sialkot region, Pakistan*, Environmental Earth Sciences, 80 (2021) Article Number 787 16 pages.
- [35] H. U. Khan, I. Rashid, J. Israr, G. Zhang, *Geotechnical characterization and statistical evaluation of alluvial soils of Lahore*, Arabian Journal of Geosciences 15 (2022) Article Number 845 12 pages.
- [36] M. H. Khalid, B. Alshameri, U. Abid, *Application of Kriging for development of SPT N value contour maps and USCS-based soil type qualitative contour maps for Islamabad, Pakistan*, Environmental Earth Sciences 80 (2021) Article Number 413 13 pages.
- [37] W. Hassan, B. Alshameri, M. N. Nawaz, Z. Ijaz, M. Qasim, *Geospatial and statistical interpolation of geotechnical data for modeling zonation maps of Islamabad, Pakistan*, Environmental Earth Sciences 81 (2022) Article Number 547 23 pages.
- [38] P. Anbazhagan, A. Parihar, H. N. Rashmi, *Review of correlations between SPT-N and shear modulus: A new correlation applicable to any region*, Soil Dynamics and Earthquake Engineering 36 (2012) 52–69.
- [39] S. Ohba, I. Toriumi, *Dynamic response characteristics of Osaka Plain (in Japanese)*, Proceedings of the Annual Meeting AIJ, Tokyo, 1970.
- [40] G. Athanasopoulos, *Empirical correlations V_{so} -NSPT for soils of Greece: A comparative study of reliability*, Transactions on The Built Environment 15 (1970) 8 pages.
- [41] Y. Ohsaki, R. Iwasaki, *On dynamic shear moduli and Poisson's ratios of soil deposits*, Soils & Foundations 13 (4) (1973) 61–73.
- [42] T. Imai, *P and S wave velocities of the ground in Japan*, 9th International Conference on Soil Mechanics and Foundation Engineering, Tokyo, 1977, pp: 257–260.
- [43] Y. Ohta, N. Goto, *Empirical shear wave velocity equations in terms of characteristic soil indexes*, Earthquake Engineering & Structural Dynamics 6 (2) (1978) 167–187.
- [44] K. Yokota, T. Imai, M. Konno, *Dynamic deformation characteristics of soils determined by laboratory tests*. OYO Tec. Rep 3 (1981) 13–37.
- [45] T. Imai, K. Tonouchi, *Correlation of N-value with S-wave velocity*, Proceedings of 2. European Symposium on Penetrating Testing, Amsterdam, 1982.
- [46] Z. Jinan, *Correlation between seismic wave velocity and the number of blow of SPT and depth*, Chinese Journal of Geotechnical Engineering, American Society of Civil Engineers, USA, 1987, pp. 92–100.
- [47] S. H. H. Lee, *Regression models of shear wave velocities in Taipei basin*, Journal of the Chinese Institute of Engineers 13 (5) (1990) 519–532.
- [48] N. Kalteziotis, N. Sabatakakis, J. Vassiliou, *Evaluation of dynamic characteristics of Greek soil formations (in Greek)*, Second Hellenic Conference on Geotechnical Engineering, 1992, pp. 239–246.
- [49] K. Pitilakis, A. Anastasiadis, D. Raptakis, *Field and laboratory determination of dynamic properties of natural soil deposits*, 10th World Conference on Earthquake Engineering, Balkema, 1992, pp. 1275–1280.

- [50] D. Raptakis, S. Anastasiadis, K. Pitilakis, K. Lontzetidis, *Shear wave velocities and damping of Greek natural soils*, in: G. Duma, 10th European Conference Earthquake Engineering, Vienna, 1995, pp. 477–482.
- [51] K. Kayabali, *Soil liquefaction evaluation using shear wave velocity*, *Engineering Geology* 44 (1-4) (1996) 121–127.
- [52] K. Pitilakis, D. Raptakis, K. Lontzetidis, T. Tika-Vassilikou, D. Jongmans, *Geotechnical and geophysical description of EURO-SEISTEST, using field, laboratory tests and moderate strong motion recordings*, *Journal of Earthquake Engineering* 3 (03) (1999) 381–409.
- [53] H. Kiku, *In-situ penetration tests and soil profiling in Adapazari, Turkey*, 15th ICSMGE TC4 Satellite Conference on Lessons Learned from Recent Strong Earthquakes, İstanbul, 2001, pp. 259–265.
- [54] N. Hasancebi, R. Ulusay, *Empirical correlations between shear wave velocity and penetration resistance for ground shaking assessments*, *Bulletin of Engineering Geology and the Environment* 66 (2) (2007) 203–213.
- [55] R. U. Maheswari, A. Boominathan, G. R. Dodagoudar, *Use of surface waves in statistical correlations of shear wave velocity and penetration resistance of chennai soils*, *Geotechnical and Geological Engineering* 28 (2) (2010) 119–137.
- [56] G. Tsiambaos, N. Sabatakakis, *Empirical estimation of shear wave velocity from in situ tests on soil formations in Greece*, *Bulletin of Engineering Geology the Environment* 70 (2011) 291–297.
- [57] A. Sil, J. Haloi, *Empirical correlations with standard penetration test (SPT)-N for estimating shear wave velocity applicable to any region*, *International Journal of Geosynthetics and Ground Engineering* 3 (2017) Article Number 22 13 pages.
- [58] P. Mehta, T. Thaker, *Development Of correlations between shear wave velocity and Spt-N for Vadodara Region, Gujarat, India*, *Journal of GeoEngineering* 15 (3) (2020) 145–157.
- [59] F. Shahgholipour, N. Afsari, V. Ghaseminejad, *Correlation between shear wave velocity and standard penetration test for Nowshahr and Chalus, Iran*, *Iranian Journal of Geophysics* 17 (6) (2023) 37–52.



Contribution to the Molecular Phylogeny of Anthribidae (Coleoptera: Curculioniodea) Inferred from COI Sequences

Polen Döngel¹ , Ali Nafiz Ekiz² 

^{1,2}Department of Molecular Biology and Genetics, Faculty of Engineering and Natural Sciences, Uşak University, Uşak, Türkiye

Article History

Received: 28 Jul 2023

Accepted: 3 Jan 2024

Published: 15 Mar 2024

Research Article

Abstract – Fungus weevils, Anthribidae, is a relatively small family, including about 3861 species worldwide, of the diverse superfamily Curculioniodea. Currently, three subfamilies are recognized within Anthribidae (Anthribinae, Choraginae and Urodontinae); however, this subfamily division is somewhat controversial and not accepted by all authors of the field. In this study, we constructed family level evolutionary histories within Anthribidae by using COI sequences and discussed the phylogenetic relations between these three subfamilies and also between tribes. Estimates of evolutionary divergence between sequences used in this study are calculated and the overall average divergence was 0,274 where minimum was 0,133 and maximum was 0,365. Phylogenetic and evolutionary histories were inferred by using 34 COI sequences representing most of the tribes and subfamilies currently recognized within Anthribidae. The phylogenetic trees were inferred by using Neighbor-Joining (NJ) and Maximum Likelihood (ML) methods. Both method provided quite similar evolutionary histories. According to the phylogenetic trees, Anthribinae + Coraginae members together constitute a monophyletic clade, which makes currently recognized Anthribinae paraphyletic and Coraginae polyphyletic. Urodontinae seems to form a monophyletic clade with respect to used COI sequences. Tribal classification which fully seem to depends on morphological characters are useful for practical taxonomic purposes but most tribes (those represented with more than one species/sequence) does not constitute monophyletic clades.

Keywords – *Anthribidae, COI barcode, DNA barcode, fungus weevils, molecular phylogeny*

1. Introduction

Fungus weevils Anthribidae Billberg, 1820, constitute a family belonging to diverse superfamily Curculioniodea (Coleoptera) Latreille, 1802, of which most members are associated with the fungus and decaying woods [1,2]. Currently, the family Anthribidae include about 3861 species spread over worldwide [3,4]. Although it is somewhat controversial, three subfamilies are recognized within Anthribidae: Anthribinae Billberg, 1820 (28 tribes, 308 genera, 3148 species), Choraginae Kirby, 1819 (five tribes, 62 genera, 630 species) and Urodontinae Thomson, 1859 (eight genera, 83 species) [4].

Cytochrome c oxidase I (COI or COXI) gene sequences are extensively used as DNA barcodes for molecular species identification and in phylogenetic studies [5,6]. Thousands of COI barcodes belonging to all living forms are now deposited publicly in several databases including NCBI (GenBank), BOLD etc. and those barcode sequences are used by researchers freely. In GenBank nucleotide database, there are 1383 sequences belonging to species of Anthribidae, and 422 of them are COI sequences i.e., DNA barcodes (<https://www.ncbi.nlm.nih.gov/nucleotide/?term=Anthribidae+COI>).

In recent revisional and phylogenetic research, superfamily Curculionoidea includes seven families of which

¹polendongel_@hotmail.com (Corresponding Author); ²nafiz.ekiz@usak.edu.tr

Anthribidae is positioned as a basal clade [4,7]. As stated above, three subfamilies (Anthribinae, Coraginae and Urodontinae) are recognized in Anthribidae; however, there are still discussions about subfamily separations. Although Urodontinae is treated as a separate subfamily by Crowson [8] and Rheinheimer [3], Mermudes and Leschen [4] considered Urodontinae as a part of Anthribinae. These subfamilies are mainly distinguished by morphological features and this group lacks sufficient molecular phylogenetic research. Anthribinae and Choraginae are distinguished by several morphological traits; the shape of the first two antennal segments, the position of the antennal scrobe, and the shape of the female genitalia (Holloway 1982).

The main goal of this paper is to contribute current understanding of the family level phylogenetic relationships within Anthribidae, and to discuss the subfamilial and tribal classification.

2. Materials and Methods

The first papers dealing with family level classification of weevils (Curculionioidea) date back to the 19th century [10-13]. Since then, 11 to 22 families were recognized [14]. Later with the application of phylogenetic methods, the number of major lineages was reduced to 6 families [7,15,16].

The materials of this study were COI sequences belonging to 34 species/specimens, 27 genera, 14 tribes and three subfamilies currently recognized in Anthribidae. Two sequences belonging to *Cimberis attelaboides* (Fabricius, 1787) (Nemonychidae) and *Curculio glandium* Marsham, 1802 (Curculionidae) were used as outgroup taxa. All COI sequences were provided from GenBank nucleotide database and given in Table 1.

Molecular Evolutionary Genetic Analysis (MEGA-X) software was used for all analysis [17]. COI Sequences taken from GenBank nucleotide database were assembled in MEGA-X to generate alignments. Multiple Sequence Comparison by Log-Expectation (MUSCLE) [18] program was used to generate multiple alignments of COI sequences. The evolutionary distances between sequences were measured by using the Kimura 2-parameter model [19]. The evolutionary history was inferred by using Neighbor-Joining (NJ) and Maximum Likelihood (ML) methods, and phylogenetic trees are given separately.

3. Results and Discussion

In this paper, we used 34 COI sequences representing most of the tribes and genera of Anthribidae and two sequences as outgroup taxa. Estimates of evolutionary divergence between sequences are given in Table 2. The overall average divergence was 0,274 where minimum was 0,133 and maximum was 0,365.

Table 1. Taxa used in the phylogenetic analysis

Subfamily	Tribus	Genus	Species	GenBank Acc. No.
	Anthribini	<i>Anthribus</i>	<i>Anthribus fasciatus</i> Forster, 1770	KM285875
			<i>Anthribus nebulosus</i> Forster, 1770	MG055246
	Corrhecerini	<i>Disphaerona</i>	<i>Disphaerona chinensis</i> Frieser, 1995	HQ987085
Anthribinae	Cratoparini	<i>Euparius</i>	<i>Euparius marmoreus</i> (Olivier, 1800)	HM433176
			<i>Acanthopygus</i>	<i>Acanthopygus griseus</i> Montrouzier, 1860
	Discotenini	<i>Pseudeuparius</i>	<i>Pseudeuparius sepicola</i> (Fabricius, 1792)	KU908682
			<i>Eucorynus</i>	<i>Eucorynus crassicornis</i> (Fabricius, 1802)

Table 1. (Continued)

Subfamily	Tribus	Genus	Species	GenBank Acc. No.	
Anthribinae	Jordanthribini	<i>Jordanthribus</i>	<i>Jordanthribus</i> sp.	KX053540	
		<i>Dinema</i>	<i>Dinema filicornis</i> Fairmaire, 1849	KX052591	
	Platyrhinini	<i>Platyrhinus</i>	<i>Platyrhinus resinosus</i> (Scopoli, 1763)	KU917082	
		<i>Phloeobius</i>	<i>Phloeobius gigas</i> (Fabricius, 1775)	HM431488	
	Platystomini	<i>Platystomos</i>	<i>Platystomos albinus</i> (Linnaeus, 1758)	KU916837	
		<i>Toxonotus</i>	<i>Toxonotus cornutus</i> (Say, 1831)	HM433055	
	Stenocerini	<i>Allandrus</i>	<i>Allandrus therondi</i> (Tempère, 1954)	KM286294	
			<i>Allandrus undulates</i> (Panzer, 1795)	MZ607386	
	Trigonorhinini	<i>Trigonorhinus</i>	<i>Trigonorhinus alternatus</i> (Say, 1826)	MF640977	
			<i>Trigonorhinus tomentosus</i> (Say, 1826)	FJ867819	
			<i>Gonotropis</i>	<i>Gonotropis dorsalis</i> (Thunberg, 1796)	MZ610748
			<i>Tropideres</i>	<i>Tropideres albistrois</i> (Schaller, 1783)	KM452571
	Zygaenodini	<i>Dissoleucas</i>	<i>Dissoleucas niveirostris</i> (Fabricius, 1798)	MZ606968	
			<i>Noxius</i>	<i>Noxius curtirostris</i> (Mulsant, 1861)	MN183027
			<i>Ormiscus</i>	<i>Ormiscus walshii</i> (LeConte, 1876)	KR485751
	Zygaenodini	<i>Rhaphitropis</i>	<i>Rhaphitropis marchica</i> (Herbst, 1797)	HQ954422	
			<i>Rhaphitropis oxyacanthae</i> (Brisout, 1863)	KM285872	
			<i>Xynotropis</i>	<i>Xynotropis</i> sp.	KM006611
	Choraginae	Araecerini	<i>Araecerus</i>	<i>Araecerus fasciculatus</i> (DeGeer, 1775)	KM446808
		Choragini	<i>Choragus</i>	<i>Choragus sheppardi</i> Kirby, 1819	KM444886
			<i>Melanopsacus</i>	<i>Melanopsacus grenieri</i> (Barneville, 1867)	MN182766
<i>Styphlochoragus</i>			<i>Styphlochoragus trachodes</i> Frieser, 1978	KJ672228	
Urodontinae	Urodontini	<i>Bruchela</i>	<i>Bruchela conformis</i> (Gyllenhal, 1833)	KM448962	
			<i>Bruchela rufipes</i> (Olivier, 1790)	MK892264	
			<i>Bruchela schusteri</i> (Schilsky, 1912)	MK892233	
			<i>Bruchela suturalis</i> (Fabricius, 1792)	MK892262	
		<i>Urodontus</i>	<i>Urodontus mesemoides</i> Louw, 1993	FJ867818	
Outgroup taxa	Nemonychidae	<i>Cimberis attelaboides</i> (Fabricius, 1787)	MZ658256		
	Curculionidae	<i>Curculio glandium</i> Marsham, 1802	KC784023		

Table 2. Estimates of evolutionary divergence between sequences. The numbers of base substitutions per site from between sequences are shown. Analyses were conducted using the Kimura 2-parameter model

	1	2	3	4	5	6	7	8	9	10	11	12	13	14	15	16	17	18	19	20	21	22	23	24	25	26	27	28	29	30	31	32	33									
1 <i>Anthribus fasciatus</i>																																										
2 <i>Anthribus neb ulosus</i>	0.23																																									
3 <i>Disphaerona chinensis</i>	0.28	0.27																																								
4 <i>Euparius mamoreus</i>	0.26	0.31	0.25																																							
5 <i>Acanthopygus griseus</i>	0.25	0.24	0.27	0.27																																						
6 <i>Pseudeuparius spicola</i>	0.29	0.31	0.28	0.28	0.29																																					
7 <i>Enconyus crassico milis</i>	0.27	0.28	0.33	0.29	0.29	0.33																																				
8 <i>Jordanthribus</i> sp.	0.25	0.27	0.26	0.25	0.28	0.25	0.29																																			
9 <i>Dinema filicornis</i>	0.24	0.27	0.28	0.25	0.30	0.30	0.25	0.22																																		
10 <i>Platymirus resinosus</i>	0.23	0.23	0.24	0.24	0.25	0.25	0.26	0.27	0.22																																	
11 <i>Phloeobitus gigas</i>	0.27	0.26	0.29	0.32	0.31	0.32	0.33	0.28	0.25	0.28																																
12 <i>Platysto mos albinus</i>	0.27	0.29	0.24	0.24	0.28	0.27	0.33	0.29	0.27	0.24	0.25																															
13 <i>Toxonotus conutus</i>	0.29	0.33	0.22	0.25	0.34	0.30	0.31	0.29	0.28	0.29	0.28	0.25																														
14 <i>Allandrus therondi</i>	0.29	0.26	0.29	0.27	0.29	0.29	0.30	0.24	0.24	0.28	0.26	0.30	0.32																													
15 <i>Allandrus undulatus</i>	0.26	0.28	0.30	0.29	0.27	0.30	0.30	0.28	0.24	0.24	0.29	0.30	0.31	0.13																												
16 <i>Trigono rhinus alternatus</i>	0.20	0.20	0.26	0.26	0.26	0.28	0.27	0.28	0.20	0.19	0.26	0.26	0.26	0.23	0.21																											
17 <i>Trigono rhinus tomentosus</i>	0.21	0.20	0.25	0.29	0.28	0.28	0.32	0.23	0.24	0.20	0.27	0.26	0.32	0.23	0.26	0.19																										
18 <i>Gonotropis dorsalis</i>	0.28	0.31	0.31	0.28	0.30	0.29	0.27	0.28	0.26	0.28	0.29	0.22	0.27	0.28	0.27	0.27	0.28																									
19 <i>Tro pideres albistrois</i>	0.26	0.31	0.28	0.27	0.29	0.28	0.31	0.28	0.27	0.28	0.29	0.26	0.28	0.26	0.31	0.26	0.26	0.21																								
20 <i>Dissoleucas niveiro stris</i>	0.27	0.23	0.26	0.28	0.28	0.26	0.30	0.26	0.27	0.24	0.29	0.30	0.31	0.25	0.25	0.26	0.22	0.28	0.25																							
21 <i>Noxius curtirostris</i>	0.25	0.22	0.25	0.25	0.23	0.26	0.23	0.20	0.20	0.20	0.25	0.21	0.27	0.24	0.27	0.22	0.25	0.28	0.25	0.24																						
22 <i>Ormiscus ralshii</i>	0.25	0.27	0.28	0.29	0.25	0.25	0.29	0.24	0.30	0.26	0.28	0.25	0.31	0.30	0.29	0.28	0.27	0.26	0.29	0.28	0.23																					
23 <i>Rhaphitropis marchica</i>	0.25	0.27	0.29	0.28	0.28	0.23	0.31	0.21	0.23	0.26	0.28	0.25	0.29	0.24	0.24	0.25	0.26	0.23	0.26	0.28	0.23	0.28																				
24 <i>Rhaphitropis oxpacanthae</i>	0.22	0.20	0.26	0.27	0.24	0.25	0.32	0.28	0.28	0.24	0.27	0.32	0.30	0.25	0.24	0.22	0.22	0.31	0.28	0.23	0.24	0.29	0.26																			
25 <i>Xynotropis</i> sp.	0.24	0.28	0.26	0.25	0.27	0.25	0.28	0.24	0.26	0.24	0.30	0.22	0.30	0.31	0.31	0.28	0.27	0.26	0.26	0.25	0.21	0.25	0.27	0.24																		
26 <i>Araecent fasciculatus</i>	0.34	0.32	0.32	0.32	0.31	0.36	0.33	0.30	0.30	0.32	0.31	0.29	0.32	0.32	0.33	0.33	0.34	0.32	0.36	0.36	0.29	0.34	0.32	0.33																		
27 <i>Choragus sheppardi</i>	0.21	0.25	0.25	0.27	0.23	0.28	0.27	0.25	0.24	0.21	0.26	0.28	0.30	0.30	0.27	0.22	0.27	0.31	0.29	0.28	0.22	0.28	0.25	0.23	0.27	0.34																
28 <i>Melanopsacus grenien</i>	0.22	0.22	0.24	0.29	0.20	0.26	0.24	0.23	0.22	0.19	0.26	0.26	0.29	0.25	0.28	0.22	0.20	0.25	0.28	0.27	0.17	0.24	0.24	0.22	0.22	0.28	0.21															
29 <i>Styphlochoragus trachodes</i>	0.26	0.25	0.29	0.29	0.21	0.29	0.31	0.23	0.26	0.22	0.29	0.27	0.34	0.29	0.31	0.29	0.28	0.28	0.31	0.26	0.22	0.24	0.25	0.26	0.21	0.30	0.25	0.20														
30 <i>Bruchela conformis</i>	0.33	0.30	0.30	0.35	0.28	0.24	0.33	0.29	0.31	0.29	0.32	0.30	0.34	0.31	0.31	0.33	0.28	0.30	0.32	0.29	0.27	0.33	0.25	0.26	0.28	0.33	0.28	0.25	0.25													
31 <i>Bruchela rufipes</i>	0.28	0.28	0.29	0.33	0.29	0.27	0.36	0.29	0.29	0.30	0.34	0.30	0.35	0.30	0.34	0.32	0.31	0.31	0.34	0.30	0.27	0.33	0.28	0.30	0.26	0.31	0.29	0.24	0.27	0.16												
32 <i>Bruchela sch usteri</i>	0.29	0.25	0.30	0.35	0.21	0.28	0.32	0.27	0.29	0.23	0.31	0.29	0.34	0.30	0.28	0.26	0.25	0.32	0.32	0.27	0.26	0.26	0.27	0.26	0.27	0.36	0.23	0.22	0.24	0.18	0.19											
33 <i>Bruchela suturalis</i>	0.30	0.30	0.29	0.34	0.26	0.26	0.35	0.26	0.28	0.26	0.30	0.33	0.34	0.27	0.28	0.28	0.26	0.33	0.34	0.29	0.28	0.28	0.25	0.25	0.30	0.35	0.26	0.25	0.29	0.16	0.19	0.15										
34 <i>Urodontus mesemoides</i>	0.29	0.30	0.33	0.31	0.24	0.31	0.32	0.29	0.27	0.25	0.30	0.30	0.35	0.26	0.25	0.25	0.24	0.28	0.30	0.28	0.26	0.31	0.30	0.26	0.29	0.35	0.23	0.22	0.27	0.26	0.26	0.20	0.23									

We constructed evolutionary scenarios by using Neighbor-joining and maximum likelihood methods. The phylogenetic scenarios inferred from NJ and ML analyses are given in Figures 1 and 2, respectively. The topologies of both trees were similar to each other with slight differences. According to evolutionary history inferred from NJ method (Figure 1), Anthribinae+Coraginae constitute a monophyletic clade where currently recognized Anthribinae was paraphyletic with respect to Choraginae members placed within Anthribinae clades. Urodontinae seems to be monophyletic (a clade descended from a common ancestor or ancestral group) with respect to sequences used in this study. As to tribal classification, some tribes (i.e., Tropiderini and Urodontini) seems to be monophyletic, most of the tribes were paraphyletic (a clade descended from a common ancestor or ancestral group, but not including all the descendant groups) or polyphyletic (a clade derived from more than one ancestor). This shows that tribal classification doesn't reflect evolutionary history but is used for practical reasons to identify specimens. Evolutionary history inferred from ML method (Figure 2) was quite similar to NJ scenario with respect to subfamily placements. The only major difference was the placement of Coraginae members within Anthribinae clades. Tribal classification also seems mostly not monophyletic with the same few monophyletic tribes as in NJ scenario.

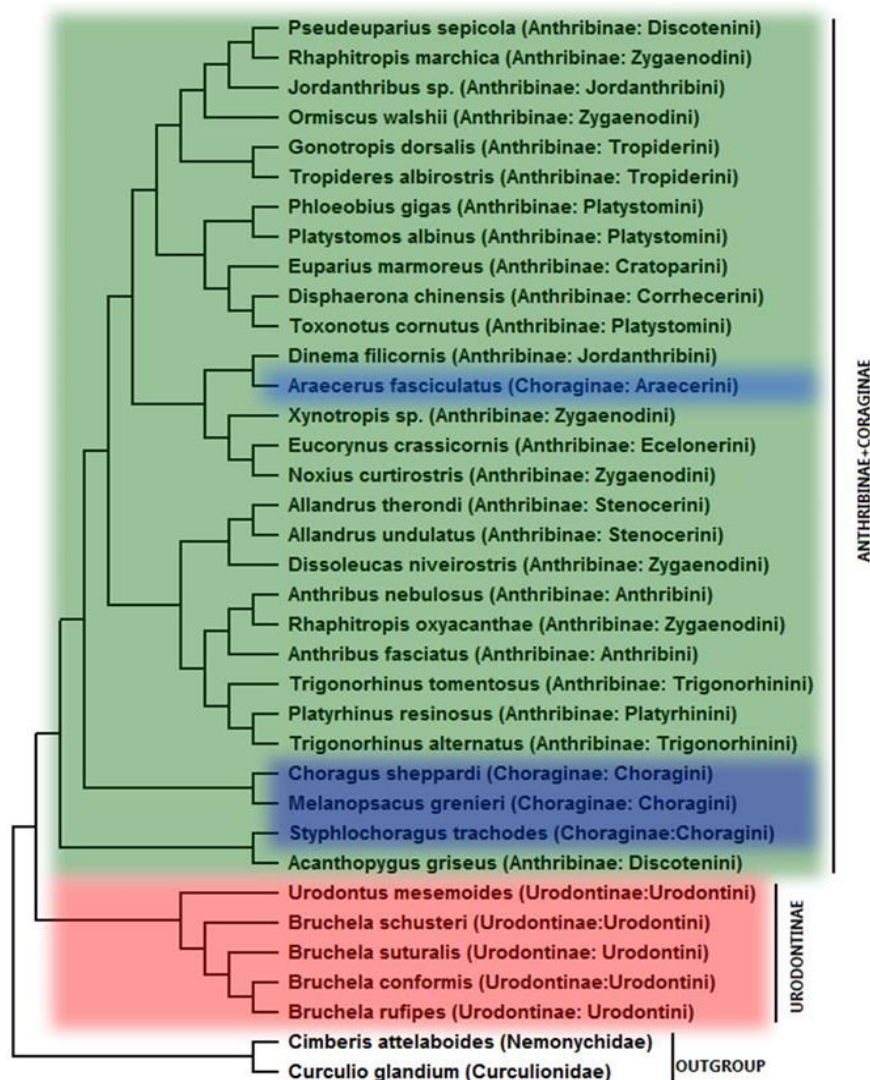


Figure 1. Evolutionary relationships within Anthribidae. The evolutionary history was inferred using the Neighbor-Joining method. The evolutionary distances were computed using the Kimura 2-parameter method and are in the units of the number of base substitutions per site. This analysis involved 36 nucleotide sequences.

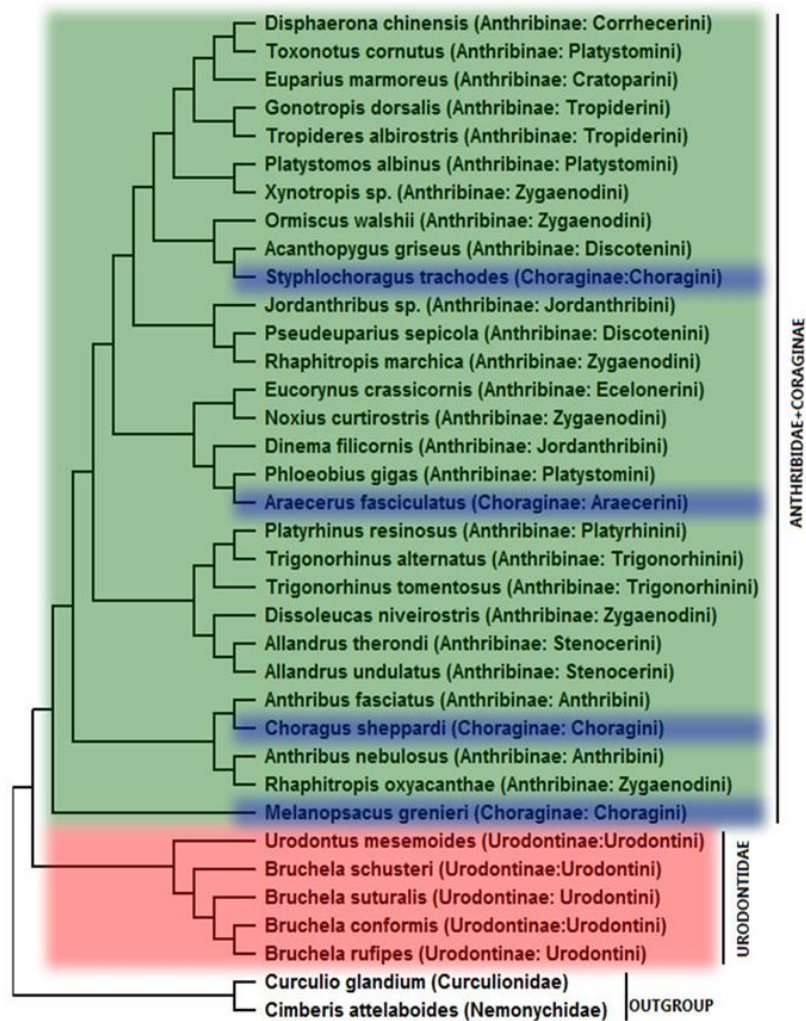


Figure 2. Evolutionary relationships within Anthribidae. The evolutionary history was inferred by using the Maximum Likelihood method and Kimura 2-parameter model. Initial tree(s) for the heuristic search were obtained automatically by applying Neighbor-Join and BioNJ algorithms to a matrix of pairwise distances estimated using the Maximum Composite Likelihood (MCL) approach, and then selecting the topology with superior log likelihood value. This analysis involved 36 nucleotide sequences.

4. Conclusion

Family Anthribidae seems to be one of the basal lineages within Curculionioidea [20]. Family level classification (subfamilies and tribes) of Anthribidae mostly depends on morphological characters and is not well resolved yet. The results of this paper show that subfamilial classification of Anthribidae needs a comprehensive revision. According to evolutionary histories presented here which inferred from COI sequences of 34 species using NJ and ML methods, members of Anthribinae + Choraginae and members of Urodontinae constitute monophyletic clades. However, the current covering of Anthribinae and Choraginae were not monophyletic, where Anthribinae was paraphyletic and Choraginae was polyphyletic. Tribal classification of Anthribidae seems to be intended for practical taxonomic purposes (i.e. morphological identification) but most of the tribes do not constitute monophyletic clades and thus not correct phylogenetically. Consequently, more phylogenetic molecular studies need to be done to resolve the current family level classification of Anthribidae.

Author Contributions

All the authors equally contributed to this work. They all read and approved the final version of the paper.

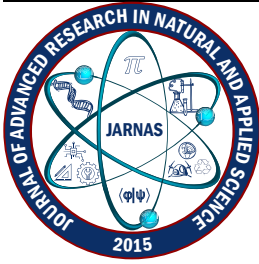
Conflicts of Interest

All the authors declare no conflict of interest.

References

- [1] M. A. Alonso-Zarazaga, C. H. C. Lyal, *A world catalogue of families and genera of curculionoidea (Insecta: Coleoptera) (Excepting scolytidae and platypodidae)*, Entomopraxis, Barcelona, 1999.
- [2] R. C. Marinoni, N. G. Ganho, M. L. Monné, J. R. M. Mermudes, *Hábitos alimentares em Coleoptera (Insecta)*, Ribeirão Preto, Holos, 2001.
- [3] J. Rheinheimer, *Illustrater katalog und bibliographie der Anthribidae der welt (Insecta: Coleoptera)*, Mitteilungen des Entomologischen Vereins Stuttgart 39 (2004) 3–242.
- [4] J. Mermudes, R. Leschen, *Anthribidae Billberg, 1820*, in: R. A. B. Leschen, R. G. Beutel (Eds.), *Morphology and Systematics*, Vol. 3 of *Handbook of Zoology*, De Gruyter, Berlin, 2014, Ch. 3.2, pp. 309–315.
- [5] P. D. N. Hebert, A. Cywinska, S. L. Ball, J. R. deWaard, *Biological identifications through DNA barcodes*, *Proceedings of the Royal Society B: Biological Sciences* 270 (1512) (2003) 313–321.
- [6] G. Yatkın, N. Güz, *The Use of DNA Barcoding in Entomology*, *Yuzuncu Yıl University Journal of Agricultural Sciences* 28 (1) (2018) 126–134.
- [7] G. Kuschel, *A phylogenetic classification of Curculionoidea to families and subfamilies*, *Memoirs of the Entomological Society of Washington* 14 (1995) 5–33.
- [8] R. A. Crowson, *On the systematic position of Bruchela Dejean (Urodon Auctt.) (Coleoptera)*, *The Coleopterists Bulletin* 38 (1) (1984) 91–93.
- [9] B. A. Holloway, *Anthribidae (Insecta: Coleoptera)*, *Fauna of New Zealand* 3 (1982) 1–269.
- [10] C. J. Schoenherr, *Curculionidum dispositio methodica, cum generum characteribus, descriptionibus atque observationibus variis, seu Prodromus ad Synonymiae, insectorum partem IV*, Fleischer, Lipsiae, 1826.
- [11] P. A. Latreille, *Suite et fin des Insectes*, Vol. 5 of *Le Règne Animal distribué d’après son organisation, pour servir de base à l’histoire naturelle des animaux et d’introduction à l’anatomie compare*, Nouvelle édition, revue et augmentée, Déterville, Paris, 1829.
- [12] T. Lacordaire, *Histoire naturelle des insectes. Genera des coléoptères, ou exposé méthodique et critique de tous les genres proposés jusqu’ici dans cet ordre d’insectes*, Vol. 6, Roret, Paris, 1863.
- [13] T. Lacordaire, *Histoire naturelle des insectes. Genera des coléoptères, ou exposé méthodique et critique de tous les genres proposés jusqu’ici dans cet ordre d’insectes*, Vol. 7., Roret, Paris, 1865.
- [14] R. G. Oberprieler, *3. Curculionoidea Latreille, 1802: Introduction, Phylogeny*, Vol. 3 of *Handbook of Zoology*, De Gruyter, Berlin, München, Boston, 2014, Ch. 3, pp. 285—300.
- [15] A. E. Marvaldi, J. J. Morrone, *Phylogenetic systematics of weevils (Coleoptera: Curculionoidea): A reappraisal based on larval and adult morphology*, *Insect Systematics & Evolution* 31 (1) (2000) 43–58.
- [16] E. Marvaldi, A. S. Sequeira, C. W. O’Brien, B. D. Farrell, *Molecular and morphological phylogenetics of weevils (Coleoptera, Curculionoidea): Do niche shifts accompany diversification?*, *Systematic Biology* 51 (5) (2002) 761–785.

- [17] S. Kumar, G. Stecher, M. Li, C. Knyaz, K. Tamura, *MEGA X: Molecular evolutionary genetics analysis across computing platforms*, *Molecular Biology and Evolution* 35 (6) (2018) 1547–1549.
- [18] R. C. Edgar, *MUSCLE: Multiple sequence alignment with high accuracy and high throughput*, *Nucleic Acids Research* 32 (5) (2004) 1792–1797.
- [19] M. Kimura, *A simple method for estimating evolutionary rate of base substitutions through comparative studies of nucleotide sequences*, *Journal of Molecular Evolution* 16 (2) (1980) 111–120.
- [20] A. A. Legalov, *The first record of anthribid beetle[s] from the Jurassic of Kazakhstan (Coleoptera: Anthribidae)*, *Paleontological Journal* 45 (6) (2011) 629–633.



Heterogeneous Photo-Fenton-like Degradation of Oxytetracycline Containing Wastewater

Ceren Orak¹ , Gülin Ersöz² 

¹Department of Chemical Engineering, Faculty of Engineering and Applied Sciences, Sivas University of Science and Technology, Sivas, Türkiye

²Department of Chemical Engineering, Faculty of Engineering, Ege University, İzmir, Türkiye

Article History

Received: 24 Nov 2023

Accepted: 20 Jan 2024

Published: 15 Mar 2024

Research Article

Abstract – Oxytetracycline (OTC) is a commonly used antibiotic. It can be absorbed to a limited extent by both humans and animals, so it can be detected at various levels in different water sources. Its presence in rivers or water and wastewater streams can pose serious problems for human and environmental health, and therefore, it needs to be treated. OTC degradation was studied using iron-doped g-C₃N₄ through a photo-Fenton-like oxidation process under simulated sunlight. In this study, the effects of key reaction parameters such as pH (3, 6, 9), catalyst amount (0-0.8 g/L), initial hydrogen peroxide concentration (HP, 0-20 mM) on the degradation of oxytetracycline were studied. The optimal reaction conditions for OTC degradation were found to be pH=6, catalyst amount of 0.4 g/L, and HP of 10 mM. Subsequently, the temperature effect was examined at the optimum reaction conditions. Based on the results, at 25, 35, and 45 °C, OTC degradation was found to be 51.1%, 60.8%, and 76.7%, respectively. The kinetic study conducted revealed that the observed reaction follows a second-order reaction kinetic model. In addition, the activation energy of observed reaction was found to be 86.96 kJ/mol.

Keywords – Oxytetracycline, Fe doped g-C₃N₄, photocatalysis, kinetic study

1. Introduction

Due to the common use of oxytetracycline (OTC) in veterinary medicine, agriculture, aquaculture, and horticulture, residues of OTC have been detected in various water flows, including natural surface waters (up to 200 ppb with a detection frequency of up to 90%) and wastewater treatment effluents (ranging from 0.061 to 23.6 ppb). Additionally, it has been found in vegetable farm soils and livestock, with concentrations reaching up to 2.98 mg/kg. OTC is acutely toxic, posing a threat to ecosystems and human health. Its limited absorption by animals and humans allows it to be excreted into the environment. Therefore, its widespread existence in the environment and its harmful effects on human and environmental health have led to the search for various ways to remove this harmful compound [1-3].

Advanced Oxidation Processes (AOPs) offer an alternative approach for breaking down recalcitrant compounds into biologically degradable compounds. Considering the studies in the literature, heterogeneous systems are found to be highly efficient in degrading organic compounds. Solar-Fenton-like oxidation, subset of AOPs, offers several advantages, including low-cost, high removal rate, easy operation, and capability to stimulate complete mineralization [4,5]. Thanks to these noteworthy properties, it has garnered interest, and it could be used to degrade oxytetracycline. Graphitic carbon nitride (CN) is sensitive to visible light owing to its narrow bandgap energy (~2.7 eV) and possesses some prominent features such as non-toxicity, low cost,

¹cerenorak@sivas.edu.tr (Corresponding Author); ²gulin.ersoz@ege.edu.tr

and chemical stability. Bandgap tuning can be achieved through metal doping, thereby enhancing the removal efficiency [6-9]. Therefore, metal-doped CN has become a promising photocatalyst to remove recalcitrant compounds under sunlight.

In this study, the aim was to remove OTC-containing wastewater in the presence of iron-doped graphitic carbon nitride (FeCN) containing 5% Fe under simulated sunlight. Within this scope, the impact of pH, catalyst amount, initial hydrogen peroxide concentration, and temperature on degradation efficiency was examined, and optimum reaction conditions were determined. Additionally, a kinetic study was conducted.

2. Materials and Methods

The chemicals, namely, urea, iron (III) chloride, NaOH, HCl, and H₂O₂ (HP), utilized during the experimental study were purchased from Sigma Aldrich. Oxytetracycline hydrochloride (OTC) was purchased from Doğa İlaç.

Catalyst preparation: Metal-doped CN (Fe/g-C₃N₄) was synthesized based on the following procedure: To synthesize 5w.% iron containing Fe/g-C₃N₄ (5FeCN), urea (20 g) and the needed amount of iron (III) chloride to obtain 5FeCN were put in a ceramic pot and then, it placed into a muffle oven. Then, N₂ atmosphere was created by feeding N₂ into the oven. Then, the mixture underwent heating to 550 °C at 30-minute intervals. Upon reaching 550 °C, it was maintained at 550 °C for a duration of 3 hours. Subsequently, it was gradually cooled to 25 °C. Following this, the solid residue underwent a washing process using ultrapure water. Then, it was filtered to separate the final residue and dried at 25 °C [10]. A characterization study was carried out by SEM (FEI QUANTA 250 FEG model) with 1000x magnification and BET (Micromeritics ASAP 2010) analyses. The catalysts (CN and 5FeCN) were coated with Au/Pd before SEM analysis, and they were degassed at 300 °C for 2 h before BET analysis. BET surface areas were determined at 77 K using a multipoint BET method.

The experimental study was performed using 10 ppm OTC solution (100 mL) for a duration of 1 h under simulated solar light illumination. In this context, a typical experiment was carried out as follows: 10 ppm OTC solution (100 mL) was placed into the beaker without any pH adjustment and then, the desired amount (i.e., 0.1 g/L) of 5FeCN and the desired amount of HP (i.e., 10 mM) were added. After that, the solar light was turned on to start the reaction. Every ten minutes throughout the reaction, liquid samples (2 mL) were collected by taking from the beaker. In the experimental study, the impact of reaction parameters such as pH (3-9), HP (0-20 mM), and catalyst amount (0-0.8 g/L) was investigated to find the optimum reaction conditions for OTC removal %. A spectrophotometer (Spectroquant® NOVA 400 spectrophotometer) was used to analyze the liquid samples.

The removal of OTC was assessed by monitoring the reduction in its distinctive absorption band, situated at 275 nm. The diminishing intensity of this band suggests the opening of rings containing N-groups during the course of the reaction.

$$\% \text{ Degradation of OTC} = \frac{A_{0 \text{ at } 275 \text{ nm}} - A_{t \text{ at } 275 \text{ nm}}}{A_{t \text{ at } 275 \text{ nm}}} \times 100$$

The investigation into the kinetics was conducted under optimal reaction conditions at temperatures of 25, 35, and 45 °C. The gathered data was then scrutinized using both first and second-order reaction kinetic models.

3. Results and Discussion

SEM analysis was employed to determine morphological changes and SEM diagrams of pristine CN and 5FeCN are given in Figure 1. Whereas CN exhibited a substantial layered structure, 5Fe-CN exhibited a sheet-like structure reminiscent of CN, indicating that the incorporation of iron did not induce any alteration in the CN structure. This observation aligns with similar morphologies reported in the literature [11-13]. BET surface area of 5FeCN was found as 3.01 m²/g. Comparatively, literature sources have reported BET areas for FeCN (0-1 wt.% Fe) ranging between 3.404 and 5.4 m²/g for various iron concentrations [14]. Thus, it could be deduced that 5FeCN was successfully synthesized.

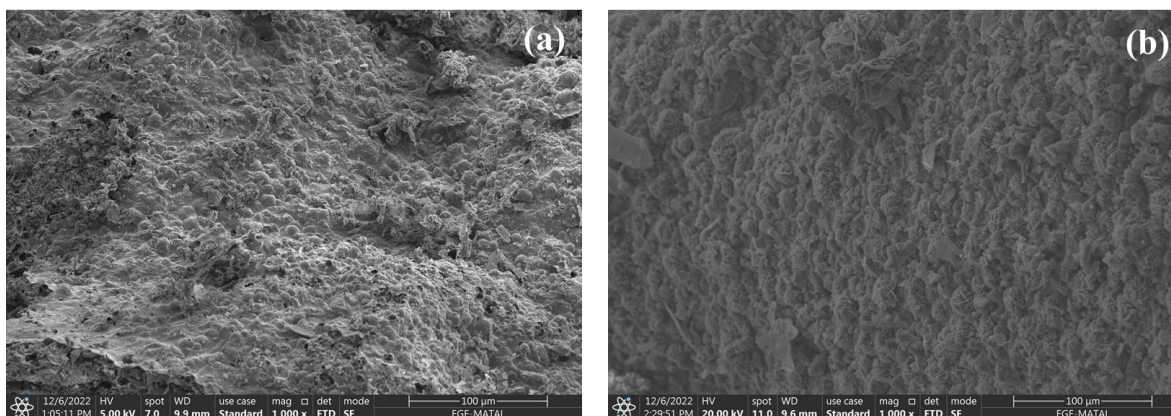


Figure 1. SEM diagrams of CN (a) and 5FeCN (b)

After the characterization study, the effect of reaction parameters was investigated to determine the optimum reaction conditions for OTC removal under simulated solar light illumination. Firstly, the effect of catalyst amount was investigated at different amounts of 5FeCN varied between 0 and 0.8 g/L, and the results are given in Figure 2. OTC degradation efficiency enhanced by increasing the amount of catalyst up to 0.4 g/L and almost the same degradation efficiency was achieved for 0.4 and 0.8 g/L of catalyst amounts. The highest degradation (51.1%) was obtained using 0.4 g/L of 5FeCN and therefore, the optimum catalyst loading was selected as 0.4 g/L and then, the effect of HP was investigated using 0, 5, 10 and 20 mM of HP, and the results are given in Figure 3.

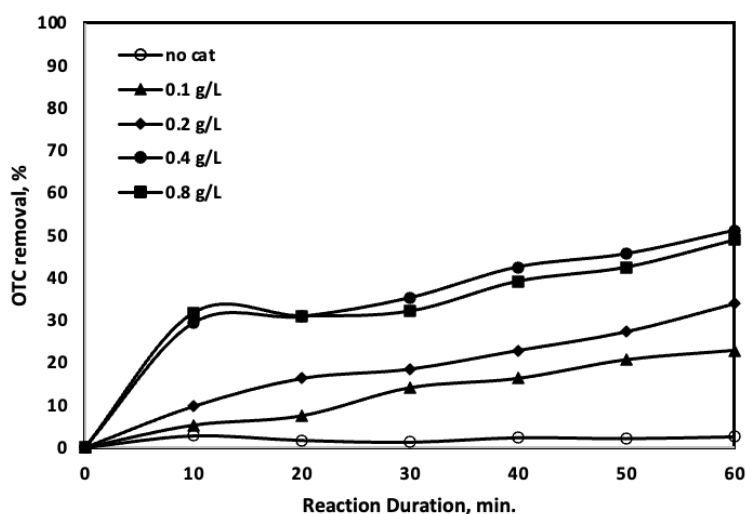


Figure 2. Effect of catalyst amount (Reaction conditions: 10 ppm OTC, pH=6, HP=10 mM)

Based on the results, the lowest efficiency (~12%) was achieved in the absence of HP on the other hand the highest efficiency was observed as 51.1% using 10 mM of HP. HP is an electron acceptor and it is better than

the molecular oxygen. It led to a decrease in the rate of electron-hole recombination and hence, an increase in degradation efficiency might be achieved. Furthermore, depending on the wavelength of the incident radiation, HP has the potential to generate hydroxyl radicals through photolytic splitting. It may help prevent oxygen starvation in the wastewater, which could otherwise occur due to insufficient oxygenation or limitations in mass transfer. In addition, the direct reaction of HP with photogenerated holes, along with its adsorption onto the photocatalyst, has the potential to enhance charge transfer rates on the semiconductor surface [15-17]. However, the excess usage of HP (20 mM) caused the scavenging effect and thus, the removal efficiency decreased. Considering the results, the optimum HP concentration was selected as 10 mM.

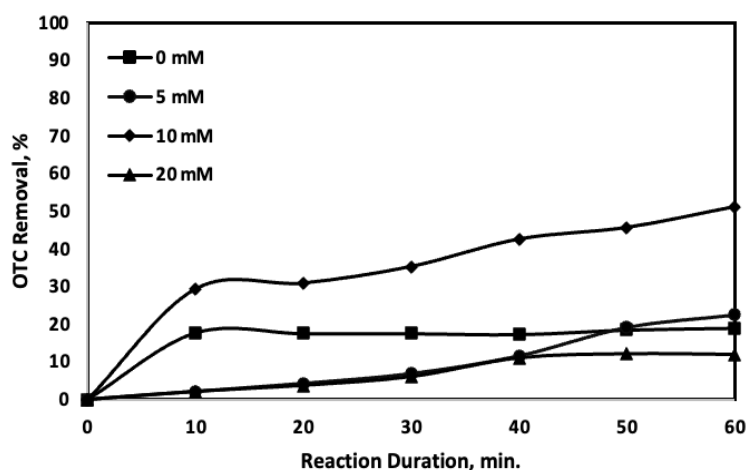


Figure 3. Effect of HP (Reaction conditions: 10 ppm OTC, pH=6, 0.4 g/L 5FeCN)

In photocatalytic degradation of organic pollutants, pH is a key parameter since it might change the ion (H^+ and OH^-) concentration. The change in ion concentration has an impact on the formation of reactive species (i.e., superoxide and hydroxyl radicals, etc.) and it is directly linked to the degradation efficiency of organic pollutants [18]. Therefore, the effect of pH was investigated at pH of 3, 6, and 9, and the results are given in Figure 4. Almost 41% and 51.1% of degradation were achieved at pH=3 and pH=6, respectively. However, 21.7% of OTC degraded at pH=9. pH_{zpc} of 5FeCN was determined as 7.2 and hence, higher degradation efficiency was observed under this value. At pH 6, there is an attraction between negatively charged 5FeCN and positively charged OTC, and thus, the degradation efficiency was high. Consequently, the optimum pH value was chosen as 6.

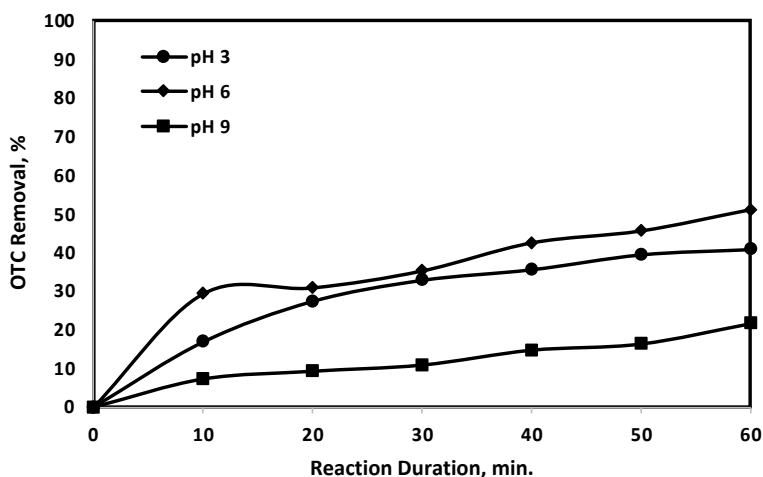


Figure 4. Effect of pH (Reaction conditions: 10 ppm OTC, 0.4 g/L 5FeCN, HP=10 mM)

Following the determination of optimal reaction conditions (pH=6, catalyst amount=0.4 g/L, and HP=10 mM), the kinetic study was conducted at varying reaction temperatures (25, 35, and 45 °C) over a 20-minute reaction duration. To comprehend the nature of OTC degradation, both first and second-order reaction kinetic models were applied. The experimental data show a strong alignment with the second-order reaction kinetic model considering the R² values. The linearized form of experimental data is given in Figure 5 and from this figure, the reaction kinetic rate constants of the observed reaction were found as 0.0004, 0.002, and 0.0036 (mg/L/min) for 25, 35, and 45 °C, respectively. From Figure 6, the activation energy of the observed reaction was found as 86.96 kJ/mol. (Figure 6, the gas constant R=8.3145 J/K mol). To understand the impact of temperature on OTC degradation, the reactions lasted for 1 hour, and based on the results, at the end of the 1 hour of reaction duration, 51.1, 60.8%, and 76.7 % of OTC was degraded at 25, 35, and 45 °C, respectively.

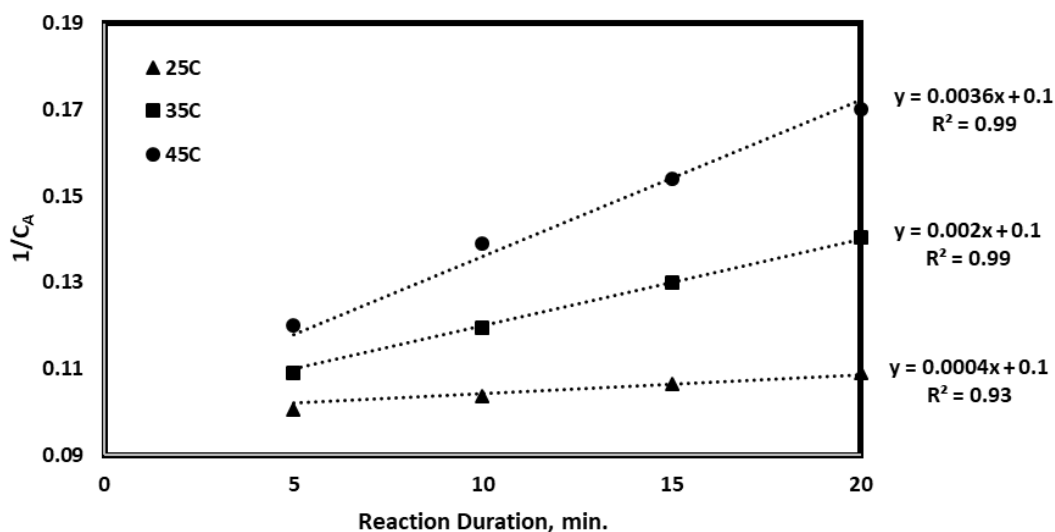


Figure 5. Linearized second-order kinetic plot (Reaction conditions: 10 ppm OTC, 0.4 g/L of 5FeCN, pH 6, 10 mM of HP)

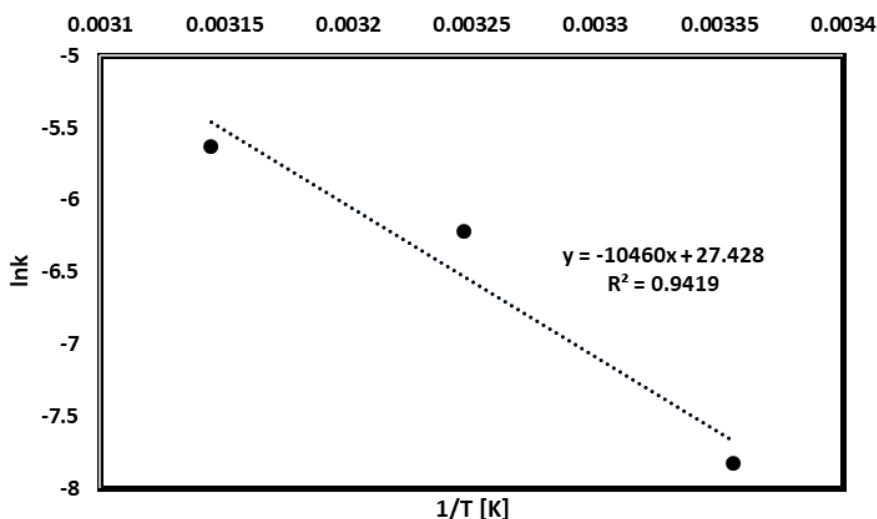


Figure 6. Arrhenius plot

In the literature, various photocatalysts were used to treat OTC. In particular, TiO₂ and TiO₂-based photocatalysts as well as semiconductor oxides were tested. A brief summary is given in Table 1.

Table 1. A brief summary of OTC degradation using various photocatalysts

Photocatalysts	OTC concentration (ppm)	Catalyst amount (g/L)	Degradation (%)	References
TiO ₂ nanoflowers	0.5	5	80	[19]
Brown TiO ₂ spheres	5	5	~50	[20]
BiOCl/TiO ₂ hollow tubes	20	0.5	51	[21]
CdS/TiO ₂	40	1	81	[22]
Fe ₃ O ₄	46	0.5	42	[23]
LaFeO ₃	40	0.5	~50	[24]
ZnO	46	0.5	41	[25]
NiFe ₂ O ₄	46	0.5	65	[7]
MnFe ₂ O ₄	46	0.5	<50	[26]
CN/LaFeO ₃ (2%)	40	0.5	90	[24]
CN/NiFe ₂ O ₄	46	10	97	[7]
N-ZnO/CdS/GO	20	0.5	50	[27]
Ag(8%)/CN	20	1	81	[28]
Fe(5%)/CN	20	0.4	51.1	This study

In this study, almost the same degradation efficiency was achieved using a relatively lower catalyst amount compared to the used amounts in the literature. For example, almost %50 of OTC degradation was achieved using 5 g/L of brown TiO₂ spheres [20] while 0.4 g/L FeCN was used to obtain almost the same degradation efficiency in this study. %41 of OTC was degraded using 0.5 g/L of ZnO [25] while relatively higher degradation efficiency was obtained in this study. 1 g/L of Ag(8%)/CN was used to treat OTC and %81 of OTC degradation was achieved [28]. However, Ag is an expensive metal so usage of a cheaper metal (iron) could be an alternative solution to treat OTC. Therefore, FeCN could be considered a promising photocatalyst for OTC degradation.

4. Conclusion

OTC is an antibiotic and due to its common usage, the unabsorbed OTC by humans and animals might be detected in different water sources and could threaten human and environmental health. Therefore, it should be treated, and in this study, OTC was degraded via photo-Fenton-like oxidation using 5FeCN under solar light irradiation, and optimum reaction conditions were selected as 6 of pH, 0.4 g/L of catalyst amount (5FeCN), and 10 mM of HP. Then, a kinetic study was conducted at the optimal reaction conditions and the observed reaction followed the second order-reaction kinetic model. In addition, the activation energy for this observed reaction was calculated to be 86.96 kJ/mol. Therefore, FeCN is a promising photocatalyst for the degradation of oxytetracycline.

Author Contributions

The first author performed the experiment and wrote the manuscript. The second author reviewed and edited the paper. All authors read and approved the final version of the paper.

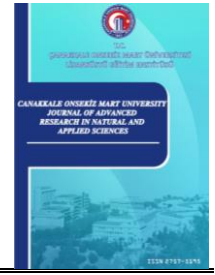
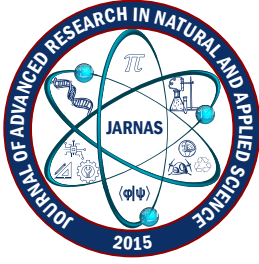
Conflicts of Interest

All the authors declare no conflict of interest.




References

- [1] P. Raizada, P. Shandilya, P. Singh, P. Thakur, *Solar light-facilitated oxytetracycline removal from the aqueous phase utilizing a H₂O₂/ZnWO₄/CaO catalytic system*, Journal of Taibah University for Science 11 (5) (2017) 689–699.
- [2] H. Wang, M. Zhang, X. He, T. Du, Y. Wang, Y. Li, T. Hao, *Facile prepared ball-like TiO₂ at GO composites for oxytetracycline removal under solar and visible lights*, Water Research 160 (2019) 197–205.
- [3] Y. Wang, J. Zhou, W. Bi, J. Qin, G. Wang, Z. Wang, P. Fu, F. Liu, *Schwertmannite catalyze persulfate to remove oxytetracycline from wastewater under solar light or UV-254*, Journal of Cleaner Production 364 (2022) 132572 10 pages.
- [4] Y. Jiang, J. Ran, K. Mao, X. Yang, L. Zhong, C. Yang, X. Feng, H. Zhang, *Recent progress in Fenton/Fenton-like reactions for the removal of antibiotics in aqueous environments*, Ecotoxicology and Environmental Safety 236 (2022) 113464 20 pages.
- [5] J. Lin, W. Tian, Z. Guan, H. Zhang, X. Duan, H. Wang, H. Sun, Y. Fang, Y. Huang, S. Wang, *Functional carbon nitride materials in photo-fenton-like catalysis for environmental remediation*, Advanced Functional Materials 32 (24) (2022) 2201743 31 pages.
- [6] J. Jiang, S. Cao, C. Hu, C. Chen, *A comparison study of alkali metal-doped g-C₃N₄ for visible-light photocatalytic hydrogen evolution*, Cuihua Xuebao/Chinese Journal of Catalysis 38 (12) (2017) 1981–1989.
- [7] A. Sudhaik, P. Raizada, P. Shandilya, P. Singh, *Magnetically recoverable graphitic carbon nitride and NiFe₂O₄ based magnetic photocatalyst for degradation of oxytetracycline antibiotic in simulated wastewater under solar light*, Journal of Environmental Chemical Engineering 6 (4) (2018) 3874–3883.
- [8] E. Fernandes, J. Gomes, R. C., Martins, *Semiconductors application forms and doping benefits to wastewater treatment: A comparison of TiO₂, WO₃, and g-C₃N₄*, Catalysts 12 (10) (2022) 1218 42 pages.
- [9] Q. Wang, Z. Fang, W. Zhang, D. Zhang, *High-efficiency g-C₃N₄ based photocatalysts for CO₂ reduction: modification methods*, Advanced Fiber Materials 4 (3) (2022) 342–360.
- [10] Z. Li, C. Kong, G. Lu, *Visible photocatalytic water splitting and photocatalytic two-electron oxygen formation over Cu- and Fe-doped g-C₃N₄*, Journal of Physical Chemistry C 120 (1) (2016) 56–63.
- [11] J. Hu, P. Zhang, W. An, L. Liu, Y. Liang, W. Cui, *In-situ Fe-doped g-C₃N₄ heterogeneous catalyst via photocatalysis-Fenton reaction with enriched photocatalytic performance for removal of complex wastewater*, Applied Catalysis B: Environmental 245 (2019) 130–142.
- [12] T. Ma, Q. Shen, B. Z. J. Xue, R. Guan, X. Liu, H. Jia, B. Xu, *Facile synthesis of Fe-doped g-C₃N₄ for enhanced visible-light photocatalytic activity*, Inorganic Chemistry Communications 107 (2019) 107451 9 pages.
- [13] M. N. Van, O. L. T. Mai, C. P. Do, H. L. Thi, C. P. Manh, H. N. Manh, D. P. Thi, B. D. Danh, *Fe-doped g-c₃n₄: High-performance photocatalysts in rhodamine b decomposition*, Polymers 12 (9) (2020) 1963 13 pages.
- [14] G. Liu, G. Dong, Y. Zeng, C. Wang, *The photocatalytic performance and active sites of g-C₃N₄ effected by the coordination doping of Fe(III)*, Chinese Journal of Catalysis 41 (10) (2020) 1564–1572.
- [15] N. S. Abbood, N. S. Ali, E. H. Khader, H. S. Majdi, T. M. Albayati, N. M. C. Saady, *Photocatalytic degradation of cefotaxime pharmaceutical compounds onto a modified nanocatalyst*, Research on Chemical Intermediates 49 (1) (2023) 43–56.

- [16] D. D. Dionysiou, M. T. Suidan, E. Bekou, I. Baudin, J.-M. L. L  n  , *Effect of ionic strength and hydrogen peroxide on the photocatalytic degradation of 4-chlorobenzoic acid in water*, Applied Catalysis B: Environmental 26 (3) (2000) 153–171.
- [17] R. Ullah, F. Khitab, H. Gul, R. Khattak, J. Ihsan, M. Khan, A. Khan, Z. Vincevica-Gaile, H. A. Aouissi, *Superparamagnetic zinc ferrite nanoparticles as visible-light active photocatalyst for efficient degradation of selected textile dye in water*, Catalysts 13 (7) (2023) 1061 19 pages.
- [18] Z. Ur Rahman, U. Shah, A. Alam, Z. Shah, K. Shaheen, S. Bahadar Khan, S. Ali Khan, *Photocatalytic degradation of cefixime using CuO-NiO nanocomposite photocatalyst*, Inorganic Chemistry Communications 148 (2023) 110312 9 pages.
- [19] J. Singh, R. K. Soni, *Fabrication of hydroxyl group-enriched mixed-phase TiO₂ nanoflowers consisting of nanoflakes for efficient photocatalytic activity*, Journal of Materials Science: Materials in Electronics 31 (15) (2020) 12546–12560.
- [20] J. Singh, S. Palsaniya, R. K. Soni, *Mesoporous dark brown TiO₂ spheres for pollutant removal and energy storage applications*, Applied Surface Science 527 (15) (2020) 146796 10 pages.
- [21] S. Bao, H. Liang, C. Li, J. Bai, *A heterostructure BiOCl nanosheets/TiO₂ hollow-tubes composite for visible light-driven efficient photodegradation antibiotic*, Journal of Photochemistry and Photobiology A: Chemistry 397 (2020) 112590 10 pages.
- [22] Y. B. Du, L. Zhang, M. Ruan, C. G. Niu, X. J. Wen, C. Liang, X. G. Zhang, G. M. Zeng, *Template-free synthesis of three-dimensional porous CdS/TiO₂ with high stability and excellent visible photocatalytic activity*, Materials Chemistry and Physics 212 (2018) 69–77.
- [23] P. Raizada, J. Kumari, P. Shandilya, R. Dhiman, V. Pratap Singh, P. Singh, *Magnetically retrievable Bi₂WO₆/Fe₃O₄ immobilized on graphene sand composite for investigation of photocatalytic mineralization of oxytetracycline and ampicillin*, Process Safety Environmental Protection 106 (2017) 104–116.
- [24] K. Xu, X. Yang, L. Ruan, S. Qi, J. Liu, K. Liu, S. Pan, G. Feng, Z. Dai, X. Yang, R. Li, J. Feng, *Superior adsorption and photocatalytic degradation capability of mesoporous LaFeO₃ /g-C₃N₄ for removal of oxytetracycline*, Catalysts 10 (3) (2020) 301 18 pages.
- [25] P. Raizada, J. Kumari, P. Shandilya, P. Singh, *Kinetics of photocatalytic mineralization of oxytetracycline and ampicillin using activated carbon supported ZnO/ZnWO₄ nanocomposite in simulated wastewater*, Desalination and Water Treatment 79 (2017) 204–213.
- [26] S. Gautam, P. Shandilya, B. Priya, V. P. Singh, P. Raizada, R. Rai, M. A. Valente, P. Singh, *Superparamagnetic MnFe₂O₄ dispersed over graphitic carbon sand composite and bentonite as magnetically recoverable photocatalyst for antibiotic mineralization*, Separation and Purification Technology 172 (2017) 498–511.
- [27] P. Huo, M. Zhou, Y. Tang, X. Liu, C. Ma, L. Yu, Y. Yan, *Incorporation of N-ZnO/CdS/Graphene oxide composite photocatalyst for enhanced photocatalytic activity under visible light*, Journal of Alloys and Compounds 670 (2016) 198–209.
- [28] Z. Ren, F. Chen, K. Wen, J. Lu, *Enhanced photocatalytic activity for tetracyclines degradation with Ag modified g-C₃N₄ composite under visible light*, Journal of Photochemistry and Photobiology A: Chemistry 389 (2020) 112217 12 pages.



Polielektrolitlerin Molekül Ağırlığı ve Harman Oranının Çok Tabakalı Filmlerin Gelişimine Etkisinin ve İlaç Adsorpsiyon/Desorpsiyon Uygulamalarında Kullanımlarının QCM-D Tekniğiyle Takibi

Dilara Yılmaz-Ayktut¹ , Öznur Yolaçan² , Hüseyin Deligoz³ 

^{1,2,3}Kimya Mühendisliği Bölümü, Mühendislik Fakültesi, İstanbul Üniversitesi-Cerrahpaşa, İstanbul, Türkiye

Öz – Bu çalışmada, harman zayıf ve kuvvetli polielektrolit çiftlerinin kullanımı ile tabakalı kaplama, layer-by-layer (LbL), yöntemi ile çok tabakalı fonksiyonel ince filmlerin kontrol edilebilir kalınlıkta, kompozisyonda, morfolojide hazırlanması ve ilaç salımında kullanımları araştırılmıştır. Kuartz Kristal Mikrobalsan-Dissipasyon (QCM-D) tekniği ile kendi kendine bir araya gelen saf/harman yapıları LbL ince filmlerin gelişimlerinin nanogram seviyesinde takibi, ilaç yükleme/salım karakterizasyonu, model ilaç ile LbL film yüzeyi arası etkileşimler ve filmlerin ilaçla etkileşimde viskoelastik değişimleri başarıyla incelenmiştir. Ayrıca, hazırlanan çok tabakalı harman fonksiyonel ince filmlerin gelişiminin takibi için UV ve QCM-D analizi gerçekleştirilerek harman film yapısındaki polielektrolit oranları tespit edilmiştir. Ek olarak, LbL saf/harman yapıları ince filmlerin kontrol edilebilir yüzey ve topografik özelliklerinin kullanılan biyobozunur ve sentetik polielektrolit çiftlerine, harman oranına ve LbL kaplama koşullarına bağlı olarak değişimlerinin incelenmesi amacıyla taramalı elektron mikroskopu (SEM) analizleri ve yüzey temas açısı çalışmaları gerçekleştirilmiştir. Hazırlanan LbL saf/harman yapıları fonksiyonel filmlerde ibuprofen sodyum ilacı için yükleme ve salım çalışmaları QCM-D tekniği ve UV-Vis analizleriyle nötral (pH:6,8), asidik (pH:2) ve bazik (pH:11) fosfat tampon çözeltisinde (PBS) gerçekleştirilmiştir. Çalışmada, ilaç salım sistemleri için yenilikçi, ekonomik ve pratik bir yaklaşımın sunulmasının yanı sıra; LbL kaplama koşullarına bağlı olarak (i) morfolojisi ve kompozisyonu kontrol edilebilen, (ii) ilaç yükleme ve salım özellikleri ayarlanabilen ve geniş bir pH (pH:2-11) aralığında ilaç salımı yapabilen sistemler geliştirilmiştir. Elde edilen sonuçlar, ilaç uygulamaları için LbL fonksiyonel filmlerin yapısına, yüzey özelliklerine, ortamın pH'ına ve ilaç-film arası etkileşimine bağlı olarak farklılıklar taşınması gerektiğini göstermiştir. LbL tekniğiyle fonksiyonel filmlerin kontrol edilebilen özelliklerde hazırlanması ve ilaç salım uygulamalarında kullanılması oldukça ümit verici sonuçlar vermiştir.

Makale Tarihiçesi

Gönderim: 20 Aralık 2023

Kabul: 20 Ocak 2024

Yayın: 15 Mart 2024

Araştırma Makalesi

Anahtar Kelimeler – İbuprofen adsorpsiyon/desorpsiyon, ince film, polielektrolit çok tabakalar, QCM-D, tabakalı kaplama

Monitoring the Effect of Molecular Weight and Blend Ratio of Polyelectrolytes on the Development of Multilayer Films and Their Use in Drug Adsorption/Desorption Applications by QCM-D Technique

^{1,2,3}Department of Chemical Engineering, Faculty of Engineering, İstanbul University-Cerrahpaşa, İstanbul, Türkiye

Article History

Received: 20 Dec 2023

Accepted: 20 Jan 2024

Published: 15 Mar 2024

Research Article

Abstract – In this study, the preparation of multilayered functional films with controllable thickness composition and morphology using the Layer-by-Layer (LbL) technique from weak and strong polyelectrolyte couples and the use of dairy in the release of different structured drugs have been studied. Besides, following the growth of self-assembled pure/blend LbL thin films at the nanogram level, interaction with the model drug LbL film surfaces in drug loading and release characterizations and viscoelastic changes of films intructed with drugs have been

¹dilarayilmaz77@gmail.com; ²oznur.yolacan@hotmail.com; ³hdeligoz@iuc.edu.tr (Corresponding Author)

successfully investigated. Moreover, UV-Vis and QCM-D analyses have been performed to follow the growth of LbL functional thin films and to find polyelectrolyte ratios in film structure. In addition, scanning electron microscopy (SEM) and contact angle measurements have been carried out to investigate the controllable surface of LbL pure/blend structured thin films depending on the use of biodegradable and synthetic polyelectrolyte couples, blend ratio, and LbL deposition conditions. Subsequently, drug loading and release stabilities for the ibuprofen sodium drug have been performed using QCM-D and UV-Visible at neutral (pH: 6.8) acidic (pH: 2) and basic (pH: 11) PBS solutions. In addition to offering an innovative, economic, and practical approach, new drug release platforms with (i) surfaces of controllable morphology and composition, (ii) adjustable loading and release properties for model drugs, and (iii) sustainable drug release in wide range of pH: 2-11, have been developed. The obtained results show that LbL functional films must have different properties considering the surface properties of the film, the pH of the media, the interaction between drug and film for drugs, and their applications. In this respect, the preparation of functional films with controllable properties using the LbL technique and their use in drug release applications exhibit quite promising results.

Keywords – *Ibuprofen adsorption/desorption, thin films, polyelectrolyte multilayers, QCM-D, Layer-by-Layer (LbL)*

1. Giriş

Günümüzde fonksiyonel ince film teknolojisinin gelişmesine bağlı olarak biyoteknoloji [1], enerji [2] ve membran [3] teknolojileri gibi alanlarda önemli gelişmeler yaşanmaktadır. Fonksiyonel ince filmlerin ilaç salım uygulamalarında kullanımlarının son yıllarda büyük ilgi çekmesi, yeni ve alternatif yaklaşımların araştırılmasına neden olmaktadır. Bu yaklaşımlar arasında farklı kullanım alanlarına sahip ince filmlerin yüzey özelliklerini kontrol edebilmek için tabakalı kaplama (Layer-by-Layer) (LbL) yöntemi ümit verici bir teknik olarak geçen yıllarda öne çıkmıştır. LbL tabakalı kaplama yöntemine ait ilk çalışmalar 1990'lı yıllarda yüzeyi hidrofille edilmiş nano ya da mikro gözeneklere sahip membran destekler üzerinde Gero Decher tarafından gerçekleştirilmiştir [4]. Bu yöntemde, yüzeyi hidrofille edilen membran desteğin pozitif yüklü ve negatif yüklü polielektrolitin sulu çözeltisine daldırılmasıyla yüzeyinde ince bir tabaka adsorbe olur. Ardından bu malzemenin tekrar zıt yüklü polielektrolit çözeltisine daldırılmasıyla membran desteğin yüzey yükü değişir. Bu adsorpsiyon adımlarının ardışık olarak çoklu tekrarlanmasıyla, sıralı pozitif veya negatif yüklerden oluşan çok tabakalı film meydana gelmektedir.

Harman polielektrolitlerden LbL tekniği kullanılarak fonksiyonel ince filmlerin hazırlanması ve bu sistemlerin ilaç salım uygulamalarında kullanımlarına yönelik grubumuz ve P. T. Hammond'ın grubunun gerçekleştirdiği öncü araştırmalar bulunmaktadır [5-9]. Sunulan bu yeni yaklaşımla birlikte LbL harman yapıları fonksiyonel ince filmlerin konvansiyonel filmlere göre; daha hassas film kalınlığı, morfolojisi, kompozisyonu ve ıslatılabilirlik özelliği kontrolü nedeniyle geniş bir pH (pH: 2-10) aralığında sürdürülebilir, kontrol edilebilir ilaç salımına sahip olması beklenmektedir [10]. Kuartz Kristal Mikrobals-Dissipasyon (QCM-D) sistemi, son yıllarda LbL ince film tekniği ile üretilen filmlerin karakterizasyonu için kullanılan tekniklerden birisi olarak dikkat çekmektedir [11-13]. Bu tekniğin tercih edilmesinin en önemli nedenleri, çok küçük kütle değişimlerine bile hassas olması ve adsorban ile adsorbent arasındaki etkileşimin hassas biçimde belirlenebilmesidir [14,15]. Tekniğin bu özelliği, çok tabakalı LbL ince filmlerin üretilebilirliği ve yapıların tabaka kontrolü için de kullanılmasına olanak sağlamasıdır.

Bu çalışmada, ilaç salım sistemleri için yenilikçi, LbL yöntemiyle kontrol edilebilen kalınlıkta, morfolojide çok tabakalı saf ve harman yapıları polielektrolit fonksiyonel filmlerin hazırlanması, ilaç uygulamalarında kullanımlarının incelenmesi, QCM-D tekniği ile tabaka gelişimlerinin incelenmesi, çeşitli karakterizasyon uygulamaları araştırılmıştır. Bu kapsamda; QCM-D tekniği ile saf ve harman yapıları çok tabakalı fonksiyonel filmlerin zayıf Poli(alilamin hidroklorit) (PAH) ve zayıf anyonik polielektrolit olarak Poliakrilik asit (PAA), kuvvetli anyonik polielektrolit olarak Poli(4-stiren sülfonik asit) sodyum tuzu (PSS) kullanımıyla saf ve harman yapıları çok tabakalı fonksiyonel filmlerin hazırlanması ve tabaka sayısına bağlı olarak adsorplanan

madde miktarı deęişimlerinin QCM-D teknięi ile izleme çalıřmaları gerekleřtirilmiřtir. Ayrıca iki farklı molekül aęırlıęına sahip (Mw: 450.000, Mw: 5.000) PAA kullanımı incelenmiřtir. Hazırlanan ok tabakalı filmlerin QCM-D ve zel UV-Suprasil kuartz cam yzeyle kaplanarak gerekleřtirilen UV-Vis, yzey temas aısı ve SEM analizleriyle detaylı karakterizasyonu tamamlanmıřtır.

İla uygulamalarında kullanılmak zere, yeni tip ok tabakalı saf ve harman polielektrolit fonksiyonel filmlerin hazırlanması ve QCM-D teknięi ile tabaka geliřimlerinin incelenmesi arařtırılmıřtır. alıřma kapsamında bařlıca bařlıca; (a) ok tabaka oluřumu/geliřimi zerine farklı molekül aęırlıęı ve zelliklere sahip polielektrolit zeltilerinin kullanımı, (b) ila adsorbsiyon/desorpsiyonu ve ok tabakalı film ile model ila etkileřimi, (c) model ilacın LbL ok tabaka hazırlanmasında kullanımı, (d) ok tabaka oluřumu/geliřiminin pH ve harman kompozisyonuna baęlı olarak UV-Vis analiziyle takibi, (e) saf ve harman LbL film detaylı yzey zelliklerinin (morfoloji ve ıslanabilirlik) SEM analizi ve temas aısı ile belirlenmesi, (f) saf ve harman LbL filmlerin aęırlıka bileřimlerinin ve kalınlıklarının tespiti ile (g) cam yzey zerine kaplanan model ila ieren filmlerin fosfat tampon zeltisi (PBS) ierisinde salımı řeklinde dir.

2. Materyal ve Yntem

Poli(alilamin hidroklorit) (PAH) (Mw: 15.000 g/mol), poli(4-stiren slfonik asit) sodyum tuzu (PSS) (Mw: 70.000 g/mol), sodyum klorr (NaCl) ($\geq\%99$), sodyum hidroksit (NaOH), hidroklorik asit (HCl) (%37), potasyum klorr (KCl), potasyum fosfat monobazik (KH_2PO_4), sodyum fosfat dibazik (Na_2HPO_4), izopropanol (2-propanol) ($\geq\%99,8$), metanol ($\geq\%99,9$), toluen ($\geq\%99,9$) ve 3-Aminopropilmetil-dietoksisilan Sigma-Aldrich (ABD) firmasından temin edilmiřtir. Slfrik asit (H_2SO_4) (%95-97), amonyum hidroksit (%26) Riedel-de-Haen (Kuzey Carolina, ABD) ve Poli(akrilik asit) (PAA) (Mw: 450.000 g/mol, Mw:5,000 g/mol) ise Polysciences (ABD) firmasından satın alınmıřtır. Azot gazı (%99,9) ise Linde (Wiesbaden, Almanya) firmasından tedarik edilmiřtir. Satın alınan kimyasallar herhangi bir ileri saflařtırma olmadan alıřmalarda kullanılmıřtır. Tabaka geliřim deneylerinin hepsinde $R=18.2 \text{ M}\Omega$ deęerine sahip ultra saf su kullanılmıřtır. Fosfat tampon zeltisinin hazırlanması iin KCl, KH_2PO_4 , Na_2HPO_4 ve NaCl belirli oranlarda 2 litre ultra saf su iinde manyetik karıřtırıcı yardımı ile zlmř ve denemelerde kullanılmak zere stok hazırlanmıřtır. Fosfat tampon zeltilerinin pH ayarları, 1 N HCl ve 1 N NaOH damla damla ilave edilerek pH=2/6,8/11 olarak ayarlanmıř ve oda sıcaklıęında muhafaza edilmiřtir.

2.1. Malzemeler ve Hazırlama Teknikleri

PAH (Mw: 15.000 g/mol), PSS (Mw: 70.000 g/mol), NaCl ($\geq\%99$), NaOH, HCl (%37), KCl, KH_2PO_4 , Na_2HPO_4 , 2-propanol ($\geq\%99,8$), metanol ($\geq\%99,9$), toluen ($\geq\%99,9$) ve 3-Aminopropilmetil-dietoksisilan Sigma-Aldrich firmasından temin edilmiřtir. H_2SO_4 (%95-97), amonyum hidroksit (%26) Riedel-de-Haen ve PAA (Mw: 450.000 g/mol, Mw:5,000 g/mol) ise Polysciences firmasından satın alınmıřtır. Azot gazı (%99,9) ise Linde firmasından tedarik edilmiřtir. Satın alınan kimyasallar herhangi bir ileri saflařtırma olmadan alıřmalarda kullanılmıřtır. Tabaka geliřim deneylerinin hepsinde $R=18.2 \text{ M}\Omega$ deęerine sahip ultra saf su kullanılmıřtır. Fosfat tampon zeltisinin hazırlanması iin KCl, KH_2PO_4 , Na_2HPO_4 ve NaCl belirli oranlarda 2 litre ultra saf su iinde manyetik karıřtırıcı yardımı ile zlmř ve denemelerde kullanılmak zere stok hazırlanmıřtır. Fosfat tampon zeltilerinin pH ayarları, 1 N HCl ve 1 N NaOH damla damla ilave edilerek pH=2/6,8/11 olarak ayarlanmıř ve oda sıcaklıęında muhafaza edilmiřtir.

2.2. Polielektrolit Çözeltilerinin Hazırlanması

Polielektrolit çözeltileri hazırlanırken, çözeltilerin konsantrasyonu hepsinde standart olup daha önceki literatür çalışmalarından 0,01 M olarak belirlenmiştir [16]. Polimer elektrolitlerin hazırlanmasında çözücü olarak, iletkenliği 25°C’de 18.2 mΩ olan ultra saf su kullanılmıştır. Homojen polielektrolit çözeltilerin pH ayarları, tabakalı kaplama işleminden önce 1N %37 HCl ve 1N NaOH kullanılarak gerçekleştirilmiştir. Polielektrolit çözeltilerinin pH değerlerinin LbL kaplamalar üzerindeki etkisini incelemek amacıyla anyonik/katyonik polielektrolit çözeltisinin iyonizasyon derecesine göre iki farklı pH değerinde (pH=1,8-5,5) çalışılmıştır.

2.3. Çok Tabakalı Saf ve Harman Yapılı LbL Filmlerin QCM-D Cihazı ile Hazırlanması

Altın kaplı kuartz kristal sensör, LbL çok katmanlı film oluşumu için öncelikle ultra saf su, %25 amonyak ve hidrojen peroksit (5:1:1, hacim) karışımı ile temizlendi ve 10 dakika süreyle 75°C’ye ısıtıldı. Ardından ultra saf su ile iyice yıkanmış olup takiben sensörler azot gazı akımında iyice kurutulmuştur. Son olarak, QCM-D ölçümüne başlanmadan önce kuartz kristal sensör 10 dakika boyunca UV/Ozon (Bioforce Nanosciences, UV Ozon Temizleyici - ProCleaner™) sisteminde bekletilerek yüzeyi hidrofilize edilip ve sensörün yüzeyindeki tüm organik maddeler uzaklaştırılarak kullanıma hazır hale getirilmektedir. Takiben ultra saf su ile taban çizgisi işleminin ardından belirli konsantrasyonda ve pH değerinde hazırlanmış olan pozitif ve negatif yüklü polielektrolit çözeltileri belirli bir debide kristal sensör üzerinden devamlı olarak geçirilmiştir. Tüm denemeler 22±0,2 °C’de gerçekleştirilmiş ve istenen tabaka sayısına ulaşıncaya kadar devam edilmiştir. LbL kendi kendine bir araya gelen saf ve harman yapıları filmlerin hazırlanmasında, polielektrolit çözeltileri sırasıyla 10 dakika boyunca kuartz kristal sensör üzerinden geçirilmiştir. Zıt yüklü polielektrolit çözeltilerinin yüzeyden geçirilmesi arasında 5 dakika boyunca ultra saf su ile yıkama işlemi gerçekleştirilmiştir. Bu sürelerin tercih edilmesindeki en temel kriter, kuartz kristal sensör üzerindeki frekans değişimlerinin kararlı hale gelmesi için yeterli görülmesidir. Yıkama işlemi yüzeye sıkı biçimde bağlanmayan polielektrolitin uzaklaştırılması amacıyla yapılmıştır. Polielektrolit çözeltilerinin farklı debilerde sensör yüzeyinden geçirilmesi sırasında yüzeyde meydana gelen değişimler frekans ve dissipasyon değişimi olarak Q-Soft 401 adlı programda hesaplanarak takip edilmiştir. LbL kendi kendine bir araya gelen filmler tek bir katyonik ve anyonik polielektrolit çözeltisinden hazırlanıyor ise saf, iki veya daha fazla polielektrolit çözeltisinin karıştırılmasıyla hazırlanırsa harman olarak adlandırılır. Harman polielektrolit çözeltileri hacmen 75/25, 50/50 ve 25/75 olacak şekilde belirlenmiştir. 10 tabakalı saf bir LbL film (PAH/PSS)₁₀ şeklinde gösterilirken, hacmen %50 PSS ve %50 PAA içeren polielektrolit çözeltisinden hazırlanan harman yapıları LbL film (PAH/PSS50PAA50)₁₀ şeklinde kısaltılarak gösterilmiştir.

2.4. Hidrofilize Cam Destek Üzerinde LbL Fonksiyonel Filmlerin Hazırlanması

UV-Vis analizlerinde özel olarak temin edilen kuartz cam destekler (Suprasil, Hellma GmbH, Müllheim/Baden, Almanya), bir seri kimyasal işlemle modifiye edilerek yüzeyi LbL kaplamaya uygun hale getirilmiştir. Öncelikle piranha solüsyonu (H₂SO₄:H₂O₂, 7:3 hacimce) ile temizlendikten sonra (dikkat: kuvvetli oksitleyici madde, organik malzeme ile temas ettiğinde patlama meydana gelebilir), kuvars destekler 3-aminopropilmetildietoksisilan ile ön işleme tabii tutulmuştur. Hidrofilize kaplama sonrası UV çalışmalarından önce, kuvars substratlar zayıf bir nitrojen akışında kurutulmuştur. Ardından daha önce 0,01 M konsantrasyonda hazırlanan pozitif ve negatif yüklü polielektrolit çözeltilerine sırasıyla 10 dakika boyunca daldırılmıştır. Zıt yüklü polielektrolit çözeltilerinin yüzeyden geçirilmesi arasında 5 dakika boyunca ultra saf su ile yıkama işlemi gerçekleştirilmiştir. Tüm denemeler oda sıcaklığında gerçekleştirilmiş ve 20 tabaka

tamamlanincaya kadar devam edilmiştir. Yıkama işlemi yüzeye sıkı biçimde bağlanmayan polielektrolitin uzaklaştırılması amacıyla yapılmıştır.

2.5. Model İlaç Çözeltisinin Hazırlanması

Nano yapıli fonksiyonel ince filmlere ilaç yüklemesi amacıyla ibuprofen sodyum tuzu model ilacın stok çözeltisi hazırlanmıştır. Bu model ilacın tercih edilmesinin sebebi, ilaç salımı konusunda literatürde en sık kullanılan ilaçlar arasında yer almasıdır. Çözünürlük sınırları nedeniyle model ilaçlardan ibuprofen sodyum tuzu $2,42 \cdot 10^{-3}$ molar olarak çalışmalarda kullanılmıştır. Model ilaçların hazırlanmasında çözücü olarak, iletkenliđi 25°C 'de $18.2 \text{ m}\Omega$ olan ultra saf su kullanılmıştır.

2.6. Malzemelerin Karakterizasyonu

2.6.1. QCM-D Analizi

Saf ve harman polielektrolitlerden hazırlanan fonksiyonel LbL filmlerin destek üzerinde çok tabakalı hazırlanması sırasında adsorplanan polielektrolit film ağırlılıđının, filmin kalınlılıđının, adsorplanan madde özelliklerinin daldırma sayısına (n), daldırma çözeltisinin pH deđerine, kullanılan polielektrolitin türü ve yük yoğunluđuna bađlı olarak kantitatif olarak hesaplanabilmesi için QCM-D E1 sistemi kullanılmıştır. QCM-D cihazı ile frekans deđişimi (ΔF), birim alan başına adsorplanan kütle deđişimi ($\Delta M/A$) ve dissipasyon deđişimi (ΔD) Sauerbrey eşitliđi kullanarak hesaplanabilmektedir. Tüm QCM-D hesaplamalarında birim alan olarak sensör yüzey alanı kullanılmış olup bu alan $0,785 \text{ cm}^2$ 'dir. QCM-D analizleri altın kaplı (Qsx 301) piezoelektrik kuvars kristali (Biolin Scientific (Q-sense), AT-cut, $4,95 \text{ MHz} \pm 50 \text{ kHz}$) kullanılarak Q-Sense QCM-D E1 sistemi ile gerçekleştirilmiştir.

2.6.2. UV-Vis Analizi

Çalışmalarda hazır destek üzerine farklı katyonik ve anyonik çözeltiler kullanılarak kaplamalar yapılmış ve oluşan çok tabakanın takibi için UV-Vis analizleri gerçekleştirilmiştir. UV-Vis analizleri "integrating sphere" ünitesi içeren Perkin-Elmer marka Lambda 35 model (Massachusetts, ABD) cihazda gerçekleştirilmiştir. Saf ve harman yapıli filmlerin tabaka geliřimi için $190\text{-}600 \text{ nm}$ dalga boyu aralıđı kullanılmıştır.

2.6.3. Temas Açısı Analizi

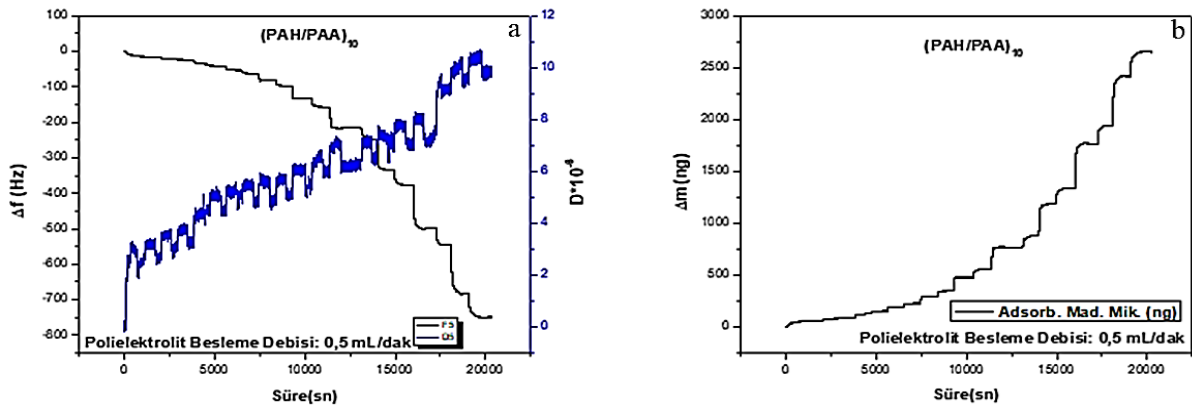
Cam destek üzerine hazırlanan filmlerin yüzey özelliklerinin ve ıslatılabilirliklerinin incelenmesi amacıyla temas açısı analizleri KSV Attension THETA marka (Biolin Scientific) optik temas açısı ve yüzey gerilimi ölçüm cihazı ile gerçekleştirilmiştir. Yüzey temas açısı (θ), oda sıcaklıđında katı yüzeye damlatılan sıvının tanjantının statik olarak tespiti ile belirlenmektedir. Ölçümlerde sesile drop tekniđi kullanılarak $5 \mu\text{l}$ ultra saf su vasıtasıyla örnek üzerinde en az 3 noktadan ölçüm alınarak analizler gerçekleştirilmiştir.

2.6.4. Taramalı Elektron Mikroskopu Analizi

Hazırlanan filmlerin morfolojik yapısının incelenmesi amacıyla SEM analizleri gerçekleştirilmiştir. Bu kapsamda Philips FEI Quanta FEG-EDS 450 marka FE-SEM (Field-Emission Scanning Electron Microscopy) cihazı kullanılarak farklı büyütme oranlarında yüzeyden görüntüler alınmıştır. SEM analizleri hidrofilik cam destek üzerine kaplanan çok tabakalı filmlerden görüntü alınması suretiyle gerçekleştirilmiştir.

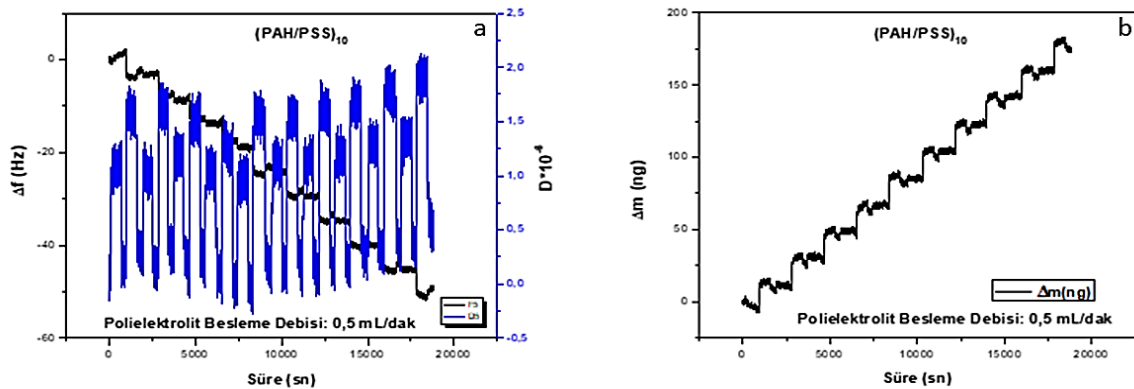
3. Bulgular ve Tartışma

Çalışma kapsamında pH'a bağlı yapısal değişikliklerin çok tabaka oluşumuna, ilaç adsorpsiyonuna ve desorpsiyonuna etkilerini incelemek amacıyla zayıf polielektrolitlerin kullanımı hedeflenerek PAA tercih edilmiştir. PAA'nın molekül ağırlığının çok tabaka oluşumuna ve çok tabaka adsorpsiyonuna etkilerini incelemek amacıyla iki farklı molekül ağırlığında (Mw: 450.000 ve Mw: 5.000) PAA kullanımı araştırılmıştır. Katyonik polielektrolit olarak PAH ve anyonik polielektrolit olarak PSS ve PAA'nın kullanıldığı LbL saf ve harman filmlerin frekans değişimleri Şekil 1-9'da gösterilmiştir. Yüksek molekül ağırlıklı PAA kullanılarak hazırlanan on tabakalı PAH/PSS-PAA (pH: 5,5) saf ve harman filmlerin QCM-D eğrileri Şekil 1-5'te sunulmuştur.



Şekil 1. 10 tabakalı LbL PAH/PAA filmin süreye bağlı (a) frekans-dissipasyon ve (b) kütle değişimleri

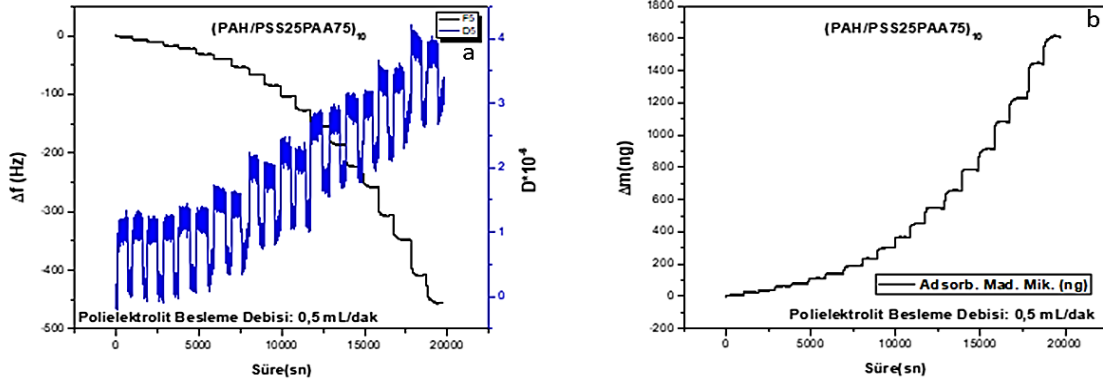
Şekil 1'de görülen (PAH/PAA)₁₀ çok tabakalı filmin beklendiği üzere artan tabaka sayısına bağlı olarak frekans değişiminin arttığı diğer bir ifadeyle yüzeyde adsorplanan madde miktarının geliştiği görülmektedir. (PAH/PAA)₁₀ filminin on tabaka sonrasında frekans değişimi -751,4 Hz olarak bulunmuştur. Sauerbrey denklemini kullanılarak on tabaka sonrasında 2.660 ng polielektrolit tabakasının yüzeye adsorplandığı gözlenmiştir. (PAH/PAA)₁₀' un dissipasyon eğrisinde ise on tabaka sonrasında dissipasyon değeri $10 \cdot 10^{-6}$ olarak gözlenmiştir. Artan tabaka sayısına bağlı olarak dissipasyon değerinin artması yüzeye adsorplanan polielektrolitler arasındaki etkileşimin zayıflayarak yapının daha esnek hale gelmesi şeklinde yorumlanmaktadır [17].



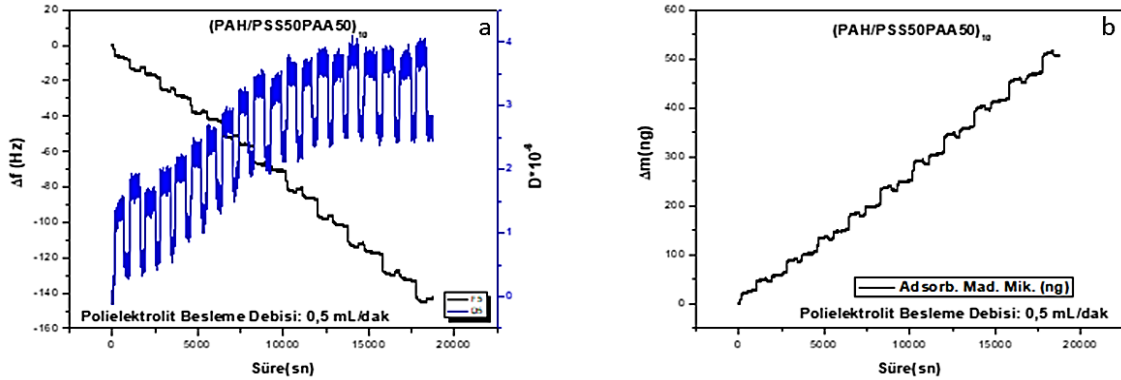
Şekil 2. 10 tabakalı LbL PAH/PSS filmin süreye bağlı (a) frekans-dissipasyon ve (b) kütle değişimleri

Şekil 2'de görülen (PAH/PSS)₁₀ filminin oluşumuna ait QCM-D grafiği incelendiğinde on tabaka sonrasında frekans değişimi -51,4 Hz ve buna karşı gelen adsorplanan madde miktarı 182 ng olarak bulunmuştur. Benzer şekilde Şekil 2 (a)'da görülen dissipasyon değişimi (PAH/PSS)₁₀'da oldukça sınırlı kalmış ve on tabaka

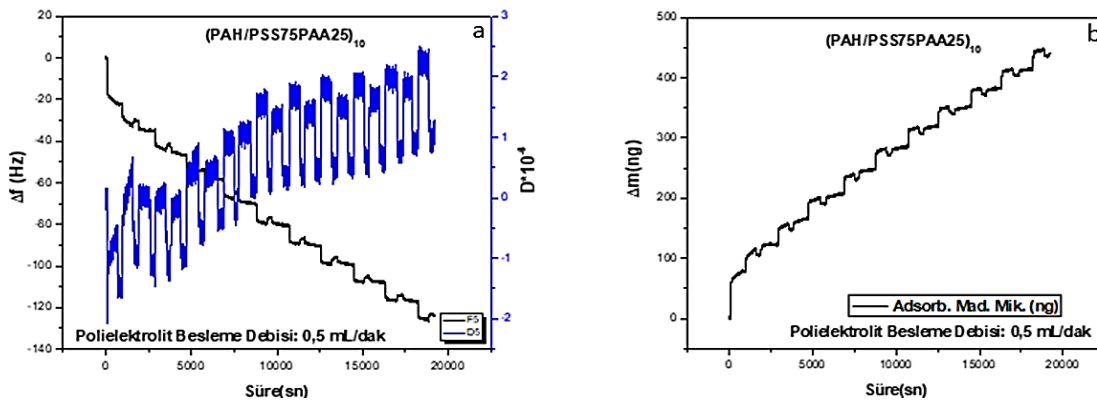
sonrasında dissipasyon değişimi yaklaşık $0,5 \cdot 10^{-6}$ olarak görülmüştür. Bu durum PAH ile PSS arasındaki etkileşimin yüksek olması ve buna bağlı olarak sert yapılı polielektrolit kompleks yapılı çok tabakalı filmlerin oluşumuyla açıklanabilir [18]. Yüksek molekül ağırlıklı PAA kullanılarak hazırlanan $(PAH/PAA)_{10}$ 'un $(PAH/PSS)_{10}$ 'a göre yüzeyde daha fazla miktarda adsorplanması, pH 5,5'te zayıf bir polielektrolit olan PAA'nın kısmen iyonize olması ve yumağimsi konformasyonu nedeniyle söz konusu pH değerinde PAH'ın iyonize yüklerinin karşılanmasında daha fazla miktarda zıt yüklü polielektrolit adsorpsiyonun gerekli olması ile açıklanabilir.



Şekil 3. 10 tabakalı LbL PAH/PSS25PAA75 filmin süreye bağlı (a) frekans-dissipasyon ve (b) kütle değişimleri



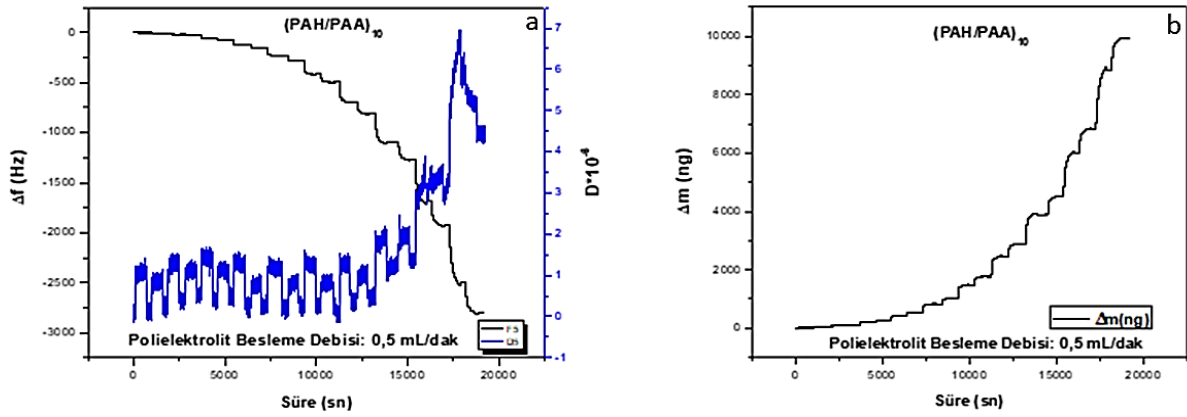
Şekil 4. 10 tabakalı LbL PAH/PSS50PAA50 filmin süreye bağlı (a) frekans-dissipasyon ve (b) kütle değişimleri



Şekil 5. 10 tabakalı LbL PAH/PSS75PAA25 filmin süreye bağlı (a) frekans-dissipasyon ve (b) kütle değişimleri

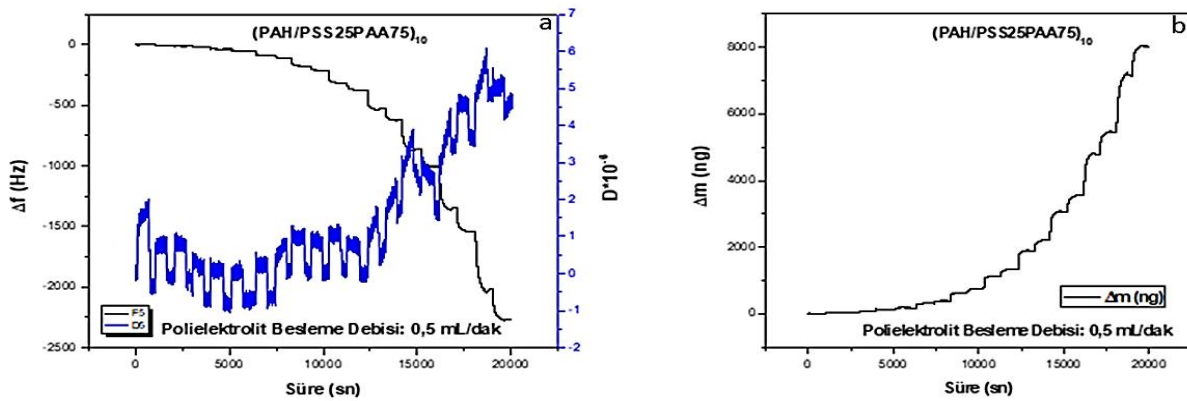
Şekil 3-4'te yüksek molekül ağırlıklı PAA kullanılarak harman yapıları LbL çok tabakalı filmlerin frekans ve dissipasyon değişimleri ile zamana bağlı adsorplanan madde miktarları gösterilmiştir. Buna göre harman filmlerin frekans değişim değerleri saf (PAH/PAA)₁₀ ve (PAH/PSS)₁₀ arasında değişmektedir. Benzer şekilde hesaplanan adsorplanan madde miktarları da 446 ng ile 1.607 ng arasında değişmektedir. Bununla birlikte, harman yapıları filmlerde PAA miktarlarının artışına bağlı olarak dissipasyon değerinin arttığı ve (PAH/PSS25PAA75)₁₀ filminin dissipasyon değeri $3,5 \cdot 10^{-6}$ olarak belirlenmiştir. Bu sonuç, harman çok tabakalı filmler için dissipasyon değişiminin frekans değişimine benzer şekilde saf filmlerin dissipasyon değerleri arasında olduğunu göstermektedir.

PAA'nın düşük molekül ağırlıklı kullanımıyla hazırlanan (pH: 5,5) çok tabakalı filmlere ait QCM-D grafikleri ve süreye bağlı olarak adsorplanan madde miktarı grafikleri Şekil 6-9'da sunulmuştur.



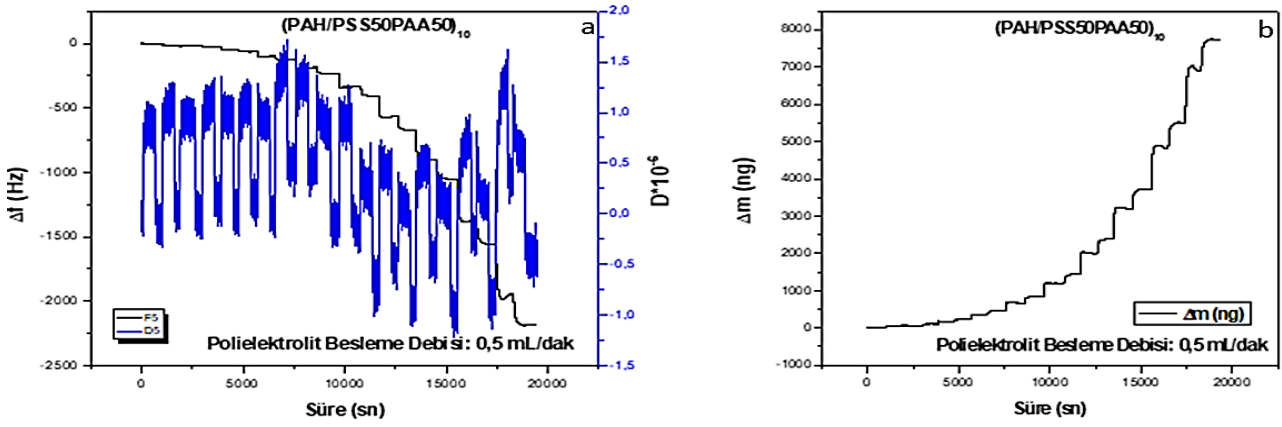
Şekil 6. 10 tabakalı LbL PAH/PAA (PAA Mw:5,000 g/mol) filmin süreye bağlı (a) frekans-dissipasyon ve (b) kütle değişimleri

Düşük molekül ağırlıklı PAA'dan hazırlanan (PAH/PAA)₁₀ LbL filminin frekans değişimi -2.828,8 Hz olduğu buna karşılık adsorplanan madde miktarının 10 mikrogram olduğu tespit edilmiştir. Molekül ağırlığı 5.000 olan PAA'dan hazırlanan çok tabakalı filmin dissipasyon değişimi yaklaşık $4 \cdot 10^{-6}$ olarak tespit edilmiştir. Bu değer özellikle 8 tabaka sonrasında artış göstermektedir. Molekül ağırlığı 450.000 olan PAA kullanılarak hazırlanan filmler ile karşılaştırıldığında düşük molekül ağırlıklı PAA kullanılarak hazırlanan filmlerin yüzeyde daha fazla adsorlandığı ve adsorplanan bu LbL filmlerin de yüksek molekül ağırlıklı PAA'dan hazırlanan LbL filmlere göre daha sert yapıda olduğu tespit edilmiştir.

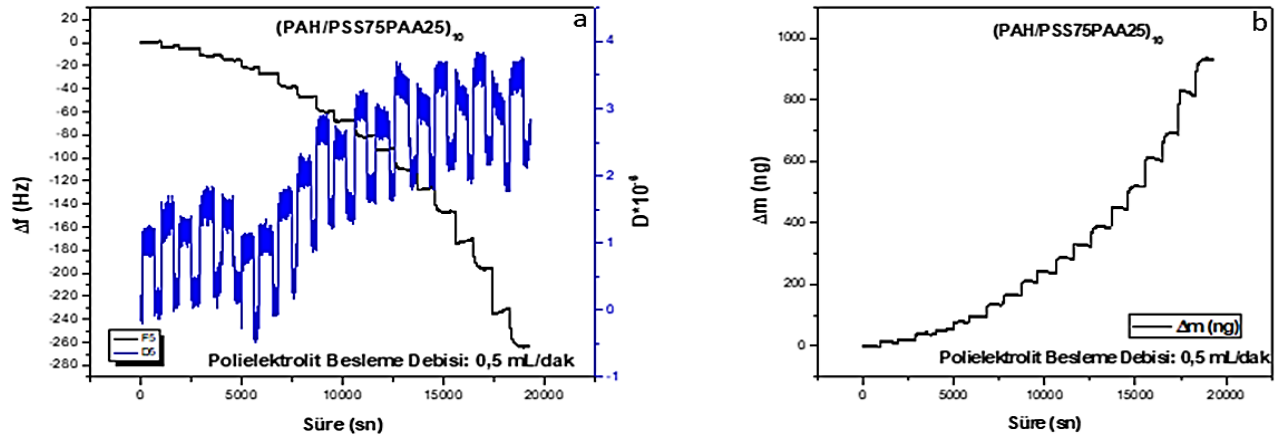


Şekil 7. 10 tabakalı LbL PAH/PSS25PAA75 (PAA Mw:5,000 g/mol) filmin süreye bağlı (a) frekans-dissipasyon ve (b) kütle değişimleri

Düşük molekül ağırlıklı PAA kullanılarak hazırlanan LbL filmin PAA adsorpsiyonunun yüksek olmasının nedeninin, düşük zincir uzunluğuna bağlı olarak polielektrolit kompleks oluşumu sırasında PAA'nın gerek yüzeye gerekse de kompleksin içerisine difüzyonu (interpenetrating diffusion) ve buna bağlı olarak adsorpsiyonun arttığı düşünülmektedir [19].



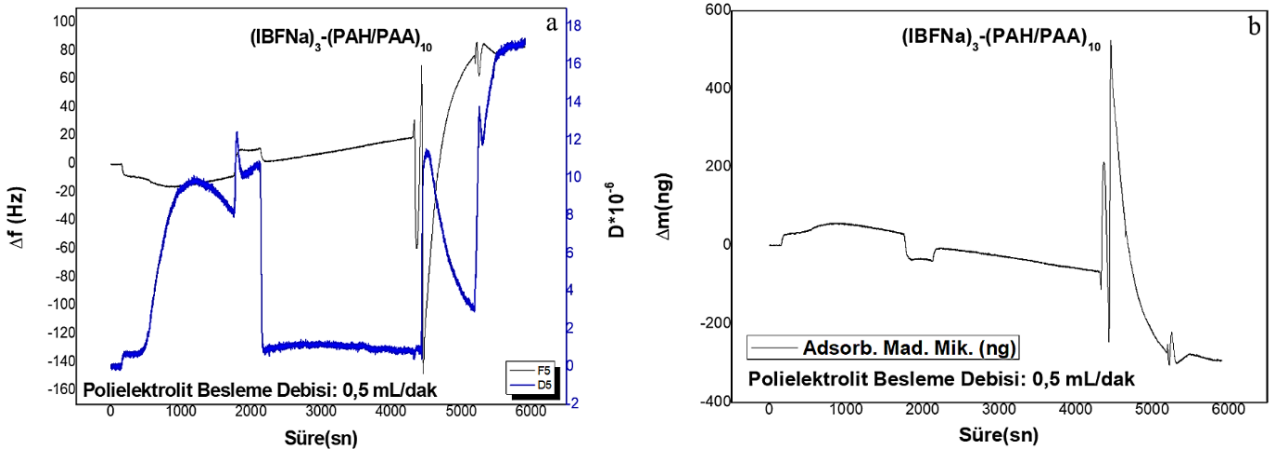
Şekil 8. 10 tabakalı LbL PAH/PSS5025PAA50 (PAA Mw:5,000 g/mol) filmin süreye bağlı (a) frekans-dissipasyon ve (b) kütle değişimleri



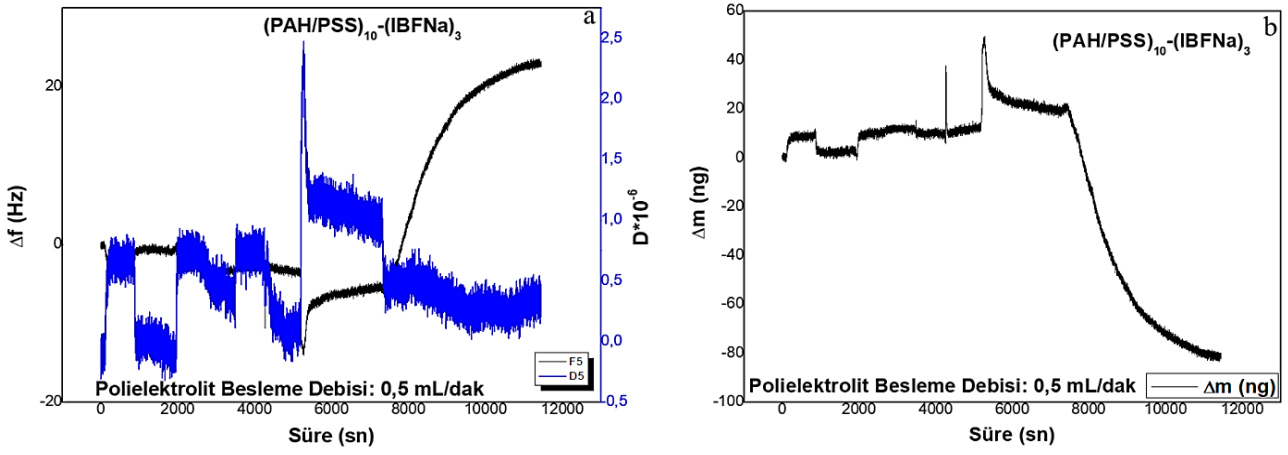
Şekil 9. 10 tabakalı LbL PAH/PSS75PAA25 (PAA Mw:5,000 g/mol) filmin süreye bağlı (a) frekans-dissipasyon ve (b) kütle değişimleri

Molekül ağırlığı 5,000 olan PAA'dan hazırlanan LbL harman filmlerin frekans değişimleri saf (PAH/PAA)₁₀ ve saf (PAH/PSS)₁₀ filmlerin arasında olup -265,6 Hz ile -2,281 Hz arasında değişmektedir. Bunlara tekabül eden adsorplanan madde miktarları ise 940,4 ng ile 8 mg arasında değişmektedir. Şekil 7-9 arasında görülen harman LbL filmlerin dissipasyon değerlerinin PSS oranının artmasına bağlı olarak düştüğü ancak PAA miktarının artmasına bağlı olarak çok az miktarda geliştiği gözlenmektedir.

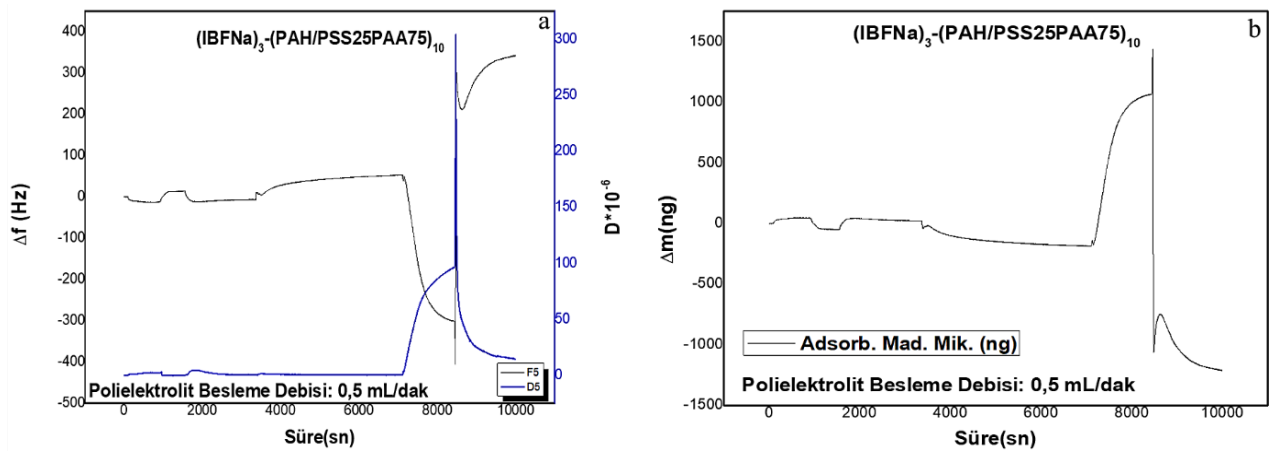
PAH/PSS-PAA'dan hazırlanan LbL saf ve harman filmlerin (PAA Mw: 450.000 ve 5.000) on tabaka film oluşturulmasının ardından ilaç adsorpsiyon ve desorpsiyon çalışmaları gerçekleştirilmiştir. Bu kapsamda on tabakalı filmin hazırlanmasından sonra öncelikle IBF-Na yüklemesi yapılmış ardından ultra saf su ile yıkanmıştır. pH değerine bağlı olarak ilaç adsorpsiyon ve desorpsiyonunun incelenmesi açısından sırasıyla önce model ilaç ardından da pH 2'deki ve 11'deki çözeltilerle yıkama işlemleri gerçekleştirilmiştir. Örnek bir adsorpsiyon/desorpsiyon çalışmasının QCM-D cihazı ile takibine yönelik grafik Şekil 10-14'te gösterilmiştir.



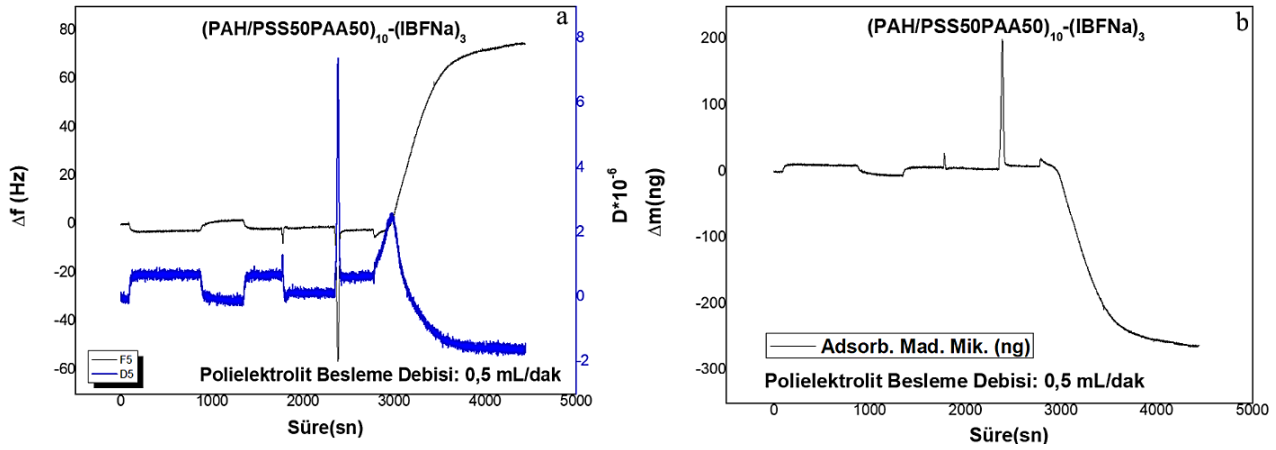
Şekil 10. 10 tabakalı LbL PAH/PAA filmin IBF-Na ile etkileşiminde süreye bağlı (a) frekans-dissipasyon ve (b) kütle değişimleri



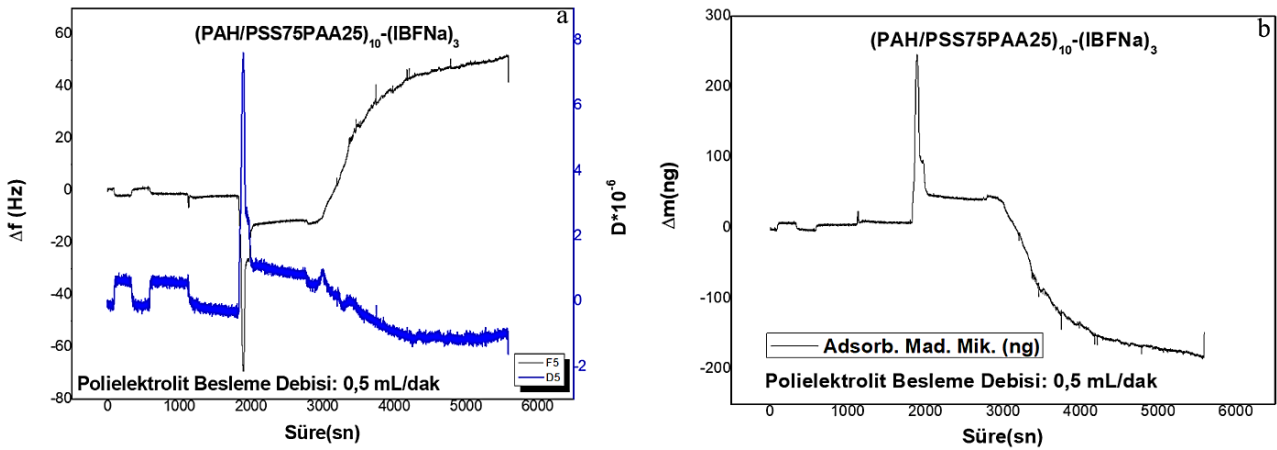
Şekil 11. 10 tabakalı LbL PAH/PSS filmin IBF-Na ile etkileşiminde süreye bağlı (a) frekans-dissipasyon ve (b) kütle değişimleri



Şekil 12. 10 tabakalı LbL PAH/PSS25PAA75 filmin IBF-Na ile etkileşiminde süreye bağlı (a) frekans-dissipasyon ve (b) kütle değişimleri



Şekil 13. 10 tabakalı LbL PAH/PSS50PAA50 filmin IBF-Na ile etkileşiminde süreye bağlı (a) frekans-dissipasyon ve (b) kütle değişimleri



Şekil 14. 10 tabakalı LbL PAH/PSS75PAA25 filmin IBF-Na ile etkileşiminde süreye bağlı (a) frekans-dissipasyon ve (b) kütle değişimleri

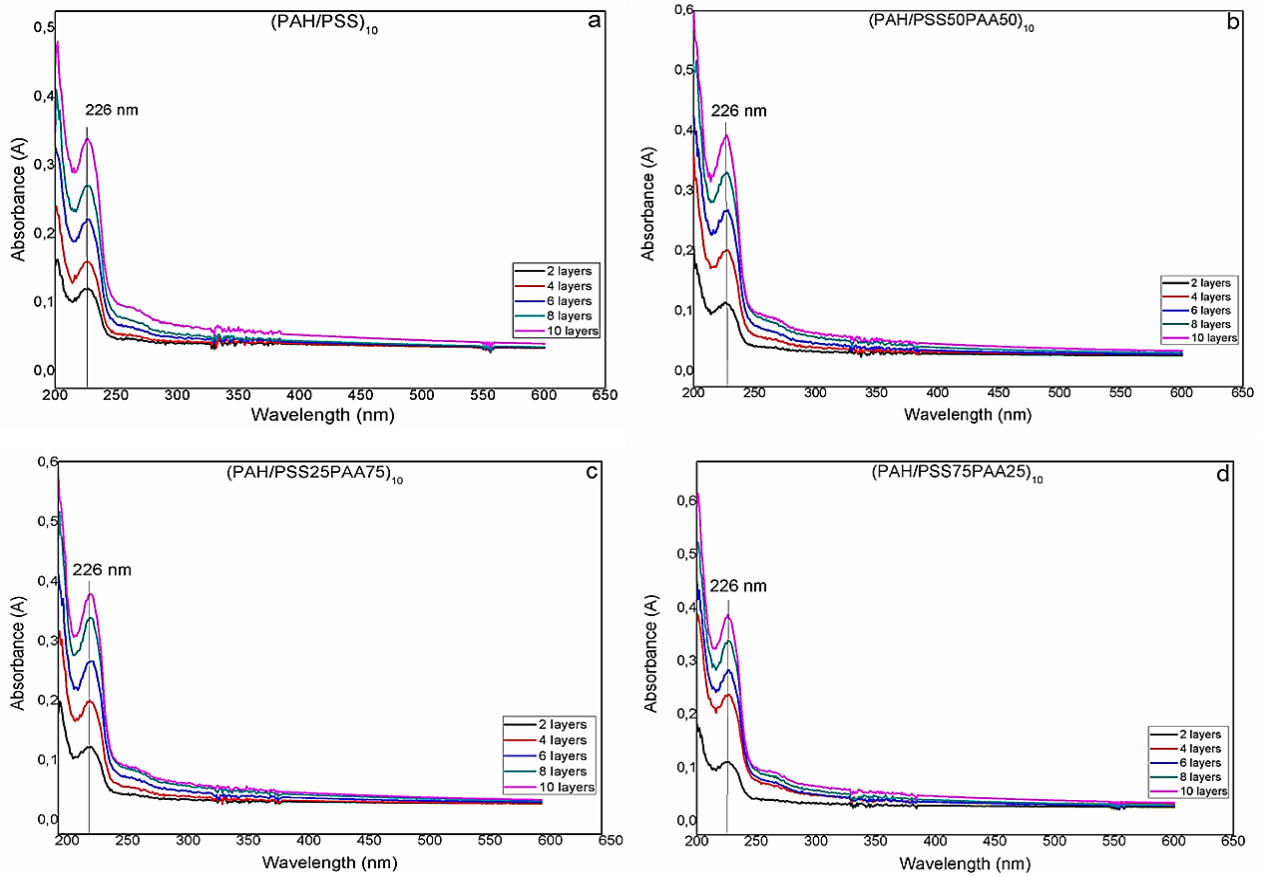
Yüksek molekül ağırlıklı PAA'dan hazırlanan PAH/PSS-PAA LbL filmlerin IBF-Na adsorpsiyonunda 3 ile 45 ng arasında adsorpsiyon tespit edilmiştir. Saf (PAH/PAA)₁₀ ürünün en yüksek model ilaç adsorpsiyonuna ulaştığı buna karşın harman filmlerde PSS miktarının artışına bağlı olarak ilaç adsorpsiyonunun belirgin şekilde düştüğü gözlenmiştir. Örneğin IBF-Na'nın ilk adsorpsiyonunda (PAH/PAA)₁₀ için 39,4 ng IBFNa adsorplanırken (PAH/PSS75PAA25)₁₀ için adsorplanan ilaç miktarı 9,7 ng seviyesindedir. (PAH/PAA)₁₀ ürününün pH=2 ve 11'de çok tabaka degradasyonuna uğradığı buna karşın PAH/PSS-PAA harman ürünün pH=2 ve 11'de herhangi bir degradasyona uğramadığı tespit edilmiştir. PAH/PAA ürününde asidik ve bazik koşullarda LbL çok tabaka degradasyonu farklı pH'larda PAA'nın zayıf polielektrolit olmasına bağlı olarak disosiyasyon olması ve ilaç molekülü ile çok tabaka arasındaki PAA'nın etkileşiminin zayıflamasından kaynaklandığı düşünülmektedir. Buna karşın yüksek oranda PSS yüklenen harman filmlerin asidik ve bazik koşullarda çok tabaka degradasyonuna uğramaması PSS'in kuvvetli polielektrolit olması ve farklı pH değerlerinde yapısal entegrasyonunda bütünlüğün bozulmaması şeklinde açıklanabilir [20].

İlaç adsorpsiyon ve desorpsiyonuna bağlı olarak PAH/PAA-PSS ürünlerinin dissipasyon değerleri saf filmler için yüksek buna karşın PAH/PSS-PAA'dan hazırlanan harman filmler için sıfıra yakın olduğu tespit edilmiştir. Saf filmlerin yüksek dissipasyon göstermesi ilaç ilavesine bağlı olarak çok tabakasının şişmesine bağlanabilir. Ancak yapıdaki PSS miktarının fazla olmasına bağlı olarak dissipasyon değerleri düşük kalmakta bu da yapının ilaçla şişmediğini göstermektedir. Bu sonuç, PSS'in kuvvetli polielektrolit olmasına bağlı olarak

zincirsel (train like) yapıya polielektrolit kompleks oluşturmasından kaynaklanmaktadır [16].

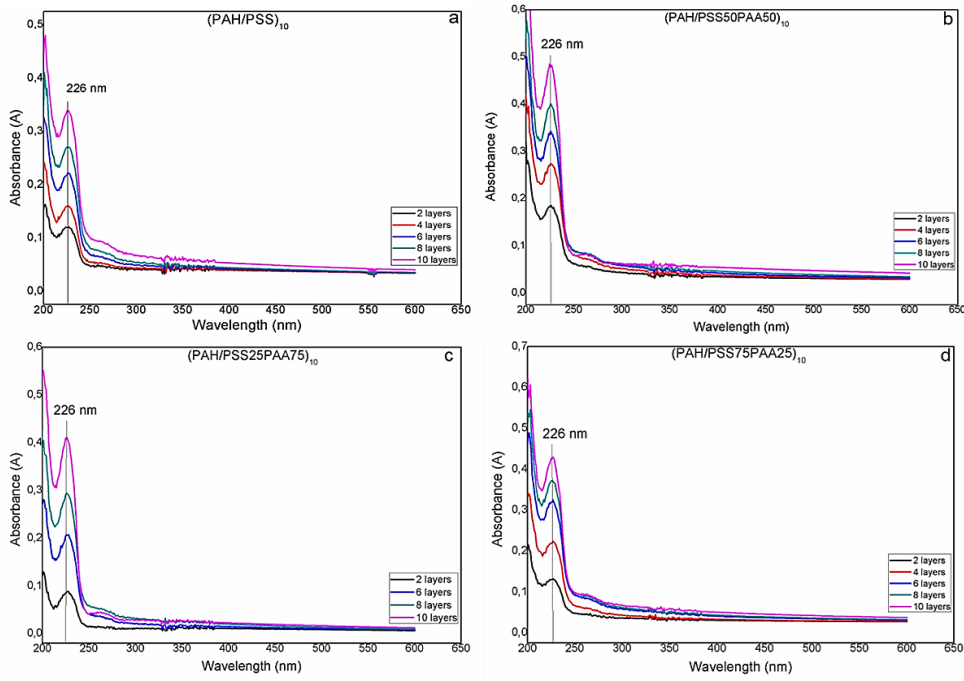
Diğer bir seri çalışmada, düşük molekül ağırlıklı PAA (Mw: 5.000) ve PSS'ten hazırlanan PAH/PSS-PAA filmlerinin IBF-Na çalışmaları sunulmuştur. Bu tür filmlerin ilaç adsorpsiyonunda PAH/PSS ve PAA içeren tüm harman filmlerde ilaç yüklemesine bağlı olarak LbL çok tabakaya ait frekans değişimleri negatif yerine pozitif alana geçtiği diğer bir ifadeyle çok tabaka degradasyonunun kuvvetli bir şekilde başladığı tespit edilmiş ve ne su ile yapılan ne de farklı pH değerlerindeki çözeltilerle yapılan yıkama işlemleri yapılamamıştır. Bu ilginç durum düşük molekül ağırlığında PAA kullanımı durumunda model ilacın tuz olarak davranması ve polielektrolit kompleks oluşumuna atfedilen denklemi tersine çevirdiği diğer bir ifadeyle polielektrolit kompleksin bozularak çok tabakaların degrade olarak yüzeyden uzaklaştığı şeklinde değerlendirilmektedir [21]. Özellikle düşük molekül ağırlıklı polielektrolit çözeltilerinden hazırlanan LbL filmlerin ilaç adsorpsiyon ve desorpsiyon çalışmaları için uygun olmadığı tespit edilmiştir.

Çok tabakalı LbL fonksiyonel filmlerin oluşumunu incelemek amacıyla UV-Vis analizleri gerçekleştirilerek hazırlanan saf ve harman yapıya filmlere ait grafikler Şekil 15-16'da gösterilmiştir.



Şekil 15. (PAH/PSS-PAA)₁₀ LbL filmlerine ait UV-Vis grafiği

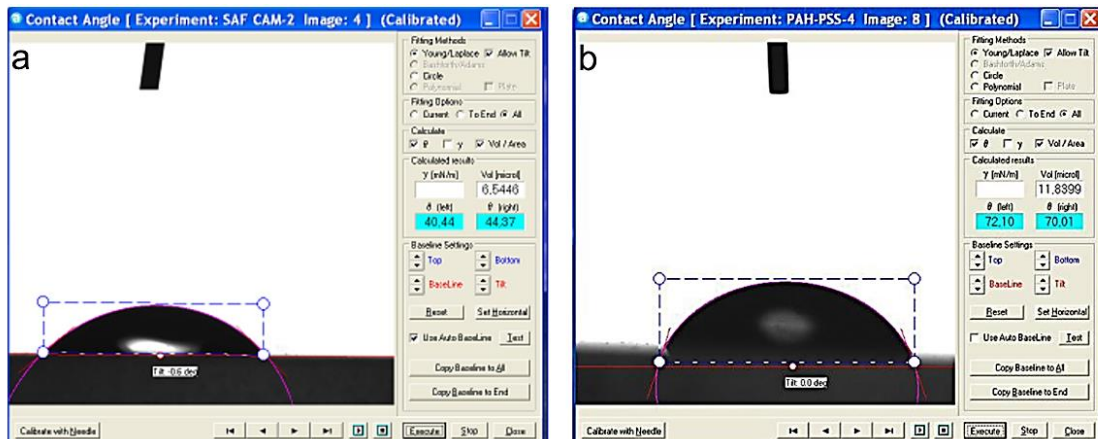
PAH-PSS ve PAA'dan oluşan LbL çok tabakalı harman filmlerin UV-Vis absorbans grafikleri çizilerek PAA'nın iki farklı molekül ağırlığı ve harman kompozisyonuna bağlı absorbans değerleri araştırılmıştır. Bu değerlerin belirlenmesinde PSS'in 226 nm'deki karakteristik piki esas alınmıştır [22].



Şekil 16. (PAH/PSS-PAA)₁₀ LbL filmlerine ait UV-Vis grafiği

Buna göre hacimce %25 PSS ve %75 PAA içeren anyonik polielektrolit ve PAH'dan hazırlanan ürünlerin absorbans değerleri poliakrilik asitin molekül ağırlığı 450.000 iken 0,4 yine poliakrilik asitin 5.000 iken 0,37 olarak tespit edilmiştir. Bu durum poliakrilik asitin molekül ağırlığındaki düşmeye bağlı olarak yüzeyin harman içerisindeki PSS ile kaplanmaya eğilim gösterdiğini düşündürmektedir. Molekül ağırlığı düşük poliakrilik asitten hazırlanan bir başka harman film (PAH/PAA25PSS75)₁₀ için absorbans değeri 0,38 olarak bulunmuştur. Bu durum düşük molekül ağırlıklı PAA kullanıldığı durumlarda PSS miktarı artsa bile LbL film kompozisyonundaki PSS'in artmadığını ve bununla PSS'in pH 1,8'de tamamen iyonize olması nedeniyle yüzeyi düşük miktarlarda dahi kaplayabildiğini göstermektedir [23].

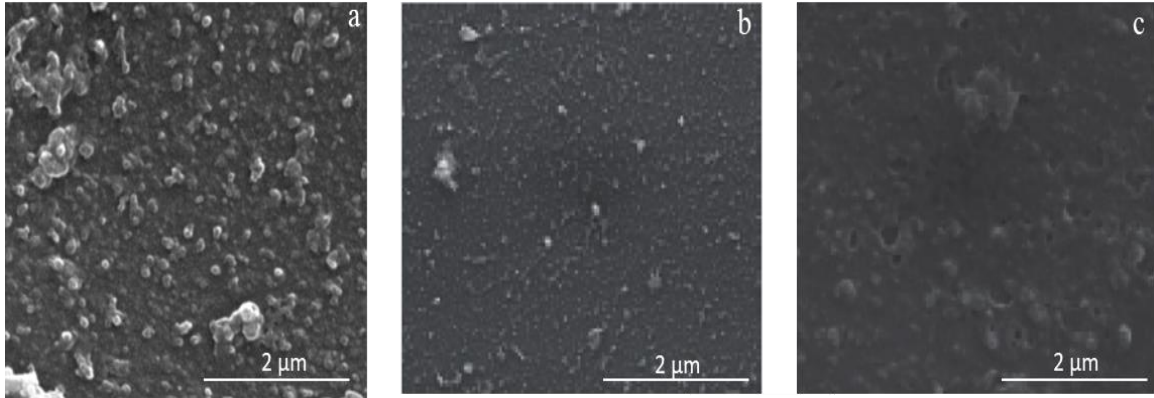
Hazırlanan filmlerin kullanılan polielektrolit türüne ve kompozisyonuna bağlı olarak yüzey ıslanabilirlik özellikleri değişimlerini incelemek amacıyla temas açısı ölçüm analizleri gerçekleştirilmiştir. Ortalama temas açısı değerleri Şekil 17'de verilmiştir. Literatürden bilindiği üzere θ açısının 90° ve üzerinde olması durumunda yüzey hidrofobik ve 90° 'nin altında olması durumunda ise hidrofilik olarak değerlendirilmektedir [24]. Filmlerin hazırlanmasında taşıyıcı yüzey olarak kullanılan UV Suprasil özel camın temas açısı değeri ortalama $42,4 \pm 2,0^\circ$ olarak tespit edilmiştir. Bu sonuç kimyasal olarak ön işleme tabi tutulan camın yüzeyinin hidrofilik (su seven) yapıda olduğunu göstermektedir.



Şekil 17. (a) Kuartz cam desteğin, (b) (PAH/PSS)₁₀ filmin yüzey temas açısına ait görünüm

Saf PAH ve PSS'ten hazırlanan filmin ortalama temas açısı değeri ise $71,1 \pm 1,1^\circ$ olarak tayin edilmiştir. Harman filmlerin hazırlanmasında beslemede PSS kullanıldığında temas açısı değerlerinin arttığı görülmektedir [25]. Bu durumun PSS yapısındaki aromatik halkanın hidrofobik yapısından kaynaklandığı ve hazırlanan filmin su sevmeyen karakterinin gelişmesi şeklinde yorumlanmıştır.

Hazırlanan LbL çok tabakalı filmlerin yüzey özelliklerinin incelenmesi amacıyla 10 çift tabakalı PAH/PSS-PAA'dan hazırlanan saf ve harman yapıları filmlerin SEM analizleri gerçekleştirilmiştir. İlgili fotoğraflar Şekil 18'te sunulmuştur.



Şekil 18. (a) (PAH/PSS)₁₀, (b) (PAH/PAA)₁₀ ve (c) (PAH/PSS50PAA50)₁₀ filmlerine ait 50.000 büyütmedeki SEM görüntüleri

Farklı büyütme oranlarında çekilen fotoğraflardan (PAH/PSS)₁₀ filminin 50,000 büyütmedeki resminde yüzeyin pürüzsüz olmadığı ve farklı boyutlarda kümelenmiş taneciklerin (aglomeratların) olduğu tespit edilmiştir. Gözlenen bu aglomeratların interpolielektrolit kompleks yapı nedeniyle meydana geldiği düşünülmektedir. (PAH/PAA)₁₀'dan hazırlanan 10 tabakalı filmin genel olarak yoğun bir yüzeye sahip olduğu bununla birlikte yüzeye yaklaşıldığında yüzeyde bazı heterojen oluşumların bulunduğu görülmüştür. LbL harman filmin (PAH/PAA50PSS50)₁₀ SEM görüntüsünde saf (PAH/PAA)₁₀ filme benzer şekilde heterojen oluşumların yanı sıra (PAH/PAA)₁₀ filmde görülmeyen farklı mikron boyutlarında gözeneklerin bulunduğu tespit edilmiştir. Bu durum, harman yapısındaki PSS'e bağlı olarak yüzeyde gözenekliliğin arttığını göstermektedir [26].

4. Sonuçlar

Çalışmada çok tabakalı saf ve harman polielektrolit fonksiyonel filmlerin hazırlanması ve QCM-D tekniği ile tabaka gelişmelerinin incelenmesi araştırılmıştır. Düşük molekül ağırlıklı PAA kullanılarak hazırlanan filmlerin yüzeyinde daha fazla madde adsorplandığı ve daha sert yapıda olduğu tespit edilmiştir. Bu durumun sebebi, düşük zincir uzunluğuna bağlı olarak polielektrolit kompleks oluşumu sırasında PAA'nın gerek yüzeye gerekse de kompleksin içerisine difüzyonu (interpenetrating diffusion) ve buna bağlı olarak adsorpsiyonun arttığı şeklinde açıklanmaktadır. IBFNa'nın LbL filme yüklenmesi ve salım çalışmaları QCM-D cihazında yapılan analizlerle takip edilmiştir. (PAH/PAA)₁₀ ürününün pH=2 ve 11'de çok tabaka degradasyonuna uğradığı buna karşın PAH/PSS-PAA harman ürünün pH=2 ve 11'de herhangi bir degradasyona uğramadığı tespit edilmiştir. PAH/PAA ürününde tabaka degradasyonu farklı pH'larda PAA'nın zayıf polielektrolit olmasına bağlı olarak disosiyasyon olması ve ilaç molekülü ile çok tabaka arasındaki PAA'nın etkileşiminin zayıflamasından kaynaklandığı düşünülmektedir. Yüksek oranda PSS yüklenen harman filmlerin asidik ve bazik koşullarda çok tabaka degradasyonuna uğramaması PSS'in kuvvetli polielektrolit olması ve farklı pH değerlerinde yapısal entegrasyonunda bütünlüğün bozulmaması şeklinde açıklanabilir. PAH/PSS-PAA sistemi

için, aynı koşullarda hazırlanan (PAH/PAA) filminin (PAH/PSS)'ten hazırlanan filmlere göre ilaç adsorpsiyonunun son derece yüksek olduğu tespit edilmiştir. LbL filmlerin tabaka gelişimlerinin lineer olarak arttığı UV-Vis analizi ile tespit edilmiştir. Hazırlanan filmlerin SEM analizlerinde yüksek yoğunluklu ve kuvvetli polielektrolitlerin kullanılması durumunda polielektrolit kompleks oluşumunun yanı sıra polielektrolitler arası etkileşimlerinde olması nedeniyle bölgesel olarak çeşitli yapılar gözlenmiştir. Daha zayıf ve düşük yük yoğunluklu polielektrolitlerden hazırlanan filmlerde ise daha gözeneksiz ve homojen yapılar elde edilmiştir. Sonuçlar değerlendirildiğinde, polielektrolit filmlerin tabakalı kaplama yöntemiyle istenilen özelliklerde hazırlanabilmesi, ilaç uygulamalarında kullanılması için ümit vericidir.

Yazar Katkıları

Birinci yazar analizleri planlamış ve tasarlamıştır. Birinci ve ikinci yazarlar veri toplamış ve analizleri yapmıştır. Üçüncü yazar çalışmanın kurgusunu, yenilikçi yönlerini ve analizleri planlamıştır. Birinci yazar makaleyi yazmıştır. Üçüncü yazar makaleyi düzenlemiş ve kontrol etmiştir. Bu çalışma birinci yazarın üçüncü yazar danışmanlığındaki yüksek lisans tezinden üretilmiştir. Tüm yazarlar makalenin son hâlini okuyup onaylamıştır.

Çıkar Çatışması

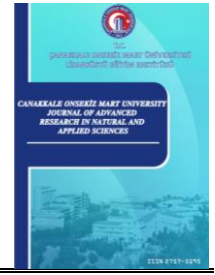
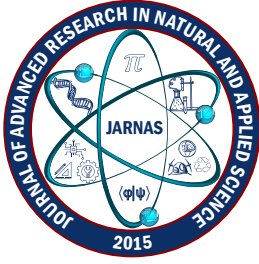
Yazarlar hiçbir çıkar çatışması olmadığını beyan etmektedir.

Kaynaklar

- [1] S. Bhusari, J. Kim, K. Polizzi, S. Sankaran, A. del Campo, *Encapsulation of bacteria in bilayer Pluronic thin film hydrogels: A safe format for engineered living materials*, Biomaterials Advances 145 (2023) 213240 8 pages.
- [2] A. Qasem, M. S. Mostafa, H. A. Yakout, M. Mahmoud, E. R. Shaaban, *Determination of optical bandgap energy and optical characteristics of Cd30Se50S20 thin film at various thicknesses*, Optics and Laser Technology 148 (2022) 107770 13 pages.
- [3] H. Yılmaz, M. Özkan, *Micropollutant removal capacity and stability of aquaporin incorporated biomimetic thin-film composite membranes*, Biotechnology Reports 35 (2022) e00745 12 pages.
- [4] G. Decher, *Fuzzy nanoassemblies: Toward layered polymeric multicomposites*, Science 277 (5330) (1997) 1232–1237.
- [5] A. E. Barberio, S. G. Smith, I. S. Pires, S. Iyer, F. Reinhardt, M. B. Melo, H. Suh, R. A. Weinberg, D. J. Irvine, P. T. Hammond, *Layer-by-layer interleukin-12 nanoparticles drive a safe and effective response in ovarian tumors*, Bioengineering and Translational Medicine 8 (2) (2023) e10453 12 pages.
- [6] J. Pickering, N. G. Lamson, M. H. Marand, W. Hwang, J. P. Straehla, P. T. Hammond, *Layer-by-layer polymer functionalization improves nanoparticle penetration and glioblastoma targeting in the brain*, ACS Nano 17 (2023) 24154–24169.
- [7] J. P. Straehla, C. Hajal, H. C. Safford, G. S. Offeddu, N. Boehnke, T. G. Dacoba, J. Wyckoff, R. D. Kamm, P. T. Hammond, B. Harley, S. Mitragotri, R. Satchi-Fainaro, *A predictive microfluidic model of human glioblastoma to assess trafficking of blood-brain barrier-penetrant nanoparticles*, Proceedings of the National Academy of Sciences (PNAS) 119 (23) (2022) e2118697119 12 pages.
- [8] D. Yılmaz-Aykut, O. Yolacan, H. Deligoz, *A comparative QCM-D study for various drug sorption behaviors and chemical degradation of chitosan/PAA LbL multilayered films*, Journal of Polymer Research 30 (8) (2023) Article Number 307 16 pages.

- [9] D. Yilmaz-Ayktut, H. Deligöz, *Examining layer-by-layer assembly of polyelectrolyte-drug interactions using quartz crystal microbalance with dissipation*, *Polymer Engineering and Science* 63 (11) (2023) 3625–3638.
- [10] J. Hong, B. S. Kim, K. Char, P. T. Hammond, *Inherent charge-shifting polyelectrolyte multilayer blends: A facile route for tunable protein release from surfaces*, *Biomacromolecules* 12 (8) (2011) 2975–2981.
- [11] S. Amorim, I. Pashkuleva, C. A. Reis, R. L. Reis, R. A. Pires, *Tunable layer-by-layer films containing hyaluronic acid and their interactions with CD44*, *Journal of Materials Chemistry B* 8 (17) (2020) 3880–3885.
- [12] R. Lu, B. Zhao, L. Yang, S. Zheng, X. Zan, N. Li, *Role of driving force on engineering layer-by-layer protein/polyphenol coating with flexible structures and properties*, *ACS Applied Materials and Interfaces* 15 (16) (2023) 20551–20562.
- [13] J. T. O’Neal, E. Y. Dai, Y. Zhang, K. B. Clark, K. G. Wilcox, I. M. George, N. E. Ramasamy, D. Enriquez, P. Batys, M. Sammakorpi, J. L. Lutkenhaus, *QCM-D investigation of swelling behavior of layer-by-layer thin films upon exposure to monovalent ions*, *Langmuir* 34 (3) (2018) 999–1009.
- [14] Z. Dong, C. Liang, J. Zhao, *Quartz crystal microbalance with dissipation (QCM-D) as a way to study adsorption and adsorbed layer characteristics of hemicelluloses and other macromolecules on thin cellulose films: A review*, *BioResources* 18 (2) (2023) 1–19.
- [15] X. Huang, Q. Chen, W. Pan, Y. Yao, *Advances in the mass sensitivity distribution of quartz crystal microbalances: A review*, *Sensors* 22 (14) (2022) 5112 20 pages.
- [16] H. Deligöz, B. Tieke, *QCM-D study of layer-by-layer assembly of polyelectrolyte blend films and their drug loading-release behavior*, *Colloids and Surfaces A: Physicochemical and Engineering Aspects* 441 (2014) 725–736.
- [17] Szilagyi, G. Trefalt, A. Tiraferri, P. Maroni, M. Borkovec, *Polyelectrolyte adsorption, interparticle forces, and colloidal aggregation*, *Soft Matter* 10 (15) (2014) 2479–2502.
- [18] E. Konyali, H. Y. Cengiz, A. Müftüler, H. Deligöz, *Monitoring the salt stability and solvent swelling behavior of PAH-based polyelectrolyte multilayers by quartz crystal microbalance with dissipation*, *Polymer Engineering and Science* 63 (10) (2023) 3328–3342.
- [19] M. Anwar, F. Pervaiz, H. Shoukat, S. Noreen, K. Shabbir, A. Majeed, S. Ijaz, *Formulation and evaluation of interpenetrating network of xanthan gum and polyvinylpyrrolidone as a hydrophilic matrix for controlled drug delivery system*, *Polymer Bulletin* 78 (1) (2021) 59–80.
- [20] Y. Jang, B. Akgun, H. Kim, S. Satija, K. Char, *Controlled release from model blend multilayer films containing mixtures of strong and weak polyelectrolytes*, *Macromolecules* 45 (8) (2012) 3542–3549.
- [21] A. Ghiorghita, F. Bucatariu, E. S. Dragan, *Influence of cross-linking in loading/release applications of polyelectrolyte multilayer assemblies. A review*, *Materials Science and Engineering C* 105 (2019) 110050 20 pages.
- [22] H. Zhang, L. Yu, L. Han, X. Liu, S. Ruan, J. Hu, *Fast modulation of surface amphiphobicity/amphiphilicity via bidirectional substitution between perfluorinated surfactants and polyanions throughout pre-assembled polyelectrolyte multilayers*, *Langmuir* 35 (52) (2019) 17122–17131.
- [23] H. Y. Cengiz, E. Konyali, A. Müftüler, H. Deligöz, *Investigating the effect of weak polyelectrolytes on the chemical stability and swelling recovery of multilayered coatings*, *Progress in Organic Coatings* 183 (2023) 107775 10 pages.
- [24] C. Li, J. Zhang, J. Han, B. Yao, *A numerical solution to the effects of surface roughness on water–coal contact angle*, *Scientific Reports* 11 (1) (2021) Article Number 459 12 pages.

- [25] A. Quinn, E. Tjipto, A. Yu, T. R. Gengenbach, F. Caruso, *Polyelectrolyte blend multilayer films: Surface morphology, wettability, and protein adsorption characteristics*, *Langmuir* 23 (9) (2007) 4944–4949.
- [26] W. Zhang, Q. Zhao, J. Yuan, *Poröse polyelektrolyte: Zusammenspiel zwischen Poren und Ladung für neue funktionen*, *Angewandte Chemie* 130 (23) (2018) 6868–6889.



Recent Engineering Applications for Noise Reduction in an Automotive Industry

Ülge Taş¹ , Ender Pak² , Berkay Uğur³ 

¹Department of Industrial Engineering, Faculty of Engineering, Aksaray University, Aksaray, Türkiye

Article History

Received: 6 Nov 2023

Accepted: 22 Jan 2024

Published: 15 Mar 2024

Research Article

Abstract – Industrialization harms as it results in the emission of noise into the surroundings and employees. Especially noise is one of the most common causes of hearing disorders and one of the most common occupational diseases in the industry. Reducing the main noise sources has become increasingly urgent since the effect on employee health was negative. Although noise reduction is an important issue in the industry, previous research has not addressed it adequately, particularly in the automotive industry. This paper presented a detailed case study on the reduction of noise in a pilot area of an automotive assembly line. The paper aimed to improve the quality of the working environment by reducing the use of Personal Protective Equipment (PPE) and noise reduction. For this purpose, noise measure tools were used: a Svantec-type noise dosimeter and a sound level meter. In the course of studies, it was creating noise maps (before/after), in order to verify whether the proposed measures will be sufficient. Once the proposed measures have been implemented, a 14.2% reduction in noise levels helped ensure employees' safety by reducing the need for mandatory PPE. Meanwhile, the noise reduction percentage for AGV is the highest among the five noise sources, at 20.9%. Results showed that the sound pressure levels dropped from 110 dBA to 87 dBA and reduced on average for AGV. Reducing reliance on PPE and implementing noise reduction measures enhances pilot area safety and contributes to a more ergonomic and sustainable work environment. The implementation of this case, the application of the suggested measures, and the subsequent verification approved a considerable reduction in the noise levels in the influenced pilot area, and the measures applied were assessed as highly effective with result rates.

Keywords – Noise mapping, noise reduction, noise sources, sound pressure level

1. Introduction

As a result of technological development and globalization, a significant point related to the hazards of employees comes to the forefront, namely, noise. Noise is among the most frequently occurring worldwide occupational threats, especially in the industry [1]. Various studies have reported that noise exposure can lead to hearing loss, sleep disturbances, psychological disorders, coronary heart disease, hypertension, and stress [2]. Nowadays, a widely used concept for preventing these diseases and improving life standards is to reduce industrial noise, above all in the industrial [3].

The industrial noise problem was explained as the industrial noise generated by industrials, and then how to consider the additional effect of other types of noise from the machine and equipment activities in the area [4]. Noise reduction has become an important part of the production process for all industries. Nowadays, especially in the production industry, with the increase in overall noise, the noise inside the production line is more and more related to equipment or technical machines. Noise-induced hearing loss is a prevalent form of industrial disease [5]. Therefore, reducing PPE use when sound levels fall below a certain threshold is

¹ulge.tas@aksaray.edu.tr (Corresponding Author); ²ender.pak@daimlertruck.com; ³berkay.ugur@daimlertruck.com

necessary. In this context, conducting a comprehensive case study is required to minimize the impact of industrial noise on employees [6].

Although noise reduction is an important issue in the automotive industry, previous research has not addressed it adequately. This study aimed to improve the quality of the working environment by reducing the use of PPE and noise reduction. This gap in this field is not well-covered by existing case studies. That can be said to be the originality of this study. In this context, the paper presents the original research of the researchers, which is expected to contribute to the literature on noise reduction in the automotive industry.

This case study employs a unique approach to contributing to the automotive industry and literature. Conducted in a functioning production facility, the study fills a gap in the existing literature. The research results may aid in reducing noise and promoting Personal Protective Equipment (PPE) usage in industries. This paper describes the noise sources and presents the main noise issues. The conducted investigations are detailed, and the results are shared with all involved parties. Furthermore, the noise reduction strategies outlined in this study may serve as a guide for future research.

2. Literature Review

One of the troubles effects of industrialization is noise spreads into the surrounding environment. Therefore, with the increase in industrial manufacturing, more and more employees are exposed to the negative impacts of noise. According to recent studies, research aimed at reducing noise pollution is often linked to various health issues. However, there are only a few works that address both noise reduction and its related health outcomes. Table 1 provides details of some of the most noteworthy research studies in this area, along with their significant findings.

Table 1. Literature review

Authors	Focus of Interest	Methods	Findings
Deryabin [7]	In the automotive industry, it helps to partially improve sound insulation in the car interior.	Simulation	The method to reduce noise implies using acoustic plugs in the car interior.
Akmal and Bharathiraja [8]	A new design of the automotive engine mount for noise reduction	Simulation	The results showed that noise reduction of the engine mount was suppressed by approximately 14% to 26%.
Bennouna et al. [9]	The France automotive supplier aims to provide quiescence inside the car cabin by reducing Climate System noises during its operation.	Experimental investigations	The results for the considered climate systems induce a significant noise reduction on both structure radiation and aeraulic paths.
Mahadhir et al. [10]	Automotive muffler manufacturer in Malaysia	Experimental investigations (simulation)	The most suitable model for reducing the tailpipe noises is the model, which manages to reduce the noise by 3.07%, reduce the perforates number and shorten the length.
Qiu and He [6]	Noise reduction in a cigarette factory (The case of China)	Case study	Findings indicated that the average sound pressure levels were reduced by 6.5 dB(A).
Chang et al. [11]	They recruited 948 male workers in an aircraft manufacturing company in Taiwan.	Surveys	Findings indicate that noise-induced hearing loss may be related to the risk of hypertension.
Gan et al. [12]	This study included 6,307 participants of the USA National Health and Nutrition Examination Survey.	Surveys	Continually exposure to occupational noise is strongly associated with widespread coronary heart disease and hypertension, especially for young male current smokers.
Nawaz and Hasnain [13]	389 samples in the Pakistani population.	Surveys	Findings indicate that noise-induced hearing loss may be related to the risk of hypertension.
Van Kempen et al. [14]	A meta-analysis of 43 epidemiologic studies published 1970 - 1999.	Meta-analysis in literature	They present noise exposure hypertension and heart illness, which is consistent with an increase in cardiovascular disease risk in populations exposed to environmental noise.

Previous research has been conducted to explore relevant studies that analyzed noise reduction. Most researchers focus on changing worker behavior rather than noise. However, the case study could be rare, even though studies address the issue of noise reduction in the automotive industry, especially. This study aimed to improve the quality of the working environment by reducing the use of PPE and addressing noise reduction. Above all, the scarcity of case studies in the literature highlights a gap in this field.

3. Materials and Methods

The study was conducted as a case study in the organization known as ABC, which operates in the automotive field in Turkey on a large scale. The measurements were carried out during the production in June 2023, within the routine workflow of the facilities, which employ 2,000 personnel and are built on a closed area of 152,000 m² and an open area of 696,000 m². This case study analyzed the improvement steps taken based on actual data identified and eliminated the dominant noise sources by a team. The team building utilized managers, engineers, and a researcher in the present case study. The research data was collected from the assembly line, chosen as a pilot area. In ABC firm, 1 of 6 production lines called assembly line was observed.

Based on the sound pressure level measurement, the Svantec type 140 (SVAN 140) noise dosimeter with the Svantec type 971 (SVAN 971) sound level meter was used. The SVAN 104 is a noise dosimeter that meets the specifications for measuring workplace noise levels and hearing protection by health and safety regulations. The device measures noise dose and noise levels in the large-scale measurement range of 55 dBA to 140 dBA [15]. SVAN 971 sound level meter is a tremendous precision with options for octave analysis. The SVAN 971 is the best choice for many applications, including industrial, environmental, and general noise measurements. Another feature of SVAN 971 is providing data about the level of vibration that influences the measurement results [16].

The paper outlines the case study stages: determining the current status, taking measures, data collection, data analysis, and reporting.

(a) The initial stage of the whole process is to comprehend the current status of the noise conditions in the chosen operation, a significant part of which is the measurement of severe noise sources. The creation of current noise mapping aimed to visualize the process, determine an actual noise measure for the current assembly line, and consider the production effect. Noise maps are created to acquire data for studying noise reduction, and noise mapping illustrates the best way to identify noise sources [17].

(b) In the second step of mapping, all noise sources defined as point sources, with various types of noises disturbing the production workers were determined, which reduced concentration and productivity. The noise decibel (dBA) in the assembly line has increased in recent years due to the usage of more equipment with PPE warning sounds in the ABC firm. Therefore, one of the aims of this study was to reduce the use of PPE materials. According to noise-related regulations, the commonly confirmed standard to diminish hearing risk relies on exposure to 85 dBA for a maximum limit of eight hours per day, followed by at least ten hours of healing time at 70 dBA or lower (URL 1) [18]. Thus, reducing the impact of industrial noise on people requires a comprehensive study of noise sources and their mitigation strategies.

(c) In this context, the analysis of the noise levels to account for noise exposure time was determined in the third step. According to the Occupational Safety and Health Administration (OSHA) [19], permissible noise exposure time is provided in Table 2.

Table 2. Permissible noise exposure time [19]

Per day noise exposure time (hours)	Sound level slow response (dBA)
8	90
6	92
4	95
3	97
2	100
1½	102
1	105
½	110
¼ or less	115

Based on the information presented in this table, it appears that an employee has been exposed to certain levels of noise for particular durations: 110 dBA ¼ hour, 100 dBA ½ hour, 90 dBA 1½ hours, etc. Since the exposure time value is within allowable limits, the exposure is within permissible limits.

(d) The next step generated an analysis of noise sources, noise pressure levels, and solution proposals based on the research team’s data. Based on these measurements, dominant noise sources were recognized in the plant. With thorough information-gathering, team suggestions and measurements were taken to reduce the noise from sources, thereby reducing the negative impact on workers in the surroundings.

(e) Finally, in the fifth step, the implementation of the proposed measures, noise measurements were again performed in the area of the ABC plant. The noise measurements from various sources were conducted at 1 foot (30.48 centimeters) to ensure a comprehensive case. Specifically, measurements were taken 15 times, and distances between the noise source and the measuring device were maintained at 1 foot. The proposed measures were implemented thoroughly by the team proposal. The proposed noise measures were compared to both current and new conditions. It is evident from the noise measurements that there has been a substantial decrease in noise in the region following the implementation of the measures.

4. Results and Discussion

The team identified a pilot area on the assembly line with a current noise map, measured using SVAN 140 and 971. The noise level (dBA) in the assembly line has recently increased due to more equipment with relevant warning sounds for Occupational Safety and Health (OSH). Therefore, the assembly line was chosen as the pilot region. The model for the given dimensions of the assembly line was created using AutoCAD software, as shown in Figure 1, and exported to reflect the current status.



Figure 1. The current status pilot area

Figure 1 shows that the ‘noise from the pilot area’ is evaluated as a loud sound by almost all the devices compared to other assembly lines because of the loud sound of their operation. In the next phase of the case study, to gain knowledge of the current noise situation in the sources, noise measurements were carried out in the pilot area. While measuring this, noise exposure measurement devices (SVAN 140 and SVAN 971) were attached to the employees, and measurements were made in accordance with TS EN ISO 9612 - Measurement and evaluation of noise exposure in an acoustic working environment. The type of noise sources in Table 3 indicates significant sound impact, as determined by measuring devices and the measured results.

Table 3. Noise sources’ sound level

Type of Noise Source for Pilot Area	Sound Level (dBA)
AGV (Automated Guided Vehicle)	110
Motor crane	105
Pneumatic nut runner	95
Concrete slabs	94
Internal logistic	85

4.1. AGV

In the pilot area, noise intensity was measured on AGVs. Figure 2 shows the results before and after installing sound-absorbing materials on the fans of AGVs.



Figure 2. Elimination of noise fans of AGVs

The team recommended the installation of yellow stoppers on the AGV fans. Installing a sound-absorbing yellow stopper has reduced sound pressure levels by 110 to 87 dBA. As a result, it can reduce the noise intensity by 20.9%.

4.2. Motor Crane

Illustrate Figure 3, based on the noise measurements in the motor crane, which was broadband and evenly distributed, peaking at 105 dBA.

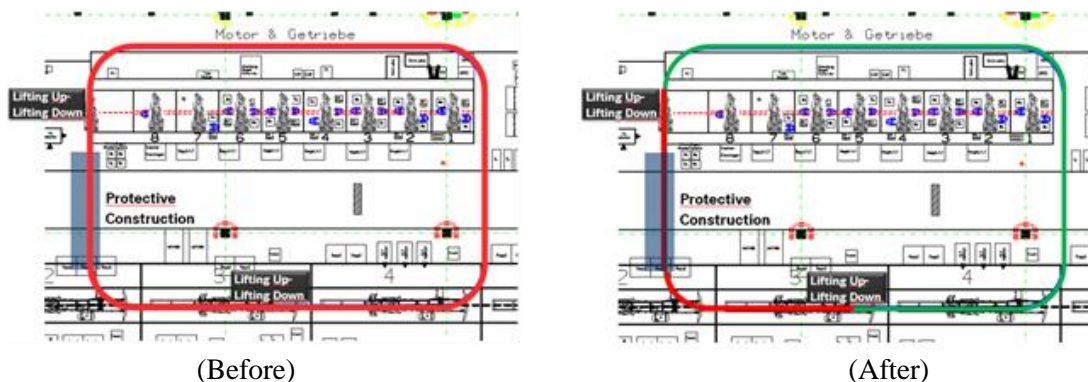


Figure 3. Reduction of crane buzzer noise level

After reducing the crane buzzer noise level, the sound pressure level of each frequency was lowered, and the noise was reduced to a maximum of 95 dBA. The employees' noise exposure time was reduced from 9 to 4 minutes because 95 dBA is considered high. The green area is where the noise level is appropriate, and the red area is where it is high. As a result, noise was reduced by 9.5% by turning off the buzzer during idle operation on the motor hoist.

4.3. Pneumatic Nut Runners

Due to the complex design of the engine, many noise issues of various origins occur within the pneumatic nut runners before and after, as shown in Figures 4 and 5. Most importantly, regarding the noise problem of the engine, pneumatic nut runners have been running with high noise.



Figure 4. Pneumatic nut runners of the engine

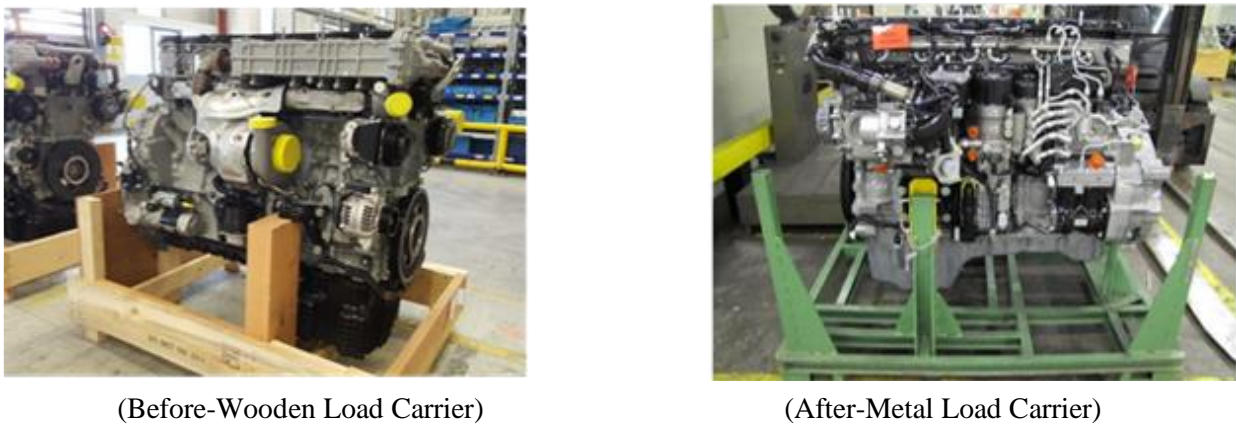


Figure 5. Load carrier of the engine

In Figure 4, inside the engine compartment, the pneumatic nut runners have been replaced with quieter ones, and the wooden load carriers have been changed to metal load carriers to reduce the car engine acoustic noise as shown in Figure 5. Replacement of the pneumatic nut runner and load carrier has reduced sound pressure levels from 95 to 78 dBA. The noise intensity has been reduced by 17.9% at the new status.

4.4. Concrete Slabs

Load carriers, forklifts, transport cars, and lifts cause noise while driving over concrete slabs. Expansion joints have been implemented to reduce noise, as shown in Figure 6.



Figure 6. Renewal of concrete slabs

Expansion joints have reduced sound pressure levels from 94 to 85 dBA. The noise intensity has been reduced by 9.6% at the new status.

4.5. Internal Logistic

Both LPG engine forklifts and handle cars are considered transportation options in internal logistics. Electric forklifts generate less noise than LPG forklifts due to their quieter operation. Therefore, replacing the LPG forklifts with electric ones has been decided. Moreover, drawbars were covered with rubber bearings for handle cars, and springs were changed with softer ones, as shown in Figure 7.



Figure 7. Changes in internal logistics

Handle cars, rubber bearings, and springs have reduced sound pressure levels from 85 to 74 dBA. The noise intensity has been reduced by 12.9% at the new status.

The contribution of the noise reduction was to improve the new status. Then, the resulting noise reduction was visualized through improvements in sound pressure levels, as shown in Figure 8.

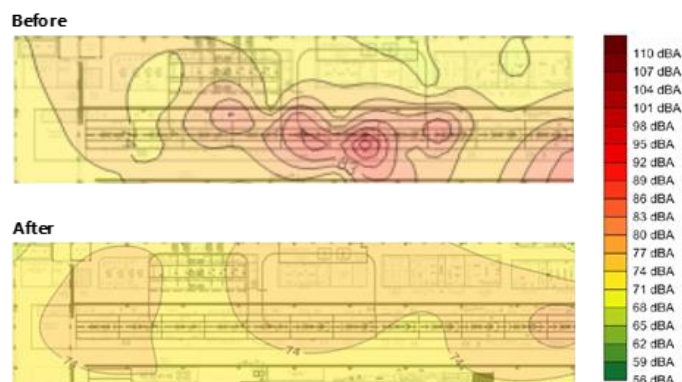


Figure 8. The new status pilot area

As a result of the studies, the overall noise level in the pilot area decreased to the target range. This result indicates that the noise level is below the target that could be achieved to prevent the usage of personal protective equipment. Measurements were taken 15 times, and distances between the noise source and the measuring device were maintained at 1 foot. The measurements conducted are presented in Table 4.

Table 4. Noise measurement (dBA)

	AGV	Motor crane	Pneumatic nut runner	Concrete slabs	Internal logistic
1	101	95	80	92	80
2	98	95	79	85	82
3	87	100	77	86	70
4	60	101	78	85	74
5	88	95	82	85	75
6	87	99	78	85	74
7	87	98	78	80	64
8	88	97	78	85	78
9	87	67	78	86	74
10	91	99	78	85	74
11	95	98	79	85	74
12	87	98	78	91	74
13	80	95	78	82	74
14	89	95	78	85	74
15	87	94	78	85	74
Average	87,47	95,07	78,47	85,47	74,33
Standard Deviation	8,86	7,78	1,15	2,80	3,93

The measures applied to assess the expected effects of a change in the sound pressure level process resulted in improvements as follows. Figure 9 shows the difference between the before and after situations.

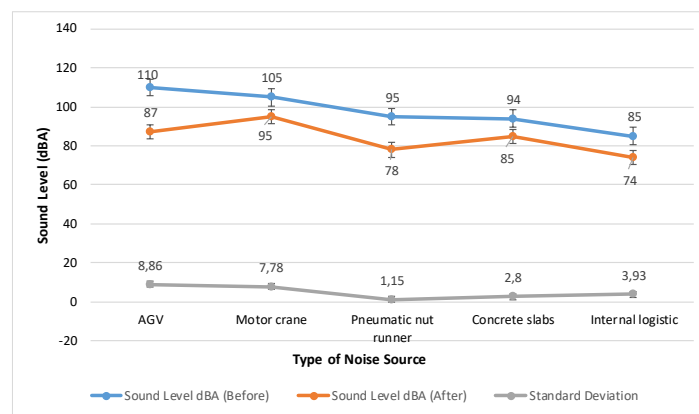


Figure 9. Sound level variation in noise sources after noise reduction

The literature aimed to improve the effectiveness of noise reduction in the automotive industry through sound absorption. This study’s results are consistent with related literature [6,10,20-22]. According to the case study, there was a 14.2% reduction in noise levels, reducing the need for mandatory PPE. Meanwhile, the noise reduction percentage for AGV is the highest among other noise sources, at 20.9%. Also, according to standards, sound-absorbing solutions have been applied to control noise above 85 dBA, and no PPE materials to control noise below 85 dBA.

5. Conclusion

Noise is a common cause of hearing disorders and occupational diseases in industry. Due to the negative impact on employees’ health, reducing the main noise sources has become increasingly urgent. Although noise

reduction is an important issue in the industry, previous research has not adequately addressed it, especially in the automotive industry. This present study aimed to improve the quality of the working environment by reducing the use of PPE and the noise level in a pilot area of an automotive assembly line. For this case study, we used noise measuring tools such as a Svantec noise dosimeter and a sound level meter. We took 15 measurements while maintaining a distance of 1 foot between the noise source and the measuring device. During the study, we created noise maps to compare the noise levels before and after implementing the proposed measures. This allowed us to verify if the measures were sufficient. This paper concludes with applications of techniques to reduce noise by the main five important noise sources. Results showed that the sound pressure levels were dropped from 110 dBA to 87 dBA and reduced by 20.9% on average for AGV; from 105 dBA to 95 dBA and reduced by 9.5% on average for Motor Crane; from 95 dBA to 78 dBA and reduced by 17.9% on average for Pneumatic Nut Runner; from 94 dBA to 85 dBA and reduced by 9.6% on average for Concrete Slabs, and from 85 dBA to 74 dBA and reduced by 12.9% on average for Internal Logistic. The average noise reduction for three of five noise sources is beneath 85 dBA. Meanwhile, the noise reduction percentage for AGV is the highest among the five noise sources, at 20.9%. Results showed that the sound pressure levels dropped from 110 dBA to 87 dBA and reduced on average for AGV. The case study showed a 14.2% reduction in noise levels, which helped ensure the safety of employees by reducing the need for mandatory PPE. When noise levels are below 85 dBA, using PPE is not required. In addition to sound pressure level and noise reduction, a map was created with the noise level in the case area before and after the noise reduction strategy. Reducing reliance on PPE and implementing noise reduction measures enhances pilot area safety and contributes to a more ergonomic and sustainable work environment.

This case study contributes to the automotive industry and literature due to its novel approach. Therefore, the research results can foster dissemination and reduce the noise and use of PPE in industries. Furthermore, the noise reduction strategies outlined in this case study guide are for future studies.

Author Contributions

The first author managed the research endeavor, overseeing the entire study's progression. The first and second authors conceived the fundamental conceptual notions and formulated the overarching theoretical framework. Data collection from the case study was executed by the third author. Manuscript composition was spearheaded by the first author, with collaborative input from the second and third authors. The analysis, article composition, results documentation, and paper review and editing were undertaken collectively by all authors. The final version of the paper garnered unanimous approval following a thorough examination by each author.

Conflicts of Interest

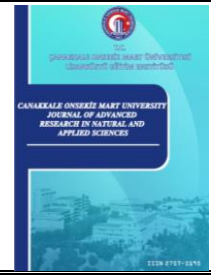
All the authors declare no conflict of interest.

References

- [1] D. I. Nelson, R. Y. Nelson, M. Concha-Barrientos, M. Fingerhut, *The global burden of occupational noise-induced hearing loss*, *American Journal of Industrial Medicine* 48 (6) (2005) 446–458.
- [2] W. Passchier-Vermeer, W. F. Passchier, *Noise exposure and public health*, *Environmental Health Perspectives*, 108 (2000) 123–131.

- [3] R. Nagy, D. Simoiu, K. Menyhardt, L. Bereteu, *Noise source monitoring in industrial and residential mixed areas*, Applied Mechanics and Materials 430 (2013) 262–265.
- [4] B. Sadler, *Environmental assessment in a changing world. In evaluating practice to improve performance – Final report*, Canadian Environmental Assessment Agency, Edmonton, 1996.
- [5] S. Tak, G. M. Calvert, *Hearing difficulty attributable to employment by industry and occupation: an analysis of the national health interview survey–United States, 1997 to 2003*, Occupational Environment Medicine 50 (2008) 46–56.
- [6] J. Qiu, X. He, *Evaluation of noise reduction in a cigarette factory, China*, International Journal of Physical Science 8 (44) (2013) 2035–2039.
- [7] I. Deryabin, *Noise reduction method in vehicle interior*, Transportation Research Procedia, 68 (2023) 642–646.
- [8] S. A. Akmal, G. Bharathiraja, *Analysis of engine mount material for automotive vibration and noise reduction*, Materials Today Proceedings 62 (2022) 2235–2239.
- [9] S. Bennouna, T. Matharan, O. Cheriaux, *Automotive HVAC noise reduction* (Technical Paper), 10th International Styrian Noise, Vibration & Harshness Congress: The European Automotive Noise Conference, 2018.
- [10] M. Mahadhir, M. M. A. Buang, A. A. Dahlan, M. H. Khairuddin, M. F. M. Said, *Simulation of automotive exhaust muffler for tail pipe noise reduction*, Jurnal Teknologi 79 (7-4) (2017) 37–45.
- [11] T. Y. Chang, C. S. Liu, K. H. Huang, R. Y. Chen, J. S. Lai, B. Y. Bao, *High-frequency hearing loss, occupational noise exposure, and hypertension: A cross-sectional study in male workers*, Environmental Health 10 (2011) Article Number 35 8 pages.
- [12] W. O. Gan, H. W. Davies, P. A. Demers, *Exposure to occupational noise and cardiovascular disease in the United States*, Occupational Environment Medicine 68 (2011) 183–190.
- [13] S. K. Nawaz, S. Hasnain S. *Noise-induced hypertension and prehypertension in Pakistan*, Bosnian Journal of Basic Medical Sciences 10 (2010) 239–244.
- [14] E. E. Van Kempen, H. Kruize, H. C. Boshuizen, C. B. Ameling, B. A. Staatsen, A. E. De Hollander. *The association between noise exposure and blood pressure and ischemic heart disease: A meta-analysis*, Environmental Health Perspectives 110 (2002) 307–317.
- [15] M. Moravec, M. Badida, N. Mikušová, L. Sobotová, J. Švajlenka, T. Dzuro, *Proposed options for noise reduction from a wastewater treatment plant: Case study*, Sustainability 13 (4) (2021) 2409–2431.
- [16] D. Czopek, K. Sochaczewska, J. Wiciak, *The soundscape of the Kościeliska Valley in the Tatra National Park – Case study*. in: J. Patricio (Ed.), Euronoise, Madeira, 2021, pp. 727–732.
- [17] T. S. Bozkurt, S. Y. Demirkale, *The field study and numerical simulation of industrial noise mapping*, Journal of Building Engineering 9 (2017) 60–75.
- [18] Türkiye - Legal Gazette (T. C. Resmi Gazete), *Çalışanların Gürültü ile İlgili Risklerden Korunmalarına Dair Yönetmelik* (28 Jul 2013 - 28721), <https://www.resmigazete.gov.tr/eskiler/2013/07/20130728-11.htm>, Accessed 6 Nov 2023.

- [19] Occupational Safety and Health Administration (OSHA) Standards, Code of Federal Regulations (29 CFR) (2017), U. S. Government Publishing Office, Washington, <https://www.govinfo.gov/content/pkg/CFR-2020-title29-vol8/pdf/CFR-2020-title29-vol8.pdf>, Accessed 6 Nov 2023.
- [20] W. Fiebig, D. Damian, *Use of acoustic camera for noise source localization and noise reduction in the industrial plant*, Archives of Acoustics 45 (1) (2020) 111–117.
- [21] B. Kukulski, T. Wszolek, *The research on impulsive events in railway noise generated during passage through a railroad switch*, Archives of Acoustics 42 (2017) 441–447.
- [22] C. Tomozei, F. Nedeff, G. Paraschiv, O. Irimia, G. Ardeleanu, A. C. Petrovici, *Mathematical modeling of sound pressure level attenuation transmitted by an acoustic screen in industrial environment*, Environmental Engineering and Management Journal 13 (2014) 1743–1749.



Effect of Venlafaxine on The Vitamins Contents of *Saccharomyces Cerevisiae* (NRRLY-12632)

Meltem Çakmak¹ , Dursun Özer² , Fikret Karataş³ , Sinan Saydam⁴ 

^{1,2}Department of Chemical Engineering, Faculty of Engineering, Firat University, Elazığ, Türkiye

^{3,4}Department of Chemistry, Faculty of Science, Firat University, Elazığ, Türkiye

Article History

Received: 28 Nov 2023

Accepted: 23 Jan 2024

Published: 15 Mar 2024

Research Article

Abstract – In this study, *Saccharomyces cerevisiae* (NRRLY-12632) was grown in YPD medium containing different concentrations of Venlafaxine ((RS)-1-[2-dimethylamino-1-(4-methoxyphenyl)-ethyl] cyclohexanol). To counteract the effect of venlafaxine, vitamin C was added to the growth medium, and vitamins content of *S. cerevisiae* were investigated by HPLC. It was found that the amounts of water-soluble vitamins and lycopene concentration in *S. cerevisiae*, decreased with increased venlafaxine concentration compared to the control ($p < 0.05$). On the other hand, the amounts of fat-soluble vitamins A, E, and β -carotene concentration were found to be increased ($p < 0.05$). The addition of vitamin C to the growth medium containing venlafaxine at different concentrations increased the number of water-soluble vitamins and lycopene content of *S. cerevisiae*, while decreasing the amount of fat-soluble vitamins A, E, and β -carotene, depending on vitamin C concentration. With the addition of vitamin C to the growth medium containing venlafaxine, all the vitamin concentrations get close to the control group. From these findings, it can be said that the negative effect of venlafaxine on *S. cerevisiae* is reduced by adding vitamin C to the growth medium of *S. cerevisiae*.

Keywords – *S. cerevisiae*, venlafaxine, vitamins, HPLC

1. Introduction

The term microorganism describes many living things broadly, including bacteria, yeast, fungi, and algae. Although humans and microorganisms have many genes in common, microorganisms carry some genes that are not present in humans. Yeast is a single-celled and eukaryotic organism widely found in biological systems. It is a highly adaptable organism that manufactures various food products, making it a group of organisms with a high biotechnological importance [1].

From yeasts, especially *S. cerevisiae* is widely used in scientific studies such as eukaryotic biology and the study of human diseases, its worldwide production is higher than that of other microorganisms. Yeast is used in many industries because it reproduces at a high rate quickly by using cheap renewable food sources and providing low cost [2]. Depression, which is a psychiatric disorder, is a complex disease with symptoms such as irritability, insomnia, fatigue, agitation, psychomotor changes, feelings of guilt, and self-devaluation, leading to serious dysfunctions in patients. Since depression, which is frequently seen in societies, brings with it the use of antidepressant drugs. Investigation of the effects of antidepressants on cellular structures has also become an important issue [3].

Like other drugs, antidepressants also cause oxidative stress by affecting cell metabolism, and the resulting

¹cakmak_meltem@hotmail.com; ²dozer@firat.edu.tr; ³fkaratas@firat.edu.tr (Corresponding Author); ⁴ssaydam@firat.edu.tr

free radicals can affect many parameters, such as cell membranes, proteins, amino acids, vitamins, total oxidant, and antioxidant capacity. Determining the damage to the cells due to the aforementioned harmful effects is important in preventing this damage [4]. Vitamins are organic molecules that have regulatory functions in the living system, act as a catalyst in metabolic events and help efficiently use nutrients in energy production. Vitamins are divided into two groups: water-soluble and fat-soluble [5]. Vitamin C has a strong antioxidant effect which is effective in releasing some hormones in the event of stress in living organisms [6].

In this study, the microorganism *S. cerevisiae* (NRRLY-12632) was used because of easy to culture, has at least 23% common genes among humans, and is similar to humans in terms of protein [7]. The effect of antidepressants on vitamins in *S. cerevisiae* cells was investigated by adding Venlafaxine, which humans widely use. In addition, it was aimed to examine the effect of vitamin C on the vitamin content of *S. cerevisiae* by adding vitamin C in the growth medium containing Venlafaxine.

2. Materials and Methods

2.1. Material

S. cerevisiae (NRRLY-12632) used in this study was obtained from Firat University, Department of Chemical Engineering, Biotechnology Laboratory. *S. cerevisiae* produced in yeast peptone dextrose (YPD) broth (10.0 g peptone, 5.0 g yeast extract, 10.0 g Dextrose per liter) was used. Solutions of 1000 ppm venlafaxine chloride and 500 ppm vitamin C were prepared freshly and used. The microorganism was produced in 250 mL flasks containing 50 mL nutrient medium. Experiments were carried out by forming the following groups for the study.

- 1. Control group:** Microorganisms were grown by inoculating *S. cerevisiae* in the YPD medium.
- 2. Venlafaxine group:** Microorganisms were grown by adding venlafaxine stock solution at desired concentrations (100 - 500 ppm) to the control.
- 3. Vitamin C group:** Microorganisms were produced by adding vitamin C at the desired concentration (10-75 ppm) to the venlafaxine group.

The medium was incubated on an orbital shaker (Selecta Rotabit) for 72 hours at 150 rpm at 30 °C. The concentration of *S. cerevisiae* was determined by measuring the absorbance at 600 nm with a spectrophotometer (CHEBIOS s.r.l.). After centrifugation of the medium containing the microorganism at 8000 rpm at 10 °C for 10 minutes (Nüve NF 800 R), the supernatant was removed, and the microorganism was washed twice with distilled water for further analysis.

2.2. Determination of Water Soluble Vitamins

The microorganism of known weight was vortexed by adding 3.0 mL of distilled water, and the mixture was sonicated (Wise Clean, WUC-AO3H, 170 W) 10 times for 30 seconds in an ice water bath. 1.0 mL, 0.5 M HClO₄ was added to the sonicated samples, the vortexed mixture was centrifuged at 8000 rpm for 10 minutes, and 1.0 ml of the supernatant was taken into HPLC vials. As the mobile phase in HPLC, the sodium salt of 5 mM heptanosulfonic acid was dissolved in methanol, and a solution of (A) and a solution of 0.1% triethylamine (B) were prepared. Then, solutions A and B were mixed at a volume ratio of 25:75, then the pH of the mixture was adjusted to 2.8 with phosphoric acid. Vitamins B and C were determined using a C18-DB column (15 cm x 4.6 mm x 5 µm) at a mobile phase flow rate of 1.0 mL/min [8].

2.3. Determination of Fat-Soluble Vitamins and Lycopene

6.0 mL of ethanol was added to the microorganism of known weight and vortexed; then, the microorganism solution was sonicated in an ice water bath (Wise Clean, WUC-AO3H, 170 W) for 30 seconds 10 times for each sample. The sonicated samples were centrifuged at 8000 rpm for 10 minutes, then 1.0 mL n-hexane was added to each tube and centrifuged again for 6 minutes at 4000 rpm. The n-hexane phase was transferred to a glass tube, and this process was repeated twice. Hexane was removed under vacuum at 30 °C, then 1.0 mL of methanol was added to the residue in the tube, transferred to HPLC vials, and analyzed by HPLC using an ODS-2 (25 cm, 4.6 mm ID, 5 µm) column. [9,10].

Intraday repeatability, linear working range, regression equation, regression coefficient, and % recovery values for water- and fat-soluble vitamins are given in Table 1.

Table 1. Some validation values in the determination of fat- and water-soluble vitamins

Parameters	Intra-day repeatability µg/mL	Range µg/mL	Regression equation	R ²	Recovery %
Vitamin A (1.0 µg/mL)	0.96	0.20 – 20	$y = 142378x$	0.999	98.2
Vitamin E (2.0 µg/mL)	1.90	0.30 – 70	$y = 1594.9x$	0.998	98.4
β-carotene (4.0 µg/mL)	3.90	0.10 – 60	$y = 14504x$	0.996	97.8
Lycopene (1.0 µg/mL)	0.95	0.05 – 50	$y = 5249.3x$	0.996	98.0
Vitamin C (5.0 µg/mL)	4.80	0.25 – 35	$y = 48528x$	0.999	97.6
Vitamin B1 (5.0 µg/mL)	4.90	0.15 – 50	$y = 43129x$	0.999	96.8
Vitamin B2 (2.0 µg/mL)	1.85	0.15 – 10	$y = 82893x$	0.999	96.5
Vitamin B3 (4.0 µg/mL)	3.90	0.30 – 40	$y = 40858x$	0.999	98.0
Vitamin B5 (3.0 µg/mL)	2.90	0.30 – 30	$y = 7435.1x$	0.999	96.5
Vitamin B6 (5.0 µg/mL)	4.85	0.35 – 45	$y = 45099x$	0.994	97.4
Vitamin B9 (5.0 µg/mL)	4.80	0.40 – 50	$y = 1758.9x$	0.993	97.9
Vitamin B12 (5.0 µg/mL)	4.80	0.10 – 30	$y = 19168x$	0.999	95.8

2.4. Statistical Analysis

All measurements were triplicated, and Mean ± Standard Deviation was determined. The results were subjected to one-way ANOVA by SPSS 26.0 for Windows. Differences between the group's means were analyzed for significance using the Tukey HSD test. The level of statistical significance was expressed as $p < 0.05$. The superscripts in the table columns are indicated as **a** if the effect of antidepressants compared to the control group is statistically significant ($p < 0.05$), **b** if the effect of vitamin C in growth medium containing antidepressants is statistically significant ($p < 0.05$), and **c** if it is not statistically significant ($p > 0.05$).

3. Results and Discussion

The concentrations of water and fat-soluble vitamins determined in *S. cerevisiae* for different experimental groups are given in Tables 2-4, respectively.

Table 2. Concentrations of vitamins C, B1, B2, and B3 in *S. Cerevisiae* produced in a nutrient medium containing varying concentrations of antidepressants and vitamin C

Application	Vitamin C ($\mu\text{g/g dw}$)	Vitamin B1 ($\mu\text{g/g dw}$)	Vitamin B2 ($\mu\text{g/g dw}$)	Vitamin B3 ($\mu\text{g/g dw}$)
Control	69.80 \pm 1.05	8.02 \pm 0.25	39.10 \pm 0.85	451.40 \pm 7.25
Ven-1	66.75 \pm 0.95 ^a	7.50 \pm 0.22 ^a	37.15 \pm 0.82 ^a	430.10 \pm 7.00 ^a
Ven-2	64.10 \pm 1.10 ^a	6.35 \pm 0.19 ^a	36.00 \pm 0.65 ^a	405.60 \pm 6.54 ^a
Ven-3	61.60 \pm 1.20 ^a	5.50 \pm 0.17 ^a	34.15 \pm 0.66 ^a	370.00 \pm 5.63 ^a
Ven-4	58.10 \pm 1.27 ^a	4.28 \pm 0.15 ^a	32.40 \pm 0.63 ^a	335.80 \pm 4.86 ^a
Ven-5	55.10 \pm 1.32 ^a	3.40 \pm 0.13 ^a	30.10 \pm 0.58 ^a	300.70 \pm 4.74 ^a
Ven-1+C10	67.60 \pm 0.90 ^c	7.65 \pm 0.23 ^c	37.50 \pm 0.80 ^c	436.80 \pm 6.05 ^c
Ven-1+C25	68.30 \pm 0.70 ^c	7.80 \pm 0.24 ^c	38.10 \pm 0.72 ^c	441.00 \pm 6.00 ^c
Ven-1+C50	69.10 \pm 0.68 ^b	7.90 \pm 0.20 ^c	38.61 \pm 0.70 ^c	445.30 \pm 6.10 ^b
Ven-1+C75	70.00 \pm 0.72 ^b	8.05 \pm 0.19 ^b	39.02 \pm 0.65 ^b	450.00 \pm 5.00 ^b
Ven-2+C10	65.60 \pm 0.90 ^c	6.42 \pm 0.18 ^c	36.65 \pm 0.68 ^c	410.85 \pm 4.50 ^c
Ven-2+C25	67.10 \pm 0.70 ^b	6.90 \pm 0.15 ^b	37.25 \pm 0.66 ^c	420.90 \pm 4.58 ^b
Ven-2+C50	68.30 \pm 0.66 ^b	7.15 \pm 0.17 ^b	38.00 \pm 0.70 ^b	428.60 \pm 4.61 ^b
Ven-2+C75	69.60 \pm 0.70 ^b	7.50 \pm 0.18 ^b	38.66 \pm 0.67 ^b	435.00 \pm 4.65 ^b
Ven-3+C10	63.60 \pm 0.86 ^c	5.95 \pm 0.14 ^b	35.00 \pm 0.56 ^c	378.10 \pm 5.06 ^c
Ven-3+C25	64.45 \pm 0.80 ^b	6.40 \pm 0.15 ^b	35.85 \pm 0.57 ^b	387.40 \pm 4.50 ^b
Ven-3+C50	65.70 \pm 0.75 ^b	6.90 \pm 0.17 ^b	36.58 \pm 0.60 ^b	395.00 \pm 4.65 ^b
Ven-3+C75	67.60 \pm 0.70 ^b	7.20 \pm 0.19 ^b	37.10 \pm 0.63 ^b	402.80 \pm 4.70 ^b
Ven-4+C10	60.00 \pm 0.92 ^c	4.50 \pm 0.15 ^c	33.00 \pm 0.55 ^c	341.50 \pm 5.00 ^c
Ven-4+C25	62.30 \pm 0.83 ^b	4.85 \pm 0.16 ^b	33.75 \pm 0.54 ^b	349.75 \pm 5.05 ^b
Ven-4+C50	64.60 \pm 0.80 ^b	5.35 \pm 0.18 ^b	34.30 \pm 0.56 ^b	359.00 \pm 4.86 ^b
Ven-4+C75	66.30 \pm 0.85 ^b	6.00 \pm 0.17 ^b	35.10 \pm 0.55 ^b	369.50 \pm 4.80 ^b
Ven-5+C10	57.60 \pm 0.81 ^c	3.90 \pm 0.14 ^b	31.00 \pm 0.50 ^c	308.80 \pm 3.95 ^c
Ven-5+C25	59.70 \pm 0.78 ^b	4.40 \pm 0.15 ^b	31.90 \pm 0.45 ^b	317.90 \pm 4.00 ^b
Ven-5+C50	62.45 \pm 0.75 ^b	5.20 \pm 0.17 ^b	32.85 \pm 0.48 ^b	328.00 \pm 4.08 ^b
Ven-5+C75	64.60 \pm 0.80 ^b	5.86 \pm 0.16 ^b	33.70 \pm 0.51 ^b	340.00 \pm 4.15 ^b

Ven-1: 100 ppm venlafaxin, Ven-2: 200 ppm venlafaxin, Ven-3: 300 ppm venlafaxin, Ven-4: 400 ppm venlafaxin, Ven-5: 500 ppm venlafaxin, C10: 10 ppm Vitamin C, C25: 25 ppm Vitamin C, C50: 50 ppm Vitamin C, C75: 75 ppm Vitamin C

It is reported that vitamin C is a good singlet oxygen scavenger that neutralizes reactive oxygen species (ROS), reduces oxidative stress, and eliminates free radicals with its scavenging effect [11].

It is reported that vitamin C has important roles such as tissue repair, protein formation, inactivation of toxic metals, and protection from the harmful effects of oxidants [6].

As shown in Tables 2 and 3, as the concentration of antidepressants increases in the medium, the vitamin C concentration of *S. cerevisiae* decreases. In addition, the vitamin C content of the microorganism increases as the increased vitamin C is added to the growth medium. It has been reported that adding vitamin C to the medium reduces the oxidative stress caused by Cr (III) [12]. A study said that the amount of ascorbic acid in the tissues of mice given CrO₃ was lower than that of the control group [13].

Table 3. Concentrations of vitamins B5, B6, B9, and B12 in *S. Cerevisiae* produced in a nutrient medium containing varying concentrations of antidepressants and vitamin C

Application	Vitamin B5 ($\mu\text{g/g dw}$)	Vitamin B6 ($\mu\text{g/g dw}$)	Vitamin B9 ($\mu\text{g/g dw}$)	Vitamin B12 ($\mu\text{g/g dw}$)
Control	168.90 \pm 2.75	385.00 \pm 4.38	21.80 \pm 0.45	6.10 \pm 0.20
Ven-1	160.20 \pm 2.56 ^a	375.40 \pm 4.20 ^a	19.50 \pm 0.41 ^a	5.70 \pm 0.18 ^a
Ven-2	151.35 \pm 2.40 ^a	363.85 \pm 4.10 ^a	17.00 \pm 0.38 ^a	5.00 \pm 0.16 ^a
Ven-3	139.50 \pm 2.34 ^a	348.70 \pm 4.00 ^a	15.10 \pm 0.38 ^a	4.15 \pm 0.15 ^a
Ven-4	130.75 \pm 2.10 ^a	339.10 \pm 4.05 ^a	13.35 \pm 0.33 ^a	3.60 \pm 0.13 ^a
Ven-5	120.68 \pm 2.00 ^a	330.25 \pm 3.80 ^a	11.90 \pm 0.28 ^a	3.30 \pm 0.14 ^a
Ven-1+C10	162.55 \pm 2.42 ^c	378.60 \pm 4.00 ^c	20.10 \pm 0.37 ^b	5.80 \pm 0.16 ^c
Ven-1+C25	165.10 \pm 2.45 ^c	380.50 \pm 3.95 ^c	20.70 \pm 0.36 ^b	5.90 \pm 0.17 ^c
Ven-1+C50	167.35 \pm 2.15 ^b	383.20 \pm 3.90 ^c	21.20 \pm 0.35 ^b	5.94 \pm 0.16 ^c
Ven-1+C75	169.40 \pm 2.00 ^b	385.80 \pm 4.00 ^b	21.75 \pm 0.40 ^b	6.05 \pm 0.18 ^c
Ven-2+C10	154.00 \pm 2.35 ^c	367.30 \pm 3.70 ^c	17.85 \pm 0.36 ^b	5.35 \pm 0.15 ^b
Ven-2+C25	158.45 \pm 2.18 ^b	371.20 \pm 3.73 ^b	18.95 \pm 0.35 ^b	5.60 \pm 0.16 ^b
Ven-2+C50	163.20 \pm 2.15 ^b	374.80 \pm 3.68 ^b	19.50 \pm 0.38 ^b	5.85 \pm 0.14 ^b
Ven-2+C75	167.10 \pm 2.05 ^b	379.00 \pm 3.70 ^b	20.60 \pm 0.36 ^b	6.00 \pm 0.15 ^b
Ven-3+C10	142.40 \pm 2.00 ^c	352.10 \pm 3.80 ^c	16.50 \pm 0.27 ^b	4.45 \pm 0.13 ^b
Ven-3+C25	146.10 \pm 2.05 ^b	356.85 \pm 3.84 ^b	18.00 \pm 0.29 ^b	4.82 \pm 0.14 ^b
Ven-3+C50	150.00 \pm 2.10 ^b	361.20 \pm 3.80 ^b	19.45 \pm 0.28 ^b	5.15 \pm 0.16 ^b
Ven-3+C75	154.60 \pm 2.20 ^b	365.85 \pm 3.90 ^b	20.90 \pm 0.29 ^b	5.60 \pm 0.17 ^b
Ven-4+C10	134.10 \pm 1.95 ^c	342.45 \pm 3.26 ^c	15.00 \pm 0.30 ^b	3.85 \pm 0.15 ^c
Ven-4+C25	139.25 \pm 2.00 ^b	347.80 \pm 3.25 ^b	16.20 \pm 0.29 ^b	4.10 \pm 0.16 ^b
Ven-4+C50	144.20 \pm 2.07 ^b	351.20 \pm 3.30 ^b	17.25 \pm 0.31 ^b	4.65 \pm 0.18 ^b
Ven-4+C75	148.34 \pm 2.11 ^b	356.40 \pm 3.40 ^b	18.40 \pm 0.32 ^b	5.00 \pm 0.20 ^b
Ven-5+C10	124.50 \pm 2.00 ^c	336.00 \pm 3.00 ^c	12.68 \pm 0.25 ^b	3.55 \pm 0.15 ^c
Ven-5+C25	130.05 \pm 2.10 ^b	345.05 \pm 3.05 ^b	13.35 \pm 0.24 ^b	3.90 \pm 0.17 ^c
Ven-5+C50	135.90 \pm 2.14 ^b	353.30 \pm 3.10 ^b	15.00 \pm 0.25 ^b	4.30 \pm 0.16 ^b
Ven-5+C75	140.80 \pm 2.17 ^b	360.00 \pm 3.00 ^b	16.45 \pm 0.27 ^b	4.80 \pm 0.19 ^b

Ven-1: 100 ppm venlafaxin, Ven-2: 200 ppm venlafaxin, Ven-3: 300 ppm venlafaxin, Ven-4: 400 ppm venlafaxin, Ven-5: 500 ppm venlafaxin, C10: 10 ppm Vitamin C, C25: 25 ppm Vitamin C, C50: 50 ppm Vitamin C, C75: 75 ppm Vitamin C

It has been reported that the deficiency of B vitamins, which are involved in all areas of the catabolic process for energy production, adversely affects cells. In particular, the active forms of thiamine, riboflavin, niacin, and pantothenic acid are essential coenzymes in cellular energy production through their role in the electron transport chain [14,15]. Vitamins B1 and B6 are necessary for the health of the nervous system; vitamin B3 regulates blood circulation. Vitamin B6 and B9 play a role in forming red blood cells, while vitamin B12 is important in nucleic acid metabolism and myelin synthesis [16].

As seen in Tables 2 and 3, it was observed that the number of vitamins B1, B2, B3, B5, B6, B9, and B12 in the microorganism decreased depending on the concentration of Venlafaxine added to the medium. In addition, it was found that increased vitamin C concentration in the growth medium containing venlafaxine led to an increase in the amount of B vitamins in the microorganism. As a result of the addition of 100 ppm venlafaxine to the control group, decrease in the amounts of vitamins as percentage 4.37, 6.48, 4.99, 4.49, 5.15, 2.49, 10.55, 6.55 were C, B1, B2, B3, B5, B6, B9, B12 respectively, on the other hand 400 ppm venlafaxine added, the

ratio of the same vitamins was found to be 16.76, 46.63, 17.14, 25.61, 22.58, 11.92, 38.76, 40.98, respectively. As a result of adding 25 ppm vitamin C to the medium containing 300 ppm venlafaxine, the percentage increase in the amounts of vitamins C, B1, B2, B3, B5, B6, B9, B12 was 4.63, 16.36, 4.98, 4.70, 4.73, 2.34, 19.21, 16.14. In comparison, 75 ppm of vitamin C was added to the same medium, and the ratio of increase in the same vitamins was found to be 9.74, 30.91, 8.64, 8.82, 10.82, 4.93, 38.41, and 34.94, respectively.

Table 4. Concentrations of fat-soluble vitamins in *S. cerevisiae* produced in a nutrient medium containing various concentrations of antidepressants and vitamin C

Application	Vitamin A (µg/g dw)	Vitamin E (µg/g dw)	β-Carotene (µg/g dw)	Lycopene (µg/g dw)
Control	4.50±0.16	30.50±0.50	1.35±0.09	0.69±0.05
Ven-1	5.30±0.18 ^a	32.60±0.52 ^a	1.50±0.10 ^a	0.61±0.04 ^a
Ven-2	5.95±0.17 ^a	35.00±0.60 ^a	1.85±0.11 ^a	0.54±0.04 ^a
Ven-3	6.50±0.20 ^a	37.70±0.56 ^a	2.10±0.13 ^a	0.47±0.03 ^a
Ven-4	7.00±0.22 ^a	40.00±0.61 ^a	2.50±0.12 ^a	0.41±0.03 ^a
Ven-5	7.70±0.19 ^a	43.00±0.63 ^a	2.90±0.14 ^a	0.35±0.02 ^a
Ven-1+C10	5.10±0.17 ^c	32.25±0.50 ^c	1.46±0.10 ^c	0.63±0.03 ^c
Ven-1+C25	4.90±0.15 ^b	31.90±0.48 ^c	1.42±0.08 ^c	0.65±0.04 ^c
Ven-1+C50	4.72±0.11 ^b	31.45±0.45 ^b	1.39±0.07 ^c	0.67±0.04 ^c
Ven-1+C75	4.51±0.10 ^b	30.90±0.43 ^b	1.36±0.07 ^c	0.69±0.03 ^b
Ven-2+C10	5.76±0.15 ^c	34.60±0.50 ^c	1.79±0.12 ^c	0.59±0.03 ^c
Ven-2+C25	5.50±0.13 ^b	34.00±0.47 ^c	1.73±0.11 ^c	0.62±0.03 ^b
Ven-2+C50	5.15±0.12 ^b	33.35±0.48 ^b	1.68±0.10 ^c	0.66±0.04 ^b
Ven-2+C75	4.90±0.10 ^b	32.80±0.44 ^b	1.60±0.08 ^b	0.70±0.04 ^b
Ven-3+C10	6.15±0.18 ^c	37.25±0.52 ^c	2.00±0.12 ^c	0.51±0.03 ^c
Ven-3+C25	5.90±0.16 ^b	36.85±0.50 ^c	1.92±0.10 ^c	0.56±0.03 ^b
Ven-3+C50	5.57±0.15 ^b	36.25±0.48 ^b	1.84±0.10 ^b	0.60±0.03 ^b
Ven-3+C75	5.35±0.15 ^b	35.80±0.45 ^b	1.76±0.09 ^b	0.64±0.02 ^b
Ven-4+C10	6.71±0.19 ^c	39.50±0.53 ^c	2.38±0.13 ^c	0.46±0.03 ^c
Ven-4+C25	6.30±0.15 ^b	38.90±0.50 ^c	2.24±0.11 ^b	0.51±0.03 ^b
Ven-4+C50	5.93±0.16 ^b	38.20±0.47 ^b	2.11±0.11 ^b	0.57±0.03 ^b
Ven-4+C75	5.50±0.14 ^b	37.75±0.45 ^b	1.93±0.10 ^b	0.61±0.04 ^b
Ven-5+C10	7.41±0.20 ^c	42.55±0.56 ^c	2.80±0.16 ^c	0.39±0.02 ^c
Ven-5+C25	7.06±0.19 ^b	42.00±0.53 ^c	2.69±0.13 ^c	0.45±0.02 ^b
Ven-5+C50	6.82±0.17 ^b	41.25±0.50 ^b	2.56±0.11 ^b	0.51±0.03 ^b
Ven-5+C75	6.34±0.14 ^b	39.85±0.42 ^b	2.40±0.10 ^b	0.58±0.03 ^b

Ven-1: 100 ppm venlafaxin, Ven-2: 200 ppm venlafaxin, Ven-3: 300 ppm venlafaxin, Ven-4: 400 ppm venlafaxin, Ven-5: 500 ppm venlafaxin, C10: 10 ppm Vitamin C, C25: 25 ppm Vitamin C, C50: 50 ppm Vitamin C, C75: 75 ppm Vitamin C

As seen from these results, the number of water-soluble vitamins decreased. When vitamin C, which has antioxidant properties, is added to the growth medium of *S. cerevisiae*, led to an increase in the number of water-soluble vitamins. As a result, it might be said that the metabolic stress caused by venlafaxine in microorganisms is reduced by vitamin C.

A study reported that cadmium added to the medium of *C. freundii* decreased the amount of water-soluble vitamins C and B in the microorganism. In contrast, vitamin C addition to the same medium increased the

amount of vitamins C and B [17]. A study investigating resistance to oxidative, osmotic, and thermal stress reported that thiamine increased the stress resistance of *S cerevisiae* [18].

It has been reported that lipid peroxidation increases in rats' tissues due to insufficient riboflavin in nutrition [19]. It has been reported that niacin added to the feed of rats caused a significant increase in superoxide dismutase (SOD), catalase (CAT), glutathione peroxidase (GPx), glutathione and zinc levels and a decrease in lipid peroxidation (LPO) levels compared to the control group [20]. It has been reported that when fish under oxidative stress are fed a diet deficient in pantothenic acid, SOD and CAT activities in the liver were found to be low, and there was a positive relationship between pantothenic acid and antioxidant defense [21].

In a study investigating the effect of pyridoxine on oxidative stress on erythrocyte membrane protein, it was shown that pyridoxine can significantly reduce lipid peroxidation and protein carbonylation in the red cell membrane exposed to high concentrations of oxidant agents [22].

Koyama et al. [23] reported that when heat stress was applied to mouse embryos, the curative effects of folic acid on the development of mouse embryos were observed.

Investigation of the effects of different concentrations and application times of vitamin B12 on the antioxidant response of *Physiophora alceae*, conducted by Abdelfattah [24], was reported that administered that vitamin B12 reduced superoxide anion radical ($O_2 \bullet^-$) and hydrogen peroxide (H_2O_2) levels. At all venlafaxine concentrations, while vitamin B1 concentration decreased significantly ($p < 0.05$), the addition of vitamin C to a medium containing 200, 300, 400, and 500 ppm venlafaxine significantly increased the amount of vitamin B1 ($p < 0.05$).

Vitamins B3, B5, and B12 were significantly decreased ($p < 0.05$) at 200, 300, 400, and 500 ppm with the increased venlafaxine concentrations. When 25, 50, and 75 ppm of vitamin C were added to the growth medium containing the same concentrations of venlafaxine, the number of vitamins B3, B5, and B12 increased significantly ($p < 0.05$). The decrease in vitamins B2 and B6 was significant at all venlafaxine concentrations ($p < 0.05$). The increase in vitamin B2 and B6 amounts was significant, adding 25, 50, and 75 ppm of vitamin C to media containing 300, 400, and 500 ppm of venlafaxine ($p < 0.05$). The amounts of vitamin C and B9 were significantly reduced ($p < 0.05$) at all concentration values of venlafaxine added to the medium. Adding vitamin C to the growth medium containing venlafaxine at 25, 50, and 75 ppm led to significantly increased vitamins C and B9 in the microorganism ($p < 0.05$).

In a study conducted to investigate the effect of vitamin A treatment on yeast strains with SOD deficiency, it was observed that the addition of vitamin A to the medium at certain concentrations increased CAT and GSH Px activities and GSH levels in yeast [25].

Vitamin E has been found to reduce free radicals in the plasma, lungs, and brains of mice exposed to arsenic. It has also been determined that vitamin E supplementation facilitates the work of stress enzymes in animals [26]. Finaud et al. [27] reported that β -carotene deactivates ROS and reduces lipid peroxidation. In a study on cats with kidney failure, it was reported that the concentration of 8-hydroxy 2-deoxygenase, which is a marker of oxidative stress, in the blood serum decreased as a result of the administration of vitamins E, C, and β -carotene [28].

Investigation of the role of lycopene in oxidative stress: various forms of lycopene were reported to reduce markers of lipid peroxidation and oxidative stress [29]. It was reported that applying heavy metal stress on *C freundii* decreased lycopene concentrations due to stress. At the same time, the addition of vitamin C increased the amount of lycopene concentration [17]. It was found that vitamin A increased significantly ($p < 0.05$)

depending on the concentration of venlafaxine added to the medium, and the amount of vitamin A observed decreased significantly ($p < 0.05$) at all concentrations except 10 ppm of vitamin C. While vitamin E concentration increased significantly with the increase of venlafaxine added to the medium ($p < 0.05$), it was found that 50 and 75 ppm of vitamin C added to the medium decreased vitamin E ($p < 0.05$) (Table 4).

The amount of β -carotene was significantly increased at all venlafaxine concentrations ($p < 0.05$); the addition of vitamin C to the medium containing 100 and 200 ppm venlafaxine did not cause a significant change in the concentration of β -carotene ($p > 0.05$) (Table 4).

It was observed that Lycopene concentration was decreased significantly ($p < 0.05$) at all venlafaxine concentrations. On the other hand, the addition of vitamin C to the growth medium (25, 50, and 75 ppm) containing 200, 300, 400, and 500 ppm venlafaxine increased lycopene concentrations significantly ($p < 0.05$).

A study reported that cadmium added to the growth medium of *S. cerevisiae* increased the amount of vitamin E [30]. A survey conducted by [17] said that adding vitamin C to the nutrient medium containing cadmium increases the concentration of fat and water-soluble vitamins by reducing cadmium's toxic and negative effects on the metabolism of microorganisms.

4. Conclusion

It has been observed that the addition of Venlafaxin to the YPD medium of *S. cerevisiae* led to decreased water-soluble vitamins and lycopene concentration while increasing the A, E vitamins, and β -carotene concentrations. The addition of vitamin C to the growth medium of *S. cerevisiae* containing Venlafaxin caused the opposite effect on the concentration of all the parameters studied. It can be concluded that vitamin C reduced the negative effect of all the parameters studied caused by Venlafaxine.

Author Contributions

All the authors equally contributed to this work. They all read and approved the final version of the paper.

Conflicts of Interest

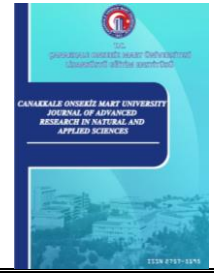
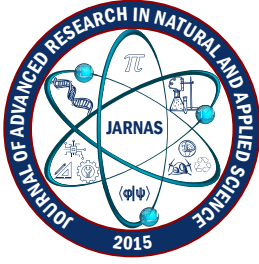
All the authors declare no conflict of interest.

References




- [1] A. M. Gil-Rodriguez, A. V. Carrascosa, T. Requena, *Yeasts in foods and beverages: In vitro characterisation of probiotic traits LWT*, Food Science and Technology 64 (2) (2015) 1156–1162.
- [2] H. Albergaria, N. Arneborg. *Dominance of Saccharomyces cerevisiae in alcoholic fermentation processes: Role of physiological fitness and microbial interactions*, Applied Microbiology and Biotechnology 100 (2016) 2035–2046.
- [3] R. Gadassi, N. Mor. *Confusing acceptance and mere politeness: Depression and sensitivity to Duchenne smiles*, Journal of Behavior Therapy and Experimental Psychiatry 50 (2016) 8–14.
- [4] H. J. Möller, I. Bitter, J. Bobes, K. Fountoulakis, C. Höschl, S. Kasper, *Position statement of the European Psychiatric Association (EPA) on the value of antidepressants in the treatment of unipolar depression*, European Psychiatry 27 (2012) 114–128.
- [5] D. O. Kennedy, *B vitamins and the brain: Mechanisms, dose and efficacy-A review*, Nutrients 8 (68) (2016) 1–29.

- [6] S. J. Devaki, R. L. Raveendran, *Vitamin C: Sources, functions, sensing and analysis*, in: A. H. Hamza (Ed.), *Vitamin C*, IntechOpen, 2017, Ch. 1, pp. 3–20.
- [7] G. Cazzanelli, F. Pereira, S. Alves, R. Francisco, L. Azevedo, P. Dias Carvalho, A. Almeida, M. Côrte-Real, M. J. Oliveira, C. Lucas, M. J. Sousa, A. Preto, *The yeast saccharomyces cerevisiae as a model for understanding RAS proteins and their role in human tumorigenesis*, *Cells* 7 (2) (2018) E14 36 pages.
- [8] R. Amidžić, J. Brborić, O. Čudina, S. Vladimirov, *Rp-HPLC determination of vitamins, folic acid and B12 in multivitamin tablets*, *Journal of the Serbian Chemical Society C* 70 (2005) 1229–1235.
- [9] K. W. Miller, N. A. Lorr, C. S. Yang, *Simultaneous determination of plasma retinol, α -tocopherol, lycopene, α -carotene, and β -carotene by high-performance liquid chromatography*, *Analytical Biochemistry* 138 (2) (1984) 340–345.
- [10] M. S. Ibrahim, Y. I. Ibrahim, Z. G. Mukhtar, F. Karatas, *Amount of vitamin A, vitamin E, vitamin C, malondialdehyde, glutathione, ghrelin, beta-carotene, lycopene in fruits of Hawthorn, Midland (Crataegus laevigata)*, *Journal of Human Nutrition and Food Science* 5 (3) (2017) 1112–1117.
- [11] K. S. El-Gendy, N. M. Aly, F. H. Mahmoud, A. Kenawy, A. K. H. El-Sebae. *The role of vitamin C as antioxidant in protection of oxidative stress induced by imidacloprid*, *Food and Chemical Toxicology* 48 (1) (2010) 215–221.
- [12] E. Çöteli, F. Karataş, *The research of the effects on antioxidant enzymes of yeasts exposed to chromium III chloride salt by adding vitamin C*, *Gümüşhane University Journal of Science and Technology* 11 (4) (2021) 1071–1081.
- [13] S. Acharya, U. R. Acharya, *In vivo lipid peroxidation responses of tissues in lead-treated Swiss mice*, *Industrial Health* 35 (1997) 542–544.
- [14] F. Depeint, W. R. Bruce, N. Shangari, R. Mehta, P. J. O'Brien, *Mitochondrial function and toxicity: Role of B vitamins on the one-carbon transfer pathways*, *Chemico-Biological Interactions* 163 (2006) 113–132.
- [15] F. Depeint, W. R. Bruce, N. Shangari, R. Mehta, P. J. O'Brien, *Mitochondrial function and toxicity: Role of the B vitamin family on mitochondrial energy metabolism*. *Chemico-Biological Interactions* 163 (2006) 94–112.
- [16] L. M. Young, A. Pipingas, D. J. White, S. Gauci, A. Scholey, *A systematic review and meta-analysis of B vitamin supplementation on depressive symptoms, anxiety, and stress: Effects on healthy and 'At-Risk' individuals*, *Nutrients* 11 (9) (2019) 2232 19 pages.
- [17] M. S. Ibrahim, M. Çakmak, D. Özer, F. Karataş, S. Saydam, *Effect of vitamin C on cadmium depending growth and vitamin C contents of Citrobacter Freundii*, *Journal of Advanced Research in Natural and Applied Sciences* 7 (3) (2021) 333–342.
- [18] R. Medina-Silva, M. P. Barros, R. S. Galhardo, L. E. S. Netto, P. Colepicolo, C. F. M. Menck. *Heat stress promotes mitochondrial instability and oxidative responses in yeast deficient in thiazole biosynthesis*, *Research in Microbiology* 157 (3) (2006) 275–281.
- [19] H. Liang, Q. Liu, J. Xu, *The effect of riboflavin on lipid peroxidation in rats*, *Wei Sheng Yan Jiu* 28 (1999) 370–371.
- [20] R. S. Tupe, S. G. Tupe, V. V. Agte, *Dietary nicotinic acid supplementation improves hepatic zinc uptake and offers hepatoprotection against oxidative damage*, *British Journal of Nutrition* 105 (2011) 1741–1749.
- [21] S. Zehra, M. A. Khan, *Dietary pantothenic acid requirement of fingerling Channa punctatus (Bloch) based on growth, feed conversion, liver pantothenic acid concentration and carcass composition*, *Aquaculture Nutrition* 24 (5) (2018) 1436–1443.

- [22] M. Velásquez, D. Méndez, C. Moneriz, *Pyridoxine decreases oxidative stress on human erythrocyte membrane protein*, The Open Biochemistry Journal 13 (1) (2019) 37–44.
- [23] H. Koyama, S. Ikeda, M. Sugimoto, S. Kume, *Effects of folic acid on the development and oxidative stress of mouse embryos exposed to heat stress*, Reproduction in Domestic Animals 47 (6) (2012) 921–927.
- [24] E. A. Abdelfattah, *Effect of different concentration and application time of vitamin B12 on antioxidant response of *Physiophora alcea**, African Journal of Biological Sciences 17 (1) (2021) 189–203.
- [25] R. Roehrs, D. R. Freitas, A. Masuda, J. A. Henriques, T. N. Guecheva, A. L. L. Ramos, J. Saffi, *Effect of vitamin A treatment on superoxide dismutase-deficient yeast strains*, Archives of Microbiology 192 (3) (2010) 221–228.
- [26] D. Satapathy, T. K. Dutta, A. Chatterjee, M. Karunakaran, M. K. Ghosh, A. Mohammad, *Evaluation of ameliorative efficiency of vitamin E and *Saccharomyces cerevisiae* yeast on arsenic toxicity in Black Bengal kids*, Small Ruminant Research 202 (2021) 106473 9 pages.
- [27] J. Finaud, G. Lac, E. Filaire, *Oxidative stress: Relationship with exercise and training*, Sports Medicine 36 (2006) 327–358.
- [28] S. Yu, I. Paetau-Robinson, *Dietary supplements of vitamins E and C and β -carotene reduce oxidative stress in cats with renal insufficiency*, Veterinary Research Communications 30 (2006) 403–413.
- [29] P. D. Sarkar, T. Gupt, A. Sahu, *Comparative analysis of lycopene in oxidative stress*, The Journal of the Association of Physicians of India 60 (2012) 17–19.
- [30] O. A., Kireççi, *Effect of Heavy Metals (Manganese, Magnesium, Cadmium, and Iron) added *Saccharomyces cerevisiae* Culture Medium on Some Biochemical Parameters*, Journal of Agriculture and Nature 20 (3) (2017) 175–184.



Assessment of Construction Site Management Practices: A Case Study of a Construction Project in Hargeisa

Abdirisak Mohamed Abdillahi¹ , Zübeyde Özlem Parlak Biçer² , Savaş Bayram³ 

¹Institute of Natural and Applied Science, Erciyes University, Kayseri, Türkiye

²Department of Architecture, Faculty of Architecture, Erciyes University, Kayseri, Türkiye

³Department of Civil Engineering, Faculty of Engineering, Erciyes University, Kayseri, Türkiye

Abstract – The effective management of construction sites is crucial for minimizing risks such as lost productivity, injuries, and theft and ensuring the successful completion of projects. Site management encompasses applying scientific methods and evaluation criteria to plan and organize various production factors, including workforce, machinery, and materials. Managing these factors is vital for transforming raw materials into the final product. Inefficiencies in site management often lead to increased rework, defects, delays, disputes, and cost overruns, affecting construction projects. This study evaluated a construction project in Hargeisa, utilizing six established construction site management practices as assessment criteria. The findings reveal significant shortcomings in the site management practices, with 15 key items within these practices either partially performed or not performed. These inadequacies mirror the broader challenges construction sites face in Hargeisa, highlighting the need for a more robust and comprehensive site management approach. The study's findings indicate that implementing an improved site management procedure is critical for the long-term sustainability of the construction industry in Hargeisa. Such improvements are essential for enhancing project efficiency, reducing costs, and safeguarding the health and safety of workers and all individuals involved in the construction projects. Based on the evaluation, the study proposes specific recommendations to address these shortcomings, aiming to contribute to advancing construction site management practices in the region. These recommendations could significantly improve project outcomes, worker safety, and industry standards.

Article History

Received: 18 Apr 2023

Accepted: 30 Jan 2024

Published: 15 Mar 2024

Research Article

Keywords – Construction, management practices, site management, Somaliland

1. Introduction

The construction industry is critical to the economic development of countries. It contributes directly and indirectly to the economic productivity of especially developing and underdeveloped countries [1]. Due to its close links with other sectors of the economy, the industry contributes significantly to the development and expansion of human settlements. It also promotes employment and income through development and economic growth [2]. The construction sector in Somaliland plays a crucial role in the country's economic growth and sustainability, much like in other low-income countries. However, the sector in Somaliland faces unique challenges due to the absence of building codes or regulations, leading to safety standards primarily maintained by building owners and contractors [3]. Against this backdrop, our study specifically focuses on examining construction site management practices within the scope of a public construction project in Somaliland.

The primary aim of this study is to systematically assess and identify the prevailing construction site management practices in Somaliland, particularly focusing on a public construction project. We intend to

¹abdirisaksajin@gmail.com (Corresponding Author); ²parlako@erciyes.edu.tr; ³sbayram@erciyes.edu.tr

evaluate these practices against established standards and identify areas for improvement. In doing so, we hope to enhance construction site management, fostering better safety standards, efficiency, and overall project success in Somaliland's construction sector.

While there have been numerous studies on construction site management practices, this research is distinctive in its focus on the specific context of Somaliland, a region with unique challenges due to the absence of formal building codes and regulations. This study comprehensively assesses current construction site management practices in Somaliland and offers a pioneering analysis by benchmarking these practices against international standards. Furthermore, our exploration of six basic site management practices is tailored to address the specific context and requirements of the Somaliland construction sector. This novel approach aims to yield contextually relevant insights and broadly applicable to similar regions facing comparable challenges. Through this study, we aim to contribute to the body of knowledge in construction site management, particularly in under-researched regions, and offer practical recommendations for enhancing safety, efficiency, and success in construction projects within such unique contexts. Following the framework outlined by Jimoh [4] and Mohamed [5], our study will explore six basic practices for site management, providing a comprehensive analysis of their application and effectiveness in Somaliland's construction sector.

• **Management, Supervision, and Administration of Construction Sites:** The management of construction sites is a critical process that hinges on effectively disseminating and exchanging information. This exchange encompasses a wide array of information, such as meeting minutes, requests for information, labor allocation documents, payrolls, progress reports, notices or requests, instructions, drawings, and technical information [6]. The efficiency and effectiveness of the construction process largely depend on the quality of this communication. Improved communication between various stakeholders, including construction and project teams, managers, and contractors, reduces the likelihood of project failure [7].

Each construction project involves stakeholders collaborating relatively quickly to develop the required facilities. However, the physical separation between construction sites and offices exacerbates the complexity of exchanging information between design teams and contractors. This distance often poses significant challenges in accessing and sharing project information promptly and efficiently. It is also crucial to consider the impact of leadership styles and team dynamics on project outcomes. The study by Ju et al. [8] highlights the effects of toxic leadership and project team member's silence on mega construction projects providing valuable insights into these dynamics. It reveals that toxic leadership negatively influences project success by fostering a culture of silence among team members. This finding is significant as it underscores the importance of positive leadership and open communication in construction site management.

Furthermore, the dynamic nature of construction projects, characterized by frequent changes and adjustments, necessitates a robust and flexible communication system. Therefore, Effective communication strategies must accommodate the project's evolving needs, enabling stakeholders to respond quickly to changes and make informed decisions. To address these challenges, it is essential to implement advanced communication technologies and practices that facilitate seamless information flow. These may include digital collaboration tools, project management software, and mobile communication platforms that enable real-time updates and access to project information, regardless of the participants' location. By enhancing communication channels and adopting a more integrated approach, construction projects can achieve greater coordination, reduce misunderstandings and errors, and ultimately improve project outcomes.

The management of construction sites extends beyond the mere exchange of documents and information; it encompasses the creation of a communication ecosystem that supports the collaborative and dynamic nature

of construction projects. Emphasizing effective communication strategies and leveraging technology can significantly contribute to the success of construction projects, ensuring timely completion, adherence to quality standards, and overall project efficiency.

• **Commercial Management of Construction Sites:** Construction sites serve as the operational grounds for mobilizing resources to produce built environments. Commercializing these sites involves a multifaceted process ensuring effective utilization and control of financial resources. This process is integral to the success of construction projects, as it encompasses a range of activities, including estimations, valuations, variations, day-to-day work, cost-value reconciliation, final accounts, and cash flow management [6].

At the core of commercial management is developing a cost control system. This system enables the site management team to collect and produce financial information accurately, tracking actual costs and comparing them with estimated costs. The relevance of such a system cannot be overstated, as it provides the basis for informed decision-making and financial oversight throughout the project lifecycle. Moreover, extracting relevant information from project models and specifications is pivotal in producing realistic cost estimates [9]. These estimates are critical in planning and guiding resource allocation and expenditure during project implementation. Vivek and Hanumantha Rao [10] highlight that cost overruns are a primary source of conflict in construction projects, underscoring the importance of accurate and realistic cost planning.

Effective commercial management extends beyond cost estimation; it encompasses cost integration with other key project dimensions such as time, quality, and scope. The cost performance of a project, being a crucial indicator of its success, can be effectively managed using the fifth dimension (5D) of Building Information Modeling (BIM) [11]. This tool is a potential solution for efficient cost management, enabling better control over financial resources. Cost management is not limited to estimation but involves the application of management accounting concepts and methods for data collection, analysis, and presentation [12]. This comprehensive approach is necessary to provide the information needed to plan, monitor, and control costs effectively.

These elements collectively form the foundation of comprehensive project management. Managing costs effectively across all project stages is a financial necessity and a strategic imperative influencing the overall project trajectory. Commercial management in construction sites is a critical function that requires meticulous attention to detail and strategic foresight. It demands a holistic approach that balances financial considerations with project objectives, ensuring that projects are completed within budget and meet the desired quality and scope. By implementing robust commercial management practices, construction projects can mitigate the risks of cost overruns, reduce conflicts, and enhance their overall success.

• **Legal, Health, and Safety Management:** Legal, Health, and Safety Management is a crucial aspect of construction site management, encompassing a range of responsibilities to ensure the safety and well-being of all employees and users involved in the project. According to Kömürlü and Toltar [13], this includes providing adequate training to personnel, monitoring compliance with safety standards, and enforcing penalties when necessary to maintain high safety levels. However, the construction sector's inherent complexity and diversity present significant challenges for safety managers. As Kulinan et al. [14] note, this complexity often makes conducting thorough and effective safety inspections difficult, essential for preventing accidents and ensuring a safe working environment.

Effective health and safety management at construction sites involves more than just adherence to safety protocols; it requires a comprehensive approach legally backed by security policies, insurance, standards, and building/enforcement rules [6]. Ensuring compliance with these legal requirements is crucial for avoiding legal

disputes and maintaining a safe and secure work environment. Moreover, the project plan often serves as a formal document outlining the project's performance standards. Therefore, any deviation from the standards presented in the project plan can lead to disagreements and legal issues.

In this context, it is essential to implement proactive measures to manage health and safety risks on construction sites effectively. This includes regular risk assessments, appropriate personal protective equipment (PPE), the implementation of safety training programs, and the development of emergency response plans. Fostering a safety culture among workers and management ensures that health and safety practices are consistently applied and respected.

In the context of Somaliland, as highlighted by Fashina et al. [3], the absence of official building codes and regulations presents a significant challenge for legal, health, and safety management in construction projects. Without standardized regulations, contractors and builders often rely on their judgment and experience, potentially leading to inconsistencies in safety standards and practices. This situation complicates efforts to ensure the safety and well-being of workers but also increases the risk of legal disputes and conflicts related to construction quality and safety.

Furthermore, Fashina et al. [3], one of a few studies conducted in this context, emphasize that in Somaliland, building owners and contractors are primarily responsible for maintaining safety standards, varying significantly from one project to another. This lack of uniformity and formal regulatory oversight can result in varied levels of compliance with basic health and safety measures. The study also points out that there is a need for the government to actively involve various stakeholders, including building occupants, owners, builders, and public health professionals, in developing and implementing building codes. Such involvement is crucial for reducing risks, enhancing public safety, and promoting health in the built environment.

Implementing proactive measures to effectively manage health and safety risks on construction sites is essential. This includes regular risk assessments, appropriate personal protective equipment (PPE), the implementation of safety training programs, and the development of emergency response plans. Promoting a safety culture among workers and management is key to consistently applying and respecting health and safety practices. Furthermore, given this local context in Somaliland, construction projects must adopt best practices in legal, health, and safety management, even without formal building codes. This includes conducting regular risk assessments, ensuring the use of proper safety equipment, providing adequate training to workers, and developing emergency response plans. Additionally, there is a need for advocacy and efforts to establish official building codes and regulations in Somaliland to standardize safety practices and provide a legal framework for resolving disputes and ensuring compliance with safety standards.

• **Planning, Monitoring, and Control:** Planning, Monitoring, and Control in construction site management encompass a comprehensive process that begins with the identification, evaluation, development, and organization of the necessary resources for executing a construction project. This practice extends beyond mere resource allocation; it involves strategically arranging these resources to facilitate smooth project progression and successful delivery [6].

In every construction project, detailed planning is crucial. Plans are meticulously crafted to ensure work is conducted according to desired quality standards, completed within the predetermined timeframe, and maintained within the budget. However, due to the inherent uncertainties and complex construction work, deviations from the original plan are common. In contrast, some divergence is expected and manageable, and significant gaps between planned and actual performance warrant immediate corrective action. This alignment is necessary to steer the project back on course with its original objectives [15].

Regularly monitoring and comparing the project's progress against the plan are vital. This ongoing evaluation allows for the early detection of discrepancies, enabling project managers to implement timely control measures. Effective monitoring includes tracking resource utilization, schedule adherence, cost management, and quality control. It ensures that any deviation from the plan is promptly identified and addressed.

The importance of a robust monitoring and control system cannot be overstated. Such a system is pivotal in minimizing project deviations and ensuring the project adheres to its planned trajectory. It gives decision-makers real-time insights into the project's status, facilitating informed decision-making. When variations from the planned status are observed, decision-makers can take swift and appropriate action to rectify the situation, thus preventing further escalation of issues [16].

Planning, Monitoring, and Control form the backbone of effective construction site management. This practice guides the project through its various phases and ensures each stage aligns with its goals. By diligently applying these practices, construction projects can achieve their quality, time, and cost objectives, ultimately leading to successful project delivery.

• **Delivery and Storage of Materials:** This construction site management application is crucial in managing resource management on construction sites, particularly concerning materials and facilities. It encompasses the management of deliveries and requisitions, purchase orders, material recalls, factory returns, and other related processes, handling these aspects from various perspectives [6]. Since the cost of materials in construction projects can range from 30 to 70 percent of the total project cost [17], effectively managing these materials is essential for controlling both efficiencies and costs in construction projects.

Recent studies underscore the need to transform materials management processes to improve efficiency and effectiveness in handling materials. Inadequate construction material handling significantly impacts a construction project's entire cost, time, quality, and productivity. Therefore, improving the delivery and storage of materials is about maintaining an inventory and enhancing the overall construction process. Effective management in this area is crucial to reduce material waste during the construction phases, which is essential to avoid loss of profits and ensure project sustainability [18].

Furthermore, effective delivery and storage of materials can address potential causes of project delays, such as late purchase, late delivery, weak transport systems, and stringent public procurement procedures. Properly managed materials deliveries and storage systems can ensure timely availability of materials, preventing project timeline disruptions.

Properly managing materials in construction sites can benefit construction project management. It assists in speeding up the completion period, saving execution time, delivering high-quality works, reducing materials wastage, and improving project cash flow management. Thus, the delivery and storage of materials play a pivotal role in the overall success and efficiency of construction projects.

• **On-site Production Management:** On-site Production Management is a critical component of construction site management, focusing on applying quality procedures to on-site and off-site production. This practice is essential for maintaining high-quality levels and reducing the occurrence of malfunctions during construction. Operations supporting production include quality assurance plans and reports, adherence to contract terms, and careful review of drawings, specifications, and measurements.

One of the most common reasons for delayed activities in construction projects is issues related to construction design. The intricate design process involves multiple disciplines with strong reciprocal interdependencies. Frequent iterations are required to mature the design, and even when the design is considered complete,

managers often encounter problems with outdated drawings, incorrect measurements, and the need for further clarification of specific details [19]. These challenges can significantly impact the smooth execution of the construction process.

Quality issues, in particular, can lead to substantial delays. In addition to the extra time spent on rework, these issues can be costly and disrupt the project's schedule. Quality assurance plans and reports, contract terms, drawings, specifications, and measurements are all examples of operations that support production. Quality assurance focuses on consumer protection and provides customers with the confidence that the building has been constructed adequately under acceptable quality control conditions and is fit for its intended use [6].

It is crucial for the site manager to closely monitor production and promptly address any issues of delay or poor quality. Early identification of problems allows managerial actions to improve quality, expedite production, or update production schedules to reflect the new situation and mitigate further delays.

Effective on-site production management, therefore, requires a proactive approach to identify and address design-related issues and challenges in connecting work. By staying vigilant and responsive to these common challenges, site managers can ensure that production activities are carried out efficiently and according to plan, ultimately contributing to the successful and timely completion of construction projects.

2. Methodology

This study assessed the alignment of a public project's management approach with six established construction site management practices, as outlined in the previous section. We selected a public construction project in Hargeisa, Somaliland, as a representative case for this evaluation. Our methodology involved conducting on-site observations to closely examine the application of these six construction management practices, as defined by Jimoh [4] and Mohamed [5].

We systematically observed and recorded various aspects of the construction project's management during our site visits. This included scrutinizing practices related to planning, resource allocation, safety measures, material management, communication, and quality control. The data gathered from these observations were then meticulously evaluated and organized in a tabulated format.

This approach allowed us to comprehensively analyze how much the construction project adhered to the six key site management practices. We aimed to identify strengths and areas for improvement in the project's management approach, providing insights into the effectiveness of current practices in the context of Hargeisa's construction industry. The findings from this analysis are presented in the following sections, offering a detailed evaluation of the project's management practices and their compatibility with the established standards.

2.1. The Construction Site

The construction industry is pivotal in developing infrastructure and educational facilities, particularly in regions striving for economic and social progress. In this context, the construction site of the Somaliland National College of Education in Hargeisa stands as a prime example of how public projects can significantly contribute to educational advancement and community development. Located approximately 10 km from the city center, this project, initiated in January 2021, is a testament to the ongoing efforts to enhance the educational landscape in Somaliland.

The site encompasses two major parcels, Lot 5 and Lot 6, each with distinct structures designed to cater to the diverse needs of the college. Lot 5 features the construction of a girls' dormitory building. This two-story (Z+1) structure spans an area of 564 square meters and is meticulously designed to provide a safe and comfortable living space for female students. The dormitory is envisioned as a nurturing environment supporting its residents' academic and personal growth.

In Lot 6, the project is more expensive, comprising several key facilities. The centerpiece is a laboratory and library building, covering a single-story area of 898 square meters. This building is poised to become a hub of learning and research, equipped with modern laboratory facilities and a comprehensive collection of academic resources. Adjacent to it is the kitchen and dining hall building, encompassing a space of 402 square meters. This building is designed to be a communal area where students and faculty can gather for meals, fostering a sense of community and collaboration. An essential component of Lot 6 is constructing an underground water tank with a capacity of 425 cubic meters. This facility ensures a reliable water supply for the new buildings and the college campus.



Figure 1. Location of the project on Google Maps showing previously existing buildings

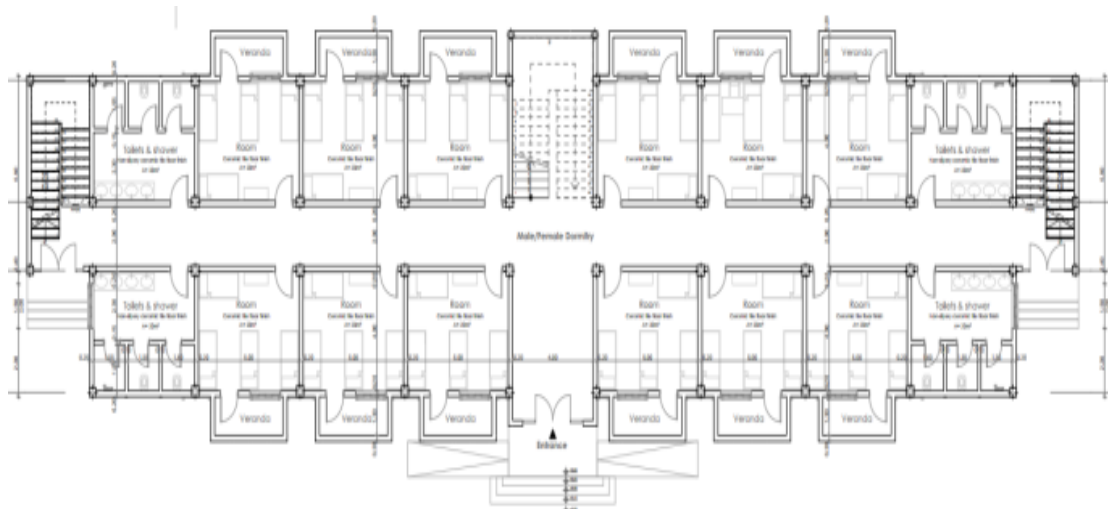


Figure 2. Lot 5 Floor Plan (Girls' Dormitory)

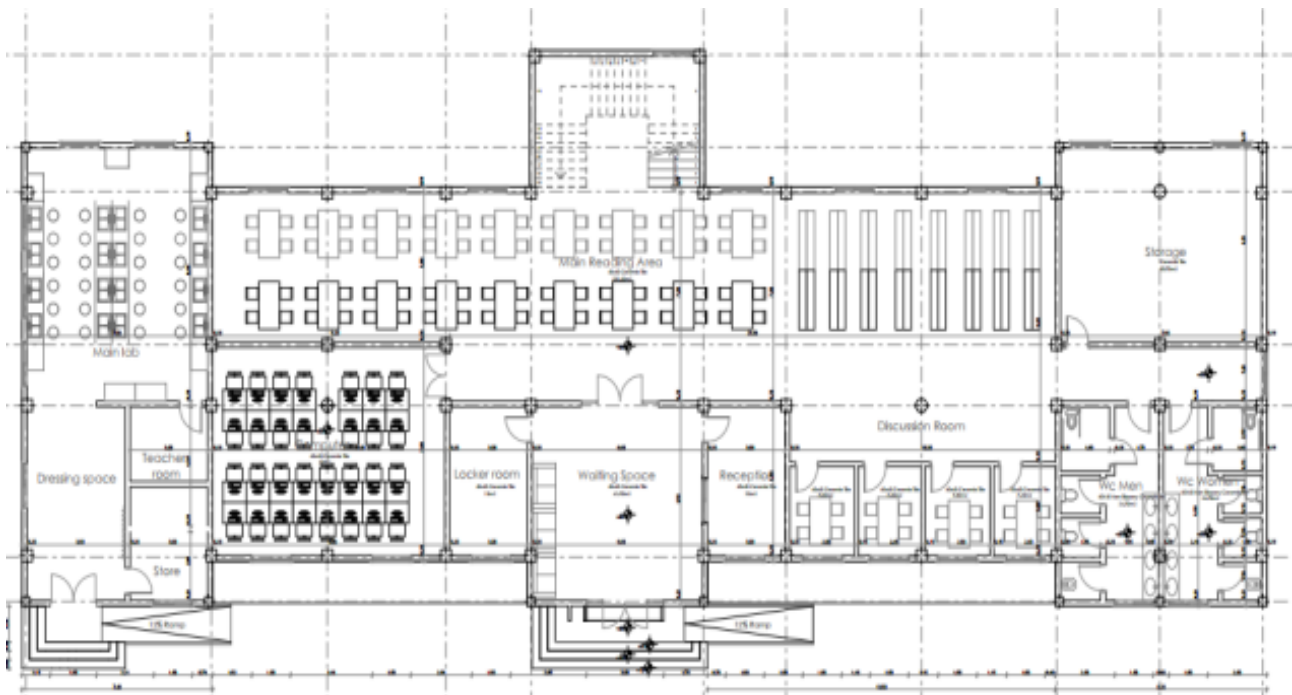


Figure 3. Lot 6 Floor Plan (Laboratory and Library)

Overall, the construction site of the Somaliland National College of Education represents a significant endeavor in the realm of educational infrastructure. The development of these new facilities is set to provide enhanced learning environments, accommodation, and essential services, thereby enriching the educational experience for students and staff at the college. This project serves as a beacon of progress and is a key contributor to the educational and socio-economic development of the region.

2.2. Current Situation of the Construction Site

This section provides a snapshot of the current state of the construction site, highlighting both the physical infrastructure in place and the progress made on specific building structures. The construction site houses two material warehouses and a single guard room, the primary facilities. However, notable absences include a dedicated management office, a technical office for project planning and execution, restrooms for workers, and a cafeteria. These missing facilities are essential for efficient site operation and worker welfare. Additionally, there is a lack of an appointed Occupational Health and Safety (OHS) expert for the project, which is a significant concern considering the importance of safety in construction sites.

As for the progress of the construction project as of April 2022, the development of various structures varies. The laboratory and library building in Lot 6 is approximately 59% complete, showcasing considerable advancement. The kitchen and dining hall in the same lot are less advanced, with around 28% completion. In contrast, the underground water tank in Lot 6 has seen significant progress, with 85% of the construction completed. On a different note, the girls' dormitory in Lot 5 is relatively less developed, with only 26% of the construction completed.



Figure 4. The current stage of the construction

The lack of critical facilities and an OHS expert points to areas that require immediate attention to ensure the smooth functioning and safety of the site. The varied completion rates across different structures indicate the ongoing nature of the project and the need for continued management and coordination to achieve completion.

In addition to the physical attributes of the construction site, it is crucial to acknowledge the broader regulatory environment in which these projects operate. The study by Fashina et al. [3] reveals that Somaliland currently lacks official building codes or standards. This absence has led to contractors relying primarily on their judgment and experience, often referencing the standards of other countries. Such a situation inevitably results in numerous legal disputes and a general lack of clarity in construction practices. The lack of standardized codes and regulations poses challenges to ensuring consistent quality and safety standards and complicates the management and administration of construction sites. This regulatory vacuum is a significant concern in the current construction landscape of Somaliland. It highlights the need to develop and implement official building codes to guide construction practices more effectively.

3. Results

This study comprehensively observed a public construction project in Hargeisa, Somaliland, to evaluate construction site management practices. The project was selected to represent typical construction practices in the region. Through a detailed and systematic approach, we aimed to identify key areas of strength and areas needing improvement in site management.

Our field observations involved multiple visits to the construction site, during which we methodically recorded various aspects of site management. We employed a systematic approach to observation, drawing on established criteria and best practices in construction management. This allowed for a thorough and unbiased evaluation of the site's operations.

The methodology for the field observations included a direct visual inspection of the site and a review of project documentation when available. This approach ensured a comprehensive understanding of the on-site management practices and their effectiveness. The main findings from our detailed field observations are presented below, providing insights into key aspects of site management that require attention:

• **Waste Management and Safety Concerns:**

Our observations revealed extensive waste scattered across the construction site floor. This creates an untidy and hazardous work environment and significantly increases the risk of injuries, particularly in the absence of personal protective equipment (PPE) usage among construction workers. The lack of PPE is a critical concern, as it exposes workers to potential harm and reflects a disregard for standard safety practices. This situation is further compounded by a widespread lack of knowledge and awareness about the risks of poor waste management, as noted by [20]. Their study highlights that both the local population and workers often have limited understanding of the dangers associated with improper waste handling, a situation likely exacerbated by the low level of education and the insufficient emphasis on awareness campaigns in Somaliland. This lack of awareness heavily impacts waste collection and disposal operations on construction sites, contributing to the unsafe conditions observed. Addressing this knowledge gap and increasing awareness among workers and the local community about proper waste management practices are essential to improving site safety and environmental health.

• **Material Storage Issues:**

We observed that construction materials were frequently stored improperly on the site, with materials often left exposed to weather conditions and rain, risking damage and degradation. This indicates a lack of adherence to proper storage protocols and could lead to increased costs due to material spoilage or the need for replacement. The importance of effective material management is further emphasized by a study conducted in Mogadishu, Somalia, by [21], which identified material-related issues as the most significant cause of construction activity cost overruns. The study highlights that selecting the winning supplier based on a lower price often leads to a lack of materials in the local market, exacerbated by the absence of dependable suppliers. This situation is particularly crucial when considering the scale and demands of the work.

According to a study by Fashina et al. [22], issues related to materials, such as increase/fluctuation in prices and procurement difficulties (Lateness), are among the most influential delay factors in construction projects in Hargeisa. Furthermore, the study highlights the shortage/lack of materials in the marketplace as a significant factor in project delays. These findings underscore the importance of proper storage and management of construction materials. Ensuring effective storage practices is essential for maintaining the integrity and usability of materials and mitigating the broader challenges of material cost fluctuations and availability, thereby ensuring the smooth progression of the construction project.

These findings underscore the critical nature of proper material storage and management practices in construction projects. Effective storage practices are essential for maintaining the integrity and usability of materials and mitigating broader challenges, such as material availability and cost fluctuations. Ensuring that materials are stored correctly, and that supplier selection is based on reliability and quality rather than solely on price can significantly contribute to construction projects' smooth progression and cost-effectiveness.

• **Lack of Occupational Health and Safety Oversight:**

A notable finding was the absence of Occupational Health and Safety (OHS) officers on the construction site. This situation mirrors the broader challenges observed in regions like Somaliland, where national occupational health and safety policies or standards are not well-established or enforced. As highlighted in the study by Fashina et al. [3], the lack of OHS oversight in construction projects is a significant concern, as it often leads to insufficient measures to ensure worker safety and health. The absence of such oversight in Somaliland's construction sector underscores the critical need to develop and implement comprehensive OHS policies and

standards. Establishing these policies is essential for safeguarding the well-being of construction workers and other stakeholders in the industry, ensuring that health and safety are prioritized and effectively managed on construction sites.

This study conducted an in-depth site investigation of a public construction project in Hargeisa, Somaliland, focusing on six key practices for site management. The main findings from this investigation are as follows:

➤ **Management, Supervision, and Administration:** Meetings are held sporadically, only deemed necessary, lacking regularity and formal structure. Workforce allocations are conducted informally without a standardized process. Progress reports are generated on an ad-hoc basis only upon request, indicating a lack of proactive project monitoring. Furthermore, there is no established format for sharing technical information, suggesting gaps in communication and information dissemination.

➤ **Commercial Management:** There is a noticeable absence of a structured cost control system. This lack of a formal system for monitoring and managing costs may lead to inefficiencies and budget overruns, highlighting a critical area for improvement in commercial management practices.

➤ **Legal, Health, and Safety Management:** The contractor has not implemented any formal health and safety policy, and the use of insurance is limited. Workers are observed performing tasks without proper safety equipment or training, indicating significant shortcomings in health and safety management. This exposes workers to potential hazards and reflects non-compliance with safety standards.

➤ **Planning:** Essential planning activities, such as creating work breakdown structures, work program development with bar diagrams, and resource leveling, are only partially executed. This incomplete planning process can lead to inefficiencies and challenges in project execution.

➤ **Delivery and Storage of Materials:** While some storage facilities are provided, they are inadequate for the project's needs. Materials are frequently left exposed to environmental elements, risking damage. This highlights deficiencies in the management and protection of construction materials.

➤ **On-site Production Management:** There is a lack of formal quality control and quality assurance plans. This absence suggests potential risks to the project's quality outcomes and underscores the need for more robust quality management processes.

The study employed site observations to systematically assess the six key site management practices. Data was collected through direct observation and analysis of available project documentation. The methods were chosen based on their alignment with best practices in construction management research and were supported by previously published references to ensure reliability and validity. This comprehensive approach allowed for a detailed assessment of site management practices and contributed to the reproducibility of the study.

In addition to the detailed observations, our findings are further elucidated in Table 1, titled 'Evaluation of the sample project according to six construction site management practices.' This table systematically evaluates the construction site's adherence to each of the six key practices. It categorizes the practices into 'Performed,' 'Partially Performed,' and 'Not Performed,' offering a clear visual representation of the project's strengths and areas for improvement.

Table 1. Evaluation of the sample project according to six practices of construction site management

Application	Work Definition	Performed	Partially Performed	Not Performed
1. Management, Supervision, and Administration of Construction Sites	1.1. Planning of meeting arrangements		√	
	1.2. Making labor allocations	√		
	1.3. Progress reporting		√	
	1.4. Technical information sharing			√
2. Commercial Management of Construction Sites	2.1. Making cost estimates	√		
	2.2. Cost-value reconciliation			√
	2.3. Implementation of cost control system			√
3. Legal, Health, and Safety Management	3.1. Health and safety policy			√
	3.2. Insurance			√
	3.3. Building Regulations			√
	3.4. Providing health and safety training to staff			√
4. Planning, Monitoring and Control	4.1. Making the work breakdown structure (WBS)		√	
	4.2. Preparation of the work program		√	
	4.3. Resource leveling		√	
5. Delivery and Storage of Materials	5.1. Management of material requests	√		
	5.2. Management of material deliveries	√		
	5.3. Proper storage of materials		√	
6. On-site Production Management	6.1. Quality control policy			√
	6.2. Quality assurance plan			√

Key findings from Table 1 include:

➤ In ‘Management, Supervision, and Administration of Construction Sites,’ labor allocations were regularly performed while planning of meeting arrangements and progress reporting were only partially performed. Technical information sharing was not observed at all.

➤ ‘Commercial Management of Construction Sites’ revealed that cost estimates were made, but cost control systems or cost-value reconciliation were not implemented.

➤ For ‘Legal, Health and Safety Management,’ none of the evaluated practices, including health and safety policy, insurance, building regulations, or staff training, were implemented.

➤ ‘Planning, Monitoring and Control’ showed partial implementation in work breakdown structure, work program preparation, and resource leveling.

➤ In ‘Delivery and Storage of Materials,’ management of material requests and deliveries were performed, but proper storage of materials was only partially implemented.

➤ ‘On-site Production Management’ lacked a quality control policy and assurance plan.

The results from Table 1 underscore the project’s significant shortcomings in several critical site management practices, particularly in legal, health and safety management, and on-site production management.

In summary, the findings from this comprehensive site investigation reveal significant shortcomings in several key areas of construction site management in Hargeisa. Notable issues include inadequate waste management and safety protocols, improper storage and handling of materials, and a lack of structured management practices across various domains, including commercial management, planning, and on-site production management. The absence of Occupational Health and Safety officers and the lack of formal health and safety policies further exacerbate these challenges.

These observations point to a pressing need for general improvements in construction site management practices in Hargeisa and Somaliland. Addressing these gaps is essential for enhancing the efficiency, safety, and overall success of construction projects in the region. The findings underscore adopting more systematic and effective management approaches, including implementing safety standards, proper material management, and structured administrative procedures.

Drawing attention to these critical issues, this study contributes to a deeper understanding of the current state of construction site management in Hargeisa. It provides a foundation for future efforts to improve practices in the region. Concerted action is required to address these challenges to ensure the successful completion of construction projects and safeguard the well-being of workers and stakeholders involved.

4. Conclusion

In conclusion, this study has shed light on the significant areas needing improvement in construction site management practices in Hargeisa. Our findings resonate with those from similar studies in other regions, highlighting universal challenges in construction management. For instance, similar to insights from the Nigerian construction industry [4], we identify inadequacies in enforcing building regulations as a critical issue. Furthermore, the Nigerian study points to the negative impact of poor communication within contractors' organizations, a challenge we also observed in Hargeisa. This reinforces the need for effective communication and information sharing for efficient site management.

Additionally, the emphasis in [4] on self-motivation and team spirit for successful project execution mirrors our findings in Hargeisa, suggesting a universally beneficial approach towards more humane and encouraging management styles in construction. This comparative analysis corroborates our findings and indicates broader systemic issues in construction site management that transcend geographical boundaries. Moreover, our study aligns with research conducted by [23] on public building construction projects in Ethiopia, which found that effective materials management practices, including construction material testing, planning, transportation, and handling systems, are crucial for project success. This study also highlighted slow responses from consultant engineers and ineffective procurement processes as primary root causes of materials management problems, paralleling issues we observed in Hargeisa. These insights emphasize the importance of efficient material management and well-planned site layout as key mitigation measures.

In summary, our research contributes to the growing body of knowledge in construction site management, underscoring the necessity of a global perspective in addressing these challenges. Future research should continue to explore parallels and differences across various geographical contexts, enriching our understanding and shaping effective strategies for construction site management globally. The findings from our study, supported by insights from similar studies, advocate for addressing common challenges such as regulatory enforcement, effective communication, positive leadership, and efficient material management to improve construction project efficiency and safety worldwide.

Author Contributions

The third author actively contributed to the editing and revision of the article, ensuring that the research findings and arguments were presented in a clear, coherent, and accurate way. The second author conceptualized the research topic, offered intellectual direction throughout the project, and significantly improved the composition and organization of the manuscript. The first author conducted data collection and analysis and wrote the manuscript with support from the second and third authors.

Conflicts of Interest

All the authors declare no conflict of interest.

References

- [1] H. Mallick, M. K. Mahalik, *Constructing the Economy: The role of construction sector in India's growth*, The Journal of Real Estate Finance and Economics 40 (3) (2010) 368–384.
- [2] C. İnak, *The impact of the construction industry on economic growth: Empirical study on Turkey*, Master's Thesis Aydın Adnan Menderes University (2019) Aydın.
- [3] A. A. Fashina, A. A., Sheikh, F. F., Fakunle, C. Opiti, *The drawbacks of the lack of building codes and regulations in Somaliland: Public health and safety implications*, PM World Journal 9 (8) (2020) 1–24.
- [4] R. A. Jimoh, *Improving site management practices in the Nigerian construction industry: The builders' perspective*, Ethiopian Journal of Environmental Studies and Management 5 (4) (2012) 366–372.
- [5] S. F. Mohamed, *Improving construction site management practices through knowledge management*, Doctoral Dissertation Loughborough University (2006) Loughborough.
- [6] O. A. Olubunmi, A. I. Olaniyi, A. Fisayo, *Diversity among construction professionals: A study of their perception of construction site management practices*, International Journal of Organization, Technology and Management 6 (2) (2014) 1010–1019.
- [7] M. Hoezen, I. Reymen, and G. P. Dewulf, *The problem of communication in construction*, in: International Conference on Adaptable Building Structures, ADAPTABLES 2006, Eindhoven University of Technology, 2006, pp. 12–14.
- [8] L. Ju, Y. P. Ji, C. Wu, X. Ning, Y. He, *Relationship between abusive supervision and workers' well-being in construction projects: Effects of guanxi closeness and trust in managers*, Engineering, Construction and Architectural Management (in press).
- [9] S. Bayram, S. Al-Jibouri, *Efficacy of estimation methods in forecasting building projects' costs*, Journal of Construction Engineering and Management 142 (11) (2016) 05016012 9 pages.
- [10] A. Vivek, C. H. Hanumantha Rao, *Identification and analyzing of risk factors affecting cost of construction projects*, Materials Today: Proceedings 60 (3) (2022) 1696–1701.
- [11] S. Azhar, *Building information modeling (BIM): Trends, benefits, risks, and challenges for the AEC industry*, Leadership and Management in Engineering 11 (3) (2011) 241–252.
- [12] M.-A., Vigneault, C. Botton, H.-Y. Chong, B. Cooper-Cooke, *An innovative framework of 5D BIM solutions for construction cost management: A systematic review*, Archives of Computational Methods in Engineering 27 (4) (2020) 1013–1030.
- [13] R. Kömürlü, L. Toltar, *Project Management in Construction and Its Effect on Project's Success*, Architecture and Life 3 (2) (2018) 249–258.

- [14] A. S. Kulinan, M. Park, P. P. W. Aung, G. Cha, S. Park, *Advancing construction site workforce safety monitoring through BIM and computer vision integration*, *Automation in Construction* 158 (2024) 105227 14 pages.
- [15] S. H. Al-Jibouri, M. J. Mawdesley, *A management game for evaluating the selection of project plans in construction*, in: G. Maas, F. Van Gassel (Eds.), *Proceedings of the 20th International Symposium on Automation and Robotics in Construction ISARC 2003 – The Future Site*, Eindhoven, 2003, pp. 383–388.
- [16] R. Maalek, F. Sadeghpour, *Reliability assessment of ultra-wide band for indoor tracking of static resources on construction sites*, in: *Proceedings of the CSCE 2012 Conference*, Edmonton, 2012.
- [17] C. Ayegba, *An assessment of material management on building construction sites*, *Civil and Environmental Research* 3 (5) (2013) 18–22.
- [18] M. Y. Wayrah, N. Sarpin, S. Mohamed, M. A. N. Masrom, *The impact of material management on construction project delivery in Somalia*, *Journal of Technology Management and Business* 8 (1) (2021) 59–72.
- [19] S. M. Lindhard, H. Neve, B. Terje Kalsaas, D. E. Møller, S. Wandahl, *Ranking and comparing key factors causing time-overruns in on-site construction*, *International Journal of Construction Management* 22 (14) (2022) 2724–2730.
- [20] V. Di Bella, M. Vaccari, *Constraints for solid waste management in Somaliland*, *Proceedings of the Institution of Civil Engineers - Waste and Resource Management* 167 (2) (2014) 62–71.
- [21] A. K. Ibrahim, M. N. B. Yasin, M. H. Hassan, *A study on causative factors of cost overrun in construction projects in Mogadishu, Somalia*, *Tropical Scientific Journal* 3 (1) (2024) 1–16.
- [22] A. A. Fashina, M. A. Omar, A. A. Sheikh, F. F. Fakunle, *Exploring the significant factors that influence delays in construction projects in Hargeisa*, *Heliyon* 7 (4) (2021) 1–9.
- [23] M. F. Taddesse, B. B. Mitikie, *Assessment of Materials Management Practice on Public Building Construction Project*, *International Journal of Engineering Science and Computing* 13 (1) (2023) 29924–29931.